

STRUCTURE-PROPERTY RELATIONS IN HIGH-MANGANESE-CHROMIUM-COPPER WHITE IRONS

A THESIS

*submitted in fulfilment of the
requirements for the award of the degree*

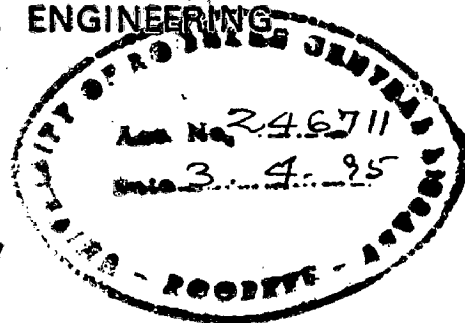
of

DOCTOR OF PHILOSOPHY

in

METALLURGICAL ENGINEERING

By

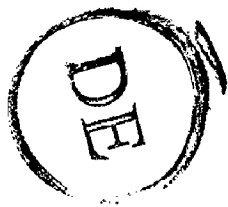


CHETANYA PRAKASH SHARMA



**DEPARTMENT OF METALLURGICAL ENGINEERING
UNIVERSITY OF ROORKEE
ROORKEE-247 667 (INDIA)**

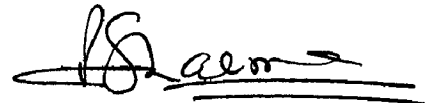
OCTOBER, 1993



CANDIDATE'S DECLARATION

I hereby certify that the work which is being presented in the thesis entitled "**STRUCTURE-PROPERTY RELATIONS IN HIGH MANGANESE-CHROMIUM-COPPER WHITE IRONS**" in fulfilment of the requirement for the award of the Degree of Doctor of Philosophy and submitted in the Department of Metallurgical Engineering of the University is an authentic record of my own work carried out during a period from October, 1987 to October, 1993 under the supervision of **Dr. A.K.Patwardhan**.

The matter presented in this thesis has not been submitted by me for the award of any other degree of this or any other University.



(**CHETANYA PRAKASH SHARMA**)

This is to certify that the above statement made by the candidate is correct to the best of my knowledge.




(**Dr. A.K. PATWARDHAN**)


Professor, Metallurgical Engg.

Date: Oct '16, 1993

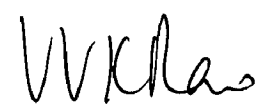
The Ph.D. Viva-Voce examination of Mr. **CHETANYA PRAKASH SHARMA**, Research Scholar, has been held on 9th February, 1994



Signature of Supervisor 9/2/94



Signature of Head of the Department 9/2/94



Signature of External Examiner

WITH THE BLESSINGS
OF
OMNISCIENT, ALMIGHTY

DEDICATED
TO
MY GRAND PARENTS
LATE SHRI (PANDIT) M.L. SHARMA & LATE SMT. H.D. SHARMA

AND

MY PARENTS
SHRI B.S. SHARMA & LATE SMT. N.D. SHARMA

AND

BROTHERS & SISTER

AND

MRS USHA (WIFE), AVANTIKA (DAUGHTER) AND ANU AYAM (SON)

PREFACE

The thesis comprises a total of eight chapters. The first chapter introduces cast irons as materials of construction. It deals with important varieties of gray cast irons such as Compacted graphite Silal, Nicrosilal, High Silicon irons and Ni-Resist irons. The second chapter deals with 'in depth' information on corrosion, wear, and heat resistant white irons. The usefulness of the Fe-Mn-Cr-Cu alloys, in resisting corrosion and wear, forms the basis of formulating the present problem highlighted in Chapter-III.

Chapter IV deals with the experimental techniques and procedures employed with major emphasis on the X-ray diffractometry, EPMA, DTA, corrosion testing, compression testing, and quantitative optical metallography.

Results and discussion have been divided into three chapters. Chapter V includes the effect of heat treating parameters on the hardness and microstructure characterized qualitatively as well as quantitatively. This has led to the development of a number of models and some new ideas encompassing 'quantitative characterization of 2nd phase particles' and 'homogeneity/heterogeneity' of the alloy(s)/system.

Chapter VI deals with the (i) structural investigations by X-ray diffractometry and EPM analysis to carry out a detailed phase analysis and for assessing the partitioning behaviour of Mn, Cr, Si, and Cu into the matrix, massive carbide, dispersed second phase (spherical & plate like) and the hitherto unobserved gray etching phase (formed on heat treating from 1000°C and (ii) study of the transformation behaviour of the alloys by DTA primarily to assess the suitability of selected microstructures for high temperature applications.

Chapter VII is devoted to an assessment of the deformation behaviour of selected microstructures in the as-cast and in the heat treated conditions by compression testing, electro-chemical characterization of selected microstructures by weight loss methods, and a study of the corroded specimens by scanning electron microscopy.

A salient feature of the present study has been the development of a number of mathematical models interrelating the

- (i) heat treating parameters with the hardness,
- (ii) microstructure (especially the effect of second phase corresponding MC & DC) with the corrosion rate,
- (iii) hardness with the compression strength,
- (iv) compressive strength with the corrosion behaviour,

- (v) distribution of the massive & dispersed second phase with homogeneity/heterogeneity
- (vi) size distribution of the dispersed second phase with coarsening

Based on the above findings, conclusions have been drawn with regard to the transformation behaviour of the alloys under various heat treating conditions and the suitability of different microstructures from the point of view of corrosion resistance, and mechanical properties finally leading to the optimization of microstructure for obtaining the aforesaid properties. They (conclusions) are enumerated in the chapter VIII.

The key features of the present investigation are (i) the development of corrosion resistant cast iron having corrosion resistance comparable to that obtained in the conventional Ni-Resist cast irons with an additional advantage of improved mechanical properties, (ii) defining a new parameter to represent the homogeneity/heterogeneity of the structure, (iii) development of several 'models' very useful for optimizing microstructure & for quantifying structure-property relations, and (iv) extensive use of computational techniques and the development of application software, of immense use for materials development/characterization, for the IBM compatible PC-AT & PC-486 systems.

SYNOPSIS

[A] OBJECTIVE(S)

The present study essentially comprised a detailed investigation of certain newly designed Fe-Mn-Cr-Cu white irons, containing 10Mn-7Cr-3.7C and alloyed with 1.5, 3.0, and 5.0%Cu, in the air cooled condition. The investigation forms a part of an 'on-going' research programme, aimed at developing a new generation of 'corrosion resistant irons', to overcome the limitations of highly alloyed 'Ni' containing proprietary compositions called 'Ni-Resist' irons. The study comprised assessing the heat treatment response of the experimental alloys with a view to establish interrelation between structure and properties. Establishing the transformation characteristics, which formed the base of the study, was carried out by employing hardness measurements, optical and scanning metallography, quantitative metallography, X-ray diffractometry, electron probe micro analysis and differential thermal analysis.

Electrochemical characterization was carried out by the weight loss method. Compression testing proved useful in assessing the deformation behaviour. Computational techniques were extensively employed for data analysis using IBM compatible PC-XT and PC-486 systems.

Round specimens of the three alloys C1, C2, and C3 were aircooled from 800, 850, 900, 950, 1000 and 1050°C after holding for 2, 4, 6, 8 and 10 hours. The microstructure, which was influenced by the Cu content and heat treating schedule, comprised : (i) Austenite (A) + Martensite (M) + MC in the as-cast state and on heat treating up to 850°C, (ii) A + MC + dispersed second phase (DSPs) on heat treating up to 950°C, (iii) A + MC (mostly rounded/hexagonal) + some stray dispersed carbides (DCs) on heat treating up to 1000°C, and (iv) A + agglomerated MCs treating up to 1050°C.

Increasing the temperature and/or soaking period decreased the amount of massive carbides (MCs). This tendency was marked at >950°C. Carbides were mostly discontinuous on heat treating from 900°C and the 'rounding-off' tendency set in at 950°C.

Dispersed second phase (DSPs) formed on heat treating at 800°C and 850°C directly from austenite. They either had a needle shaped or a rounded morphology and coarsened with temperature and time, the tendency being marked at 900°C and 950°C. Coarsening has been represented by a newly evolved parameter called the 'coarsening index'(CI). The dispersed carbides dissolved on heat treating from 1000°C.

Hardness measurements provided a reliable measure of the mechanical properties of the transformation product(s). The relationship between hardness, temperature & time is of the form:

$$H = K_1 e^{K_2/T} + (K_3 + K_4.T).t$$

where, H = hardness (VHN₃₀); T = temperature (°K); t = time (seconds); and K₁, K₂, K₃ and K₄ are constants and are different for different alloys.

This model has been shown to be valid and physically consistent with the structural changes with the first term modelling the matrix transformations and the second term the 'carbide' transformations. 3D plots between hardness - temperature - time and the 'iso-hardness' plots gave a useful insight into the hardness sustaining ability of the alloys.

It has been demonstrated that the transformation behaviour, arrived at on the basis of 30 experiments can be equally accurately predicted based on merely 4 or 6 experimental data points by 'simulating' the 'modelled' transformation behaviour. The new idea put forth could greatly help in minimizing arduous experimentation and needs further exploring.

The variation in volume fraction of MCs and DCs for a given heat treatment has been utilized to evolve a new parameter called the homogeneity/heterogeneity index of the alloy/alloy system. Its fuller implications need further exploring.

X-ray diffractometry was helpful in identifying the matrix microstructure in 'marginal' cases (e.g. in confirming whether 'M' existed in the as-cast condition) and in establishing the identity of the carbides to form namely M_3C , M_5C_2 and M_7C_3 in the as-cast / heat treated conditions. Additionally, the presence of Cu and of Fe-Si-carbide (Fe_3Si_2C) was also established. A complete indexing of diffractograms was possible only if the formation of $CrMn_3$ and Cu_2S was also considered.

EPMA proved helpful in establishing the partitioning behaviour of Mn, Cr and Cu into the matrix and carbide phases which was influenced by heat treatment. It alone established that :

- (i) MCs and DCs are M_7C_3/M_3C type carbides,
- (ii) 'haloed' regions within the matrix are carbides,
- (iii) dark etching regions between adjoining MCs represented 'matrix regions' with different alloy concentration, and
- (iv) Cu enriched regions existed in the as-cast/heat treated conditions.

Differential thermal analysis (DTA) revealed two transformations at $540-575^\circ C$ (matrix transformation) & $960-980^\circ C$ (carbide transformation). The thermogravimetric data obtained with the help of the DTA demonstrated that the as-cast

microstructures are suitable for high temperature applications upto a service temperature of 600°C . It also proved useful in evaluating the merits of different heat treated microstructures for high temperature applications.

A mathematical model interrelating the weight gain (%TG) with temperature was developed and is of the form

$$\%TG = A_1 + A_2 e^{-A_3/T}$$

Where, TG = weight gain; T= temperature; A1, A2 and A3 are constants.

Weight loss studies , carried out in 5% NaCl solution under stagnant condition clearly brought out the effect of the second phase (MC + DC) [namely the morphology and volume fraction of the MC and the size , shape and distribution of the DCs] in influencing corrosion e.g. plate like morphology and a large volume fraction of the MC had an adverse effect. Similarly a favourable morphology e.g. a rounded or hexagonal morphology of MCs (produced on heat treating from higher temperatures) reduced the adverse effect. In comparison to this, heat treating from lower temperatures adversely affected corrosion resistance due to the diverse nature of the DSPs present (needle and spherical particles). The data thus obtained has useful implications in developing improved corrosion resistant microstructures .

Considering the modelling of the corrosion behaviour (interrelating corrosion rate with the microstructure), the different models developed during the 'on-going' alloy development programme

$$CR = [K1 + K2 (VMC) + K3 (VMC)^2] (NOP)^{K4}$$

where, VMC = volume fraction of MCs only and,

$$CR = [K1' + K2'(VMC) + K3' (VMC)^2] (DF)^{K4'}$$

where, DF = newly evolved term distribution factor (DF) defining DCs & other abbreviations have the same meaning were examined afresh in the light of the experimental data generated in the present study.

Through a critical appraisal it emerged that the final models arrived at in the present investigation are on similar lines as the ones developed before. 3D-plots between CR, VMC & NOP and CR, VMC & DF proved extremely useful in optimizing the microstructures so as to obtain the best in terms of corrosion resistance and deformation behaviour in each of the alloy.

From the point of view of mechanical properties even the as-cast microstructure responded favourably. The austenite bearing microstructures containing needle type DSPs showed somewhat lower compressive strength(CS). However, the

microstructures generated on heat treating from higher temperatures attained high values of CS. The amount and stability of austenite has emerged as the key parameter in influencing the deformation behaviour. The effect of massive carbides on the deformation behaviour was a function of the compatibility, volume fraction and morphology while the effect of DCs was governed by their size, shape and distribution .

Model interrelating compressive strength with hardness is of the form

$$R = A1 + A2 (H) + A3 (H)^2$$

where $R = CS/H$; $H = \text{hardness}$; $A1$, $A2$ and $A3$ are constants.

Thus, summing up, the present investigation is a useful critique on developing new corrosion resistant materials based on basic physical metallurgical principles. Its high points are the modelling of structure-property relations and microstructural optimization .

ACKNOWLEDGEMENT

I express my profound sense of gratitude to my reverend guide, Professor A.K. Patwardhan, Department of Metallurgical Engineering, University of Roorkee, Roorkee for his astute research methodology and inspiration coupled with assiduity and deep insight into the subject. I am greatly indebted to him for his stimulating input of ideas, thought provoking discussions, erudite and meticulous guidance throughout the tenure of my research work.

I am highly grateful to Professor V. Srinivasan, V.C., Jai Narayan Vyas University, Jodhpur and former Principal, MR Engineering College, Jaipur for permitting me to pursue my research work at the University of Roorkee, Roorkee under QIP scheme. I am highly thankful to Dr. Sudhir Verma (IAS), Technical Secretary, Govt. of Rajasthan and Principal, M.R. Engineering College, Jaipur for extending me all the help at all times.

I am highly thankful to my teacher, Prof. T.V. Rajan, Department of Metallurgical Engineering, M.R. Engineering College, Jaipur for his punctilious guidance, perpetual encouragement, ardent and poignant moral support and personal help at various stages. I am thankful to Prof. M.K. Bhargava, Prof. & Head Dr. H.N. Dharwadkar, Department of Metallurgical

Engineering, M.R. Engineering College, Jaipur for helping me at all the critical moments in every respect.

I am thankful to Dr. D.B. Goel, Professor & Head, Dr. M.L. Kapoor, Professor and all O.C.'s of the concerned laboratories, Department of Metallurgical Engineering, University of Roorkee, Roorkee for extending the help by providing the laboratories and other facilities which enabled me to present the thesis in the present form well in time. I virtually fall short of words while expressing my respect to Prof. D.B. Goel and Dr. M.L. Kapoor who helped me from the very beginning till the completion of the thesis work.

I am thankful to Mr. P.N.V.R.S.S.V. Prasada Rao, Lecturer, Department of metallurgical Engineering, M.R. Engineering College, Jaipur and the then Research Scholar for his help throughout my period of stay at Roorkee. His generous help greatly eased the task.

I am grateful to Dr. J.L. Gaindher, Professor, Department of Mechanical and Industrial Engineering, Prof. S. Prakash, Dr. V.K. Tewari, Dr. S.K. Nath, Department of Metallurgical Engineering for their continuous help, support and for their useful discussions and suggestions extended to me. The help from Dr.

J.L. Gaindher, MIE Department, Dr. S.Ray, Dr. S. Singh, Dr. S. Prakash, Dr. R.D. Agarwal, Dr. R.C. Agarwal, and Dr. V.K. Tewari of Metallurgical Engineering Department is greatly acknowledged.

I am extremely thankful to Dr. S.R. Mediratta, DGM, R&D Centre for Iron and Steel, SAIL, Ranchi for providing the laboratories facilities to do EPMA, quantitative metallography, and DTA. In this regard, the help rendered by Mr. U.N. Jha and Mr. Mahapatra is highly acknowledged. I am also grateful to Mr. B.K. Jha and Mr. B. Singh for their help during my stay at Ranchi.

I wish to record my sincere thanks to Professor P. Rama Rao, former Director, Defence Metallurgical Research Laboratory, Hyderabad (Presently Secretary, Department of Science & Technology, New Delhi) for providing the melting facilities for alloy preparation and laboratory facilities for carrying out some part of the experimental work. The help rendered by Dr. M.L. Bhatia and Dr. R.D.K. Misra and Mr. V.V. Rama Rao for E.P.M.A. and of Dr. K.K. Sharma, Dr. N.C. Birla and Mr. Vikas Kumar for compression testing is highly acknowledged.

I am greatly thankful to Dr. Kailash Chandra, Director, USIC, University of Roorkee for providing facilities for x-ray diffractometry, scanning electron microscopy. I am also thankful

to Mr. Anil Kumar, Mrs. Rekha Sharma and Mr. K.N.R. Jaul for the help rendered.

I express my sincere gratitude to Prof. K.R. Soni, Head and Dr. C.L. Arora, Professor, Department of Physics, MREC, Jaipur for their family-and-generous touch during the period of my research work.

It is with stupendous delight I express my whole-hearted indebtedness to Dr. Surendra Kumar, Chemical Engineering Department, University of Roorkee, who always boosted my morale with his brotherly touch. I sincerely appreciate his deep personal involvement. The constant and continuous help by Sarvasri S.C. Kaushik, S.K. Seth, S.P. Anand, J.P. Sharma, Madhu Kumar, S.N. Kaushik, V.K. Tyagi, Vidya Prakash, Kailash Chand, Prem Singh and Ms. Vijay Laxmi is highly appreciated.

I fall short of words to express my inner core of heart for my eldest brother, Dr. T.P. Sharma, Head, Fire Research Laboratory, CBRI, Roorkee, who not only provided me the best facilities available at Roorkee but also took away lion's share out of my responsibilities at the critical juncture of the thesis work by rendering me his moral, monetary and physical help.

I would like to emphasize the support, forbearance and inspiration from my in-laws.

I sincerely express my grateful to Mr. Suvir Singh, Mr. R.S. Chimote, Mr. Sushil Kumar, Mr. Jalaj Prashar, Mr. Sewa Ram, Mr. Rajiv Bansal, Mr. Rajiv Kasyap and Ms. Deepti Gupta for their timely and constant efforts during the completion of my thesis work.

I am thankful to all the family members of Dr. A.K. Patwardhan, Dr. S. Kumar, Mr. Suvir Singh, Mr. R.S. Chimote for their kind support and help. I too sincerely apologise to family members of Mr. Suvir Singh, Mr. R.S. Chimote, Mr. Sushil Kumar, Mr. Jalaj Prashar, Mr. Sewa Ram, Mr. Rajiv Bansal, Mr. Rajiv Kasyap and Ms. Deepti Gupta for inconvenience caused due to strenuous work load of the thesis work.

Last but not the least, I wish to record most affectionately and with great indebtedness, the patience and excellent understanding shown by my wife Usha, daughter Avantika and son Anu Ayam to bear the gross negligence during the entire period of my research work.

In the strenuous task of my doctoral research, I received directly and indirectly assistance and help from my innumerable

colleagues with special reference to Mr. K.L. Narang and Mr. A.K. Bhargava. To acknowledge their whole-hearted assistance, I virtually fall short of words; therefore, I am leaving this acknowledgement incomplete in their reminiscences.

(C.P. SHARMA)

CONTENTS

	Page No.
CANDIDATE'S DECLARATION	i
PREFACE	ii
SYNOPSIS	v
ACKNOWLEDGEMENT	xii
LIST OF TABLES	xxvi
LIST OF FIGURES	xxxi
ABBREVIATIONS	xxxix
CHAPTER I INTRODUCTION TO CAST IRONS	
1.1 Introduction	1
1.2 Effect of elements normally present on iron-graphite/cementite 'equilibrium'	4
1.3 General classification	10
1.3.1 General purpose cast irons	12
1.3.2 Special purpose cast irons	14
1.3.2.1 Silal	15
1.3.2.2 Microsilal	20
1.3.2.3 High silicon irons	23
1.3.2.4 Ni-resist cast irons	27
1.4 Conclusions	38
CHAPTER II WHITE CAST IRONS	
2.1 Introduction	41
2.2 Plain carbon white irons	42

2.2.1 Applications	45
2.3 Alloy white cast irons	46
2.3.1 Nickel-chromium white irons	48
2.3.1.1 Morphology of carbides in Ni - hard iron	51
2.3.1.2 Ni-hard 4 vs Ni-hard 1 and 2 irons	52
2.3.1.3 Heat treatment of Ni-hard irons	54
2.3.1.4 Applications of Ni-hard irons	55
2.3.2 Chromium irons	56
2.3.2.1 Carbide morphology in chromium irons	58
2.3.2.2 Wear resistant chromium irons	60
2.3.2.3 Heat resistant chromium irons	65
2.3.2.4 Corrosion resistant chromium irons	67
2.3.3 Chromium-molybdenum irons	70
2.3.4 Chromium-manganese irons	74
2.4 Conclusions	76
CHAPTER III STUDIES IN THE Fe-Mn-Cr-Cu SYSTEM; FORMULATION OF THE PROBLEM	
3.1 Introduction	79
3.2 The approach	83
3.3 Design of alloys	86
3.4 Planning of experiments	89
CHAPTER IV EXPERIMENTAL TECHNIQUES AND PROCEDURE	

4.1	Alloy preparation	91
4.2	Specimen preparation	92
4.3	Heat treatment	93
4.4	Hardness measurement	93
	4.4.1 Macro-hardness	93
	4.4.2 Micro-hardness	94
4.5	Compression testing	95
4.6	Metallography	95
	4.6.1 Optical metallography	95
	4.6.2 Quantitative metallography	96
	4.6.3 Scanning electron microscopy	96
4.7	Electron probe micro-analyser	96
4.8	X-ray diffractometry	97
4.9	DTA studies	99
4.10	Corrosion studies	100
	4.10.1 Weight loss method	100
4.11	Data analysis	101
CHAPTER V EFFECT OF HEAT TREATMENT ON HARDNESS AND MICROSTRUCTURE		
5.1	Results	103
	5.1.1 Effect of heat treatment on hardness	103
	5.1.2 Microstructure	109

5.1.3 Quantitative metallography	123
5.1.3.1 Massive carbides	123
5.1.3.2 Dispersed second phase(DSPs)	125
5.2 Discussion	128
5.2.1 Structural changes during heating	128
5.2.2 Changes during cooling to room temperature	130
5.2.3 Strengthening response of different transformations	133
5.2.4 Interrelation between microstructure and hardness	134
5.2.4.1 As-cast state	134
5.2.4.2 Heat treated condition	136
5.2.4.3 Alloy C1	137
5.2.4.4 Alloys C2 and C3	145
5.2.4.5 Hardness-microstructure interrelation	147
5.2.4.6 Comparative changes in hardness in C1, C2, and C3 as influenced by heat treating parameters	151
5.2.5 Hardness and time interrelation	153
5.2.6 Hardness-temperature interrelations	154
5.2.6.1 Nature of variation	154
5.2.6.2 Effect of temperature on hardness and microstructure	155
5.2.6.3 Comparative hardness vs temperature data	157

5.2.7	Effect of temperature and time on the morphology and volume fraction of massive carbides	157
5.2.8	Effect of time and temperature on the distribution of dispersed second phase	160
5.2.9	Mathematical modelling of the transformation behaviour	167
5.2.9.1	Physical consistency of the proposed model	171
5.2.9.2	'Simulation' of the transformation behaviour through modelling	173
5.2.10	Mathematical modelling of the distribution factor	178
5.2.11	Homogeneity/heterogeneity of the alloys	178
5.2.11.1	3D plots representing interrelation amongst temperature, time and hardness	185
5.2.11.2	Iso-hardness plots	186
5.3	Conclusion	187
CHAPTER VI PHASE ANALYSIS AND PHASE IDENTIFICATION		
6.1	Structural analysis by X-ray diffractometry	189
6.1.1	Results	189
6.1.1.1	As-cast condition	189
6.1.1.2	Heat treated condition	190
6.1.1.2.1	Effect of heat treatment on the matrix microstructure	190

6.1.1.2.2	Effect of heat treatment on the nature of carbides	191
6.1.1.2.3	Other features	192
6.1.2	Discussion	193
6.1.2.1	Matrix microstructure	193
6.1.2.2	Carbide transformation	194
6.1.2.2.1	The M_3C	196
6.1.2.2.2	The M_7C_3	197
6.1.2.2.3	The M_5C_2	198
6.1.2.2.4	Fe_8Si_2C	200
6.1.2.2.5	Presence of elemental Cu and other phases	200
6.1.2.3	Concluding remarks	202
6.2	Electron probe micro analysis results	203
6.2.1	Elemental distribution	203
6.2.1.1	As-cast condition	203
6.2.1.2	Effect of heat treatment on elemental distribution	204
6.2.1.3	Nature of MCs	205
6.2.1.4	Identity of the different carbides	206
6.2.1.5	Identity of DSPs	206
6.2.1.6	Identity of 'haloed' regions & dark etching areas adjoining MCs	207
6.2.1.7	Identification of Cu	207
6.2.2	Discussion	208
6.2.3	Concluding remarks	215
6.3	Thermal Analysis	216
6.3.1	Results	217
6.3.1.1	Critical/transformation temperatures	217

6.3.1.2 DTA	217
6.3.1.3 Thermogravimetric studies	217
6.3.2 Discussion	218
6.3.2.1 Critical/transformation temperature(s)	219
6.3.2.2 Thermogravimetric studies	221
6.3.3 Modelling of the TG data	225
CHAPTER VII DEFORMATION & CORROSION BEHAVIOUR	
7.1 Introduction	231
7.2 Effect of heat treatment on the deformation behaviour	231
7.2.1 Modelling of the deformation behaviour	232
7.2.1.1 Interrelation between compressive strength and hardness	233
7.2.2 Effect of heat treating temperature/time	234
7.2.3 Discussion	236
7.3 Corrosion studies	240
7.3.1 Analysis of data based on "weight loss" studies	240
7.3.1.1 Weight loss data	240
7.3.1.2 Nature of corroded surfaces	242
7.3.1.3 Discussion	243
7.4 Modelling of the corrosion behaviour	248
7.4.1 Background information	248

7.4.2 Modelling of the corrosion behaviour of the experimental alloys	252
7.4.2.1 The VMC-NOP model	252
7.4.2.2 The VMC-DF model	256
7.4.3 Interrelation between corrosion and deformation behaviour	258
7.5 Concluding remarks	259
CHAPTER VIII GENERAL DISCUSSION, CONCLUSIONS AND SUGGESTIONS FOR FUTURE WORK	
8.1 General discussion	261
8.2 Conclusions	265
8.3 Suggestions for future work	278
REFERENCES	279-297

LIST OF TABLES

1.1	Conditions favouring each of the eutectic reactions in cast irons	T1
1.2	Mechanical and physical properties of C.G. irons	T2
1.3	Mechanical and physical properties of compacted graphite, grey and nodular irons	T2
1.4a	Ranges of alloy content for the corrosion & heat resistant alloyed grey cast irons	T3
1.4b	Typical mechanical properties of corrosion resistant cast irons	
	Typical mechanical properties of heat resistant alloy cast irons	T4
1.5a	Chemical composition of Ni-resist irons, percent	T5
1.5b	Mechanical properties of Ni-resist irons	T6
1.6a	Chemical composition of S.G. Ni-resist irons, percent	T7
1.6b	Mechanical properties of S.G. Ni-resist irons	T7
1.7	Commercial applications for Ni-resist ductile irons	T8
2.1	Composition and properties of some representative plain carbon white irons	T9
2.2	Chemical analysis and properties of Ni-hard	T10
2.3	Composition, properties and applications of carious Cr-Ni-white cast irons	T11
2.4	Composition and properties of some representative chromium white irons	T13

2.5	Ranges of alloy content for the corrosion & heat resistant alloyed grey cast irons	T14
2.6a	Iron carbide in Fe-C-Cr alloying system	T15
2.6b	Information of chromium, manganese, and iron bearing carbides	T16
2.7a	Composition of Cr-Mo type abrasion resistant alloy cast irons	T17
2.7b	Properties of Cr-Mo irons (from Sl.no. 5 to 10 of table 1.5a)	T18
2.8a	Composition of Cr-X type abrasion resistant irons	T19
2.8b	Typical properties of Cr-X type irons	T19
3.1	Summary of the structure-property relations in some Fe-Mn-Cr-Cu corrosion resistant cast irons	T20a
4.1	Chemical analysis of raw materials	T21
4.2	Chemical analysis of the alloys (weight percent)	T21
5.1- 5.18	Effect of soaking period on hardness in A.C. condition	T22 -T30
5.19- 5.33	Effect of soaking temperature on hardness in A.C. condition	T31 -T39
5.34	Summary table of effect of heat treatment on hardness	T40
5.35- 5.37	Effect of heat treatment on volume percent of massive carbide	T41 -T46
5.38	Summary table of effect of heat treatment on volume percent of massive carbides	T47

5.39	Effect of heat treatment on the average no. of dispersed carbides in different classes	T48
5.40	Effect of heat treatment on percent number of dispersed carbides in different classes	T49
5.41	Effect of heat treatment on the average no. of dispersed carbides	T50
5.42	Effect of heat treatment on volume percent of dispersed carbides	T51
5.43	Effect of heat treatment on the mean diameter of dispersed carbides	T52
5.44	Effect of heat treatment on distribution factor	T53
5.45	Relative coarsening behaviour of the alloys	T54
5.46- 5.48	Effect of heat treatment on size and distribution of dispersed carbides	T55 -T57
5.49- 5.51	Effect of heat treatment on the contribution of Distribution Factor of different classes	T58 -T60
5.52	Effect of heat treatment on the percent . distribution factor in classes	T61
5.53- 5.55	Relative contribution of factors constituting the model	T62 -T64
5.56- 5.58	Effect of temperature and time on hardness	T65 -T67
5.59	Massive carbide based Heterogeneity Index of the alloys as influenced by heat treating parameters	T68
5.60	Dispersed second phase based Heterogeneity Index of the alloys as influenced by heat treating parameters	T68
6.1	Phases under consideration	T69

6.2-	Summary table of diffractogram indexing	T70
6.22		-T90
6.23	Summary of X- ray diffractometric data	T91
6.25		-T93
6.26	Element distribution into the matrix as influenced by heat treatment	T94 -T95
6.27	Element distribution into the massive carbide as influenced by heat treatment	T96 -T97
6.28	Element distribution into the massive carbide(gray) as influenced by heat treatment	T98 -T99
6.29-	Element distribution within flower type	
6.32	carbide, gray phase, DC (globular feature) & copper-rich phase as influenced by heat treatment	T100 -T103
6.33	Partitioning ratios of Mn and Cr between carbide and matrix	T104
6.34	Transformation temperatures	T105
6.35	DTA	T106
6.36	Effect of heating temperature on %TG	T107
6.37	Percent increase in %TG on heating in the different temperature ranges	T108
7.1-	Effect of heat treatment on compressive	T109
7.3	behaviour	-T111
7.4	Summary table of predicted and experimentally determined compressive strength values	T112
7.5	Corrosion data in 5% NaCl solution	T113
7.6	Comparative corrosion rates of the experimental alloys in the heat treated condition	T114

7.7	Summary table of predicted vs experimentally determined CR values based on NOP	T115
7.8	Summary table of predicted vs experimentally determined CR values based on NOP(unified model)	T116
7.9	Summary table of predicted vs experimentally determined CR values based on DF	T117
7.10	Summary table of predicted vs experimentally determined CR values based on DF(with constraints)	T118
7.11	Summary table of predicted vs experimentally determined CR values based on DF(unified model)	T119
7.12	Experimentally determined and predicted compressive strength values	T120

LIST OF FIGURES

- Fig. 1.1 : The iron-carbon phase diagram showing the relationship between the stable iron-graphite equilibria (solid lines) and the metastable iron-cementite reaction (dashed lines) F1
- Fig. 1.2 : Variation of growth kinetics of graphite and carbide eutectics F2
- Fig. 1.3 : The effect of silicon (a) the eutectic temperature and (b) the phase F3
- Fig. 1.4 : Cooling curves superimposed on the eutectic temperatures of cast iron F4
- Fig. 1.5 : Schematic drawings of the five types of cast iron : (a) gray iron, (b) white iron, (c) malleable iron, (d) ductile iron, and (e) compacted graphite iron F5
- Fig. 2.1 : Vertical Sections in Fe-C-Si system F6
- Fig. 2.2 : Maurer diagram F7
- Fig. 2.3 : Section through the iron-iron carbide - silicon ferrary equilibrium diagram at 2% silicon F8
- Fig. 2.4 : Pseudo-binary phase diagrams of Ni - hard irons F9
- Fig. 5.1 : Effect of h/t time on hardness (base curves) Alloy C1 F10
- Fig. 5.2 : Effect of h/t time on hardness (base curves) Alloy F11

Fig. 5.3 : Effect of h/t time on hardness (base curves) Alloy C3	F12
Fig. 5.4 : Effect of h/t time on hardness (comparative plots) (800 deg C)	F13
Fig. 5.5 : Effect of h/t time on hardness (comparative plots) (850 deg C)	F14
Fig. 5.6 : Effect of h/t time on hardness (comparative plots) (900 deg C)	F15
Fig. 5.7 : Effect of h/t time on hardness (comparative plots) (950 deg C)	F16
Fig. 5.8 : Effect of h/t time on hardness (comparative plots) (1000 deg C)	F17
Fig. 5.9 : Effect of h/t time on hardness (comparative plots) (1050 deg C)	F18
Fig. 5.10 : Effect of h/t temperature on hardness as influenced by h/t time (Alloy C1)	F19
Fig. 5.11 : Effect of h/t temperature on hardness as influenced by h/t time (Alloy C2)	F21
Fig. 5.12 : Effect of h/t temperature on hardness as influenced by h/t time (Alloy C3)	F23
Fig. 5.13 : Effect of h/t temperature on hardness (2 hours)	F25
Fig. 5.14 : Effect of h/t temperature on hardness (4 hours)	F26
Fig. 5.15 : Effect of h/t temperature on hardness (6 hours)	F27
Fig. 5.16 : Effect of h/t temperature on hardness (8 hours)	F28

Fig. 5.17 : Effect of h/t temperature on hardness (10 hours)	F29
Fig. 5.18 : Summary bar diagram depicting the effect of alloy composition on hardness (variable h/t temperature)	F30
Fig. 5.19 : Summary bar diagrams depicting the effect of alloy composition on hardness (variable h/t time)	F32
Fig. 5.20 : Summary bar diagrams depicting the effect of h/t time on hardness (variable h/t temperature)	F34
Fig. 5.21 : Summary bar diagrams depicting the effect of h/t temperature on hardness (variable h/t time)	F36
Fig. 5.22 : Optical micrographs	F38
- 5.42	- F66
Fig. 5.43 : Effect of heat treatment on volume fraction of massive carbide (Alloy C1)	F67
Fig. 5.44 : Effect of heat treatment on volume fraction of massive carbide (Alloy C2)	F69
Fig. 5.45 : Effect of heat treatment on volume fraction of massive carbide (Alloy C3)	F71
Fig. 5.46 : % area of DCs in different classes at different locations (850°C, 2 hours heat treatment)	F73
Fig. 5.47 : % area of DCs in different classes at different locations (1000°C, 8 hours heat treatment)	F75
Fig. 5.48 : Effect of heat treatment on DF of DCs (Alloy C1)	F77

Fig. 5.49 : Effect of heat treatment on DF of DCs (Alloy C2)	F79
Fig. 5.50 : Effect of heat treatment on DF of DCs (Alloy C3)	F81
Fig. 5.51 : Experimental vs predicted hardness values of the experimental alloys	F83
Fig. 5.52 : 3D plot depicting the effect of heat treating parameters on hardness (Alloy C1)	F84
Fig. 5.53 : 3D plot depicting the effect of heat treating parameters on hardness (Alloy C2)	F85
Fig. 5.54 : 3D plot depicting the effect of heat treating parameters on hardness (Alloy C3)	F86
Fig. 5.55 : Iso-hardness plot of alloy C1	F87
Fig. 5.56 : Iso-hardness plot of alloy C2	F88
Fig. 5.57 : Iso-hardness plot of alloy C3	F89
Fig. 6.1 : Back scattered electron images of the alloys	F90
Fig. 6.2 : Differential thermal analysis plot of alloy C1	F92
Fig. 6.3 : Differential thermal analysis plot of alloy C2	F93
Fig. 6.4 : Differential thermal analysis plot of alloy C3	F94
Fig. 6.5 : Experimental vs predicted %TG plots of experimental alloys	F95

- Fig. 7.1 : Variation in C.S. with temperature as influenced by soaking period (Alloy C1) F98
- Fig. 7.2 : Variation in C.S. with temperature as influenced by soaking period (Alloy C2) F100
- Fig. 7.3 : Variation in C.S. with temperature as influenced by soaking period (Alloy C3) F102
- Fig. 7.4 : Effect of heat treatment on deformation behaviour under compression F104
- Fig. 7.5 : Effect of heat treatment on deformation behaviour under compression F106
- Fig. 7.6 : Effect of heat treatment on deformation behaviour under compression F108
- Fig. 7.7 : 3D plot depicting the effect of VMC & NOP on corrosion rate (based on equation 7.17) F110
- Fig. 7.8 : 3D plot depicting the effect of VMC & NOP on corrosion rate (based on equation 7.17) F111
- Fig. 7.9 : 3D plot depicting the effect of VMC & NOP on corrosion rate (based on equation 7.17) F112
- Fig. 7.10 : Contour plot depicting the combined effect of VMC & NOP on corrosion rate (based on equation 7.17) F113
- Fig. 7.11 : 3D plot depicting the effect of VMC & DF on corrosion rate (based on equation 7.21) F114

- Fig. 7.12 : 3D plot depicting the effect of VMC & DF on corrosion rate (based on equation 7.21) F115
- Fig. 7.13 : 3D plot depicting the effect of VMC & DF on corrosion rate (based on equation 7.21) F116
- Fig. 7.14 : Contour plot depicting the combined effect of F-113 VMC & DF on corrosion rate (based on equation 7.21) F117
- Fig. 7.15 : 3D plot depicting the effect of VMC & DF on corrosion rate (based on equation 7.22) F118
- Fig. 7.16 : Contour plot depicting the combined effect of F-113 VMC & DF on corrosion rate (based on equation 7.22) F119
- Fig. 7.17 : 3D plot depicting the effect of VMC & DF on corrosion rate (based on equation 7.22) F120
- Fig. 7.18 : 3D plot depicting the effect of VMC & DF on corrosion rate (based on equation 7.22) F121
- Fig. 7.19 : 3D plot depicting the effect of VMC & DF on corrosion rate (based on equation 7.23) F122
- Fig. 7.20 : 3D plot depicting the effect of VMC & DF on corrosion rate (based on equation 7.23) F123
- Fig. 7.21 : Contour plot depicting the combined effect of F-113 VMC & DF on corrosion rate (based on equation 7.23) F124

- Fig. 7.22 : 3D plot depicting the effect of VMC & DF on corrosion rate (based on equation 7.23) F125
- Fig. 7.23 : 3D plot depicting the effect of VMC & DF on corrosion rate (based on equation 7.24) F126
- Fig. 7.24 : 3D plot depicting the effect of VMC & DF on corrosion rate (based on equation 7.24) F127
- Fig. 7.25 : 3D plot depicting the effect of VMC & DF on corrosion rate (based on equation 7.24) F128
- Fig. 7.26 : 3D plot depicting the effect of VMC & DF on corrosion rate (based on equation 7.24) F129
- Appendix:
- Fig. A1- : Percent area of particles in A3 different classes at different locations as influenced by heat treating parameters A1-A3
- Fig. A4 : Variation in Vf of MC as influenced by h/t temperature (2 hours soaking period) Alloy C1 A4
- Fig. A5 : Variation in Vf of MC as influenced by h/t temperature (2 hours soaking period) Alloy C2 A5
- Fig. A6 : Variation in Vf of MC as influenced by h/t temperature (2 hours soaking period) Alloy C3 A6
- Fig. A7 : Variation in Vf of MC as influenced by h/t temperature (10 hours soaking period) Alloy C1 A7

Fig. A8 : Variation in Vf of MC as influenced
by h/t temperature (10 hours soaking
period) Alloy C2

A8

Fig. A9 : Variation in Vf of MC as influenced
by h/t temperature (10 hours soaking
period) Alloy C3

A9

ABBREVIATIONS

A	Austenite
AC	Air cooled
AVE, Ave, ave	Average
B	Bainite
BCC	Body centered cubic
BHN	Brinell hardness number
C	Carbon
C1, C2, C3	Alloy designation
Cb	Carbide
C.C	Correlation coefficient
CE	Carbon equivalent
CI	Coarsening Index
COND	Condition
CONF	Confidence
COP	Cross over point
CR	Corrosion rate
CS	Compressive strength, MN/m ²
DC	Dispersed carbide
DCs	Dispersed carbides
DF	Distribution factor
DIFF	Diffraction angle

DSPs	Dispersed second phase particles
DTA	Differential Thermal Analysis
EPMA	Electron probe micro analysis
exp, Exp	Experimentally determined
FCC	Face centered cubic
GB	Grain boundary
Gms, gms	Grams
H	Hardness
Hm	Heterogeneity of the structure based on volume fraction of massive carbides
Hm(dist)	Distributional heterogeneity related with precipitated second phase
HRS, h, hr, hrs, Hrs	Hours; austenizing period; test duration
HT, H/T, h/t	Heat treatment
HV30	Vickers hardness at 30 kg load
INT	Intensity
IPY, ipy	Inch penetration per year
M	Martensite
mA	Milliampere
mV	Millivolt
Max, max	Maximum
Max.Dev	Maximum deviation
MC	Massive carbide

MCs	Massive carbides
M3	M3C (orthorhombic)
M5	M5C2 (monoclinic)
M7	M7C3 (hexagonal)
M23	M23C6 (cubic)
MDD, mdd	Milligram per decimeter ² / day
Meas, MEAS	Measured
MN/M ² , MN/m ²	Mega newton per square meter
MPa	Mega Pascal
mpy	mils per year
Min	Minimum
NOP	Number of particles
NP	New phase
OQ	Oil quenched
P	Pearlite
per	permissible
pre, Pre	Predicted from model/equation
RA	Retained austenite
R.T	Room temperature
SD, S.D.	Standard deviation
S.N, S.No.	Serial number
SP	Soaking period/austenitizing period
ST	Soaking temperature
SA, S. AREA	Surface area

CHAPTER I

INTRODUCTION TO CAST IRONS

1.1 INTRODUCTION

Cast iron is a generic term used to identify a large family of ferrous alloys which in the simplest form are regarded as binary alloys of iron and carbon [Stickle (S15), Walton (W1)]. The lower limit of carbon may exceed its maximum solubility in austenite. Although the upper limit may approach the carbon content of iron carbide (Fe_3C), it rarely exceeds 4 per cent [Avner (A8)] because it is difficult to produce binary alloys with 'C' in excess of 4 % commercially owing to economic and technical limitations. Besides carbon, varying quantities of other elements such as silicon, manganese, phosphorus and sulphur are always present in cast irons. The role of silicon is so dominant that the term cast iron is usually applied to a series of iron, carbon and silicon alloys [Lakhtin (L3)].

Because production cost of pig iron, the raw material for making cast irons, is relatively low as compared with other alloys, and since no expensive refining process is necessary, cast iron is regarded as low priced engineering material.

Cast irons offer a wide range of properties namely strength, hardness, machinability, wear resistance, abrasion resistance, corrosion & oxidation resistance . Further more, the founding characteristics of cast irons such as yield, fluidity, shrinkage, soundness, ease of production, and others make it an ideal choice as a cast material. In fact the ease with which a wide range of properties can be attained in them makes them an important class of engineering material but also ensures their continued and wide-spread use even as ' high-tech ' materials [Heine (H5)].

Since many types of cast irons have been developed and are in use, it is desirable to review the underlying physical metallurgical principles critically in order to project an over all picture of the family of cast irons to arrive at the 'technologically significant ' and ' technologically deficient ' regimes. Evidently the starting point for such an agenda is the Fe-C diagram.

Though Fe-C diagram is of great value, it is not an equilibrium diagram in the true sense since cementite has a natural tendency to decompose into iron (ferrite) and carbon (graphite). However, once formed, cementite is quite stable and for practical purposes is regarded as an equilibrium phase.

The equilibrium between iron and graphite is shown in solid lines whereas the dashed lines represent the metastable relationship between iron and cementite (Figure. 1.1) [Askeland (A4)]. Although the former represents stable reactions (i.e. all structures should eventually have graphite), nucleation of graphite in iron-carbon alloys is so difficult that one almost always obtains undercooling ($> 6^{\circ}\text{C}$) which allows the metastable reactions to occur [Askeland (A4)]. Figure 1.2 [Hillert (H9)] shows the variation of the growth kinetics of the graphite and carbide eutectics as a function of temperature. The diagram shows that in the temperature range $1155-1148^{\circ}\text{C}$ only the graphite phase can exist. If nucleated, it will grow without competition from the carbide. Just below the equilibrium temperature for the carbide phase, its growth rate is lower than that for graphite. This changes rapidly with decreasing temperature, so that the curves cross at approximately 2°C below the carbide equilibrium; in the prevailing situation carbide phase will grow faster than graphite and hence will dominate the structure as the temperature further decreases [Minkoff (M13)].

Addition of silicon increases the temperature difference between the "stable" and "metastable" eutectic reactions (Figure. 1.3) [Askeland (A4)]. When a liquid iron-carbon-silicon alloy cools, there is a large temperature interval within which stable

iron-graphite eutectic reaction can take place. If solidification occurs between the two eutectic temperatures (Figure. 1.4) [Askeland (A5)], a graphite-containing iron, such as grey, ductile or compacted graphite, is produced. If solidification occurs below the lower eutectic temperature, a white iron forms. Conditions favouring the occurrence of the two eutectic reactions are shown in Table 1.1 [Askeland (A4)]. In some instances, both the eutectic reactions may occur e.g. mottled irons begin to solidify above the lower eutectic temperature (LET) and solidification is completed below it (LET) [Askeland (A4)].

1.2 EFFECT OF ELEMENTS NORMALLY PRESENT ON IRON-GRAPHITE / CEMENTITE 'EQUILIBRIUM'

Presence of elements would influence the general state of equilibrium as well as the state in which carbon could exist. Carbon may be present either in the combined form (as carbide) or in free form (as graphite). This aspect has a major influence on the physical and mechanical properties. The term total carbon (TC) represents the sum of the free and combined carbon (including carbon in solution).

For the Fe-C alloys, the eutectic occurs at 4.3 per cent carbon. Alloys above this carbon level are termed hypereutectics and those below it as hypoeutectics. The hypereutectic compositions may develop coarse open-grained structure and comparatively large flakes of "kish" graphite when cooled slowly. Hypoeutectic alloys, on the other hand, attain relatively fine graphite and denser and tighter structures. The aforesaid tendencies become more marked as the carbon content of the hypereutectics is raised and that of the hypoeutectics lowered.

Presence of unintentionally added elements affects the solubility of carbon. Both silicon and phosphorus reduce the amount of carbon required to form the eutectic by 0.3 per cent for each 1 weight per cent of the element added [Strauss (S16)]. This gives rise to a concept known as the "carbon equivalent" which is employed as a basis to define cast irons. Carbon equivalent (CE) is given by the expression,

$$CE = \%TC + (\%Si + \%P)/3$$

For alloyed irons, the expression would also include effect(s) from other elements. The eutectic composition is always near 4.3% CE. Any cast iron with a CE less than 4.3% is hypoeutectic whereas any with a CE greater than 4.3% is

hypereutectic. A hypoeutectic alloy will have lower carbon and silicon contents whereas hypereutectic alloy will have higher carbon and silicon contents. In general, the lower the CE value, the greater the tendency for an iron to solidify white or mottled [Askeland (A4)].

The total carbon and silicon contents of an alloy, as reflected in the CE value, not only establish the solidification temperature range of the alloy, but are also related to its foundry characteristics and properties. Cast irons of the same CE value may be obtained with different carbon and silicon values and consequently differing in properties.

The lower the carbon equivalent value below 4.3 the more likely it is that undercooling will take place and graphitization occurs with increasing reluctance and will become completely suppressed if the undercooling attains the temperature at which the carbide eutectic forms. Very slow cooling encourages the precipitation and growth of graphite [Strauss (S16)].

Addition of silicon shifts the eutectic composition to the left and lowers the eutectic temperature. Silicon is a potent graphitizer and therefore the silicon bearing cast irons solidify as per the stable iron-graphite system unless the graphitizing tendency is offset by adding carbide forming element(s). Carbon

separates as primary graphite in the form of flakes. Such an happening would preclude any alteration of its shape. Presence of graphite flakes imparts discontinuity to the matrix and is responsible for the low strength and low ductility of grey irons [Avner (A9)]. Silicon dissolves in the iron forming a solid solution which increases hardness as silicon increases. The presence of this dissolved silicon in the matrix, up to a certain point also adds to its strength. This can be understood by the fact that the strength of Fe-4% Si alloy is almost double and that of Fe - 2% Si alloy is about 1.6 times the strength of pure iron [Lorig (L5)].

The main function of manganese in cast irons is to counteract the undesirable effect of sulphur by forming manganese sulphide. It is lighter than iron sulphide and floats out of the molten iron as slag. In the absence of Mn, sulphur is present as iron sulphide which is retained in the melt and deposited around the grain boundaries inducing hot shortness.

The indirect effect of Mn, therefore, is to promote graphitization by combining with sulphur [Higgins (H7)]. For manganese to act as an alloying element, its amount present must exceed that which will combine with sulphur i.e. theoretically it should be 1.7 times the sulphur content [Walton

(W2)]. However, a formulation of practical interest is given by the relation :

$$\% \text{ Mn} = \% \text{ S} \times 1.7 + 0.15$$

Manganese in excess of that required to combine with the sulphur stabilizes carbide. This leads to an increase in the chilling tendency and therefore the hardness [Askeland (A5), Avner (A9)].

When present in amounts ranging from 0.40 to 1.00 per cent, manganese may increase machinability. In amounts less than 1.00 per cent, manganese has little effect on mechanical properties. The addition of manganese in excess of 1.25 per cent increases strength, hardness, chill and resistance to wear but decreases machinability [Higgins (H7)]. As will be evident, manganese can play an effective role in developing alloyed irons.

Sulphur has a marked influence on hardening. In the absence of sufficient manganese, sulphur increases stability of the iron carbide very markedly and also the chilling tendency. Sulphur renders molten iron sluggish which leads to defects such as short running and pinholes due to entrapment of mould and other gases. Undesirable effects of sulphur can be counteracted by manganese additions. Manganese also raises the fluidity of the molten cast

iron [Avner (A9), Higgins (H7)].

The solid solubility of phosphorus is limited in austenite and so phosphorus in cast irons is present as iron phosphide, which is a constituent of iron-iron phosphide eutectic in grey irons and the iron-iron phosphide-cementite eutectic in mottled and white irons. Phosphides are similar to carbides. They cause machining problems but are not eliminated by heat treatment. The eutectic has a relatively low melting point (960°C) and consequently phosphorous bearing irons have better fluidity.

Phosphorus has a negligible effect on the stability of cementite, but its direct effect is to promote hardness and brittleness due to the large volume of phosphide eutectic which a comparatively small amount of phosphorus will produce. Phosphorus must be kept low in irons where shock resistance is important. Increasing amounts of silicon reduce the effect of phosphorus.

Phosphorus bearing cast irons exhibit improved wear resistance and good resistance to severe corrosive attack, notably from hydrochloric, sulphuric and acetic acids .

High phosphorus content has been associated with the segregation of molybdenum, chromium, vanadium and tungsten. This leaves areas of the matrix depleted in these elements and reduces

strength. 'Phosphide eutectic liquid' at cell boundaries creates a mushy state that is difficult to feed. This condition creates high eutectic solidification forces within the outer solidifying shell, causing mould wall movement and a requirement for feed metal in the final stages of solidification. This can lead to shrinkage porosity. Phosphorus increases fluidity and extends the range of eutectic freezing, thus increasing primary graphitization when the silicon content is high and phosphorus content is low. It is therefore useful in very thin castings where a less fluid iron may not take a perfect impression of the mould.

The elements (Si, Mn, S & P) discussed above, though normally present in all varieties of cast irons, have a major influence on the soundness of the castings. Once they are taken care of, it becomes relatively simpler to add the main alloying elements for the specific effect(s) they impart.

1.3 GENERAL CLASSIFICATION

Cast irons are most extensively used casting alloys despite a considerable decrease in their production during the past decade. Ability to produce complex shapes at relatively low cost and the wide range of properties that can be achieved by careful control of chemical composition, solidification process and heat

treatment make them an ideal choice for a number of applications so much so that there could be a strong case for classifying them as high-tech materials. Cast irons can be categorized depending upon the (i) form of carbon, (ii) matrix microstructure and (iii) applications.

A simple classification would be to categorize them into general purpose and special purpose [Elliott (E1)]. The former, as the name suggests, are cast irons used for general engineering applications and include grey irons, malleable irons, nodular irons and compacted graphite irons. Specifications exist for all types except for the recently developed compacted graphite variety .

Special purpose cast irons include white and alloy cast irons which are mainly used for applications demanding enhanced abrasion, corrosion or heat resistance.

Austempered ductile irons are a new introduction to the family of cast irons. A detailed and critical review of literature on austempered cast irons is available in few recent publications [Janowak (J6), Janowak (J7), Shiokawa (S8), Dorazil (D6)].

1.3.1 GENERAL PURPOSE CAST IRONS

The commonly employed cast irons namely grey, malleable and nodular are shown schematically in Figure. 1.5 [Askeland (A4)] which also illustrates features of a more recently developed iron called the compacted graphite cast iron. The typical properties and principal applications of each of the grades has been discussed in detail by Gillbert [Gillbert (G1)]. The basis of deciding whether to select an ordinary grey iron, or an S.G. iron or a malleable iron for an end application comprises the economic and the technical considerations. Grey irons offer the lowest cost in cost option of producing sound castings. It is, however, not easy to choose between the remaining ones, namely between the S.G. and the malleable irons, malleable irons are more difficult to cast because the starting microstructure is a white iron. This automatically introduces section size limitations. Moreover, the cost incurred in malleabilizing is large. As against this S.G. irons although not requiring a long duration heat treatment may not be able to attain the expected/stipulated levels of toughness. Similarly, it may become necessary to heat treat an S.G. iron to introduce uniformity in properties; similarly annealing may be necessitated to improve machinability [Higgins (H8)].

Compacted graphite cast irons [Higgins (H8), Minkoff (M14), Cox (C4), Metals Hand Book (M9), Walton (W3)], which were originally considered to be a degenerate form of spheroidal iron, exhibit a microstructure midway between grey irons and spheroidal irons. Graphite appears as short, thick flakes with rounded ends and can therefore be distinguished from the conventional flake graphite [Minkoff (M14)]. SEM studies have revealed that compacted graphite comprises interconnected branches and is more akin to flakes than the completely isolated nodules present in spheroidal grey irons [Minkoff (M14)].

Compacted graphite iron is produced when molten iron of near eutectic composition is first de-sulphurised in the ladle and then treated at 1400°C with a single alloy containing appropriate amounts of magnesium, titanium and cerium so that the resultant iron contains Mg (0.015-0.030%), Ti (0.06 - 0.13%) and Ce (a trace). The presence of magnesium tends to produce spheroidal graphite (as it does in S.G. iron) and this is controlled by the restraining tendency of titanium which makes the amount of the magnesium less critical [Higgins (H8)].

A compacted iron exhibits superior tensile strength, stiffness and ductility, fatigue life, impact resistance and elevated temperature properties compared with grey iron of a

similar matrix structure. In general, compacted graphite irons effectively fill the mechanical and physical property void between grey and nodular irons. Table 1.2 [Cox (C4)] shows mechanical and physical properties of compacted irons whereas Table 1.3 [Metals Hand Book (M9), Walton (W3)] provides a comparison between the mechanical and physical properties of compacted graphite, grey and nodular irons.

A unique combination of high strength, good ductility and high thermal conductivity coupled with superior resistance to cracking and distortion (as compared to both grey and nodular iron) make compacted graphite irons an ideal engineering material. These irons are very well suited as materials for ingot moulds. In so doing the service life is improved by as much as 70 per cent. Good elevated temperature properties have resulted in their being used for cylinder heads, gear pumps, eccentric gears, exhaust manifolds, brake drums, discs and piston rings.

1.3.2 SPECIAL PURPOSE CAST IRONS

The term "special purpose cast irons" has been used to designate white irons and alloy grey cast irons exhibiting resistance to corrosion, abrasion and thermal shock. Presence of alloying element(s) is primarily responsible for introducing

these attributes. Extensive information is available on the effect of alloying elements on the properties of different grades of cast irons. As such these effects are not being separately discussed and would be considered as a part of the discussion on different grades of cast irons.

Special purpose cast irons [Elliott (E1)] can be divided into two broad classes namely white and grey irons depending upon whether carbon is present in the combined form or in the free form. The following sections describe some alloy grey irons of commercial importance.

1.3.2.1 SILAL

Silal [Barton (B3), walton (W4)] one of the earliest heat resistant irons developed by Norbury and Morgan of the British Cast Iron Research Association (BCIRA), is a trade name given to silicon bearing heat resisting irons. Basically silal can be categorized as silicon alloyed grey iron containing 4 to 6% silicon. The general microstructure of Silal consists of graphite in a completely ferritic matrix.

The size and the distribution of the graphite flakes has an important bearing on the heat and oxidation resistance. Fine undercooled graphite has been found to impart the best heat

resistance. Similarly, the formation of the undesirable hypereutectic "kish" graphite should be avoided.

The carbon content of silal depends upon the silicon content and is adjusted so as to retain a hypoeutectic composition and avoid primary graphitization.

For the production of a 5 per cent silicon iron the total carbon content should be less than 2.7 per cent and lower values will reduce the amount of graphite present and thereby improve mechanical properties.

Silicon increases oxidation resistance, up to 6 per cent, by forming a resistant oxide film and then a silicate film which provides resistance to the transport of oxygen atoms into the metal and to the diffusion of metal atoms towards the surface. Silicon also raises the critical temperature at which ferrite transforms to austenite thereby expanding the useful temperature range of application with respect to resistance to growth.

Silicon content of silal is governed by the service temperature. The necessity of relating the silicon content to the service temperature has been well illustrated by White, Rice and Elsea [White (W7)] and Maitland and Huges [Maitland (M3)]. Scaling and growth resistance are increased by increasing the

silicon content, provided that the temperature of service is lower than the critical temperature range. In amounts exceeding 5 per cent, silicon reduces toughness and increases the brittle-ductile transition to above room temperature. The aforesaid considerations form the basis of the optimizing the silicon content to prevent/resist growth. For optimum in terms of properties, the Si content should be approximately 4.5 to 6.5%. Such a composition is very well suited for temperatures ranging from room temperature up to 900°C.

It has been suggested that the benefit of increasing the silicon content up to 4.5 - 5.5 per cent, is due to (a) the production of a completely ferritic matrix, thereby avoiding the growth associated with the decomposition of pearlite; (b) a degree of surface passivation conferred by the silicon which, however, probably breaks down at high service temperature; (c) raising the critical transformation temperature, and thus avoiding the stresses and growth associated with the ferrite to austenite change.

For use at higher service temperatures (>900°C), the silicon content is raised to about 11%. The disadvantage of a higher silicon content is that the iron is weaker and more brittle at room temperature than a 5% silicon iron.

The inherent brittleness of Silal at normal temperatures restricts its applications. However this brittleness is not a problem if the service temperatures are above 260°C. These irons have been used successfully for furnace and stoker parts, for burner nozzles, and for trays used in heat treating other metals.

Mechanical properties of Silal can be improved through alloying. Addition of small quantities of chromium (0.5-1.0%) refines the graphite and increases the density and strength significantly. A further increase in the chromium content makes the microstructure uniform but also leads to the formation of free carbides.

Small amounts of copper and nickel in the presence of chromium favourably influence the mechanical and heat resistant properties.

The ductile grades (consisting of spheroidal graphite) containing 4 to 6% silicon account for the major tonnage presently used by the industrial sector. The higher strength and ductility of these irons qualify them for more rigorous service. Through the mechanism of solution strengthening, silicon contributes to the enhancement of the mechanical properties of ductile irons, particularly in the temperature range 370 to 540°C.

Spheroidal graphite Silal is superior to conventional Silal (flake graphite Silal) from the view point of oxidation resistance at elevated temperature. This is mainly due to the fact that the oxide layer formed in S.G. Silal is not broken by graphite precipitation, shows less cracking and adheres well to the surface. Thus penetration by oxygen is difficult and the S.G. Silal even after oxidation exposes less surface areas and oxygen penetration through these is less.

The as-cast microstructure of the ductile (S.G.) Silal containing 4 to 5% silicon is predominantly ferritic, but small amounts of eutectic carbide and pearlite may persist at grain boundaries. The presence of these constituents contributes to a tendency towards brittleness. These irons are generally annealed to eliminate the eutectic carbides and pearlite, or, to at least, minimise their adverse effect.

The 4% silicon ductile irons can be alloyed with 0.6 to 2.0% molybdenum to obtain a combination of adequate strength and ductility at room temperature and good strength properties and resistance to oxidation at elevated temperatures. Molybdenum although added primarily to develop high temperature mechanical properties in the 4% ductile silicon irons, also increases the strength at room temperature.

Although there is a continuous increase in the creep rupture strength and a reduction in creep rates as molybdenum contents are increased up to 2.5%, the greatest response to increased molybdenum contents is realised from the additions of 0.5 to 1.0% molybdenum.

Because of their relatively low cost, their low creep rates at temperatures in the 700 to 820°C range and good resistance to oxidation, the molybdenum alloyed, 4% silicon irons are attractive materials for the production of some automobile and truck turbochargers. A 1% molybdenum content is used for special engine exhaust manifolds and heat treating racks.

1.3.2.2 NICROSILAL

It is a heat resistant alloy cast iron developed by BCIRA in 1930. The approximate range of composition of Nicrosilal is: total carbon 1.6 - 2.2 per cent; silicon 4.0 - 4.5 per cent; manganese 0.6 - 1.2 per cent; nickel 18.0 - 22.0 per cent; chromium 2.0 - 4.0 per cent; phosphorus 0.1 - 0.5 per cent. The basic purpose of the development of Nicrosilal [Barton (B3)] was to have a cast iron with superior or at least equivalent heat resistance to that of Silal but with better ductility and toughness. This was achieved through alloying with nickel and chromium.

The general microstructure comprises of graphite in a predominantly austenitic matrix. For the best mechanical properties and oxidation resistance the graphite should be fine and preferably undercooled. Chromium bearing carbides are also present when chromium content exceeds about 1.8 per cent. The morphology of the carbides varies with the graphite structure, being acicular with the undercooled graphite, and relatively coarse and massive when random graphite flakes are produced/present.

Optimum properties are obtained at 4.5-5.0 per cent silicon. Lowering the silicon content reduces heat resistance. A higher silicon content lowers the solubility of carbon in austenite. An increase in silicon content thus adversely affects the stability of austenite and favours the formation of silico-ferrite, a brittle phase. Stability of austenite can be restored to a desired level by adding austenite stabilizer Ni.

The addition of nickel to this material imparts an initial hardening up to about 10 per cent nickel followed by a gradual softening of the material until a fully austenitic matrix is obtained.

As both silicon and nickel decrease the carbon content in eutectic the carbon content of these cast irons rarely exceeds

1.8 to 2.0 per cent. Increased carbon content results in the production of coarse primary graphite. A minimum of 18 per cent nickel is maintained to stabilize austenitic matrix. A chromium content of at least 1.8 per cent is also always present.

A small amount of the chromium enters into solution in the austenite, but most of it is present as carbide and thus imparts strength to the matrix. Enhanced wear and heat resistance can be obtained by increasing the chromium content up to about 4 per cent.

The heat resistance of Nicrosilal is dependent upon its high silicon content coupled with the presence of a stable austenitic matrix. Heating this iron within the range 400-700°C causes instability of the austenite resulting in the formation of martensite and thus making the material magnetic and hard. Subsequent cooling to room temperature from the temperature range results in the dimensional changes and embrittlement which lead to cracking. This problem can be overcome by increasing the nickel content.

Nicrosilal exhibits excellent physical and mechanical properties at room temperature as well as at elevated temperatures. It is superior to Silal in terms of toughness,

thermal shock resistance and resistance to scaling. It offers very high (even better than Ni-Resist) oxidation resistance up to 1000°C and can be safely employed in sulphur bearing atmospheres.

1.3.2.3 HIGH SILICON IRON

High silicon cast irons [Barton (B3), Metals Hand Book (M10), Shreir (S9)], containing silicon between 14-16 per cent, are perhaps the cheapest corrosion resistant irons offering maximum resistance to acids. The alloys resist oxidizing and non-oxidizing acids better than any other commonly employed metallic materials. For this reason, these cast irons are popularly known as acid - resisting cast irons. Their discovery is normally credited to Jouve, a french metallurgist, in 1908.

Their microstructures (upto 15.2 per cent silicon) comprise a solid solution (silico-ferrite) containing free carbon distributed as fine graphite flakes [Hurst (H13)]. In amounts in excess of 15.2 per cent silicon, both η and ϵ phases appear in the microstructure [Shreir (S9)]. Their presence considerably increases the brittleness of the material. These phases can be identified under polarized light. In view of this, the silicon content is normally restricted within the range 14.25 to 15.25 per cent though a higher level of silicon is required to give maximum corrosion resistance, specially to hydrochloric acid.

Compositions and properties of the high silicon irons are given in the Table 1.4(a) & 1.4(b) [Boyer (B10)].

High silicon irons are basically low strength brittle materials exhibiting poor thermal and mechanical shock resistance. An attempt has been made to produce high silicon iron with a nodular graphite structure for improving the mechanical properties [Dumitseseu (D7)]. It has been observed that nodular graphite silicon irons have not proved useful which confirms that the low strength and brittleness of high silicon irons is essentially due to the brittle matrix rather than the graphite form.

Their excessive hardness makes them virtually unmachinable except by grinding. The mechanical properties of high silicon irons are summarized in Table 1.4(b) [Boyer (B10)]. Mechanical strength and shock resistance can be improved by lowering the silicon content to about 12 per cent; however the corrosion resistance is significantly reduced thereby restricting the applications to those situations wherein the loss in corrosion resistance has a minimal effect on service life or is offset by the benefit derived from a higher strength [Metals Hand Book (M10)].

Resistance to attack by hydrochloric acids can also be improved by adding 3 to 4 per cent molybdenum or 3 to 5 per cent chromium to the basic composition. These additions also tend to increase the brittleness of the iron. The improved corrosion resistance of molybdenum bearing high silicon irons may be attributed to the formation of extremely stable complex carbides with the consequent elimination of graphite [Hurst (H13)]. Chromium also gives a similar beneficial effect. Good corrosion-erosion resistance is primarily due to its high inherent hardness.

High silicon cast irons are highly resistant to solutions of organic acids at all concentrations and temperatures but inferior to ordinary grey irons in their resistance to alkali attack [Hurst (H13)].

High silicon cast irons are a low strength, brittle materials and are very susceptible to cracking owing to a build up of internal stresses associated with differential cooling rates of various sections. These stresses may be removed by stripping the castings from the moulds before a temperature of 800°C is reached and placing them in an annealing furnace at 800-850°C. The castings are allowed to remain in the furnace for 4-5 hours, after which they are cooled to room temperature over a period of about 30 hours [Angus (A2)].

The excellent corrosion resistance of high silicon irons is largely due to the presence of silica-like oxide film. This film is a corrosion product which forms during exposure to the environment. This film prevents further corrosion in many media. On initial exposure to a corrosive medium, the iron is attacked by aggressive ions and iron atoms are leached out of the silico-ferrite lattice; the corrosion rate is high during initial exposure. The silicon atoms remaining in the matrix of the iron are oxidized to form silicon-oxygen compounds which react with water at the metal surface to form an adherent film. The film continues to develop and harden with time thereby improving the efficacy of the protection it imparts [Walton (W4)]. The maximum advantage of protective film is achieved at silicon contents $\geq 14.25\%$ [Dumitsescu (D7)]. Hydrofluoric acid is capable of dissolving this film and thus the material offers no resistance to hydrofluoric acid. Also the resistance to sulphurous acid is very poor.

High silicon irons exhibit good resistance to sulphuric, nitric and mixed (sulphuric and nitric) acids at all concentrations and temperatures. The resistance to hydrochloric acid is somewhat inferior but can be improved upon by increasing the silicon content to levels of 16 to 18 per cent, a modification which causes the irons to become more brittle.

High silicon cast irons are used extensively in equipment for the production of sulphuric and nitric acid; for fertilizer, textile, and explosives manufacturer; for sewage disposal and water treatment; for handling mineral acids in petroleum refining, and in metal cleaning or pickling; in electroplating; for processing of paper, beverages, and paints and pigments; and as anodes for the impressed current, cathodic protection of iron pipes or other ferrous vessels buried in the soil. Specific castings of high silicon irons include pump rotors, agitators, kettles, evaporators, separator towers and Rachid rings, tank outlets, crucibles, insoluble anodes, and pipe and fitting for plumbing in chemical laboratories of hospitals, colleges, and industry. The size of castings may vary from small pump rotors and laboratory sink fittings to tower sections 1.22m in diameter and 1.22 mm high.

1.3.2.4 NI-RESIST CAST IRONS

'Ni-Resist' is a trade name used for a group of high nickel cast irons containing sufficient nickel to produce an austenitic matrix. This matrix is tough, heat-resisting and stable under chemical attack giving the irons outstanding performance in contact with a wide range of commonly occurring corrosives. The irons are not completely stainless, but they form a thin, closely

adhering film of rust which prevents further corrosion and does not flake off to contaminate the product handled [Anant Narayan (A1)].

These (Ni-Resist) irons contain nickel ranging from 14 to 36 per cent, chromium from 1.6 to 6.0 per cent and molybdenum up to 1 per cent. As does in stainless steels, the alloy content of the Ni-Resist irons gives them good resistance to corrosion, erosion and the destructive effects of moderately high temperatures. They show advantage in many environments when compared with carbon steel and ordinary cast irons. Tougher than grey irons, Ni-Resist irons have good castability and machinability [Anant Narayan (A1)].

There are two main classes of Ni-Resist, the copper containing and the copper free (Table 1.5a) [Metals Hand Book (M10), Inco (I2)]. Both the types contain chromium which imparts hardness and stiffness to the material. Presence of chromium also ensures good machinability which is otherwise poor due to greater toughness of the austenitic matrix.

Microstructure of Ni-Resist irons comprises of graphite flakes in an austenitic matrix. Presence of carbides would depend upon the presence of chromium [Barton (B3)].

Though the Ni-Resist irons are tougher and more resistant to shock than conventional grey cast irons, the fact that the graphite is present in the same weakening flake form inhibits possible improvements. Much better strength and impact properties can, however, be obtained by treating the iron so that the graphite appears in the spheroidal form whose weakening effect on the austenitic matrix is negligible. The improved Ni-Resist irons of the S.G.Ni-Resist series have better mechanical properties than those of their-flake graphite counterparts and this has considerably extended their field of use [Anant Narayan (A1)].

Ni-resist irons, thus, are also classified on the basis of graphite morphology - flake and spheroidal graphite. To distinguish the spheroidal graphite irons from the flake ones, the prefix 'D' has been used. The composition ranges are given in Table 1.6a [INCO (I2)],

Unlike high silicon and high chromium irons, corrosion resistance of Ni-Resist irons is due to high nickel content rather than to the presence of an inert oxide surface film [Metals Hand Book (M10), INCO (I2)]. Ni-Resist irons offer high resistance to the corrosive action of sulphuric acid and are perhaps the most economical in resisting attack by sulphuric

acid. Ni-Resist irons do not perform well in hydrochloric acid and are unsuitable in resisting attack by nitric acids. They offer excellent resistance to caustic soda over a wide range of concentrations and temperatures.

Ni-Resist irons, unlike the high silicon and high chromium irons, are not truly rustless. However, the rust film which develops over the first few years restricts further corrosion [INCO (I2), INCO (I5)]. Copper bearing Ni-Resist irons produce a blue coloured corrosion product not looked at favourably by food, soap and cosmetic industries. Although the mechanical properties (Table 1.5b & 1.6b) [INCO (I2)] of flake graphite and spheroidal graphite vary considerably (the latter one having superior properties), the corrosion behaviour of the two varieties is nearly similar. This is a reflection of the superiority of flake morphology in resisting corrosion.

(A) FLAKE GRAPHITE NI-RESIST IRONS

There are five basic types of Ni-Resist irons (Table 1.5a) two of which have specified modifications [INCO (I2), (I3), (I4)] : Types 1 and 2 are used interchangeably in many corrosion and wear resistant applications. Both are specially suited to heavy metal-to-metal wear service. Type 1 has some advantages over the other types in handling mineral-acid

corrosives and salt water and where maximum expansivity is desired such as in piston ring inserts for matching the expansivity of aluminium. Type 1b has superior corrosion-erosion resistance in comparison with Type 1, and is harder and stronger.

Type 2, because of its wide use in corrosive environments, is the most commonly used. It is preferred for heat and oxidation resistance to 700°C and in steam service. It is also used for handling caustics, alkalies, ammonical solutions, food products, rayon, plastics and similar environments where freedom from copper contamination is desired. Type 2b is specially recommended for heat applications up to 815°C. Uses include gas turbine parts, exhaust manifolds and turbochargers. If machining is required, the chromium level should be kept between 3.0 to 4.0%. The greater hardness of type 2b makes it suitable for resistance to abrasive wear with corrosion, but it is not suited for metal-to-metal wear.

Type 3 is recommended for severe thermal shock service between room temperature and 230°C. At temperatures between 230 and 815°C without severe thermal shock, Type 3 can also be used for applications such as diesel exhaust manifolds and

turbochargers. This type offers high resistance to erosion in wet steam and corrosion slurries.

Type 4 is recommended when stain resistance is required. This type is superior to other types of Ni-Resist in resisting erosion, corrosion and oxidation.

Type 5 offers minimum thermal expansivity which provides dimensional stability for machine tool parts, forming dies, steam turbines, scientific instruments and expansion joints. It can be preferred over the other types of Ni-Resist to minimize thermal shock stresses up to 420°C.

(i) HEAT TREATMENT

Ni-Resist castings can be stress relieved at 620-675°C to remove residual casting stresses. However, large, relatively thin section casting such as large pump diffusers or water boxes should be mould-cooled to 315°C before shakeout rather than furnace stress relieved.

If Ni-Resist castings are fully alloyed but are higher in hardness than expected, they can be softened by heat treatment. Annealing at 980-1040° C for 1/2 to 5 hours will break down some of the carbides and most of those remaining will be spheroidized.

Castings with hardness values greater than 190 BHN can be softened in this manner without any adverse effect upon the strength. This does not apply to types containing 4% or more chromium such as type 4. The best results are obviously obtained when the carbides have become completely spheroidized.

(ii) WEAR AND GALLING RESISTANCE

Because Ni-Resist, (just as grey iron) has graphite particles distributed throughout its structure, it is highly resistant to galling and to metal - to - metal wear. In the hardness range of 130-175 BHN, the alloys have optimum metal - to - metal wear properties and exhibit a fine carbide structure. For moving parts operating to 815°C Ni-Resist can be used to combat rubbing wear, galling and heat oxidation.

The Ni-Resist alloys have shown unusual ability to resist a combination of corrosion and erosion, specially in applications such as pump and valve parts subjected to marked erosion effects by suspended solids, velocity of the liquid and by the water droplets in wet steam.

(iii) CORROSION RESISTANCE

The austenitic Ni-Resist alloys are intermediate in corrosion resistance between grey cast iron and austenitic Cr-Ni

stainless steels. There are exceptions to this. For instance, in very mild environments, both grey cast irons and the Ni-Resists may corrode at low rates.

The largest application of the Ni-Resist alloys is in the petroleum industry. In hydrogen sulphide environments Ni-Resist alloys develop a protective sulphide corrosion product that results in a very low corrosion rate. Ni-Resist pumps and valves are particularly well suited for offshore oil well applications where their resistance to brines and marine atmospheres make them preferred construction materials.

Generally Ni-Resist alloys are ideally suited to seawater handling systems for a number of important applications [INCO (I2)]. They provide significant "corrosion" advantages over unalloyed cast irons. The excellent erosion-corrosion resistance of the Ni-Resist alloys has resulted in extensive applications for pump and valve components in seawater handling systems.

Ni-Resist is cathodic to galvanized steel, aluminium alloys, steel and unalloyed cast irons, and is anodic to the various copper alloys, stainless steels and nickel alloys. The latter alloys, particularly the austenitic stainless steels, are

frequently used in combination with Ni-Resist alloys in seawater without introducing serious galvanic corrosion problems.

The adherent character of the scale formed on Ni-Resist castings at elevated temperatures is important for applications such as gas turbines, exhaust manifolds and turbocharger components.

(B) S.G. NI-RESIST IRONS

Ductile Ni-Resists [INCO (I2), (I3), (I4)] are similar to conventional Ni-Resist compositions but have been treated with Mg to convert the graphite from flake form to spheroids. The ductile family of Ni-Resists is available in every type except Type 1 which because of its high Cu content, does not respond properly to Mg treatment. There are, in addition, several modifications of Type 2 to 5 including a low temperature grade, D-2M and a high temperature, dimensionally stable grade, D-5B.

Type D-2 is recommended for service requiring resistance to corrosion, erosion, frictional wear and temperature up to 760° C.

Type D-2B is recommended for superior resistance to neutral and reducing salts and where higher resistance to erosion and oxidation than that afforded by Type D-2 is desired.

Type D-2C is recommended where resistance to heat and corrosion is less severe and where high ductility is desired.

Type D-2M was developed for use at cryogenic temperatures. Its austenitic matrix is stable to at least as low as -250°C and thus it retains toughness adequate for most applications down to that temperature.

Type D-3 is recommended for thermal shock service. This type, in addition to having excellent elevated temperature properties, also offers high resistance to erosion.

Type D-3A is recommended for use where a high degree of wear and galling resistance is required along with intermediate thermal expansion.

Type D-4 is superior to type D-2 or D-3 in resisting corrosion, erosion and oxidation.

Type D-5 is used whenever minimum thermal expansion is desired. It can also be preferred over other types of Ni-Resists to reduce thermal stresses.

Type D-5B is recommended for applications requiring a very low order of thermal stress. In addition, this type has a high

level of heat and oxidation resistance as well as good mechanical properties at elevated temperatures.

Type D-5S is recommended where oxidation resistance in air to 980° C is desired. It also resists embrittlement and offers thermal stability and strength in cyclic heating to 870° C.

(i) HEAT TREATMENT

To relieve residual casting and machining stresses Ni-Resist ductile castings are annealed at 620-675° C.

Annealing at 950-1040° C followed by uniform air cooling, or furnace cooling if preferred, will decrease the hardness to about 180 BHN or less while increasing elongation. Obviously the best results are obtained when the carbides have become completely spheroidized, which usually indicates that the minimum hardness has been reached.

(ii) WEAR AND GALLING RESISTANCE

The presence of dispersed graphite, as well as the work-hardening character of ductile Ni-Resist castings, provide a high level of resistance to frictional wear and galling. Type D-2, D-2C, D-3A and D-4 offer good wear properties with a wide variety of other metals and at temperatures from sub-zero to 815° C.

Ductile Ni-Resist castings provide excellent service where resistance to erosion and corrosion are required. For handling wet steam, salt slurries and relatively high velocity corrosive liquids, all of the types containing higher chromium levels, such as Types D-2B and D-3, have shown superior service.

(iii) CORROSION RESISTANCE

Corrosion properties of the ductile Ni-Resist alloys are comparable to those of conventional Ni-Resist. It is desirable to have two or more per cent of Cr present in the material for exposure in most corrosive media.

The Cr-Containing ductile Ni-Resists (D-2, D-2B, D-3, D-4 and D-5B) provide resistance to oxidation and maintain satisfactory mechanical properties to about 760° C. As such, they can be specified for applications including furnace parts, turbochargers and gas turbine parts. Table 1.7 [INCO (I3)] shows various commercial applications of the ductile Ni-Resist irons.

1.4 CONCLUSIONS

Starting from the basics, an effort has been made to highlight how the two broad categories of cast irons (white and grey) emerged as a consequence of differing solidification histories. Main stress has been laid on the development of

different grades of grey irons culminating in the design and development of the high alloy grades. The discussion also touches upon compacted graphite irons.

As the main thrust of the work is on white irons, the next chapter deals with unalloyed and alloyed white irons.

CHAPTER II

WHITE CAST IRONS

2.1 INTRODUCTION

White cast irons are so referred due to their characteristic silvery white fracture resulting from the absence of free graphite in the microstructure [Metals Hand Book, (M9), (M10), Charles (C2)]. The carbon is present in the form of massive carbides [Metals Hand Book (M9)]. These irons are hard, brittle and difficult to machine and therefore did not attract attention of metallurgists and materials engineers, as an engineering material for many years. In fact researching into white irons was not given credence and more than 90 per cent of total white irons produced was utilized in producing malleable iron castings. However, due to the possibility of exercising a closer control over the metallurgy and chemistry of the melts, a more efficient use of alloying element(s) along with appropriate inputs of heat treatment in improving properties, a better understanding of phenomenon occurring during service, improved testing facilities and availability of reliable experimental data interrelating theory with practice, have brought about a sea-change in this attitude. Economic aspects have contributed in no small a measure in giving a phillip to the R&D activities in

white irons. To sustain this interest, it would be relevant to critically examine the physical metallurgical thinking that has gone into the development of white irons in general and alloy white irons in particular. The following sections deal with this aspect.

2.2 PLAIN CARBON WHITE IRONS

Unalloyed white cast irons are metastable alloys of iron and carbon. A basic understanding of their behaviour stems from a study of the iron-iron carbide equilibrium [Charles (C2)].

The formation of cementite in place of graphite leads to a lowering in free energy but kinetically the formation of iron carbide is more probable [Lakhtin (L4)]. On the basis of metastable equilibrium (Fe-Fe₃C) diagram, the formation of different microconstituents on cooling is now well understood. For a hypoeutectic composition (most of the white irons are hypoeutectic alloys), the microstructure comprising cementite and pearlite resembles that of hypereutectoid steel except that the proportion of cementite is larger. Hypereutectic compositions contain undesirable free Fe₃C plates. The overall hardness of such a white iron (pearlite + cementite) lies in

the range of 400-600 VHN, the microhardness of the constituents being 200-300 and 800-1100 VHN respectively [Pearce (P11)].

Hardness can be controlled by controlling the proportion of these constituents through a control of carbon content/carbon equivalent [Rollason (R8), Angus (A2), Heine (H5)]. For most applications, a carbon content $\approx 3\%$ is considered as an optimum.

White irons exhibit high hardness due to a continuous interdendritic network of cementite. This imparts excellent wear resistance although machinability is adversely affected. Therefore engineering applications of these materials are based on this single attribute (high hardness) as utilized in liners for cement mixers, ball mills, certain types of drawing dies and extrusion nozzles [Rollason (R8)].

Hardness of white cast irons increases with an increase in carbon content. This is explained on the basis of an increase in the proportion of the ledeburitic carbide. An unalloyed white cast iron containing 2.5 per cent carbon has a hardness of about 375 VHN which increases to ≈ 500 VHN on raising the carbon content to ≈ 3.5 per cent. The simplest method to attain a high resistance to wear is by increasing the 'C' content. In high carbon white irons, silicon is kept low. Taking an overall view,

the normal range of carbon content in unalloyed versions is 2.2 to 3.6 per cent. The hardness of a white cast iron can also be increased further by the substitution of the pearlitic matrix by a tempered martensitic one. In plain carbon white irons, a martensitic matrix can only be obtained in thinner sections with a drastic quench from the austenitic region. Such a treatment although likely to produce cracks is not effective in generating a martensitic matrix in thick sections in absence of alloying elements .

The carbon equivalent of white cast irons is so adjusted that for a given cooling rate, graphite is not formed during solidification. This effect is achieved by maintaining a high carbon to silicon (C/Si) ratio. The silicon content of white cast irons ranges from 0.3 to 1.2 per cent. Increasing the Si content lowers the carbon content of the eutectic and steadily lowers the eutectic temperature (Fig.2.1) [Minkoff (M13)]. A convenient way of representing the influence of silicon on the different structures in Fe-C-Si alloys is through a diagram which incorporates the effect of cooling rate and C/Si ratio on the microstructure. This is designated as the Maurer diagram (Fig. 2.2) [Rollason (R9)]. It in fact serves as the basis for designing plain carbon white iron compositions. The

favourable effect of a high C/Si ratio in ensuring the formation of a white iron structure can be further accentuated by employing chilling. However, there are practical limitations to doing so. Representative compositions, properties and applications of plain carbon white irons are summarized in Table 2.1 [Angus (A2), Metals Hand Book (M11), Patwardhan (P10)].

Figure 2.3 [Metals Hand Book (M9)] shows Fe-C-2%Si system. The system is of particular interest as most of the white irons have a silicon content less than 2 per cent. The well defined sharply delineated eutectic and eutectoid temperatures, exhibited by Fe-Fe₃C system, change into a temperature regime by the addition of silicon. The eutectic and eutectoid points are also shifted towards lower carbon contents. Silicon, in this amount, is soluble both in ferrite and austenite and therefore the composition of carbide phase remains unaltered [Metals Hand Book (M9)].

2.2.1 APPLICATIONS

The applications of white irons as a wear resistant material dates back to over hundred years. Higher carbon lower silicon irons were developed for use specifically as wear resistant castings and are in use even today. The main limitation of these irons is their extreme brittleness coupled with poor toughness

and shock resistance. This tendency can be improved upon to some extent by restricting phosphorus to a low (<0.1%) level and also by adjusting carbon content to $\leq 3\%$. Toughness can be further improved by the addition of chromium up to 0.5 per cent [Durman (D9)]. This enables a graphite free structure to be achieved in thicker sections. The main advantages of unalloyed white irons are their relatively low price and, to a lesser extent, the fact that they can be melted in cupola [Durman (D9)].

The main advantage with unalloyed white irons is their low cost. One such example is associated with wet grinding (signifying a high rate of metal removal) wherein there is little economic justification to using alloyed cast iron grinding balls. In such instances where a wear rate of over 1 kg of balls per tonne of product ground is not unusual, high 'C' forged steel and unalloyed white irons find wide applications [Durman (D9)].

2.3 ALLOY WHITE CAST IRONS

Unalloyed and low alloy white irons attain a microstructure comprising a continuous and massive ledeburitic carbide (Fe_3C) in a predominantly pearlitic matrix. Due to their extreme brittleness, they have been largely replaced by the more tougher alloyed white irons. With an ever increasing use of materials in

applications involving resistance to wear, the major developmental efforts in alloyed white irons have centred around this application.

An important class of alloy white irons was developed by The International Nickel Company, Inc. (INCO) is known by their proprietary name 'Ni-Hard' irons. This class of materials represent an improvement over unalloyed white irons and owe their superior properties to the presence of nickel and chromium. Their microstructures essentially comprise iron-chromium carbides in a predominantly martensitic matrix.

Alloy white irons other than Ni-Hard irons are referred to as chromium irons or more precisely high chromium irons. These special purpose grades which have numerous applications contain chromium ranging from 12 to 30 per cent. Additionally, they frequently contain elements such as molybdenum and copper which are useful in enhancing the performance of these materials.

Manganese, which was rarely employed in developing cast irons, is now being extensively used and development of Cr-Mn cast irons has received major attention during the last decade. These efforts have reached a stage such that commercialization is a definite possibility .

2.3.1 NICKEL-CHROMIUM WHITE IRONS

These alloys are available in four different grades-the lower alloy versions designated as Ni-Hard 1,2 and 3 and their higher alloy counterpart Ni-Hard 4. Their chemical composition and the corresponding mechanical properties have been indicated in Table 2.2 [Patwardhan (P10), Inco (I1)].

When added to low chromium white iron [Metals Hand Book (M10)] in amounts up to about 2.5%, nickel produces a harder and finer pearlite in the structure, which improves its abrasion resistance. Nickel in somewhat larger amounts up to about 4.5% is needed to completely suppress pearlite formation, thereby ensuring that a martensitic iron results when the castings cool in their moulds. This latter practice forms the basis for production of the Ni-Hard cast irons (which are usually identified in standard specifications as nickel-chromium martensitic irons). With small castings such as grinding balls, which can be shaken out of the moulds while still hot, air cooling from the shake out temperature will produce the desired martensitic structure even when the nickel content is as low as 2.7%. On the other hand, an excessively high nickel content (more than about 6.5%) will so stabilize the austenite that little martensite, if any, can be formed in castings of any size.

Appreciable amounts of retained austenite in Ni-Hard cast irons can be transformed to martensite by refrigerating the castings at -55 to -75°C, or by the use of special tempering treatments [Metals Hand Book (M10)].

Ni-Hard cast irons are essentially Ni-Cr cast irons possessing outstanding resistance to wear. These irons in the mould cooled condition attain a matrix microstructure akin to that of heat treated steels. In addition they contain a multitude of refined carbides which make an important contribution to their abrasion wear resistance [INCO (I1)]. Chromium is useful in attaining a white iron structure and in hardening (and therefore strengthens through martensite formation) whereas nickel enhances hardenability and is useful in rendering carbides discontinuous through its graphitizing tendency.

Ni-Hard types 1 and 2 which contain relatively lower amounts of nickel and chromium were primarily developed as higher hardness and improved wear resisting materials, their fundamental property being high hardness. Microstructurally they comprise bainite/tempered martensite plus carbide [INCO (I1), Boyes (B12)]. An important observation concerning Ni-Hard 1 and 2 is that their shock resistance in general is low. However, the

shock resistance of Ni-Hard irons particularly of the low carbon and heat treated varieties is substantially better than unalloyed white cast irons. Ni-Hard 1 is used in applications where abrasion resistance is of prime consideration. For this, the carbon content is maintained in the range 3.2-3.6 per cent. However, if impact loading is involved, it is usual to restrict the carbon to \approx 2.7-3.2 per cent (Ni-Hard 2).

The main drawback (poor shock resistance due to the presence of massive and continuous eutectic carbide network) of Ni-Hard type 1 limits its use in larger diameter grinding mills as liners or balls. It is still true, but to a less extent, for Ni-Hard type 2 with low carbon content. For this reason, low carbon Ni-Hard type 3 was developed. Due to its much lower carbon content (Table 2.2) it has lower hardness but higher impact strength. In fact, Ni-Hard type 3 is a high carbon steel and is being replaced by Ni-Hard type 4 in many applications.

A modified version of Ni-Hard 1 and 2 containing higher proportions of nickel and chromium and designated as Ni-Hard 4 was developed by INCO around the mid-fifties [INCO(I1), Boyes(B12)]. The chemical composition and properties of Ni-Hard type 4 are summarized in Table 2.2. Important changes brought about in the composition of the type 4 namely 5 to 7% Ni in place

246711.

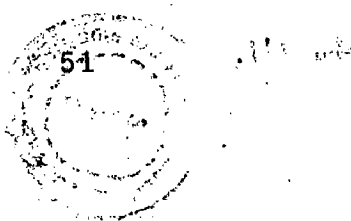


of 5.5 to 6.5%, 7 to 11% Cr as against 7 to 9% and 1.3% Mn (maximum) in place of 0.4 to 0.7% as per the recent literature published by INCO are noteworthy. The main objective in doing so was to improve the resistance to fracture under repeated impact. In view of a higher alloy content, the Ni-Hard type 4 variety is harder and has a greater resistance to corrosion. In fact Ni-Hard type 4 possesses the highest strength and greatest resistance to impact amongst the different grades of Ni-Hard irons. The advantage of a lower carbon content coupled with a somewhat tough high nickel matrix makes Ni-Hard 4 a very useful abrasion resistant material.

Besides the standard compositions described as Ni-Hard, a number of other nickel-chromium white iron compositions are also in use. Their representative compositions, properties and applications are summarised in Table 2.3 [Angus(A2), Metals Hand Book (M11), Patwardhan (P10)].

2.3.1.1 MORPHOLOGY OF CARBIDES IN NI-HARD IRON

The morphology of eutectic carbides is identical in Ni-Hard type 1, 2 and 3. These irons display a quasi-regular eutectic structure with the major phase being the massive continuous M_3C carbide. But the type 1 alloy is inferior to the rest in respect of shock resistance on account of its maximum carbon content. The



difference in the eutectic structure, in type 1 and 4 irons may be explained by the pseudo-binary phase diagrams (Figure 2.4) [Chakraborty (C1)].

Carbide contents in type 1 are about 50 per cent and that in type 4 are 31 per cent (Figure 2.4), the latter being discontinuous and plate-like eutectic type. Through intensive investigations involving special etching technique it is opined that if an eutectic comprises constituents in equal amounts, they are continuous in three dimensions. However, if they are in unequal amounts, the minor phase will be discontinuous and embedded in the major phase. Applying this observation, it was inferred that in the type 4 alloy, the minor phase (carbide) will be discontinuous and embedded in the major phase (austenite) just after solidification [Chakraborty (C1)]. Carbides are further rendered discontinuous in type 4 through a heat treatment comprising heating to the austenitic state, holding, to be followed by air cooling. This flexibility is not available in the lower alloy grades 1 to 3 as there is a danger of graphitization occurring during heat treatment.

2.3.1.2 NI-HARD 4 VS NI-HARD 1 AND 2 IRONS

Fracture in Ni-Hard type 1 and 2 castings normally results from the initiation and propagation of a crack in the continuous

brittle carbide . The susceptibility to failure by this mechanism is considerably reduced in Ni-Hard type 4 as the carbides [trigonal $(Cr,Fe)_7C_3$] are discontinuous and in a less massive form due to the modified composition. In fact for all practical purposes the carbides are regarded as discontinuous. As already stated, heat treatment may prove additionally beneficial. Similarly, controlled quantities of austenite present in the type-4 alloy can be used to advantage in blunting crack propagation.

Until recently, the increased toughness and better resistance to fracture of Ni-Hard type 4 and other high chromium irons was attributed to the presence of discontinuous carbide as described in the preceding paragraphs. According to Powell [Powell (P14)] the term "discontinuous" is misleading and both eutectic phases are continuous. The difference in mechanical properties of Ni-Hard type 1 and 2 and Ni-Hard type 4 is due to different types of anomalous eutectic structures. Powell could not assign any reason for the similarity in morphology of the carbide in type 4 and that of carbide in high chromium irons (27 per cent chromium and 17 per cent chromium - 1.5 per cent molybdenum white irons) but explained that eutectic carbide (M_7C_3) in Ni-Hard type 4 comprises of blades and hollow rods of hexagonal cross-section. This carbide is not discontinuous in

three dimensions and is continuous as rods and blades. This structure is akin to that of composites (hard carbide being present in the softer austenite) and therefore exhibits better toughness compared with that attained in Ni-Hard 1 and 2.

2.3.1.3 HEAT TREATMENT OF NI-HARD IRONS

Practically, all Ni-Hard castings are heat treated before being used in service. Heat treatment of these castings enhances impact resistance and reduces stresses in the casting.

Ni-Hard type 1,2 and 3 are subjected to two main types of heat treatments i.e. (i) single heat treatment : tempering at 275°C for 4 to 16 hours followed by air cooling and (ii) double heat treatment : (a) tempering at 450°C for 4 hours followed by air cooling/furnace cooling to 275°C, (b) tempering at 275°C for 4 to 16 hours followed by air cooling. For Ni-Hard type 4 iron, any one out of following heat treatments is employed.

- (i) 8 hours soaking at 750°C followed by air cooling.
- (ii) 4 hours soaking at 750°C followed by air cooling. Again 4 hours soaking at 75°C followed by air cooling.
- (iii) 4 hours at 550°C, air cooled and 16 hours at 450°C, air cooled.

These heat treatments result in considerable improvement in strength and impact resistance (sometimes by 50 to 80 per cent or more). It is accomplished without any loss in hardness or abrasion resistance [INCO (I1)].

2.3.1.4 APPLICATIONS OF NI-HARD IRONS

Ni-Hard irons are famous for their outstanding resistance to wear. Their use in the mining, power, cement, ceramic, paint, dredging, coal, coke, steel and foundry industries is now well established as an outcome of the experience gained over nearly fifty years. Typical applications include rolling mill rolls, grinding media balls, grinding mill liners, slurry pump parts, pulverizer rings, roll heads, pipe and elbows; and mixer blades etc [Patwardhan (P10)].

Ni-Hard iron castings have demonstrated outstanding ability to resist abrasion at temperatures upto red heat. Sand cast Ni-Hard which possess a hardness level of 600 BHN at room temperature maintains a hardness of approximately 475 BHN at 480°C. This accounts for its ability to resist abrasive and metal-to-metal wear even at elevated temperatures. Ni-Hard can be considered for service at temperatures upto 815°C as long as operating conditions do not involve severely rapid or localized heating and cooling [INCO (I1)]. Ni-Hard liner plates and flight

segments can successfully resist the abrasion of cement clinker at temperatures up to 815°C [INCO (I1)].

2.3.2 CHROMIUM IRONS

Chromium, by virtue of being a strong carbide former markedly influences the behaviour of cast irons and when present in large amounts, imparts outstanding wear, corrosion and heat resistance [Ohide (O1)]. The range of chromium contents used in high chromium irons varies from 12 to 30 per cent. Presence of chromium in large amounts alters different phase fields, the stability of phases and the eutectic temperature and composition. The precise nature of change will depend upon the chromium and carbon contents and whether or not other elements are added e.g. the nature of the matrix could vary from ferrite to austenite [Barton (B4)]. An equally important effect is the formation of stable Cr-carbide in preference to iron carbide (Fe_3C).

There are two main reasons for the success of high chromium irons. Firstly, the modification of the iron-carbon solidification process at approximately 12% chromium leading to the formation of chromium carbides (Cr_7C_3) in place of cementite (Fe_3C). The chromium carbides are harder than cementite and thus improve wear resistance. Further, they tend to be far more

compact and do not form the cellular eutectic structure characteristic of unalloyed white and martenstic irons. This leads to a significant improvement in toughness [Durman (D9)]. Secondly, the matrix microstructure of high chromium irons can be altered from a fully heat treated martenstic matrix to a completely austenitic work-hardenable matrix so as to cater to differing end requirements.

Depending upon the chromium content, the high chromium irons may be divided for practical purposes into three groups [Barton (B3)];

- (i) 15-17% Cr for heat and wear resistance applications.
- (ii) 26-28% Cr for abraion resistance applications
- (iii) 30-35 Cr for heat and corrosion resistance applications.

Typical compositions and properties of some representative (abrasion and wear resistant) chromium irons are shown in Table 2.4 [Angus (A2), Patwardhan (P10)]. Table 2.5 [Angus (A2), Metals Hand Book (M11), Patwardhan (P10)] summarizes information on chromium irons used for corrosion resistant applications.

The principal effect of carbon in chromium irons is to form carbides and since it also controls the amount of eutectic carbon present, the carbon content is important in determining the

hardness of the material. It is usually found that as the eutectic carbon content is approached, the fineness of carbides increases resulting in improved strength. When the carbon content exceeds the eutectic concentration coarse carbides appear which have a deleterious effect on the properties [Barton (B3)].

For applications demanding maximum heat and corrosion resistance, the bulk of the chromium present should be in solution in the matrix. It is usual to limit the carbon to 1.2-1.8 per cent. However, for attaining a high resistance to abrasion, the carbon content is controlled around 2.7-2.8 per cent which in combination with 27-28 per cent chromium gives an iron of eutectic composition [Barton (B3)].

2.3.2.1 CARBIDE MORPHOLOGY IN CHROMIUM IRONS

The as-cast microstructure of high chromium irons consists principally of eutectic carbides in a chromium-rich ferritic matrix. Between about 5 and 10 per cent chromium, the dominant carbide is the $(\text{FeCr})_3\text{C}$ which has a needle-like morphology, is coarse and primarily responsible for the extremely high hardness. More recent work [Torpe (T1)] suggests that at $\approx 8-10\%$ Cr, the eutectic carbide is of a duplex type comprising an inner core of M_7C_3 and an outer shell of M_3C formed during cooling within the solid state. It is possible that the $(\text{Cr,Fe})_7\text{C}_3$ is the first

carbide to form by a reaction similar to the eutectic reaction observed in the high chromium irons and controls the subsequent growth of the $(\text{FeCr})_3\text{C}$ carbide from the melt either by a peritectic or by an eutectic transformation. It is believed that these carbides constitute the matrix [Torpe (T1)].

Three dimensional studies carried out on M_7C_3 carbides by Powell [Powell (P14)] suggest that the true carbide morphology is fibrous, the fibres being hexagonal in cross section with adjacent fibers frequently attached together to form blades. The high hardness (≈ 1600 HV) of this carbide and its relatively 'enhanced discontinuity' within the eutectic colony result in an optimum resistance against wear and impact.

However, at chromium contents in excess of 10 per cent, eutectic carbides of the type M_7C_3 are formed in preference to the M_3C . More significantly, the increased chromium content causes a change in the solidification pattern such that the M_7C_3 carbides are surrounded by a matrix of austenite/its transformation products. This difference in the solidification characteristics makes the hypoeutectic irons containing M_7C_3 carbides more stronger and tougher than irons containing M_3C carbides. Information on different carbides observed in Fe-C-Cr system and their possible impact on properties is summarized in

the Table 2.6 [Ohide (O1), Goldschmidt (G2), Metals Hand Book (M10)].

The high chromium irons [Sare (S3)] are most frequently used in the heat treated condition, in which the austenitic as-cast matrix is rendered less stable by the precipitation of secondary carbides at high temperatures so as to enable its transformation to martensite on cooling. However, some alloys, namely the 27% Cr white irons, are frequently used in the austenitic condition to utilize the amenability of the matrix to work hardening (as in Hadfield steels) even though the service conditions may not entail severe impact loading.

From an application point of view the chromium white irons can be grouped into three classes namely wear resistant, heat resistant and corrosion resistant irons. The following sections are devoted to a critical reappraisal of these varieties.

2.3.2.2 WEAR RESISTANT CHROMIUM IRONS

High chromium cast irons effectively resist different forms of wear encountered in crushing and grinding of ores, coal and cement- pulverising materials. Wear resistance is controlled by hardness of the carbide and the type of matrix present. A detailed analysis of the effect of metallurgical parameters in

influencing the wear behaviour of alloyed white irons has been put forth by Singh and Patwardhan [Patwardhan (P10)]. In the present context, a carbon/chromium ratio to yield an eutectic composition will produce the finest distribution of carbides and help attain an optimum balance between hardness and toughness. In the as-cast state the matrix of the high chromium irons is ferrite although Hughes and Monaghan [Hughes (H12)] state that some austenite is also present. It is generally agreed that a matrix comprising unstable or 'transformable' austenite is most suitable for attaining a high wear resistance and this can be effectively attained in high chromium irons through heat treatment. Hughes et al [Hughes (H12)] have also shown that if pure sliding wear is experienced, a fully hardened martensitic matrix is most useful.

Generally, abrasion resistance increases with an increase in material hardness, which in turn is influenced by microstructural features such as the volume fraction of carbides, its morphology and the structure of the matrix.

On the other hand, as the toughness of cast irons is also affected by microstructure, high chromium cast irons, which contain discontinuous eutectic carbides of the type M_7C_3 , have a higher toughness than low alloyed white irons attaining

continuous M_3C carbides. It is therefore expected that control of the shape, size and distribution of eutectic carbides should not only improve their toughness but also the abrasion resistance.

The carbides in the microstructure, depending upon their type, morphology and volume fraction, provide the hardness required for crushing materials without degradation. The supporting matrix microstructure, which controls the abrasion and crack propagation characteristics, can be controlled by alloy content and/or heat treatment to develop pearlitic, austenitic or martensitic structures to provide the most cost effective balance between abrasive wear resistance and toughness [Elliott (E2)].

The complex dependence of wear on microstructure is illustrated in a recent study on the grinding abrasion resistance of chromium irons in the as-cast and heat treated conditions [Pearce (P12)]. A martensitic matrix displayed higher abrasion resistance than austenitic or pearlitic matrix structures. The 10-15% chromium irons were more resistant than 25-30% chromium irons due to the low carbon martensite produced on reducing the stability of the higher chromium irons. The 5% chromium irons exhibited a good wear resistance than the 10-15% chromium irons. This was because cracking in the carbide phase did not lead to its immediate removal from the structure due to the 'continuous'

structure of the carbide as in the 5% chromium irons. On the other hand the fractured carbide rods in the 'discontinuous' eutectic in the 15% chromium irons became detached readily during wear.

These findings differed when impact loading accompanied wear. Under these conditions, structures with continuous carbides showed insufficient toughness and suffered gross fracture. However, a microstructure with a discontinuous eutectic withstood impact loading effectively and gross failure was avoided at the expense of greater wear, particularly if the carbide is not adequately supported by a hard matrix.

For counteracting high stress abrasion there is the feasibility of attaining a tough austenitic matrix to room temperature through controlled solidification, forming a self replacing hard case while retaining a comparatively softer core. In applications where metal-to-metal contact is insufficient to result in work hardening, or under conditions of severe repeated impact when the development of internal stresses is a problem, high chromium irons can be heat-treated to provide a hard martensitic structure throughout the cross-section [Durman (D9)].

Lining plates, grinding balls and auxiliary castings for the attrition of various materials in tubular ball mills is probably the largest single application of chromium white irons. High carbon high chromium castings are generally employed as lining plates. In instances involving very high impact or where exceptionally large sized alloyed balls are used, the lower carbon heat treated versions are used. High chromium iron grinding balls are manufactured and used in all sizes, although it is important to use a composition suitable for a specific application. Higher carbon irons are generally used for small diameter balls and the lower carbon compositions in the heat treated conditions are more suitable for larger sized balls [Durman (D9)].

High chromium irons have also met with a major success in the cement industry. The requirement of good toughness associated with high wear resistance against a highly abrasive product, is achieved with ease in a series of low carbon high chromium heat treated white irons [Durman (D9)].

High chromium cast irons have been well-known for their abrasive wear resistance. Typical applications are materials such as balls, liners, rollers, rings for pulverizer mills, impeller

blades for shotblast equipment and impact crushers, dredge pump parts and wearing parts for steel making plants [Matsuraba (M7)].

2.3.2.3 HEAT RESISTANT CHROMIUM IRONS

The scale on pure iron consists of three layers : an outer one of Fe_2O_3 ; an intermediate one of Fe_3O_4 ; and an inner one of FeO . Scale on cast irons is more adherent than on steels and hinders free access of the atmosphere to the metal below, so that attack is reduced unless the scale is cracked or removed mechanically. Scale is usually continuous and adherent at least up to 800°C . It is usual to assess the heat resistance of cast irons by exposing them to air at a given temperature for a given period of time and by assessing how effectively they are able to resist such an exposure.

The excellent heat resistance of the high chromium irons is due to the formation of an adherent oxide scale which reduces further progressive oxidation to a minimum, and also to the stability of the iron-chromium carbides which do not break down on exposure to high temperatures. The work of Burgess [Burgess (B13)] suggests that a 12 per cent chromium iron is satisfactory up to $840\text{-}850^\circ\text{C}$, a 15-17 per cent chromium iron up to 900°C , 25 per cent chromium upto 980°C and a 33 per cent chromium iron upto

1050°C. Hallett [Hallett (H1)] has confirmed the excellent growth and scaling resistance of the high chromium irons.

High chromium white irons offer excellent resistance to growth and oxidation at elevated temperatures and are cost effective alternatives to stainless steels in applications that are not subjected to severe impact loading [Elliott (E2)].

For developing resistance to the softening effect of heat, and for protection against oxidation, chromium is the most effective element. It stabilizes iron carbide and therefore prevents breakdown of carbides at elevated temperatures. 1% chromium gives adequate protection against oxidation up to about 750°C in many applications. For temperatures above 750°C, the chromium content should be greater than 15% for long-term protection. This percentage of chromium suppresses the formation of graphite and makes the alloy solidify as white cast iron [Boyes (B12)].

Chromium cast irons have better mechanical properties than those of high silicon irons and respond better to heat [Metals Hand Book (M10)].

It may be noted that no research on the heat-resisting properties of high chromium irons has been done since the

detailed investigations made by Corti et al [Corti (C3)]. The literature published by Climax-Molybdenum Co. is not readily available.

2.3.2.4 CORROSION RESISTANT CHROMIUM IRONS

High chromium white irons have useful corrosion and heat-resisting properties but there has been little recent research on these materials. In fact, limited data are available on their corrosion resistance in some environment. Patwardhan and co-workers [Patwardhan (P2)], working in this area since last several years, are now in a position to predict corrosion behaviour of alloyed white irons based on models interrelating corrosion rate with the microstructure. Dodd [Dodd (D2), (D3)] has reviewed corrosion characteristics of chromium white irons and pointed out that irons containing 0.5-2.0 per cent carbon and 20-28 per cent chromium offer a useful compromise between resistance to corrosion and to abrasion.

High chromium irons owe their excellent corrosion resistance to the presence of an impervious and highly tenacious surface film of chromium oxide. In a particular corrosive medium, the corrosion behaviour would depend upon whether the film is formed or repaired more rapidly than it is broken down. Since the corrosion resistance of the alloy is basically due to the oxide

film, oxidising agents/atmospheres maintain the oxide film while reducing conditions give rise to rapid attack [Barton (B3)].

To ensure maximum corrosion resistnace, the chromium content should exceed the amount required to form carbides by atleast 10 per cent. An increase in the silicon content further increases the corrosion resistance by refining carbides. This leads to the development of a more continuous oxide film over the metal surface. Addition of molybdenum has a similar effect. It may enhance corrosioin resistance by displacing some chromium by combining with carbon, thereby increasing the chromium content of ferrite [Barton (B3)].

High chromium irons resist nitric acid well. Corrosion rates in this medium are less than 5 mil/year at all temperatures up to the boiling point and in concentrations upto 70 per cent. However boiling concentrated nitric acid is very corrosive to high chromium irons. No reliable information is available on the behaviour of these irons in sulphuric acid. Similarly not much is known about the response to hydrochloric acid; apparently the concentration would be the deciding factor. The high chromium cast irons have a useful resistance to sulphurous acid in all concentrations up to 80°C.

As regards the organic acids, high chromium cast irons offer excellent resistance to acetic acid at all temperatures and concentrations. The corrosion rate in this medium is less than 5 mil/year. However, the poorer resistance to formic acid is essentially due to its reducing nature. Even then, exposure of a 10 per cent solution at 20°C and the 100 per cent acid at all temperatures upto boiling point, result in corrosion rates of less than 5 mil/year. These irons exhibit good resistance to lactic and citric acids in dilute solutions.

High chromium irons offer no useful resistance to alkalis. In the absence of solid deposits or crevice effects, high chromium cast irons are practically immune to corrosion by aerated sea-water and most mine waters. In fact, these irons are most suitable for pumping acid mine waters.

High chromium irons show outstanding resistance to atmospheric corrosion. It is claimed that the iron containing about 34 per cent chromium and 1.1 per cent carbon do not rust when exposed to the atmosphere in the as-cast state. A similar alloy containing 2.3 per cent carbon is stated to be only slightly inferior in this regard, but on increasing the carbon to 3.1 per cent, a marked rust film develops. However, in the

machined and polished state, all these alloys were found to be fully resistant i.e. stainless.

Increasing use is being made of high chromium cast irons [Corti (C3), Boyes (B11)] for applications at high temperatures as well as moderate to high temperatures where their high resistance to abrasion, wear and corrosion is well known. Besides their excellent corrosion resistance, these irons can be centrifugally cast as tubes and are inexpensive compared to wrought high alloy steels despite their high chromium content.

These irons are most usefully used in environment containing a plentiful supply of oxygen or oxidising agents. Anaerobic or reducing conditions would lead to rapid corrosion. Low carbon versions are useful for annealing pots, lead, zinc or aluminium melting pots, conveyor links and other parts exposed to corrosion at high temperature. An important area of application is when high temperatures (upto 1000°C) are encountered [Metals Hand Book (M10)].

2.3.3 CHROMIUM-MOLYBDENUM IRONS

Massive castings, with section sizes of the order of 250 mm or larger and weighing several tonnes, are being utilized as mill liners, pulverizer rolls, slurry-pump impellers and rolling mill

rolls. Abrasive wear and failure by spalling or fracture are the limiting factors in the performance and reliability of these thick-section castings. Large tonnage of high chromium-molybdenum irons are currently being produced for thick-section castings which require a combination of abrasive wear resistance and toughness not obtainable in other alloyed irons or steels.

High chromium irons, in general, contain hard, relatively discontinuous M_7C_3 primary or eutectic carbides or both. Molybdenum is soluble in M_7C_3 carbides, and significant amount of molybdenum partition to the M_7C_3 phase. Molybdenum-rich M_2C eutectic carbides and M_6C carbides have been observed in high Cr-Mo irons. Manganese also has similar tendency as that of molybdenum. The alloying elements namely silicon, nickel and copper have limited solubility in the carbide phases and, therefore, are concentrated in the metallic matrix.

The as-cast matrix microstructure (in thin sections) is predominantly austenite with a very small amount of pearlite and some martensite adjacent to the eutectic carbides. The microstructure in thick-sections comprises a larger proportion of martensite and secondary carbides precipitated in the centre of the austenite dendrites.

The microstructures of heat treated thick-section castings are similar in nature to those in thin-sections. The heat treatment consists of heating to high temperature, usually in the range 950 to 1060°C and cooling (quenching) to obtain a martensitic matrix. Such heat-treated high Cr-Mo irons show the best combination of abrasion resistance and toughness, particularly resistant to spalling and fracture under conditions of severe repeated impact.

However, cast irons (Cr-Mo ones) with either austenitic or austenitic-martensitic matrix microstructures have been used successfully for castings which do not encounter severe impact in service. The most obvious advantage of using high Cr-Mo irons in the as-cast condition is the cost savings and energy conservation that results from eliminating the high temperature heat treatment.

The as-cast Cr-Mo irons during mould cooling as well as heat-treated irons cooled or quenched after reaustenitizing treatments may have ferrite-carbide constituents present in the matrix microstructure if hardenability is not properly controlled. Presence of ferrite-carbide constituents, even in small amounts, reduces the abrasion wear resistance. Since it is difficult to control cooling rates, specially of a thicker

section casting, the hardenability of Cr-Mo irons is usually controlled by adjusting the carbon and chromium contents. Another way is through alloying (Mo, Mn, Ni or Cu).

The addition of molybdenum to high chromium white irons suppresses the decomposition of austenitic matrix to form pearlite. Maratray and Usseglio-Nanot [Maratray (M6)] concluded that one-half of the molybdenum in the alloy forms the carbide (Mo_2C), one-fourth dissolves in the M_7C_3 carbide, and the remaining one-fourth remains in the matrix.

The high Cr-Mo irons currently produced generally have carbon contents in the range 2.4 to 3.0% and chromium contents in the range 18 to 22%. At these levels, the amount of eutectic carbide is large enough to ensure good abrasion resistance and adequate toughness, and the amount of chromium in the matrix makes a moderate contribution to hardenability.

High Cr-Mo irons are used for abrasion-resistant castings ranging in size from very small (12 mm) diameter grinding balls up to massive (335 mm) thick table segments for roller pulverizers.

The high Cr-Mo white cast irons [Frost (F1)] exhibit substantially improved toughness than the unalloyed white irons, high chromium irons, and high nickel martensitic irons mostly due

to improved carbide morphology and distribution. These alloys have stood to benefit from the superior abrasion resistance provided by the M_7C_3 chromium carbides in applications such as grinding balls and ball mill liner plates where high impact loading is observed.

A martensitic matrix may be obtained on heat treating Cr-Mo white irons by soaking for 4 hours at a temperature of 982°C , followed by an air cool. This heat treatment results in the precipitation of M_7C_3 carbides and a martensitic matrix on cooling. Dodd, et al, have shown that the martensitic transformation is not complete and up to 40% austenite may remain in the microstructure [Frost (F1), Dodd (D4), (D5)].

Compositions and properties of some Cr-Mo white cast irons are summarized in Tables 2.7 and 2.8 [Angus (A2), Patwardhan (P10), Metals Hand Book (M10)].

2.3.4 CHROMIUM-MANGANESE IRONS

Nickel is an expensive alloying element and so nickel bearing materials are costly. An attempt, to replace this costly element in Ni-Hard irons by a comparatively cheaper element manganese, has been recently tried in chromium cast irons [Tsypin (T2)]. Manganese can be used successfully to suppress the

pearlitic transformation in cast irons. Depending on the manganese content of the chromium-manganese cast irons, the matrix microstructure in the as-cast condition could be either a mixture of pearlite, austenite and martensite or fully austenitic. The carbide morphology of chromium-manganese white irons is similar to that of high chromium white irons (discontinuous M_7C_3 type).

Manganese, an efficient carbide stabilizer but a weak carbide former, partially joins the M_7C_3 carbides. Most of the reported literature on Cr-Mn cast irons deal with high chromium contents i.e. more than about 12% chromium except a few [Srinivasan (S12), Sudan (S17)] with lower chromium contents (about 7%). In these reports [Srinivasan (S12), Sudan (S17)] in addition to the effect of manganese, the effect of copper has also been studied. The as-cast structure comprises of retained austenite. This retained austenite can be minimized by various heat treatments. Depending upon the service conditions, the alloys with austenitic matrix, obtained either in as-cast or heat treated condition, may exhibit very good performance specially in impact-abrasive wear applications. In this case, the austenitic matrix gets strained due to impact and subsequently gets transformed probably into strain martensite [Rozhkov (R10)].

The microstructure [Stefanescu (S14)] of the 15% chromium white cast iron (without manganese) consists of pearlite and carbides of the $(Cr, Fe)_7C_3$ type. As the manganese content of the alloy increases, the pearlite/austenite ratio decreases and at 5% manganese (15% Cr-5% Mn cast iron) a matrix being mainly austenitic is obtained. The increase in manganese content also influences carbide morphology e.g. a large proportion of lamellar carbides are observed in a 15% Cr - 4.5% Mn cast iron at room temperature. With differential etching, two different types of carbides are observed : some with dark-grey colour and the others with light-grey colour. The dark carbides, revealed by Murakami etchant, are of the $(Cr, Fe)_7C_3$ type. They grew during eutectic solidification. The light-grey carbides also appear during eutectic solidification. The light- grey carbides are not present in the structure at lower manganese contents. From the microprobe examination, it was found that both carbides are chromium carbides. It was concluded that the difference in colour is due to different chromium contents, manganese partitioning being uniform enough [Stefanescu (S14)].

2.4 CONCLUSIONS

This chapter essentially dealt with the development of (i) unalloyed white irons and (ii) the proprietary alloy white irons

compositions namely the Ni-Hard and Cr-Mo cast irons already in use. The advantages and limitations of lower alloyed grades of Ni-Hard have been discussed. It is clearly brought out as to how these problems have been overcome through the development of Ni-Hard 4 irons.

A critique on the development of high Cr-irons revealed their apparent superiority over Ni-Hard irons. However, a more closer analysis and detailed experimentation is necessary to establish whether such a superiority really exists. An important variety of white irons excluded from the discussion are the Mn-Cr-Cu white irons. The physical metallurgical aspects related with their development leading to the formulation of the problem are discussed in the next chapter.

CHAPTER III

STUDIES IN THE Fe-Mn-Cr-Cu SYSTEM: FORMULATION OF THE PROBLEM

3.1 INTRODUCTION

A critical survey of the literature revealed that Ni-Cr and high Cr white irons (with or without Mo, the latter being more popular) are in extensive use for a wide range of applications. Whereas the major applications of the former, commonly known by their proprietary name NI-HARD, are as wear resistant materials (Ni-Hard 4 also shows excellent corrosion and high temperature resistance), the Cr-Mo/Cr-irons are well known for their excellent wear, heat and corrosion resistance.

The high cost and scarcity of the major alloying elements (Ni, Mo) in the abovesaid irons in the Indian context lead to an interest in developing low cost substitutes for Ni-Hard/Cr-Mo cast irons. Although the initial indigeneous attempts were aimed at substituting the scarce elements partly or fully, it soon emerged that developing substitutes was no more a local necessity in view of the high prices of metals in the International market. Based on fundamental considerations, it was surmised that Ni can be replaced either partially by Mn and Cu.

Manganese, like Ni is a complete austenite stabilizer and

therefore can be successfully employed to (i) refine pearlite and (ii) promote the formation of any desired matrix (eg. bainite/martensite/austenite) in the as-cast condition. It has a mild carbide forming tendency [Bain (B1)]. The carbide morphology of Mn-bearing Chromium irons was found to be similar to that observed in high Cr-irons (i.e. M_7C_3 type) because Mn and Cr have a similar carbide forming tendency [Stefanescu (S14), Basak (B6)]. In a nut shell Mn could effectively perform the functions of both Ni and Cr.

Cu cannot fully stabilise austenite because of its low stability in ferrite [Bain (B1)] and therefore for it to be effective the presence of another austenite stabilizer is essential. On the basis of a comparison between a 4Ni-2Cr and a 1.5Ni-2Cr-3Cu white irons, Henon [Henon (H6)] concluded that Ni-Cr-Cu irons could be used in place of Ni-Cr irons in a number of applications thereby substantiating the point mentioned above.

Going by the aforesaid favourable evidence, and realizing the immense economic implications that lay in store, developmental efforts were initiated by Patwardhan in the early seventies [Patwardhan (P2)] with a view to develop low cost substitutes for Ni-Hard cast irons based on the utilization of indigenously available elements. Some of the early results based on the work

of Srinivasan [Srinivasan (S12)] later to be reported by Srinivasan, Patwardhan and Mehta [Srinivasan (S13)] revealed that Fe-Cr-Mn-Cu alloy white irons could attain microstructures similar to those observed in Ni-Cr white irons. However the carbides formed were massive and were rendered discontinuous only on heat treating from high temperatures ($>850^{\circ}\text{C}$).

Work related to the optimization of copper and manganese was carried out by Sudan [Sudan (S17)] and Sharma [Sharma (S7)] respectively. Sudan, Patwardhan and Mehta [Sudan (S18)] while studying the effect of 0.5, 1, 2 and 3%Cu on the microstructure and hardness of a 7%Cr, 1.5%Si and 3.1%C cast iron, reported that hardness in excess of 650VHN could be attained only on quenching. However, copper was extremely effective in rendering the carbide network discontinuous. Taking an overall view, the optimum copper content appeared to be $\approx 1\%$.

Patwardhan, Mehta and Sharma [Patwardhan (P7)] while reporting on the possible effects of 2, 4, and 6% Mn on the transformation behaviour of 7%Cr-1.5%Si-3.1C, observed that although Mn was extremely useful in attaining a high hardness ($>650\text{VHN}$) without the necessity of quenching, it was not effective in making the carbide network discontinuous. The optimum Mn content was $\approx 4\%$.

Based on the above studies Patwardhan conceived that a composition containing $\approx 4\% \text{Mn}$, $\approx 1\% \text{Cu}$, $\approx 7\% \text{Cr}$ and about $1.5\% \text{Si}$ could be a useful alternative to Ni-Hard 4 cast iron and was investigated partly for the effect of heat treatment on the nature of microstructure. Through such a study Jha et.al [Jha (J11)] showed that microstructures and hardness similar to those attained in Ni-Hard are also attainable in the Fe-Mn-Cr-Cu alloys.

Around this time Patwardhan opined that two possible lines of approach existed. The first essentially comprised developing low cost wear resistant compositions. This line of approach was pursued by Singh [Singh (S10)] who examined a series of Fe-Mn-Cr-Cu alloys to arrive at optimum alloy composition(s) which could serve as low cost substitutes for Ni-Hard/Cr-Mo wear resistant cast irons.

The second line of approach comprised developing corrosion resistant microstructures by following the white iron route. The reasons for following this line of approach have been elaborated upon in the next section. This discussion would also highlight the advantages that will accrue and also summarise the salient results obtained. All these aspects formed the basis of formulating the present problem.

3.2 THE APPROACH

The present investigation was primarily undertaken to assess the feasibility of developing low cost corrosion resistant white irons. It was felt appropriate to undertake such a study as the backup information, as discussed above (Section 3.1), had revealed that the Fe-Mn-Cr-Cu system held promise.

A comprehensive review of literature on corrosion resistant alloy cast irons currently in use namely ferritic (high Si), austenitic (high Ni) and high Cr with or without Mo (ferritic/martensitic/austenitic) revealed that the high Si irons are most usefully utilized under oxidising conditions [Shreir (S9), Kumar (K7), Jain (J3), (J4)]. Their poor mechanical strength and shock resistance preclude their general engineering applications [Shreir (S9)]. Ni-Resist irons although useful in a variety of environments, have a low strength and are unsuitable at service temperatures $>800^{\circ}\text{C}$ [Jain (J2), (J3), (J4); Kumar (K9)]. A major drawback with the high Ni and high Si irons is that they suffer from graphitic corrosion- a phenomenon that is highly undesirable. The higher Cr irons, which can develop all matrices and which should be essentially classified as wear resistant materials, can in principle be employed upto higher service temperatures owing to the presence of a large Cr

content. Their shock resistance is improved by lowering 'C' content [Metals Hand Book (M11)]. Dodd [Dodd (D2), (D3)] has demonstrated that irons containing 0.5-2.0% C and 20-28% Cr can offer a useful compromise between resistance to corrosion and abrasion. Nonavailability of published literature lead to a possible inference that not much effort has gone into the study of electrochemical and deformation behaviour of high Cr irons.

Realizing the above, Patwardhan propounded the idea that the development of corrosion resistant cast irons was feasible by following the 'white iron' route. He was encouraged in his belief by the realization that the difference in electrochemical potentials between austenite and carbide was lesser than that between austenite and graphite. A major advantage foreseen was the possible elimination of graphitic corrosion- a severe problem associated with high alloyed corrosion resistant grey irons. Such a study was expected to become additionally meaningful if it were possible to develop alloys at a minimum of cost i.e. by utilizing low cost indigenously available alloying elements. Patwardhan [Patwardhan (P2), Kumar (K9)] further opined that Fe-Mn-Cr-Cu white irons can be successfully developed to resist corrosion, wear and corrosive wear as the system provided flexibility in attaining different matrices (pearlite, bainite, martensite and austenite) through the use of relatively lower amounts of

alloying elements. The work done by Singh [Singh (S10)] and Basak et.al [Basak (B5)] proved useful in strengthening this belief.

This prompted Patwardhan [Patwardhan (P2)] to initiate an alloy development programme for developing low cost alternatives to the existing high nickel austenitic corrosion resistant cast irons. The idea thus propounded was investigated upon by Jain [Jain (J2)] in a study which dealt with the characterization of microstructures encountered in a series of Fe-Mn-Cr-Cu white irons, based on their electrochemical and deformation response. Major conclusions of design interest (Table 3.1) [Patwardhan (P4), (P5), (P6); Jain ((J5)] emerged, one of the highlights being the quantization of different correlations. On the basis of these relations, Jain and Patwardhan [Patwardhan (P4), (P5), (P6); Jain (J5)] were able to propose models interrelating microstructure with the transformation, corrosion and deformation behaviour. The data thus obtained proved helpful in designing future compositions to reach to the final objective.

The present investigation was accordingly undertaken in order to study the various microstructures encountered in low cost white iron compositions incorporating Mn, Cr and Cu as the main alloying elements and to correlate the effect of matrix/

microconstituent(s) with the hardness, deformation behaviour and resistance to corrosion. As would be clear, the alloys investigated differ in their composition significantly from those investigated by Jain. The compositions were to be so designed that the microstructures of interest could be attained at a minimum of alloying either in the as-cast condition or through simple heat treatment(s). It was decided to develop microstructures comprising austenite and carbide since single phase austenite was adjudged to be most effective in resisting corrosion. Additionally, austenite based microstructures can be made to respond favourably to work hardening, useful in imparting high resistance to wear and perhaps corrosion if the need so arose. It was decided to concentrate on optimizing second phase present in the form of massive and dispersed carbides. Priority was accorded to the possible elimination of dispersed carbides as they were found to adversely affect the corrosion resistance.

3.3 DESIGN OF ALLOYS

The Fe-Mn-Cr-Cu system was chosen for the present investigation in view of the following:

- (i) Mn improves hardenability significantly at a low cost, helps in retaining austenite, stabilises carbide, and does not adversely effect fluidity.

- (ii) Cu is a useful graphitizer (helpful in rendering carbides discontinuous and in altering carbide morphology during heat treatment), solution hardens and improves resistance to corrosion in the presence of dilute acids (acetic, sulphuric, hydrochloric) and acid mine waters.
- (iii) Cr stabilizes carbide, is helpful in attaining a uniform microstructure (i.e. with a minimum of segregation) and may prove useful in attaining martensite/austenite even if present singly in large proportions.

Since the aim was to obtain an austenitic matrix and to assess whether it is necessary to aim for a near eutectic microstructure, the primary element i.e carbon was kept around 3.7%. A different carbon content was also selected in a parallel study [Rao (R3)] to arrive at the relevance or otherwise of adjusting the alloy composition close to the eutectic. Carbon, besides increasing fluidity, stabilizes austenite and enhances solubility of copper in cast irons. Silicon was controlled $\approx 1.5-2\%$ - a range in which it is normally present in white cast irons. Chromium was restricted to $\approx 6\%$, in order to ensure that compositions were cast white. The amount was based on the data of Singh [Singh (S10)] which revealed that raising Cr level from $\approx 6\%$ to $\approx 9\%$ did not significantly alter the behaviour of the alloys. Mn content was fixed at $\approx 10\%$ so as to ensure attainment of a

completely or nearly complete austenitic matrix even in the as-cast state. Mn, like Ni and carbon, is also expected to raise the solubility of Cu in cast irons.

A great stress has been laid on the stability of austenitic matrix as a pre-requisite to attaining good corrosion resistance. Its importance can be assessed on the basis of findings in a recent study by Prasada Rao and Patwardhan [Rao(R2)], wherein it was shown that stress relieving adversely affected the corrosion behaviour of Fe-Mn-Cr-Cu cast irons. One of the prime reasons putforward to explain the anomolous behaviour is that stress relieving (at 650°C) lead to the decomposition of the austenitic matrix thereby implying that the matrix was not stable enough.

Copper was added in three distinct amounts $\approx 1.5, 3.0$ and 5.0% . Besides aiding the formation of austenite and enhancing its stability, its presence (Cu) was expected to further improve corrosion resistance. Thus in all three alloys were designed with the same base composition i.e. $3.7\%C, 6\%Cr, 10\%Mn$ and $1.5-2.0\%Si$ but with different Cu contents as indicated below:

C1 $\approx 1.5\%Cu$

C2 $\approx 3.0\%Cu$

C3 $\approx 5.0\%Cu$

3.4 PLANNING OF EXPERIMENTS

The experiments were planned as follows:

PHASE I

A study of structure-property relation by subjecting the alloys to different heat treatments, assessing their hardness and conducting structural investigations by (optical) metallography.

PHASE II

Electrochemical characterisation of the alloy by weight loss method and further detailed structural examination by x-ray diffractometry and by quantitative optical metallography and work on optimization of microstructures.

PHASE III

Deformation behaviour of different microstructures by compression testing and structural investigation by EPMA.

CHAPTER IV

EXPERIMENTAL TECHNIQUES AND PROCEDURE

4.1 ALLOY PREPARATION

Raw materials used for preparing alloys were pig iron, low carbon ferro-alloys (ferro-chrome, ferro-manganese and ferro-silicon), graphite powder, electrolytic copper and mild steel scrap. Composition of the pig iron and the ferro-alloys are reported in the Table 4.1.

The charge consisted of the aforesaid raw materials in the requisite proportions so as to ensure that the desired compositions are attained. Due consideration was given to the metal content of the ferro-alloys and to the melt losses while making charge calculations. Alloys were air melted in clay bonded graphite crucibles in a medium frequency induction furnace.

Initially a base alloy, weighing 65 kgs and containing 3%C, ~5-6%Cr and 10%Mn was prepared by first melting requisite proportions of pig iron, mild steel scrap and graphite to a super-heat followed by deslagging and subsequent addition of ferro-chromium, ferro-silicon and ferro-manganese. After ensuring complete dissolution of alloy additions, small samples were taken out of the melt for estimation of carbon by LECO analyser. In the

intervening period the melt temperature was lowered to reduce losses. After ensuring that the carbon content had reached the desired level, the liquid metal temperature was raised to about 1400°C and slag removed. The molten alloy was then cast into three cylindrical blocks of approximately equal weight. Thus in all three castings were poured.

Finally, the Cu content was adjusted to the desired level (i.e. ~1.5, 3.0 and 5%) by adding requisite amount of electrolytic copper to each of the three base alloy castings in the molten condition. Carbon content was rechecked even at this stage to ensure that it was maintained at the desired level. After deslagging, temperature of the molten metal was measured with an optical pyrometer. The alloys were then poured at about 1425°C into ~18 mm diameter X 250 mm long cylindrical moulds and 8x22x120 mm rectangular strips in resin bonded self setting sand moulds.

Alloys were analysed for C,S,P,Si,Mn,Cr on X-ray fluorescence spectrometer. Detailed chemical analysis is reported in Table 4.2.

4.2 SPECIMEN PREPARATION

Alloys were very hard and could not be cut either with a

power saw or with high speed steel tools. Disc samples (height 14 to 18 mm) were sliced off from the cylindrical ingots with the help of a cut-off wheel. Heating of the specimens during slitting was kept to a minimum through water cooling. Specimens thus obtained were ground to have parallel faces and paper polished in the usual manner.

For corrosion studies by weight loss method, specimens of the size $\sim 8 \times 6 \times 4$ mm were employed. They were cut from rectangular strips by a procedure outlined above. As before they were ground to have parallel faces and paper polished to the 4/0 stage to obtain mirror finish.

4.3 HEAT-TREATMENT

Heat-treatments primarily comprised soaking at 800, 850, 900, 950, 1000, 1050°C for 2, 4, 6, 8 & 10 hours followed by air cooling. They were carried out in muffle furnaces whose temperatures were measured with a Pt-Pt/Rh thermocouple and controlled to an accuracy of $\pm 3^\circ\text{C}$.

4.4 HARDNESS MEASUREMENT

4.4.1 MACROHARDNESS

Hardness testing was extensively employed because it provides a quick yet reliable indication of the effect of heat-treatment

on properties.

Heat treated specimens were initially ground to a uniform depth of about 1mm to remove any decarburized layer. Thereafter they were paper polished upto the 3/0 stage in the usual manner. Hardness measurements were carried out on both the faces of a specimen on a Vicker's hardness testing machine employing a 30 kg load. A minimum of 20 impressions were taken on each specimen. The permissible scatter in the hardness values was ± 17 VHN [Angus (A3)]. In the event of the variation exceeding this limit, hardness has been represented as a band denoting both the maximum and the minimum values.

As the alloy system under investigation is hetrogeneous in character, the representative hardness readings as well as the average values have been reported.

4.4.2 MICROHARDNESS

Microhardness measurements were carried out on polished and etched selected specimens using a TUKON MICROHARDNESS TESTER (MODEL 300) at 50 grams load and an objective magnification of X200.

Microhardness measurements were made at different locations within a region as also in a number of carbide and matrix regions.

4.5. COMPRESSION TESTING

Deformation behaviour of the different microstructures was assessed by carrying out compression tests. They were carried out on cylindrical specimens (size approx. 10 mm dia x 10 mm height) on a 60 ton capacity West German made MFL microprocessor based universal testing machine, at a cross-head speed of 1.0 mm/min.

4.6. METALLOGRAPHY

4.6.1. OPTICAL MICROSCOPY

This has been extensively employed to study how heat-treatment influenced microstructure. Specimens were paper polished in the usual manner (section 4.2). The final (wheel) polishing was carried out using 1 and 0.1 micron alumina as the abrasives. After proper cleaning, specimen surfaces were etched in freshly prepared alkaline picrate and 2% nital solutions. Metallographic examination was carried out on a REICHERT -JUNG MeF-3 microscope.

4.6.2. QUANTITATIVE METALLOGRAPHY

It was carried out on a LEITZ image analyser (Auto-scan) at a magnification of 3000X. Specimen size was the same as that used during optical metallography. Ten different fields of view were examined on each specimen. Quantitative estimations including plotting of histograms were carried out with the help of computational techniques.

4.6.3. SCANNING ELECTRON MICROSCOPY

Scanning electron microscopy was also extensively employed on specimens, that had been subjected to corrosion studies in different environments, to assess the nature of damage.

To ensure good electrical contact, specimens were glued to the specimen holder using a silver base paint. They were then allowed to dry before being examined on a Phillips 501 scanning electron microscope at an opening voltage of 15 KV.

4.7. ELECTRON PROBE MICRO-ANALYSER

This study was carried out for assessing the partitioning behaviour of different alloying elements, particularly Mn, Cr, Cu, C and Si, as influenced by heat-treatment. This was

carried out on CAMEBAX EPMA/SEM at 15 KV and $\sim 60\mu\text{A}$ beam current using the crystals LiF (for Fe, Cr, Ni and Cu), TAP (for Mn and Si) and ODPb (for Carbon) using the fixed-probe technique.

Specimens for electron probe micro-analysis were cut from rectangular strips, heat treated, and after removing approximately 1mm thick layer from all the faces were cold mounted (mount size: 25 mm dia X 7 mm height). The samples, after being prepared for metallographic examination in the usual manner, were etched just enough to reveal the microstructure. This way it was ensured that the composition of different phases/microconstituents was practically unaltered.

4.8 X-RAY DIFFRACTOMETRY

As-cast and the heat-treated specimens of the alloys were subjected to structural investigations on a PHILLIPS diffractometer PW 1140/90, employing an iron target and a manganese filter, at a voltage of 35 KV and a current of 12mA.

Specimens, which were polished and lightly etched, were scanned from 40 to 150°. Time constant and scanning speed were kept at 2 seconds and 1° per minute respectively. Diffractograms were analysed/indexed by adopting the following procedure.

INDEXING OF X-RAY DIFFRACTOGRAMS

Indexing of the diffractograms and a detailed analysis of the probable microconstituents present were done with the help of a computer software package 'XRAY' [Kumar (K5)] as follows:

1. Based on the chemical composition of the alloy and the heat - treatment employed, a list of 196 probable micro - constituents was prepared. This included all constituents that were likely to form as a consequence of possible interactions amongst the alloying elements present eg. carbides, sulphides, phosphides, oxides, silicides etc. including the possible presence of metals (Cu) in an elemental form.
2. Standard 'd'-values, relative intensities, their miller indices of planes, and lattice parameter(s) for the abovesaid constituents were noted down from the ASTM powder diffraction data cards [JCPOS (J8),(J9),(J10)]. This served as the input data for carrying out the analysis.
3. The experimental error limit for 2θ -matching was taken as $\pm 0.2^\circ$ (the minimum value of 2θ -which can be measured accurately at a chart speed of 1° per cm). The experimental error limit for d-matching was calculated on the basis of this assumption.
4. The computer software performs the following functions:
 - a. Experimental error determination for d- matching.

- b. Calculation of d-values from 2θ -values and vice-versa.
- c. Matching of the calculated d-values or the 2θ -values with the standard values.
- d. Prediction of the confidence limit of peak angle/d-value matching as well as the confidence limit of the possible presence of a phase.
- e. Reporting of the result of matching in the form of a 2-D matrix and/or in the descending order of confidence limits of the possible phase(s)/microconstituents that may be present.
- f. Reporting the miller indices of planes (arising out of the abovesaid exercise) of the possible phases present.
- g. Calculation of the possible peak-angles corresponding to the $K\alpha$ -radiation.

4.9 DTA STUDIES

DTA was extensively employed to investigate the phase transformation characteristics and for assessing the high temperature response of the different microstructures.

This was carried out on NETZSCH Simultaneous Thermal Analyser STA 409 using KEOLINE as a reference material. A powder sample weighing 45 mg. was taken in an alumina

crucible and heated at a rate of 10°C per minute in air. The experimental data were analyzed and integrated plots of DTA (mV), TG(mg.) and DDTA were obtained as plots through the plotter by NETZSCH DATA ACQUISITION SYSTEM.

4.10. CORROSION STUDIES

Corrosion studies were carried out by the weight loss method.

4.10.1. WEIGHT LOSS METHOD

These tests were carried out in accordance with the relevant ASTM standards [ASTM (A6)]. Specimens were prepared by adopting a procedure outlined in the section 4.2 and cleaned as per the standard procedure laid down [ASTM (A7)]. A specimen was tied to glass rod by a nylon thread/cord. It was then suspended in a 100 ml capacity beaker containing 5% NaCl solution upto a preset level. Each specimen was weighed and its surface area determined prior to being subjected to the test. Tests was conducted for 7 days. After completion of a test, the specimen was cleaned by scrubbing followed by washing in double distilled water, degreasing in acetone and finally air drying [ASTM (A7)]. It was then weighed again and the loss in weight calculated. Corrosion

rates were calculated by using the formula [ASTM (A7)]:

$$\text{Corrosion rate} = \frac{\text{K.W.}}{\text{A.T.D.}}$$

K= Constant (3.45 x 10²) for ipy

K= Constant (2.40 x 10⁶XD) for mdd

T= exposure time in hours to the nearest 0.01 hour

A= area in cm² to the nearest 0.01cm²

W= Weight loss in gms. nearest 1 mg

D= Density in g/cm³

Corrosion rates have been reported in inches per year (ipy) and in mdd(milligrams per square decimeter per day). The latter unit is more reliable since density does not figure in the final calculations.

4.11 DATA ANALYSIS

Analysis of the data obtained was carried out with the help of computational techniques using PC-AT/486.

CHAPTER V

EFFECT OF HEAT TREATMENT ON HARDNESS AND MICROSTRUCTURE

The present investigation was primarily aimed at assessing the heat treatment response of the three alloys namely C1, C2, C3 with the help of hardness measurements, optical metallography, and quantitative metallography.

The results thus obtained have been summarized in the following sections.

5.1 RESULTS

5.1.1 EFFECT OF HEAT TREATMENT ON HARDNESS

Transformation behaviour of the alloys was investigated in the first instance (i) to ascertain the different microstructures that can be generated, (ii) to determine how the heat treating schedule influenced the as-cast hardness, (iii) to assess the effect of composition and heat treatment on hardness and (iv) to characterise the microstructures initially on the basis of hardness. This was achieved by heat treating round specimens (18-20 mm diameter x 14-18 mm height) of the three alloys by air cooling from 800, 850, 900, 950, 1000, and 1050°C after holding for periods ranging from 2 to 10 hours.

Effect of time and temperature on the hardness is summarized in the Tables 5.1-5.34 (Table 5.34 summarizes data contained in the Tables 5.1-5.33) and in the Figures 5.1-5.3 (the base curves). The data contained in the figures represents the experimentally determined values whereas the actual plots conform to the best fit data. A perusal of the tables and the figures revealed that :

1. The overall transformation behaviour of the alloys could be classified as follows :

- (a) Hardness remaining independent of soaking period on air cooling from 800°C (valid for C1); however for C2 and C3, hardness decreasing marginally with soaking period.
- (b) Hardness decreasing marginally with the soaking period on air cooling from 850°C (valid for all the alloys), the decrease being more pronounced in C2.
- (c) Hardness decreasing marginally with the soaking period on heat treating from 900°C (valid for all alloys); the decrease being more pronounced in C2.
- (d) A slight decrease in hardness with soaking period on heat treating from 950°C (valid for all the alloys); the decrease being a maximum in C3.
- (e) Hardness decreasing with soaking period on heat treating from 1000 and 1050°C (valid for all the

alloys).

(f) The hardness, in general, decreasing with the soaking temperature in the order

$$H_{1050} < H_{1000} < H_{950} < H_{900} < H_{850} < H_{800}$$

2. There is a general decrease in hardness on heat treating from temperatures between 800 and 1050°C vis-a-vis the as-cast state [valid for all alloys] (Figures 5.1 - 5.3).

3. The aforesaid data (Figures 5.1-5.3) although providing useful information fell short of revealing a comprehensive understanding of the transformation behaviour. The additional information required was obtained by replotting the data contained in the Tables 5.1-5.33 in the following manner :

- (i) Effect of time on the hardness as influenced by the heat treating temperature (Figures 5.4-5.9).
- (ii) Effect of temperature on the hardness as influenced by the holding period for each alloy (Figures 5.10-5.12).
- (iii) Effect of temperature on the hardness at each of the five soaking periods for all the alloys (Figures 5.13-5.17).
- (iv) Effect of alloy composition on the hardness as influenced by the heat treating parameters [for each alloy] (Figures 5.18-5.21 which are in the form of bar

diagrams).

The following deductions would reveal the usefulness of the Figures 5.4-5.21 when considered along with the Figures.5.1-5.3, in providing further useful information on the (a) individual and (b) comparative behaviour of the alloy(s).

4. The comparative hardness vs time plots, as influenced by temperature, further confirmed the similarity between C2 and C3 upon heat treating from 800°C; alloy C1 responded differently as is evidenced by hardness remaining unchanged (Figure 5.4).
5. On air cooling from 850 and 900°C, the alloys C1 and C3 responded similarly as revealed by an equivalent rate of decrease in their hardness with time. However, the response of C2 differed showing a constancy in hardness (Figures 5.5-5.6).
6. On air cooling from 950°C, hardness was found to be dependent on time for all the alloys, thereby revealing a basic similarity (a general decrease in hardness with increased soaking time) in their transformation characteristics (Figure 5.7). However the response of C3 (showing steep fall in hardness with time) differed from C1 and C2 (exhibiting an almost similar decrease).

7. On air cooling from 1000 and 1050°C, whereas the alloy C1 showed a marginal decrease in hardness with time, the alloys C2 and C3 revealed a marked decrease which became pronounced at and beyond 6 hours soaking period (Figures 5.8 - 5.9).
8. On heat treating from 1000 and 1050°C, the transformation behaviour was found to be similar for the alloys C2 and C3. Alloy C1 showed the best resistance to softening amongst the three alloys. Alloys C2 and C3 exhibited almost similar hardness levels at 8 hours soaking period both at 1000 and 1050°C (Figures 5.8 - 5.9).
9. (a) The hardness vs temperature plots as influenced by time (Figures 5.10-5.12) represented how effectively each alloy sustained its hardness on heat treating.
(b) These curves had an inverted parabolic shape.
(c) The slope of the curve altered around a threshold temperature called the 'cross over point' (COP). The overall slope varied with the Cu content, its effect being marked at 3%Cu (in alloy C2).
10. The (qualitative) profile of the hardness vs temperature plots (Figures 5.10-5.12) for the three alloys is nearly the same. It was further evident that with an increase

in the heat treatment temperature, the hardness vs temperature plots are acquiring a sharp profile, the effect being marked in all the alloys beyond 900°C.

11. A clear cut COP could not be obtained in most instances for the experimental alloys. However it was observed to be in the range 800-850°C.

12. A comparison of the hardness vs temperature plots as influenced by time (Figures 5.13-5.17), further revealed that:

(i) At 2 and 4 hours soaking period, the three alloys C1, C2 & C3 responded similarly as is evident from the similarity in the slope of the hardness vs temperature plots. However, C1 sustained a higher level of hardness.

(ii) At 950°C, 6 hours soaking period, alloys C1 & C2 attained almost identical hardness. On raising the temperature to 1000°C and 1050°C, the overall change in hardness level in C1 and C2 was found to be marginal whereas the response of C3 was different i.e. the decrease in hardness was larger. The rate of decrease in hardness in all the three alloys is not directly related with the Cu content.

(iii) The nature of hardness vs temperature plots at 8 hours soaking period is different from the rest of the plots as the differences in the hardness levels in C2 and C3 evened out. The hardness values were almost similar except at 950°C. The alloy C1 although showing a decrease in hardness with temperature, retained a higher level of hardness than either to C2 or C3.

13. The bar diagrams summarized in Figures 5.18-5.21 clearly bring out the individual and comparative behaviour of the three alloys at a glance besides reinforcing the different deductions arrived at earlier.

5.1.2 MICROSTRUCTURE

Effect of heat treatment on the hardness was substantiated by carrying out microstructural examination. Initially the experiments were confined to assessing qualitative changes in the microstructure and these are summarized as photomicrographs in the Figures 5.22-5.42. Subsequently, quantitative estimations involving massive and dispersed carbides were also carried out. This data have been dealt with separately.

(a) The microstructure of the alloy C1

1. The as-cast microstructure essentially comprised martensite + austenite + carbide (Figure 5.22). Volume fraction of massive

carbides was large. (Figure - 5.22a). The carbide phase which was by and large discontinuous had different morphologies namely, (i) eutectic type, (ii) massive/platy type, and (iii) mesh type/flowering (resembling phosphide eutectics). The eutectic carbides were apparently inter-linked with platy carbides (Figures 5.22a-b). Overall the carbides were oriented in different directions. In addition to the above, certain dark etching features with 'leaf like' morphology were also observed (Figure 5.22b).

2. On heat treating from 800°C for 2 hours, the matrix showed needle like precipitation (Figures 5.23a-b) whose morphology became evident at a higher magnification (Figure 5.23b). Its volume fraction was not uniform. The needles had an obtuse plate like appearance although occasionally straight needles/plates were also observed (Figure 5.23b).

On raising the soaking period through 6 to 10 hours, the precipitation of needle type second phase was more pronounced (Figures 5.23f-g). Massive carbides rendered discontinuous and assumed a favourable morphology (Figure 5.23 g). Dispersed spherical carbides were also observed at 6 hours and more so at 10 hours (Figures 5.23c, d, e & g).

3. On heat treating at 850°C for 2 hours, there was a general coarsening of the needles as well as the dispersed carbides

(DCs). DCs appeared to have increased in amount. The matrix now mainly comprised austenite as is evident from the observations carried out at higher magnification (Figures 5.24a-b).

On raising the soaking period to 6 hours, features similar to the above were observed. Apparently, the extent of coarsening was more (Figure 5.24e-f). The matrix mainly comprised austenite and some martensite (Figures 5.24 d,f). It occasionally showed variable etching characteristics (Figure 5.24f). Dispersed particles coalesce (Figure 5.24e-f). Similarly the needles/plates were also seen to link up (Figure 5.24f). The needle "ends" acquired a rounded morphology (Figure 5.24f).

On raising the soaking period to 10 hours, was a general coarsening of the 'obtuse needles'/plates as well as the dispersed spherical carbides (Figure 5.24h). Disintegration/delinking of massive carbides (MCs) which had acquired rounded edges was also observed without any graphite forming (Figures 5.24a-i). An interesting feature was that the dispersed particles acquired a tendency to align themselves along specific directions (Figure 5.24h).

4. On heat treating at 900°C for 2 hours, volume fraction of the needles greatly diminished (Figures 5.25a-b). Simultaneously,

the formation of 'aligned' DCs was observed (Figures 5.25a-b). The disintegration of MCs continued as observed earlier. At 6 hours soaking period, the above said features were somewhat coarsened (Figures 5.25c-d). The volume fraction of the needle type phase had greatly diminished (Figures 5.25 c-d).

On raising the soaking period to 10 hours, there was general coarsening of the DCs (Figures 5.25f-g). The volume fraction of the needles/plates was very small (Figure 5.25 f-g). An interesting feature is that the MCs and the coarsened DCs tended to align themselves. Simultaneously, 'rounding off' at their edges confirmed (Figures 5.25f-g). The austenite matrix showed differently etching regions (Figure 5.25 e-f).

5. On heat treating from 950°C, microstructural features at 2 hours soaking period are not much different from those observed on heat treating at 900°C for 10 hours (Figures 5.26 a-f). An equally important aspect was that the MCs were seen to be linking themselves/approaching one another to link up. A similar tendency was also observed amongst DCs (Figures 5.26b&f).

On raising the soaking period through 6 to 10 hours, the basic features were similar to those mentioned above. However, the morphology of MCs was either near spherical or with

'rounded edges' (Figures 5.26c-d). Occasionally hexagonal shaped carbides were seen (Figure 5.26d). The austenitic matrix etched somewhat differently around some massive / dispersed carbide regions (Figure-5.26b,d&f).

6. On heat treating from 1000°C for 2 hours, there were some marked but interesting structural changes. First of all no needles were present (Figure 5.27a-b). Secondly, linking of DCs, which had by now acquired a favourable morphology, continued resulting in their merging together or interdiffusing (Figure 5.27b). Similarly, the aligned MCs also appeared to link-up with one another (Figure 5.27a). The disintegration and rounding off amongst MCs continued and was more prevalent at 6 hours soaking period (Figures 5.27c-d). The existence of differently etching regions around MCs continued as before (Figure 5.27 d).

On raising the soaking period through 6 to 10 hours, the microstructure now comprised massive carbide regions with favourable morphologies in a matrix of austenite (Figures 5.27e-g). The various tendencies especially the ones involving 'alignment' and 'rounding off' in MCs were in evidence. Dark grey etching regions appeared to develop both around massive as well as around dispersed carbides. The austenite matrix was very 'evenly' / uniformly 'textured' (Figures 5.27e-g).

7. On raising the temperature to 1050°C and at 2 hours soaking period, the 'rounding off' and coalescing tendencies among the MCs were greatly enhanced (Figures 5.28a-c) giving rise to the formation of large 'agglomerates' at higher soaking periods (Figures 5.28d-j). Very often these agglomerates had either a massive or sometimes a 'plate like' morphology. Occasionally regions having either massive or 'plate like' morphologies but with 'rounded edges' were also observed. It appeared as though some of the original DCs have become MCs with rounded or hexagonal morphologies as observed on heat treating for 6 and 10 hours (Figures 5.28e-f & i-j). The 'rounding off' tendency was clearly dominant but equally dominant was also the tendency of 'aligned linking' amongst MCs. In certain areas, 'dark etching' regions appeared to form essentially around MCs or at the interface between two or more massive carbide regions which were joining one another (Figure 5.28g&j). In some instances, stray DCs were also seen to form (Figures 5.27j). All in all, a large number of interrelated changes appeared to be occurring. From the point of morphology of massive carbides, the 1050°C, 6 hours heat treatment appeared beneficial.

(b) Alloys C2 and C3

The structural changes in C2 & C3 are on similar lines as

those in C1 barring some areas of difference centering around:

- (i) type of carbides present in the as-cast state and the nature of the matrix
- (ii) the type of the needle morphology, the main precipitating second phase at 'lower temperatures'
- (iii) stage(s) at which disintegration/rounding off within massive carbide sets in,
- (iv) possible interaction between coarsening/growing needles and dispersed carbides(DCs),
- (v) general state of MCs at high temperature, and
- (vii) the extent of the formation of dark/grey etching regions at the highest heat treating temperature, namely, at 1000°C & 1050°C.

Alloy C2

- (a) As-cast : -same basic features as in Alloy C1 (Figures 5.29a-d)
 -carbides are compact, discontinuous, and less platy compared to C1(Figure-5.29b)
- (b) 800°C, 2hours -needles & DCs are present in the matrix; presence of austenite more readily detected austenite. (Figures 5.30a-b)
 6hours -needles mostly obtuse in character (as in C1) (Figure 5.30d-e)

-feathering is present(Figure 5.30e)

10hours -basic structure as in 6 hours (Figure 5.30f)

-structure more uniform

-some coarsening of needles seen (Figure 5.30f)

-feathering not apparent

-MCs developing rounded edges (Figure 5.30f)

(c) 850°C, 2hours -general coarsening of DCs(Figure 5.31a)

-feathering seen(Figure 5.31a)

-DCs are more

-discontinuity in MCs(Figure 5.31a)

6hours -general coarsening of DSPs/DCs; volume fraction of needles low (Figures 5.31 b-d).

-Massive carbide morphology discontinuous, favourable.(Figure 5.31b-e)

10hours -general coarsening of needles/DCs (Figures 5.31e-g)

-‘needle’ volume fraction less

-alignment of DCs

-needles approaching/joining DCs (Figures 5.31g)

(d) 900°C, 2hours -‘uneven’ matrix etching(Figures 5.32a-d)

-needles & DCs coarsened(Figure 5.32b-e)

- needles & DCs less than in C1
- needles and DCs aligning themselves
- linking up of needles/DCs
- dark etching spots around MCs(Figure 5.32a,b & d)
- 6hours -discontinuous MCs with rounded edges (Figures 5.32 e-g)
- dark etching spots around MCs (Figures 5.32 e-g)
- less DCs & needles; linking up/agglomeration of coarsened DCs
- 10hours -as above(Figures 5.32h-j)
- DCs appear more in some regions(some of them may be disintegrated MCs)(Figure 5.32i)
- needles approaching DCs(Figure 5.32i-j)
- rounding of MCs at edges(general)
- (e) 950°C, 2hours -rounding of MCs(Figures 5.33a-c)
- dissolved MCs and interlinking of MCs & DCs observed(Figure 5.33a)
- joining/approaching of MCs(Figure 5.33b)
- both needles & DCs present
- 6hours -pronounced general disintegration and 'rounding off' of MCs(Figures 5.33d-f)

-DCs are present(Figures 5.33 d-f)

- 'haloed' regions(Figure 5.33f)

-linking tendency among needles & DCs (Figure
5.33 f)

10hours -same as above(Figures 5.33g-i)

-DCs coarsened(Figure 5.33g)

-morphology of MCs favourable; they are
discontinuous (Figure 5.33 i)

-coarsened DCs appearing as MCs linking up
with MCs (Figures 5.33 h)

(f) 1000°C,2hours -matrix plain(Figures 5.34a-c)

-needles almost nonexistent

-DCs are a part of disintegrated MCs (Figure
5.34c)

-linking as before among MCs(Figure 5.34b) and
amongst DCs & MCs (Figure 5.34 c) -aligned
MCs & DCs

-hexagonal or rounded 'carbides' are present
(Figure 5.34b)

6hours -as above(Figures 5.34d-f)

10hours -rounded MCs(Figures 5.34h-i)

-dark grey/light grey regions adjoining MCs
(Figures 5.34h - i)

- 'haloed' regions around MCs (Figure 5.34g)
- Hexagonal, rounded & some elongated MCs (Figures 5.34 g-i)
- interdiffusion amongst DCs & MCs and between DCs & MCs seen (Figures 5.34 g-i)

(g) 1050°C, 2 hours - rounded, hexagonal, and rectangular carbides observed (Figures 5.35 b,d)

- favourable carbide morphology (Figures 5.35 a,b&d)

6 hours - grey/dark regions around MCs (Figures 5.35e-h)

- linking up or joining together of MCs

10 hours - joining of large MCs (Figures 5.35 i-l)

- perforated MCs (Figures 5.35k-l)
- general 'morphology' of MCs useful

Alloy C3

(a) As-Cast - carbides compact, less platy, more discontinuous and lesser in amount (Figures 5.36 a-c)

(b) 800°C, 2 hours - minute platelets/DCs (Figures 5.37a-b)

- straight platelets / needles - curving type (Figures 5.37a-b)
- obtuse needles/plates also present (Figure 5.37b)

-Overall DSPs mostly comprise DCs

6hours -as above(Figures 5.37c-e)

-Morphology of MCs favourable & discontinuous

-DCs marked/prominent(Figure 5.37d)

10hours -MCs discontinuous(Figures 5.37f-h)

-DCs are present and somewhat coarsened
(Figure 5.37h)

(c) 850°C, 2hours -discontinuous MCs with hexagonal shape
(Figure 5.38b)

-discontinuous MCs with massive morphology
also observed(Figure 5.38b)

-‘rounding off’ at edges already initiated
(Figure 5.38a)

-DCs somewhat more coarsened (Figure 5.38 b)

6hours -as above(Figures 5.38c-d)

-DCs apparent(Figure 5.38d)

-agglomerating & linking tendency amongst DCs
(Figure 5.38d)

10hours -matrix ‘even textured’ than at 2 & 6 hours
(Figure 5.38e-f)

-coarsening of DCs(Figure 5.38f)

-alignment amongst DCs

(d) 900°C, 2hours -‘rounding off’ at edges of MCs (Figures

5.39b-c)

-general coarsening

-MCs linking and discontinuous; both platy & rounded/favourable morphologies present (Figure 5.39c)

-feathering absent

-formation of dark/grey regions seen (showing concentration difference) (Figures 5.39b-c)

6hours -same as above (Figures 5.39d-f)

-DCs coarsening (Figures 5.39e-f)

-needles 'rounding off' at edges (Figure 5.39e)

10hours -rounding off as before (Figures 5.39h-i)

-disintegration of MCs (Figures 5.39g-i)

-aligned DCs and agglomerating tendency amongst DCs and MCs (Figure 5.39i)

-coarsening of DCs

(e) 950°C, 2hours -as above (Figures 5.40a-b)

-MCs linking and alignment observed (Figures 5.40a-b)

6hours -hexagonal carbides (Figures 5.40c-e)

-rest as before

-existence of dark/grey patches continues

(Figures 5.40d-e)

-formation of 'haloed regions' around MCs

(Figure 5.40d)

10hours -same as above(Figures 5.40f-g)

-directional growth amongst MCs and DCs

(Figures 5.40f-g)

-general coarsening(both needles and DCs)

mostly latter, (Figure 5.40f)

(f) 1000°C, 2hours -clean matrix(Figures 5.41a-c)

-rounding of MCs

-no needles

-interlinking amongst MCs(Figures 5.41b-c)

-some 'haloeing' around MCs(Figure 5.41c)

6hours -same as above(Figures 5.41d-e)

-interlinking marked(Figure 5.41e)

-rounded MCs(both at the edges and overall)

10hours -MCs coarsening(Figures 5.41f-h)

-aligned MCs/DCs(Figure 5.41f)

(g) 1050°C, 2hours -general rounding of MCs & agglomeration /

interlinking (Figures 5.42a-d)

-formation of grey/dark regions around MCs

lesser than in C1 and C2 (Figures 5.42b-c)

-light grey regions also seen(Figure 5.42a)

-morphology of MCs mostly rounded and also platy

6hours -basic features as before(Figures 5.42e-h)

-interlinking of MCs

10hours -general features as before(Figures 5.42i-l)

-perforated carbides are also seen (Figures 5.42i-j)

-some reprecipitation of DCs observed

On comparing the three alloys(i.e. on increasing the Cu content), the following observations emerged:

- (i) DCs formed at an early stage and were more in number,
- (ii) no trend was observed with regard to the amount of needles,
- (iii) matrix microstructure was cleaner and comprised lesser grey/dark regions(at 1000 and 1050°C); carbide morphology and distribution was better,
- (iv) better morphology of carbides even on heat treating at high temperature.

5.1.3 QUANTITATIVE METALLOGRAPHY

5.1.3.1 MASSIVE CARBIDES

Effect of heat treatment on the volume fraction of massive carbides was investigated with the help of a LEITZ image analyzer. The data thus obtained have been summarized in Tables

5.35-5.38 (Table 5.38 summarizes data contained in the Tables 5.35-5.37).

A perusal of these tables revealed that :

1. Volume fraction of the massive carbides in the as-cast condition ranged from 30-45%, it being the highest in C1 and the least in C3. Volume fraction of MCs in C2 was not much different from that in C3.
2. In a majority of instances, an increase in the temperature/time, in general, led to a decrease in the amount of massive carbides.
3. Up to 900°C, the decrease in volume fraction was gradual/minimal.
4. Raising the temperature from 900°C to 1000°C led to a marked decrease in the amount of MCs except in C3 which contained the least amount of MCs even in the as-cast condition. On heat treating from 1050°C, a general marked decrease in the volume fraction of massive carbides with time was observed (valid for alloy C1 and C2). Alloy C3 exhibited marginal decrease in volume fraction of massive carbides both at 1000 and 1050°C.
5. An interesting observation to emerge from the quantitative data is that in most instances with an increase in the copper content, there is a general

decrease in the volume fraction of massive carbides with temperature/time.

6. Increasing the copper content also made the micro-structure(s) more uniform with regard to the variation in and the average volume fraction of massive carbides.
7. To understand the nature of variation at (5) and (6) above, the volume fraction of MCs was plotted as a function of temperature as influenced by soaking period (Figures 5.43-5.45).

(i) such a perusal revealed that the variations conform to a second order polynomial, i.e.

$$\% \text{ MCs} = K_1 + K_2.T + K_3.T^2 \text{ (at } t \text{ in hours).}$$

- (ii) On increasing the Cu content, the overall volume fraction of MCs in the as-cast state decreased, and (iii) the decrease in the volume fraction of MCs with temperature was a function of time, it being slow at lower soaking periods and gaining in momentum with time.

5.1.3.2 DISPERSED SECOND PHASE(DSPs)

Dispersed second phase(both needles and dispersed carbides) were characterized on the basis of the following parameters :

- (i) Total number of DSPs
- (ii) their 'size based' distribution

- (iii) Volume fraction of the DSPs
- (iv) their average particle size and
- (vi) Percent number and percent area occupied by the DSPs
in different size ranges

In the present study also[Jain (J2)] particles have been classified on the basis of different size ranges with a mean of 0.58 μ ; a total of four classes existed.

The data thus generated are summarized in the Tables 5.39-5.43, Figures 5.46-5.47, and in Appendix A-1 to A-3. Figures 5.46-5.47 depict representative histograms showing a variation in the amount of DSPs at five different locations as influenced by heat treating. The aforesaid data were analyzed in two ways, (a) by assessing whether any general trend existed and (b) by laying down a detailed account of how the heat treating variables affected the parameters employed to characterize the dispersed second phase.

Considering to start with the former, the following general trends were observed for all the alloys:

- (i) Dispersed carbides predominantly belonged to class I(0-0.58 μ) and II i.e. size 0.58-1.16 microns(Tables 5.39-5.40 and Appendix A-1 to A-3).

- (ii) The number of particles was a maximum for heat treatments carried out at 800°C and 850°C. (Table 5.41).
- (iii) The effect of heat treating parameters on the average number and per cent number of particles, their volume fraction, mean diameter did not conform to a definite trend (Tables 5.39-5.42). Hence this aspect is not being commented upon.
- (iv) In a general way, it can be stated that for a given time, the number of particles in classes I & II decreased or remained unaltered with an increase in temperature. A similar trend was observed on increasing the heat treating time at a given heat treating temperature (Tables 5.39-5.40).
- (v) The changes described in (iv) above were supplemented by a spilt over of DSPs/DCs in class III (Tables 5.39 - 5.40). The extent of these changes was a minimum in C1 and increased with Cu content (Tables 5.39-5.40).
- (vi) Representative histograms summarized in Figures 5.46-5.47 proved extremely helpful in appreciating as to how the distribution of the particles varied with temperature and time at different fields of view/specimen cross section.

5.2 DISCUSSION

The main aim of the present investigation was to establish the transformation behaviour of the alloys. This was achieved by heat treating the alloys from different temperatures after holding for different lengths of time followed by assessing the microstructural changes by hardness measurements. Subsequently, the microstructures were quantitatively characterized by studying the variation in (i) the volume fraction of massive carbide and (ii) the size and distribution of dispersed second phase as influenced by heat treating parameters. The data thus generated proved helpful in modelling (i) the transformation behaviour, (ii) the coarsening behaviour of dispersed carbides, and (iii) the heterogeneity based on the distribution of massive carbides and dispersed carbides as influenced by heat treating parameters.

5.2.1 STRUCTURAL CHANGES DURING HEATING

Before embarking upon this analysis, it would be useful to mention once again that the alloys investigated in the present study were designed to ensure that the matrix comprised austenite with higher stability. This has been achieved by maintaining the Mn content at 10%. The Cr content of the alloys was maintained at 7% on the basis of data generated by Singh [Singh (S10)] who studied the abrasion resistance of 6% and 9% Cr cast irons alloyed with 1% Cu and varying amounts of Mn. The 7% limit

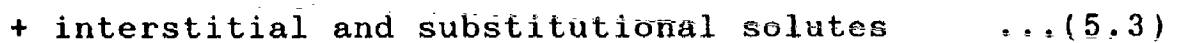
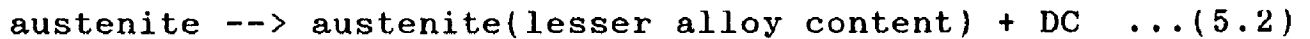
ensured that there was no danger of graphitization occurring even if Cu was employed in larger amounts (as has been presently done). Thus the present set of alloys contained Cr higher than the ones investigated by Jain & Kumar [Jain (J2), Kumar (K6)]. Similarly, the copper levels presently used (up to 5%) are higher than the ones employed earlier [Jain (J2), Kumar (K6)]. Further, whereas the earlier alloys contained up to 7.5% Mn, the alloys presently investigated contain 10% Mn.

It has been established that (a) nearly 45% of the Mn added partitions to austenite and the balance to the carbide phase, (b) bulk of the chromium partitions to the carbide phase, and (c) bulk of the Cu partitions to austenite [Singh (S10)]. This enables an understanding of the ensuing structural changes that will occur which comprise (i) a reduction in the volume fraction of the massive carbides due to the presence of Si and Cu (attributed to their graphitizing tendency), (ii) an increase in the stability of austenite arising out of the dissolution of the additional alloying elements made available as a consequence of (i), and (iii) a possible 'rounding off' of the massive carbides and their being rendered discontinuous due to (i), (iv) occurrence of a carbide transformation which would be governed by the nature of the phase diagrams, and (v) the possible

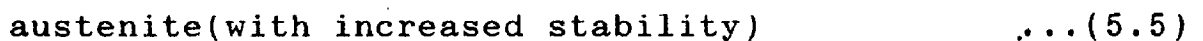
precipitation of carbides from austenite on prolonged soaking as represented by the reaction



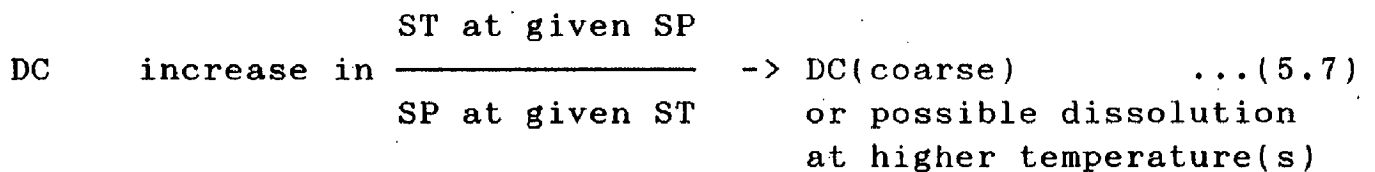
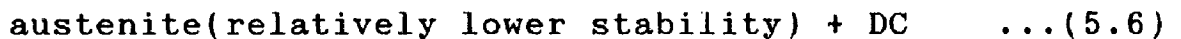
The likely structural changes therefore, can be summarized with the help of the following equations :



Interstitial + substitutional solutes + austenite \rightarrow



austenite(with higher stability) increase in SP/ST \rightarrow



5.2.2 CHANGES DURING COOLING TO ROOM TEMPERATURE

They will be governed by the cooling rate and the alloy content and would primarily be confined to austenite. Some changes may also occur in the massive carbides and the DCs that have formed. The possible changes in austenite would depend upon the temperature and time as they govern the relative stability of austenite in accordance with the Equations (5.2), (5.5), and

(5.6). If air cooling is done, austenite may reject excess solute in the form of dispersed carbides and would subsequently transform to either B/M and or remain untransformed. Since the minimum Mn content in the alloys is appreciably higher(10%) to ensure that no martensite can form on air cooling from 800 and 850°C, it is evident that the transformation product in the present alloys on air cooling would essentially be austenite independent of the temperature from which they are cooled. This tendency is further aided by the amount of Cr that would partition to τ in spite of its being a carbide former. Similarly, Cu would essentially partition to τ only. Any martensite if at all present, may at best be observed on air cooling from 800 and/or confined to the as-cast state.

Carbide precipitation during cooling mainly occurs because of a decrease in the solid solubility of carbon with temperature in the austenite. If austenite is supersaturated after heat treatment, it would reject out excess solute as carbides and these would be inherited by the transformation product of austenite on cooling which in the present situation is most likely to be austenite only and therefore the chances of excess carbon precipitating as carbides are greatly reduced since part of Cr partitioning to it also has large solubility in austenite. If however the austenite is not supersaturated and is in a state

wherein the solute is fully or 'near completely' dissolved (requiring a higher heat treating temperature), it will be retained as such on cooling.

Taking an overall view, the possible structural changes on cooling can be summarized with the help of the following equations :

Slow cooling(as during casting)

austenite --> austenite(τ) + some martensite(M) ? ... (5.8)

(relative proportion of the τ & M depending upon the Cu content)

Carbide --> unchanged or otherwise, depending upon

carbide transformation ... (5.9)

Final likely structure : τ + M(?) + MCs

Heat treated condition

(a) lower temperatures 800 and 850°C

austenite --> austenite* + DC ... (5.10)

austenite* --> τ mostly + M(?) or exclusively τ ... (5.11)

(extent of M, if any, depends upon soaking period i.e. less at lower soaking period and likely to be negligible at higher soaking period)

Massive carbide --> M'C' + M''C'' etc. ... (5.12)

DC --> DC(coarse) ... (5.7)

Final likely structure : τ + M(?) + MC + DC

(b) Temperatures 900 & 950°C

austenite* --> austenite ... (5.13)

DC --> DC(coarse) ... (5.7)

MC --> M'C' + M"C" + --- (volume fraction reduced) ... (5.12)

Likely final structure : austenite + DC + MC

(c) 1000 and 1050°C

austenite* --> austenite(matrix completely austenitic) ... (5.14)

DC --> DC(coarse) and possible dissolution at higher
soaking period(s) and temperature(s) ... (5.7)

MC --> M'C' + M"C" + --- (volume fraction low, possible rounding
off may be observed) ... (5.12)

Final likely structure : austenite + MC + some DC(?)

or austenite + MC

5.2.3 STRENGTHENING RESPONSE OF DIFFERENT TRANSFORMATIONS

Before analyzing the structure-property relations it would be appropriate to consider the strengthening associated with different transformations.

The austenite to martensite transformation leads to hardening and to simultaneous embrittlement. It is of little significance in so far as the present study is concerned. The attainment of austenitic matrices would lead to an improvement in the ease of deformation. In such instances, the stacking fault

energy(SFE) of the matrix would determine the strength-ductility interrelation as it(SFE) controls the extent of work hardening. It is relevant to record here that Mn-austenites have a low SFE and hence exhibit a high rate of work hardening [Patwardhan (P3)].

Massive carbides have a higher hardness and the strengthening response would be directly related to their volume fraction. Its morphology and compatibility with the matrix are also equally important. The latter is governed by the crystal structure. The effect of dispersed carbides would be governed by the volume fraction, compatibility with the matrix, size, shape and distribution [Jain (J5)].

5.2.4 INTERRELATION BETWEEN MICROSTRUCTURE AND HARDNESS

The general microstructural changes that may occur in the experimental alloys, highlighted in the earlier sections, facilitate interpretation of the structural changes that would occur in C1, C2, and C3. As hardness is governed by the microstructure, the two have been discussed together.

5.2.4.1 AS-CAST STATE

The microstructure of the alloys in the as cast condition namely, $m + \tau + MCs$. (Figures 5.22c, 5.29c & 5.36b), could be explained on the basis of the analysis outlined in the sections 5.2.1-5.2.3(Equation-5.8). At 10% Mn the matrix is expected to be

predominantly austenitic. However the high hardness of the alloys in the 'as-cast' state clearly indicates that a fair proportion of martensite is present as is duly supported by microstructural examinations (Figures 5.22 a-b, 5.29a-b & 5.36a-b). This is due to a higher carbon content of the experimental alloys which tends to combine with a relatively larger concentration of alloying elements thereby reducing the overall alloy content of the matrix to an extent that on air cooling a fair proportion of martensite is formed in addition to retained austenite. Quite evidently the lower the overall carbon content the larger would be the tendency to form martensite. Thus the analysis put forth in the section 5.2.1 to 5.2.3 is in no way isolated and explain why the volume fraction of MCs is large in the as-cast state. Apparently the three alloys do differ in some respects especially with regard to the morphology of the massive carbides. While describing the microstructure, three types of massive carbides have been identified, namely, (a) eutectic type, (b) massive/platy type, and (c) mesh type. The amount of type (a) & (b) carbides will be governed by the carbon equivalent of the composition and its (compositions's) disposition with respect to the modified eutectic composition. The (c) type carbide is governed by the phosphorous content which is approximately the same in all the three alloys. Considering the

carbon equivalent of the compositions being investigated on the basis of the data reported by Merchant [Merchant (M8)], the modified eutectic composition is ~ 3.8%. Thus effectively the compositions being investigated are hypoeutectic in nature. The microstructure of alloy C1 does in fact conform to its being hypoeutectic in character by exhibiting a fair proportion of platy carbides (Figures 5.22a-c). With an increase in the copper content of the expected changes would comprise a reduction in the volume fraction of MCs and their being rendered less platy and more eutectic type and discontinuous. This is what has been observed (Figures 5.22, 5.29 & 5.36). Thus the microstructures in the as-cast condition are appropriately explained. In the present set of alloys, the strengthening is essentially governed by the amount of martensite and MCs. The latter is directly related to the amount of copper present (the levels of Mn and Si being nearly the same in the three alloys). Accordingly the hardness in the as-cast condition would be the highest in C1 and the least in C3 as has been observed although the overall difference may not be large (Figures 5.1 - 5.3).

5.2.4.2 HEAT TREATED CONDITION

The structural changes in the heat treated condition have been outlined with the help of equations in the sections 5.2.2.1-

5.2.2.3. The prominent changes would be the precipitation of carbides from the austenite during soaking and a reduction in the amount of MCs and their eventual 'rounding off'. In the present context equally important would be the resultant of the breakdown of the martensitic structure in the as-cast state on heating while heat treating.

For the sake of simplicity, transformations in C1 will be initially discussed and subsequently the similarities/ differences between C1 and the transformations observed in C2 and C3.

5.2.4.3 ALLOY C1:

(a) 800°C: The matrix is a combination of martensite + austenite. The interesting aspect is the formation of 'a needle like' and dispersed second phase (Figure 5.23). At 2 hours soaking period the needles formed (Figures 5.23a-b) appear to have etching characteristics similar to the dispersed carbides, more clearly seen at higher soaking periods (Figures 5.23f-g). This leads to an inference that they could either be carbides which is most likely and/or some intermetallics. It is not possible to identify them through optical metallography except on the basis of microhardness measurements. As this proved difficult, the identification aspect has been separately dealt with and would be discussed in the next chapter. The obtuse morphology of some of

the needles, more prominent at higher heat treating temperatures/periods(Figures 5.23f-g), may lead to a mistaken inference that the precipitated phase is martensite. However in the present instance since the matrix is partly martensite, such a possibility is rather remote. Moreover, the 'obtuse plate' feature is observed even on heat treating from higher soaking temperatures. This establishes beyond doubt that the obtuse plates do not represent martensite because the alloys are so designed so as to exclude its formation and to ensure the retention of austenite over a wide range of heat treating temperatures especially on heat treating from higher temperatures. The observation that the tendency to precipitation/coarsen is enhanced at higher soaking period is logical since a larger activation is available for the intended changes at higher soaking periods. The matrix is martensitic independent of the soaking period. Since the precipitation of dispersed second phase lowers the solute concentration of the matrix to a level such that austenite cannot be fully retained.

850°C: On heat treating at 850°C for 2 hours, the major expected changes are a general coarsening and the formation of a larger volume fraction of DCs and DSPs(needle/plate)(Figure 5.24) because the temperature is higher. The coarsening tendencies would be marked at higher soaking periods. This is what has been

observed(Figures 5.24f-h).

The formation of differentially etching regions within the austenitic matrix(Figures 5.24a,c&i) is an indication of 'heterogeneity' which is being sustained/accentuated due to the possible disintegration of MCs(Equation-5.12). As the heat treating temperature is low, the concentration gradients thus formed persist. It is expected to be evened out as the temperature increases. The disintegration of MCs is occurring because of the combined graphitizing action of Cu and Si(as already discussed) whose intensity will increase with temperature. This leads to a reduction in the volume fraction of MCS(which is minimal at this temperature) and in their being rendered discontinuous to begin with(Figures 5.24b & h).

The most interesting feature i.e. the formation of aligned DCs(Figure 5.24h) suggests the 'precipitating tendency' to be directional which appears reasonable as the precipitating phase will pick out directions of closest packing. This could also be interpreted differently by stating that the 'aligned' carbides are in fact the 'globularized segments' of the precipitating needle morphology being so rendered due the combined graphitizing tendency of Cu and Si. Otherwise no specific reasons exist as to why the carbides should be 'aligned'.

The matrix is now almost entirely austenitic more so at higher soaking periods since solute enrichment of the matrix due to a dissolution of MCs is enough to retain nearly austenitic matrix on air cooling.

900°C: The structural changes at 900°C as influenced by an increase in the soaking period are essentially on similar lines as those observed on heat treating at 850°C (Figure 5.25). Evidently the temperature being higher, the extent of coarsening of DCs and needles and disintegration of MCs will be more marked (Figures 5.25b-d & f). The etching characteristics of the matrix are more or less uniform (Figures 5.25f&g) because the nonuniformity of the matrix vis-a-vis the solute concentration is evened out at a higher temperature (as the present one). However, the special features namely the 'needle ends' (now plate ends) acquiring rounded shapes and 'aligned' precipitation of carbides (both dispersed and massive) are strikingly distinctive in character representing 'preferred directional growth' and needing a more careful analysis (Figures 5.25). Rounding off amongst MCs is occurring to enable them to acquire lower energy configuration(s) at higher heat treating temperatures (section 5.2.1). The austenitic matrix showed differently etching regions revealing a nonuniformity in composition resulting due to the

structural changes mentioned above.

950°C: The microstructures observed at this temperature as influenced by soaking period (Figure 5.26a) are consistent with the reasoning put forward to explain similar changes earlier. Presence of needles is at best limited up to 6 hours which is logical since around this temperature or higher a near spherical morphology is more preferred, more so at higher soaking periods. Rounding off of MCs will be more, the extent of coarsening will be larger and the remaining portions of MCs will acquire lower energy configuration (spherical/hexagonal) particularly so at higher soaking periods since this temperature is the same as that employed for malleablizing [Heine (H5)]. All of these features can be attributed to enhanced diffusion rates at 950°C. Only hereafter would pronounced changes occur in the massive carbide morphology and a marked reduction in their volume fraction (Figures 5.26).

Massive carbide regions are seen approaching one another in an effort to reduce their volume fraction and also perhaps to acquire low energy configurations (Figures 5.26a,d-f). This is a unique feature observed, which although similar to 'diffusion bonding', has neither been hitherto reported nor observed so distinctly in alloyed white irons or in other materials where

large sized carbides are present in the microstructure. Although Ostwald-ripening does come close enough to this situation but its occurrence has been mostly observed/confined to dispersed second phase. What is bringing about a similar situation amongst MCs is perhaps the tendency of the alloy to pronounced directional precipitation/growth and a desire to minimize the volume fraction of the second phase with a view to reduce energy.

At some locations 'haloed' regions (representing a different etching character within the matrix) are observed especially around MCs/coarsening DCS (Figures 5.26b,d&e). They may represent regions with a different alloy concentration (indicative of a different strain field compared to the matrix) during the process of carbide growth/coalescence.

1000°C: On heat treating at 1000°C for 2 hours, the changes described at 950°C especially at 10 hours heat treating period are further accelerated.

The observation that the austenitic matrix is relatively clean especially at higher soaking periods is an indication that compositional heterogeneities are minimized and simultaneously the number of transformations occurring within the matrix are at a minimum. This is to be expected in view of the temperature

being high which would contribute to the structure attaining as high a stability as possible. None the less the formation of some small sized dispersed second phase perhaps through a process of reprecipitation is still in evidence(Figures 5.27b-c).

The absence of needles, as on prolonged soaking at 950°C, is a welcome feature and signifies the process of growth to be equiaxial rather than directional as would be expected at high temperatures. For similar reasons, the MCs would acquire morphologies such as 'near spherical' or 'hexagonal'(Figures 5.27d & g) and their volume fraction would reduce. The latter is aided by the observed 'linking up' amongst massive carbides.

The formation of localized dark grey etching regions around massive and dispersed carbides(Figures 5.27c & d) needs commenting upon. Such regions are apparently forming as a prelude to either the DCs or the MCs linking up/agglomerating. There are also instances where isolated MCs are developing dark etching regions around themselves which may be due to the initiation of the formation of a new phase(Figures 5.27c-d). All the aforesaid tendencies will be marked at higher heat treating temperatures/soaking periods.

1050°C: The prominent features observed on heat treating at 1050°C are essentially an extension of changes occurring on heat

treating at 1000°C (Figures 5.28), namely, (a) general 'rounding off' of MCs, (b) their linking/agglomerating along specific directions, (c) formation of dark grey/dark etching regions around MCs and in the regions separating adjoining MCs, and (d) formation of linkages and eventual 'spherodization'* and/or formation of hexagonal MCs. The only difference is that all of the aforesaid tendencies are marked due to the temperature being higher. The driving force for marked 'agglomeration' amongst MCs is the tendency of the microstructure to reduce its energy. Further, the 'dark grey' and 'dark etching' regions are definitely austenitic depicting solute concentration different from the austenitic matrix- so essential to facilitating the agglomerating/linking up processes (Figures 5.28).

It is of significance that a greater unevenness within the austenitic matrix and the formation of small sized DCs have been observed. In fact the former and the latter add up to suggest that the unevenness is because of initiation of certain precipitation based transformation(s) afresh. The reason for the formation of 'linkups' (Figures 5.28g&i&j) appears to be that they are acting as initiators for the formation of a new (carbide) phase.

* Refers to small sized MCs as distinct from the usual MCs or DCs

When these alloys are compared with those investigated by Jain and Kumar [Jain (J2), Kumar (K6)], it then becomes evident that the microstructures in the 6-8% Mn and 5% Cr and 1.5-3.0% Cu white irons examined by them were less complex than the ones being presently observed with regard to (i) the initiation of transformation(s) afresh at a number of points within the matrix even on heat treating at 1050°C and (ii) the formation of varied dispersed second phases. In fact the earlier alloys although free from these changes, none the less suffered from problems resulting from the formation of an 'eutectic type' of platy carbide at lower soaking periods on heat treating at 1050°C. The presently investigated alloys are free from this problem.

5.2.4.4 ALLOYS C2 AND C3

Structural changes observed in C2 (Figures 5.29-5.35) and C3 (Figures 5.36-5.42) are on similar lines as those described in the alloy C1 (Figures 5.22-5.28). Therefore no specific comment is being made so as to avoid repetition.

Taking an overall view, the difference on proceeding from C1 to C3 can be attributed to copper increasing from 1.5% to 5%.

The differences between C1 and the alloys C2 & C3, namely- (a) the overall incidence of needle morphology being lesser/negligible.

- (b) dispersed carbides forming at relatively lower temperatures/
soaking period(s),
- (c) disappearance of plates at relatively lower temperature(s)
and soaking period(s),
- (d) disintegration amongst MCs being faster and initiated at
lower heat treating temperature(s)/soaking periods,
- (e) unevenness of the matrix being lesser except on heat treating
at 1050°C,
- (f) overall distribution of MCs being better, and
- (g) the overall distribution of MCs at higher temperature being
better, confirm the above reasoning to be correct as the
aforesaid changes are duly related with an increase in the
carbide destabilizing tendency and austenite stabilizing
tendencies thereby enabling structural changes to be
initiated/occur at lower temperature(s) and/or lower
period(s).

A similar reasoning explains why dark grey/dark etching regions at higher heat treating temperatures are the least in the alloy C3.

This in essence would conclude the discussion on the nature of the structural changes. The aforesaid similarities and differences are clearly reflected in the hardness data and the next

section would therefore be devoted an interrelation between hardness and microstructure. Being a useful indicator of the likely properties, the hardness-microstructure interrelations assume major significance as a precursor to an understanding of the microstructure-property correlations.

5.2.4.5 HARDNESS-MICROSTRUCTURE INTERRELATION

The aforesaid analysis provides a basis for explaining the hardness changes as influenced by the temperature and time.

(a) Alloy C1

Considering the alloy C1(Figure 5.1), on heat treating at 800°C for 2 hours, the hardness is lower than the as-cast hardness because the amount of martensite has decreased with respect to that in the as-cast state. On increasing the soaking period up to 10 hours there is negligible change in the overall martensite content as the tendency to precipitate balances the tendency towards solute enrichment due to the dissolution of massive carbides. A very general gradual increase in hardness with time is due to an increase in the amount of precipitated second phase(needles and/or DCs) (Table 5.35).

On raising the temperature to 850°C, there is little change in the hardness levels over that observed at 800°C as there is

little change in the microstructure. The small decrease in hardness on increasing the period further is an indication that coarsening of the DCs has perhaps set in and at the same time the reduction in the amount of MCs is marginally higher than at 800°C. Similar to the situation at 800°C, the overall hardness is in general dependent of the soaking time. However marginal difference in the hardness levels is an indication that the factors promoting increase and decrease in hardness approximately balance one another.

On heat treating at 900°C, the coarsening of precipitated second phase and a somewhat larger reduction in the amount of MCs (an indirect increase in the amount of austenite) has resulted in the hardness decreasing with soaking period. Evidently, the overall hardness at 900°C is lower than that at 850°C for reasons already stated. A similar analysis would also explain the reasons for a decrease in hardness with time on heat treating at 950°C and also its overall level being lower than the one attained on heat treating at 900°C. It is noteworthy that the decrease in the amount of MCs would be marked hereafter for reasons already discussed (section-5.2.4.3).

On comparing the hardness levels at 850°C, 900°C, and 950°C at higher soaking periods, the decrease in hardness is getting

marked with an increase in temperature. This is due to (i) the coarsening of dispersed second phase up to 900°C, (ii) its more or less complete disappearance at 950°C, and (iii) more importantly because of an enhanced tendency at reducing the volume fraction of MCs. All these add up to an increase in the amount of austenite and its stability (Equation-5.5).

On raising the temperature to 1000°C, the matrix is practically free from DCs and the reduction in hardness with time is basically due to a reduction in the volume fraction of MCs. A similar situation also exists at 1050°C except that changes occurring are more marked than at 1000°C. The maximum reduction in hardness is occurring at 10 hours soaking period on transiting from 1000 to 1050°C due to (i) a marked decrease in volume fraction of MCs (as a result of enhanced graphitizing/carbide destabilizing tendency) and (ii) an enhanced interdiffusing/agglomerating tendencies amongst MCs.

(b) Hardness changes in alloys C2 and C3

The hardness changes in C2 and C3 (Figures 5.2-5.3) can be interpreted on similar lines. In as-cast state, both C2 and C3 attain almost equal volume fraction of MCs which is lower than that of C1 (C3 attains the least) and accordingly heat treating would have little effect on the volume fraction of MCs in the

heat treated condition to begin with (Tables 5.35-5.37), i.e. hardness change is being controlled by the volume fraction of DSPs.

Apart from the above, the other major difference between C1 and, C2 & C3 is that whereas in C1 the hardness remains unaltered or marginally changes with time on heat treating from all temperatures, it is decreasing with time on heat treating, the decrease being more pronounced at 1000 and 1050°C, for C2 and C3. The rate of decrease is maximum in C2 and a minimum in C3 with C2 falling in between. However, the overall hardness is lowest in C3 and highest in C1. All the aforesaid differences are essentially related to the carbide destabilizing/DSPs forming tendencies.

On comparing C2 and C3, the commonality exists heat treating is that the difference in hardness levels even out with increasing soaking periods except at 950°C where the alloys exhibited broadening (more difference) with increasing soaking periods. The aforesaid observations, namely, the decreasing trend in hardness setting early in C3 and the overall hardness being lower at higher soaking periods can be attributed to a larger copper content in C3 and hence to a larger carbide destabilizing and austenite stabilizing effects. Accordingly the

least hardness is observed in alloy C3 on soaking for 10 hours at 1050°C.

5.2.4.6 COMPARATIVE CHANGES IN HARDNESS IN C1, C2, AND C3 AS INFLUENCED BY HEAT TREATING PARAMETERS

The discussion up till now centered around explaining the base curves(Figures 5.1-5.3). It would now be appropriate to compare the relative behaviour of the three alloys as influenced by time(Figures 5.4-5.9).

The general behaviour of the alloys C2 and C3 is similar on heat treating at 800°C because, overall, the volume fraction of MCs is playing a major role in controlling it. C1 however responded differently(Figure 5.4) more due to a higher initial volume fraction of massive carbides(Table 5.38). A careful study of Table 5.38 can explain the above said behaviour of the alloys. The almost matching hardness levels at higher soaking periods can be attributed to similar V_f of MCs.

The three alloys on heat treating from 850°C are behaving in a similar manner as stated above i.e. at 800°C (Figure 5.5). It is a pointer that the overall contributions of an increasing second phase and decreasing MCs approximately balanced out, the lower initial volume fraction of MCs notwithstanding(Tables 5.8 & 5.14).

The similarity in C1 and C3 on heat treating from 900 (denoting only a marginal decrease in hardness with time) is due to the overall contributions of DSPs and MCs. At 950°C, the situation is different as the alloys C1 and C2 are showing less rate of reduction in hardness as compared to C3. Such a behaviour can be attributed to almost complete absence of DSPs and to the sufficiently higher temperature (950°C) affecting significantly the stability of the matrix and the carbide transformation (formation) behaviour.

On heat treating at 1000°C, the precipitating second phase is practically absent and the differentiating factor are the rate at which volume fraction of MCs is decreasing with time and the structural changes. The former (Vf of MCs) being equivalent, leads to the similarity in the overall behaviour of the experimental alloys, the latter might account for behaviour of C1 in particular (Figure 5.8, Tables 5.11 and 5.17).

On heat treating at 1050°C, the changes are on similar lines as those indicated at 1000°C, including the 'hardness arrest' at 8 hours soaking period (Figure 5.9, Tables 5.12 and 5.18) and an enhanced carbide destabilizing tendency. Reasons for the former are not clearly understood whilst that for the latter are explained.

Thus overall, the Figures 5.4-5.9 reiterate the commonality and differences amongst the three alloys discussed individually on the basis of the Figures 5.1-5.3.

5.2.5 HARDNESS AND TIME INTERRELATION

The data contained in the Tables 5.1-5.18 and Figures 5.1-5.9 were analyzed with the help of a computer programme to arrive at the aforesaid interrelation. Constants for the first, second and third order variations were calculated using the least square technique [Himmelblau (H10), Mangasarain (M4)] and are also reported at the bottom of each of the Tables 5.1-5.18. Although the variance decreased as the order of equations increased, plotting of the data revealed that the hardness-time interrelation and its interpretation (already discussed) can be best explained on the basis of a first order equation. The calculated values of hardness on this basis (also indicated in the Tables) are in excellent agreement with the experimental values. Thus, hardness H can be expressed by an equation :

$$H = K_1 + K_2.t \text{ (at a constant temperature) } \dots(5.15)$$

The values of the constants K1 and K2 for each of the alloys at different heat treating temperatures are indicated in the Tables 5.1-5.18.

5.2.6 HARDNESS-TEMPERATURE INTERRELATIONS

5.2.6.1 NATURE OF VARIATION

In order to arrive at the aforesaid correlation, the hardness vs temperature data for each of the alloys (summarized in the Tables 5.19-5.33) were analyzed and the constants for the first to third order variations calculated (Tables 5.19-5.33). It is not reasonable to assume that hardness varies linearly with temperature especially so when changes in the microstructure are being brought about by at least two major transformations. On a similar ground a third or a fourth order variation is also ruled out. Of the available options a second order variation represents the microstructural changes most appropriately which comprise an initial gradual/minimal decrease in hardness which is followed by a marked decrease in hardness at $T \geq 950^{\circ}\text{C}$. Hence the variation in hardness with temperature at each of the soaking periods can be most appropriately represented by a second order polynomial :

$$H = K_1 + K_2.T + K_3.T^2 \quad \dots(5.16)$$

The values of the constants K_1 , K_2 , and K_3 have been indicated in the Tables 5.19-5.33. This analysis forms the basis of arriving at the hardness vs temperature plots (Figures 5.10-5.17) which are in the form of an inverted parabola.

5.2.6.2 EFFECT OF TEMPERATURE ON HARDNESS AND MICROSTRUCTURE

The aforesaid data summarised in the Figures 5.10-5.12 can be interpreted on a basis similar to the one employed for interpreting the data contained in the Figures 5.1-5.3. However, it is the shape of the hardness vs temperature plots that needs analyzing. As already stated (section 5.2.6.1), the hardness vs temperature plots should have an inverted parabolic configuration i.e. the hardness decreasing somewhat slowly to begin with and gaining momentum after a threshold temperature is exceeded. Since the base microstructure is nearly identical in all the three alloys (austenitic matrix), the hardness changes would be governed by the overall outcome of the two transformations namely, (i) formation of precipitated second phase and (ii) decrease in MCs. As already noted the former increases the hardness whereas the latter decreases it. Evidently, the overall change in hardness with temperature will be very slow to begin with especially at lower soaking periods and in alloy(s) exhibiting the least austenite stabilizing/carbide destabilizing tendencies (i.e. alloy C1) and would gain momentum as more activation is provided by increasing time (Figure 5.10). The extent of activation provided increases with temperature & time at a given temperature and would be more at higher temperatures. This analysis satisfactorily explains the general features of the hardness vs temperature plots (Figures 5.10a-e).

The higher Cu alloys C2 and C3 exhibit a near linear behaviour to begin with since the austenite stabilizing/carbide destabilizing tendency in them is larger though no direct relationship with the copper content is observed. Thus the transformation products conducive to sustaining a higher level of hardness may not be so effective (due to their reduced Vf) and therefore the decrease in hardness with temperature and time sets in early in C2 and C3. This explains the data summarized in Figures 5.11-5.12.

The aforesaid analysis would also explain why the COP (signifying a change in the slope of the hardness vs temperature plots) would occur within a narrow temperature range for all the alloys (Figures 5.10-5.12). The maximum decrease in the hardness (hardness band) in the alloys has occurred at 1050°C firstly because this is the highest heat treating temperature employed and secondly because at this temperature the different structural changes leading to a decrease in hardness occur the fastest and to the maximum extent. At 1050°C, the higher the soaking period, the smaller would be the volume fraction of massive carbide and larger the volume fraction of austenite and therefore, the lower would be the hardness (Figures 5.10-5.12).

5.2.6.3 COMPARATIVE HARDNESS VS TEMPERATURE DATA

The comparative hardness vs temperature plots (Figures 5.13-5.17), essentially derived from the data summarized in the Figures 5.10-5.12, indicate the effect of soaking period in influencing H vs T relation and can essentially be interpreted on a similar basis as the one employed for interpreting the Figures 5.10-5.12. The usefulness of the Figures 5.13-5.17 is that they reveal the comparative data at a glance and this is further summarized in the form of bar diagrams depicted in Figures 5.18-5.21.

5.2.7 EFFECT OF TEMPERATURE AND TIME ON THE MORPHOLOGY AND VOLUME FRACTION OF MASSIVE CARBIDES

Although the effect of massive carbides in controlling the overall hardness has been discussed at length in sections 5.2.4.5 & 5.2.6.2, it would be appropriate to comment upon the effect of heat treating parameters on their morphology and volume fraction. Massive carbides present in the as-cast structure (Figures 5.22, 5.29, and 5.36) are partly discontinuous (though still massive) and have been so rendered due to the graphitizing action of Cu and Si (sections 5.2.1- 5.2.3). This tendency, which increases with Cu content, temperature and time, also reduces the volume fraction of massive carbides on heat treating.

Based on physical metallurgical considerations associated with malleablizing in so far as carbide destabilization/disintegration is concerned [Heine (H6)], it is expected that the tendency towards attaining (a) a discontinuous morphology and (b) a reduced volume fraction would become marked at temperature $\geq 950^{\circ}\text{C}$. Another reason why volume fraction of massive carbides may not significantly decrease until 950°C is that other transformation(s) involving the formation of precipitated second phase as needles and DCs (highlighted earlier) take precedence over the carbide transformation. This is because they require lesser activation in terms of temperature.

However, unlike in malleable irons, the carbide phase in the experimental alloys has been rendered stable by Cr additions. Additionally a fair proportion of Mn also partitions to it, thereby enhancing its stability [Singh (S10)]. Therefore, as the heat treating temperature and time are increased the massive carbides instead of decomposing into graphite, will acquire a low energy near rounded or hexagonal morphologies. The precise nature would be governed by the crystal structure of the massive carbides as influenced by heat treating temperature and time. This analysis explains why (i) carbides are rendered discontinuous, (ii) their volume fraction reduced with temperature and time, and (iii) the 'rounding off' tendency is

observed on heat treating from higher temperatures/periods (Figures 5.22-5.42).

Considering the decrease in the Vf of massive carbides, the Cr containing carbides, as already stated, are further rendered stable because Mn (55-60% of the added amount) partitions to them [Singh (S10)]. Therefore, normally the decrease in the volume fraction of massive carbides will be faster only at temperatures around 950°C or higher (i.e. 1000°C) because this is the temperature at which carbide is destabilized during malleablizing. This is duly supported by the observations discussed earlier (Figures 5.43- 5.45). This process (involving a reduction in the volume fraction of massive carbides) will be further aided by the presence of a fully austenitic matrix and this occurs in the experimental alloys even in the as-cast state. This may account for a reasonable reduction in the Vf of MCs even at temperatures lower than 950°C.

Although copper is a mild graphitizer, the carbide destabilizing tendency is directly proportional to the copper + silicon content. An important effect of raising Cu content will be that the volume fraction of MCs in the as-cast state will reduce and the reduction in the Vf of MCs will set in at lower temperatures/soaking periods. Thus the data summarized in Table

5.38 and in Figures 5.43-5.45 thus stand appropriately explained. The least volume fraction of massive carbides will be observed at the highest soaking temperature and time (Table 5.38).

An analysis of the manner in which MCs decreased revealed that an increase in the soaking period had only a marginal effect at least to begin with and gathers momentum with time more markedly at higher temperatures. It was therefore felt appropriate to quantify the decrease as a function of temperature at different soaking periods (Figures 5.43-5.45). On doing so it emerged that the plots should logically follow a second order variation, namely, the same as the one observed when the variation in hardness with temperature as influenced by soaking period was considered (Figures 5.10-5.12). Evidently the data in Figures 5.43-5.45 would be interpreted similarly as the one in Figures 5.10-5.12.

5.2.8 EFFECT OF TIME AND TEMPERATURE ON THE DISTRIBUTION OF DISPERSED SECOND PHASE

Sections 5.2.1-5.2.2 highlight the mechanism of formation of dispersed second phase from austenite. The results summarized in the Tables 5.39-5.43, Figures 5.46-5.47, and in Appendix A-1 to A-3 prove helpful in characterizing them comprehensively. Particles constituting the dispersed carbides have a size up to

1.16 μ because they exclusively fall into classes I and II at the formation stage. This is valid for all the alloys. On heat treating, their distribution is altered in a manner consistent with the attributes of nucleation and growth type of transformations. Simultaneously, coarsening would also set in. This would lead to a reduction in the number of particles in the first two classes and a simultaneous increase in their number in the class III or higher. Additionally, the mean diameter would also increase. This is what has been observed in a majority of the instances. The main deviation is that a 'general coarsening' is followed by a phenomenon in reverse. This is because, after a certain stage of heat treating the matrix begins to dissolve the DSPs leading to a decrease their mean diameter as well as in their numbers(which is also reflected in the V_f getting reduced(Tables 5.39-5.43). The extent and the stage at which this sets in would be governed by the τ - stabilizing tendency of the matrix and the carbide destabilizing tendency. This in the present instance is being controlled by the Cu content as well as by heat treatment parameters and accordingly the extent of coarsening is lesser in C2 and C3 and the 'carbide' dissolution tendency sets in early(at lower heat treating temperature/time) in C3. In fact, for similar reasons C2 and C3 does not exhibit a marked tendency towards coarsening. Such a thinking could also

form a useful basis for analyzing the data related with DSPs in a general sense.

The comparative data given in the Tables 5.39-5.43 reveal that it would not be easy to arrive at a broad based correlation between composition and heat treating parameters with coarsening. Arriving at such an understanding is of interest as the coarsening behaviour & heterogeneity of distribution would govern the overall properties of the alloys. Till date Ostwald's equation [Burke (B-14)] given below is the most authentic formulation for studying the coarsening behaviour of second phase particles, i.e.

$$r_1^3 - r_0^3 = k(t_1 - t_0) \quad \dots(5.17)$$

where r_1 = particle radius at time t_1 , and

r_0 = particle radius at time t_0

A major limitation of this equation is that a large number of data points are required to ascertain its validity/to ensure its application under a given set of experimental conditions. Moreover the equation merely correlates the arithmetical mean of particle radius with time but in no way reflects upon how the particle distribution is influenced by heat treating parameters. Further, finding out the arithmetical average of particle radius does not represent the true picture since the particle size distribution is statistical in nature. In the present investigation the data related with the second phase are available for

all soaking periods at a given temperature. Generally, this should have sufficed for any further analysis of the data but not so with the above equation especially when it is intended to represent distribution. The difficulties arising thus were resolved by evolving a new parameter called the 'coarsening index'(CI) [Jain (J2)].

In order to calculate coarsening index, it is necessary to first evolve a parameter which can represent particle size distribution for a given heat treating schedule. Development of such a parameter was greatly facilitated by the manner in which the quantitative metallographic data was generated, namely, the (a) categorization of particles into different classes, (b) assessment of the number of particles in different classes, (c) calculation of percent number and area occupied by particles in different classes, and (d) measurement of the average particle diameter. The new parameter termed the 'distribution factor'(DF) which incorporated the variables (a) to (d) is defined as [Jain (J2), Patwardhan (P6)]

$$DF = \frac{\sum_{i=1}^n X_i \cdot N_i}{\sum_{i=1}^n N_i} \quad \dots(5.18)$$

where, n = the number of classes,

N_i = the number of particles in i^{th} class,

X_i = volume fraction in the i^{th} class /VDC,

and, VDC = total volume fraction of dispersed carbides.

Distribution factors, calculated on the basis of the aforesaid formula, are summarized in the Table 5.44.

Having defined this parameter(DF), the coarsening index can now be calculated with respect to a specified reference base - a concept also implicitly in-built into the Ostwald's formula. In the present instance, this reference base was taken to be the heat treating schedule at which the dispersed carbide particles/DSPs just about formed namely the heat treating schedule corresponding to which dispersed carbides/DSPs were present in classes I and II only.

The coarsening index(CI) is thus defined as

$$CI = \frac{\text{DF for a given heat treatment}}{\text{DF for the h/t with particles in classes I \& II}} \quad \dots(5.19)$$

Based on the above formulation, the coarsening index for the different alloys was calculated and is summarized in the Table 5.45.

As already discussed above, the aforesaid table proved

extremely useful in assessing the relative coarsening tendency of the different alloys (Table 5.45).

The data on the relative coarsening behaviour of the alloys is relevant to an understanding of their deformation and the corrosion behaviour as would be evident from an analysis put forth in Chapter VII.

Although the aforesaid analysis does explain the data obtained in a majority of instances for all the alloys, a number of data points did not follow a specific trend (Table 5.45). A possible reason could be that the system under investigation is intrinsically 'heterogeneous'. This is evident from the representative histograms summarized in Figures 5.46-5.47 and from the data given in Appendix A-1 to A-3. This reporting notwithstanding, it became prudent to analyze/interpret the entire data more comprehensively/methodically. A possible methodology is to assess the percent number and percent area occupied by particles of different classes as influenced by heat treating parameters [Jain (J2), Kumar (K6)]. This may lead to incomplete/erroneous assessments as is evident from the data summarized in the Tables 5.46-5.48. To overcome this problem, instead, DF was calculated for each heat treatment (Tables 5.49-5.51). Subsequently for each heat treating temperature, the

DF was plotted as a function of time for the experimental alloys (Figures 5.48-5.50). Their perusal revealed that-

- (i) particles predominantly precipitate in class II (size 0.58-1.16 μ)
- (ii) with an initial increase in temperature (800/850°C), further precipitation in the same ranges occurs; this is followed by coarsening
- (iii) with an increase in temperature or time at a given temperature, an initial tendency towards precipitation gave way to the coarsening tendency predominates.
- (iv) the changes in class I sized particles are mostly prefunctory in alloys C2 & C3 in general. However in C1 they seemed to assume relevance even at 900°C and their importance persisted even on heat treating at 950°C and 1000°C.
- (v) the relevance of Class III type particles was a function of the alloy (Cu) content and heat treating schedule. Class III particles had little relevance in alloy C1. Its relevance appeared to increase with Cu content and was a maximum in alloy C3 (especially on heat treating at 950°C and 1000°C). A similar situation had partly existed in C2 upon heat treating from 950° at higher soaking periods. Thus taking an overall view, alloy C1 exhibited DSPs

belonging to class I and II, the alloy C2 mostly comprised DSPs in size range 0.58-1.16 μ (Class II) with a spillover into class III whereas DSPs in the C3 comprised a size fraction 0.58-1.16 μ upon heat treating up to 900°C and in the size range 1.16-1.74 μ (Class III) upon heat treating from 950°C and 1000°C.

The aforesaid analysis is quantitatively re-substantiated through the data summarized in the Table 5.52 which reveal the percent contribution of DF in each class as influenced by heat treatment. An important objective of doing so is to arrive at homogeneity/heterogeneity based on the size and distribution of the DSPs. This aspect has been separately dealt with in a later section 5.2.11.

5.2.9 MATHEMATICAL MODELLING OF THE TRANSFORMATION BEHAVIOUR

Figures 5.1-5.3 reveal how time and temperature control the transformation behaviour and therefore, the hardness of the experimental alloys. It was concluded that hardness, H varies linearly with time, t and can be represented by

$$H = K1 + K2t \quad \dots (5.15)$$

The values of K1 and K2 were found to be different for different temperatures(T) and therefore can be expressed as a function of temperature in the form of equations

$$K1 = f(T) \quad \dots(5.20)$$

$$K2 = f(T) \quad \dots(5.21)$$

The plots of K1 vs T and K2 vs T revealed that the K2 vs T is linear and gives a relationship $K2 = A3 + A4T$. However, the $\ln K1$ vs $1/T$ plots indicated a linear behaviour and hence, the relation between K1 and T can be expressed as :

$$\ln K1 = \ln A1 + A2.(1/T) \quad \dots(5.22)$$

or
$$K1 = A1.e^{A2/T} \quad \dots(5.23)$$

Substituting for K1 and K2 in the equation 5.15, the final relationship is

$$H = A1.e^{A2/T} + (A3+A4T)t \quad \dots(5.24)$$

The constants A1, A2, A3, A4 were calculated for different alloys using the multi-variable nonlinear constraint optimization technique [Hiemmenai (H10), magasarain (M4)]. The final equations along with the overall standard deviations are reported below :

$$C1 : H = 271.701 e^{838.513/T} + (0.005809-0.5476 \times 10^{-5} T)t$$

$$\text{Overall SD} = 1.593 \quad \dots(5.25)$$

$$C2 : H = 342.517 e^{551.093/T} + (0.01686-0.158 \times 10^{-4} T)t$$

$$\text{Overall SD} = 4.524 \quad \dots(5.26)$$

$$C3 : H = 287.256 e^{692.334/T} + (0.01777-0.163 \times 10^{-4} T)t$$

$$\text{Overall SD} = 3.053 \quad \dots(5.27)$$

Where T = temperature in °K

t = time in seconds

H = hardness, HV₃₀

The theoretical hardness values calculated from the above equations were plotted against the corresponding experimental values and are shown in Figure 5.51. It reveals that barring a few instances, the calculated values are well within $\pm 5\%$.

It is observed that the constants A₁, A₂, and A₃ are positive for all the alloys. Hence their effect would be similar and additive. The constant A₄ is negative and therefore, its effect needs to be analyzed. This calls for assessing the contribution of second factor of the Equation 5.24. Its values, as influenced by the heat treating temperature and time are given below. As will be evident, the contribution of the factor becomes negative at temperatures $\geq 800^\circ\text{C}$ for C₁ & C₂ and 850°C for C₃.

Contribution of the second factor

Heat-treatment		Contribution of the second factor		
		C1	C2	C3
800	2 AC	0	0	2
800	4 AC	0	-1	4
800	6 AC	-1	-2	5
800	8 AC	-1	-3	6
800	10 AC	-2	-4	9
850	2 AC	-2	-6	-4
850	4 AC	-4	-13	-8
850	6 AC	-7	-19	-12
850	8 AC	-9	-26	-16
850	10 AC	-12	-33	-20

900	2	AC	-4	-12	-9
900	4	AC	-8	-24	-19
900	6	AC	-13	-37	-29
900	8	AC	-17	-49	-39
900	10	AC	-22	-61	-49
950	2	AC	-6	-18	-15
950	4	AC	-12	-36	-31
950	6	AC	-19	-54	-47
950	8	AC	-25	-72	-63
950	10	AC	-31	-90	-79
1000	2	AC	-8	-23	-21
1000	4	AC	-16	-47	-43
1000	6	AC	-25	-71	-65
1000	8	AC	-33	-94	-86
1000	10	AC	-41	-118	-108
1050	2	AC	-10	-29	-27
1050	4	AC	-20	-58	-55
1050	6	AC	-31	-88	-82
1050	8	AC	-41	-117	-110
1050	10	AC	-51	-147	-138

It will be seen that the contribution of this factor to the overall hardness varies linearly with time for a given h/t temperature.

The above discussion reveals that the term $(A_3 + A_4.T)t$ has a significant impact on the overall hardness especially when the alloys are being heat treated either from 'higher' temperatures or for longer soaking periods.

Because of a difference in the nature of the contribution of the second factor, as influenced by temperature, further calcula-

tions were made to find out the temperature at which the contribution of the aforesaid factor became negative. The change over occurred at 802, 800, and 817°C in C1, C2, and C3 respectively, which are in fact, the temperatures representing the cross-over point(section 5.2.6.2). This deduction is valid for all the alloys, duly remembering that the value of the COP would differ from alloy to alloy.

When the values of COP(obtained from the Figures 5.10-5.12), namely, 850-900°C are compared with those observed on the basis of the model, the apparent difference can be explained by stating that whereas the equations represent transformations without reflecting upon their complexities, the actual situation is to the contrary due to heterogeneity of the system and also because a large number of phases with greatly different 'inherent' characteristics are participating in the transformations. The lag between the 'ideal' and 'actual' situations is what is contributing to the difference and evidently can not be computed mathematically.

5.2.9.1 PHYSICAL CONSISTENCY OF THE PROPOSED MODEL

The data summarized in the Tables 5.53-5.55 , when viewed in the context of the structural changes already discussed, leads to certain important inferences. Firstly, the hardness is essen-

tially controlled by the parameter $A_1 \cdot e^{A_2/T}$. This is independent of the matrix microstructure, i.e, independent of whether the matrix is martensitic/austenitic, or simply austenite as in the present case. Recalling the basis on which the alloys are designed, it is easy to visualise why the matrix is austenitic irrespective of the heat treating temperature employed. Its hardness values vary inversely with temperature, with time at best playing a secondary role, as has been observed (Tables 5.53-5.55).

The contribution from the second factor, although less significant to begin with, assumes prominence at higher temperatures and soaking periods. The parameter $(A_3 + A_4 \cdot T)t$ can therefore, be said to represent the carbide transformation. At lower temperatures ($\sim 800^\circ\text{C}$ for C1 and C2 and 850°C for C3), its contribution is positive and increases with time because the precipitated second phase (DSPs/DCs) is in a condition to harden/strengthen in view of its size and distribution. The correctness of this analysis is proved by the data obtained on heat treating from 850°C , wherein the contribution has decreased due to some coarsening of the DSPs. The contribution, on heat treating from 850°C is quite significant thereby signifying that the precipitated second phase is still playing an effective role.

The negative contribution is seen to have a sizable effect only on heat treating from upwards of 950°C, a temperature at which hardness begins to decrease with time markedly. It is thus noteworthy that the negative contribution is assuming reasonable proportions just when the V_f of MC is beginning to decrease. By this temperature, the DSPs have grown considerably and become less in number, it can be assumed safely that the DSPs seized to be effective and hence the second factor is now representing 'massive carbide' related transformations. Therefore its (second factor) magnitude will increase steeply (i) as the temperature is raised beyond 950°C and (ii) at higher soaking periods at a given temperature. The reasons for the negative contribution of this parameter, with an increase in temperature, have already been analyzed in the section 5.2.7. Therefore, the two parameters constituting the model are physically consistent with the attendant microstructural changes; the first term representing the matrix transformations and the second term the carbide transformations.

5.2.9.2 'SIMULATION' OF THE TRANSFORMATION BEHAVIOUR THROUGH MODELLING

As is known, the overall transformation behaviour of the alloys has been arrived at on the basis of a total of 30 experi-

ments per alloy. This is a time consuming exercise. If it were possible to arrive at/or simulate the transformation behaviour of the alloys on the basis of a minimum yet optimal number of experiments with an accuracy equivalent or thereabouts to that of the models developed, then it would greatly help in cutting down on arduous experimentation and would also lead to a saving on energy and the overall costs.

Recent studies by Patwardhan, Mukundan, Rao, Sharma, and Kumar [Patwardhan (P9)] have shown that the transformation behaviour of Fe-5Cr-1.5Cu cast irons containing 7.5% Mn and 6% Mn with austenitic and martensitic matrices studied on the basis of 30 arduous experiments and mathematically modelled [Patwardhan (P10)], could be 'simulated' on the basis of either 4 or at the maximum 6 data points. They comprise hardness values at two extremes of heat treating temperature & time, namely, 800°C (2 hours & 10 hours) and 1050°C (2 hours & 10 hours) and at an intermediate temperature namely 850°C/900°C (2 hours and 10 hours). The logic of selecting the intermediate is that the hardness should be independent of time i.e. $dH/dt = 0$. This also made the choice of the heat treatments, selected for the purpose of simulation, more representative/broad based.

It was felt appropriate to apply the concept thus developed

to assess whether the transformation behaviour of the alloys C1, C2, and C3 could be similarly 'simulated'.

On following the procedure outlined by Patwardhan et.al. [Patwardhan (P9)], the following emerges-

The 'models' representing the transformation behaviour of the experimental alloys(section 5.2.9) are-

$$C1 : H = 271.7 e^{838.513/T} + (0.005809 - 0.54 \times 10^{-5} T)t$$

$$\text{Overall SD} = 1.5931 \quad \dots(5.25)$$

$$C2 : H = 342.517 e^{551.093/T} + (0.01686 - 0.158 \times 10^{-4} T)t$$

$$\text{Overall SD} = 4.524 \quad \dots(5.26)$$

$$C3 : H = 287.256 e^{692.334/T} + (0.01777 - 0.163 \times 10^{-4} T)t$$

$$\text{Overall SD} = 3.053 \quad \dots(5.27)$$

The hardness values predicted on the basis of the above models are summarized in the Tables 5.56-5.58.

On selecting the hardness values at the two extremities of heat treating temperature & time, namely, 800°C(2 hours & 10 hours) and 1050°C (2 hours & 10 hours), the 'simulated' models are-

$$C1 : H = 204.5 e^{1051.1/T} + (0.0114 - 0.1111 \times 10^{-4} T)t$$

$$\text{Overall SD} = 14.844 \quad \dots(5.28)$$

$$C2 : H = 222.4 e^{1013/T} + (0.00872 - 0.9167 \times 10^{-4} T)t$$

$$\text{Overall SD} = 6.752 \dots(5.29)$$

$$\text{C3 : } H = 204.5 e^{1051/T} + (0.01144 - 0.1111 \times 10^{-4} T)t$$

$$\text{Overall SD} = 4.955 \dots(5.30)$$

On the basis of the above models, hardness values at different temperatures and periods were computed and are summarized in the Tables 5.56-5.58. Interestingly the correlation coefficients for C1 and C3 match closely and approach unity, where this is not so for C2. Thus, there appeared to be no direct relationship between correlation coefficients and the Cu content of the alloys.

On selecting the hardness values at two extremities of heat treating periods (2 hours & 10 hours) at 800 & 1050°C and at an additionally selected heat treating temperature(900°C), the simulated models are-

$$\text{C1 : } H = 235.87 e^{902.75/T} + (0.0143 - 0.1334 \times 10^{-4} T)t$$

$$\text{Overall SD} = 12.683 \dots(5.31)$$

$$\text{C2 : } H = 265.34 e^{835.39/T} + (0.01229 - 0.1199 \times 10^{-4} T)t$$

$$\text{Overall SD} = 4.824 \dots(5.32)$$

$$\text{C3 : } H = 235.87 e^{902.75/T} + (0.0143 - 0.1334 \times 10^{-4} T)t$$

$$\text{Overall SD} = 3.448 \dots(5.33)$$

On the basis of the above models, hardness values at different temperatures and times were computed and are summarized

in the Tables 5.56-5.58. The correlation coefficients of this model are slightly better than the ones obtained on the basis of similar models outlined in Equations 5.28-5.30. Higher correlation coefficients (revealing improved relation between the 'actual' & the 'simulated' behaviour) have been obtained because the selection of hardness values at two extremities of periods at the three heat treating temperatures has made the exercise more representative vis-a-vis transformation behaviour.

Thus the transformation behaviour can be simulated with reasonably high accuracy on the basis of either four or six data points. The correlation coefficients first decrease and then increase with copper content and are minimum in alloy C2 whereas maximum in C1. No satisfactory reasoning based on theory could be assigned to this because it is understood that high Cu content will reduce the level of heterogeneity through exercising better control over the 'carbide related' transformations. For example, at higher copper contents (alloy C3) the starting volume fraction of massive carbides is low (38.2% in as-cast condition) compared to alloys C1 and C2 which contain 44.9% and 38.7% volume percent of MCs in the as-cast state. The same trend was followed on heat treating from lower temperatures (upto 900°C) as evident from Table 5.38. However, on heat treating from higher

temperatures ($\geq 950^\circ\text{C}$), the trend is changed and the alloy C3 exhibit more Vf of MCs than C2, and in some cases even more than C1 (Table 5.38). This increased Vf of MCs, with attendant heterogeneity, might account for the above said behaviour i.e. there is a first decrease and then increase in the correlation coefficients with increase in copper.

5.2.10 MATHEMATICAL MODELLING OF THE DISTRIBUTION FACTOR

A critical analysis reveals that the DF can be mathematically represented with the help of the following equations :

$$C1: 0.04049 e^{2646.47/T} - (7000 - 5.818T) \times 10^{-8}.t \quad \dots(5.34)$$

$$C2: 0.00407 e^{4905.09/T} - (7000 - 5.980) \times 10^{-8}.t \quad \dots(5.35)$$

$$CP3: 0.00079 e^{6945.10/T} - (7162 - 6.040T) \times 10^{-8}.t \quad \dots(5.36)$$

The basis of arriving at these equations is the same as the one on which the mathematical modelling of the transformation behaviour of the alloys was carried out (section 5.2.9).

5.2.11 HOMOGENEITY/HETEROGENEITY OF THE ALLOYS

A careful perusal of the data summarized in the Tables 5.35-5.37 and especially the one pertaining to the volume fraction of massive carbides as influenced by heat treating parameters reveals that for a given heat treatment, the amount of massive

carbides varied over a considerable range. Higher values are obtained close to the core of the specimens and lower values were obtained towards the periphery. This is primarily due to the inhomogeneities which are intrinsic to alloys/system. The usual statistical methods available to analyze such a data did not prove useful since if mean and the $\pm 3\sigma$ limit (indicative of 95% reliability) are applied to find out the permissible range over which the parameter being assessed could vary, then all the experimental values fall within the ambit of 'permissible' data. The aforesaid observation and the resulting implications are being analyzed separately.

It was however opined by Patwardhan [Patwardhan (P2)] that variations in the data indicate a lack of homogeneity and therefore this could become a basis for calculating the homogeneity/heterogeneity of the alloy(s)/alloy system under investigation.

In a broad sense homogeneity of the experimental alloys can be adjudged on the basis of:

- (i) a variation in the alloy concentration within the austenitic matrix- chemical homogeneity/heterogeneity,
- (ii) uneven distribution of MCs, leading to a highly variable volume fraction of MCs and thereby to a variable homogeneity

which may be termed as distributional heterogeneity; additionally carbide transformations and carbide destabilizing tendency will also contribute to this situation.

(iii)uneven distribution of precipitated second phase(variation in size, distribution, and volume fraction discounting the morphology to begin with).

Assessing homogeneity/heterogeneity at (i) would require an accurate assessment of the (a) alloy concentration and (b) the concentration gradients, if any. Such an information could be generated through extensive electron-probe micro analysis which although used in the present study may not prove sufficient to arrive at the desired assessments. Thus the main emphasis would be on assessing the homogeneity/heterogeneity at (ii) and (iii). To begin with the one at (ii) would be addressed to.

In order to fully appreciate the nature of variation, curves were plotted for the experimental alloys depicting all 20 observations(Vf of MCs) as influenced by heat treating parameters. Representative data thus obtained is summarized in the (figures) Appendix A-4 to A-9. Interestingly the data points do not reveal the existence of 'median points'(or similar data points) which otherwise could have enabled 'assessment' of the

'average'/reasonably relevant value. It was therefore decided to consider all the data points and to arrive at the 'mean' in the usual manner. Having done so, the overall homogeneity/heterogeneity of the alloy as influenced by heat treating has been defined as

$$H_M = \frac{\text{The net variation in } V_f \text{ of MCs around the mean}}{\text{Permissible variation around a mean}} \quad \dots(5.37)$$

$$= \frac{V_{f_{exp}} \times \text{overall standard deviation}(exp)}{[V_{f_{max,exp}} - V_{f_{min,exp}}]} \quad \dots(5.38)$$

$$= \frac{\text{permitted standard deviation around the mean} \times V_{f_{exp}}}{[V_{f_{max,per}} - V_{f_{min,per}}]}$$

$$= \frac{V_f \times SD_{exp}}{[V_{f_{max,exp}} - V_{f_{min,exp}}]} \times \frac{[V_{f_{max,per}} - V_{f_{min,per}}]}{V_f \times SD_{per}} \quad \dots(5.39)$$

$$= \frac{SD_{exp}}{SD_{per}} \times \frac{[V_{f_{max,per}} - V_{f_{min,per}}]}{[V_{f_{max,exp}} - V_{f_{min,exp}}]} \quad \dots(5.40)$$

To calculate SD_{per} , we recall that a given parameter being measured can have values $V_{fave} \pm 3\sigma$. This concept can be extended further by stating that under the existing constraints(i.e. for a permitted variation of 15%),

$$\frac{3\sigma_{per}}{\sqrt{n}} = 15\% \times V_{fave} \quad \dots(5.41)$$

where n = number of readings

σ_{per} = permissible variance

$$\text{Hence } \sigma_{per} = SD_{per} = 15\% \times \frac{\sqrt{n} \times Vf_{ave}}{3}$$

$$SD_{per} = 0.15 \times \frac{\sqrt{n} \times Vf_{ave}}{3} \quad \dots(5.42)$$

and for a 15% permissible variation in the Vf of MCs

$$Vf_{max,per} = Vf_{ave} + 0.15 \times Vf_{ave} \quad \dots(5.43)$$

$$Vf_{min,per} = Vf_{ave} - 0.15 \times Vf_{ave} \quad \dots(5.44)$$

H_M could be expressed as a fraction or percent. Under ideal condition $H_M = 1$. $Vf_{max,per}$, $Vf_{min,per}$, and SD_{per} could be computed on the basis of the error limit permissible e.g. $\pm 15\%$ or higher as the case may be except in a situation where H_M exceeds 1.

This homogeneity can be described as 'intrinsic' or compositional homogeneity. However, if it were possible to predict 'theoretically' the Vf of MCs an alloy should attain for a given heat treatment, then another parameter 'theoretical homogeneity' can be defined which would be given by the expression-

Homogeneity (theoretical/optimal),

$$Vf_{exp} \times SD_{exp} \times [Vf_{max,per} - Vf_{min,per}]$$

$$H_M(\text{Th/opt}) = \frac{\text{SD}_{\text{per}} \times V_{\text{ftheo}} \times [V_{\text{fmax,exp}} - V_{\text{fmin,exp}}]}{\dots} \dots(5.45)$$

This would additionally require estimating V_{ftheo} . To do so a possible basis would be to theoretically compute the V_f from the V_f vs t (at a given T) and also from V_f vs T (for a given t) model and to arrive at a mean of the two values. Thereafter the permissible variation ($\pm 20\%$ or $\pm 15\%$) will have to be considered to arrive SD_{per} as before. The ratio of the compositional to the optimum/ theoretical homogeneity could then reflect upon the deviation exhibited by the alloy/alloy system to heat treating.

To begin with H_M was calculated on the basis of the equation 5.40 for a variation of $\pm 15\%$. The data thus computed is summarized in the Table 5.59. The implications of this data are being analyzed and this aspect does not form a part of this thesis.

The other form of heterogeneity namely, distributional heterogeneity could result from the unevenness of size/distribution of the precipitated dispersed second phase whose nature has already been commented upon. Variation in it could then be utilized for expressing 'distributional heterogeneity and as per the concept developed [Patwardhan (P2)] could be defined on the basis of the following consideration.

Distributional heterogeneity, $H_M(\text{dist})$ (related with precipitated second phase) could then be expressed as

$$= \frac{\text{Deviation in distribution function/factor with respect to the majority size fraction}}{\text{Overall distribution function/factor}} \dots (5.46)$$

or more precisely

$$H_M(\text{dist}) = \frac{\text{underspill ratio} \times \text{spillover ratio}}{\text{overall distribution factor}} \dots (5.47)$$

expressed as a ratio or as percentage.

The data summarized in the Table 5.60 puts forth such an information and this proves additionally useful in understanding the structural changes already quantitatively and qualitatively discussed. It would be interesting to analyze the impact of such a variation on properties- a theme which has been left out of the ambit of the present investigation.

The concept of determining the homogeneity/heterogeneity based on the data generated through quantitative metallography has not been hitherto pursued/evolved and the following additional steps are suggested to explore this idea/concept further:

- (i) a systematic and detailed reporting of the quantitative data on the lines outlined in the present investigation and some of the earlier investigations [Jain (J2), Kumar (K6)].

(ii) a more detailed and comprehensive analysis of the data to assess the nature of 'events' it represents and the implications thereof.

It is however certain that the earlier assessments regarding the possible effect of heat treating parameters and copper on the extent of homogeneity/heterogeneity are perhaps over simplistic as would be evident from a perusal of the Figures A-4 to A-9 and the data summarized in Tables 5.59-5.60.

5.2.11.1 3D PLOTS REPRESENTING INTERRELATION BETWEEN TEMPERATURE, TIME AND HARDNESS

Till now the effect of heat treatment on the hardness has been analyzed on the basis of varying one of the parameters while keeping the other a constant. This has been represented in Figures 5.1-5.21. Although, these plots provided useful and necessary explanations of the transformation behaviour, they failed to provide the overall effect of heat treatment at a glance.

This difficulty was resolved by constructing 3-dimensional plots (Figures 5.52-5.54) using the Equations 5.25-5.27, at rotation angles 45° and 225° around the Z-axis and at a tilt angle of 30° . For each of the alloy, Figure (a) represents a gradual change in the slope of the hardness vs time plots as influenced by temperature which are represented over a surface. The Figure

(b) clearly reveals that the so called COP is not a sharply delineated temperature but that the change over is occurring over a narrow dark region represented by a surface.

A comparison of the Figures (a) for the experimental alloys further brings out that the slope of the hardness vs temperature/time plot is generating a surface which has been depicted in Figures (b). The 3-D plots reaffirm the relative differences in the transformation behaviour of the three alloys.

5.2.11.2 ISO-HARDNESS PLOTS

Iso-hardness plots were made by plotting out hardness (as influenced by temperature and time) as contours (Figures 5.55-5.57). Evidently, the hardness is a constant along a contour and as such it would be possible to determine the different temperature and time combinations (from the plot) to get a desired hardness. The existence of approximately equally spaced contours with a gradual change over of the slope/orientation in alloy C1 is because it sustains hardness over a longer range of heat treating temperature(s) and period(s). A nearly similar situation exists in C2 and C3 at lower temperature regions, however significant change is observed in these alloys at higher temperatures which exhibit greater flexibility in attaining hardness levels lower than what could be attained in C1.

The aforesaid observations while reinforcing the earlier deductions vis-a-vis the transformation behaviour of the alloys do bring about additional useful information. The data thus obtained could be related to enhanced austenite stabilizing/ carbide destabilizing tendencies resulting from an increase in the copper content.

5.2 CONCLUSION

This chapter has dealt at length with the transformation behaviour of the experimental alloys characterized on the basis of hardness measurements and the attendant microstructural changes. A detailed analysis of the latter proved extremely helpful in arriving at a qualitative understanding of the interrelation between microstructure and properties (indicated by hardness). The behaviour of the dispersed second phase as influenced by heat treating schedule has been mathematically represented by evolving a parameter called the 'distribution factor'. This enabled calculation of the coarsening behaviour of the second phase on the basis of a parameter called as the 'coarsening index'. The evolution of these parameters has proved extremely helpful in overcoming the limitations of the Ostwald's ripening formula which is regarded as the sole basis for

characterizing the distribution of the second phase particles. The development of these models has proved useful in establishing models interrelating properties with the microstructure. This has been discussed in Chapter VII. An equally interesting aspect has been to quantify/define 'heterogeneity'/'homogeneity' on the basis of the distribution of massive second and dispersed second phase as influenced by heat treating parameters.

Finally mathematical models have been developed interrelating hardness with the heat treating temperature and time (microstructures). It has been established that the model is physically consistent i.e. it truly represents the structural changes occurring on heat treating. With the help of empirical modelling, it has been possible to establish that the transformation behaviour of the alloys could be 'simulated', with nearly equivalent accuracy as the modelled ones, on the basis of 4 to 6 experiments as against the original thirty. This is an important contribution which is of major technological significance.

Although much has been said about the characterization of different phases, the presence of martensite could not be unequivocally established in marginal cases. Similarly, the nature and types of carbides needed identifying. Therefore, a detailed study comprising X-ray diffractometry and EPMA was carried out. The data thus obtained have been discussed in the next chapter.

CHAPTER VI

PHASE ANALYSIS AND PHASE IDENTIFICATION

6.1 STRUCTURAL ANALYSIS BY X-RAY DIFFRACTOMETRY

Specimens of the alloys in the as-cast, as well as in the heat treated conditions were extensively examined by X-ray diffractometry to identify/confirm (i) the nature of matrix microstructure, and (ii) the nature of different carbides that formed during heat treatment. The data emerging from an analysis of the x-ray diffractograms has been summarized in the Tables 6.1-6.22. Summary tables (Tables 6.23-6.25) have also been prepared to make the discussion more concise. With the help of diffraction data, it was possible to interpret the microstructures more or less fully as would be evident from the ensuing analysis in spite of restricting the experimental work to specimens that were cast and heat treated for 6 hours at different temperatures primarily due to time constraints. None the less it just about sufficed to surmise the likely events occurring on heat treating for 2 hours and 10 hours.

6.1.1 RESULTS

6.1.1.1 AS-CAST CONDITION

The microconstituents attained in the experimental alloys comprise a matrix of austenite with some martensite and carbides.

namely M_3C (isomorphous with Fe_3C) + M_7C_3 (isomorphous with Cr_7C_3) and M_5C_2 . Additionally, Fe_8Si_2C , $CrMn_3$ and elemental copper were also indexed. Lower angle peaks corresponding to α/M were observed in all the alloys. However, the higher angle peaks characterizing martensite were found to be absent in all the three alloys.

6.1.1.2 HEAT TREATED CONDITION

On heat treating, the 2θ values of the matrix differed from the standard 2θ -values as obtained from the diffraction data cards (Tables 6.2-6.22). Further the nature of carbides formed and the presence/absence of other constituents observed in the as-cast state also differed. This along with the effect of heat treating temperature and time on the possible transformations occurring within the matrix and the carbides, and any additional features that were observed, have been discussed below.

6.1.1.2.1 EFFECT OF HEAT TREATMENT ON THE MATRIX MICROSTRUCTURE

- (i) On heat treating from $800^\circ C$ the matrix essentially comprised austenite and martensite.
- (ii) A similar situation existed on heat treating from $850^\circ C$.
- (iii) Increasing the temperature further resulted in the attainment of austenitic matrices.

6.1.1.2.2 EFFECT OF HEAT TREATMENT ON THE NATURE OF CARBIDES

On heat treating, a clear cut carbide transformation sequence was observed. However, the main difference was with regard to the carbide stability as influenced by heat treating parameters and the alloy (copper) content.

(i) M₃C

- (a) This is a commonly occurring carbide in the as-cast condition. It was clearly indexed in C1 and C2 but not in C3.
- (b) On heat treating, it was indexed in C1 up to 950°C, (6 hours heat treatment) and in traces for the 1050°C, 6 hours heat treatment.
- (c) Amongst the three alloys, it was indexed at best in traces on heat treating from 1050°C in C1.
- (d) The behaviour of alloy C2 was similar to C1 except on heat treating at 900°C where it could not be indexed.
- (e) In C3, the indexing of the M₃C carbide is random i.e. the regularity of its occurrence as in C1 and C2 is missing. However, the M₃C carbide was indexed up to 1000°C, 6 hours heat treatment (except at 950°C, 6 hours heat treatment).

(ii) M₇C₃

This carbide formed in all the alloys both in the as-cast as well as in the heat treated condition. Heat treating parameters

seemed to have little effect on its formation/indexing. In all the three alloys, it has been indexed with greater certainty as compared to the M_3C carbide. It was indexed best in C2.

(iii) M_5C_2

Its presence in the experimental alloys was detected in as-cast and heat treated condition (up to the maximum heat treatment temperature i.e. $1050^\circ C$, 6 hours heat treatment). Its indexing showed a trend approaching to that observed for the presence of M_7C_3 carbide and certainly better than that for M_3C carbide.

6.1.1.2.3 OTHER FEATURES

(a) Elemental copper :

Copper was indexed in the as-cast condition as well as in the heat treated condition in all the alloys. Overall its presence appeared to be less marked in C1 whereas it was indexed best in C3, whereas in C2 its indexing was almost approaching that observed in C3.

(b) Fe_8Si_2C :

It was invariably indexed both in as-cast as well as at all the heat treatments.

(c) CrMn₃ :

It was present in the as-cast and in the heat treated conditions. It was indexed only upto 900 °C though found on traces at 1000°C, 6 hours heat treatment for C1. Overall the alloy C3 appeared less susceptible to its formation. The needle like constituent observed through optical metallography may represent this constituent since inter-metallics are known to have a needle like appearance.

6.1.2 DISCUSSION

6.1.2.1 MATRIX MICROSTRUCTURE

A summary of the findings relating to the matrix microstructure has been presented in the Section 6.1. The alloys presently investigated were primarily designed to attain an austenitic matrix on air cooling from all temperatures. Optical metallography had revealed that there is in fact a deviation from this premise and that the matrix comprised austenite and martensite on heat treating from 800°C (all soaking periods) and 850°C (up to 6 hours soaking period). Reasons for the deviation observed have been critically analysed and explained in the section 5.2.4. The x-ray observations have proved useful in supporting and confirming these findings. The matrix microstructure is expected to be only austenitic (refer alloy design) on heat treating from 850°C (higher soaking period) or

from higher temperatures (independent of the soaking period). This is duly confirmed from the diffractometric studies (Tables 6.2 - 6.25).

As the heat treating temperature is raised or time at a given temperature is raised, the volume fraction of MCs decreased (Equation=5.3). The solute atoms thus made available will dissolve into austenite increasing its stability/the lattice parameter. This tendency would be marked at or above a threshold temperature at which the tendency to dissolve the MCs/DCs is also marked. An increase in the lattice parameter will mean that the diffracted beam will shift towards lower 2θ values for austenite. Its magnitude is not easy to assess. To overcome this problem, the maximum intensity peak in each diffractogram (heat treating temperatures $\geq 900^{\circ}\text{C}$) has been attributed to austenite.

6.1.2.2 CARBIDE TRANSFORMATION

Based on an analysis of the data contained in Section-6.1.1.2 (Tables 6.2-6.22 and summary (Tables 6.23-6.25), it is evident that the general carbide transformation sequence in the experimental alloys is as follows:

Carbide(s)	Temperature regime
$\text{M}_3\text{C} + \text{M}_5\text{C}_2 + \text{M}_7\text{C}_3$	As-cast state in all the investigated alloys

|
M₃C + M₅C₂ + M₇C₃

up to 850°C (M₃C present
in traces in C₃)

M₅C₂ + M₇C₃

up to 1000°C in C₁ and C₃
up to 1050°C in C₂.

|
M₅C₂ + M₇C₃

up to 1000°C, in C₂ and C₃

+ M₃C (reforming)

up to 1050°C in C₁.

|
M₅C₂ (some/traces)

+ M₇C₃

up to 1050°C

|
Predominant carbides at high temperature are M₇C₃ + M₅C₂
(small traces)

A study of the Fe-Mn-C and Fe-Cr-C ternary diagrams revealed that M₇C₃, M₅C₂ and M₂₃C₆ are essentially high temperature carbides and the last mentioned one has a relatively lower dissolution temperature/thermal stability as compared to the other two [Owen (02)]. Further, the predominant carbide at lower temperatures is M₃C. Accordingly, the carbide expected to be present in the as-cast state should be M₃C as this is the stable form at room temperature. The possible presence of higher temperature forms of carbides can be explained by stating that because of the complexity of the alloy system under study, the different high temperature carbides have not fully transformed

successively to their lower temperature variants due to the reactions being sluggish. This can also be looked at differently as would be evident from the discussion below.

The attainment of M_5C_2 and M_7C_3 carbides in the as-cast/heat treated condition with the M_3C carbides playing at best a secondary role affirms that what was outlined in 'design of alloys' (attainment of high temperature microstructure/carbides with a minimum of processing) has in fact been achieved. Equally satisfying is the absence of 'boundary carbide' $M_{23}C_6$.

Looking to the general trend of the data summarized in the Tables 6.23-6.25, it is evident that the carbide transformation occurring in the alloys could be visualized as follows:

- (i) retention of the 'high temperature carbides' M_5C_2 & M_7C_3 , attained in the as-cast condition, even on heat treating
- (ii) gradual phasing out of M_3C (room temperature/lower temperature form) upon heat treating which is governed by the "temperature regime" of stability. This is what has been observed. The only additional feature is that M_3C is reforming on heat treating from 1000°C and 1050°C .

6.1.2.2.1 THE M_3C

This carbide (in massive/platy form) was present up to

950°C. It was found to be isomorphous with Fe_3C , although small amounts of Mn and Cr were also present in it as confirmed through EPMA (Tables 6.26-6.28) to be discussed later. This in fact made the Fe_3C more stable [Goldschmidt (G2)] otherwise it might have dissolved/transformed even at relatively lower temperature(s) and soaking period(s). On the other hand the presence of Cu in the alloys (although not partitioning to Fe_3C) has an opposite effect and therefore, the dissolution of this carbide is enhanced. This could also be gauged from the subtle differences in the temperature range of stability of M_3C in the alloys C1 (1.5% Cu) and C2 (3% Cu) (Tables 6.23 & 6.24) although C3 totally differed from C1 and C2 in this regard (Table 6.25). Further, it appears that the phasing out of M_3C is in some way linked with the formation of higher volume fraction/larger proportions of M_5C_2 and M_7C_3 carbides. Whether M_3C could directly transform to M_7C_3 or via an intermediate carbide M_5C_2 carbide needs to be looked at carefully.

6.1.2.2.2 THE M_7C_3

This carbide was present in the as-cast condition and upon heat treating from practically all temperatures. It may be Cr based (Cr_7C_3), Fe based (Fe_7C_3), or Mn based (Mn_7C_3), but Cr_7C_3 is the only carbide to form singly. Others namely Fe_7C_3 or Mn_7C_3 are always present in combination as $(Cr, Fe)_7C_3$, $(Fe, Mn)_7C_3$, or

(Cr₇C₃+Mn₇C₃)(103) [Goldschmidt (G2)]. In the present study the carbide formed was a mixed carbide of Fe, Cr & Mn (Table 6.27) with a preponderance of Fe & Cr atoms (Table 6.27).

The formation of M₇C₃ has been the subject matter of a number of studies and its mechanism of formation from M₃C has been described as (i) in-situ [Wever (W6), Smith (S11), Pickering (P13), Nutting (N1), Woodhead (W8), Mills (M12), Kuo (K10)] (ii) combination of in-situ and separate nucleation [Honeycombe (H11), Bilby (B9)] and (iii) also as separate nucleation [Balluffi (B2)]. In the presently investigated alloys, a part of the MCs comprise M₇C₃. Its appearance was not similar to the one described in earlier studies [Jain (J2), Kumar (K6)] nor could it have formed "in-situ" as suggested earlier. The additionally forming M₇C₃, coinciding with the phasing out of M₃C, is most likely to be 'nucleated' at the M₃C-matrix interface. In the absence of any M₂₃C₆ forming, the earlier hypothesis that it is the dissolution of M₂₃C₆ carbide which may initiate the formation of M₇C₃ [Rao (R2), (R4)] would not hold good under the existing conditions. Thus one could visualize a transformation sequence

$$M_3C \rightarrow \text{metal atoms} \rightarrow \text{nucleation/formation of } M_7C_3 \quad \dots(6.1)$$

6.1.2.2.3 THE M₅C₂

As has already been stated, the M₅C₂ carbide is present even

in the as-cast condition; reasons for its presence have already been stated. Its persistence even upon heat treating (even when the dispersed second phase is absent) could be attributed to the successful implementation of alloy design strategy which aims at attaining the high temperature carbides even in the as-cast state. Inertness and sluggishness of M_5C_2 to transform to the 'other carbide' forms have also contributed to its retention in the microstructure. Evidently, M_5C_2 carbide constitutes a part of the MCs. Additionally, a part of the DSPs comprise M_5C_2 in addition to M_3C . This observation is consistent with the carbide transformation sequence as observed in the Fe-Cr-C and Fe-Mn-C ternary systems [Metals Hand Book (M11)]. By careful perusal of Table 5.42, it can be deduced that there is a general decrease in the volume fraction of dispersed carbides with soaking period up to 6 hours and thereafter an increase on raising the soaking period to 10 hours (Table 5.42). The volume fraction of dispersed carbides initially increased in all the experimental alloys with increasing heat treatment temperature (up to 850°C). It was followed by either little change or an increase at 900 and 950°C (barring few exceptions) and finally an increase at 1000°C . Both these observations in a nut shell reveal that some new carbide is definitely forming and it would not be incorrect to deduce that this is in fact M_5C_2 . Further, a carbide such as the one

presently under consideration i.e. forming through a precipitation process by ageing of austenite is more likely to be of a dispersed type. Hence at least a part of the dispersed carbides comprise M_5C_2 . This can be established unequivocally only through selective etching techniques and or by EPMA.

6.1.2.2.4 Fe_8Si_2C

Even after considering various possibilities of indexing diffractograms, some peaks still remained unidentified. One of the possible options considered was the presence of the aforesaid phase. From the Tables 6.2-6.22, it can be observed that this phase is indexed in all the alloys up to 1050°C either in traces or in small amounts. Other than this no further comment is being made as to its mechanism of formation and/or the morphology it assumes.

6.1.2.2.5 PRESENCE OF ELEMENTAL Cu AND OTHER PHASES

The possible presence of Cu in the as-cast condition and its being indexed even on heat treating in spite of the matrix being by and large austenitic (exceptions heat treating at 800°C and 850°C up to 6 hours) is additionally an unexpected result. However, results (Tables 6.23-6.25) are in agreement with the composition of investigated alloys the presence of Cu being best indexed for C3 i.e. alloy with maximum Cu (5% Cu) and with less

certainty in C1 (1.5% Cu). Quite clearly its difficult to putforth a highly satisfactory explanation as to its presence on the basis of physical metallurgical principles especially when the matrix is austenitic. Its presence is easier to comprehend when the matrix is either martensitic or ferritic as Cu has low solubility in them. A detailed EPM analysis confirmed the presence of Cu-rich phase (Table 6.32) in C3 (5% Cu).

After considering all possibilities, some reflections still remained unindexed. It was observed that this problem could be partly resolved by considering the formation of CrMn_3 and Cu_2S phases. The possibility of the formation of inter-metallics such as CrMn_3 is more on heat treating from higher temperatures. The formation of Cu_2S is feasible in all the alloys perhaps more so in the higher Cu containing alloys. It is suggested that a more detailed investigation is required to confirm the presence of phases such as CrMn_3 and Cu_2S etc. in future studies especially since even the possible presence of a carbide of the type Cr_3C_2 is indicated.

Before concluding, a comment regarding the possible indexing of Mn_{15}C_4 would be in order. Evidently this carbide is not forming in the experimental alloys. Its inclusion in the Tables 6.23-6.25 meant to convey that the mixed carbides to form come

close enough to a composition not much different from $Mn_{15}C_4$.

6.1.2.3 CONCLUDING REMARKS

The above said analysis can be concised to pin point the deductions/tentative conclusions arrived on the basis of x-ray diffractometry:

- (i) matrix of the experimental alloys is affirmed to be austenite and martensite in the as-cast condition and upon heat treating from $800^{\circ}C$ and $850^{\circ}C$ and fully austenite upon heat treating from temperatures $\geq 900^{\circ}C$.
- (ii) bulk of the MCs comprise M_3C , M_5C_2 and M_7C_3 upto $900^{\circ}C$ and mostly M_7C_3 and some M_5C_2 thereafter.
- (iii) DSPs (needle & globular morphology) mostly comprise M_3C and M_5C_2 ; the plate/needle morphologies etch similarly as the MCs and therefore there are reasons to believe that they are carbides rather than being inter-metallics of the type $CrMn_3$; this needs a more detailed analysis through EPMA.
- (iv) indications of the possible presence of Cu and other phases such as Fe_8Si_2C , $CrMn_3$ etc. make it incumbent to carry out detailed EPM analysis
- (v) the above said line of approach would also help in identifying the 'haloed' regions around MCs (light grey &

dark grey) as well as dark etching regions often present between two bridging massive carbide regions on heat treating from 1000/ 1050°C.

6.2 ELECTRON PROBE MICRO ANALYSIS RESULTS

This was carried out on the experimental alloys to ascertain (i) the distribution of major alloying elements into the matrix and the carbide phase, (ii) the manner in which the distribution was affected by heat treating/alloying(copper content), (iii) the type of carbides constituting the MCs, DCs and DSPs(needle/plate type), (iv) whether Cu was present, and (v) the identity of the 'haloed' regions around MCs and new regions/ phases such as dark etching areas abridging agglomerating MCs. The relevant data is summarized in the Tables 6.26-6.32 and in the Table 6.33 and in Figure 6.1a-1.

The analysis of the data will be specific to the points that have been mentioned above.

6.2.1 ELEMENTAL DISTRIBUTION

6.2.1.1 AS-CAST CONDITION

The distribution of alloying elements into the matrix and carbide phases is illustrated in the Tables 6.26-6.28. Representative micrographs are summarized in the Figure 6.1.

- (i) A larger amount of Mn partitioned to the carbide than to the matrix phase. The ratio of Mn in the carbide to Mn in the matrix was approximately 1.6 and this was uniformly so for all the three alloys except in C2 wherein it was still higher (Tables 6.26, 6.27 and 6.33).
- (ii) Majority of the Cr partitioned to the carbide phase as is evident from the high ratio of Cr in the carbide to that in the matrix (Tables 6.26, 6.27 and 6.33).
- (iii) Bulk of the Cu and Si were present in the matrix (Tables 6.26 and 6.27).
- (iv) Carbon distribution into the carbide and matrix phases is on the expected lines (Tables 6.26 and 6.27).

6.2.1.2 EFFECT OF HEAT TREATMENT ON ELEMENT DISTRIBUTION

The above said observations concerning element distribution are also valid in the heat treated condition. However there are certain additional observations meriting consideration (Tables 6.26-6.33), namely:

- (i) The amount of Mn partitioning into the matrix was a maximum in C1, minimum in C2 and intermediate in C3 (though it showed minimum variation with time and temperature) irrespective of the fact that all the three experimental alloys had similar Mn content. There is apparently no

relationship between the amount partitioned and heat treatment temperature/time.

- (ii) The concentration of 'C' within the matrix decreased on raising heat treatment temperature/time for C2 and C3 in general. However, in C1, the variation in 'C' concentration as influenced by heat treating parameters did not conform to a specific trend. Alloy C2 showed a more consistent partitioning of carbon into matrix, compared to the other two alloys.
- (iii) Cr partitioning into the matrix showed a much better consistency in comparison to either Mn or C. The amount partitioned was found to be a maximum in the as-cast condition (valid for C1 and C3).
- (iv) As stated earlier, Cu & Si mainly partitioned to the matrix, and heat treating did not have an appreciable effect on their partitioning.
- (v) An important observation is that heat treating did not have a tangible effect on the amount of Mn & Cr present in the MCs.

6.2.1.3 NATURE OF MCs

While discussing the microstructural changes, three types of carbide had been mentioned, (a) massive/platy and (b) eutectic/discontinuous type and (c) flower and perforated type.

All of them etched bright during optical metallography. However, on observing under an electron micro-probe analyzer, the eutectic/discontinuous type and massive carbides appeared differently as grey and dark etching areas respectively (Figure 6.1 a, b & e)

On heat treating the distinction in the etching characteristics between two types of carbides persisted (Figures 6.1a-c, h & c). A perusal of Tables 6.27 & 6.28 indicated that the compositions of the two carbides also differed.

6.2.1.4 IDENTITY OF THE DIFFERENT CARBIDES

Based on the element distribution data, it can be inferred with reasonable certainty that -

- (i) In all alloys, the MCs present are of M_7C_3 & M_3C type :
- (ii) The higher the temperature the more favoured the presence of M_7C_3 .

6.2.1.5 IDENTITY OF DSPs

Identifying the 'needle' like phase and dispersed carbides proved extremely difficult because of their size and the difficulty in focussing. The limited information available suggested these to be carbides (Table 6.29 & Figure 6.1i).

6.2.1.6 IDENTITY OF HALOED REGIONS & DARK ETCHING AREAS ADJOINING MCs

Representative electron density images of the aforesaid regions are shown in Figures 6.1a,b,c,d,e,h,i,k and l. Considering the former (haloed regions) to begin with, it is clearly seen that these represent a carbide whose composition is similar to that of the MCs except for the Cr content which is less by 10 % (Tables 6.27, 6.28 and 6.31). Similarly the "C" content of these regions was also somewhat lower than normally associated with carbides.

The dark etching regions adjoining the agglomerating carbides (Figure 5.1e, h) contained approximately the same amounts of Mn, Cr and C as the massive carbides but additionally also contained Cu & Si (Table 6.30). This indicates that these regions represent areas having an alloy concentration different from the rest of the matrix.

6.2.1.7 IDENTIFICATION OF Cu

Copper was observed in the as-cast as well as in the heat treated conditions. This has been duly supported by EPMA observations (Table 6.32 & Figure 6.1f and g).

6.2.2 DISCUSSION

The EPMA data which has been critically represented in the above sections needs to be carefully analyzed to arrive at useful inferences regarding the partitioning behaviour and its consequent impact on alloy design. Equally important would be to resolve the unanswered queries arising out of x-ray diffractometry and optical metallographic analyses such as the identity of the MCs and DSPs and the identity of the differently etching matrix regions obtained on heat treating from high temperatures. Although a more extensive EPM analysis would have proved substantially more beneficial, the experience gained thus far could serve as a basis of arriving at useful conclusions.

The primary interest in such studies centers around the basic partitioning data and as Mn is being given primacy, the initial interest would centre around its partitioning. Subsequently partitioning behaviour of Cr has also been commented upon. Overall, the partitioning ratio $Mn_{carbide}/Mn_{matrix}$ in the present study has varied from 1.35 (only in a few instances) to 1.75. This appears to be in fair agreement with an earlier study conducted by Singh [Singh (S10)] in which this partition ratio was found to be 1.5. and by Kumar [Kumar (K6)] where the partition ratio was found to be 1.5-1.8. The difference, however, is that in the former the heat treating temperatures did not

exceed 850°C, whereas in the latter temperatures have been relatively higher as is also the case in the present study. This difference in itself can account for the slightly larger partition ratios presently obtained.

Looking to the heterogeneous nature of the microstructure certain generalizations can be arrived at regarding the partitioning data which have also been appropriately explained.

- (i) $Mn_{carbide}/Mn_{matrix}$ ratio in the as-cast state is relatively unaffected by heat treatment except on heat treating from high temperature when the ratio reduced (valid for C1 & C2). This could have resulted from two possible sources, firstly that the nature of the carbide(s) formed at higher temperature(s) require(s) a higher concentration of alloying elements and carbon content (i.e. high concentration of metal atoms such as Mn & Cr) and/or secondly that Mn is preferentially partitioning to the matrix phase (austenite) due to its intrinsic tendency to stabilize austenite or perhaps a combination of the two (Table 6.33). Thirdly, a considerably altered V_f of MCs on heat treating from high temperatures should not be overlooked.

(ii) The said ratio appeared to follow a general trend, though not strictly, namely that it appeared to increase marginally with Cu content (least in C1). The possible reasons are that (a) a carbide with a higher metal concentration is forming and/or (b) an increase in the Cu content (τ - stabilizer) is allowing a larger concentration of Mn to partition to the carbide since Cu is now additionally playing the role of a τ -stabilizer (Table 6.33).

Having discussed the Mn partitioning it would be pertinent to comment upon the partitioning of Cr. The partition ratio $C_{\text{carbide}}/C_{\text{matrix}}$ in the as-cast state is 6.5-7.5 somewhat lower than the expected partitioning ratio [Sandoz (S1),(S2)] thereby indicating that the carbides formed incorporates lesser Cr content than normal. This is perhaps due to a part of Cr being replaced by Mn. On heat treating, the ratio increased with temperature/ time for reasons already discussed while considering Mn partitioning, although a consistent trend was not observed. Exception is C2 which showed an initial decrease in ratio followed by increase at high temperatures. On heat treating from 1000°C , 10 hours, the $C_{\text{carbide}}/C_{\text{matrix}}$ is larger than what was observed in the as-cast condition thereby implying that the carbide to form is richer in Cr (Table 6.33) and lower in Mn

content as has already been discussed and commented upon. The inference is that the preferred carbides to form would be of the type M_7C_3 and/or M_5C_2 . X-ray diffractometric analysis has suggested this to be so and this is duly corroborated by EPM analysis as discussed in the ensuing sections.

The important implications of these observations are that although Mn is considered to be an austenite stabilizer (implying a large partitioning into austenite), its known carbide forming tendency is enabling a larger proportion of it to partition into the carbide phase. This is further made apparent when the partition ratio of a conventional austenite stabilizer like Ni is considered (based on data reported by Sandoz [Sandoz (S2)]). Therefore, in order to ensure that the requisite amount of Mn is available in austenite a substantially larger amount of Mn would have to be added.

Talking about Cu partitioning it is seen that bulk of the Cu partitions into the matrix. This is to be expected in view of its (i) inherent tendency to stabilize austenite and (ii) negligible carbide stabilizing tendency. On raising the heat treating temperature, the amount of Cu in the carbide is negligible. This is again as per expectations and consistent with the behaviour of other graphitizing elements Ni and Si, which

are essentially found in the matrix [Sandoz (S1), (S2)]. It may, however, be remembered that the graphitizing tendency of Cu is not as marked as that of either Ni or Si and that it is effective only at higher temperatures and when added in larger amounts.

Having thus discussed the general partitioning pattern, it would now be appropriate to comment upon the nature of the carbides formed in the as-cast condition and the effect of heat treatment on their nature. The observation that both Mn and Cr partition to the carbide phase alongwith Fe makes it evident that the carbides formed are mixed Fe, Mn, Cr type. Based on the element distribution, the MCs forming in C1 in the as-cast state mostly comprise M_3C and M_9C_3 . Thus the possible indexing of the M_5C_2 carbide, as revealed through the analysis in the sections 6.1.1.1 & 6.1.1.2 (Tables 6.23-6.25) may have to be revised. The observation that the carbides formed contain Fe, Mn, and Cr whereas only Fe and Mn are known to form M_5C_2 type carbide [Kuo (K11)] further suggests that the possible presence of M_5C_2 will have to be conclusively established (Table 6.27).

Similarly the presence of M_7C_3 type carbide in C2 and C3 in the as-cast state is on the expected lines since an increase in Cu content (compositions of C2 & C3) enables a larger

partitioning of Cr into the carbide phase thereby enhancing the tendency to form Cr enriched M_7C_3 type carbide (Figure 6.1, Tables 6.26-6.32).

The identity of the "haloed regions" has been confirmed as a carbide although with a Cr content about 10% less than in the MCs. The formation of such massive carbides has been reported in the literature [Stefanascu (S14)]. Irrespective of the reasons for their formation, such an occurrence reflects upon the heterogeneity of the alloys (Figures 6.1a-d,i,k,l; Table 6.30).

As already appropriately resoned (section 5.2.4.2), the dark etching areas represent those regions within the matrix whose composition differs from the rest of the matrix (Table 6.30). Their composition approximates to M_7C_3 type carbide except for the high concentration of Cu and Si. In fact with time these regions would have developed into well formed carbide(s) thereby abridging the two agglomerating carbide regions into a whole mass.

In the light of the above, it may not be out of place to suggest that the DSPs are mostly M_7C_3 and/or M_3C type (Table 6.29, Figure 6.1i). Thus the conclusions arrived at on the basis of x-ray diffractometric analysis regarding the possible

attainment of M_5C_2 have to be modified by excluding its presence. This conclusion is also in agreement with the deductions arrived at in a study involving the transformation behaviour of Cr-Ni in the heat treated condition wherein the formation 'needle shaped' DSPs of the type M_3C has been reported [Laird - II (L1), (L2)]. This further confirms the analysis put forth while analyzing the structures that the needle type DSPs based on their etching characteristics and growth behaviour are in fact carbides and not intermetallics. The observation that part of the DSPs are needle like & partly dispersed may also be differently interpreted to mean that the DSPs are essentially in the form of needles and the DCs observed may in fact represent the 'end view' of the needles that are oriented perpendicular to the plane of observation. This may be considered as an appropriate justification for treating the DSPs and DCs as one entity while carrying out quantitative metallographic studies although in the present investigation the volume fraction of needle type DSPs is rather small.

Finally it becomes incumbent to comment upon the influence of one element on the partitioning of the others into different phases.

Considering now the effect of Cu on the partitioning of Mn, it is seen that Cu is either having little effect or is perhaps

promoting Mn to perform its customary function (of being a τ -stabilizer/carbide former). A somewhat similar effect is observed on Cr partitioning. In fact, as expected, the amount of Cr in the matrix appears reduced (Table 6.26) thereby further confirming that Cu is promoting Cr to perform its usual function of forming/stabilizing carbide(s).

The formation of copper in the as-cast condition (Table 6.23-6.25), although not expected, may be explained by stating that in the as-cast condition, the alloys contain martensitic regions and elemental copper could have been present in those regions. However its formation even in the heat treated condition in the form of Cu enriched regions (Table 6.32, Figure 6.1 f-g) especially on heat treating for higher temperatures is a surprising result since the matrix under these conditions is fully austenitic and Cu has a large solubility in austenite. None the less the result is an important one and its implications could be examined only after a more detailed EPM analysis.

6.2.3 CONCLUDING REMARKS

Based on the above critique, it can be concluded that-

- (i) MCs are mostly a combination of M_7C_3 and/or M_3C depending upon the condition/heat treating regime.
- (ii) DSPs mostly comprise M_7C_3/M_3C

- (iii) Cu is present both in the as-cast/heat treated condition
- (iv) the dark etching regions observed on heat treating from high temperature(s) represent regions with an 'alloy concentration' different from that of the matrix. They represent a composition close to an M_7C_3 type carbide but containing large amounts of Cu and Si.
- (v) Mn partitioned more to the carbide phase and less to the matrix. This situation was not altered even on heat treating from high temperature(s)
- (vi) the distribution of Cr, Si, and Cu was on the expected lines.

A more conclusive and detailed investigation is required to unequivocally conclude upon the absence of M_5C_2 type of carbides. For this reason their indexing has not been deleted while analyzing the x-ray diffractometric data (Tables 6.23-6.25).

6.3 THERMAL ANALYSIS

Differential thermal analysis comprised (i) assessment of the critical/transformation temperatures, and (ii) compilation of the thermogravimetric (TG) data, and (iii) modelling of the TG data, carried out to a limited extent. The data thus obtained have been summarized in the Tables 6.34-6.37 and in the Figures 6.2-6.3. Results have been discussed in the following sections.

6.3.1 RESULTS

6.3.1.1 CRITICAL/TRANSFORMATION TEMPERATURES

- (i) First transformation occurred 540-575°C (Table 6.34).
- (ii) The second transformation similarly occurred in the temperature range of 960-980°C (Table 6.34).
- (iii) In C1 and C2 third transformation was seen to occur at 740-760 °C (Table 6.34).
- (iv) C1 also revealed a phase change occurring at 900°C.

6.3.1.2 DTA

- (i) For the first transformation (540-575°C), DTA values were negative and were in the range of 3.2-4.6 μ V (Table 6.35).
- (ii) For the higher transformation (960-980°C), DTA values were positive and ranged from 10.0-18.0 μ v (Table 6.35).
- (iii) For the transformation observed in C1 and C2 only (740-760°C), the DTA value was positive for C1 and negative for C2 (Table 6.35).
- (iv) For the transformation (900°C), occurring only in C1, the DTA value was positive and 3.4 μ V (Table 6.35).

6.3.1.3 THERMOGRAVIMETRIC STUDIES

This data, summarized in the form of plots between %TG as a function of temperature, are shown in the Figures 6.2-6.5 and

Tables 6.36-6.37(Figure 6.5 summarizing the overall information).

From the figures, the following inferences were drawn:

- (i) %TG increased very slowly with an increase in temperature. This was followed by an exponential increase on raising the temperature further.
- (ii) The nature of these plots was a function of the microstructure.
- (iii) In the as-cast state, the weight gain was nearly a constant up to approximately 600°C. %TG corresponding to this condition was a minimum for C3 followed by C1 & C2. A steep increase in the %TG was observed on moving from 900°C to 1000°C. In fact up to 800°C, the increase in %TG with temperature was gradual(Figure-6.5).
- (iv) Taking an overall view, an increase in the Cu content accounted for a decrease in %TG at least in the as-cast condition i.e. a higher Cu content was conducive to improving high temperature oxidation resistance.

6.3.2 DISCUSSION

The DTA studies proved useful in substantiating the structural observations reported earlier(section 5.1.2). Such a study was expected to prove helpful in resolving some of the existing inconsistencies and in providing additional information

on the possibility of employing the experimental alloys for high temperature applications. The least that was expected from the study was by way of information on the transformation/critical temperatures.

6.3.2.1 CRITICAL/TRANSFORMATION TEMPERATURE(S)

The first set of transformation temperature(s) occurring at 540-575°C evidently represent the $\alpha \rightarrow \tau$ transformation in the experimental alloys. Evidently, those regions which were α/α' would transform. A near similarity in the DTA values suggests that the three alloys have roughly similar τ forming tendency thereby suggesting that an increase in the copper content has little effect on the τ stabilizing tendency. This deduction belies the normally held view since Cu is known to be a τ -stabilizer and should prove effective in doing so since another austenite stabilizer is already present. Moreover, the $\alpha \rightarrow \tau$ transformation temperature has been considerably reduced due to the presence of 10% Mn (common to all the alloys). A more plausible explanation is that this temperature represents the formation of FeO through a process of internal oxidation. In the presence of Mn, Si, P, & Si, the formation of FeO is mildly exothermic as has been observed in the present study for alloys both in the as-cast and heat treated conditions.

The next important set of transformation temperatures (960-980°C) evidently represents carbide transformation which is duly suggested by optical metallographic studies (Figures 5.22-5.42) and confirmed through x-ray diffractometric analysis (Tables 6.23-6.25). The possible transformation in the temperature range 960-980°C will comprise the (a) precipitation/growth of carbides constituting the DSPs (M_3C and/or M_7C_3) and (b) conversion of M_3C/M_5C_2 (?) into the higher temperature carbide forms. While saying so it should also be remembered that the magnitude of the peak in the DTA plot does suggest that more than one transformation is occurring perhaps involving a change of state otherwise it would be difficult to account for the pronounced peak (Figures 6.2-6.4) [Rao (R5)]. At the same time it is equally true that optical metallography does not in any way suggest a change of state (formation of a liquid phase). A close scrutiny of the data summarized in the Tables 6.23-6.25 and the aforesaid discussion supplementing these observations reveal that the DTA data is in fact representing a carbide transformation involving a change over from M_3C to M_7C_3 via the formation of a transition carbide of the type M_5C_2 . Although the reasons for the occurrence of a third transformation in C1 are not clearly understood, it is quite likely that the eventual carbide transformation observed at 960-980°C may have initiated in C1 at

~ 900°C.

Although an attempt has been made to arrive at definitive deductions on the basis of DTA results, perhaps a more rigorous experimentation would have enabled doing so with greater certainty. Such an experimentation would comprise (i) employing different heating rates starting from the lowest value e.g. of the order of 0.1°C/min., (ii) plotting out of the initial and peak transformation temperatures, (iii) extrapolating the initial and peak transformation temperatures to a heating rate equivalent to zero to obtain the equilibrium transformation temperatures, and (iv) calculation of heat of reaction based on the peak area finally culminating in the calculation of heat capacities of the reactants and that of the products [Schute (S4), Mackenzie (M1), Kofstad (K1)]. It is suggested that the DTA studies be more rigorously carried out in order to arrive at precise information on the transformation behaviour of the experimental alloys.

6.3.2.2 THERMOGRAVIMETRIC STUDIES

Thermogravimetric studies proved helpful in drawing inferences regarding the usefulness of the experimental alloys for high temperature applications. Since, the basic aim of the study was to optimize the microstructure for obtaining the best in terms of corrosion and heat/oxidation resistance and

deformation behaviour, even the as-cast microstructure was expected to respond favourably when exposed to high temperature. Therefore to begin with, its high temperature behaviour was investigated to arrive at some initial data especially with regard to the effect of copper content. It was reasonable to do so since "alloy design" had been aimed at stabilizing the high temperature microstructure to room temperature in as large a measure as possible.

From a perusal of the thermogravimetric data (Figure 6.5 & Tables 6.36-6.37), it emerges that the TG data for as-cast microstructure has two distinct regions, (i) up to 600°C and (ii) beyond 600°C and extending up to 1050°C. The first of these is characterized by a very small and more or less uniform increase in %TG suggesting the usefulness of as-cast structure up to 600°C. An equally important aspect is that till a temperature of 600°C the behaviour of the alloy C3 was superior to the other two (though comparable with C1), at $T > 600^\circ\text{C}$ the behaviour varied significantly in the sense that alloy C3 was found to be much superior than the other two behaving similarly. The observation that the higher the copper content the lesser the weight gain is true for high temperatures ($\geq 700^\circ\text{C}$) and partially true at lower temperatures (C1 better than C2 though C3 is best). This difference in the behaviour can be attributed to the presence of

more amount of MCs (predominantly M_7C_3 type) at lower temperatures. M_3C was better indexed in C1 and C2 in Comparison to C3 (Tables 6.23-6.25). Presence of M_3C is disadvantageous from the point of view of high temperature oxidation resistance because (i) to begin with it has a high coarsening tendency and (ii) its transition to a higher temperature form. A temperature of 600°C could be considered as representing the transition stage. At temperature $\geq 900^\circ\text{C}$, the high temperature behaviour is being governed by the volume fraction of the MCs (the nature of carbide being mostly M_7C_3 and stability of matrix (austenite) which is controlled by the Cu content. The larger the Cu content the better will be the stability of austenite.

To understand the interrelation, if any, between the TG data and the DTA results, the data summarized in the Tables 6.36-6.37 and Figure 6.5 were reexamined. From this comparison, it also emerges that the sharp increase in %TG may be related with the susceptibility to carbide transformation; the more marked the susceptibility the less useful the alloy. This can be explained by stating that an alloy susceptible to carbide transformation essentially exhibits proneness to configurational changes at the atomistic level. And this would lead to enhanced oxidation. Thus the key aspect would be to employ heat treatments to exclude such

transformations.

Before concluding it would be pertinent to record that a more comprehensive understanding of the high temperature behaviour would have emerged if thermogravimetric studies were carried out on alloys in the heat treated condition. None the less on the basis of the studies carried out (data not reported) it can be concluded that the basic parameters controlling the high temperature performance are (i) the stability and volume fraction of austenite, (ii) volume fraction of the "high temperature" carbide forms $M_7C_3/M_{2-3}C_6/M_5C_2$, and (iii) presence/absence of "low temperature" carbide forms. Based on the quantitative metallographic data, the most useful microstructures in the as-cast condition may comprise a minimum of 15-20% carbide and balance austenite (in the present alloys the amount of carbides is higher). This situation changes when heat treated micro-structures are considered as the volume fraction of carbides reduces. This will certainly not be useful from the point of view of high temperature properties in the sense that the strength will reduce but the absence of susceptibility to "carbide transformation" is advantageous. Thus if we could attain all the merits of the 'high temperature heat treated' microstructure and yet retain a larger volume fraction of the MCs, that would be ideal. The existence of lower

temperature carbides is not desirable since their effectiveness is greatly reduced at (high) temperatures at which they could coarsen and/or may undergo transformation, either of which is undesirable.

Finally, the occurrence of a phase transformation during heating at or below the temperature at which the alloy is intended to be used would adversely affect high temperature performance as the base/expected microstructure is prone to a change in its configuration at the atomistic level i.e. it is susceptible to enhanced rate of migration of atoms/material flow.

6.3.3 MODELLING OF THE TG DATA

The discussion contained in the Section 6.3.2.1 essentially dealt with the high temperature response of some selected microstructures and of the possible impact of various transformations, occurring during heating/treating, in affecting the overall high temperature performance. Having done so, it would now be appropriate to look into modelling aspect of the TG data. In order to do so, it would be necessary to examine the processes involving high temperature oxidation per se and arrive at the possible rate laws relevant to the present study, which would eventually form the basis for modelling.

Oxidation of metals can be expressed by a simple chemical reaction as



However, the reaction path and the oxidation behaviour of a metal may depend on a variety of factors, and reaction mechanism(s) may as a result prove complex.

The initial step in the metal-oxygen reaction involves the adsorption of gas on the metal surface. As the reaction proceeds, oxygen may dissolve in the metal forming an oxide on the surface either as a film or as a separate oxide nuclei. Adsorption and the initial oxide formation are both functions of surface orientation and condition, concentration of crystal defects at the surface, and impurities in both the metal and the gas [Kofstad (K1)].

The surface oxide separates the metal from the gas. This oxide may either be in the form of thin tenacious film or as a porous oxide scale.

For a particular metal, the reaction mechanism is a function of the pre-treatment and surface condition, temperature, gas composition and pressure, and elapsed time of reaction. Looking to the possibility of a large variation in the properties of

different metals and alloys and their oxides, a number of theories are needed to describe the oxidation behaviour of metals [Kubaschewski(K3), Hauffi (H3), Benard (B7)].

A detailed understanding of this phenomenon requires knowledge of reaction rates and kinetics, the temperature and oxygen pressure dependence of the reaction, the composition, structure, and growth mechanism of the reaction products.

Rate equations describing oxidation may be classified as logarithmic, parabolic, and linear. These are discussed in detail elsewhere [Kubaschewski (K3), Hauffi (H3), Benard (B7), Evans (E3), Loviers (L6), Webb (W5), Haycock (H4)] and are not relevant to the present study because temperature dependence of oxidation behaviour alone has been studied.

Numerous oxidation reactions have shown empirically that the temperature dependence of oxidation rate constants at a constant ambient oxygen pressure obeys an Arrhenius-type equation

$$k = k_0 \exp(-Q/RT) \quad \dots(6.3)$$

where Q is the activation energy commonly given in cal/mole, R is the gas constant(1.986 cal/°K mole), and the T the absolute temperature. The pre-exponential factor, k_0 , is within experimental accuracy, usually found to be independent of

temperature. Using Equation 6.3, the activation energy Q is determined by plotting $\log_{10}k$ as a function of $1/T$, in which case the slope of the curve is given by $Q/2.303R$. The rate constant at different temperatures is commonly determined from isothermal measurements, but may also be determined from a single run under conditions of linearly increasing temperature [Kofstad (K2)].

Nucleation and growth phenomena may give rise to unusual oxygen pressure-dependence of the process of oxidation [Sewell (S5), (S6); Rahmel (R1)]. Considering oxidation of Fe as an example, Fe_3O_4 is initially formed on the surface (FeO is unstable below $570^\circ C$), and Fe_2O_3 is subsequently nucleated in the Fe_3O_4 surface. When Fe_2O_3 has grown to form a continuous layer, the oxidation rate is substantially reduced.

A scrutiny of the Figure 6.5 reveals that although the %TG varies exponentially with temperature, the plot has two distinct parts, the nature of variation in one being opposite to that of the other. The first part (from ambient temperature to $200^\circ C$) can be represented by an asymptotic curve as

$$\%TG = A_1'(\exp^{-A_2/T} - 1) \quad \dots(6.4)$$

and the second part can be represented as

$$\%TG = A_1 + A_2(\exp^{-A_3/T}) \quad \dots(6.5)$$

where, A_1' , A_2' , A_1 , A_2 , and A_3 are constants, and T is temperature in $^{\circ}K$.

The %TG increase in the first part is very small (~2%) compared to the overall increase of up to (18-25%) attained at highest heating temperature. It was therefore, felt appropriate to neglect the former in arriving at the proposed model. As before multi-variable nonlinear constraint optimization technique [Himmelblau (H10), Mangasarain (M4)] was employed to do so.

The correlations thus obtained are summarized as follows:

$$\text{Alloy C1} \quad \%TG = 2.2761 + 7999.65 \exp(-7929.25/T) \quad \dots(6.6)$$

$$\text{Alloy C2} \quad \%TG = 2.5190 + 7426.91 \exp(-7999.98/T) \quad \dots(6.7)$$

$$\text{Alloy C3} \quad \%TG = 1.9690 + 6046.54 \exp(-7999.98/T) \quad \dots(6.8)$$

The %TG was calculated from the aforesaid correlations and a plot of predicted %TG as a function of temperature obtained (Figures 6.6). The predicted %TG values lie very close to the experimentally determined values thereby indicating the validity of the models developed.

CHAPTER VII

DEFORMATION & CORROSION BEHAVIOUR

7.1 INTRODUCTION

Having established the transformation characteristics of the alloys and carried out the phase analysis and phase identification with a reasonable accuracy and certainty, it becomes essential to carry out an in depth analysis of the deformation and corrosion behaviour as this alone would decide as to how far the objectives outlined in the introduction/alloy design have been achieved. While the deformation behaviour was assessed through compression testing, the corrosion characterization has been carried out with the help of weight loss studies.

7.2 EFFECT OF HEAT TREATMENT ON THE DEFORMATION BEHAVIOUR

As already stated, the deformation behaviour was assessed through compression testing and the data have been reported in Tables 7.1-7.3.

Apparently, the data thus summarized did not conform to a specific trend. However it can be attributed to the fact that some of the specimens might have fractured prematurely due to the existence of pipe not visible outwardly. This problem was resolved through a normalization process carried out in the

following manner-

- (i) by modelling the hardness-strength interrelation on a basis adopted by Kumar [Kumar (K6)].
- (ii) by computing the predicted value(s) of CS based on the above model, and
- (iii) by indirectly computing the likely experimental values on the basis of their differing from the predicted values by $\pm 15\%$.

7.2.1 MODELLING OF THE DEFORMATION BEHAVIOUR

Hardness is a very useful measure of the mechanical properties (deformation behaviour) of materials. Therefore, it is regarded as a quick yet a reliable measure of strength. Normally higher the hardness the larger is the UTS/CS and smaller the % elongation value. In ferrous materials (steels) hardness and tensile strength are related empirically through a conversion factor

$$5 \text{ VHN}_{30} \cong 1 \text{ tsi UTS} \cong 15.5 \text{ MPa}$$

A similar empirical law is not expected to be obeyed in cast irons in general and white irons in particular because, as engineering materials, they are a class apart from steels due to their brittleness and due to a generally complex microstructure. An attempt was, therefore, made to examine the possibility of

establishing a quantitative relation between hardness and deformation behaviour in the experimental alloys. The information thus generated was expected to provide a back up to the mathematical modelling work being actively pursued.

7.2.1.1 INTERRELATION BETWEEN COMPRESSIVE STRENGTH AND HARDNESS

To begin with CS was plotted as a function of hardness. As no definite relationship emerged, it was decided to plot CS/H as a function of hardness. On doing so a second order polynomial functional relationship between the two parameters emerged and therefore hardness can be represented as

$$R = A_1 + A_2 (H) + A_3 (H)^2 \quad \dots(7.1)$$

where $R = CS/H$,

$H =$ hardness, HV₃₀,

A_1, A_2 and A_3 are constants.

The constants A_1, A_2 , and A_3 were computed as before and the correlations thus obtained are :

$$\text{Alloy C1 : } R = -11.58 + 0.0667H - (0.6926E-04)H^2 \quad \dots(7.2)$$

$$\text{Alloy C2 : } R = 36.92 - 0.1299H + (0.1227E-03)H^2 \quad \dots(7.3)$$

$$\text{Alloy C3 : } R = 24.98 - 0.0629H + (0.4240E-04)H^2 \quad \dots(7.4)$$

CS values for the experimental alloys were computed on the basis of above models. On comparing them with the experimentally

determined values, it emerged that the difference in most cases does not exceed $\pm 10\%$ (Table-7.4). In some instances the experimental and the predicted values differed by a larger margin which might be due to casting defects present in the test specimens.

7.2.2 EFFECT OF HEAT TREATING TEMPERATURE/TIME

(i) For the alloy C1 (2 hours soaking period), the CS initially increased over that in the as-cast state on heat treating from 900°C (Tables 7.1 & 7.4). A further increase in the temperature upto 1050°C lead to a decrease in the CS. The predicted values did not follow the same trend, the decrease was negligible and for all practical purposes the variation could be considered as being linear.

A similar trend was observed on heat treating for 6 hours soaking period except that the predicted values of CS followed a pattern in reverse. As stated earlier, the magnitude of increase/decrease was small and it could well be stated that heat treating has had little effect i.e. the expected benefits have not accrued (Table 7.4).

On increasing the soaking period to 10 hours there was a decrease in strength on raising the temperature from 1000 to

1050°C; the predicted values followed a similar trend.

(ii) In alloy C2, CS increased significantly over that in the as-cast state on heat treating from 900°C for 2 hours soaking period. An increase in the heat treating upto 1000°C had an adverse effect followed by an increase in the strength on heat treating from 1050°C. The predicted values followed a decreasing trend (Tables 7.2 & 7.4).

For the 6 hours soaking period CS decreased continuously with temperature although the predicted values remained more or less unchanged.

At 10 hrs soaking period, the variation in CS with temperature followed a trend similar to the one observed at 2 hrs soaking period. The predicted values of CS also followed a similar trend.

(iii) In alloy C3 (6 hrs soaking period), the CS initially increased on raising the temperature from 900°C to 950°C. This was followed by a significant decrease in CS on heat treating from 1000°C. Contrary to C1 and C2 an increase in CS was observed on raising the temperature to 1050°C. The predicted values exhibited a continuously increasing trend.

On raising the soaking period to 10 hrs, CS to begin with was low, it increased with temperature and became a constant. The predicted values, although revealing an increasing trend with temperature, showed a marked increase on raising the temperature from 1000°C to 1050°C. The experimentally determined values had remained unaltered on heat treating from this temperature range.

7.2.3 DISCUSSION

The aforesaid data can be suitably interpreted on the basis of the initial volume fraction of MCs, the effect of temperature/time in influencing the formation and morphology of DSPs and their effect in decreasing the volume fraction of MCs. That this contention is true can be judged by recalling that the property changes are being by and large controlled through the aforesaid structural changes (the partially martensitic matrix on heat treating from 800° and 850°C notwithstanding).

Before setting out to explain the trends for the 2 hrs, 6 hrs and 10 hrs soaking periods, which are analysed in the form of plots summarized in the Figures 7.1 to 7.3 (some of the plots contain 3 points). It may be mentioned that % strain has not been reported since it could not be determined with accuracy and certainty for all the heat treatments.

DSPs are expected to strengthen and also embrittle the material somewhat especially when their morphology is adverse (needle like/platy). This is applicable at the lower heat treating temperatures and soaking periods. With an increase in time, their embrittling response is expected to reduce because their volume fraction reduces as a result of coarsening and also because the DSPs then predominantly comprise DCS. However on raising the temperature at either of the soaking periods, embrittlement reduces because the Vf of DSPs and MCs is reducing and the morphology of latter is assuming favourable configurations. With an increase in temperature the DSPs/DCs are less relevant and therefore the overall properties would be governed by the volume fraction, distribution and morphology of MCs as the matrix in combination with the MCs/DCs is constituting a composite comprising MCs and DSPs upto 950°C and mostly MCs at $T > 950^{\circ}\text{C}$. Based on this analysis, the data summarized in the Figure 7.1 to 7.3 can be reasonably well understood; only the trends would be analysed in the following section.

In C1 at 2 hours (Figure 7.1) soaking period, a CS higher than in the as-cast state (900°C) is due to the formation of an austenitic matrix and the presence of DSPs mostly as DCs which would compensate for the reduced strengthening response due to a

decrease in the volume fraction of MCs (Figure 5.25). On raising the temperature to 1000°C the volume fraction of DSPs decreases and no needle type structure is present (Figure 5.27). This alongwith a reduced volume fraction of MCs and a higher stability of the austenitic matrix accounts for an increase in CS. However on further raising the temperature to 1050°C, the expected improvement in CS for reasons already stated has not occurred due to the formation of degenerate structure (dark patches) and aligned MCs giving rise to an appearance as though MCs are acquiring afresh a platy/needle type morphology (Figure 5.28). It may be mentioned that absence of DSPs/DCs, a reduced Vf of MCs and a higher stability of austenite should have proved helpful in enhancing CS. However, this has not happened and the adverse features have prevailed. At 10 hrs soaking period, the overall CS values are lower than the ones attained on heat treating for 2 hrs. Furthermore they appear to decrease with temperature. This is not easy to comprehend. Since a similar situation exists at 6 hrs soaking period, it may be inferred that the adverse microstructural features for the 6 hrs and 10 hrs soaking period (heat treating temperatures 1000° & 1050°C namely the linking up of platy carbides and microstructural degeneracy are having a dominant effect (Figures 5.27 - 5.28).

In alloy C2 at 2 hrs soaking period the best in terms of CS has occurred at a lower temperature (900°C) compared to C1 (Table 7.4). This is followed by a decrease on heat treating from 950° and 1000°C due to inhomogeneity of the matrix and to the existence of a degenerate microstructure (Figure 5.33 - 5.34). An improvement in CS on heat treating from 1050°C but not to the extent one would have expected can be explained on a basis similar to that put forward earlier to analyse the data observed in C1 (Table 7.4). On increasing the soaking period to 10 hrs, the overall CS values are higher than the ones attained at 2 hrs soaking period and increase with an increase in the heat treating temperature thereby implying that the favourable structural features are dominating and that the overall effect of the adverse microstructural features is reducing (Table 7.4, Figures 5.33 - 5.35). This would also explain why the alloy C2, overall and especially on heat treating at 10 hrs soaking is attaining higher CS than C1.

This being so, the better overall CS attained in C3 over that in C2 can be easily explained on the basis of an inter-play between the favourable and unfavourable microstructural changes as discussed earlier. It may be worth noting that the best CS has been attained in C3 on heat treating for 10 hrs at 1050°C when the volume fraction of MCs is the least. This has been made

possible due to a favourable morphology of MCs, minimum microstructural degeneracy, a reasonably uniform distribution, a good compatibility of MCs with the matrix (Figure 5.42). The favourable changes on transiting from the composition of C1 to C3 could be attributed to an increase in the Cu content.

7.3 CORROSION STUDIES

The results reported thus far dealt with the transformation behaviour of the experimental alloys arrived at on the basis of hardness measurements, optical metallography, X-ray diffraction, EPMA, and compression testing. Having achieved this target, it was appropriate to characterize the alloys for their corrosion behaviour. Corrosion behaviour was studied with the help of weight loss method as it is deemed to be reliable method as the results are reproducible. The data thus obtained have been summarized and discussed in the following sections.

7.3.1 ANALYSIS OF DATA BASED ON "WEIGHT LOSS" STUDIES

7.3.1.1 WEIGHT LOSS DATA :

Weight loss were studies were carried out on as-cast/heat treated specimens of the experimental alloys as per the relevant ASTM specifications. The data presented in the Tables 7.5-7.6 revealed that-

- (a) The corrosion rate even in the as-cast state was reasonably good, it being the maximum in C1 and minimum in C3.
- (b) On heat treating from lower temperatures, the corrosion rate increased over that in the as-cast state up to a particular heat treating temperature/time and began decreasing there after.
- (c) The adverse effect persisted up to 900°C and for lower soaking periods for all the experimental alloys. However, situation was quite encouraging for 10 hours soaking period at 900°C where corrosion rate was found to be lower than that observed in as-cast condition.
- (d) Although the beneficial effect of increasing the heat treating temperature in improving corrosion resistance was in evidence as early as at 900°C, 10 hours heat treatment (marked in C1 and C2 & marginal in C3), a tangible effect set in only on heat treating from 1000°C. The magnitude of improvement was proportional to the amount of copper present (minimum in C1 and a maximum in C3) and soaking period.
- (e) This is duly reflected in the alloy C3 attaining the least corrosion rate & marginally better than that attained in C1 or C2.

The data contained in the Tables 7.5-7.6 could be looked at differently on the basis of the plots summarized in Figures 7.4-7.6. The plots besides revealing a second order variation between corrosion rate and temperature, revealed the relative usefulness of microstructures generated in the experimental alloys, in resisting corrosion e.g. in all investigated alloys the microstructure attained on heat treating at 900°C(2 hours) had an adverse effect & it(adverse effect) decreased gradually by increasing the heat treating temperature/time. The adverse effect of this microstructure however was not observed at the 10 hour soaking period. The plots further revealed the usefulness of the following structures in resisting corrosion:

- C1 -- microstructures at 10 hours soaking period,
- C2 -- microstructures at 10 hours soaking period,
- C3 -- microstructures at 2 and 10 hours soaking periods

7.3.1.2. NATURE OF CORRODED SURFACES

The corroded surfaces on being examined under a scanning microscope revealed absence of pitting and or graphitic corrosion. The attack was uniform and even after the completion of the test, the specimen surfaces retained a fair amount of polish revealing negligible surface attack. The corrosion product was non-adherent. The photographs merely showing the surface

topography of the polished specimens have not been included.

7.3.1.3. DISCUSSION

The weight loss data give a substantial and authentic information on the corrosion behaviour of different microstructures. In a general sense it reveals reasonably good corrosion resistance in the as-cast condition, its marginal deterioration, at best, on heat treating up to a certain temperature (900°C) and 2 hrs for each alloy, the maximum deterioration occurring at a specified heat treatment to be followed by a substantial improvement in corrosion resistance on heat treating from high temperatures (1000/1050°C) preferably on soaking for larger periods. This is indeed a welcome trend because in the temperature range of 800- 950°C needle or plate shaped DSPs as well as DCs have formed in all the three alloys (Figures 5.23-5.25, 5.30-5.32, and 5.37-5.39). That the corrosion rate on heat treating from temperatures within 'this range' is not much different from that in the corresponding as-cast state reveals that the adverse morphology/distribution of the DSPs & the alignment of DCs and MCs (Figures 5.23-5.25, 5.30-5.32, and 5.37-5.39) have had a minimal adverse effect on corrosion behaviour thereby reflecting favourably upon the τ /DSP & τ /MC couple in resisting aqueous corrosion in 5% NaCl solution. In fact the data summarized in the Table 7.6 and Figures 7.4 -

7.6 further indirectly indicate that the DSPs are of a similar character as the MCs i.e. the DSPs & DCs should in fact be either M_7C_3 and or M_3C type carbides. It is surmised that the possible formation of M_5C_2 may have adversely affected the corrosion behaviour more than what is reflected by the data summarized in Table 7.6 due to its monoclinic structure inducing enhanced incompatibility between second phase and the τ -matrix.

Having said so it would be pertinent to examine the microstructures/heat treatments which have given rise to a substantial increase in corrosion rate.

A careful perusal of the microstructures for the 900°C , 2 hrs heat treatment for the experimental alloys (Figures 5.25, 5.32 & 5.39) revealed that the features common to the three alloys which could have affected corrosion resistance adversely are (i) unevenness of the matrix(matrix heterogeneity), and (ii) bunching & alignment of carbides MCs & DCs (more apparent in C2 and C3). Interestingly the other parameters used to define distributional heterogeneity (Tables 5.99-5.60) apparently do not show the aforesaid microstructures in a poorer light, except the distribution heterogeneity associated with DCs in C3, thereby suggesting that chemical heterogeneity(associated with the matrix) may be the dominant factor in adversely affecting the

corrosion resistance. This analysis also suggests that the presence of DSPs with unfavourable morphology appeared to have a minimal adverse effect whereas the matrix unevenness (heterogeneity) appeared to have a more dominant effect in adversely affecting corrosion resistance. On the other hand unfavourable morphology of the DSPs has a definite adverse impact on the deformation behaviour of the alloys as already discussed in section-6.2.3. This explains the corrosion data on heat treating from temperatures up to 950°C.

On heat treating from 1000°C, the three alloys showed a marked improvement in corrosion resistance due to the elimination of DSPs, the MCs attaining spherical/hexagonal morphologies (favourable), 'rounding off' at the edges of MCs, and due to a reduction in the V_f of MCs. Alloy C3 with the highest Cu content (at 2 hours soaking period) attained a marginally lower corrosion rate than either C1 or C2 due to its lowest V_f of MCs, a more stable τ , and a better morphology of MCs. These beneficial effects are further accentuated at 10 hours soaking period leading to considerable improvement in corrosion resistance in C1 & C2. However the beneficial changes are attained, in general, on heat treating from 1050°C leading to the attainment of minimum corrosion rates in the experimental alloys (Table 7.6, Figure

7.4-7.6). It is of significance to note that in spite of a heterogeneity arising out of the formation of 'degenerate' dark regions around MCs and a general unevenness of the matrix due to reprecipitation of DCs (attributed to enhanced graphitizing action resulting from an increase in the Cu content from 1.5% in C1 to 5% in C3), the alloys are attaining very low corrosion rates and yet not exhibiting any kind of localized attack. It is evident that in the absence of the above mentioned heterogeneities, the alloys would have exhibited still lower corrosion rates. The discussion would imply that to reduce heterogeneity the process(es) responsible for accelerating different transformations (already discussed) have to be contained. There is thus a need to optimize the Cu content keeping in mind the seemingly contradictory effects it is producing namely (i) the transformation 'accelerating effect' promoting a reduction in the amount of second phase (partly beneficial & partly retrograde), (ii) increasing the Cu content of the matrix thereby improving corrosion resistance (beneficial), and (iii) microstructural degeneracy/heterogeneity that is being created due to an enhancement in the transformation kinetics (retrograde).

The SEM examination carried out to a limited extent none-the-less is very encouraging, reaffirms the findings of Jain, Kumar, and Rao, Patwardhan & Jain [Jain (J2), Kumar (K6),

Rao (R5)] regarding the absence of pitting, graphitic corrosion, and the nature of attack being 'uniform dissolution'. The retention of mirror finish on the specimen surfaces even in the corroded condition is a clear indication that some kind of passive layer is perhaps forming. This is concluded from the observation that the corrosion product is non-adherent and 'falls off' merely on shaking the specimen in the aqueous media.

The corrosion rates attained in the experimental alloys are substantially better than the ones reported by Jain [Jain (J2)] in the Fe-Mn-Cr-Cu alloys containing 7.5% Mn & up to 3% Cu. The deformation behaviour of the presently investigated alloys has already been adjudged to be promising. On the strength of these observations the key elements of the alloy design, outlined in the Chapter III, stand vindicated.

Corrosion rates attained on heat treating from higher temperatures are comparable or better than the ones attained in standard Ni-Resist(both flake & S.G. type) compositions being very extensively used under marine conditions. Incidentally the strength of the Ni-Resist compositions is approximately half of that obtained in the experimental alloys. These observations may be regarded as the highlights of the present study with major technological fall out. This aspect has been considered in the

next chapter, in detail, in the section dealing with general discussion.

7.4 MODELLING OF THE CORROSION BEHAVIOUR

An analysis of the corrosion data in the previous section reveals how the different microconstituents influenced corrosion behaviour. Excluding the matrix to begin with, their effect depends upon their nature and size, shape and distribution. When the matrix is also considered, its characteristics (crystal structure and stability) and difference in the electro-chemical potentials between the matrix and the constituents also assume significance. Interestingly, most of the correlations have been qualitative in character. Any effort aimed at modelling the corrosion behaviour will have to incorporate the above said aspects.

7.4.1 BACKGROUND INFORMATION

The first effort in this regard was made by Jain and Patwardhan [Jain(J2); Patwardhan(P4),(P6)] who attempted to correlate corrosion rate with the microstructural features comprising austenitic matrix, massive carbides and dispersed carbides. They selected heat treatments carried out at 900 & 950°C primarily because the different alloys constituting the study attained nearly constant hardness values at these

temperatures. Whereas the hardness was more or less independent of the soaking period, the volume fraction of MCs & DCs varied. It was felt appropriate to examine the methodology adopted by him before enlarging upon the ideas conceived in his work reported recently by Patwardhan & Jain [Patwardhan (P4),(P6)].

It was conceived that the CR could be expressed as a function of different parameters namely,

$$CR \approx f(\text{austenite Vf/ stability})$$

$$CR \approx f(\text{Vf of MC})$$

$$CR \approx f(\text{Vf of DC})$$

$$CR \approx f(\text{distribution of the DC})$$

or
$$CR \approx F [(\text{Vf/stability of } \tau) \cdot (\text{Vf of MC}) \cdot (\text{Vf of DC}) \cdot (\text{distribution of DC})] \dots(7.5)$$

To begin with, the last term was excluded and the volume fraction of MCs & DCs was combined into a single term to develop the initial stage model. This was justified on the assumption that since the second phase in general would enhance CR, their overall effect can be cumulated into a single factor.

From the experimental data it was concluded that the functional relationship interrelating corrosion rate with the total volume fraction of carbides(VCb) can be represented by a second order polynomial :

$$CR = A_1 + A_2(VCb) + A_3(VCb)^2 \dots(7.6)$$

where VCb = total volume fraction of MC + DC

The contribution of the second phase, i.e. the role of dispersed carbides, was included in the above expression by incorporating a factor based on the number of particles, NOP.

This led to the following expression :

$$CR = [A_1' + A_2'(VCb) + A_3'(VCb)^2](NOP)^{A_4'} \dots(7.7)$$

The constants A1', A2', A3', and A4' were calculated by using the multi-variable constraint optimization technique [Himmelblau (H10), Mangasarain (M4)] and the final equations are:

Alloy C1:

$$CR = (19.982 - 0.37157(VCb) + 0.02125(VCb)^2)(NOP)^{-0.26838} \dots(7.8)$$

Alloy C2:

$$CR = (12.316 - 0.26605(VCb) + 0.00652(VCb)^2)(NOP)^{0.22482} \dots(7.9)$$

Alloy C3:

$$CR = (13.354 - 0.45377(VCb) + 0.01147(VCb)^2)(NOP)^{0.23459} \dots(7.10)$$

Through a suitable analysis involving the effect of two factors in contributing to corrosion, it can be shown that the model is neither physically consistent nor theoretically justifiable since NOP do not truly represent the DC and that the

constants were calculated without adequately understanding the physical implications of their effect on the corrosion rate. Further the effect of DCs was getting considered twice as it figured as a part of VCb and again as NOP. This was also observed by Jain and Patwardhan [Jain (J2), Patwardhan (P4), (P6)]. Therefore further stress was laid on developing models interrelating the corrosion behaviour with massive second phase and dispersed second phase. Thus the two models developed were CR vs VMC/NOP and CR vs VMC/DF.

Kumar's (K6)] work reiterated that the VMC-NOP and VMC-DF models were a satisfactory representation of the corrosion behaviour of the alloys developed. Of the two models, the former emerged as a more effective representation of the corrosion behaviour, somewhat surprisingly, although his and Jain's [Jain (J2)] studies had convincingly demonstrated that DF was a far better representation of the DCs than the NOP. Through 3-D plotting the idea of 'microstructural optimization' was mooted which proved useful in assessing what best to expect in terms of properties from a given composition. The method to arrive at the optimal minimal values of MC, DF/NOP to obtain the best in terms of performance was also indicated. This enabled optimization of the heat treating parameters to be carried out. Finally the idea of developing a 'unified model', wherein a single model could

predict the corrosion behaviour of all the experimental alloys, was also mooted (Kumar (K26)).

It was decided to expand upon the ideas initially proposed by Jain and Kumar [Jain (J2), Kumar (K6)] and to arrive at a rationalized assessment of the modelling of the corrosion behaviour of the alloys being presently investigated. It was also proposed to compare the data presently obtained with that reported by Kumar [Kumar (K6)] so that a considered appraisal of the state of the art (of this new area) was made possible.

7.4.2 MODELLING OF THE CORROSION BEHAVIOUR OF THE EXPERIMENTAL ALLOYS

7.4.2.1 THE VMC-NOP MODEL

The basis for this model is the qualitative formulation represented by equation (7.5)

$$CR \approx F [(Vf/stability\ of\ \tau).(Vf\ of\ MC).(Vf\ of\ DC).(distribution\ of\ DC)] \dots(7.5)$$

As proposed earlier [Jain(J2), Kumar(K6)], the effect of the parameter Vf/stability of τ was considered as constant to begin with so that the equation could be rewritten as

$$CR \propto F [.(Vf\ of\ MC).(Vf\ of\ DC).(distribution\ of\ DC)] \dots(7.11)$$

From the experimental data, it was considered that relationship between CR & Vf of MCs could be represented by a

second order polynomial

$$CR = A1 + A2.VMC + A3.(VMC)^2 \quad \dots(7.12)$$

The role of dispersed second phase in influencing corrosion was considered by incorporating the total number of particles (NOP) into the equation 7.12, which now assumes the form

$$CR = (A1 + A2.VMC + A3.(VMC)^2)(NOP)^{A4} \quad \dots(7.13)$$

The constants A1, A2, A3, and A4 were calculated by the nonlinear optimization technique permitting the constants to vary over a large unlimited range. The models arrived at are

Alloy C1:

$$CR = (20.427 - 0.51259(VMC) + 0.02069(VMC)^2)(NOP)^{-0.16212} \quad \dots(7.14)$$

Alloy C2:

$$CR = (8.525 - 0.17197(VMC) + 0.00432(VMC)^2)(NOP)^{0.041145} \quad \dots(7.15)$$

Alloy C3:

$$CR = (18.653 - 0.90156(VMC) + 0.022076(VMC)^2)(NOP)^{0.22502} \quad \dots(7.16)$$

The values of the two factors constituting the models were computed and the data are summarized in the Table 7.7.

A scrutiny of the data summarized in the Table 7.7 revealed that the corrosion rates predicted on the basis of the models agree well with the experimentally determined values. Secondly, the contribution of factor I to the corrosion rate follows a

systematic pattern, namely, with an increase in temperature/time of the heat treating its contribution reduces in all the three alloys and so also does the corrosion rate. Moreover its contribution to corrosion is inversely proportional to the Cu content(or the τ -stabilizing/carbide destabilizing tendency). This result is consistent with the analysis put forth in the earlier sections(sections 7.3-7.4) to explain the corrosion behaviour of the experimental alloys. However the contribution of the factor II did not appear to be consistent either in itself or with the corresponding variation in the NOP as influenced by temperature & time in the three experiential alloys(Table 7.7). A possible reason could be that the constants A1,A2,A3, and A4 have been calculated without exercising any constraint on the range over which they can vary. Alternatively, it was likely that the NOP is not a relevant representation of the effect of the dispersed second phase.

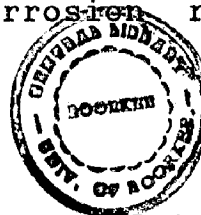
A single model(called the unified model) was also developed which could predict the corrosion behaviour of the three experimental alloys and is of the form:

$$CR = (18.653 - 0.53144(VMC) + 0.01497(VMC)^2)(NOP)^{0.04524} \quad \dots(7.17)$$

The predicted values of corrosion rate estimated on the basis of this model, were found to be in good agreement with the

experimentally determined values, barring few instances where considerable difference appeared (Table 7.8). However looking into the differences in the transformation behaviour of the experimental alloys elaborately discussed in Chapter-VI, the overall agreement between the predicted values of CR based on the 'unified model' and the experimentally determined values should be regarded as excellent.

3D-plots corresponding to the unified model (based on equation 7.17) is generating a surface in the form of an inverted parabola. Its operative profile over the admissible levels of VMC & NOP and the likely admissible levels of corrosion rates are shown in Figure 7.7. Although an impression is generated that lower corrosion rates could be attained, but practically this is not the situation since negative corrosion rates can not be attained.



The contour plot shown in the Figure 7.8 very usefully represent an interplay between NOP and VMC in controlling corrosion and the information summarized in it can be explained on a similar basis as the data contained in the Figures 7.7. An additional advantage of this figure is that it would be possible to predict corrosion rates for those heat treatments/conditions at which experimental data are not

available.

7.4.2.2 THE VMC-DF MODEL

Models(based on DF) Evaluated without constraints

Alloy C1:

$$CR = (13.388 - 0.38353(VMC) + 0.01394(VMC)^2)(DF)^{-0.15490} \quad \dots(7.18)$$

Alloy C2:

$$CR = (32.881 - 1.2331(VMC) + 0.03053(VMC)^2)(DF)^{-0.21524} \quad \dots(7.19)$$

Alloy C3:

$$CR = (22.692 - 1.0355(VMC) + 0.02842(VMC)^2)(DF)^{-0.07608} \quad \dots(7.20)$$

Models(based on DF) Evaluated with constraints

Alloy C1:

$$CR = (9.999 - 0.16190(VMC) + 0.00999(VMC)^2)(DF)^{-0.17935} \quad \dots(7.21)$$

Alloy C2:

$$CR = (9.999 + 0.13269(VMC) + 0.00304(VMC)^2)(DF)^{-0.05403} \quad \dots(7.22)$$

Alloy C3:

$$CR = (9.998 - 0.04625(VMC) + 0.00911(VMC)^2)(DF)^{-0.08734} \quad \dots(7.23)$$

Unified Model

$$CR = (16.066 - 0.36040(VMC) + 0.01274(VMC)^2)(DF)^{-0.05233} \quad \dots(7.24)$$

The data pertaining to the modelling of the corrosion behaviour based on the VMC-DF combination, as summarized in Tables 7.9-7.11 & Figures 7.9-7.12 can be explained on similar lines as the data pertaining to the VMC-NOP model. The

differences, if any, center around the figures depicting the data emerging from the unified model.

The profile of the resulting surface emerging from the unified model based on VMC-DF combination (Figure 7.12), although in itself planar, is essentially similar to the surface profile observed in the VMC-NOP unified model (Figure 7.7). It may be further mentioned that the overall data depicted in Figure 7.12 (in terms of attainable corrosion rates) is realistic in the sense that no negative corrosion rate values are envisaged. Thus, taking an overall view, the VMC-DF unified model provides a more realistic representation of the actual state of affairs when compared with the projections emerging from the VMC-NOP unified model.

Thus summing up, it is a happy augury that the explanation put forward to explain the corrosion behaviour of the alloys based on the VMC-NOP model is duly reflected in its behaviour based on the VMC-DF model namely the range over which DF varies having no effect in controlling the corrosion behaviour although the DF in itself does make a small yet uniform contribution. Further the role of the matrix and of a low V_f of MCs in controlling corrosion is more specifically highlighted. Thirdly, of the two 'unified models', the VMC-DF & VMC-NOP the former

combination appears to yield a more balanced picture of the relative effects of factors I and II in controlling corrosion as already discussed above. This appears reasonable since 'size distribution' as represented by DF is a more precise representation of an assembly of particles rather than their actual number more so as the former also takes into consideration the number of particles.

7.4.3 INTERRELATION BETWEEN CORROSION AND DEFORMATION BEHAVIOUR

A perusal of the data on the corrosion and the deformation behaviour indicated that an 'improvement' in the deformation behaviour in general 'improved' corrosion resistance. It was therefore felt appropriate to establish such an interrelation. Mathematically it meant that

$$CS = A_1 + A_2 (X) \quad \dots(7.25)$$

where X represents ^{CR}CS. On calculating the constants as before, the models are

$$\text{Alloy C1} \quad CS = 1892 + 25.43 (CR) \quad \dots(7.26)$$

$$\text{Alloy C2} \quad CS = 2475 - 1.79 (CR) \quad \dots(7.27)$$

$$\text{Alloy C3} \quad CS = 3768 - 84.02 (CR) \quad \dots(7.28)$$

CS calculated on the basis of the above formulations are summarized in the Tables 7.12. Barring a few instances (wherein there was an error in estimating CS_{exp} due to defects in

specimens), there is an excellent agreement between the predicted and experimentally determined values of CS.

The above said formulations also reveal the possibility of estimating CR from CS values and if this is done, the agreement between the experimentally determined and predicted CR is very good.

7.5 CONCLUDING REMARKS

The data analyzed in sections 7.1-7.4 touches upon a number of new ideas, namely, assessment/modelling of the deformation behaviour, an analyses of the corrosion behaviour based on the weight loss studies to arrive at an overall 'performance' appraisal. The final sections deal with the modelling of the corrosion behaviour, efforts aimed at microstructural optimization with a view to assess the key parameter involved in corrosion control, checking on the 'physical consistency' of the models developed, plotting contour maps of CR vs VMC/NOP and CR vs VMC/DF not only to have a birds eye view but also with a view to finding out the corrosion behaviour under those conditions at which it has not been experimentally determined e.g. for 800°C and 850°C heat treatments.

CHAPTER VIII

GENERAL DISCUSSION, CONCLUSIONS, AND SUGGESTIONS FOR FUTURE WORK

8.1 GENERAL DISCUSSION

The present investigation has succeeded in assessing the transformation behaviour of the experimental alloys in a fair detail. The alloys intended to resist corrosion, were designed to include low cost indigenously available alloying elements Mn, Cr and Cu. Possible clues to their transformation behaviour were provided by their compositions and from previous work of Jain and Kumar [Jain (J2), Kuamr (K6)].

The alloys were so designed that austenite is retained in the as-cast condition itself thereby implying it to be the matrix. Optical metallography and x-ray diffractometry duly confirm this to be so. This is further confirmed through microhardness measurement which indicates the matrix hardness to be 350-360 VPN. However, in as-cast state and on heat treating from 800° and 850°C (independent of soaking period), microstructure comprises martensite. The reasons for it have already been explained at appropriate place. The black areas having differeing etching characteristics, identified as martensite, have a microhardness of 660 VPN. On heat treating from 900°C, the matrix is essentially austenitic and has microhardness ~ 400

VPN. The stability and volume fraction of austenite increased with an increase in the heat treating temperature/time but the same trend could not be related to copper content [i.e. while moving from alloy C1 (1.5% Cu) to C3 (5% Cu)]. It (stability of austenite) is, in general, accompanied by a simultaneous decrease in the volume fraction of massive carbides. This was corroborated through the EPMA, macrohardness and microhardness measurements; e.g. the microhardness of the matrix increased from 400 VPN as above to 420 VPN obtained on heat treating at 1000°C, thereby confirming increased stability of the matrix due to increased solute enrichment. X-ray diffractometric studies confirmed this through a decrease in the diffraction angle. The above changes, brought about by increasing the heat treating temperature/soaking period, were conducive to improving the corrosion resistance (which showed improvement with increased copper content) and the deformation behaviour.

The second phase in the as-cast microstructure is massive carbide only. Three types of massive carbides were observed, namely, massive/platy type, eutectic type, and mesh type. Massive carbides have a hardness of 650-700 VPN and flower type carbides 1000-1100 VPN. On heat treating, the following changes have been observed:

1. Mesh type carbide disappeared(dissolved) and dispersed second phase precipitated from the austenitic matrix.
2. There was a considerable variation in the chemical composition of the carbides as ascertained through EPMA and corroborated by micro-hardness measurements. As already discussed, the Vf of MCs decreased with an increase in the heat treating temperature/time and the 'rounding off' tendency was observed at 950/1000°C heat treatments. On heat treating from higher temperatures massive carbides assumed different morphologies such as rounded, hexagonal etc. So also it appeared that there was an increase in the Vf of discontinuous free carbides, some of which appeared to form though agglomeration of DCs.

Massive/platy carbides have a micro-hardness of 800 VPN at 800°C, 1000 VPN at 1000°C, and 1120 VPN at 1050°C whereas the free carbides have micro-hardness of 1100 VPN at 800°C, 1500-1600 VPN at 1000°C, and 1600-1800 VPN at 1050°C heat treatments.

At 1050°C, 6 & 10 hours heat treatment, a 'peculiar' feature involving 'agglomeration' of massive carbides was observed. These carbides have micro-hardness of 1800 VPN and the dark phase in between the agglomerating carbides has a micro-hardness of 850 VPN. EPMA studies revealed that the dark grey

regions in between the agglomerating MCs would become MCs except for their Cu and Si content.

3. Optical metallography and EPMA studies have revealed two types of massive carbides on heat treating at 900/950°C differing in their Cr content by about 10%. The inherent nature of the white cast irons to form heterogeneous structures may have lead to such an occurrence. This could be one of the reasons for deterioration in the corrosion resistance and deformation behaviour on heat treating from these temperatures.

As already discussed, dispersed second phase(DSP) precipitated from the austenitic matrix on heat treating from 800°C and 850°C. They essentially comprised needles(plates) + DCs up to 900°C, 10 hours heat treatments, only DCs up to 950°C, 10 hours heat treatments, and reprecipitated particles of Class I size upon heat treating up to 1050°C, 6 hours. DCs finally dissolved on raising the temperature/time. The dispersed second phase adversely influences corrosion behaviour due to an unfavorable morphology and enhanced galvanic action. However, it is the heterogeneity of the matrix which appears to have a more dominant effect on the corrosion behaviour than the dispersed second phase. The DSPs and MCs have more pronounced effect on the deformation behaviour. Deformation behaviour was assessed on the

basis of compression testing. In some of the instances the experimentally determined values have been low due to defects in specimen present in the form of a pipe running right through the casting.

Optical metallography revealed a similarity between the needle type DSPs and DCs. X-ray diffractometric studies have shown them to be M_5C_2/M_3C whereas EPMA indicated them to be M_3C/M_7C_3 type carbide. Not much is known as to whether M_5C_2 could form in the experimental alloys. The possibility that these needles are partly M_3C and/or partly M_7C_3/M_5C_2 type carbides can not be ruled out.

EPMA studies also revealed the possibility of the formation of extraneous phases besides providing the useful data on the partitioning behaviour of Mn, Cr and also Cu.

Extensive 'modelling work' has provided a wealth of the information on the transformation behaviour, 'second phase' characteristics, and the 'overall performance' which has major 'fundamental and applied implications'.

8.2 CONCLUSIONS

Under the experimental conditions, the following conclusions are arrived at:

1. Corrosion resistant cast irons can be developed through 'white iron' route employing low cost indigenously available alloying

on selecting the hardness values at two extremities of heat treating periods(2 hours & 10 hours) at 800 & 1050°C and at an additionally selected heat treating temperature(900°C). The simulated models are-

$$C1 : H = 204.5 e^{1051/T} + (0.01144 - 0.1111 \times 10^{-4} T)t$$

$$\text{Overall SD} = 14.844$$

$$C2 : H = 222.4 e^{1013/T} + (0.00872 - 0.9167 \times 10^{-5} T)t$$

$$\text{Overall SD} = 6.752$$

$$C3 : H = 204.5 e^{1051.1/T} + (0.01144 - 0.1111 \times 10^{-4} T)t$$

$$\text{Overall SD} = 4.955$$

Thus the transformation behaviour can be simulated with reasonably high accuracy on the basis of only six data points as against the original thirty.

12.3-D plots interrelating temperature and time with hardness revealed that the 'change over' at which the second factor in the above model becomes negative can be represented by a surface. Iso-hardness plots for the experimental alloys revealed the range over which hardness varied and the different temperature and time combinations to arrive at a desired hardness.

13.A new parameter 'distributional homogeneity/heterogeneity' of the microstructure has been defined.

(i) The overall homogeneity/heterogeneity(based on Vf of

basis of compression testing. In some of the instances the experimentally determined values have been low due to defects in specimen present in the form of a pipe running right through the casting.

Optical metallography revealed a similarity between the needle type DSPs and DCs. X-ray diffractometric studies have shown them to be M_5C_2/M_3C whereas EPMA indicated them to be M_3C/M_7C_3 type carbide. Not much is known as to whether M_5C_2 could form in the experimental alloys. The possibility that these needles are partly M_3C and/or partly M_7C_3/M_5C_2 type carbides can not be ruled out.

EPMA studies also revealed the possibility of the formation of extraneous phases besides providing the useful data on the partitioning behaviour of Mn, Cr and also Cu.

Extensive 'modelling work' has provided a wealth of the information on the transformation behaviour, 'second phase' characteristics, and the 'overall performance' which has major 'fundamental and applied implications'.

8.2 CONCLUSIONS

Under the experimental conditions, the following conclusions are arrived at:

1. Corrosion resistant cast irons can be developed through 'white iron' route employing low cost indigenously available alloying

elements Mn, Cr, and Cu. The microstructures that were characterized for their deformation and corrosion behaviour (in 5% NaCl solution) are A + MC + DSPs, A + MC + DC, A + MC, A + MC (agglomerated). All these microstructures were generated through heat treatments. The temperature ranges over which the different microstructures exist are given below:

As-cast	: A + M + MC
up to 850°C	: A + M + DCs
up to 950°C	: A + MC + DCs
up to 1050°C	: A + MC

2. The volume fraction of MC decreased with temperature or with soaking period at a given heat treating temperature. The decrease was marked at temperatures $\geq 950^\circ\text{C}$. MCs were rendered discontinuous on heat treating from 900/950°C. The 'rounding off' tendency (in MCs) set in at 950°C; and an increase in Cu content accelerated this process. Agglomeration amongst MCs was observed at 1050°C. This has perhaps stalled the expected marked decrease in the Vf of MCs at 1050°C, 10 hours heat treatment.

3. Dispersed second phase formed on heat treating at $\geq 800^\circ\text{C}$ comprised (a) needles + dispersed carbides up to 950°C, 10 hours heat treatment, only dispersed carbides up to 1000°C, 10 hours heat treatment, (b) then dissolved into matrix, and (c) again

reappeared at 1050°C, 2 hours heat treatment as class-I particles. The DSP forms by a mechanism involving precipitation from austenite and also during air cooling. Particles constituting them belonged to Classes I and II (size up to 1.16 microns). As the heat treating temperature/soaking duration is raised the overall spread of the particles is increased to Class IV (size up to 3.32 microns).

4. Dispersed carbides underwent coarsening which was characterized by the 'spill over' of the particles into classes III and IV. Coarsening was assessed with the help of coarsening index.
5. DCs get dissolved at 1000°C heat treatment and reappeared on heat treating at 1050°C, 2 hours as Class I size particles and again dissolved at 1050°C 6 hours heat treatment.
6. The carbides to form in the experimental alloys are M_3C , M_7C_3 , and M_5C_2 . The massive carbides are mostly of the type M_3C/M_7C_3 . The haloed regions observed are essentially massive carbides but with 10% less Cr. The dark grey regions between 'agglomerating massive carbides' approximately exhibit the same composition as the agglomerating MCs except for their Cu and Si content. The dispersed carbides and needles are M_3C/M_5C_2 type. The carbide transformation sequence is:

Carbide

Stability range

M₃C + M₅C₂ + M₇C₃

As-cast state in all the investigated alloys.

|

M₃C + M₅C₂ + M₇C₃

up to 850°C (M₃C present in traces in C₃)

|

M₅C₂ + M₇C₃

up to 1000°C in C₁ & C₃
up to 1050°C in C₂

|

M₅C₂ + M₇C₃
+ M₃C (reforming)

up to 1000°C in C₂ & C₃
up to 1050°C in C₁

|

M₅C₂ (some/traces) + M₇C₃ up to 1050°C

|

M₃C + M₅C₂ (?)
+ M₇C₃ (some amount)

up to 1050°C; higher SP

|

Predominant carbides at high temperature are M₇C₃ & M₅C₂ (small/traces)

7. Hardness in general decreased with an increase in the heat treating temperature in the order :

H₁₀₅₀ < H₁₀₀₀ < H₉₅₀ < H₉₀₀ < H₈₅₀ < H₈₀₀

8. For a given heat treating temperature, hardness varied linearly with the soaking period. There is a general decrease in hardness with increase in soaking period for all

the alloys. However, the effect is more marked at higher heat treating temperatures ($\geq 950^{\circ}\text{C}$). The increase/decrease exhibited by the alloys with increase in soaking period at low temperatures say 800° and 850°C is very marginal for a given heat treating temperature.

9. For a given heat treating period, the variation in hardness with temperature was in the form of inverted parabola.

10. Transformation behaviour of the alloys, over the entire range of temperature and soaking period, on being modelled is of the form:

$$C1 : H = 271.701 e^{838.513/T} + (0.005809 - 0.547 \times 10^{-5} T)t$$

$$\text{Overall SD} = 1.593$$

$$C2 : H = 342.517 e^{551.093/T} + (0.01688 - 0.158 \times 10^{-4} T)t$$

$$\text{Overall SD} = 4.524$$

$$C3 : H = 287.256 e^{692.334/T} + (0.01777 - 0.163 \times 10^{-4} T)t$$

$$\text{Overall SD} = 3.053$$

Where T = temperature in $^{\circ}\text{K}$

t = time in seconds

H = hardness, HV_{30}

The first parameter models the matrix transformation and the second parameter the carbide transformation

11. The aforesaid transformation behaviour of the experimental alloys can be 'simulated' through mathematical modelling based

on selecting the hardness values at two extremities of heat treating periods(2 hours & 10 hours) at 800 & 1050°C and at an additionally selected heat treating temperature(900°C). The simulated models are-

$$C1 : H = 204.5 e^{1051/T} + (0.01144 - 0.1111 \times 10^{-4} T)t$$

$$\text{Overall SD} = 14.844$$

$$C2 : H = 222.4 e^{1013/T} + (0.00872 - 0.9167 \times 10^{-5} T)t$$

$$\text{Overall SD} = 6.752$$

$$C3 : \bar{H} = 204.5 e^{1051.1/T} + (0.01144 - 0.1111 \times 10^{-4} T)t$$

$$\text{Overall SD} = 4.955$$

Thus the transformation behaviour can be simulated with reasonably high accuracy on the basis of only six data points as against the original thirty.

12.3-D plots interrelating temperature and time with hardness revealed that the 'change over' at which the second factor in the above model becomes negative can be represented by a surface. Iso-hardness plots for the experimental alloys revealed the range over which hardness varied and the different temperature and time combinations to arrive at a desired hardness.

13.A new parameter 'distributional homogeneity/heterogeneity' of the microstructure has been defined.

(i) The overall homogeneity/heterogeneity(based on Vf of

MCs) of an alloy as influenced by heat treating parameters has been defined as

$$H_M = \frac{\text{The net variation in } V_f \text{ of MCs around a mean}}{\text{Permissible variation around a mean}}$$

or

$$= \frac{SD_{exp}}{SD_{per}} \times \frac{[V_{fmax,per} - V_{fmin,per}]}{[V_{fmax,exp} - V_{fmin,exp}]}$$

This could be expressed as a fraction or percent. Under ideal condition $H_M = 1$. Homogeneity can be assessed depending upon the permissible variation in the parameter(s) being measured.

$$\text{Heterogeneity} = 1 - \text{Homogeneity}$$

(ii) Distributional heterogeneity, $H_M(\text{dist})$ (related with precipitated second phase) has been expressed as

$$= \frac{\text{Deviation in distribution function/factor with respect to the majority size fraction}}{\text{Overall distribution function/factor}}$$

or more precisely

$$H_M(\text{dist}) = \frac{\text{underspill ratio} \times \text{spillover ratio}}{\text{overall distribution factor}}$$

expressed as a ratio or as percentage.

14. The dispersed second phase has been represented by a parameter called the 'distribution factor' which is given by the expression

$$DF = \frac{\sum_{i=1}^n X_i \cdot N_i}{\sum_{i=1}^n N_i}$$

where, n = the number of classes,

N_i = the number of particles in i^{th} class,

X_i = volume fraction in the i^{th} class /VDC,

and, VDC = total volume fraction of dispersed carbides.

15. X-ray diffractometric studies proved helpful in establishing the presence of 'martensite islands' in the as-cast structure and in deciding upon the likely identity of the MCs and the DSPs.

16. EPMA confirmed that the carbides to form mostly comprised M_3C and M_7C_3 , the needle like DSPs are in fact carbides, that on heat treating at 900/950°C two types of carbides differing in their Cr content by about 10% formed and that the dark etching regions abridging agglomerating carbides in fact have a composition close to M_7C_3 except for their Cu and Si content. In addition to the above, useful partitioning data on the distribution of Mn and Cr into the matrix and carbide phases has been generated.

17. DTA data showed that whereas the alloys C1, C2, and C3 undergo the (i) martensite → austenite as well as internal

oxidation reaction at 540-575°C, and (ii) carbide transformation(s) involving a transition of M_3C to M_7C_3 via M_5C_2 transition carbide at 960-980°C, an additional transformation occurred in C1 and C2 at 740-760°C.

18. TG data showed that the as-cast microstructure was suitable up to 600°C.

19. Mathematical modelling of the TG data showed that %TG is related to the temperature by the equation

$$\text{Alloy C1} \quad \%TG = 2.2761 + 7999.65 \exp(-7929.25/T)$$

$$\text{Alloy C2} \quad \%TG = 2.5190 + 7426.91 \exp(-7999.98/T)$$

$$\text{Alloy C3} \quad \%TG = 1.9690 + 6046.54 \exp(-7999.98/T)$$

20. The deformation studies carried out on the experimental alloys have established that compressive strength improved on heat treating. CS is not linearly interrelated with hardness as is found in the case of steels. It is because of the heterogeneous nature of the microstructure generally found in cast irons. It was established that the CS can be related with hardness through a second order polynomial.

$$\text{Alloy C1} : R = -11.58 + 0.0667H - (0.6926E-04) H^2$$

$$\text{Alloy C2} : R = 36.92 - 0.1299H + (0.1227E-03) H^2$$

$$\text{Alloy C3} : R = 24.98 - 0.0629H + (0.4249E-04) H^2$$

where $R = CS/H$,

$H = \text{hardness, HV}_{30}$,

21. From the point of view of mechanical properties, austenite based microstructure with little dispersed second phase and containing 'appropriate' volume fraction of 'massive second phase' with near 'rounded' morphology are the most suitable. Accordingly high CS is obtained on heat treating from high temperatures (1050°C). The effect of DCs on the deformation behaviour depends upon their size, shape, and distribution. Similarly the effect of MC is governed by their volume fraction, morphology, and compatibility with the matrix.

22. Corrosion rate in the as-cast condition is consistent with its microstructure. It, in general, decreased with an increase in the heat treating temperature/soaking duration and also with an increase in Cu content (i.e. while moving from alloy C1 to C3) due to enhanced stability and a larger volume fraction of austenite and simultaneous decrease in the Vf of MCs; the exceptions are those heat treatments which produced adverse microstructural feature namely matrix heterogeneity, and aligned DCs.

23. The effect of dispersed second phase on corrosion resistance depends on their size, shape and distribution. In the present study dispersed particles affected the corrosion resistance adversely to some extent as is seen on heat treating from 900 and 950°C. Heat treatment 1050°C, 10 hour, AC provided the

best corrosion resistance and most useful deformation behaviour.

24. Corrosion rate is interrelated with the volume fraction of VCb (MC + DC) and NOP through the following equations

$$\text{Alloy C1: CR} = (19.982 - 0.37157(\text{VCb}) + 0.02125(\text{VCb})^2)(\text{NOP})^{-0.26838}$$

$$\text{Alloy C2: CR} = (12.316 - 0.26605(\text{VCb}) + 0.00652(\text{VCb})^2)(\text{NOP})^{0.22482}$$

$$\text{Alloy C3: CR} = (13.354 - 0.45377(\text{VCb}) + 0.01147(\text{VCb})^2)(\text{NOP})^{0.23459}$$

where CR = corrosion rate in mdd

VCb = total volume fraction of MCs + DCs

NOP = number of particles(DSPs)

This model when modified as

$$\text{CR} = (C1 + C2(\text{VMC}) + C3(\text{VMC})^2)(\text{NOP})^{C4}$$

gave a more representative idea of the true physical happenings

Alloy C1:

$$\text{CR} = (20.427 - 0.51259(\text{VMC}) + 0.02069(\text{VMC})^2)(\text{NOP})^{-0.16212}$$

Alloy C2:

$$\text{CR} = (8.525 - 0.17197(\text{VMC}) + 0.00432(\text{VMC})^2)(\text{NOP})^{0.041145}$$

Alloy C3:

$$\text{CR} = (18.653 - 0.90156(\text{VMC}) + 0.02207(\text{VMC})^2)(\text{NOP})^{0.22502}$$

25. On incorporating the effect of DC on the basis of the distributional factor(DF), the above equations are modified as:

$$\text{Alloy C1: CR} = (13.388 - 0.38353(\text{VMC}) + 0.01394(\text{VMC})^2)(\text{DF})^{-0.15490}$$

$$\text{Alloy C2: CR} = (32.881 - 1.2334(\text{VMC}) + 0.03053(\text{VMC})^2)(\text{DF})^{-0.21524}$$

$$\text{Alloy C3: CR} = (22.692 - 1.0355(\text{VMC}) + 0.02842(\text{VMC})^2)(\text{DF})^{-0.07608}$$

and again when constraints are imposed on the constants of the equation while optimizing, the equations so obtained are-

Alloy C1:

$$\text{CR} = (9.999 - 0.16190(\text{VMC}) + 0.00999(\text{VMC})^2)(\text{DF})^{-0.17535}$$

Alloy C2:

$$\text{CR} = (9.999 + 0.13269(\text{VMC}) + 0.00304(\text{VMC})^2)(\text{DF})^{-0.05403}$$

Alloy C3:

$$\text{CR} = (9.998 - 0.04625(\text{VMC}) + 0.00911(\text{VMC})^2)(\text{DF})^{-0.08734}$$

and 'truly' represented the effect of second phase on the corrosion resistance.

26.A 'unified model' describing the corrosion behaviour of all the experimental alloys has been obtained and is of the form

(i) CR vs VMC & NOP

$$\text{CR} = (18.653 - 0.53144(\text{VMC}) + 0.01497(\text{VMC})^2)(\text{NOP})^{0.04524}$$

(ii) CR vs VMC & DF

$$\text{CR} = (16.066 - 0.36040(\text{VMC}) + 0.01274(\text{VMC})^2)(\text{DF})^{-0.05233}$$

The aforesaid models especially the latter predict the corrosion behaviour of the alloys with excellent accuracy.

27. On the basis of specially constructed contour plots, it is possible to predict the corrosion behaviour for those heat

treatments at which experimental assessment of the corrosion rates has not been carried out. An equally important aspect is that from the 3-D and contour plots it is possible to determine the 'performance controlling features' for the experimental alloys, e.g. in the present study corrosion essentially centers around reducing the volume fraction of MCs and matrix heterogeneity seemed to have a larger adverse effect than the adverse effect associated with unfavorable morphology of the DSPs. For controlling the deformation behaviour, a careful control over the distribution of massive and second phase particles is more specifically required.

28. From the 'overall performance' point of view alloy ^{C3} C2 has been found to be better than C1 and ^{C2} C3. Hence it is recommended that the future modifications in the alloy chemistry should incorporate the beneficial features of the composition ^{C3} C2 which have many positive features. Further, the alloying elements should be so adjusted that the microstructures of interest (formed in the present investigation at 1000 and 1050°C) should form in the as-cast condition or on heat treating at lower temperatures i.e. say up to 800°C heat treatment.

29. The above said discussion reveals that a detailed study of the phase transformations and of the resulting microstructures

has major technological fallout and major implications in the design of future alloy compositions to obtain the best corrosion resistance and deformation behaviour.

8.3 SUGGESTIONS FOR FUTURE WORK

The future work should be carried out on the following lines:

1. Detailed study of the nature and formation of needles at lower heat treating temperature and dark grey phase at high temperature heat treatments.
2. Further work on the defining the 'homogeneity/heterogeneity' index of the microstructure.
3. Extensive electro-chemical characterization of different microstructures by potentiostatic methods.
4. Crystal structure determination of carbides by x-ray diffractometry.
5. Detailed study of the high temperature behaviour of the alloys in the heat treated condition.
6. Studying the founding characteristics of the alloys
7. Detailed investigations of the performance of the experimental alloy C2.

REFERENCES

- A1. Anant Narayan, S.N.,
Ni-Resist Irons for Pumps in Corrosion-Resisting
Applications", International Nickel Co. In Corp., 1980,
p. 1-2.
- A2. Angus, H.T.,
'Cast Iron- Physical and Engineering Proper- ties',
Butterworths, London, 1976, pp.161-253 and 286-354
- A3. Angus, H.T.,
'Cast Iron- Physical and Engineering Properties',
Butterworths, London, 1976, p.53.
- A4. Askeland, Donald R.,
The Science and Engineering of Materials, 2nd Edition,
PWS-KENT Publishing Co., Boston. 1984, p. 396-399.
- A5. Askeland, Donald R.,
The Science and Engineering of Materials, 1st Edition,
PWS-KENT Publishing Co., Boston. p. 393.
- A6. ASTM Standards:
G-1-72, 'Standard recommended practice for preparation,
cleaning, and evaluating corrosion test specimens', Annual
book of ASTM standards, part 10, Philadelphia, 1978.

- A7. ASTM Standards
:G-31-72, 'Standard recommended practice for laboratory immersion corrosion testing of materials', Annual book of ASTM standards, part 10, Philadelphia, 1978.
- A8. Avner, S.H.,
'Introduction to Physical Metallurgy', McGraw-Hill, 1984, P.423.
- A9. Avner, S.H.,
'Introduction to Physical Metallurgy', McGraw-Hill, 1984, P.437.
- B1. Bain, E.C., and Paxton, H.W.,
'Alloying Elements in Steels' ASM, Metals Park, Ohio, 1962, pp.59-87.
- B2. Balluffi, R.W., et.al.,
Trans. ASM, 1951,43,p.493.
- B3. Barton, R.,
"Special Cast Irons", Report No. 576, BCIRA Journal , Nov. 1960, vol.8, no.6, p.857-882.
- B4. Barton, R.,
"Influence of Alloying Elements in Cast Irons", Report No. 576, BCIRA Journal , Nov. 1960, vol.8, no.6.
- B5. Basak, A., Penning, J., and Dilewijns,
AFS International Cast Metal Journal, vol. 6, no.3,

September 1981, p12-17.

- B6. Battelle, B.L., Minkoff, I. and Mollard, F., Editors,
"The metallurgy of cast irons", Proc.of 2nd International
Symposium, Geneva, Switzerland , May 29-31, 1974.
- B7. Benard, J.,
'Oxydation des Metaux', Gauthier Villars etc., Paris, 1962.
- B8. Benz, R., Elliott, J.F., and Chipman, J.,
Metallurgical Transactions, vol.5, pp.2235-40 (1974).
- B9. Bilby, B.A., and Pickering, F.B.,
ISI Sp. Report-64, 313.
- B10. Boyer, H.E., and Gall, T.L.,
Metals Hand Book, Desk Edition, Ed. ASM, Metals Park,
Ohio, 1984, p.5.1645.19 and 5.19.
- B11. Boyes, J.W.,
Iron and Steel, March 1966, p2-9
- B12. Boyes, J.W.,
Iron and Steel, 42 (1), February, 1968, pp.57-63
- B13. Burgess, C.O.,
Proceedings of the American Society for Testing of
Materials, 1939, V39, p.604-622 and 623-625.
- B14. Burke, J.,
" The kinetics of phase transformation in metal, Pergamon

Press, 1965, p93-98

- C1. Chakraborty, I.,
Ph.D. Thesis, I.I.T, Kharagpur, India, 1988
- C2. Charles, Arthur, N. and Kenneth, E. Rose,
"Engineering Metallurgy Series, 19, p.408-437.
- C3. Corti, C.W., Boyes, J.W., and King, C.W.,
Iron and Steel, October, 1969, pp.337-342.
- C4. Cox, G.J.,
"British Foundrymen", Vol. 76, 1983, p. 129-144.
- D1. Dawson, R.J., and Craig, G.B.,
AFS Transactions, vol.91, 1983, pp.235-242.
- D2. Dodd, J.,
Corrosion vol.I; Newnes Butterworth Ltd., 1976, B, p.111.
- D3. Dodd, J.,
Proc. of Conference : Materials to supply the energy
demand, Harrison, British Columbia,1980, ASM Publication,
1981, p.17.
- D4. Dodd, J and Parks, J.L.,
Metals Forum, vol.3, No.1,1980, pp.4
- D5. Dodd, J., and Parks, J.L.,
AFS International Cast Metal Journal, September 1980, p.48
- D6. Dorazil E. and Barta, B., Munssterova, E.,
"AFS International Cast Metals Journal", Vol. 7, No. 2,

1982, p 52-62.

- D7. Dumitsescu, T., Medeleanu, V., Nicolaid, M., and Dinu, I.,
Rev. Metall. (Roumania), vol.3, No.2, 1958, p.19
- D8. Durman, R.W.,
Foundry Trade journal, vol.134, 1973, pp.645- 651.
- D9. Durman, R.W.,
'The applications of alloyed white cast irons in crushing,
grinding, and materials handling processes', conference
paper, reprinted from 'Modern Castings' journal
- E1. Elliott, R.,
'Cast Iron Technology', Butterworths, 1988, p.5
- E2. Elliott, R.,
'Cast Iron Technology', Butterworths, 1988, pp.24-36.
- E3. Evans, U.R.,
'The corrosion and oxidation of Metals', Edward Arnold
Ltd., London, 1960.
- F1. Frost, R.H., Majewski, T., and Krauss, G.,
AFS Transa- ctions, vol.94, 1986, pp.297-332.
- G1. Gilbert, G.N.J.,
"The properties of cast irons", Engineering Materials and
Methods, The Institute of Mechanical Engineers, London,

1971, p.10-17.

- G2. Goldschmidt, H.J.,
'Interstitial Alloys', Butterworths, London, 1967, p.94-95.
- G3. Greene, N.D.,
'Experimental electrode kinetics' Ressenlaer Polytechnic
Institute, Troy, New York, 1965.
- H1. Hallett, M.M.,
Journal of the Iron and Steel Institute, 1952, Vol. 170,
April p. 321-329.
- H2. Hassen, Peter,
'Physical Metallurgy', Cambridge University press, 1986,
pp.214-216
- H3. Hauffi, K.,
'Oxydation Von Metallen Und Metallefierungen Springer'
Berlin, 1957.
- H4. Haycock, E.W.,
J.Electrochem. Soc.,106,1959,p.771.
- H5. Heine, R.W., Loper, C.R., and Rosenthal, P.C.,
"Principles of Metal Casting", McGraw Hill New York,
1967, p.491 & 504.
- H6 Henon, G.,
Properties and Uses of Irons alloyed with nickel, copper
and chromium, Foundry Trade Journal, March 28, 1966, p.

507-519.

- H7. Higgins, Raymond. A.,
Engineering Metallurgy Pt.I-Applied Physical Metallurgy",
5th Edition, E.L.B.S.,1983, p.369.
- H8. Higgins, Raymond. A.,
Engineering Metallurgy Pt.I-Applied Physical Metallurgy",
5th Edition, E.L.B.S.,1983, p.380-381.
- H9. Hillert, M., and V.V. Subba Rao,
"The Solidification of Metals", Iron and Steel Inst. Publ.
110, London 1968.
- H10. Himmelblau, D.M.,
'Applied Non-linear Programming', McGraw-Hill book
company, 1975.
- H11. Honeycombe, R.W.K., and Seal, A.K.,
JISI, 188, 1958, p.9.
- H12. Hughes, H.P., and Monaghan, J.,
Foundence Belge, 1955, No.10, p. 177-185, 188-190.
- H13. Hurst, J.E., and Piley, R.V.,
JISI, Vol. 155, Feb. 1947, p. 172-178.
- I1. INCO
'Engineering Properties and applications of Ni-Hard Cast
irons'; International Nickel Co., Inc., New York, 1978,
pp.2-15

- I2. INCO
'Engineering Properties of Ni-Resists and Ductile Ni-Resists': International Nickel Co. In Corp., 1976, P. 1-40
- I3 INCO
"Nickel as an Alloy in Cast Iron" International Nickel Co. Incorp., Publication No. A-1271, 1977, p. 17-30.
- I4 INCO
"Ni-Resist Austenitic Cast Irons-Properties and Applications", International Nickel Co. Incorp., 1965, p.1-21.
- I5 INCO
"Ni-Resist Irons for Fluid Handling in the Chemical Industry", International Nickel Co. Incorp., Publication No. 2773, p. 2-8.
- J1. Jackson, R.S.,
Journal of Iron & Steel Institute, 1970, Vol. 208, p. 163-167
- J2. Jain, N.C.,
Ph.D. Thesis, University of Roorkee, Roorkee, India, 1986.
- J3. Jain, N.C., Patwardhan, A.K., and Kumar, V.,
Tool & Alloy Steels, Vol.22, No.7 & 8, July & August 1988, pp.215-227
- J4. Jain, N.C., Patwardhan, A.K., and Kumar, V.,

Tool & Alloy Steels, September, 1988, Vol.22, No.9,
pp.271-278

- J5. Jain, N.C., and Patwardhan, A.K.,
Metallurgical Transactions, Vol.23A, March 1992, p.891-901.
- J6. Janowak, J.F., Gundlach, R.B., Eldis, G.T., & Rohrig, K.,
"Technical Advances in Cast Iron Metallurgy" AFS
International Cast Metals Journal, Vol.6, No.4, 1981,
p.28-42.
- J7. Janowak, J.F., and Gundlach, R.B.,
"Report XGI-RBG-83-01 (June 13, 1983), Climax Molybdenum
Co., Michigan.
- J8. JCPOS
'Selected powder diffraction data' Metals and alloys data
book, JCPOS, vol. I, 1978
- J9. JCPOS
'Selected powder diffraction data' Metals and alloys data
book, JCPOS, vol. II, 1978
- J10. JCPOS
'Selected powder diffraction data' Metals and alloys data
book, JCPOS, Inorganic, sets 1-22, 1967.
- J11. Jha, B.K., Sharma, P.K.,
B.E. Project Report, University of Roorkee, Roorkee, May,
1978.

- K1. Kofstad, P.,
'High temperature oxidation of Metals', John Wiley & Sons
Inc., New York, 1966.
- K2. Kofstad, P.,
Acta Chem. Scand. 12, 1959, p. 501
- K3. Kubaschewski, O., and Hopkins, B.E.,
'Oxidation of Metals and Alloys', Butterworths, London,
1962.
- K4. Kumar, V.,
M.E. Dissertation, University of Roorkee, Roorkee, 1985.
- K5. Kumar, V., and Mohanty, B.,
'Indexing of x-ray diffractograms', software section,
Scripta Metallurgica, Vol. 20, 1986.
- K6. Kumar, V.,
Ph.D. Thesis, University of Roorkee, Roorkee, 1990
- K7. Kumar V., Rao, P.N.V.R.S.S.V.P., and Patwardhan, A.K.,
Proceedings of the International Conference on 'Corrosion
and Corrosion control for Offshore and Marine Construction'
held on September 6-9, 1988, Xiamen, China; Pergamon Press,
Incorp, New York (USA), pp. 623-628.
- K8. Kumar, V., Rao, P.N.V.R.S.S.V.P., and Patwardhan, A.K.,

- Tool & Alloy Steels, Vol.25, No.6, June, 1991, pp.221-225
- K9. Kumar, V., Rao, P.N.V.R.S.S.V.P., and Patwardhan, A.K.,
Materials Performance, Vol.30, No.8, August, 1991, pp.72-74
- K10. Kuo, K.,
JISI, 1953,173,pp.363-374.
- K11. Kuo, K., and Persson, L.E.,
JISI, Sept.1954, pp.39-44.
- K12. Kutner, C.,
Tech. Mitt. Krup., No.1, March, 17, 1933.
- L1. Laird-II, G., Brown, R.R., and Neilson, R.L.,
Material Science and Technology, July, 1991, vol.7,
pp.631-642.
- L2. Laird-II, G., Nielsen, R.L., and MacMillan, N.H.,
Material Science and Technology, Vol.22A, August, 1991,
pp.1709-1720
- L3 Lakhtin, Yu,
"Engineering Physical Metallurgy and Heat Treatment", Mir
Publishers, Moscow, 1983, p. 171-177.
- L4 Lakhtin, Yu, "Engineering Physical Metallurgy and Heat
Treatment", Mir Publishers, Moscow, 1983, p. 154.
- L5. Lorig, C.H. ,
Metallurgy of Cast Iron, Cast Metals Hand Book, American
Foundrymen's Association, Chicago III, 1944, p. 363-365.

- L6. Loviers, J.,
Compt. rend., 229(1949), p.547., Gordon and Beach, New
York, 1968, p.50
- M1. Mackenzie, R.C.,
Differential Thermal Analysis', vol.1., Academic Press,
London, 1970,p.32.
- M2. Magee, C.L., and Davis, R.G.,
'Low Alloy Steels'; Iron and Steel Instt, London, Special
Report No.111, 1968
- M3. Maitland, R.J., and Huges, I.C.H.,
B.C.I.R.A., Journal of Research and Development, 1958,
Vol. 7, April, p. 203-223.
- M4. Mangasarain, O.L., Meyer, R.R., and Robinson, S.M.,
Non-linear programming-2, Academic Press, Inc., New York,
San Francisco, London, 1975.
- M5. Maratray, F.,
AFS Transactions, Vol. 79, 1971, p. 121-124.
- M6. Maratray, F., Ussenglio-Nanot, R.,
Climax-Molybdenum company, S.A., 1971, pp.1-31.
- M7. Maturaba, Y., Ogi, K., and Matsuda, K.,
AFS Transactions, vol.89, 1981, pp.183-196.

- M8. Merchant, H.D.(Editor),
'Recent Research on Cast Irons', G.B. Science Publications,
New York, 1968, p.7
- M9. Metals Hand Book,
Vol.1, 9th edition, ASM, Metals Park, Ohio, 'Properties
and Selection of Irons and Steels', 1978, p.3-9.
- M10. Metals Hand Book,
Vol.1, 9th edition, ASM, Metals Park, Ohio, 'Properties
and Selection of Irons and Steels', 1978, p.75-96.
- M11. Metals Hand Book,
8th edition, ASM, Metals Park, Ohio, 1961, pp.394-406
- M12. Mills, K.C., Argent, B.B., and Quarrell, A.G.,
JISI, Jan., 1961, p. 9-21.
- M13. Minkoff, I.,
"Solidification and Cast Structure", John Wiley & Sons,
1986, p. 195.
- M14. Minkoff, I.,
"Solidification and Cast Structure", John Wiley & Sons,
1986, p. 207.
- N1. Nutting, J.,
JISI, vol.207, June 1969, pp.872-893.
- O1. Ohide, T., and Ohira, G.,
British Foundry, Vol. 76, Part 1, January, 1983, p.9.

- O2. Owen, W.S., and Wilson, E.A.,
'Physical properties of Martensite and Bainite', Iron and
Steel Instt., London, Special Report No. 93, 1965, p.103
- P1. Parks, J.L.,
AFS Transactions, vol.86, 1978, pp.93-102
- P2. Patwardhan, A.K.,
Personal communication
- P3. Patwardhan, A.K.,
Ph.D.Thesis, University of Roorkee, Roorkee, 1979.
- P4. Patwardhan, A.K., and Jain, N.C.,
AFS Transactions, Vol.96, 1988, pp.329-338
- P5. Patwardhan, A.K., and Jain, N.C.,
AFS Transactions, Vol.97, 1989, pp.201-206
- P6. Patwardhan, A.K., and Jain, N.C.,
Metallurgical Transactions, Vol.22A, October, 1991, pp.
2319-2325.
- P7. Patwardhan, A.K., Mehta, M.L., and Sharma, C.P.,
AFS International Cast Metal Journal, March, 1981, pp.3-9.
- P8. Patwardhan, A.K., Mehta, M.L., and Viswanadham, Ch.,
AFS Transactions, 1988, pp.919-924.
- P9. Patwardhan, A.K., Mukundan, R., Rao, P.N.V.R.S.S.V.,
Sharma, C.P., and Kumar, S.,

'Simulation of the Transformation behaviour of 7.5% and 6% manganese C-Cr-1.5Cu corrosion resistant white irons through mathematical modelling', accepted for publication in Metallurgical Transactions-A.

- P10. Patwardhan, A.K., Singh, S.S., and Jain, N.C.,
Tool & Alloy Steels, October, 1987, pp.369-377.
- P11. Pearce, J.G., and Bromage, K.,
'Copper in Cast Iron', C.D.A. publication No.65, Copper Development Association, London, 1964, pp.41-43
- P12. Pearce, J.T.H.,
British Foundryman, vol.78, part-1, 1985, pp.13-23
- P13. Pickering, F.B.,
4th Int. Cof. on Electronmicroscopy, 1958, Berlin, 668.
- P14. Powell, G.L.F.,
Metals Forum, vol.3, No.1, 1980, pp.37-46
- R1. Rahmel, a., Z.Elektrochem.,
66, 1962, 363, p.284.
- R2. Rao, P.N.V.R.S.S.V.P.,
M.E. Dissertation, University of Roorkee, Roorkee, 1988.
- R3. Rao, P.N.V.R.S.S.V.P.,
Ph.D. Thesis, 1993, Submitted, University of Roorkee,
Roorkee.
- R4. Rao, P.N.V.R.S.S.V.P., and Patwardhan, A.K.,

Materials Forum, vol.16, 1992, pp.51-67

- R5. Rao, P.N.V.R.S.S.V.P., Patwardhan, A.K., and Jain, N.C.,
Metallurgical Transactions, Feb., 1993, p. 445-457.
- R6. Rickard, J., The British Foundryman,
Vol.77, part 6, July 1984, pp.313-317
- R7. Roberts, M.J., and Owen, W.S.,
Trans. ASM Quart., vol. 60, 1967, p.679
- R8. Rollason, E.C.,
'Metallurgy for Engineers', Edward Arnold, London, 1973,
pp.270-285.
- R9. Rollason, E.C.,
'Metallurgy for Engineers', Edward Arnold, London, 1973,
p. 272.
- R10. Rozhkove, E.V. et.al.,
Materials Science and Heat treatment, 23, 1, 1981, p.59.
- S1. Sandoz, G.,
The partitioning of alloying elements in malleable irons,
NRL Report 5268, US Naval Research Laboratory, Washington,
D.C., Feb. 1959, p. 1-25.
- S2. Sandoz, G.,
Gordon and Beach, New York, 1968, p. 50. 'Recent research
in Cast Iron', (Merchant, H. Ed.)
- S3. Sare, I.R.,

Metals Technology, November, 1979, pp.412-419.

- S4. Schute, D.,
'Differential Thermal Analysis', Weinheim Verlag, Cherie,
1969.
- S5. Sewell, P.B., and Cohen, M,
J.Electrochem. Soc., 111, 1964, p.501.
- S6. Sewell, P.B., and Cohen, M,
J.Electrochem. Soc., 111, 1964, p.508.
- S7. Sharma, C.P.,
M.E. Dissertation, University of Roorkee, Roorkee, 1976
- S8. Shiokawa, T.,
59th Japan Ductile Cast Iron Assoc. Licencee Conf., Nov.
1978.
- S9. Shreir, L.L., Editor,
'Corrosion', Newnes-Butterworths, London, vol.1, 1976,
p.3:77 to 3:126.
- S10 Singh, S.S.,
Ph.D.Thesis, University of Roorkee, Roorkee, 19
- S11 Smith, E., and Nutting, J.,
JISI, 1957, 187, p. 314-329.
- S12 Srinivasan, T.,
M.E. Dissertation, University of Roorkee, Roorkee, 1975

- S13. Srinivasan, T, Patwardhan, A.K., and Mehta, M.L.,
AFS International Cast Metal Journal, March, 1977,
pp.57-60.
- S14 Stefanescu, D.M., Mitea, D., and Cracium, S.,
AFS International Cast Metal Journal, June, 1976, vol.1.
No.2, pp.19-26
- S15 Stickle, R. Donald.,
"Corrosion of Cast Irons", Metals Handbook, Vol. 13, 9th
Edition, ASM, Metals Park, Ohio, 1979, p. 566.
- S16 Strauss, K.,
Applied Science in the Casting of Metals", Pergamon Press,
1970, p. 179-206.
- S17. Sudan, A.S.,
M.E. Dissertation, University of Roorkee, Roorkee, 1976.
- S18 Sudan, A.S., Mehta, M.L., and Patwardhan, A.K.,
AFS Internanational Cast Metal Journal, March, 1980,
p.42-46
- T1. Torpe, W.R., Chicco, B.,
Material Science and Engineering, 51, 1981, p.11-19
- T2. Tsy-pin, T.I. et.al.,
Materials science and Heat treatment,12, 1970, p.612.

- V1. Viswanadham, Ch.,
M.E. Dissertation, University of Roorkee, Roorkee, 1981
- V2. Viswanadham, Ch., Patwardhan, A.K. & Mehta, M.L.,
'Gisserei' (FGR), 73(4), 1986, p.238
- W1 Walton, C.F., and Opar, T.J.,
'Iron Castings Hand Book', Iron Castings Society, Des
Plaines, IL, 1981, p. 121
- W2 Walton, C.F., and Opar, T.J.,
'Iron Castings HandBook', Iron Castings Society, Des
Plaines, IL, 1981, p. 138
- W3 Walton, C.F., and Opar, T.J.,
'Iron Castings Hand Book', Iron Castings Society, Des
Plaines, IL, 1981, p. 63, 381-397.
- W4. Walton, C.F., and Opar, T.J.,
'Iron Castings Hand Book', Iron Castings Society, Des
Plaines, IL, 1981, p. 409-411,
- W5 Webb, W.W., Norton, J.J., and Wagner, C.,
J. electrochem Soc., 103,1956,p.107.
- W6 Wever, F., and Koch, W., Stehl Eisen ,
1954, 74, p.989
- W7 White, W.H.; Rice, L.P., and Elsea, A.R.,
Transactions of the American Foundrymen's Society, 1951,
Vol. 59, p. 337-345, Discussions, p. 345-347.
- W8. Woodhead, J.H., and Quarrell, A.G.,
JISI, 605, 1965, p.203

TABLE 1.1

CONDITIONS FAVOURING EACH OF THE EUTECTIC REACTIONS IN CAST IRONS

A. Formation of grey iron, ductile iron, compacted graphite iron

1. High Carbon Equivalent
2. High Silicon
3. Presence of Graphitizers eg. Cu, Ni
4. Slow Cooling
5. Thick Casting
6. Inoculation

B. Formation of white iron

1. Low Carbon Equivalent
 2. Low Silicon
 3. Presence of Carbide Formers eg. Cr, Mo, V
 4. Fast Cooling
 5. Thin Castings
 6. No Inoculation
-

TABLE 1.2

MECHANICAL AND PHYSICAL PROPERTIES OF C.G. IRONS

Property	Microstructure	
	Ferrite	Pearlite
Tensile strength N/mm ²	310	420
Yield strength N/mm ²	270	345
Elongation %	4	2
Hardness	150	200
C.V.N. impact, J	5	3
Fatigue strength (N/mm ²)	150	180
Elastic modulus GN/m ²	165	165
Poissons ratio	0.265	0.265
Thermal conductivity W/(mK)	44	36
Specific heat at 100°C, J/g°C	0.5	0.5
Coefficient of linear thermal expansion, X10 ⁻⁶ /°C	11	13

TABLE 1.3

MECHANICAL AND PHYSICAL PROPERTIES OF COMPACTED GRAPHITE, GREY AND NODULAR IRONS

Property	Grey irons	CG irons	SG irons
Tensile strength N/mm ²	160-320	300-600	400-700
Ton/in ²	11-20	20-38	26-45
Elongation %	Nil	3-6	6-25
Modulus of elasticity lb/in ²	14-16x10 ⁻⁶	20-23x10 ⁻⁶	25-27x10 ⁻⁶
Charpy impact (J) at room temperature	Nil	3-7	17
Thermal conductivity Cal/cm °C/sec	0.11-0.14	0.10-0.12	0.08-0.09
Damping capacity	13.2x10 ⁻⁴	4-6x10 ⁻⁴	2-5x10 ⁻⁴
Fatigue limit un-notched ton/in ²	7-8	15-20	12-18
Machineability	Very good	Very good	Good
Corrosion Resistance	Moderate	Intermediate	Good

TABLE-1.4a

RANGES OF ALLOY CONTENT FOR THE CORROSION & HEAT RESISTANT ALLOYED GREY CAST IRONS

Description	TC(a)	Mn	COMPOSITION, (Wt %) (b)							Matrix structure as-cast(c)
			P	S	Si	Ni	Cr	Mo	Cu	
Corrosion-Resistant Irons										
High silicon iron(d)	0.4-1.1	1.5	0.15	0.15	14-17	...	5.0	1.0	0.5	F
Ni-Cr grey iron(e)	3.0	0.5-1.5	0.08	0.12	1.0-2.8	13.5-36	1.5-6.0	1.0	7.0	A
Ni-Cr ductile iron(f)	3.0	0.7-4.5	0.08	0.12	1.0-3.0	18-36	1.5-5.5	1.0	...	A
Heat-Resistant Grey Irons										
Medium silicon iron(g)	1.6-2.5	0.4-0.8	0.30	0.10	4.0-7.0	F
High Cr-iron	1.2-4.0	0.3-1.5	0.15	0.15	0.5-3.0	5.0	12-35	4.0	3.0	F, CP
Ni-Cr iron(e)	1.8-3.0	0.4-1.5	0.15	0.15	1.0-2.7	13.5-36	1.8-6.0	1.0	7.0	A
Ni-Cr-Si iron(h)	1.8-2.6	0.4-1.0	0.10	0.10	5.0-6.0	13-43	1.8-5.5	1.0	...	A
Heat-Resistant Ductile Irons										
High Al-iron	1.3-2.0	0.4-1.0	0.15	0.15	1.3-6.0	...	20-25 Al	F
Medium Si-ductile iron	2.8-3.8	0.2-0.6	0.08	0.12	2.5-6.0	1.5	F
Ni-Cr ductile iron(f)	3.0	0.7-2.4	0.08	0.12	1.75-5.5	18-36	1.75-3.5	1.0	...	A

(a) Where a single value is given rather than a range, that value is a maximum limit

(b) Total Carbon (c) F, Ferrite; A, austenite; CP, coarse pearlite

(d) such as Duriron, Durichlor 51, Superchlor

(e) Such as Ni-Resist austenitic iron (ASTM A436)

(f) Such as Ni-Resist austenitic ductile iron (ASTM A439)

(g) Such as Silal (h) Such as Nicrosilal

TABLE-1.4b

TYPICAL MECHANICAL PROPERTIES OF CORROSION RESISTANT CAST IRONS

Type of iron	Hardness, HB	Tensile strength		Compressive strength		Impact energy J	Transverse breaking load(b)		Transverse deflection(b)	
		MPa	ksi	MPa	ksi		kg	lb	mm	in.
High-silicon iron	480 to 520	90 to 180	13 to 26	690	100	2.7 to 5.4(c)	2 to 4(c)	545 to 1200 to 1000	2200	0.65 to 0.026
High-chromium iron	250 to 740	205 to 830	30 to 120	690	100	0.1 to 3(d)	0.1 to 2(d)	910 to 2000 to 1590	3500	1.5 to 0.06 to 3.8
High-nickel gray iron	120 to 250	170 to 310	25 to 45	690 to 1240 to 1100	100 to 160	80 to 200(c)	60 to 150(c)	820 to 1800 to 1590	3500	5 to 0.20 to 1.00
High-nickel ductile iron	130 to 240	380 to 480	55 to 70	1380	180 to 200	14 to 40(d)	10 to 30(d)

(b) For as-cast 30.5-mm (1.2-in.) diam bar broken over a 457-mm (18-in.) span. (c) Unnotched 30.5-mm diam test bar broken over a 152-mm (6-in.) span in a Charpy testing machine. (d) Standard Charpy.

TYPICAL MECHANICAL PROPERTIES OF HEAT RESISTANT ALLOY CAST IRONS

Type of iron.	Hardness, HB	Tensile strength		Compressive strength		Impact energy J	Transverse breaking load(b)		Transverse deflection(b)	
		MPa	ksi	MPa	ksi		kg	lb	mm	in.
Medium-silicon gray iron	170 to 250	310	25 to 45	1040	90 to 150	20 to 31(c)	15 to 23(c)	455 to 1090	1000 to 2400	4.6 to 0.16 to 8.9
High-chromium gray iron	250 to 500	620	30 to 90	690	100	27 to 47(c)	20 to 35(c)	910 to 1590	2000 to 3500	1.5 to 0.06 to 3.8
High-nickel gray iron	130 to 250	310	25 to 45	1100	100 to 160	200(c)	80 to 150(c)	820 to 1360	1800 to 3000	5 to 0.2 to 1.0
Ni-Cr-Si gray iron	110 to 210	310	20 to 45	480 to 690	70 to 100	110 to 200(c)	80 to 150(c)	820 to 1130	1800 to 2500	7 to 0.3 to 1.4
High-aluminum gray iron	180 to 350	620	34 to 90
Medium-silicon ductile iron	140 to 300	690	60 to 100(c)	7 to 155(d)	5 to 115(d)
High-nickel ductile iron (20 Ni)	140 to 200	415	55 to 60(e)	1240 to 1380	180 to 200	16(f)	12(f)
High-nickel ductile iron (23 Ni)	130 to 170	450	58 to 65(g)	38(f)	28(f)

(b) Unnotched 30.5-mm (1.2-in.) diam test bar broken on 152-mm (6-in.) supports in a Charpy testing machine. (c) Yield strength, 310 to 520 MPa (45 to 75 ksi); elongation, 0.2%. (d) Standard Charpy test on 10-mm unnotched specimen. (e) Yield strength, 210 to 240 MPa (30 to 35 ksi); elongation, 8 to 20%. (f) Standard Charpy test on 10-mm notched specimen. (g) Yield strength, 195 to 240 MPa (28 to 35 ksi); elongation, 20 to 40%.

TABLE-1.5a

CHEMICAL COMPOSITION OF Ni-RESIST IRONS, PERCENT

	Type 1 ¹	Type 1B	Type 2 ²	Type 2B	Type 3	Type 4	Type 5
	Aus 101a	Aus 101b	Aus 102a	Aus 102b	Aus 105		
C	3.00 max	3.00 max	3.00 max	3.00 max	2.60 max	2.60 max	2.40 max
Si	1.00-2.80	1.00-2.80	1.00-2.80	1.00-2.80	1.00-2.00	5.00-6.00	1.00-2.00
Mn	1.00-1.50	1.00-1.50	0.80-1.50	0.80-1.50	0.40-0.80	0.40-0.80	0.40-0.80
Ni	13.50-17.50	13.50-17.50	18.00-22.00	18.00-22.00	28.00-32.00	29.00-32.00	34.00-36.00
Cu	5.50-7.50	5.50-7.50	0.50 max	0.50 max	0.50 max	0.50 max	0.50 max
Cr	1.75-2.50	2.75-3.50	1.75-2.50	3.00-6.00 ³	2.50-3.50	4.50-5.50	0.10 max ⁴

1 Where the presence of copper offers corrosion-resistance advantages, Type 1 is recommended.

2 For handling caustics, food, etc., where copper contamination cannot be tolerated, Type 2 is recommended.

3 Where some machining is required, the 3.0-4.0 chromium level is recommended.

4 Where higher hardness, greater strength and added heat resistance are desired, the chromium may be 2.5-3.0% at the expense of increased expansivity.

TABLE-1.5b

MECHANICAL PROPERTIES OF Ni-RESIST IRONS

	Type 1 Aus 101a	Type 1B Aus 101b	Type 2 Aus 102a	Type 2B Aus 102b	Type 3 Aus 105	Type 4	Type 5
Tensile Strength ton/in ² (kg/mm ²)	11-13.5 (17-21)	11-15.5 (17-24)	11-13.5 (17-21)	11-15.5 (17-24)	11-15.5 (17-24)	11-15.5 (17-24)	9-11 (14-17)
Compressive Strength ton/in ² (kg/mm ²)	44-53 (69-84)		44-53 (69-84)	58-71 (91-112)	44-50 (69-79)	36 (57)	36-44 (57-69)
Torsional Strength lb/in ² x 10 ⁴ (kg/mm ²)	35-40 (25-28)		35-40 (25-28)	45-60 (32-42)	35-45 (25-32)	29 (20)	30-35 (21-25)
Torsional Modulus lb/in ² x 10 ⁶ (kg/mm ² x 10 ³)	4.5 (3.2)		4.5 (3.2)	5.5 (3.9)	5.0 (3.5)	4.0 (2.8)	4.5 (3.2)
Modulus of Elasticity lb/in ² x 10 ⁴ (kg/mm ² x 10 ³)	12-14 (8.4-9.8)	14-16 (9.8-11.2)	15-16.2 (10.5-11.4)	15-16.5 (10.5-11.6)	15-15.5 (10.5-10.9)	15 (10.5)	10.5 (7.4)
Permanent Set Point lb/in ² (kg/mm ²)	3,000 (2.1)		3,000 (2.1)				
Transverse Properties (18 in) load — lb x 10 ³ (kg x 10 ³) deflection — inch (cm)	2.0-2.2 (0.9-1.0) 0.3-0.6 (0.8-1.5)		2.0-2.2 (0.9-1.0) 0.3-0.6 (0.8-1.5)	2.4-2.8 (1.1-1.3) 0.2-0.4 (0.5-1.0)	2.0-2.4 (0.9-1.1) 0.5-0.6 (1.3-1.5)	1.8 (0.8) 0.3-0.6 (0.8-1.5)	1.8-2.0 (0.8-0.9) 0.5-1.0 (1.3-2.5)
Vibration Damping Capacity	High	Medium	High	Medium	High	Medium	High
Endurance Limit lb/in ² (kg/mm ²)	12,000 (8.4)		12,000 (8.4)	18,000 (12.6)	13,500 (9.5)	9,000 (6.3)	9,900 (7.0)
Hardness Brinell	130-170	150-210	125-170	170-250	120-160	150-210	100-125
Toughness by Impact (Izod) ft. lbf (kgm)*	100 (14)	80 (11)	100 (14)	60 (8)	150 (21)	30 (11)	150 (21)

*1.2 inch (3cm) diameter bar unnotched — struck 3 inches (7.6 cm) above supports (Grey iron shows 25-35 ft-lbf (3.46-4.48 kgm))

TABLE-1.6a

CHEMICAL COMPOSITION OF S.G. Ni-RESIST IRONS, PERCENT

	Type D-2 Aus 202a	Type D-2B Aus 202b	Type D-2C Aus 203	Type D-2M Aus 205	Type D-3 Aus 205	Type D-3A	Type D-4	Type D-5	Type D5B
C	3.00 max	3.00 max	2.90 max	2.7 max	2.60 max	2.60 max	2.60 max	2.40 max	2.40 max
Si	1.75-3.00	1.75-3.00	2.0-3.0	1.5-2.6	1.50-2.8	1.50-2.80	5.0-6.0	1.50-2.75	1.50-2.75
Mn	0.70-1.0	0.70-1.0	1.80-2.40	3.75-4.50	0.50 max	0.50 max	0.50 max	0.50 max	0.50 max
P	0.08 max	0.08 max	0.08 max	0.08 max	0.08 max	0.08 max	0.08 max	0.08 max	0.08 max
Ni	18.0-22.0	18.0-22.0	21.0-24.0	21.5-24.0	28.0-32.0	28.0-32.0	29.0-32.0	34.0-36.0	34.0-36.0
Cr	1.75-2.50	2.75-4.0	0.50 max	0.2 max	2.50-3.50	1.00-1.50	4.50-5.50	0.10 max	2.0-3.0

TABLE-1.6b

MECHANICAL PROPERTIES OF S.G. Ni-RESIST IRONS

	Type D-2 Aus 202a	Type D-2B Aus 202b	Type D-2C Aus 203	Type D-2C Aus 205	Type D-3 Aus 205	Type D-3A	Type D-4	Type D-5	Type D-5B
Tensile Strength ton/in ² (kg/mm ²)	24-30 (38-47)	26-31 (41-49)	24-29 (38-46)	24-30 (38-47)	24-29 (38-46)	24-29 (43-50)	24-27 (38-43)	24-29 (38-46)	24-29 (38-46)
Yield Strength (2% Offset) ton/in ² (kg/mm ²)	14-16 (22-25)	14.5-16.5 (23-26)	13.5-15.5 (21-24)	14.5-16.5 (23-26)	14-17 (22-27)	17-20 (27-32)	13.5-16.5 (21-26)	16.5-19 (26-30)	16.5-19 (26-30)
Elongation, % on 2 in (5.1 cm)	8-20	7-15	20-40	7-18	13-18	15-40	20-40	5-10	5-10
Proportional Limit ton/in ² (kg/mm ²)	7.3-8.3 (11.6-13.0)	7.1-8.5 (11.2-13.4)	5.4-7.1 (8.4-11.2)	7.1-8.5 (11.2-13.4)	6.7-8.5 (10.5-13.4)	5.4-7.1 (8.4-11.2)	4.2-4.9 (6.7-7.7)	4.7-5.8 (7.4-9.1)	4.7-5.8 (7.4-9.1)
Modulus of Elasticity lb/in ² x 10 ⁶ (kg/mm ² x 10 ³)	16.5-18.5 (11.6-13.0)	16.5-19	15	13.5-14.5 (9.5-10.2)	16-18.5 (11.2-13.0)	13	16-20 (11.2-14.1)	16-17.5 (11.2-12.3)	16-17.5 (11.2-12.3)
Hardness Brinell	140-200	150-210	130-170	140-200	130-190	170-240	130-180	140-190	140-190
Impact ft-lbf (kgm/cm ²) Charpy V-notch	12 (2.075)	10(1.73)	28(4.84)	7(1.21)	14(2.42)		17(29.4)	6(1.04)	6(1.04)
Room Temperature									

TABLE-1.7

COMMERCIAL APPLICATIONS FOR NI-RESIST DUCTILE IRONS

INDUSTRY	APPLICATIONS	REASONS FOR USE	INDUSTRY	APPLICATIONS	REASONS FOR USE
Chemical Process	pumps, valves	corrosion resistance heat resistance	Liquid Handling (Cont.)	valves	for high temperature service up to 1400 F
	supports and frames	corrosion resistance		body, bushing, butterfly gates, glands, pistons, piston rings	
	kettles	corrosion resistance erosion resistance wear resistance	Petroleum	pumps, valves	corrosion resistance
	filters	corrosion resistance erosion resistance wear resistance		tube supports	heat resistance high temperature strength
Electrical	nonmagnetic housings	low magnetic permeability	Power (Steam)	furnace castings	heat resistance
	switchgear	low magnetic permeability machinability		pumps, valves	corrosion resistance heat resistance
	pole line hardware	low magnetic permeability corrosion resistance	turbine diaphragms	corrosion resistance steam erosion resistance wear resistance	
Internal Combustion Engines	ring bands and hot spot buttons for aluminum pistons	heat resistance high temperature strength wear resistance erosion resistance high expansion machinability	Pulp and Paper	control valves	corrosion resistance steam erosion resistance wear resistance selected expansion
	exhaust manifolds, turbocharger cases and diffusers	heat resistance erosion resistance wear resistance high temperature strength selected expansion		shaft seals	erosion resistance wear resistance
	valve guides	heat resistance wear resistance corrosion resistance erosion resistance selected expansion	pipe and fittings	corrosion resistance erosion resistance	
	cylinder liners	corrosion resistance wear resistance erosion resistance high strength	pumps, valves	refer to liquid handling field	
	water pump bodies and impellers	corrosion resistance erosion resistance wear resistance	sweat rolls	corrosion resistance	
	turbine cases	heat resistance high temperature properties selected expansion	cowan screen frames	high strength corrosion resistance	
	pumps—stationary parts	corrosion resistance	supports and frames	corrosion resistance	
	cases or bodies	graphitic corrosion resistance	furnace castings	heat resistance	
	end plates	wear	glass molds	high temperature strength heat and scale resistance selected expansion	
	wear rings	wear resistance	winch drums and brakes	corrosion resistance high strength nonmagnetic properties wear resistance	
cylinder liners	machinability	sewage plant castings	erosion resistance corrosion resistance wear resistance		
diaphragms	high strength	water works, valves, flood gates	corrosion resistance erosion resistance		
pumps—moving parts	cavitation erosion resistance	dishwasher pumps and manifolds	corrosion resistance erosion resistance high temperature strength		
impellers		textile rolls	heat resistance		
shaft sleeves	galvanic corrosion resistance	hot forming dies	heat resistance high temperature strength wear resistance		
pistons	for high temperature service up to 1400 F	glass rolls	minimum coefficient of thermal expansion heat resistance high temperature strength		
seals, valves, gears		sintering machine pallets	heat oxidation resistance high temperature strength		
fittings, meters, pipe	same reasons apply as for pumps				

TABLE-2.1

COMPOSITION AND PROPERTIES OF SOME REPRESENTATIVE PLAIN CARBON WHITE IRONS

Sl. No.	Type/Class/Designation	TC	COMPOSITION				S	P	Hardness BHN	Micro-structure	Wear Rate (relative)	Application
			Mn	Si	Mn	P						
1.	Pearlitic Iron	2.80	0.3	0.4	0.15	0.1-0.12	—	415-477	C+P	179.0	Grinding Balls	
2.	Unalloyed, low hardness Iron	3.0	0.75	0.25	0.4	0.12	—	320-440	C+P	—	Iron Rolls	
3.	Unalloyed high hardness Iron	3.5	0.5	0.25	0.4	0.12	—	440-520	C+P	—	Iron Rolls	
4.	Unalloyed chill Cast Iron	2.78	0.53	0.42	—	—	—	444	Carbide in C.P.	174.0	—	
5.	Unalloyed Iron (Sand Cast)	3.05	0.4	0.5	—	—	—	444	C+P	122.0	Grinding Balls	
6.	Chill Cast unalloyed Iron	3.59	0.7	0.8	—	—	—	495	C+P	100.0	Grinding Balls	
7.	Pearlitic Iron	2.9	0.5	0.5	0.12	0.1	—	415-460	C+P	—	—	
8.	Cupola White Iron	3.3-3.6	0.4-1.0	0.5-0.7	0.15	0.3	—	400	C+P	—	—	
9.	Unalloyed high hardness alloys	3.2-3.8 3.0-3.4	0.4-0.8 0.9-1.3	0.3-0.7 0.6-1.0	max. 0.1	max. 0.2	—	380-600 380-520	C+P C+P	— —	— —	

*Wear rates are relative to an assigned rate of 100 for Chill Cast Unalloyed Iron

PHYSICAL AND MECHANICAL PROPERTIES

1.	Hardness (DPN)	410-520 (sand Cast) 435-550 (Chill Cast) (abrasion resistant)	53-72
2.	Tensile strength (ton/in ²)	400 (L.C., 2.5-2.6%C) 650 (H.C., 3.75-4.0%C) 15-30 (sand Cast) 18-30 (Chill Cast) 16-18 (H.C., 3.0-3.5%C) (Pearlitic, Hard)	6-11 (impact strength of white cast iron is about one third that of gray iron)
3.	Modulus of elasticity (lb/in ² x 10 ⁶)	18-30 (L.C., 2.75-2.9%C) (Pearlitic, Tough)	0.035-0.076
4.	Transverse rupture stress 1.2 bar, 12 in span (ton/in ²)	30 (Sand Cast, Chill Cast)	10-11 x 10 ⁻⁶ 15.9-16.4 x 10 ⁻⁶
5.	Transverse deflection	0.05-0.1 (H.C., 3.0-3.5%C) 0.07-0.11 (L.C., 2.75-2.9%C)	Usually not determined because of low ductility of white irons. The yield strength is considered to be close to the tensile strength.
6.	Specific gravity	7.6-7.8	
7.	Electrical resistivity (microhm-cm ³ at 78°F)		
8.	Impact strength (0.798 in dia machined from 0.875 in as-cast dia.) (ft. lb.)		
9.	Thermal conductivity (Cal/cm ³ s °C)		
10.	Thermal expansion coefficient 0-276°C		
11.	Yield strength		

TABLE-2.2

CHEMICAL ANALYSIS AND PROPERTIES OF Ni-HARD

	Type 1-Regular (ASTM A 532 1-B)		Type 2-HI-Stren. (ASTM A 532 1-C)		Type 3 (ASTM A532 1-D)		Type 4 (ASTM A 532 1-D)	
	Sand Cast	Chill Cast	Sand Cast	Chill Cast	Sand Cast	Chill Cast	Sand Cast	Chill Cast
Chemical Analysis, %								
Total Carbon	3.0-3.6		2.90 max		2.9 -3.7		2.5 -3.6	
Silicon	0.8 max		0.8 max		0.8 (max)		1.0 -2.2	
Manganese	1.3 max		1.3 max		1.3 max		1.3 max	
Sulfur	0.15 max		0.15 max		0.15 max		0.15 max	
Phosphorus	0.30 max		0.30 max		0.30 max		0.10 max	
Nickel	3.3 -5.0		3.3 -5.0		2.7 -4.0		5.0 -7.0	
Chromium	1.4 -4.0		1.4 -4.0		1.1 -1.5		7.0 -11.0	
Engineering Properties								
Brinell Hardness, Minimum	550	600	550	600	550	600	550	550
Trans. Strength, 1.20" DIA.	4000 to	4500 to	4500 to	5500 to	5000 to	5500 to	5000 to	5500 to
Test Bars, 12" Span, lb. Trans. Defl., 1.20" DIA.	5000	6800	5500	7000	6000	7000	6000	7000
Test Bars, 12" Span, in. Tensile Strength, 1.20" DIA. Test Bars, psi.	0.080 to	0.080 to	0.100 to	0.100 to	0.08 to	0.10 to	0.08 to	0.10 to
Modulus of Elasticity, million psi	0.110	0.120	0.120	0.120	0.11	0.15	0.11	0.15
IZOD AB impact, ft-lb	40 to	50 to	45 to	60 to	75 to	80 to	75 to	80 to
	50,000	60,000	55,000	75,000	85,000	110,000	85,000	110,000
	24-26	24-26	24-26	24-26	24-26	24-26	24-26	24-26
	20-30	25-40	25-35	35-55	35-45	35-55	35-45	35-45

TABLE-2.3

COMPOSITION, PROPERTIES AND APPLICATIONS OF VARIOUS Cr-Ni-WHITE CAST IRONS

Sl. No.	Type/Class Designation	I.C.	COMPOSITION							S	P	Other element	Hardness	Wear rate relative to Pearlitic White Iron
			Si	Mn	Cr	Ni	Mo	Other element	Hardness					
1	2	3	4	5	6	7	8	9	10	11	12	13		
1.	Martensitic Ni-Cr	3.2	0.5	0.6	2.0	4.5	0.12	0.2	—	—	60	Wear rate relative to Pearlitic White Iron		
													Ball mill end liner	
													55	
													80	
													Application	
													Mill liners	
2.	Martensitic Ni-Cr	3.2	0.5	0.6	2.0	4.5	0.12	0.2	—	550-650 BHN	Microstructure M A			
3.	Martensitic Ni-Cr	3.5	0.5	0.6	2.0	3.0	0.12	0.1	1.0 Mo	600-650 BHN	M A			
4.	Martensitic Ni-Cr	3.2	0.5	0.3	1.4	3.5	0.15	0.2	—	555-627 BHN	M A		Mill liners	
5.	L.C. White Iron	2.2-2.8	1.0-1.6	0.2-0.6	1.0	1.5	0.15	0.15	0.5 Mo	—	—	CP (as-cast)	Grinding balls	
													(a) Where a single value is given rather than a range that value is a maximum limit.	
6.	H.C.L. Si, White Iron	2.8-3.6	0.3-1.0	0.3-2.0	3.0	2.5	0.15	0.5	1.0 Mo	—	CP (as-cast)	CP	Coarse Pearlites	
													MA — Martensite Austenite	
7.	Martensitic Ni-Cr Iron	2.5-3.7	0.8	1.3	1.1-4.0	2.7-5.0	0.15	0.3	1.0 Mo	—	M A			
8.	Alloyed Intermediate	3.4	0.6	0.3	1.25	4.5	0.1	0.35	0.4 Mo	690-830 VP	Precise hardness obtained will depend on specific composition & section size			
9.	Alloyed Intermediate hardness	3.4	0.8	0.3	0.6	2.5	0.1	0.35	0.4 Mo	610-690 VP				
10.	Chill Cast Ni-Cr iron	2.85	0.56	0.48	0.98	1.67	—	—	—	600 BHN	Micro-structure Carbides in Fine Pearlite	Wear rate (Relative)		
													134	
11.	Chill Cast Ni-Cr iron	2.83	0.60	0.50	1.33	2.2	—	—	—	627 BHN	Carbides in very fine pearlite		124	
12.	Chill Cast Ni-Cr iron	2.87	0.60	0.50	1.55	2.54	—	—	—	600 BHN	Carbides in Martensitic matrix		59	

	1	2	3	4	5	6	7	8	9	10	11	12	13
13. Chill Cast Ni-Cr iron		3.79	0.55	0.50	1.49	2.61						744 BHN	Carbides in Martensitic Matrix
14. Martensitic Ni-Cr iron		2.8	0.5	0.3	1.4	2.5	0.15	0.1					Relative wear rate 106 (Where Martensitic forged steel — (0.8% C, 0.3% Si, 0.7% Mn, 0.2% Cr, 0.2% Mo, 0.3% S, 0.01% P) had a nominally assigned relative wear rate of 100)
15. ASTM I A-532 Grade 1		3.0-3.6	0.3-0.8	0.3-0.8	1.4-2.5	3.3-0.5	0.15	0.3	0.75	Mo		500 SC 600 CC	
16. I -750 Grade 2		2.5-3.0	0.3-0.8	0.3-0.8	1.4-2.5	3.3-5.0	0.15	0.3	0.75	Mo		450 SC 500 CC	MHN
17. I Grade 3		2.9-3.7	0.3-0.6	0.2-0.5	1.1-1.5	2.7-4.0	0.15	0.3	0.75	Mo		525 SC 600 CC	

SC-SAND CAST, CC-CHILL CAST

PHYSICAL AND MECHANICAL PROPERTIES

1. Specific gravity	7.6-7.8 (Ni-Cr cast iron)	Martensitic white	4. Modulus of elasticity lb./in. ² x 10 ⁸	24-26 (2.5-4.75% Ni, 2.75-3.5% C) 16-17 (2.5-4.75% Ni, H.C. 3-3.5% C)
2. Coefficient of thermal expansion (Micro-in per in per °F)	8-9 x 10 ⁻⁶ (2.5-4.75% Ni, H.C) 3-3.5% C 12.2-14.2 x 10 ⁻⁶ (2.5-4.75% Ni, L.C. 2.75-2.9% C)		5. Tensile strength, ton/in. ²	21-36 (2.5-4.75% Ni, L.C 2.75-2.9% C)
	0-430°C 0-95°C		6. Hardness (DPN)	590-800 (2.5-4.75% Ni, H.C. 3-3.5% C)
3. Electrical resistivity microhm/cm ³ at 78°F	80-100		7. Transverse rupture stress ton/in. ²	550-650 (2.5-4.75% Ni, L.C. 2.75-2.9% C)
			8. Transverse deflection (12 in bar, 12 in span) in.	31-53 (H.C. 2.5-4.75% Ni) 35-55 (L.C. 2.5-4.75% Ni) 0.08-0.11 (H.C. 2.5-4.75% Ni) 0.1-0.12 (L.C. 2.5-4.75% Ni)

TABLE-2.4

COMPOSITION AND PROPERTIES OF SOME REPRESENTATIVE CHROMIUM WHITE IRONS

Sl. No.	Type/class/Designation	T.C.	Si	Mn	Composition Cr	P	S	Hardness BHN
1.	Cupola white iron (1% Cr)	3.30-3.60	0.40-1.0	0.5-0.70	0.80-1.00	0.3 (Max)	0.15 (Max)	444
2.	High Cr white iron	2.25-2.85	0.25-1.0	0.5-1.25	24.00-30.00	0.3 (Max)	0.15 (Max)	500
3.	Pearlitic	3.3	0.5	0.5	1.0	0.20	0.12	444
4.	Sand cast** Pearlitic	3.2-3.5	—	—	1.2	—	—	—
5.	Plain Cr white iron	3.50	0.5	0.5	1.0	0.30	0.12	444-477
6.	Plain Cr white iron	3.20	0.6	0.5	2.0	0.15	0.15	477-555
7.	Low Cr Iron (chill cast)	3.20	1.7	0.4	0.9	—	—	477
8.	Low Cr iron (sand cast)	3.00	0.9	0.6	0.8	—	—	477
9.	Sand cast 5% Cr Iron	3.65	0.6	0.6	5.0	—	—	514
10.	Pearlitic Cr-iron	3.00	0.6	0.5	2.0	0.10	0.15	—
11.	30% Cr	2.5-2.9	0.33-0.65	0.6-0.8	28.00-33.0	0.10	0.10	340-420
**Transverse strength (kg)		Deflection (mm)		Toughness (kgm)				
635-815		2.0-2.3		1.27-1.87				

TABLE-2.5

RANGES OF ALLOY CONTENT FOR THE CORROSION & HEAT RESISTANT ALLOYED GREY CAST IRONS

Description	TC(a)	Mn	COMPOSITION, (Wt %)					Cr	Mo	Cu	Matrix structure as-cast(c)
			P	S	Si	Ni	Ni				
Corrosion-Resistant Irons											
High silicon iron(d)	0.4-1.1	1.5	0.15	0.15	14-17	...	5.0	1.0	0.5	F	
Ni-Cr grey iron(e)	3.0	0.5-1.5	0.08	0.12	1.0-2.8	13.5-36	1.5-8.0	1.0	7.0	A	
Ni-Cr ductile iron(f)	3.0	0.7-4.5	0.08	0.12	1.0-3.0	18-36	1.5-5.5	1.0	...	A	
Heat-Resistant Grey Irons											
Medium silicon iron(g)	1.6-2.5	0.4-0.8	0.30	0.10	4.0-7.0	F	
High Cr-iron	1.2-4.0	0.3-1.5	0.15	0.15	0.5-3.0	5.0	12-35	4.0	3.0	F,CP	
Ni-Cr iron(e)	1.8-3.0	0.4-1.5	0.15	0.15	1.0-2.7	13.5-36	1.8-8.0	1.0	7.0	A	
Ni-Cr-Si iron(h)	1.8-2.6	0.4-1.0	0.10	0.10	5.0-6.0	13-43	1.8-5.5	1.0	...	A	
Heat-Resistant Ductile Irons											
High Al-iron	1.3-2.0	0.4-1.0	0.15	0.15	1.3-6.0	...	20-25 Al	F	
Medium Si-ductile iron	2.8-3.8	0.2-0.6	0.08	0.12	2.5-6.0	1.5	F	
Ni-Cr ductile iron(f)	3.0	0.7-2.4	0.08	0.12	1.75-5.5	18-36	1.75-3.5	1.0	...	A	

(a) Where a single value is given rather than a range, that value is a maximum limit
 (b) Total Carbon
 (c) F, Ferrite; A, austenite; CP, coarse pearlite
 (d) such as Duriron, Durichlor 51, Superchlor
 (e) Such as Ni-Resist austenitic iron (ASTM A438)
 (f) Such as Ni-Resist austenitic ductile iron (ASTM A439)
 (g) Such as Silal
 (h) Such as Microsilal

TABLE-2.6a

IRON CARBIDE IN Fe-C-Cr ALLOYING SYSTEM

Type	Crystalline system	Lattice const.	Specific gravity	
$(Fe, Cr)_3C$	Rhombic	a=4.52 b=5.09 c=6.74	7.67	can contain a maximum of 18% Cr
	Hexagonal	a=6.88 b=4.54 a=4.54		
$(Fe, Cr)_3C_3$	Rhombic	b=6.88 c=11.94	6.92	can contain a maximum of 50% Cr
	Rhombohedral	a=13.98 b= 4.52		
$(Cr, Fe)_{23}C_6$	F.C.C	a=10.64 a=2.82	6.97	Max. 35% Fe
$(Cr, Fe)_3C_2$	Rhombic	b=5.52 c=11.46	6.68	little Fe

Microconstituent(s)	Microhardness
M3C	840-1100 HV
M7C3	1200-1800 HV
M3C(low Cr irons)	1060-1240 HV
M7C3(high Cr irons)	1500-1800 HV
Pearlite	300-960 HV
Pearlite(high carbon)	240-425 HV
Austenite(high Cr)	300-600 HV
Austenite(high Cr)	350-400 HV
Martensite	500-1000 HV
Martensite(high carbon)	770-800 HV

TABLE-2.6b

INFORMATION ON CHROMIUM, MANGANESE, AND IRON BEARING CARBIDES

Base Metal	Carbide	Crystal structure		Stability Range, °C	Melting Point, °C	Harness
		Type	Spacing, Å			
Cr	Cr ₂₃ C ₆	Comp. Cubic	10.60	upto 1577	1580	1000 Kg/mm ² *
	Cr ₇ C ₃	Comp. hex.	a= 4.53 c=14.01	upto 1768	1780	1600 Kg/mm ² *
	Cr ₃ C ₂	Ortho.	a= 2.82 b= 5.53 c=11.47	upto 1813	1895	1300 Kg/mm ² *
Mn	Mn ₂₃ C ₆	Comp. cubic	a=10.586	upto 1025	1010	
	Mn ₇ C ₂	-----	-----	850-1000		
	Mn ₃ C	Ortho.	a=5.0806 b=6.772 c=4.530	950-1050	1520	
	Mn ₅ C ₂	Mono-	a=5.806 b=4.573 c=11.66 β=92.75°	upto 1050	-----	
	Mn ₇ C ₃	Comp. hex.	a=13.838 c=4.539	upto 1100	1340	840 Brin
Fe	Fe ₃ C	Ortho. rhombic	a=5.088 b=6.744 c=4.524	upto 1227	1650	
	Fe ₅ C ₂	Mono-clinic	a=11.563 b=4.573 c=5.058 β=	upto 350	-----	

* hardness at 50-200 gms. load

TABLE-2.7a

COMPOSITION OF Cr-Mo TYPE ABRASION RESISTANT ALLOY CAST IRONS

Sl. No.	Type/Class/Designation	T.C.	Composition						Other element	Hardness BHN	Micro-structure
			Si	Mn	Cr	Mo	S	P			
1.	ASTM II A-532-750 Grade 1	3.1-3.6	0.3-0.8	0.4-0.9	14.0-18.0	2.5-4.5	0.06 Max	0.1 Max	0.5 Ni	—	—
2.	II Grade 2	2.4-3.1	0.3-0.8	0.4-0.9	14.0-18.0	2.5-3.5	0.06 Max	0.1 Max	0.5 Ni	—	—
3.	III Grade 2	2.3-3.0	0.2-1.5	1.5 Max	24.0-28.0	0.06 Max	0.06 Max	0.1 Max	0.5 Ni	—	—
4.	Martensitic 15% Cr, H.C.	3.25	0.6	0.7	15.0	3.0	0.03	.06	—	600-750	M.A.
5.	Martensitic 27%Cr	2.75	0.7	0.7	27.0	3.0	0.03	.06	—	653	—
6.	Martensitic 15% Cr, 3% Mo	2.75	0.7	0.7	15.0	10.5	0.03	.06	—	712	—
7.	Sand cast	2.8-3.4	—	—	12-16	2.4	—	—	—	—	—
8.	Sand cast	3.5-4.1	—	—	12-16	2.5-3.0	—	—	—	—	—
9.	Chill cast martensitic	3.2-3.4	—	—	12-16	1.5-3.0	—	—	—	—	—
10.	Chill cast martensitic	3.5-4.1	—	—	12-16	2.5-3.0	—	—	—	—	—
11.	12-18% Cr, 2-4% Mo	3.0-4.0	0.4-1.0	0.5-0.9	12-18	2-4	0.06	0.1	—	600-950	VPN

TABLE-2.7b

PROPERTIES OF Cr-Mo IRONS
(FROM SI. no. 5 TO 10 OF TABLE-1.5a)

St. No.	Type/Class/Designation	Wear rate relative to pearlitic iron*			Akin classifier wear shoes	Flotation impellers
		Crushing plant chute liners	Ball Mill end liners			
5.	Martensitic 27% Cr	70	49	48	27	
6.	Martensitic 15% Cr, 3% Mo	51	44	44	—	
—————						
		Transverse strength (kg.)	Deflection (mm)	Toughness** kgm.		
7.	Sand cast	1015-1370	3.2-3.6	3.25- 4.93		
8.	Sand cast	800-1000	2.0-2.8	1.60- 2.8		
9.	Chill cast Martensitic	1980-2300	5.1-6.5	10. 1-15.0		
10.	Chill cast martensitic	1270-1570	3.6-3.8	4.57- 5.9		

* The pearlitic white iron (3.3%C, 0.5% Mn, 0.5% Si, 1.0% Cr, 0.12% S, 0.2% P) had a nominally assigned relative wear rate of 100 in each application. The other wear rates are relative to this rate of the pearlitic white iron.

** Data from as cast 30.5mm dia. test bars broken over a 457 mm span. Relative toughness evaluated as product of transverse strength.

TABLE-2.8a

COMPOSITION OF Cr-X TYPE ABRASION RESISTANT IRONS

Class	Type	Designation	C%	Mn%	Si%	Ni%	Cr%	Mo%	P%	S%	Cu%
I	A	Ni-Cr-HC	3.0			3.3	1.4				minimum
	B	Ni-Cr-LC	3.6	1.3	0.8	5.0	4.0	1.0	0.3	0.15	maximum
I	A	Ni-Cr-LC	2.5			3.3	1.4				minimum
	B	Ni-Cr-LC	3.0	1.3	0.8	5.0	4.0	1.0	0.3	0.15	maximum
I	A	Ni-Cr-GB	2.9			2.7	1.1				minimum
	B	Ni-Cr-GB	3.7	1.3	0.8	4.0	1.5	1.0	0.3	0.15	maximum
I	A	Ni-HiCr	2.5			5.0	7.0				minimum
	B	Ni-HiCr	3.6	1.3	2.2	7.0	11.0	1.0	0.10	0.15	maximum
II	A	12% Cr	2.4	0.5	1.0	0.5	11.0	0.5	0.10	0.06	1.2
	B	15% Cr-Mo-LC	2.8	1.5	1.0	0.5	14.0	1.0	0.10	0.06	1.2
II	A	15% Cr-Mo-LC	2.4	0.5	1.0	0.5	14.0	1.0	0.10	0.06	1.2
	B	15% Cr-Mo-LC	2.8	1.5	1.0	0.5	18.0	3.0	0.10	0.06	1.2
II	A	15% Cr-Mo-HC	2.8	0.5	1.0	0.5	14.0	2.3	0.10	0.06	1.2
	B	15% Cr-Mo-HC	3.6	1.5	1.0	0.5	18.0	3.5	0.10	0.06	1.2
II	A	20% Cr-Mo-LC	2.0	0.5	1.0	1.5	23.0	1.5	0.10	0.06	1.2
	B	20% Cr-Mo-LC	2.6	1.5	1.0	1.5	23.0	1.0	0.10	0.06	1.2
II	A	20% Cr-Mo-HC	2.6	0.5	1.0	1.5	23.0	2.0	0.10	0.06	1.2
	B	20% Cr-Mo-HC	3.2	1.5	1.0	1.5	23.0	2.0	0.10	0.06	1.2
III	A	25% Cr	2.3	0.5	1.0	1.5	23.0				minimum
	B	25% Cr	3.0	1.5	1.0	1.5	28.0	1.5	0.10	0.06	1.2

TABLE-2.8b

TYPICAL PROPERTIES OF Cr-X TYPE IRONS

Class	Type	Designation	Sand cast (minimum)			Brinell hardness			Softened (minimum)	Typical section thickness (mm)
			Sand cast (minimum)	Chill cast (minimum)	Hardened (minimum)	Chill cast (minimum)	Hardened (minimum)			
I	A	Ni-Cr-HC	550	600					200	
	B	Ni-Cr-LC	550	600					200	
I	A	Ni-Cr-LC	550	600					75 diameter ball	
	B	Ni-Cr-LC	550	600					300	
I	A	Ni-HiCr	550	500				400	25 diameter ball	
	B	Ni-HiCr	550	500				400	100	
II	A	12% Cr	550	500	600	600	600	400	75	
	B	15% Cr-Mo-LC	450	500	600	600	600	400	200	
II	A	15% Cr-Mo-LC	550	500	600	600	600	400	300	
	B	15% Cr-Mo-LC	450	500	600	600	600	400	200	
II	A	20% Cr-Mo-LC	450	500	600	600	600	400	300	
	B	20% Cr-Mo-LC	450	500	600	600	600	400	200	
III	A	25% Cr	450	500	600	600	600	400	300	
	B	25% Cr	450	500	600	600	600	400	200	

TABLE-3.1

Summary of the structure-property relations in some Fe-Mn-Cr-Cu corrosion resistant cast irons

(1) Alloys studied	3%C, 5%Cr, 6.8%Mn, 1.5-3.0%Cu cast irons
(2) Heat treatments	Held at 800,850,900,950,1000 and 1050°C for 2,4,6,8, and 10 hours followed by OQ(62) and AC(83).
(3) Microstructures	(a) As-Cast: P/B + M + MC + some RA (b) Upto 900°C: M + τ + MC + DC (c) Upto 1000°C: τ + DC + MC or τ + MC (d) At 1050°C: τ + MC (M_7C_3 in eutectic form)
(4) Effect of cooling	OQ: larger τ , lesser DC AC: more DC, lesser τ , 'M' up to higher heat treating temperatures
(5) various carbides formed	M_3C , M_5C_2 , M_7C_3 , and $M_{23}C_6$ M_3C : up to 950°C prolonged soaking $M_{23}C_6$: boundary carbide up to 900°C, 10 hrs. M_5C_2 & M_7C_3 : up to 1050°C
(6) Structure-Property interrelations	
(a) Martensite :	Resists corrosion, but embrittles
(b) Austenite :	Most desirable matrix to resist corrosion & to give good strength and ductility. Increase in the amount and stability enhance properties.
(c) Dispersed Carbides:	
	-They precipitate as M_3C/M_5C_2 from matrix during heat treatment (represented as no. of particles or by distribution factor). -Overall adverse effect on properties;attains a maximum at 950°C, 10 hours treatment
(d) Massive carbides:	
	-Represented as area fraction -Platy morphology in as-cast/low temperature heat treatments -Rounding-off at $\geq 950^\circ\text{C}$ -Platy morphology detrimental to properties (corrosion & mechanical) -Near rounded/hexagonal forms preferred

(e) Grain boundary carbide $M_{23}C_6$:

-Adversely affects corrosion resistance and deformation behaviour

(f) M_7C_3 & M_5C_2 :

- M_7C_3 present in the form of MC and also as eutectic carbide (eutectic form not preferred)

- M_5C_2 present as MC and part of DC

(7) Structure-property correlations (Models):

(a) Heat treating temperature, time and hardness

(b) Weight gain as a function of temperature

(c) A correlation between corrosion rate and microstructure denoting the effect of MC & DC

(d) Interrelating corrosion & deformation behaviour

TABLE 4.1
CHEMICAL ANALYSIS OF RAW MATERIALS

Raw Material	C	Si	P	S	Mn	Cr	Cu
Pig Iron	3.55	2.15	0.40	0.05	1.12	----	----
Ferro-Chromium (low carbon)	0.10 max.	0.70 max.	0.03 max.	0.01 max.	----	67.0- 75.0	----
Ferro-Manganese (low carbon)	0.03 max.	----	0.03 max.	0.008	97.0	----	----
Ferro-Silicon (low carbon)	0.03 max.	75.0	----	----	----	----	----
Copper (Electrolytic)	----	----	----	----	----	----	99.99

TABLE 4.2
CHEMICAL ANALYSIS OF ALLOYS (WEIGHT PERCENT)

Alloy	C	S	P	Si	Mn	Cr	Cu
C1	3.66	0.041	0.30	1.83	10.38	6.80	1.48
C2	3.68	0.040	0.29	1.81	10.36	6.78	2.94
C3	3.66	0.038	0.29	1.84	10.36	6.80	4.86

EFFECT OF SOAKING PERIOD ON HARDNESS IN A.C.CONDITION

ALLOY : C 1
TABLE : 5.1

AS CAST HARDNESS(HV30)= 618
TEMPERATURE (DEG.C)= 800

TIME (HRS)	HARDNESS (HV30)										SD	AVERAGE (HV30)
2	598	598	598	594	594	594	594	594	590	590	6.59	589
	590	590	590	586	586	586	583	583	583	571		
4	586	586	586	583	583	583	583	583	579	579	7.46	576
	579	575	575	575	568	568	568	568	565	565		
6	602	602	598	598	594	594	590	590	590	583	9.35	586
	583	583	583	583	579	579	579	579	571	571		
8	610	610	598	598	598	594	594	594	594	590	8.30	591
	586	586	586	586	586	586	586	586	583	579		
10	590	590	590	590	590	590	590	590	583	583	6.65	583
	583	583	583	579	579	579	579	579	579	564		

FOR DEGREE OF 1 COEFFICIENTS ARE
584.10000000 .15000000
BEST FIT VALUES 584.4 584.7 585.0 585.3 585.6
STANDARD DEVIATION IS 6.7601650
FOR DEGREE OF 2 COEFFICIENTS ARE
586.60000000 -.92142860 .08928572
BEST FIT VALUES 585.1 584.3 584.3 584.9 586.3
STANDARD DEVIATION IS 8.2254070
FOR DEGREE OF 3 COEFFICIENTS ARE
637.00230000 -36.32302000 6.83959100 -.37501700
BEST FIT VALUES 588.7 577.1 584.3 592.1 582.7
STANDARD DEVIATION IS 2.3904570

TABLE : 5.2

TEMPERATURE (DEG.C)= 850

2	579	579	579	575	575	575	575	575	571	571	7.08	569
	571	568	568	568	561	561	561	561	561	557		
4	586	586	586	579	579	579	579	579	579	579	6.91	575
	575	575	575	575	568	568	568	568	564	564		
6	586	586	586	586	586	586	583	583	579	579	7.02	578
	579	579	579	579	575	575	571	571	564	564		
8	571	571	571	571	564	564	564	564	561	561	10.16	558
	561	561	561	557	557	543	554	543	540	540		
10	561	561	557	557	557	554	554	554	554	554	5.96	552
	554	554	550	550	550	550	547	543	540	540		

FOR DEGREE OF 1 COEFFICIENTS ARE
581.70000000 -2.55000000
BEST FIT VALUES 576.6 571.5 566.4 561.3 556.2
STANDARD DEVIATION IS 8.8147600
FOR DEGREE OF 2 COEFFICIENTS ARE
558.19900000 7.52184700 -.83932060
BEST FIT VALUES 569.9 574.9 573.1 564.7 549.5
STANDARD DEVIATION IS 6.1365370
FOR DEGREE OF 3 COEFFICIENTS ARE
534.39240000 24.24319000 -4.02771100 .17713280
BEST FIT VALUES 568.2 578.3 573.1 561.3 551.2
STANDARD DEVIATION IS 6.8128100

EFFECT OF SOAKING PERIOD ON HARDNESS IN A.C. CONDITION

ALLOY : C 1
TABLE : 5.3

AS CAST HARDNESS(HV30)= 618
TEMPERATURE.(DEG.C)= 900

TIME (HRS)	HARDNESS (HV30)										SD	AVERAGE (HV30)
2	571	571	571	571	564	564	564	564	561	561		
	561	561	561	557	557	557	554	554	550	547	6.88	561
4	561	561	557	557	557	557	557	557	557	557		
	554	554	554	554	554	554	550	550	543	543	4.82	554
6	568	568	564	564	564	561	561	561	561	561		
	557	557	557	554	554	550	550	550	550	547	6.35	557
8	561	557	557	557	554	550	550	550	547	547		
	543	543	543	543	543	540	540	540	537	537	7.25	546
10	547	547	547	547	547	547	540	540	540	540		
	537	537	533	533	533	533	533	523	523	523	8.27	537

FOR DEGREE OF 1 COEFFICIENTS ARE
567.80000000 -2.80000000
BEST FIT VALUES 562.2 556.6 551.0 545.4 539.8
STANDARD DEVIATION IS 4.1793090

FOR DEGREE OF 2 COEFFICIENTS ARE
558.80000000 1.05714300 -.32142860
BEST FIT VALUES 559.6 557.9 553.6 546.7 537.2
STANDARD DEVIATION IS 3.8247300

FOR DEGREE OF 3 COEFFICIENTS ARE
570.00150000 -6.81059200 1.17877500 -.08334464
BEST FIT VALUES 560.4 556.3 553.6 548.3 536.4
STANDARD DEVIATION IS 4.7809440

TABLE : 5.4

TEMPERATURE (DEG.C)= 950

2	550	550	550	550	547	547	547	547	547	543		
	543	543	540	537	537	537	533	533	533	533	6.43	542
4	550	550	543	543	543	543	540	540	540	540		
	537	537	533	533	533	530	530	530	530	530	6.49	537
6	540	540	537	537	533	533	533	530	530	527		
	527	527	527	527	527	527	527	523	523	523	5.35	529
8	530	530	530	530	530	530	527	527	523	520		
	517	514	514	514	514	514	508	505	505	505	9.48	519
10	523	523	520	520	520	520	517	517	514	514		
	514	514	514	514	514	514	514	511	511	511	3.80	515

FOR DEGREE OF 1 COEFFICIENTS ARE
550.00020000 -3.60002400
BEST FIT VALUES 542.8 535.6 528.4 521.2 514.0
STANDARD DEVIATION IS 1.7127020

FOR DEGREE OF 2 COEFFICIENTS ARE
550.00120000 -3.60044300 .00003488
BEST FIT VALUES 542.8 535.6 528.4 521.2 514.0
STANDARD DEVIATION IS 2.0975890

FOR DEGREE OF 3 COEFFICIENTS ARE
537.41420000 5.24035400 -1.68571000 .09365252
BEST FIT VALUES 541.9 537.4 528.4 519.4 514.9
STANDARD DEVIATION IS .8367019

EFFECT OF SOAKING PERIOD ON HARDNESS IN A.C. CONDITION

ALLOY : C 1 AS CAST HARDNESS(HV30)= 618
 TABLE : 5.5 TEMPERATURE (DEG.C)=1000

TIME (HRS)	HARDNESS (HV30)										SD	AVERAGE (HV30)
2	527	527	523	523	520	520	517	514	514	511		
	511	508	508	505	505	505	502	502	502	502	8.68	512
4	514	514	514	514	508	508	508	508	508	508		
	508	505	505	505	505	505	502	502	502	502	4.12	507
6	496	496	496	496	493	493	490	490	487	487		
	487	487	487	484	484	484	481	476	476	476	6.64	487
8	511	511	499	499	499	496	493	493	493	493		
	490	490	487	487	487	487	487	484	484	484	7.96	492
10	502	502	499	499	496	496	493	490	490	484		
	484	484	484	484	481	481	478	478	473	473	9.23	487

FOR DEGREE OF 1 COEFFICIENTS ARE
 516.50000000 -3.25000000
 BEST FIT VALUES 510.0 503.5 497.0 490.5 484.0
 STANDARD DEVIATION IS 6.5192020
 FOR DEGREE OF 2 COEFFICIENTS ARE
 529.00000000 -8.60714300 .44642860
 BEST FIT VALUES 513.6 501.7 493.4 488.7 487.6
 STANDARD DEVIATION IS 6.4364880
 FOR DEGREE OF 3 COEFFICIENTS ARE
 522.00020000 -3.69060900 -.49104600 .05208192
 BEST FIT VALUES 513.1 502.7 493.4 487.7 488.1
 STANDARD DEVIATION IS 8.9642070

TABLE : 5.6 TEMPERATURE (DEG.C)= 1050

2	511	511	499	499	499	496	493	493	493	490		
	487	487	487	487	487	484	484	484	484	478	8.79	491
4	484	484	484	481	481	481	481	476	476	476		
	476	476	473	473	470	470	465	465	465	459	7.27	474
6	499	493	493	490	490	487	484	484	481	481		
	478	478	478	478	473	473	467	467	465	465	9.96	480
8	487	478	484	481	478	476	476	473	473	470		
	470	467	467	467	467	465	465	462	462	459	7.69	471
10	462	462	462	459	459	459	451	451	451	451		
	449	449	449	449	446	444	444	441	441	441	7.23	451

FOR DEGREE OF 1 COEFFICIENTS ARE
 498.30000000 -4.15000000
 BEST FIT VALUES 490.0 481.7 473.4 465.1 456.8
 STANDARD DEVIATION IS 7.5784770
 FOR DEGREE OF 2 COEFFICIENTS ARE
 487.80000000 .34999990 -.37500000
 BEST FIT VALUES 487.0 483.2 476.4 466.6 453.8
 STANDARD DEVIATION IS 8.3904670
 FOR DEGREE OF 3 COEFFICIENTS ARE
 535.39500000 -33.07986000 5.99933900 -.35412990
 BEST FIT VALUES 490.4 476.4 476.4 473.4 450.4
 STANDARD DEVIATION IS 5.0199710

EFFECT OF SOAKING PERIOD ON HARDNESS IN A.C. CONDITION

ALLOY : C 2
TABLE : 5.7

AS CAST HARDNESS(HV30)= 583
TEMPERATURE (DEG.C)= 800

TIME (HRS)	HARDNESS (HV30)										SD	AVERAGE (HV30)
2	575	571	571	571	571	571	568	568	568	568		
	564	564	564	564	557	557	557	557	554	554	6.56	564
4	568	568	568	568	564	564	564	564	564	561		
	561	561	561	554	557	554	550	550	550	550	6.57	560
6	568	568	564	557	557	557	557	557	554	550		
	550	550	550	550	547	547	543	543	543	543	7.84	552
8	568	568	564	557	557	557	554	550	547	547		
	547	543	543	543	543	540	540	540	540	537	9.70	549
10	547	543	543	540	537	537	533	533	530	530		
	530	530	530	530	527	527	527	523	523	523	6.98	532

FOR DEGREE OF 1 COEFFICIENTS ARE
573.90000000 -3.75000000
BEST FIT VALUES 566.4 558.9 551.4 543.9 536.4
STANDARD DEVIATION IS 4.1912610
FOR DEGREE OF 2 COEFFICIENTS ARE
563.39900000 .75041870 -.37503490
BEST FIT VALUES 563.4 560.4 554.4 545.4 533.4
STANDARD DEVIATION IS 3.2557920
FOR DEGREE OF 3 COEFFICIENTS ARE
577.38960000 -9.07624900 1.49869400 -.10409600
BEST FIT VALUES 564.4 558.4 554.4 547.4 532.4
STANDARD DEVIATION IS 3.3466550

TABLE : 5.8

TEMPERATURE (DEG.C)= 850

2	568	568	564	564	564	561	561	561	561	561		
	557	557	557	554	554	550	550	550	550	547	6.35	557
4	561	557	557	557	554	550	550	550	547	547		
	547	547	543	543	543	543	543	540	540	537	6.64	547
6	547	547	547	543	543	533	530	530	530	530		
	530	530	530	527	527	527	527	523	523	523	8.23	532
8	533	533	523	523	523	523	520	517	517	517		
	517	517	517	514	514	514	514	511	511	511	6.35	518
10	527	527	527	527	527	523	523	523	523	520		
	520	520	517	517	517	517	517	517	517	514	4.35	521

FOR DEGREE OF 1 COEFFICIENTS ARE
565.30000000 -5.05000000
BEST FIT VALUES 555.2 545.1 535.0 524.9 514.8
STANDARD DEVIATION IS 5.8280840
FOR DEGREE OF 2 COEFFICIENTS ARE
578.80000000 -10.83571000 .48214290
BEST FIT VALUES 559.1 543.2 531.1 523.0 518.7
STANDARD DEVIATION IS 4.9914500
FOR DEGREE OF 3 COEFFICIENTS ARE
548.00270000 10.79575000 -3.64250100 .22914690
BEST FIT VALUES 556.9 547.6 531.1 518.6 520.9
STANDARD DEVIATION IS 1.1952140

EFFECT OF SOAKING PERIOD ON HARDNESS IN A.C. CONDITION

ALLOY : C 2 AS CAST HARDNESS(HV30)= 583
 TABLE : 5.9 TEMPERATURE (DEG.C)= 900

TIME (HRS)	HARDNESS (HV30)										SD	AVERAGE (HV30)
2	568	564	564	564	561	561	561	561	561	557	5.63	557
	557	557	557	557	554	554	550	550	550	547		
4	575	575	575	571	571	571	568	568	568	568	7.16	564
	564	564	561	561	557	557	557	557	554	554		
6	547	547	547	540	537	533	533	533	530	530	7.63	532
	530	530	530	530	527	527	527	523	523	523		
8	540	540	540	533	533	533	530	530	530	527	11.55	524
	527	523	523	520	508	517	514	508	505	505		
10	533	523	523	523	523	520	517	517	517	517	5.56	517
	517	517	514	514	514	514	511	511	511	511		

FOR DEGREE OF 1 COEFFICIENTS ARE
 574.80000000 -6.00000000
 BEST FIT VALUES 562.8 550.8 538.8 526.8 514.8
 STANDARD DEVIATION IS 9.4304480
 FOR DEGREE OF 2 COEFFICIENTS ARE
 572.80000000 -5.14285700 -.07142857
 BEST FIT VALUES 562.2 551.1 539.4 527.1 514.2
 STANDARD DEVIATION IS 11.5251300
 FOR DEGREE OF 3 COEFFICIENTS ARE
 516.80150000 34.18941000 -7.57122500 .41665540
 BEST FIT VALUES 558.2 559.1 539.4 519.1 518.2
 STANDARD DEVIATION IS 10.2789600

TABLE : 5.10 TEMPERATURE (DEG.C)= 950

2	527	527	520	517	517	517	517	517	517	517	4.40	516
	514	514	514	514	514	514	514	511	511	511		
4	527	527	523	523	520	520	517	514	514	511	8.68	512
	511	508	508	505	505	505	502	502	502	502		
6	533	533	533	533	530	530	530	530	527	527	5.45	526
	527	527	527	527	527	527	523	517	517	514		
8	511	511	508	508	508	505	505	505	502	499	7.79	499
	499	499	499	496	496	493	493	487	487	487		
10	511	511	508	505	505	502	502	499	499	499	7.44	498
	499	499	499	496	496	496	493	490	484	484		

FOR DEGREE OF 1 COEFFICIENTS ARE
 524.90000000 -2.45000000
 BEST FIT VALUES 520.0 515.1 510.2 505.3 500.4
 STANDARD DEVIATION IS 10.3392500
 FOR DEGREE OF 2 COEFFICIENTS ARE
 507.40000000 5.05000000 -.62500000
 BEST FIT VALUES 515.0 517.6 515.2 507.8 495.4
 STANDARD DEVIATION IS 10.7981600
 FOR DEGREE OF 3 COEFFICIENTS ARE
 496.19850000 12.91774000 -2.12520400 .08334464
 BEST FIT VALUES 514.2 519.1 515.2 506.2 496.2
 STANDARD DEVIATION IS 15.0599000

EFFECT OF SOAKING PERIOD ON HARDNESS IN A.C. CONDITION

ALLOY : C 2
TABLE : 5.11

AS CAST HARDNESS(HV30)= 583
TEMPERATURE (DEG.C)= 1000

TIME (HRS)	HARDNESS (HV30)										SD	AVERAGE (HV30)
2	493	493	487	487	487	484	484	484	481	481		
	481	481	481	481	478	478	478	476	476	476	5.07	482
4	517	517	514	514	511	511	508	508	502	502		
	499	496	496	496	496	496	493	493	484	484	10.18	501
6	462	462	457	457	457	454	454	454	451	451		
	449	449	449	449	449	446	446	446	441	441	5.94	451
8	409	409	409	409	406	406	406	406	406	404		
	404	404	404	404	404	402	402	402	398	398	3.22	404
10	398	398	398	398	398	393	393	393	391	391		
	387	387	383	383	381	381	377	377	375	375	8.34	387

FOR DEGREE OF 1 COEFFICIENTS ARE
531.10000000 -14.35000000
BEST FIT VALUES 502.4 473.7 445.0 416.3 387.6
STANDARD DEVIATION IS 21.2061300
FOR DEGREE OF 2 COEFFICIENTS ARE
496.60000000 .43571280 -1.23214300
BEST FIT VALUES 492.5 478.6 454.9 421.2 377.7
STANDARD DEVIATION IS 22.4614000
FOR DEGREE OF 3 COEFFICIENTS ARE
358.00740000 97.78052000 -19.79365000 1.03119500
BEST FIT VALUES 482.6 498.4 454.9 401.4 387.6
STANDARD DEVIATION IS 5.3785110

TABLE : 5.12

TEMPERATURE (DEG.C)= 1050

2	467	467	465	462	462	462	462	457	457	454		
	454	449	449	449	449	449	446	446	446	441	7.98	454
4	451	451	449	446	446	446	446	446	446	444		
	444	444	444	444	441	439	439	439	432	422	6.64	442
6	459	459	457	457	457	451	451	451	446	444		
	444	441	436	439	436	434	434	432	432	427	10.37	444
8	371	371	366	366	362	360	358	358	358	358		
	357	357	357	357	357	357	357	357	355	353	5.01	359
10	362	360	358	358	358	358	357	357	357	357		
	357	357	357	357	357	355	355	353	353	353	2.21	356

FOR DEGREE OF 1 COEFFICIENTS ARE
494.70000000 -13.95000000
BEST FIT VALUES 466.8 438.9 411.0 383.1 355.2
STANDARD DEVIATION IS 24.7918000
FOR DEGREE OF 2 COEFFICIENTS ARE
460.20000000 .83571340 -1.23214300
BEST FIT VALUES 456.9 443.8 420.9 388.0 345.3
STANDARD DEVIATION IS 27.4210500
FOR DEGREE OF 3 COEFFICIENTS ARE
365.00070000 67.70185000 -13.98204000 .70832770
BEST FIT VALUES 450.1 457.4 420.9 374.4 352.1
STANDARD DEVIATION IS 32.271800

EFFECT OF SOAKING PERIOD ON HARDNESS IN A.C. CONDITION

ALLOY : C 3 AS CAST HARDNESS(HV30)= 569
 TABLE : 5.13 TEMPERATURE (DEG.C)= 800

TIME (HRS)	HARDNESS (HV30)										SD	AVERAGE (HV30)
2	550	550	550	550	547	547	547	547	547	547		
	547	547	543	543	533	533	533	523	523	523	9.68	541
4	568	568	564	557	557	557	554	550	550	550		
	547	547	547	543	543	543	543	540	540	537	9.17	549
6	547	547	547	543	543	540	540	540	540	537		
	537	537	533	530	530	527	527	523	523	523	8.20	535
8	550	550	543	543	543	543	540	540	540	540		
	537	537	537	533	533	530	530	530	530	530	6.39	537
10	543	543	540	540	537	533	533	533	533	530		
	530	530	527	523	520	520	517	514	508	505	11.08	527

FOR DEGREE OF 1 COEFFICIENTS ARE
 550.30000000 -2.05000000
 BEST FIT VALUES 546.2 542.1 538.0 533.9 529.8
 STANDARD DEVIATION IS 6.2155900
 FOR DEGREE OF 2 COEFFICIENTS ARE
 539.80000000 2.45000000 -.37500000
 BEST FIT VALUES 543.2 543.6 541.0 535.4 526.8
 STANDARD DEVIATION IS 6.4961720
 FOR DEGREE OF 3 COEFFICIENTS ARE
 523.00230000 14.24840000 -2.62469500 .12498300
 BEST FIT VALUES 542.0 546.0 541.0 533.0 528.0
 STANDARD DEVIATION IS 8.3666220

TABLE : 5.14 TEMPERATURE (DEG.C)= 850

2	550	550	547	547	547	547	540	540	537	537		
	537	537	533	533	533	533	533	523	523	523	8.64	537
4	543	543	540	533	530	527	527	527	527	527		
	527	523	523	520	520	517	517	517	508	508	9.77	524
6	517	517	514	514	511	511	508	508	502	502		
	499	496	496	496	496	496	493	493	484	484	10.18	501
8	540	533	533	533	533	530	530	530	530	527		
	527	523	523	520	508	517	514	508	505	505	10.61	523
10	537	537	523	523	520	520	517	514	514	511		
	511	508	508	505	505	505	502	502	502	502	10.76	513

FOR DEGREE OF 1 COEFFICIENTS ARE
 534.80000000 -2.50000000
 BEST FIT VALUES 529.8 524.8 519.8 514.8 509.8
 STANDARD DEVIATION IS 12.6859500
 FOR DEGREE OF 2 COEFFICIENTS ARE
 559.80000000 -13.21429000 .89285710
 BEST FIT VALUES 536.9 521.2 512.7 511.2 516.9
 STANDARD DEVIATION IS 12.3334600
 FOR DEGREE OF 3 COEFFICIENTS ARE
 587.79930000 -32.88042000 4.64275600 -.20832770
 BEST FIT VALUES 538.9 517.2 512.7 515.2 514.9
 STANDARD DEVIATION IS 16.2551300

EFFECT OF SOAKING PERIOD ON HARDNESS IN A.C. CONDITION

ALLOY : C 3 AS CAST HARDNESS(HV30)= 569
 TABLE : 5.15 TEMPERATURE (DEG.C)= 900

TIME (HRS)	HARDNESS (HV30)										SD	AVERAGE (HV30)
2	530	530	530	530	530	530	527	527	523	523		
	517	520	517	514	514	508	508	505	505	505	9.64	519
4	540	533	533	533	533	533	530	530	530	530		
	527	523	523	520	520	508	514	508	505	505	10.72	523
6	530	530	530	530	530	530	527	527	523	523		
	523	520	517	514	514	508	508	505	505	505	9.65	519
8	527	527	523	523	520	520	517	514	514	511		
	511	508	508	505	505	505	502	502	502	502	8.68	512
10	511	511	499	499	499	496	496	493	493	493		
	493	490	487	487	487	487	487	487	484	478	8.29	492

FOR DEGREE OF 1 COEFFICIENTS ARE
 532.50000000 -3.25000000
 BEST FIT VALUES 526.0 519.5 513.0 506.5 500.0
 STANDARD DEVIATION IS 7.9895760
 FOR DEGREE OF 2 COEFFICIENTS ARE
 507.00000000 7.67857200 -.91071430
 BEST FIT VALUES 518.7 523.1 520.3 510.1 492.7
 STANDARD DEVIATION IS 1.6903100
 FOR DEGREE OF 3 COEFFICIENTS ARE
 513.99980000 2.76203800 .02676028 -.05208192
 BEST FIT VALUES 519.2 522.1 520.3 511.1 492.2
 STANDARD DEVIATION IS 1.7928430

TABLE : 5.16 TEMPERATURE (DEG.C)= 950

2	511	511	499	499	499	496	493	493	493	490		
	487	487	487	487	487	484	484	484	484	478	8.79	491
4	508	508	502	505	502	499	499	499	496	496		
	496	496	496	496	493	493	487	490	487	481	6.90	496
6	467	467	465	465	459	459	457	454	451	451		
	451	449	449	449	449	449	444	444	436	434	9.37	452
8	470	470	467	467	465	465	465	462	462	459		
	457	457	454	454	454	451	451	449	449	449	7.28	458
10	459	459	457	457	457	451	451	451	446	444		
	444	441	436	439	436	434	434	432	432	427	10.37	444

FOR DEGREE OF 1 COEFFICIENTS ARE
 507.80000000 -6.60000000
 BEST FIT VALUES 494.6 481.4 468.2 455.0 441.8
 STANDARD DEVIATION IS 12.9408800
 FOR DEGREE OF 2 COEFFICIENTS ARE
 513.80000000 -9.17142900 .21428570
 BEST FIT VALUES 496.3 480.5 466.5 454.1 443.5
 STANDARD DEVIATION IS 15.6862100
 FOR DEGREE OF 3 COEFFICIENTS ARE
 473.20470000 19.34190000 -5.22257900 .30204800
 BEST FIT VALUES 493.4 486.3 466.5 448.3 446.4
 STANDARD DEVIATION IS 20.1993700

EFFECT OF SOAKING PERIOD ON HARDNESS IN A.C. CONDITION

ALLOY : C 3
TABLE : 5.17

AS CAST HARDNESS(HV30)= 569
TEMPERATURE (DEG.C)= 1000

TIME (HRS)	HARDNESS (HV30)										SD	AVERAGE (HV30)
2	487	478	484	481	478	476	476	473	473	470		
	470	467	467	467	467	465	465	462	462	459	7.69	471
4	467	467	465	462	462	457	457	454	454	454		
	451	451	449	449	449	449	449	446	446	446	7.03	454
6	436	436	434	432	432	429	429	429	429	429		
	429	429	429	429	427	427	427	425	425	418	4.01	429
8	415	415	415	415	402	402	402	402	400	400		
	400	400	393	398	393	391	391	387	387	385	9.57	399
10	400	400	389	387	385	383	381	379	377	377		
	377	373	373	370	368	368	368	366	366	364	10.64	377

FOR DEGREE OF 1 COEFFICIENTS ARE
498.90000000 -12.15000000
BEST FIT VALUES 474.6 450.3 426.0 401.7 377.4
STANDARD DEVIATION IS 3.7903470
FOR DEGREE OF 2 COEFFICIENTS ARE
491.40000000 -8.93571400 -.26785710
BEST FIT VALUES 472.5 451.4 428.1 402.8 375.3
STANDARD DEVIATION IS 3.6761780
FOR DEGREE OF 3 COEFFICIENTS ARE
468.99690000 6.79975500 -3.26826400 .16668930
BEST FIT VALUES 470.9 454.6 428.1 399.6 376.9
STANDARD DEVIATION IS 1.1952330

TABLE : 5.18

TEMPERATURE (DEG.C)= 1050

2	436	436	434	432	432	429	429	429	429	429		
	429	429	429	429	427	427	427	425	425	418	4.01	429
4	418	418	418	418	413	413	413	413	413	413		
	411	411	411	409	409	409	406	406	398	398	5.71	410
6	418	413	413	411	409	409	406	406	406	404		
	404	404	404	404	404	402	402	402	402	398	4.80	406
8	366	366	362	362	358	358	358	357	357	357		
	355	355	349	349	348	348	341	341	339	339	8.56	353
10	355	344	344	341	341	339	339	339	334	333		
	333	333	333	333	331	331	329	326	326	326	7.29	335

FOR DEGREE OF 1 COEFFICIENTS ARE
460.10000000 -12.25000000
BEST FIT VALUES 435.6 411.1 386.6 362.1 337.6
STANDARD DEVIATION IS 13.0473500
FOR DEGREE OF 2 COEFFICIENTS ARE
436.60000000 -2.17857200 -.83928570
BEST FIT VALUES 428.9 414.5 393.3 365.5 330.9
STANDARD DEVIATION IS 13.2837200
FOR DEGREE OF 3 COEFFICIENTS ARE
408.60080000 17.48756000 -4.58918400 .20832770
BEST FIT VALUES 426.9 418.5 393.3 361.5 332.9
STANDARD DEVIATION IS 17.6893800

EFFECT OF SOAKING TEMPERATURE ON HARDNESS IN A.C. CONDITION

ALLOY : C 1 AS CAST HARDNESS(HV30)= 618
 TABLE : 5.19 TIME (HRS)= 2

TEMP (DEG. C)	HARDNESS (HV30)										SD	AVERAGE (HV30)
800	598	598	598	594	594	594	594	594	590	590	6.59	589
	590	590	590	586	586	586	583	583	583	571		
850	579	579	579	575	575	575	575	575	571	571	7.08	569
	571	568	568	568	561	561	561	561	561	557		
900	571	571	571	571	564	564	564	564	561	561	6.88	561
	561	561	561	557	557	557	554	554	550	547		
950	550	550	550	550	547	547	547	547	547	543	6.43	542
	543	543	540	537	537	537	533	533	533	533		
1000	527	527	523	523	520	520	517	514	514	511	8.68	512
	511	508	508	505	505	505	502	502	502	502		
1050	511	511	499	499	499	496	493	493	493	490	8.79	491
	487	487	487	487	487	484	484	484	484	478		

FOR DEGREE OF 1 COEFFICIENTS ARE
 903.42860000 - .38857140
 BEST FIT VALUES 592.6 573.1 553.7 534.3 514.9 495.4
 STANDARD DEVIATION IS 6.5246770
 FOR DEGREE OF 2 COEFFICIENTS ARE
 341.53150000 .83678420 - .00066235
 BEST FIT VALUES 587.1 574.2 558.1 538.7 516.0 489.9
 STANDARD DEVIATION IS 4.7371710
 FOR DEGREE OF 3 COEFFICIENTS ARE
 679.26610000 -.27291280 .00054694 -.00000044
 BEST FIT VALUES 587.2 574.0 558.0 538.9 516.2 489.7
 STANDARD DEVIATION IS 5.7676680

TABLE : 5.20 TIME (HRS)= 4

800	586	586	586	583	583	583	583	583	579	579	7.46	576
	579	575	575	575	568	568	568	568	565	565		
850	586	586	586	579	579	579	579	579	579	579	6.91	575
	575	575	575	575	568	568	568	568	564	564		
900	561	561	557	557	557	557	557	557	557	557	4.82	554
	554	554	554	554	554	554	550	550	543	543		
950	550	550	543	543	543	543	540	540	540	540	6.49	537
	537	537	533	533	533	530	530	530	530	530		
1000	514	514	514	514	508	508	508	508	508	508	4.12	507
	508	505	505	505	505	505	502	502	502	502		
1050	484	484	484	481	481	481	481	476	476	476	7.27	474
	476	476	473	473	470	470	465	465	465	459		

FOR DEGREE OF 1 COEFFICIENTS ARE
 923.55240000 - .41771430
 BEST FIT VALUES 589.4 568.5 547.6 526.7 505.8 485.0
 STANDARD DEVIATION IS 11.0578600
 FOR DEGREE OF 2 COEFFICIENTS ARE
 -261.53960000 2.16667200 - .00139697
 BEST FIT VALUES 577.7 570.8 556.9 536.0 508.2 473.3
 STANDARD DEVIATION IS 3.2543710
 FOR DEGREE OF 3 COEFFICIENTS ARE
 -200.13320000 1.96422900 - .00117709 -.00000008
 BEST FIT VALUES 577.8 570.8 556.9 536.1 508.2 473.3
 STANDARD DEVIATION IS 4.0115370

EFFECT OF SOAKING TEMPERATURE ON HARDNESS IN A.C. CONDITION

ALLOY : C 1 AS CAST HARDNESS(HV30)= 618
 TABLE : 5.21 TIME (HRS)= 6

TEMP (DEG. C)	HARDNESS (HV30)										SD	AVERAGE (HV30)
800	602	602	598	598	594	594	590	590	590	583		
	583	583	583	583	579	579	579	579	571	571	9.35	586
850	586	586	586	586	586	586	583	583	579	579		
	579	579	579	579	575	575	571	571	564	564	7.02	578
900	568	568	564	564	564	561	561	561	561	561		
	557	557	557	554	554	550	550	550	550	547	6.35	557
950	540	540	537	537	533	533	533	530	530	527		
	527	527	527	527	527	527	527	523	523	523	5.35	529
1000	496	496	496	496	493	493	490	490	487	487		
	487	487	487	484	484	484	481	476	476	476	6.64	487
1050	499	493	493	490	490	487	484	484	481	481		
	478	478	478	478	473	473	467	467	465	465	9.96	480

FOR DEGREE OF 1 COEFFICIENTS ARE
 975.40950000 - .47485720
 BEST FIT VALUES 595.5 571.8 548.0 524.3 500.6 476.8
 STANDARD DEVIATION IS 10.3159500
 FOR DEGREE OF 2 COEFFICIENTS ARE
 498.02910000 .56618890 - .00056273
 BEST FIT VALUES 590.8 572.7 551.8 528.0 501.5 472.1
 STANDARD DEVIATION IS 10.8224800
 FOR DEGREE OF 3 COEFFICIENTS ARE
 -1252.05000000 6.31643700 - .00682910 .00000226
 BEST FIT VALUES 590.1 573.9 552.3 527.2 500.3 473.1
 STANDARD DEVIATION IS 11.8800700

TABLE : 5.22 TIME (HRS)= 8

800	610	610	598	598	598	594	594	594	594	590		
	586	586	586	586	586	586	586	586	583	579	8.30	591
850	571	571	571	571	564	564	564	564	561	561		
	561	561	561	557	557	543	554	543	540	540	10.16	558
900	561	557	557	557	554	550	550	550	547	547		
	543	543	543	543	543	540	540	540	537	537	7.25	546
950	530	530	530	530	530	530	527	527	523	520		
	517	514	514	514	514	514	508	505	505	505	9.48	519
1000	511	511	499	499	499	496	493	493	493	493		
	490	490	487	487	487	487	487	484	484	484	7.96	492
1050	487	478	484	481	478	476	476	473	473	470		
	470	467	467	467	467	465	465	462	462	459	7.69	471

FOR DEGREE OF 1 COEFFICIENTS ARE
 965.57140000 - .47142860
 BEST FIT VALUES 588.4 564.9 541.3 517.7 494.1 470.6
 STANDARD DEVIATION IS 4.5355670
 FOR DEGREE OF 2 COEFFICIENTS ARE
 965.57140000 - .47142860 .00000000
 BEST FIT VALUES 588.4 564.9 541.3 517.7 494.1 470.6
 STANDARD DEVIATION IS 5.2372220
 FOR DEGREE OF 3 COEFFICIENTS ARE
 1211.19700000 -1.27848100 .00087949 - .00000032
 BEST FIT VALUES 588.5 564.7 541.2 517.8 494.3 470.4
 STANDARD DEVIATION IS 6.3623690

EFFECT OF SOAKING TEMPERATURE ON HARDNESS IN A.C. CONDITION

ALLOY : C 1		AS CAST HARDNESS(HV30)= 618											
TABLE : 5.23		TIME (HRS)= 10											
TEMP (DEG. C)	HARDNESS (HV30)										SD	AVERAGE (HV30)	
800	590	590	590	590	590	590	590	590	590	583	583		
	583	583	583	579	579	579	579	579	579	579	564	6.65	583
850	561	561	557	557	557	554	554	554	554	554	554		
	554	554	550	550	550	550	547	543	540	540	540	5.96	552
900	547	547	547	547	547	547	540	540	540	540	540		
	537	537	533	533	533	533	533	523	523	523	523	8.27	537
950	523	523	520	520	520	520	517	517	514	514	514		
	514	514	514	514	514	514	514	511	511	511	511	3.80	515
1000	502	502	499	499	496	496	493	490	490	484	484		
	484	484	484	484	481	481	478	478	473	473	473	9.23	487
1050	462	462	462	459	459	459	451	451	451	451	451		
	449	449	449	449	446	444	444	441	441	441	441	7.23	451

FOR DEGREE OF 1. COEFFICIENTS ARE
 984.39050000 -.50114290

BEST FIT VALUES 583.5 558.4 533.4 508.3 483.2 458.2

STANDARD DEVIATION IS 6.4279850

FOR DEGREE OF 2 COEFFICIENTS ARE
 519.08390000 .51357320 -.00054850

BEST FIT VALUES 578.9 559.3 537.0 512.0 484.2 453.6

STANDARD DEVIATION IS 5.6182240

FOR DEGREE OF 3 COEFFICIENTS ARE
 1716.50700000 -3.42080700 .00373902 -.00000155

BEST FIT VALUES 579.4 558.5 536.6 512.5 485.0 452.9

STANDARD DEVIATION IS 5.9143140

EFFECT OF SOAKING TEMPERATURE ON HARDNESS IN A.C. CONDITION

ALLOY : C 2
TABLE : 5.24

AS CAST HARDNESS(HV30)= 583
TIME (HRS)= 2

TEMP (DEG. C)	HARDNESS (HV30)										SD	AVERAGE (HV30)
800	575	571	571	571	571	571	568	568	568	568		
	564	564	564	564	557	557	557	557	554	554	6.56	564
850	568	568	564	564	564	561	561	561	561	561		
	557	557	557	554	554	550	550	550	550	547	6.35	557
900	568	564	564	564	561	561	561	561	561	557		
	557	557	557	557	554	554	550	550	550	547	5.63	557
950	527	527	520	517	517	517	517	517	517	517		
	514	514	514	514	514	514	514	511	511	511	4.40	516
1000	493	493	487	487	487	484	484	484	481	481		
	481	481	481	481	478	478	478	476	476	476	5.07	482
1050	467	467	465	462	462	462	462	457	457	454		
	454	449	449	449	449	449	446	446	446	441	7.98	454

FOR DEGREE OF 1 COEFFICIENTS ARE
 952.98100000 -.46628570
 BEST FIT VALUES 580.0 556.6 533.3 510.0 486.7 463.4
 STANDARD DEVIATION IS 15.5008400
 FOR DEGREE OF 2 COEFFICIENTS ARE
 -504.23650000 2.71153700 -.00171774
 BEST FIT VALUES 565.6 559.5 544.8 521.5 489.6 449.1
 STANDARD DEVIATION IS 9.4809850
 FOR DEGREE OF 3 COEFFICIENTS ARE
 -1271.81500000 5.23357500 -.00446615 .00000099
 BEST FIT VALUES 565.3 560.0 545.0 521.1 489.0 449.5
 STANDARD DEVIATION IS 11.1800000

TABLE : 5.25

TIME (HRS)= 4

800	568	568	568	568	564	564	564	564	564	561		
	561	561	561	554	557	554	550	550	550	550	6.57	560
850	561	557	557	557	554	550	550	550	547	547		
	547	547	543	543	543	543	543	540	540	537	6.64	547
900	575	575	575	571	571	571	568	568	568	568		
	564	564	561	561	557	557	557	557	554	554	7.16	564
950	527	527	523	523	520	520	517	514	514	511		
	511	508	508	505	505	505	502	502	502	502	8.68	512
1000	517	517	514	514	511	511	508	508	502	502		
	499	496	496	496	496	496	493	493	484	484	10.18	501
1050	451	451	449	446	446	446	446	446	446	444		
	444	444	444	444	441	439	439	439	432	422	6.64	442

FOR DEGREE OF 1 COEFFICIENTS ARE
 933.28580000 -.44571430
 BEST FIT VALUES 576.7 554.4 532.1 509.9 487.6 465.3
 STANDARD DEVIATION IS 22.7847000
 FOR DEGREE OF 2 COEFFICIENTS ARE
 -1134.12400000 4.06278400 -.00243703
 BEST FIT VALUES 556.4 558.5 548.4 526.1 491.6 445.0
 STANDARD DEVIATION IS 15.1014200
 FOR DEGREE OF 3 COEFFICIENTS ARE
 1.89263900 .53016690 .00163061 -.00000147
 BEST FIT VALUES 556.9 557.7 548.0 526.6 492.4 444.3
 STANDARD DEVIATION IS 18.3454600

EFFECT OF SOAKING TEMPERATURE ON HARDNESS IN A.C. CONDITION

ALLOY : C 2 AS CAST HARDNESS(HV30)= 583
 TABLE : 5.26 TIME (HRS)= 6

TEMP (DEG. C)	HARDNESS (HV30)										SD	AVERAGE (HV30)
800	568	568	564	557	557	557	557	557	554	550	7.84	552
	550	550	550	550	547	547	543	543	543	543		
850	547	547	547	543	543	533	530	530	530	530	8.23	532
	530	530	530	527	527	527	527	523	523	523		
900	547	547	547	540	537	533	533	533	530	530	7.63	532
	530	530	530	530	527	527	527	523	523	523		
950	533	533	533	533	530	530	530	530	527	527	5.45	526
	527	527	527	527	527	527	523	517	517	514		
1000	462	462	457	457	457	454	454	454	451	451	5.94	451
	449	449	449	449	449	446	446	446	441	441		
1050	459	459	457	457	457	451	451	451	446	444	10.37	444
	444	441	436	439	436	434	434	432	432	427		

FOR DEGREE OF 1 COEFFICIENTS ARE
 923.20950000 - .45085710
 BEST FIT VALUES 562.5 540.0 517.4 494.9 472.4 449.8
 STANDARD DEVIATION IS 21.4690200
 FOR DEGREE OF 2 COEFFICIENTS ARE
 -497.78650000 2.64797600 - .00167505
 BEST FIT VALUES 548.6 542.8 528.6 506.1 475.1 435.9
 STANDARD DEVIATION IS 19.8849900
 FOR DEGREE OF 3 COEFFICIENTS ARE
 -559.19270000 2.84973900 - .00189492 .00000008
 BEST FIT VALUES 548.5 542.8 528.6 506.0 475.1 435.9
 STANDARD DEVIATION IS 24.3479400

TABLE : 5.27, TIME (HRS)= 8

800	568	568	564	557	557	557	554	550	547	547	10.00	548
	547	543	543	543	543	540	540	540	540	533		
850	533	533	523	523	523	523	520	517	517	517	6.35	518
	517	517	517	514	514	514	514	511	511	511		
900	540	540	540	533	533	533	530	530	530	527	11.55	524
	527	523	523	520	508	517	514	508	505	505		
950	511	511	508	508	508	505	505	505	502	499	7.79	499
	499	499	499	496	496	493	493	487	487	487		
1000	409	409	409	409	406	406	406	406	406	404	3.22	404
	404	404	404	404	404	402	402	402	398	398		
1050	371	371	366	366	362	360	358	358	358	358	4.89	359
	357	357	357	357	357	357	357	357	355	355		

FOR DEGREE OF 1 COEFFICIENTS ARE
 1171.62900000 - .75257140
 BEST FIT VALUES 569.6 531.9 494.3 456.7 419.1 381.4
 STANDARD DEVIATION IS 31.6981300
 FOR DEGREE OF 2 COEFFICIENTS ARE
 -1695.44000000 5.49978000 - .00337965
 BEST FIT VALUES 541.4 537.6 516.8 479.2 424.7 353.3
 STANDARD DEVIATION IS 21.1690500
 FOR DEGREE OF 3 COEFFICIENTS ARE
 -436.61050000 1.36363700 .00112774 - .00000163
 BEST FIT VALUES 541.9 536.7 516.4 479.8 425.6 352.5
 STANDARD DEVIATION IS 25.8298800

EFFECT OF SOAKING TEMPERATURE ON HARDNESS IN A.C. CONDITION

ALLOY : C 2 AS CAST HARDNESS(HV30)= 583
 TABLE : 5.28 TIME (HRS)= 10

TEMP (DEG.C)	HARDNESS (HV30)										SD	AVERAGE (HV30)
800	547	543	543	540	537	537	533	533	530	530		
	530	530	530	530	527	527	527	523	523	523	6.98	532
850	527	527	527	527	527	523	523	523	523	520		
	520	520	517	517	517	517	517	517	517	514	4.35	521
900	533	523	523	523	523	520	517	517	517	517		
	517	517	514	514	514	514	511	511	511	511	5.56	517
950	511	511	508	505	505	502	502	499	499	499		
	499	499	499	496	496	496	493	490	484	484	7.44	498
1000	398	398	398	398	398	393	393	393	391	391		
	387	387	383	383	381	381	377	377	375	375	8.34	387
1050	362	360	358	358	358	358	357	357	357	357		
	357	357	357	357	357	355	355	353	353	353	2.21	356

FOR DEGREE OF 1 COEFFICIENTS ARE
 1156.17100000 - .74342860
 BEST FIT VALUES 561.4 524.3 487.1 449.9 412.7 375.6
 STANDARD DEVIATION IS 35.8102100

FOR DEGREE OF 2 COEFFICIENTS ARE
 -2035.96100000 6.21780600 - .00376283
 BEST FIT VALUES 530.1 530.5 512.2 475.0 419.0 344.2
 STANDARD DEVIATION IS 24.5671800

FOR DEGREE OF 3 COEFFICIENTS ARE
 -2204.82800000 6.77265500 - .00436748 .00000022
 BEST FIT VALUES 530.0 530.6 512.2 474.9 418.9 344.3
 STANDARD DEVIATION IS 30.0525800

EFFECT OF SOAKING TEMPERATURE ON HARDNESS IN A.C. CONDITION

ALLOY : C 3 AS CAST HARDNESS(HV30)= 569
 TABLE : 5.29 TIME (HRS)= 2

TEMP (DEG.C)	HARDNESS (HV30)										SD	AVERAGE (HV30)																																																																																																																																															
800	550	550	550	550	547	547	547	547	547	547				547	547	543	543	533	533	533	523	523	523	9.68	541	850	550	550	547	547	547	547	540	540	537	537				537	537	533	533	533	533	533	523	523	523	8.64	537	900	530	530	530	530	530	530	527	527	523	523				517	520	517	514	514	508	508	505	505	505	9.64	519	950	511	511	499	499	499	496	493	493	493	490				487	487	487	487	487	484	484	484	484	478	8.79	491	1000	487	478	484	481	478	476	476	473	473	470				470	467	467	467	467	465	465	462	462	459	7.69	471	1050	436	436	434	432	432	429	429	429	429	429				429	429	429	429	427	427	427	425	425	418	4.01	429
	547	547	543	543	533	533	533	523	523	523	9.68	541	850	550	550	547	547	547	547	540	540	537	537				537	537	533	533	533	533	533	523	523	523	8.64	537	900	530	530	530	530	530	530	527	527	523	523				517	520	517	514	514	508	508	505	505	505	9.64	519	950	511	511	499	499	499	496	493	493	493	490				487	487	487	487	487	484	484	484	484	478	8.79	491	1000	487	478	484	481	478	476	476	473	473	470				470	467	467	467	467	465	465	462	462	459	7.69	471	1050	436	436	434	432	432	429	429	429	429	429				429	429	429	429	427	427	427	425	425	418	4.01	429													
850	550	550	547	547	547	547	540	540	537	537				537	537	533	533	533	533	533	523	523	523	8.64	537	900	530	530	530	530	530	530	527	527	523	523				517	520	517	514	514	508	508	505	505	505	9.64	519	950	511	511	499	499	499	496	493	493	493	490				487	487	487	487	487	484	484	484	484	478	8.79	491	1000	487	478	484	481	478	476	476	473	473	470				470	467	467	467	467	465	465	462	462	459	7.69	471	1050	436	436	434	432	432	429	429	429	429	429				429	429	429	429	427	427	427	425	425	418	4.01	429																										
	537	537	533	533	533	533	533	523	523	523	8.64	537	900	530	530	530	530	530	530	527	527	523	523				517	520	517	514	514	508	508	505	505	505	9.64	519	950	511	511	499	499	499	496	493	493	493	490				487	487	487	487	487	484	484	484	484	478	8.79	491	1000	487	478	484	481	478	476	476	473	473	470				470	467	467	467	467	465	465	462	462	459	7.69	471	1050	436	436	434	432	432	429	429	429	429	429				429	429	429	429	427	427	427	425	425	418	4.01	429																																							
900	530	530	530	530	530	530	527	527	523	523				517	520	517	514	514	508	508	505	505	505	9.64	519	950	511	511	499	499	499	496	493	493	493	490				487	487	487	487	487	484	484	484	484	478	8.79	491	1000	487	478	484	481	478	476	476	473	473	470				470	467	467	467	467	465	465	462	462	459	7.69	471	1050	436	436	434	432	432	429	429	429	429	429				429	429	429	429	427	427	427	425	425	418	4.01	429																																																				
	517	520	517	514	514	508	508	505	505	505	9.64	519	950	511	511	499	499	499	496	493	493	493	490				487	487	487	487	487	484	484	484	484	478	8.79	491	1000	487	478	484	481	478	476	476	473	473	470				470	467	467	467	467	465	465	462	462	459	7.69	471	1050	436	436	434	432	432	429	429	429	429	429				429	429	429	429	427	427	427	425	425	418	4.01	429																																																																	
950	511	511	499	499	499	496	493	493	493	490				487	487	487	487	487	484	484	484	484	478	8.79	491	1000	487	478	484	481	478	476	476	473	473	470				470	467	467	467	467	465	465	462	462	459	7.69	471	1050	436	436	434	432	432	429	429	429	429	429				429	429	429	429	427	427	427	425	425	418	4.01	429																																																																														
	487	487	487	487	487	484	484	484	484	478	8.79	491	1000	487	478	484	481	478	476	476	473	473	470				470	467	467	467	467	465	465	462	462	459	7.69	471	1050	436	436	434	432	432	429	429	429	429	429				429	429	429	429	427	427	427	425	425	418	4.01	429																																																																																											
1000	487	478	484	481	478	476	476	473	473	470				470	467	467	467	467	465	465	462	462	459	7.69	471	1050	436	436	434	432	432	429	429	429	429	429				429	429	429	429	427	427	427	425	425	418	4.01	429																																																																																																								
	470	467	467	467	467	465	465	462	462	459	7.69	471	1050	436	436	434	432	432	429	429	429	429	429				429	429	429	429	427	427	427	425	425	418	4.01	429																																																																																																																					
1050	436	436	434	432	432	429	429	429	429	429				429	429	429	429	427	427	427	425	425	418	4.01	429																																																																																																																																		
	429	429	429	429	427	427	427	425	425	418	4.01	429																																																																																																																																															

FOR DEGREE OF 1 COEFFICIENTS ARE
 913.45720000 - .44914280
 BEST FIT VALUES 554.1 531.7 509.2 486.8 464.3 441.9
 STANDARD DEVIATION IS 11.4492700
 FOR DEGREE OF 2 COEFFICIENTS ARE
 -282.77980000 2.15954800 - .00141010
 BEST FIT VALUES 542.4 534.0 518.6 496.2 466.7 430.1
 STANDARD DEVIATION IS 4.3830290
 FOR DEGREE OF 3 COEFFICIENTS ARE
 24.25150000 1.15073300 - .00031074 - .00000040
 BEST FIT VALUES 542.5 533.8 518.5 496.3 466.9 429.9
 STANDARD DEVIATION IS 5.4140140

TABLE : 5.30 TIME (HRS)= 4

800	568	568	564	557	557	557	554	550	550	550				547	547	547	543	543	543	543	537	537	533	9.88	549	850	543	543	540	533	530	527	527	527	527	527				527	523	523	520	520	517	517	508	508	505	10.63	524	900	540	533	533	533	533	533	530	530	530	530				527	523	523	520	520	508	514	508	505	505	10.72	523	950	508	508	502	505	502	499	499	499	496	496				496	496	496	496	493	493	487	490	487	481	6.90	496	1000	467	467	465	462	462	457	457	454	454	454				451	451	451	449	449	449	449	449	446	446	6.81	454	1050	418	418	418	418	413	413	413	413	413	413				411	411	411	409	409	409	406	406	398	398	5.71	410
	547	547	547	543	543	543	543	537	537	533	9.88	549	850	543	543	540	533	530	527	527	527	527	527				527	523	523	520	520	517	517	508	508	505	10.63	524	900	540	533	533	533	533	533	530	530	530	530				527	523	523	520	520	508	514	508	505	505	10.72	523	950	508	508	502	505	502	499	499	499	496	496				496	496	496	496	493	493	487	490	487	481	6.90	496	1000	467	467	465	462	462	457	457	454	454	454				451	451	451	449	449	449	449	449	446	446	6.81	454	1050	418	418	418	418	413	413	413	413	413	413				411	411	411	409	409	409	406	406	398	398	5.71	410													
850	543	543	540	533	530	527	527	527	527	527				527	523	523	520	520	517	517	508	508	505	10.63	524	900	540	533	533	533	533	533	530	530	530	530				527	523	523	520	520	508	514	508	505	505	10.72	523	950	508	508	502	505	502	499	499	499	496	496				496	496	496	496	493	493	487	490	487	481	6.90	496	1000	467	467	465	462	462	457	457	454	454	454				451	451	451	449	449	449	449	449	446	446	6.81	454	1050	418	418	418	418	413	413	413	413	413	413				411	411	411	409	409	409	406	406	398	398	5.71	410																										
	527	523	523	520	520	517	517	508	508	505	10.63	524	900	540	533	533	533	533	533	530	530	530	530				527	523	523	520	520	508	514	508	505	505	10.72	523	950	508	508	502	505	502	499	499	499	496	496				496	496	496	496	493	493	487	490	487	481	6.90	496	1000	467	467	465	462	462	457	457	454	454	454				451	451	451	449	449	449	449	449	446	446	6.81	454	1050	418	418	418	418	413	413	413	413	413	413				411	411	411	409	409	409	406	406	398	398	5.71	410																																							
900	540	533	533	533	533	533	530	530	530	530				527	523	523	520	520	508	514	508	505	505	10.72	523	950	508	508	502	505	502	499	499	499	496	496				496	496	496	496	493	493	487	490	487	481	6.90	496	1000	467	467	465	462	462	457	457	454	454	454				451	451	451	449	449	449	449	449	446	446	6.81	454	1050	418	418	418	418	413	413	413	413	413	413				411	411	411	409	409	409	406	406	398	398	5.71	410																																																				
	527	523	523	520	520	508	514	508	505	505	10.72	523	950	508	508	502	505	502	499	499	499	496	496				496	496	496	496	493	493	487	490	487	481	6.90	496	1000	467	467	465	462	462	457	457	454	454	454				451	451	451	449	449	449	449	449	446	446	6.81	454	1050	418	418	418	418	413	413	413	413	413	413				411	411	411	409	409	409	406	406	398	398	5.71	410																																																																	
950	508	508	502	505	502	499	499	499	496	496				496	496	496	496	493	493	487	490	487	481	6.90	496	1000	467	467	465	462	462	457	457	454	454	454				451	451	451	449	449	449	449	449	446	446	6.81	454	1050	418	418	418	418	413	413	413	413	413	413				411	411	411	409	409	409	406	406	398	398	5.71	410																																																																														
	496	496	496	496	493	493	487	490	487	481	6.90	496	1000	467	467	465	462	462	457	457	454	454	454				451	451	451	449	449	449	449	449	446	446	6.81	454	1050	418	418	418	418	413	413	413	413	413	413				411	411	411	409	409	409	406	406	398	398	5.71	410																																																																																											
1000	467	467	465	462	462	457	457	454	454	454				451	451	451	449	449	449	449	449	446	446	6.81	454	1050	418	418	418	418	413	413	413	413	413	413				411	411	411	409	409	409	406	406	398	398	5.71	410																																																																																																								
	451	451	451	449	449	449	449	449	446	446	6.81	454	1050	418	418	418	418	413	413	413	413	413	413				411	411	411	409	409	409	406	406	398	398	5.71	410																																																																																																																					
1050	418	418	418	418	413	413	413	413	413	413				411	411	411	409	409	409	406	406	398	398	5.71	410																																																																																																																																		
	411	411	411	409	409	409	406	406	398	398	5.71	410																																																																																																																																															

FOR DEGREE OF 1 COEFFICIENTS ARE
 985.29520000 - .53257140
 BEST FIT VALUES 559.2 532.6 506.0 479.4 452.7 426.1
 STANDARD DEVIATION IS 15.8620500
 FOR DEGREE OF 2 COEFFICIENTS ARE
 -580.58670000 2.88222100 - .00184583
 BEST FIT VALUES 543.9 535.7 518.3 491.7 455.8 410.7
 STANDARD DEVIATION IS 8.3234440
 FOR DEGREE OF 3 COEFFICIENTS ARE
 770.35230000 -1.55656700 .00299136 - .00000175
 BEST FIT VALUES 544.4 534.8 517.9 492.3 456.7 409.9
 STANDARD DEVIATION IS 9.6311480

EFFECT OF SOAKING TEMPERATURE ON HARDNESS IN A.C. CONDITION

ALLOY : C 3 AS CAST HARDNESS(HV30)= 569
 TABLE : 5.31 TIME (HRS)= 6

TEMP (DEG.C)	HARDNESS (HV30)										SD	AVERAGE (HV30)
800	547	547	547	543	543	540	540	540	540	537		
	537	537	533	530	530	527	527	523	523	523	8.20	535
850	517	517	514	514	511	511	508	508	502	502		
	499	496	496	496	496	496	493	493	484	484	10.18	501
900	530	530	530	530	530	530	527	527	523	523		
	523	520	517	514	514	508	508	505	505	505	9.65	519
950	467	467	465	465	459	459	457	454	451	451		
	451	449	449	449	449	449	446	446	444	444	7.66	452
1000	436	436	434	432	432	429	429	429	429	429		
	429	429	429	429	427	427	427	425	425	418	4.01	429
1050	418	413	413	411	409	409	406	406	406	404		
	404	404	404	404	404	402	402	402	402	398	4.80	406

FOR DEGREE OF 1 COEFFICIENTS ARE
 963.81910000 -.52971430
 BEST FIT VALUES 540.0 513.6 487.1 460.6 434.1 407.6
 STANDARD DEVIATION IS 17.9492700
 FOR DEGREE OF 2 COEFFICIENTS ARE
 281.18380000 .95894090 -.00080468
 BEST FIT VALUES 533.3 514.9 492.4 466.0 435.4 400.9
 STANDARD DEVIATION IS 19.4653100
 FOR DEGREE OF 3 COEFFICIENTS ARE
 -517.09840000 3.58186100 -.00366302 .00000103
 BEST FIT VALUES 533.0 515.4 492.7 465.6 434.9 401.4
 STANDARD DEVIATION IS 23.6510000

TABLE : 5.32 TIME (HRS)= 8

800	550	550	543	543	543	543	540	540	540	540		
	537	537	533	533	533	530	530	530	530	530	6.49	537
850	540	533	533	533	533	530	530	530	530	527		
	527	523	523	520	508	517	514	508	505	505	10.61	523
900	527	527	523	523	520	520	517	514	514	511		
	511	508	508	505	505	505	502	502	502	502	8.68	512
950	470	470	467	467	465	465	465	462	462	459		
	457	457	454	454	454	451	451	449	449	449	7.28	458
1000	415	415	415	415	402	402	402	402	400	400		
	400	400	393	398	393	391	391	387	387	385	9.57	399
1050	366	366	362	362	358	358	358	357	357	357		
	355	355	349	349	348	348	341	341	339	339	8.56	353

FOR DEGREE OF 1 COEFFICIENTS ARE
 1175.12400000 -.76914290
 BEST FIT VALUES 559.8 521.4 482.9 444.4 406.0 367.5
 STANDARD DEVIATION IS 21.2936400
 FOR DEGREE OF 2 COEFFICIENTS ARE
 -952.65520000 3.87100500 -.00250819
 BEST FIT VALUES 538.9 525.5 499.6 461.2 410.2 346.6
 STANDARD DEVIATION IS 10.6245000
 FOR DEGREE OF 3 COEFFICIENTS ARE
 -1689.53100000 3.29215200 -.00514666 .00000095
 BEST FIT VALUES 538.6 526.0 499.8 460.8 409.6 347.0
 STANDARD DEVIATION IS 12.5726700

EFFECT OF SOAKING TEMPERATURE ON HARDNESS IN A.C. CONDITION

ALLOY : C 3 AS CAST HARDNESS(HV30)= 569
 TABLE : 5.33 TIME (HRS)= 10

TEMP (DEG.C)	HARDNESS (HV30)										SD	AVERAGE (HV30)
800	543	543	540	540	537	533	533	533	533	530		
	530	530	527	523	520	520	517	514	508	505	11.08	527
850	537	537	523	523	520	520	517	514	514	511		
	511	508	508	505	505	505	502	502	502	502	10.76	513
900	511	511	499	499	499	496	496	493	493	493		
	493	490	487	487	487	487	487	487	484	478	8.29	492
950	459	459	457	457	457	451	451	451	446	444		
	444	441	436	439	436	434	434	432	432	427	10.37	444
1000	400	400	389	387	385	383	381	379	377	377		
	377	373	373	370	368	368	368	366	366	362	10.78	377
1050	355	344	344	341	341	339	339	339	334	333		
	333	333	333	333	331	331	329	326	326	326	7.29	335

FOR DEGREE OF 1 COEFFICIENTS ARE

1196.45700000 -.80914280

BEST FIT VALUES 549.1 508.7 468.2 427.8 387.3 346.9

STANDARD DEVIATION IS 19.9018900

FOR DEGREE OF 2 COEFFICIENTS ARE

-762.28850000 3.46238600 -.00230894

BEST FIT VALUES 529.9 512.5 483.6 443.2 391.2 327.6

STANDARD DEVIATION IS 10.5614400

FOR DEGREE OF 3 COEFFICIENTS ARE

-1760.14000000 6.74103500 -.00588186 .00000129

BEST FIT VALUES 529.5 513.2 483.9 442.7 390.5 328.2

STANDARD DEVIATION IS 12.2624600

Table-5.34 Summary table of effect of heat treatment on hardness

H/T TEMP. DEG. °C	S O A K I N G P E R I O D (hrs)														
	Alloy C1					Alloy C2					Alloy C3				
	2	4	6	8	10	2	4	6	8	10	2	4	6	8	10
800	589	576	586	591	583	564	560	552	549	532	541	549	535	537	527
850	569	575	578	558	552	557	547	532	518	521	537	524	501	523	513
900	561	554	557	546	537	557	564	532	524	517	519	523	519	512	492
950	542	537	529	519	515	516	512	526	499	498	491	496	452	458	444
1000	512	507	487	492	487	482	501	451	404	387	471	454	429	399	377
1050	491	474	480	471	451	454	442	444	359	356	429	410	406	353	335

Table-5.35 Effect of heat treatment on volume fraction of massive carbide

Temp °C	Time (hours)	Volume fraction of massive carbide (Alloy C1) (%)										S.D.	Ave (%)
As-cast		52.5	49.4	48.3	48.1	47.6	47.5	47.2	47.1	46.4	46.0	4.3	44.9
		46.0	45.8	44.8	44.2	43.3	43.0	42.2	37.4	36.0	35.8		
800	2	50.9	47.4	47.1	45.1	44.4	43.4	42.8	42.6	42.5	42.4	6.2	40.1
		42.4	40.6	40.4	37.6	37.5	35.9	31.2	31.1	28.9	27.4		
800	4	47.9	43.1	42.7	42.5	42.0	41.8	41.4	39.2	38.5	37.9	4.1	38.4
		37.7	37.4	36.6	35.9	35.3	35.2	34.4	34.4	32.7	31.1		
800	6	49.5	47.3	46.8	43.9	43.8	42.2	40.8	40.5	39.1	39.1	4.9	39.6
		38.5	38.4	38.1	37.2	36.9	36.6	36.5	34.8	31.3	29.8		
800	8	45.4	44.8	44.7	44.2	42.9	40.8	40.5	39.7	39.4	39.2	7.2	36.8
		37.6	37.4	35.6	35.5	33.7	32.5	32.3	27.6	24.1	17.2		
800	10	45.6	44.6	40.5	39.9	38.6	37.4	37.3	37.0	36.8	35.8	4.0	36.4
		35.5	35.5	35.5	34.7	34.3	33.4	33.0	32.5	30.1	30.0		
850	2	49.2	46.2	45.8	44.8	43.0	42.8	42.4	41.2	40.2	40.1	5.2	39.0
		37.7	37.4	36.4	35.9	33.9	33.3	33.2	33.2	33.2	30.0		
850	4	55.2	50.0	48.1	47.2	41.2	41.1	40.9	40.3	40.0	39.7	7.3	39.0
		39.3	37.6	35.3	35.3	34.7	34.6	34.5	33.2	32.2	20.5		
850	6	49.5	42.5	42.3	39.2	38.3	37.7	36.7	35.4	35.0	35.0	6.7	34.1
		34.5	33.7	33.7	31.3	31.0	29.8	25.7	25.6	24.1	20.4		
850	8	42.5	42.0	41.9	41.6	41.1	39.4	39.2	38.8	37.9	37.3	4.8	36.1
		35.2	34.6	34.0	33.7	33.6	33.2	32.0	31.9	30.1	22.9		
850	10	38.1	35.6	35.0	34.8	33.9	33.9	32.1	31.7	31.3	31.3	3.3	31.3
		31.3	30.9	30.9	30.7	29.6	29.3	28.8	27.6	26.1	23.9		
900	2	46.9	45.7	44.7	41.8	41.1	39.7	38.5	38.4	38.1	37.4	5.7	36.5
		36.0	35.5	34.4	33.1	31.6	31.4	30.8	30.2	28.9	25.1		
900	4	49.1	48.1	46.3	45.2	44.4	44.3	41.2	38.6	38.2	37.2	6.3	37.9
		36.6	34.1	33.9	33.2	32.9	32.6	32.3	31.9	31.2	27.1		
900	6	54.8	45.0	44.0	41.9	41.1	40.6	38.9	37.1	36.7	36.6	7.9	35.7
		35.8	34.6	33.4	32.4	32.3	31.7	28.9	26.9	22.2	18.8		
900	8	40.7	39.1	38.4	37.4	36.6	36.5	36.3	36.2	36.2	35.7	3.2	34.9
		35.7	35.5	35.1	35.0	33.5	31.7	29.9	29.8	29.5	29.4		
900	10	45.2	40.3	40.1	40.1	39.1	37.5	36.0	35.6	34.5	32.7	7.1	32.1
		32.3	31.0	28.2	26.5	26.4	26.4	25.3	24.4	21.7	18.1		

contd...

950	2	44.5	43.4	43.1	42.2	40.6	40.1	38.9	37.4	37.3	36.2	6.0	35.2
		36.1	32.3	32.1	30.3	30.2	30.1	29.6	29.2	27.3	23.1		
950	4	42.6	42.1	41.9	41.4	39.6	39.2	39.1	38.4	36.9	36.2	4.7	35.7
		35.6	34.1	33.8	32.9	32.8	31.8	31.3	30.6	28.8	25.6		
950	6	43.2	41.9	39.1	38.2	37.9	37.4	36.1	35.2	31.1	29.4	6.7	31.3
		29.2	29.1	28.0	27.1	26.1	26.0	25.3	25.1	22.1	18.2		
950	8	40.3	37.3	34.6	32.8	29.3	29.1	28.8	27.6	27.3	26.7	7.6	25.5
		26.4	25.1	24.3	23.1	21.4	19.5	16.1	15.5	13.6	10.8		
950	10	33.8	30.8	27.8	27.2	25.6	24.8	24.5	23.4	22.4	22.2	4.7	22.9
		21.5	21.5	21.5	21.2	20.9	20.6	20.4	18.7	18.1	11.2		
1000	2	44.1	44.1	41.7	40.6	40.2	40.1	31.4	28.6	28.4	27.6	9.2	29.3
		26.7	26.7	25.8	25.3	25.1	22.1	18.5	17.9	16.4	15.4		
1000	4	48.6	40.2	38.1	35.7	34.8	33.7	32.7	31.8	30.7	30.7	7.5	29.8
		29.4	28.1	27.3	27.1	23.9	23.2	21.8	20.8	18.3	18.2		
1000	6	38.4	37.5	32.4	32.3	32.2	32.2	30.7	30.0	27.9	25.9	5.4	27.5
		25.8	25.1	24.8	24.2	23.8	22.6	22.2	21.9	21.9	17.5		
1000	8	37.3	32.4	31.2	28.4	28.1	27.2	26.7	25.9	23.6	22.8	7.1	22.2
		21.4	18.7	18.3	16.2	16.2	15.2	14.3	13.3	13.3	13.2		
1000	10	25.4	24.9	23.4	22.6	19.7	19.6	18.9	18.7	18.1	18.1	3.8	17.9
		17.8	16.8	15.8	15.5	14.6	14.6	14.4	13.4	13.4	12.2		
1050	2	38.8	38.7	32.6	32.4	29.6	29.5	28.4	27.8	27.3	26.8	6.2	26.2
		25.2	24.6	23.6	22.2	22.1	22.1	21.8	19.6	16.1	15.1		
1050	4	35.9	34.9	33.7	33.4	32.7	32.6	29.7	28.9	23.6	22.5	7.4	24.3
		21.7	19.8	19.7	19.5	17.8	17.7	16.9	15.7	15.3	13.5		
1050	6	27.4	27.2	25.8	24.8	24.1	24.0	23.6	23.5	23.3	22.4	3.1	22.2
		22.1	21.8	21.4	21.2	20.1	19.4	19.1	19.1	18.7	14.4		
1050	8	26.6	26.2	26.1	25.2	22.5	22.2	21.9	21.5	20.6	20.5	4.6	19.7
		19.7	19.2	18.4	18.1	17.7	16.6	14.9	12.6	11.7	10.9		
1050	10	22.3	21.2	19.1	18.6	18.6	17.3	17.2	16.8	16.7	16.6	2.5	16.5
		16.3	16.2	15.9	14.9	14.4	14.2	13.7	13.6	13.5	13.4		

Table-5.36 Effect of heat treatment on volume fraction of massive carbide

Temp °C	Time (hours)	Volume fraction of massive carbide (Alloy C2) (%)										S.D.	Ave (%)
As-cast		54.8	53.1	47.0	44.8	44.3	41.8	41.6	40.4	40.3	39.6	7.6	38.7
		38.8	36.8	35.8	34.2	33.4	33.0	31.8	29.6	29.1	24.1		
800	2	47.5	47.3	46.6	39.9	39.7	39.6	38.9	37.1	36.3	35.3	6.8	35.4
		35.1	33.0	32.7	31.8	31.5	30.7	30.2	29.3	25.8	20.3		
800	4	42.5	42.2	42.1	41.9	40.5	39.7	38.4	38.2	37.8	37.3	3.9	36.9
		36.6	36.6	35.8	35.2	34.4	34.1	32.2	31.6	30.1	30.1		
800	6	45.6	39.1	36.9	36.8	36.7	36.5	36.4	35.3	34.4	34.4	5.9	32.4
		34.2	32.3	31.4	30.1	25.9	25.7	25.3	24.2	24.2	23.5		
800	8	42.9	41.3	40.4	39.1	36.1	35.7	35.5	34.2	34.2	32.5	5.5	32.6
		32.1	30.7	30.5	29.3	28.8	27.7	26.9	25.1	24.3	23.9		
800	10	39.6	35.5	35.2	34.2	33.9	33.5	32.4	31.8	31.8	31.1	3.7	30.9
		30.5	30.4	29.5	29.5	29.4	27.4	26.3	26.1	25.9	24.9		
850	2	45.3	43.4	40.6	39.7	37.6	37.4	37.1	36.9	36.9	36.4	5.8	34.3
		34.4	32.6	31.1	31.0	30.6	30.3	28.6	27.6	24.1	23.6		
850	4	45.7	44.5	43.4	40.6	39.8	38.5	37.3	37.2	36.9	36.2	5.7	35.2
		34.8	34.3	33.1	31.9	30.3	30.2	29.6	28.9	27.7	23.8		
850	6	48.4	45.6	45.6	43.6	40.2	39.4	36.1	35.7	35.3	34.7	6.8	35.3
		33.5	33.3	33.0	32.2	31.9	31.6	30.3	29.7	25.9	19.6		
850	8	39.0	37.8	37.7	36.4	33.5	33.2	32.9	31.8	31.8	30.8	4.6	31.0
		30.7	30.5	30.4	29.7	28.3	27.5	26.6	25.7	25.6	19.9		
850	10	38.9	37.3	35.5	34.8	33.9	33.8	33.6	33.6	32.7	31.9	4.9	30.6
		31.8	30.8	28.4	27.7	27.6	26.1	25.8	25.6	20.9	20.7		
900	2	46.5	43.7	42.8	38.5	37.5	37.2	35.7	34.9	34.3	34.2	4.9	34.9
		34.0	33.2	32.8	32.6	32.1	30.9	30.8	29.4	29.1	27.7		
900	4	49.7	43.5	42.7	40.4	39.5	39.1	37.5	36.6	36.3	36.2	6.5	35.3
		35.7	34.9	34.9	33.4	32.7	31.1	27.9	26.9	25.3	21.7		
900	6	45.7	38.3	37.1	36.9	36.5	36.2	34.6	34.3	33.9	33.9	6.0	32.2
		32.9	32.6	32.5	31.2	29.9	27.0	26.3	23.3	22.7	19.0		
900	8	42.1	41.5	36.6	36.1	35.7	34.2	33.8	33.2	31.2	30.3	6.2	30.3
		30.2	29.4	28.9	27.7	24.2	23.9	23.7	22.8	20.9	20.3		
900	10	42.5	40.2	39.0	37.8	36.1	34.5	32.5	30.9	28.3	27.8	8.7	27.4
		27.1	26.1	22.0	21.4	20.1	17.8	17.1	17.1	16.6	14.1		

contd...

950	2	40.2	38.8	38.1	38.0	37.9	37.7	37.6	36.5	35.6	35.6	6.4	32.6
		35.4	33.5	33.2	32.6	26.6	25.4	24.9	24.7	23.4	17.1		
950	4	38.8	36.3	35.7	35.2	34.6	34.6	33.1	32.4	32.1	32.1	3.3	32.0
		31.9	31.6	31.6	31.4	30.3	30.1	29.5	28.3	26.7	24.6		
950	6	37.5	37.0	36.9	36.6	36.1	34.3	34.2	33.8	32.9	32.3	4.8	31.
		30.2	29.6	29.0	28.6	28.5	28.2	27.1	26.9	25.1	17.9		
950	8	35.9	33.4	32.8	32.6	31.7	31.7	29.9	29.5	29.1	29.1	3.3	29.1
		29.1	28.7	28.7	28.5	27.4	27.1	26.6	25.3	23.8	21.7		
950	10	28.5	27.2	27.1	26.7	26.3	25.7	25.0	24.4	24.1	24.1	4.4	22.4
		23.1	23.1	22.7	21.4	20.1	19.2	17.1	16.5	13.5	13.1		
1000	2	47.6	39.3	34.7	33.8	32.8	31.9	31.7	30.8	29.8	29.7	7.2	28.8
		28.4	27.4	27.1	26.3	26.1	22.9	20.7	19.8	17.3	17.1		
1000	4	34.8	34.4	31.1	30.5	30.2	29.7	27.9	27.7	27.6	27.6	3.4	27.5
		27.6	26.8	26.3	25.6	24.5	24.5	24.3	23.1	23.0	22.1		
1000	6	32.2	32.1	31.5	31.2	28.2	26.9	26.5	26.5	26.2	25.5	5.1	24.5
		25.5	23.7	23.4	22.1	21.7	20.6	18.8	17.6	15.7	14.9		
1000	8	28.3	28.1	27.5	27.2	24.2	22.9	22.5	22.5	22.2	21.6	5.1	20.6
		21.5	19.7	19.4	18.1	17.7	16.7	14.9	13.6	11.7	10.9		
1000	10	25.2	25.1	24.7	24.2	21.2	19.9	19.5	19.5	19.2	18.5	5.1	17.6
		18.4	16.7	16.4	15.1	14.7	13.7	11.9	10.7	8.7	7.9		
1050	2	38.4	31.1	30.8	28.4	27.5	26.7	26.5	26.4	23.1	20.3	6.1	22.9
		19.7	19.2	19.1	18.7	18.6	18.5	18.1	16.7	15.7	13.9		
1050	4	35.1	33.1	33.1	27.6	26.8	26.0	23.6	23.5	21.8	21.4	6.5	22.1
		21.1	20.4	19.1	18.7	18.3	18.1	17.6	13.3	12.2	11.4		
1050	6	25.3	24.2	22.1	21.6	18.9	17.5	17.3	16.8	16.6	16.5	3.9	16.7
		16.4	15.6	14.2	14.2	13.7	13.6	13.2	13.2	11.9	10.7		
1050	8	24.5	22.3	21.2	21.1	20.2	19.2	18.4	16.9	16.1	15.6	3.9	16.3
		15.3	14.3	14.2	13.8	13.5	13.3	12.8	12.4	11.2	10.5		
1050	10	22.3	21.2	19.1	18.6	15.9	14.4	14.3	13.8	13.6	13.5	3.9	13.7
		13.4	12.6	11.3	11.3	10.7	10.6	10.3	10.2	8.9	7.7		

Table-5.37 Effect of heat treatment on volume fraction of massive carbide

Temp °C	Time (hours)	Volume fraction of massive carbide (Alloy C3) (%)										S.D.	Ave (%)
As-cast		50.0	48.1	42.0	41.8	41.6	40.4	39.9	39.1	39.1	39.0	5.5	38.2
		38.6	38.6	37.4	36.8	36.1	35.0	34.2	32.9	27.3	26.1		
800	2	39.1	37.1	36.8	36.7	36.5	36.4	36.2	35.3	34.4	34.4	6.3	31.4
		34.2	32.3	32.1	31.2	25.4	24.1	23.7	23.5	22.2	15.9		
800	4	44.7	44.1	39.1	38.6	38.3	36.7	36.4	35.5	33.8	32.9	6.3	32.8
		32.3	31.8	31.4	30.0	26.8	26.4	25.9	25.4	23.2	22.8		
800	6	43.6	43.0	37.9	37.5	37.2	35.6	35.3	34.4	32.7	31.8	6.3	31.7
		31.3	30.7	30.3	28.9	25.7	25.3	24.8	24.3	22.1	21.7		
800	8	42.2	42.2	41.3	37.1	36.5	36.2	36.1	32.2	31.4	31.3	5.6	32.3
		31.3	30.6	30.2	30.0	29.4	28.8	28.1	25.1	24.9	21.4		
800	10	39.6	38.6	36.1	35.3	35.2	34.1	33.3	32.4	32.3	32.2	5.3	30.9
		31.1	30.4	30.2	29.8	28.3	27.7	27.2	26.8	19.8	17.7		
850	2	40.5	38.1	38.1	37.5	37.2	36.8	36.6	36.1	33.9	32.4	4.6	32.8
		32.4	31.8	31.7	30.1	29.5	29.2	27.4	27.1	24.9	24.9		
850	4	43.8	43.6	38.9	36.3	35.9	35.9	35.2	33.4	32.9	31.6	6.2	31.8
		31.5	29.3	29.1	28.3	27.9	27.3	26.5	25.6	22.1	20.3		
850	6	44.5	42.8	36.7	34.5	34.0	31.5	31.3	30.1	29.9	29.3	7.5	28.5
		28.5	26.6	26.5	23.9	23.1	22.7	21.5	19.3	19.1	14.6		
850	8	35.3	34.6	33.3	32.1	31.1	30.2	29.9	29.3	28.9	28.5	3.6	28.4
		28.1	27.6	27.3	26.7	26.3	25.8	24.9	24.6	22.1	21.8		
850	10	46.6	38.2	36.1	33.7	32.8	31.7	30.7	29.8	28.7	28.7	7.6	27.7
		27.4	26.1	25.3	25.0	21.9	21.3	19.1	18.8	16.2	16.1		
900	2	49.6	43.9	43.5	41.9	34.4	31.7	30.9	28.7	28.3	27.4	8.5	29.9
		26.7	26.5	26.5	25.6	25.6	24.9	24.9	22.2	19.7	15.2		
900	4	39.3	37.5	35.4	34.3	32.5	31.2	30.8	30.1	28.7	27.7	6.5	27.3
		26.9	26.4	24.9	23.5	22.1	21.6	20.4	18.6	18.1	16.4		
900	6	42.0	39.1	31.3	30.8	30.7	30.1	29.4	29.3	27.6	27.5	5.3	28.0
		26.8	26.4	26.1	25.9	25.7	25.4	22.7	22.6	21.9	19.1		
900	8	35.1	32.1	31.8	30.8	29.9	29.2	29.1	28.7	28.4	28.1	4.2	26.9
		27.2	26.2	26.1	26.1	23.6	23.4	22.3	21.7	19.3	19.2		
900	10	34.2	33.3	32.9	32.6	31.1	30.9	30.8	30.8	30.1	29.4	5.0	27.3
		27.5	25.8	25.2	25.2	24.1	22.8	22.4	20.8	17.8	17.5		

contd...

950	2	39.5	37.1	33.7	33.5	32.2	31.8	31.2	30.0	29.6	29.3	4.9	28.9
		28.4	28.4	27.3	26.2	25.9	25.4	25.3	23.5	21.2	19.1		
950	4	37.4	33.9	33.6	33.4	32.8	31.5	30.9	30.8	26.6	25.3	5.5	26.9
		25.2	24.6	23.9	23.8	22.5	21.9	21.4	21.2	20.7	17.5		
950	6	33.1	32.9	31.4	30.4	29.0	28.7	28.2	27.3	26.7	26.1	4.5	25.9
		26.1	25.3	25.2	25.2	24.1	23.5	21.1	18.2	18.2	17.2		
950	8	33.8	31.6	30.2	30.1	28.9	27.9	26.8	26.2	25.9	25.5	4.2	25.3
		25.2	24.1	23.6	23.1	22.8	22.8	20.5	20.1	18.5	18.2		
950	10	32.3	31.1	28.4	27.3	27.2	26.6	25.9	24.4	24.3	23.6	5.6	22.5
		23.2	22.7	21.3	18.7	18.3	16.2	16.1	15.1	13.2	13.1		
1000	2	36.3	35.4	32.8	32.7	28.4	28.3	27.9	25.9	25.1	24.7	4.9	25.9
		23.7	23.3	22.6	22.4	22.2	22.2	21.6	21.6	21.6	19.3		
1000	4	34.4	32.5	31.6	30.1	29.4	29.1	28.2	27.1	25.6	25.4	4.6	25.5
		25.1	23.8	22.9	22.9	22.5	20.2	20.1	19.8	19.4	19.1		
1000	6	27.7	26.7	26.3	25.6	25.2	25.1	24.6	24.0	23.3	23.3	2.3	23.2
		23.1	22.4	21.9	21.9	21.7	20.6	20.5	20.4	20.2	20.1		
1000	8	26.4	25.9	25.4	25.1	25.1	24.8	24.4	23.4	22.9	22.6	2.2	22.8
		22.6	22.5	22.4	21.3	21.3	20.5	20.5	19.8	19.3	18.9		
1000	10	26.2	25.3	24.4	23.8	23.3	23.2	22.8	22.1	21.8	21.7	2.8	21.2
		21.7	20.5	20.4	20.1	19.5	19.4	18.7	18.4	16.1	15.1		
1050	2	30.3	29.3	29.1	28.8	27.6	27.3	27.3	26.7	26.4	26.0	3.6	25.2
		25.5	25.0	24.7	24.3	23.5	23.1	22.8	21.4	19.5	14.8		
1050	4	29.6	28.9	28.8	28.7	28.5	28.4	27.3	26.4	26.4	26.2	5.0	23.6
		24.3	24.1	23.4	21.1	19.6	17.9	17.4	16.1	15.5	14.2		
1050	6	29.7	26.6	26.6	26.5	25.2	25.2	24.7	24.5	23.9	23.4	3.8	22.6
		23.4	22.3	22.2	21.1	20.2	20.0	18.9	16.2	15.8	15.7		
1050	8	29.5	29.3	26.9	26.9	25.9	25.2	25.1	24.9	22.3	21.5	4.8	21.3
		18.8	18.2	17.6	17.4	17.2	17.1	17.1	16.6	15.2	14.2		
1050	10	27.7	26.9	26.7	23.7	23.1	22.4	22.0	21.7	21.2	21.2	4.6	20.0
		20.9	19.2	18.9	17.6	17.6	17.2	16.1	14.4	12.0	10.4		

Table-5.38 Summary table of effect of heat treatment on volume fraction of massive carbides

Alloy	Temp. °C	S O A K I N G					P E R I O D (hrs)				
		2	4	6	8	10	2	4	6	8	10
C 1	800	40.1	38.4	39.6	36.8	36.4					
	850	39.0	39.0	34.1	36.1	31.3					
	900	36.5	37.9	35.7	34.9	32.1					
	950	35.2	35.7	31.3	25.5	22.9					
	1000	29.3	29.8	27.5	22.2	17.9					
	1050	26.2	24.3	22.2	19.7	16.5					
C 2	800	35.4	36.9	32.4	32.6	30.9					
	850	34.3	35.2	35.3	31.0	30.6					
	900	34.9	35.3	32.2	30.3	27.4					
	950	32.6	32.0	31.1	29.1	22.4					
	1000	28.8	27.5	24.5	20.6	17.6					
	1050	22.9	22.1	16.7	16.3	13.7					
C 3	800	31.4	32.8	31.7	32.3	30.9					
	850	32.8	31.8	28.5	28.4	27.7					
	900	29.9	27.3	28.0	26.9	27.3					
	950	28.9	26.9	25.9	25.3	22.5					
	1000	25.9	25.5	23.2	22.8	21.2					
	1050	25.2	23.6	22.6	21.3	20.0					

Table-5.39 Effect of heat treatment on the average number of dispersed carbides in different classes

Alloy	Temp. °C	S O A K I N G P E R I O D (hrs)																			
		classI					classII					classIII					classIV				
		2	4	6	8	10	2	4	6	8	10	2	4	6	8	10	2	4	6	8	10
C1	800	7	9	6	4	7	2	4	3	2	5	0	0	0	1	2	0	0	0	0	0
	850	7	4	3	7	6	4	3	2	4	3	1	0	0	1	2	0	0	0	0	0
	900	6	6	6	4	-	2	1	2	2	-	0	0	0	1	-	0	0	0	0	-
	950	6	6	1	7	-	2	2	1	1	-	0	0	0	0	-	0	0	0	0	-
	1000	6	5	6	6	-	3	2	2	2	-	0	0	0	0	-	0	0	0	0	-
C2	800	6	5	9	5	7	4	2	5	3	2	1	0	1	1	1	0	0	0	0	0
	850	6	7	6	9	6	3	4	3	6	2	2	1	1	1	1	0	0	0	0	0
	900	5	6	3	6	4	3	6	2	3	3	2	0	1	0	2	0	0	0	0	0
	950	5	4	6	4	4	4	2	4	2	1	1	1	1	1	2	0	0	0	0	0
	1000	4	3	-	-	-	2	3	-	-	-	1	1	-	-	-	0	0	-	-	-
C3	800	8	7	7	9	14	7	3	4	3	6	0	0	0	0	1	0	0	0	0	0
	850	6	9	4	7	6	0	6	2	2	2	3	1	1	1	2	0	0	0	0	0
	900	7	5	3	9	7	3	2	3	2	4	1	2	1	1	0	0	0	0	0	0
	950	4	4	3	5	5	0	0	0	0	2	2	1	2	2	0	0	0	1	0	1
	1000	4	4	4	6	-	2	0	0	0	-	2	1	2	4	-	0	1	0	0	-

Table-5.40 Effect of heat treatment on percent number of dispersed carbides in different classes

Alloy	Temp. °C	S O A K I N G P E R I O D (hrs)																			
		classI					classII					classIII					classIV				
		2	4	6	8	10	2	4	6	8	10	2	4	6	8	10	2	4	6	8	10
C1	800	78	69	67	57	50	22	31	33	29	36	0	0	0	14	14	0	0	0	0	0
	850	58	57	60	58	55	33	43	40	33	27	8	0	0	8	18	0	0	0	0	0
	900	75	86	75	57	-	25	14	25	29	-	0	0	0	14	-	0	0	0	0	-
	950	75	75	50	88	-	25	25	50	13	-	0	0	0	0	-	0	0	0	0	-
	1000	67	71	75	75	-	33	29	25	25	-	0	0	0	0	-	0	0	0	0	-
C2	800	55	71	60	56	70	36	29	33	33	20	9	0	7	11	10	0	0	0	0	0
	850	55	58	60	56	67	27	33	30	38	22	18	8	10	6	11	0	0	0	0	0
	900	50	50	50	67	44	30	50	33	33	33	20	0	17	0	22	0	0	0	0	0
	950	50	57	55	57	57	40	29	36	29	14	10	14	9	14	29	0	0	0	0	0
	1000	57	43	-	-	-	29	43	-	-	-	14	14	-	-	-	0	0	-	-	-
C3	800	53	70	64	75	67	47	30	36	25	29	0	0	0	0	5	0	0	0	0	0
	850	67	56	57	70	60	0	38	29	20	20	33	6	14	10	20	0	0	0	0	0
	900	64	56	43	75	64	27	22	43	17	36	9	22	14	8	0	0	0	0	0	0
	950	67	80	50	71	56	0	0	0	0	22	33	20	33	29	11	0	0	17	0	11
	1000	50	67	67	60	-	25	0	0	0	-	25	17	33	40	-	0	1	17	0	-

Table-5.41 Effect of heat treatment on the average numbers of dispersed carbides

Temp. °C	Alloy	S O A K I N G P E R I O D (hrs)				
		2	4	6	8	10
800	C1	9	13	9	7	14
850		12	7	5	12	11
900		8	7	8	7	-
950		8	8	2	8	-
1000		9	7	8	8	-
800	C2	11	7	15	9	10
850		11	12	10	16	9
900		10	12	6	9	9
950		10	7	11	7	7
1000		7	7	-	-	-
800	C3	15	10	11	12	21
850		9	16	7	10	10
900		11	9	7	12	11
950		6	5	6	7	9
1000		8	6	6	10	-

Table-5.42 Effect of heat treatment on the volume percent of dispersed carbides

Temp. °C	Alloy	S O A K I N G P E R I O D (hrs)				
		2	4	6	8	10
800	C1	1.641	2.953	2.166	3.084	6.694
850		4.463	2.034	1.378	4.463	5.447
900		1.575	0.984	1.575	3.084	-
950		1.575	1.575	0.656	1.050	-
1000		2.166	1.509	1.575	1.575	-
800	C2	4.397	1.509	5.184	3.741	3.281
850		5.447	4.463	3.806	5.775	3.216
900		5.381	3.938	3.019	2.166	5.316
950		4.331	3.084	4.397	3.084	4.134
1000		3.084	3.609	-	-	-
800	C3	4.659	2.231	2.822	2.363	6.013
850		5.316	5.775	3.084	3.281	4.856
900		3.872	4.791	3.609	3.413	2.822
950		3.544	1.903	6.694	3.609	6.366
1000		4.725	5.119	3.544	6.956	-

Table-5.43 Effect of heat treatment on the mean diameter of dispersed carbides

Temp. °C	Alloy	S O A K I N G P E R I O D (hrs)				
		2	4	6	8	10
800	C1	0.418	0.467	0.482	0.413	0.454
850		0.458	0.537	0.520	0.458	0.394
900		0.434	0.372	0.434	0.413	-
950		0.434	0.434	0.578	0.361	-
1000		0.482	0.454	0.434	0.434	-
800	C2	0.473	0.454	0.463	0.450	0.376
850		0.394	0.458	0.434	0.488	0.385
900		0.405	0.578	0.434	0.482	0.418
950		0.491	0.413	0.473	0.413	0.289
1000		0.413	0.496	-	-	-
800	C3	0.559	0.463	0.499	0.434	0.440
850		0.193	0.488	0.413	0.376	0.347
900		0.420	0.353	0.496	0.361	0.499
950		0.193	0.231	0.145	0.206	0.353
1000		0.361	0.193	0.193	0.173	-

Table-5.44 Effect of heat treatment on Distribution Factor

Heat Treatment	C1	C2	C3
800, 2	0.378	0.278	0.474
800, 4	0.385	0.379	0.382
800, 6	0.394	0.279	0.408
800, 8	0.234	0.255	0.375
800, 10	0.262	0.220	0.279
850, 2	0.267	0.238	0.358
850, 4	0.447	0.267	0.305
850, 6	0.429	0.245	0.234
850, 8	0.267	0.305	0.220
850, 10	0.238	0.220	0.232
900, 2	0.375	0.251	0.239
900, 4	0.429	0.500	0.245
900, 6	0.375	0.254	0.299
900, 8	0.234	0.394	0.228
900, 10	-	0.270	0.408
950, 2	0.375	0.294	0.358
950, 4	0.375	0.234	0.283
950, 6	0.500	0.278	0.258
950, 8	0.453	0.234	0.325
950, 10	-	0.283	0.155
1000, 2	0.394	0.234	0.264
1000, 4	0.379	0.299	0.192
1000, 6	0.375	-	0.358
1000, 8	0.375	-	0.411

Table-5.45 Relative coarsening behaviour of the alloys

Heat Treatment	C1	C2	C3
800, 2	1.000	1.000	1.000
800, 4	1.018	1.363	0.805
800, 6	1.042	1.003	0.860
800, 8	0.619	0.917	0.791
800,10	0.693	0.791	0.588
850, 2	0.706	0.856	0.755
850, 4	1.182	0.960	0.643
850, 6	1.134	0.881	0.493
850, 8	0.706	1.097	0.464
850,10	0.629	0.791	0.489
900, 2	0.992	0.902	0.504
900, 4	1.134	1.798	0.516
900, 6	0.992	0.913	0.630
900, 8	0.619	1.417	0.481
900,10	-	0.971	0.860
950, 2	0.992	1.057	0.755
950, 4	0.992	0.841	0.597
950, 6	1.322	1.000	0.544
950, 8	1.198	0.841	0.685
950,10	-	1.017	0.327
1000, 2	1.042	0.841	0.556
1000, 4	1.002	1.075	0.405
1000, 6	0.992	-	0.755
1000, 8	0.992	-	0.867

Table-5.46 Effect of heat treatment on size and distribution of dispersed carbides (Alloy C1)

Temp °C	Time (hrs)	Hard- ness HV30	MD µm	CLASSI		CLASSII		CLASSIII		CLASSIV	
				%area	%NOP	%area	%NOP	%area	%NOP	%area	%NOP
800	2	589	.418	27	77	71	22	0	0	0	0
	4	576	.467	20	69	80	30	0	0	0	0
	6	586	.482	18	66	81	33	0	0	0	0
	8	591	.413	8	57	38	28	53	14	0	0
	10	583	.454	6	50	44	35	49	14	0	0
850	2	569	.458	10	58	52	33	36	8	0	0
	4	575	.537	12	57	87	42	0	0	0	0
	6	578	.520	14	60	85	40	0	0	0	0
	8	558	.458	10	58	52	33	36	8	0	0
	10	552	.394	7	54	32	27	60	18	0	0
900	2	561	.434	25	75	74	25	0	0	0	0
	4	554	.372	39	85	59	14	0	0	0	0
	6	557	.434	25	75	74	25	0	0	0	0
	8	546	.413	8	57	38	28	53	14	0	0
950	2	542	.434	25	75	74	25	0	0	0	0
	4	537	.434	25	75	74	25	0	0	0	0
	6	529	.578	10	50	90	50	0	0	0	0
	8	519	.361	43	87	56	12	0	0	0	0
1000	2	512	.482	18	66	81	33	0	0	0	0
	4	507	.454	21	71	78	28	0	0	0	0
	6	487	.434	25	75	74	25	0	0	0	0
	8	492	.434	25	75	74	25	0	0	0	0

Table-5.47 Effect of heat treatment on size and distribution of dispersed carbides (Alloy C2)

Temp °C	Time (hrs)	Hard- ness HV30	MD µm	CLASSI		CLASSII		CLASSIII		CLASSIV	
				%area	%NOP	%area	%NOP	%area	%NOP	%area	%NOP
800	2	564	.473	8	54	53	36	37	9	0	0
	4	560	.454	21	71	78	28	0	0	0	0
	6	552	.463	11	60	56	33	31	6	0	0
	8	549	.450	8	55	47	33	43	11	0	0
	10	532	.376	13	70	35	20	50	10	0	0
850	2	557	.394	7	54	32	27	60	18	0	0
	4	547	.458	10	58	52	33	36	8	0	0
	6	532	.434	10	60	46	30	43	10	0	0
	8	518	.488	10	56	61	37	28	6	0	0
	10	521	.385	12	66	36	22	51	11	0	0
900	2	557	.405	6	50	32	30	60	20	0	0
	4	564	.578	10	50	90	50	0	0	0	0
	6	532	.434	6	50	39	33	54	16	0	0
	8	524	.482	18	66	81	33	0	0	0	0
	10	517	.418	4	44	33	33	61	22	0	0
950	2	516	.491	7	50	54	40	37	10	0	0
	4	512	.413	8	57	38	28	53	14	0	0
	6	526	.473	8	54	53	36	37	9	0	0
	8	499	.413	8	57	38	28	53	14	0	0
	10	498	.289	6	57	14	14	79	28	0	0
1000	2	482	.413	8	57	38	28	53	14	0	0
	4	501	.496	5	42	49	42	45	14	0	0

Table-5.48 Effect of heat treatment on size and distribution of dispersed carbides (Alloy C3)

Temp °C	Time (hrs)	Hard- ness HV30	MD µm	CLASSI		CLASSII		CLASSIII		CLASSIV	
				%area	%NOP	%area	%NOP	%area	%NOP	%area	%NOP
800	2	541	.559	11	53	88	46	0	0	0	0
	4	549	.463	20	70	79	30	0	0	0	0
	6	535	.499	16	63	83	36	0	0	0	0
	8	537	.434	25	75	75	25	0	0	0	0
	10	527	.440	15	66	58	28	26	4	0	0
850	2	537	.193	7	66	0	0	92	33	0	0
	4	524	.488	10	56	61	37	28	6	0	0
	6	501	.413	8	57	38	28	53	14	0	0
	8	523	.376	13	70	35	20	50	10	0	0
	10	513	.347	8	60	24	20	67	20	0	0
900	2	519	.420	11	63	45	27	42	9	0	0
	4	523	.353	6	55	24	22	68	22	0	0
	6	519	.496	5	42	49	42	45	14	0	0
	8	512	.361	17	75	34	16	48	8	0	0
	10	492	.499	16	63	83	36	0	0	0	0
950	2	491	.193	7	66	0	0	92	33	0	0
	4	496	.231	13	80	0	0	86	20	0	0
	6	452	.145	2	50	0	0	49	33	0	16
	8	458	.206	9	71	0	0	90	28	0	0
	10	444	.353	5	55	18	22	25	11	0	11
1000	2	471	.361	5	50	25	25	69	25	0	0
	4	454	.193	5	66	0	0	32	16	0	16
	6	429	.193	7	66	0	0	92	33	0	0

Table-5.49 Effect of heat treatment on the contribution of Distribution Factor of different classes (Alloy C1)

Temp. °C	Time (hrs)	Hardness HV30	MD μm	Volume fraction of DC	Contribution of DF from various classes				Total DF
					CLASS I	CLASS II	CLASS III	CLASS IV	
800	2	589	.418	1.641	.218	.160	.000	.000	.378
800	4	576	.467	2.953	.138	.246	.000	.000	.385
800	6	586	.482	2.166	.121	.273	.000	.000	.394
800	8	591	.413	3.084	.049	.109	.076	.000	.234
800	10	583	.454	6.694	.034	.158	.070	.000	.262
850	2	569	.458	4.463	.060	.176	.031	.000	.267
850	4	575	.537	2.034	.074	.373	.000	.000	.447
850	6	578	.520	1.378	.086	.343	.000	.000	.429
850	8	558	.458	4.463	.060	.176	.031	.000	.267
850	10	552	.394	5.447	.039	.089	.110	.000	.238
900	2	561	.434	1.575	.188	.188	.000	.000	.375
900	4	554	.372	.984	.343	.086	.000	.000	.429
900	6	557	.434	1.575	.188	.188	.000	.000	.375
900	8	546	.413	3.084	.049	.109	.076	.000	.234
950	2	542	.434	1.575	.188	.188	.000	.000	.375
950	4	537	.434	1.575	.188	.188	.000	.000	.375
950	6	529	.578	.656	.050	.450	.000	.000	.500
950	8	519	.361	1.050	.383	.070	.000	.000	.453
1000	2	512	.482	2.166	.121	.273	.000	.000	.394
1000	4	507	.454	1.509	.155	.224	.000	.000	.379
1000	6	487	.434	1.575	.188	.188	.000	.000	.375
1000	8	492	.434	1.575	.188	.188	.000	.000	.375

Table-5.50 Effect of heat treatment on the contribution of Distribution Factor of different classes (Alloy C2)

Temp. °C	Time (hrs)	Hardness HV30	MD µm	Volume fraction of DC	Contribution of DF from various classes				Total DF
					CLASSI	CLASSII	CLASSIII	CLASSIV	
800	2	564	.473	4.397	.049	.195	.034	.000	.278
800	4	560	.454	1.509	.155	.224	.000	.000	.379
800	6	552	.463	5.184	.068	.190	.021	.000	.279
800	8	549	.450	3.741	.049	.158	.049	.000	.255
800	10	532	.376	3.281	.098	.072	.050	.000	.220
850	2	557	.394	5.447	.039	.089	.110	.000	.238
850	4	547	.458	4.463	.060	.176	.031	.000	.267
850	6	532	.434	3.806	.062	.140	.043	.000	.245
850	8	518	.488	5.775	.058	.230	.018	.000	.305
850	10	521	.385	3.216	.082	.082	.057	.000	.220
900	2	557	.405	5.381	.030	.099	.122	.000	.251
900	4	564	.578	3.938	.050	.450	.000	.000	.500
900	6	532	.434	3.019	.033	.130	.091	.000	.254
900	8	524	.482	2.166	.121	.273	.000	.000	.394
900	10	517	.418	5.316	.022	.111	.137	.000	.270
950	2	516	.491	4.331	.038	.218	.038	.000	.294
950	4	512	.413	3.084	.049	.109	.076	.000	.234
950	6	526	.473	4.397	.049	.195	.034	.000	.278
950	8	499	.413	3.084	.049	.109	.076	.000	.234
950	10	498	.289	4.134	.036	.020	.227	.000	.283
1000	2	482	.413	3.084	.049	.109	.076	.000	.234
1000	4	501	.496	3.609	.023	.210	.065	.000	.299

Table-5.51 Effect of heat treatment on the contribution of Distribution Factor of different classes (Alloy C3)

Temp. °C	Time (hrs)	Hardness HV30	MD µm	Volume fraction of DC	Contribution of DF from various classes				Total DF
					CLASSI	CLASSII	CLASSIII	CLASSIV	
800	2	541	.559	4.659	.060	.414	.000	.000	.474
800	4	549	.463	2.231	.144	.238	.000	.000	.382
800	6	535	.499	2.822	.104	.304	.000	.000	.408
800	8	537	.434	2.363	.188	.188	.000	.000	.375
800	10	527	.440	6.103	.100	.166	.013	.000	.279
850	2	537	.193	5.316	.049	.000	.309	.000	.358
850	4	524	.488	5.775	.058	.230	.018	.000	.305
850	6	501	.413	3.084	.049	.109	.076	.000	.234
850	8	523	.376	3.281	.098	.072	.050	.000	.220
850	10	513	.347	4.856	.049	.049	.135	.000	.232
900	2	519	.420	3.872	.076	.125	.039	.000	.239
900	4	523	.353	4.791	.038	.055	.152	.000	.245
900	6	519	.496	3.609	.023	.210	.065	.000	.299
900	8	512	.361	3.413	.130	.058	.040	.000	.228
900	10	492	.499	2.822	.104	.304	.000	.000	.408
950	2	491	.193	3.544	.049	.000	.309	.000	.358
950	4	496	.231	1.903	.110	.000	.172	.000	.283
950	6	452	.145	6.694	.015	.000	.163	.080	.258
950	8	458	.206	3.609	.065	.000	.260	.000	.325
950	10	444	.353	6.366	.029	.041	.029	.056	.155
1000	2	471	.361	4.725	.028	.063	.174	.000	.264
1000	4	454	.193	5.119	.034	.000	.053	.105	.192
1000	6	429	.193	3.544	.049	.000	.309	.000	.358
1000	8	399	.173	6.956	.034	.000	.377	.000	.411

TABLE 5.52

EFFECT OF HEAT TREATMENT ON THE PERCENT DISTRIBUTION FACTOR IN DIFFERENT CLASSES

H/T Temp. Deg C	Soaking Time																			
	2 hours		4 hours		6 hours		8 hours		10 hours											
	I	II	III	IV	I	II	III	IV	I	II	III	IV	I	II	III	IV				
Alloy C1																				
800	58	42	00	00	36	64	00	00	31	69	00	00	21	47	32	00	13	60	27	00
850	22	67	11	00	17	83	16	00	20	80	00	00	22	67	11	00	17	37	46	00
900	50	50	00	00	80	20	00	00	50	50	00	00	21	47	32	00	--	--	--	--
950	50	50	00	00	50	50	00	00	10	90	00	00	86	14	00	00	--	--	--	--
1000	31	69	00	00	41	59	00	00	50	50	00	00	50	50	00	00	--	--	--	--
Alloy C2																				
800	18	70	12	00	41	59	00	00	24	58	18	00	19	62	19	00	44	33	23	00
850	17	37	46	00	22	67	11	00	25	57	18	00	19	75	06	00	39	37	26	00
900	12	39	49	00	10	90	00	00	13	51	36	00	31	69	00	00	08	41	51	00
950	13	74	13	00	21	47	32	00	18	70	12	00	21	47	32	00	13	07	80	00
1000	21	47	32	00	08	70	22	00	--	--	--	--	--	--	--	--	--	--	--	--
Alloy C3																				
800	13	87	00	00	38	62	00	00	25	75	00	00	50	50	00	00	36	59	05	00
850	14	00	86	00	19	75	06	00	21	47	32	00	44	33	23	00	21	21	58	00
900	32	52	16	00	16	22	62	00	08	70	22	00	57	25	18	00	25	75	00	00
950	14	00	86	00	39	00	61	00	06	00	63	31	20	00	80	00	19	26	19	36
1000	11	24	65	00	18	00	28	00	14	00	86	00	08	00	92	00	--	--	--	--

Table-5.53 Relative contribution of the factors constituting the model

ALLOY: C1

Heat treatment		Overall hardness HV30	First factor value	First factor %	Second factor value	Second factor %
800	2	594	594	100.00	0	.00
800	4	594	594	100.00	0	.00
800	6	593	594	99.83	-1	.17
800	8	593	594	99.83	-1	.17
800	10	592	594	99.66	-2	.34
850	2	571	573	99.65	-2	.35
850	4	569	573	99.30	-4	.70
850	6	566	573	98.76	-7	1.24
850	8	564	573	98.40	-9	1.60
850	10	561	573	97.86	-12	2.14
900	2	551	555	99.27	-4	.73
900	4	547	555	98.54	-8	1.46
900	6	542	555	97.60	-13	2.40
900	8	538	555	96.84	-17	3.16
900	10	533	555	95.87	-22	4.13
950	2	533	539	98.87	-6	1.13
950	4	527	539	97.72	-12	2.28
950	6	520	539	96.35	-19	3.65
950	8	514	539	95.14	-25	4.86
950	10	508	539	93.90	-31	6.10
1000	2	517	525	98.45	-8	1.55
1000	4	509	525	96.86	-16	3.14
1000	6	500	525	95.00	-25	5.00
1000	8	492	525	93.29	-33	6.71
1000	10	484	525	91.53	-41	8.47
1050	2	502	512	98.01	-10	1.99
1050	4	492	512	95.93	-20	4.07
1050	6	481	512	93.56	-31	6.44
1050	8	471	512	91.30	-41	8.70
1050	10	461	512	88.94	-51	11.06

Table-5.54 Relative contribution of the factors constituting the model

ALLOY: C2

Heat treatment		Overall hardness HV30	First factor value	First factor %	Second factor value	Second factor %
800	2	572	572	100.00	0	.00
800	4	571	572	99.82	-1	.18
800	6	570	572	99.65	-2	.35
800	8	569	572	99.47	-3	.53
800	10	568	572	99.30	-4	.70
850	2	554	560	98.92	-6	1.08
850	4	547	560	97.62	-13	2.38
850	6	541	560	96.49	-19	3.51
850	8	534	560	95.13	-26	4.87
850	10	527	560	93.74	-33	6.26
900	2	536	548	97.76	-12	2.24
900	4	524	548	95.42	-24	4.58
900	6	511	548	92.76	-37	7.24
900	8	499	548	90.18	-49	9.82
900	10	487	548	87.47	-61	12.53
950	2	520	538	96.54	-18	3.46
950	4	502	538	92.83	-36	7.17
950	6	484	538	88.84	-54	11.16
950	8	466	538	84.55	-72	15.45
950	10	448	538	79.91	-90	20.09
1000	2	505	528	95.45	-23	4.55
1000	4	481	528	90.23	-47	9.77
1000	6	457	528	84.46	-71	15.54
1000	8	434	528	78.34	-94	21.66
1000	10	410	528	71.22	-118	28.78
1050	2	491	520	94.09	-29	5.91
1050	4	462	520	87.45	-58	12.55
1050	6	432	520	79.63	-88	20.37
1050	8	403	520	70.97	-117	29.03
1050	10	373	520	60.59	-147	39.41

Table-5.55 Relative contribution of the factors constituting the model

ALLOY: C3

Heat treatment		Overall hardness HV30	First factor value	First factor %	Second factor value	Second factor %
800	2	550	548	99.64	2	.36
800	4	552	548	99.28	4	.72
800	6	553	548	99.10	5	.90
800	8	555	548	98.74	7	1.26
800	10	557	548	98.38	9	1.62
850	2	528	532	99.24	-4	.76
850	4	524	532	98.47	-8	1.53
850	6	520	532	97.69	-12	2.31
850	8	516	532	96.90	-16	3.10
850	10	512	532	96.09	-20	3.91
900	2	509	518	98.23	-9	1.77
900	4	499	518	96.19	-19	3.81
900	6	489	518	94.07	-29	5.93
900	8	479	518	91.86	-39	8.14
900	10	469	518	89.55	-49	10.45
950	2	491	506	96.95	-15	3.05
950	4	475	506	93.47	-31	6.53
950	6	459	506	89.76	-47	10.24
950	8	443	506	85.78	-63	14.22
950	10	427	506	81.50	-79	18.50
1000	2	474	495	95.57	-21	4.43
1000	4	452	495	90.49	-43	9.51
1000	6	430	495	84.88	-65	15.12
1000	8	409	495	78.97	-86	21.03
1000	10	387	495	72.09	-108	27.91
1050	2	458	485	94.10	-27	5.90
1050	4	430	485	87.21	-55	12.79
1050	6	403	485	79.65	-82	20.35
1050	8	375	485	70.67	-110	29.33
1050	10	347	485	60.23	-138	39.77

Table-5.56 Effect of temperature and time on hardness (Alloy C1)

H/T	Experi- mental hardness HV30	Original model equation (5.25)			Model according to equation (5.31)			Model according to equation (5.28)			
		(a)	(b)	(c)	(a)	(b)	(c)	(a)	(b)	(c)	
800	2	589	593	-4	-.67	547	42	7.68	541	48	8.87
850	2	569	570	-1	-.18	522	47	9.00	513	56	10.92
900	2	561	550	11	2.00	499	62	12.42	489	72	14.72
950	2	542	532	10	1.88	478	64	13.39	467	75	16.06
1000	2	512	516	-4	-.78	460	52	11.30	447	65	14.54
1050	2	491	501	-10	-2.00	442	49	11.09	429	62	14.45
800	4	576	592	-16	-2.70	546	30	5.49	537	39	7.26
850	4	575	568	7	1.23	517	58	11.22	506	69	13.64
900	4	554	546	8	1.47	489	65	13.29	478	76	15.90
950	4	537	526	11	2.09	464	73	15.73	452	85	18.81
1000	4	507	508	-1	-.20	440	67	15.23	428	79	18.46
1050	4	474	491	-17	-3.46	418	56	13.40	405	69	17.04
800	6	586	592	-6	-1.01	546	40	7.33	534	52	9.74
850	6	578	565	13	2.30	512	66	12.89	498	80	16.06
900	6	557	542	15	2.77	480	77	16.04	466	91	19.53
950	6	529	520	9	1.73	450	79	17.56	436	93	21.33
1000	6	487	499	-12	-2.40	421	66	15.68	408	79	19.36
1050	6	480	481	-1	-.21	394	86	21.83	382	98	25.65
800	8	591	591	0	.00	546	45	8.24	530	61	11.51
850	8	558	563	-5	-.89	507	51	10.06	491	67	13.65
900	8	546	537	9	1.68	470	76	16.17	455	91	20.00
950	8	519	513	6	1.17	435	84	19.31	421	98	23.28
1000	8	492	491	1	.20	402	90	22.39	389	103	26.48
1050	8	471	470	1	.21	370	101	27.30	358	113	31.56
800	10	583	591	-8	-1.35	546	37	6.78	527	56	10.63
850	10	552	561	-9	-1.60	502	50	9.96	484	68	14.05
900	10	537	533	4	.75	460	77	16.74	443	94	21.22
950	10	515	507	8	1.58	421	94	22.33	405	110	27.16
1000	10	487	483	4	.83	382	105	27.49	369	118	31.98
1050	10	451	460	-9	-1.96	346	105	30.35	335	116	34.63

C.C = 0.976	C.C = 0.965	C.C = 0.962
S.D = 1.593	S.D = 12.683	S.D = 14.844
MAX.DEV. = 17	MAX.DEV. = 105	MAX.DEV. = 118

- (a) represents the calculated hardness value from the model
- (b) represents the deviation of the calculated hardness from the experimental hardness
- (c) represents the % deviation of the calculated hardness from the observed hardness

Table-5.57 Effect of temperature and time on hardness (Alloy C2)

H/T	Experi- mental hardness HV30	Original model equation (5.26)			Model according to equation (5.32)			Model according to equation (5.29)			
		(a)	(b)	(c)	(a)	(b)	(c)	(a)	(b)	(c)	
800	2	564	571	-7	-1.23	573	-9	-1.57	563	1	.18
850	2	557	552	5	.91	549	8	1.46	536	21	3.92
900	2	557	535	22	4.11	528	29	5.49	512	45	8.79
950	2	516	519	-3	-.58	508	8	1.57	491	25	5.09
1000	2	482	504	-22	-4.37	490	-8	-1.63	471	11	2.34
1050	2	454	490	-36	-7.35	473	-19	-4.02	453	1	.22
800	4	560	570	-10	-1.75	569	-9	-1.58	555	5	.90
850	4	547	546	1	.18	541	6	1.11	525	22	4.19
900	4	564	523	41	7.84	515	49	9.51	498	66	13.25
950	4	512	501	11	2.20	491	21	4.28	473	39	8.25
1000	4	501	480	21	4.38	468	33	7.05	450	51	11.33
1050	4	442	460	-18	-3.91	447	-5	-1.12	429	13	3.03
800	6	552	569	-17	-2.99	565	-13	-2.30	547	5	.91
850	6	532	539	-7	-1.30	533	-1	-.19	514	18	3.50
900	6	532	510	22	4.31	502	30	5.98	483	49	10.14
950	6	526	483	43	8.90	474	52	10.97	455	71	15.60
1000	6	451	456	-5	-1.10	447	4	.89	429	22	5.13
1050	6	444	431	13	3.02	421	23	5.46	404	40	9.90
800	8	549	568	-19	-3.35	561	-12	-2.14	539	10	1.86
850	8	518	532	-14	-2.63	524	-6	-1.15	502	16	3.19
900	8	524	498	26	5.22	489	35	7.16	469	55	11.73
950	8	499	465	34	7.31	457	42	9.19	437	62	14.19
1000	8	404	433	-29	-6.70	425	-21	-4.94	408	-4	-.98
1050	8	359	401	-42	-10.47	396	-37	-9.34	380	-21	-5.53
800	10	532	567	-35	-6.17	557	-25	-4.49	531	1	.19
850	10	521	526	-5	-.95	516	5	.97	491	30	6.11
900	10	517	486	31	6.38	477	40	8.39	454	63	13.88
950	10	498	447	51	11.41	440	58	13.18	419	79	18.85
1000	10	487	409	-22	-5.38	404	-17	-4.21	386	1	.26
1050	10	356	372	-16	-4.30	370	-14	-3.78	355	1	.28

C.C = 0.908	C.C = 0.905	C.C = 0.901
S.D = 4.524	S.D = 4.824	S.D = 6.752
MAX.DEV. = 51	MAX.DEV. = 58	MAX.DEV. = 79

- (a) represents the calculated hardness value from the model
- (b) represents the deviation of the calculated hardness from the experimental hardness
- (c) represents the % deviation of the calculated hardness from the observed hardness

Table-5.58 Effect of temperature and time on hardness (Alloy C3)

H/T	Experi- mental hardness HV30	Original model equation (5.27)			Model according to equation (5.33)			Model according to equation (5.30)			
		(a)	(b)	(c)	(a)	(b)	(c)	(a)	(b)	(c)	
800	2	541	549	-8	-1.46	547	-6	-1.10	541	0	.00
850	2	537	528	9	1.70	522	15	2.87	513	24	4.68
900	2	519	508	11	2.17	499	20	4.01	489	30	6.13
950	2	491	490	1	.20	478	13	2.72	467	24	5.14
1000	2	471	473	-2	-.42	460	11	2.39	447	24	5.37
1050	2	429	457	-28	-6.13	442	-13	-2.94	429	0	.00
800	4	549	551	-2	-.36	546	3	.55	537	12	2.23
850	4	524	523	1	.19	517	7	1.35	506	18	3.56
900	4	523	498	25	5.02	489	34	6.95	478	45	9.41
950	4	496	474	22	4.64	464	32	6.90	452	44	9.77
1000	4	454	451	3	.67	440	14	3.18	428	26	6.17
1050	4	410	429	-19	-4.43	418	-8	-1.91	405	5	1.23
800	6	535	552	-17	-3.08	546	-11	-2.01	534	1	.19
850	6	501	519	-18	-3.47	512	-11	-2.15	498	3	.60
900	6	519	488	31	6.35	480	39	8.13	466	53	11.37
950	6	452	458	-6	-1.31	450	2	.44	436	16	3.67
1000	6	429	429	0	.00	421	8	1.90	408	21	5.15
1050	6	406	401	5	1.25	394	12	3.05	382	24	6.28
800	8	537	554	-17	-3.07	546	-9	-1.65	530	7	1.32
850	8	523	515	8	1.55	507	16	3.16	491	32	6.52
900	8	512	478	34	7.11	470	42	8.94	455	57	12.53
950	8	458	442	16	3.62	435	23	5.29	421	37	8.79
1000	8	399	407	-8	-1.97	402	-3	-.75	389	10	2.57
1050	8	353	374	-21	-5.61	370	-17	-4.59	358	-5	-1.40
800	10	527	556	-29	-5.22	546	-19	-3.48	527	0	.00
850	10	513	511	2	.39	502	11	2.19	484	29	5.99
900	10	492	468	24	5.13	460	32	6.96	443	49	11.06
950	10	444	426	18	4.23	421	23	5.46	405	39	9.63
1000	10	377	386	-9	-2.33	382	-5	-1.31	369	8	2.17
1050	10	335	346	-11	-3.18	346	-11	-3.18	335	0	.00

C.C = 0.959	C.C = 0.957	C.C = 0.955
S.D = 3.053	S.D = 3.448	S.D = 4.999
MAX.DEV. = 34	MAX.DEV. = 42	MAX.DEV. = 57

- (a) represents the calculated hardness value from the model
- (b) represents the deviation of the calculated hardness from the experimental hardness
- (c) represents the % deviation of the calculated hardness from the observed hardness

Table-5.60 Dispersed second phase based Heterogeneity Index of the alloys as influenced by heat treating parameters

ALLOY	H/T TEMP. °C	S O A K I N G D U R A T I O N (hours)				
		2	4	6	8	10
C 1	800	.58	.36	.31	.53	.40
	850	.34	.17	.20	.34	.63
	900	.50	.80	.50	.53	.50
	950	.50	.10	.85	.31	.41
	1000	.50	.50	.30	.41	.32
C 2	800	.38	.67	.63	.34	.43
	850	.25	.63	.61	.10	.49
	900	.31	.59	.26	.53	.30
	950	.53	.93	.53	.29	1.00
	1000	.13	.38	.25	.50	.41
C 3	800	1.00	.25	.53	.67	.79
	850	.48	.78	.29	.75	.25
	900	1.00	1.00	1.00	1.00	.74
	950	.77	1.00	1.00	1.00	1.00
	1000	1.00	1.00	1.00	.00	.00

TABLE-6.1 PHASES UNDER CONSIDERATION

NO. (S)	ASTM CODE	PHASE(S)	LATTICE TYPE	LATTICE PARAMETER		
				A	B	C
1	06-0696	ALPHA IRON	CUBIC(BCC)	2.8664	.0000	.0000
2	23-298	AUSTENITE	CUBIC(FCC)	3.6000	.0000	.0000
3	-----	MARTENSITE	CUBIC(BCT)	-----	-----	-----
4	14-0407	CR23C6	CUBIC	10.6380	.0000	.0000
5	-----	MN23C6	-----	-----	-----	-----
6	23-1113	FE3C(CEMENTITE)	ORTHORHOMBIC	4.5144	5.0787	6.7297
7	20-509	FE5C2	MONOCLINIC	11.5630	4.5730	5.0580
8	20-508	FE5C2(HAGG)	MONOCLINIC	11.5600	4.5600	5.0300
9	14-176	MN5C2	MONOCLINIC	5.0860	4.5730	11.6600
10	16-0038	MN5C2(PD5B2)	MONOCLINIC	11.6600	4.5730	5.0860
11	17-333	FE7C3(2)	HEXAGONAL	6.8820	.0000	4.5400
12	-----	CR7C3(2)	HEXAGONAL	13.9000	.0000	4.5400
13	11-0550	CR7C3	HEXAGONAL(TR)	13.9800	.0000	4.5230
14	05-0720	(CR, FE)7C3	HEXAGONAL	13.9800	.0000	4.5230
15	03-0975	(CR7C3+MN7C3)	-----	2.2220	.0000	.0000
16	14-519	CR2C	HEXAGONAL	2.7900	.0000	4.4600
17	14-406	CR3C2	ORTHORHOMBIC	11.4600	5.5200	2.8210
18	26-782	FE2C(NEFA)	ORTHORHOMBIC	4.7040	4.2180	2.8300
19	20-522	FE0.6MN5.4C2	HEXAGONAL	5.7700	.0000	6.9800
20	23-0064	C(GRAPHITE)	HEXAGONAL	2.4630	.0000	6.7140
21	13-534	FE2O3	RHOMBOHEDRAL	5.0340	.0000	13.7520
22	13-504	CR2O3	HEXAGONAL	4.9540	.0000	13.5840
23	26-1116	CU2S(1)	HEXAGONAL	3.9610	.0000	36.7220
24	06-518	MNS	CUBIC	5.2236	.0000	.0000
25	04-836	COPPER	CUBIC	3.6150	.0000	.0000
26	26-798	FE8SI2C	TRICLINIC	6.3470	6.4140	9.7200
27	05-0708	FE-CR	TETRAGONAL	8.7990	.0000	4.5440
28	06-645	CRMN3	TETRAGONAL	8.8000	.0000	4.5880
29	20-706	MN15C4	HEXAGONAL	7.4920	.0000	12.0700
30	17-897	FE2C	MONOCLINIC	2.7940	2.7940	4.3600

X-RAY WAVE LENGTH(A°)= 1.9373

TABLE-6.2

SUMMARY TABLE OF DIFFRACTOGRAM INDEXING

ALLOY: C1 AS-CAST		PHASE(S)																	INT													
DIFF. ANGLE	1	3	5	7	9	11	13	15	17	19	21	23	25	27	29																	
48.1	0	0	0	1	1	1	0	1	0	0	0	0	0	1	0	0	1	0	0	0	0	0	0	0	0	0	0	0	0	0	0	6.0
54.9	0	0	0	0	0	1	1	0	0	0	0	1	0	0	0	1	1	0	1	0	0	0	0	0	0	0	0	0	0	0	1	3.5
55.3	0	1	0	0	0	0	1	0	1	1	0	0	0	0	0	0	0	0	0	0	0	0	0	1	1	0	0	1	0	40.0		
55.9	0	0	1	0	0	1	0	1	1	1	0	0	0	0	0	0	1	0	0	1	0	0	0	0	1	1	1	0	0	9.0		
58.9	0	0	0	0	0	1	0	0	0	1	0	0	0	0	0	0	0	0	0	0	0	0	0	0	1	1	1	0	0	5.0		
64.7	0	0	0	0	0	0	1	0	1	0	1	0	1	1	0	0	1	0	0	0	0	1	0	0	1	1	0	0	0	15.0		
65.2	0	1	0	1	1	0	0	1	0	0	0	0	0	0	0	0	0	0	0	0	0	0	0	1	1	0	0	0	0	8.0		
* 65.7	0	0	0	1	0	0	0	0	0	0	0	1	1	0	1	0	1	0	0	0	0	0	0	0	0	1	0	0	1	4.0		
85.2	1	0	0	0	0	0	0	0	0	0	0	0	0	0	0	0	0	0	0	0	0	0	0	0	0	0	0	0	0	4.0		
98.4	0	0	0	0	0	0	0	0	0	0	0	1	0	0	0	1	0	0	0	0	0	0	1	0	1	0	0	0	0	10.0		
99.0	0	0	0	0	0	0	0	0	0	0	0	0	0	0	0	0	0	0	0	0	0	0	1	0	0	0	0	0	0	7.0		
114.6	0	0	0	0	0	0	0	0	0	0	1	0	0	0	0	0	1	1	0	0	0	0	0	0	0	0	0	0	0	5.0		
125.4	0	0	0	0	0	0	1	0	0	0	0	0	0	0	0	0	0	0	0	0	0	0	0	1	0	0	0	0	0	9.0		
0 2 0 3 2 4 3 4 3 3 2 2 3 0 2 0 5 3 0 0 0 2 2 0 4 6 2 2 3 0																																

0 = ABSENT 1 = PRESENT * = PROBABLE DIFF. ANGLE FOR K-BETA RADIATION
DETAILED ANALYSIS OF PHASE(S) ACTUALLY PRESENT

S.N.	PHASE PRESENT	DIFF. ANGLE	PEAK INT	D I/10	D MEAS	D STD	DIFF PLANE	INT STD	CONF LIMIT
(1)	AUSTENITE	55.3	100	100	2.088	2.080	111	100	99.8
		65.2	20	20	1.798	1.800	200	80	99.9
(2)	FE3C(CEMENTITE)	48.1	14	66	2.378	2.380	112	65	99.9
		54.9	8	38	2.102	2.100	121	60	99.9
		55.9	22	100	2.067	2.060	210	70	99.8
		58.9	12	55	1.971	1.970	211	55	100.0
(3)	FE5C2(HAGG)	48.1	14	66	2.378	2.390	202	20	99.7
		55.9	22	100	2.067	2.060	510	100	99.8
		65.2	20	88	1.798	1.800	312	70	99.9
		125.4	22	100	1.090	1.090	404	20	100.0
(4)	MN5C2(PD5B2)	55.3	100	100	2.088	2.078	21	100	99.7
		55.9	22	22	2.067	2.058	510	80	99.7
		58.9	12	12	1.971	1.972	600	80	100.0
(5)	FE7C3(2)	64.7	37	100	1.811	1.807	22	20	99.8
		114.6	12	33	1.151	1.153	501	10	99.7
(6)	CR7C3	64.7	37	100	1.811	1.810	431	70	100.0
		65.7	10	26	1.786	1.780	521	50	99.7
		98.4	25	66	1.280	1.280	0	60	100.0
(7)	(CR7C3+MN7C3)	48.1	14	100	2.378	2.380	333	80	99.9
		65.7	10	66	1.786	1.780	980	60	99.7
(8)	COPPER	55.3	100	100	2.088	2.088	111	100	100.0
		64.7	37	37	1.811	1.808	200	46	99.9
		98.4	25	25	1.280	1.278	220	20	99.8
		125.4	22	22	1.090	1.090	311	17	100.0
(9)	FE8SI2C	55.3	100	100	2.088	2.080	131	80	99.8
		55.9	22	22	2.067	2.070	210	80	99.9
		58.9	12	12	1.971	1.970	212	60	100.0
		64.7	37	37	1.811	1.810	15	20	100.0
		65.2	20	20	1.798	1.794	312	20	99.8
		65.7	10	10	1.786	1.780	301	20	99.7
(10)	MN15C4	55.3	100	100	2.088	2.094	213	100	99.8
		65.2	20	20	1.798	1.800	310	20	99.9
		65.7	10	10	1.786	1.780	311	50	99.7

Martensite additionally present

TABLE-6.4 SUMMARY TABLE OF DIFFRACTOGRAM INDEXING

ALLOY: C1		H/T TEMPERATURE: 850°C														SOAKING DURATION: 6HOURS				INT												
DIFF. ANGLE		1	3	5	7	9	11	13	15	17	19	21	23	25	27	29																
54.3	0	0	0	0	0	0	0	1	1	1	0	1	1	1	0	0	1	0	0	0	0	0	0	0	1	1	1	1	3.0			
55.4	0	1	0	0	0	0	1	0	1	1	0	0	0	0	0	0	0	0	0	0	0	0	0	0	1	1	0	0	1	0	5.6	
57.3	1	0	1	0	0	1	0	1	1	1	1	1	1	0	0	0	0	0	0	0	0	0	0	0	0	1	0	1	0	3.8		
58.2	0	0	0	0	0	0	0	0	1	1	1	1	0	0	0	0	0	1	0	0	0	0	0	0	0	0	0	0	0	4.0		
62.7	0	0	0	0	0	1	0	0	0	0	0	0	0	0	0	0	1	0	0	0	0	0	0	0	0	0	0	0	0	3.2		
63.5	0	0	0	0	0	0	0	0	0	0	0	0	1	0	0	0	0	0	0	0	0	0	0	1	0	0	1	0	1	0	2.9	
64.5	0	0	0	0	0	0	1	0	1	1	1	1	1	0	0	1	0	0	0	0	0	0	0	1	0	0	0	1	0	0	15.4	
114.3	0	0	0	0	0	0	0	0	0	0	1	1	0	0	0	0	1	0	0	0	0	0	0	0	0	0	0	0	0	0	3.0	
125.2	0	0	0	0	0	0	1	0	0	0	0	0	0	0	0	0	0	0	0	0	0	0	0	0	0	1	0	0	0	0	5.0	
		0	0	0	0	0	2	2	2	5	5	5	4	4	2	2	0	4	0	0	2	0	0	0	0	0	2	3	2	2	3	0

0 = ABSENT 1 = PRESENT * = PROBABLE DIFF. ANGLE FOR K-BETA RADIATION

DETAILED ANALYSIS OF PHASE(S) ACTUALLY PRESENT

S.N.	PHASE PRESENT	DIFF. ANGLE	PEAK INT	D I/I0	D MEAS	D STD	DIFF PLANE	INT STD	CONF LIMIT
(1)	FE3C(CEMENTITE)	57.3	24	100	2.021	2.020	22	60	100.0
		62.7	20	84	1.862	1.870	113	30	99.7
(2)	FE5C2	55.4	36	36	2.084	2.080	21	70	99.9
		64.5	100	100	1.816	1.814	312	25	99.9
(3)	FE5C2(HAGG)	57.3	24	75	2.021	2.030	312	100	99.7
		125.2	32	100	1.091	1.090	404	20	99.8
(4)	MN5C2(PD5B2)	54.3	19	19	2.123	2.117	112	70	99.8
		55.4	36	36	2.084	2.078	21	100	99.8
		57.3	24	24	2.021	2.016	312	80	99.8
		58.2	25	25	1.992	1.990	511	80	99.9
		64.5	100	100	1.816	1.820	312	70	99.8
(5)	FE7C3(2)	54.3	19	19	2.123	2.122	12	40	100.0
		57.3	24	24	2.021	2.019	121	100	99.9
		58.2	25	25	1.992	1.989	300	16	99.9
		64.5	100	100	1.816	1.820	301	10	99.8
(6)	CR7C3(2)	114.3	19	19	1.153	1.153	501	10	100.0
		57.3	24	24	2.021	2.020	121	100	100.0
		58.2	25	25	1.992	1.990	300	20	99.9
		64.5	100	100	1.816	1.820	301	30	99.8
(7)	(CR7C3+MN7C3)	114.3	19	19	1.153	1.154	999	30	99.9
		54.3	19	93	2.123	2.120	555	100	99.9
(8)	CR3C2	62.7	20	100	1.862	1.860	888	100	99.9
		58.2	25	25	1.992	1.990	420	20	99.9
		62.7	20	20	1.862	1.860	221	30	99.9
		64.5	100	100	1.816	1.810	130	30	99.8
(9)	COPPER	114.3	19	19	1.153	1.153	0	50	100.0
		55.4	36	100	2.084	2.088	111	100	99.9
(10)	FE8SI2C	125.2	32	89	1.091	1.090	311	17	99.8
		55.4	36	36	2.084	2.080	131	80	99.9
		63.5	18	18	1.841	1.840	15	60	99.9
		64.5	100	100	1.816	1.810	15	20	99.8
(11)	CRMN3	54.3	19	100	2.123	2.132	410	100	99.8
		63.5	18	96	1.841	1.838	222	40	99.9
(12)	MN15C4	54.3	19	53	2.123	2.129	301	10	99.8
		55.4	36	100	2.084	2.094	213	100	99.7
		57.3	24	67	2.021	2.012	6	50	99.7

Martensite additionally present

TABLE-6.5

SUMMARY TABLE OF DIFFRACTOGRAM INDEXING

ALLOY: C1	H/T		TEMPERATURE: 900°C										SOAKING DURATION: 6 HOURS																																	
DIFF. ANGLE	PHASE(S)																INT																													
	1	3	5	7	9	11	13	15	17	19	21	23	25	27	29																															
48.1	0	0	0	1	1	1	0	1	0	0	0	0	0	0	1	0	0	0	0	0	0	0	0	0	0	0	0	0	0	0	0	0	0	0	0	0	0	9.0								
51.0	0	0	0	0	0	1	0	1	0	0	1	0	0	0	0	0	0	0	0	0	0	0	0	0	0	0	0	0	0	0	0	0	0	0	0	0	1	0	1	0	8.0					
55.5	0	1	0	0	0	0	0	1	0	1	1	0	0	0	0	0	0	0	0	0	0	0	0	0	0	0	1	1	0	0	0	0	0	0	0	0	0	0	0	82.0						
56.2	0	0	1	1	1	1	1	1	1	1	0	0	0	0	0	0	0	0	0	0	0	0	0	0	0	0	0	1	1	0	0	0	0	0	0	0	0	0	0	27.0						
57.7	0	0	0	0	0	1	1	0	0	1	0	0	0	0	0	0	0	0	0	0	0	0	0	0	0	0	0	0	0	0	0	0	0	0	0	0	0	1	1	0	1	0	30.0			
58.6	0	0	0	0	0	0	0	1	0	0	1	0	0	0	0	0	0	0	0	0	0	0	0	0	0	0	1	0	0	1	0	0	0	0	0	0	0	0	0	0	0	4.0				
59.1	0	0	0	0	0	1	0	0	0	1	0	0	1	0	0	0	0	0	0	0	0	0	0	0	0	0	0	0	0	0	0	0	0	0	0	0	0	0	1	1	1	0	0	8.0		
62.4	0	0	0	0	0	1	0	0	0	0	0	0	0	0	0	0	0	0	0	0	0	0	0	0	0	0	1	0	0	0	1	0	1	0	0	0	0	0	0	0	0	0	9.0			
* 65.3	0	1	0	1	1	0	0	1	0	0	0	1	0	0	0	0	0	0	0	0	0	0	0	0	0	0	1	0	0	0	0	0	0	0	0	0	0	0	0	0	0	0	0	0	18.0	
93.7	0	0	0	0	1	0	0	0	0	0	0	0	0	0	0	0	0	0	0	0	0	0	0	0	0	0	0	0	0	0	0	0	0	0	0	0	0	0	0	0	0	0	0	6.4		
99.1	0	0	0	0	0	0	0	0	0	0	0	0	0	0	0	0	0	0	0	0	0	0	0	0	0	0	0	0	0	0	0	0	0	0	0	0	0	0	0	0	0	0	0	0	15.0	
126.8	0	1	0	0	0	0	0	0	0	0	0	0	0	0	0	0	0	0	0	0	0	0	0	0	0	0	0	0	0	0	0	0	0	0	0	0	0	0	0	0	0	0	0	0	0	9.0
0 3 0 3 4 6 3 5 2 4 2 0 2 0 0 0 0 0 2 0 0 0 0 4 0 0 0 6 6 0 4 0																																														

0 = ABSENT 1 = PRESENT * = PROBABLE DIFF. ANGLE FOR K-BETA RADIATION

DETAILED ANALYSIS OF PHASE(S) ACTUALLY PRESENT

S.N.	PHASE PRESENT	DIFF. ANGLE	PEAK INT	D I/10	D MEAS	D STD	DIFF PLANE	INT STD	CONF LIMIT
(1)	AUSTENITE	55.5	100	100	2.081	2.080	111	100	100.0
		65.3	21	21	1.796	1.800	200	80	99.8
		126.8	10	10	1.083	1.083	311	80	99.9
(2)	FE3C(CEMENTITE)	48.1	10	30	2.378	2.380	112	65	99.9
		51.0	9	26	2.251	2.260	200	25	99.8
		56.2	32	89	2.057	2.060	210	70	99.9
		57.7	36	100	2.008	2.010	103	100	99.9
		59.1	9	26	1.965	1.970	211	55	99.8
		62.4	10	30	1.870	1.870	113	30	100.0
(3)	FE5C2(HAGG)	48.1	10	33	2.378	2.390	202	20	99.7
		51.0	9	29	2.251	2.260	20	50	99.8
		56.2	32	100	2.057	2.060	510	100	99.9
		58.6	4	14	1.980	1.980	511	20	100.0
		65.3	21	66	1.796	1.800	312	70	99.8
(4)	MN5C2(PD5B2)	55.5	100	100	2.081	2.078	21	100	99.9
		56.2	32	32	2.057	2.058	510	80	100.0
		57.7	36	36	2.008	2.016	312	80	99.8
		59.1	9	9	1.965	1.972	600	80	99.8
(5)	FE7C3(2)	51.0	9	100	2.251	2.255	120	30	99.9
		58.6	4	50	1.980	1.989	300	16	99.7
(6)	CR7C3	59.1	9	100	1.965	1.960	511	70	99.8
		93.7	7	80	1.328	1.330	0	50	99.8
(7)	FE8SI2C	55.5	100	100	2.081	2.080	131	80	100.0
		56.2	32	32	2.057	2.050	121	80	99.8
		57.7	36	36	2.008	2.010	322	100	99.9
		58.6	4	4	1.980	1.980	114	60	100.0
		59.1	9	9	1.965	1.960	224	60	99.8
		65.3	21	21	1.796	1.794	312	20	99.9
(8)	MN15C4	51.0	9	26	2.251	2.262	105	50	99.7
		57.7	36	100	2.008	2.012	6	50	99.9
		62.4	10	30	1.870	1.873	220	20	99.9
		65.3	21	60	1.796	1.789	222	50	99.7

TABLE-6.6

SUMMARY TABLE OF DIFFRACTOGRAM INDEXING

ALLOY: C1	H/T TEMPERATURE: 950°C														SOAKING DURATION: 6 HOURS																	
DIFF. ANGLE	PHASE(S)														INT																	
	1	3	5	7	9	11	13	15	17	19	21	23	25	27		29																
47.0	0	0	0	0	0	1	0	0	1	0	0	0	0	0	0	1	0	0	0	0	0	0	0	0	0	0	0	1	5.0			
55.0	0	0	0	0	0	1	0	0	0	0	0	1	0	0	0	0	0	1	0	0	0	0	0	1	1	0	0	1	1	8.0		
58.0	0	0	0	0	0	0	0	0	1	1	0	1	0	0	0	0	1	0	0	0	0	0	0	0	0	0	0	0	0	6.0		
58.8	0	0	0	0	0	1	0	1	0	1	0	0	0	0	0	0	0	0	0	0	0	0	0	0	0	0	1	0	1	0	0	7.6
64.5	0	0	0	0	0	0	1	0	1	1	1	1	1	0	0	1	0	0	0	0	1	0	0	0	1	0	0	0	0	4.8		
0 0 0 0 0 2 2 0 2 4 0 3 0 0 0 0 2 0 0 0 0 0 0 0 0 0 0 3 0 0 0 2																																

0 = ABSENT 1 = PRESENT * = PROBABLE DIFF. ANGLE FOR K-BETA RADIATION

DETAILED ANALYSIS OF PHASE(S) ACTUALLY PRESENT

S.N.	PHASE PRESENT	DIFF. ANGLE	PEAK INT	I/I0	D MEAS	D STD	DIFF PLANE	INT STD	CONF LIMIT
(1)	FE3C(CEMENTITE)	55.0	100	100	2.098	2.100	121	60	100.0
		58.8	94	94	1.974	1.970	211	55	99.9
(2)	FE5C2	47.0	62	100	2.430	2.421	311	15	99.8
		64.5	60	96	1.816	1.814	312	25	99.9
(3)	MN5C2	58.0	75	100	1.999	1.994	115	80	99.9
		64.5	60	80	1.816	1.818	213	60	99.9
(4)	MN5C2(PD5B2)	47.0	62	65	2.430	2.429	311	50	100.0
		58.0	75	78	1.999	1.990	511	80	99.7
		58.8	94	100	1.974	1.972	600	80	99.9
		64.5	60	63	1.816	1.820	312	70	99.8
(5)	CR7C3(2)	55.0	100	100	2.098	2.100	12	60	100.0
		58.0	75	75	1.999	1.990	300	20	99.7
		64.5	60	60	1.816	1.820	301	30	99.8
(6)	CR3C2	58.0	75	100	1.999	1.990	420	20	99.7
		64.5	60	80	1.816	1.810	130	30	99.8
(7)	FE8S12C	55.0	100	100	2.098	2.090	130	80	99.8
		58.8	94	94	1.974	1.970	212	60	99.9
		64.5	60	60	1.816	1.810	15	20	99.8
(8)	FE2C	47.0	62	62	2.430	2.431	100	16	100.0
		55.0	100	100	2.098	2.103	101	100	99.9

TABLE-6.8

SUMMARY TABLE OF DIFFRACTOGRAM INDEXING

ALLOY: C1	H/T TEMPERATURE: 1050°C															SOAKING DURATION: 6 HOURS																
DIFF. ANGLE	PHASE(S)															INT																
	1	3	5	7	9	11	13	15	17	19	21	23	25	27	29																	
55.2	0	0	0	0	1	0	0	1	0	0	1	0	0	0	0	0	0	0	0	0	0	0	0	1	1	0	0	1	0	38.0		
57.8	0	0	0	0	0	1	1	0	0	0	0	0	0	0	0	0	0	0	0	0	0	0	0	0	0	0	1	0	0	1	0	5.4
64.6	0	0	0	0	0	0	1	0	1	1	1	1	1	1	0	0	1	0	0	0	0	1	0	0	1	1	0	0	0	0	102.0	
98.2	0	0	0	0	0	0	0	0	0	0	0	1	0	0	0	1	0	0	0	0	0	0	1	0	0	0	0	0	0	0	5.4	
0 0 0 0 0 2 2 0 2 0 0 2 2 0 0 0 2 0 0 0 0 0 0 0 0 0 2 3 0 0 2 0																																

0 = ABSENT 1 = PRESENT * = PROBABLE DIFF. ANGLE FOR K-BETA RADIATION

DETAILED ANALYSIS OF PHASE(S) ACTUALLY PRESENT

S.N.	PHASE PRESENT	DIFF. ANGLE	PEAK INT	D I/10	D MEAS	D STD	DIFF PLANE	INT STD	CONF LIMIT
(1)	FE3C(CEMENTITE)	55.2	37	100	2.091	2.100	121	60	99.8
		57.8	5	14	2.005	2.010	103	100	99.8
(2)	FE5C2	57.8	5	5	2.005	2.010	312	40	99.8
		64.6	100	100	1.813	1.814	312	25	100.0
(3)	MN5C2	55.2	37	37	2.091	2.084	120	80	99.8
		64.6	100	100	1.813	1.818	213	60	99.8
(4)	CR7C3(2)	55.2	37	37	2.091	2.100	12	60	99.8
		64.6	100	100	1.813	1.820	301	30	99.7
(5)	CR7C3	64.6	100	100	1.813	1.810	431	70	99.9
		98.2	5	5	1.282	1.280	0	60	99.8
(6)	CR3C2	64.6	100	100	1.813	1.810	130	30	99.9
		98.2	5	5	1.282	1.280	531	5	99.8
(7)	COPPER	55.2	37	37	2.091	2.088	111	100	99.9
		64.6	100	100	1.813	1.808	200	46	99.8
(8)	FE8SI2C	55.2	37	37	2.091	2.090	130	80	100.0
		57.8	5	5	2.005	2.010	322	100	99.8
		64.6	100	100	1.813	1.810	15	20	99.9
(9)	MN15C4	55.2	37	100	2.091	2.094	213	100	99.9
		57.8	5	14	2.005	2.012	6	50	99.8

TABLE-6.9 SUMMARY TABLE OF DIFFRACTOGRAM INDEXING

ALLOY: C2 AS-CAST		PHASE(S)																INT
DIFF. ANGLE	1	3	5	7	9	11	13	15	17	19	21	23	25	27	29			
48.3	0	0	0	1	1	1	0	0	0	0	0	0	0	0	0	0	5.2	
55.6	0	1	0	0	0	0	1	0	1	1	0	0	0	0	0	0	79.0	
57.5	0	0	1	0	0	1	1	0	1	1	1	1	0	0	0	0	31.0	
57.8	0	0	0	0	0	0	0	0	0	0	0	0	0	0	0	0	28.0	
58.4	0	0	0	0	0	0	1	1	1	1	1	0	0	0	0	0	8.2	
62.3	0	0	0	1	1	1	0	0	0	0	0	0	0	0	0	0	3.8	
* 64.4	0	0	0	0	0	0	1	0	1	1	1	0	0	0	0	0	4.8	
* 65.0	0	1	0	1	1	0	0	1	0	0	1	0	0	1	0	0	18.4	
112.5	0	0	0	0	0	0	0	0	0	0	0	0	0	0	0	0	2.8	
118.4	0	0	0	0	0	0	0	0	0	0	0	0	0	0	0	0	4.1	
126.4	0	0	0	0	0	0	0	0	0	0	0	0	0	0	0	0	3.2	
0 2 0 3 3 3 3 2 4 4 4 3 2 0 0 0 2 0 0 0 0 0 2 0 0 6 2 0 3 0																		

0 = ABSENT 1 = PRESENT * = PROBABLE DIFF. ANGLE FOR K-BETA RADIATION

DETAILED ANALYSIS OF PHASE(S) ACTUALLY PRESENT

S.N.	PHASE PRESENT	DIFF. ANGLE	PEAK INT	D I/I0	D MEAS	DIFF PLANE	INT STD	CONF LIMIT
(1)	AUSTENITE	55.6	100	100	2.078	2.080	111	100 99.9
		65.0	23	23	1.803	1.800	200	80 99.9
(2)	FE3C(CEMENTITE)	48.3	6	16	2.368	2.380	112	65 99.7
		57.5	39	100	2.014	2.010	103	100 99.9
		62.3	4	12	1.873	1.870	113	30 99.9
(3)	FE5C2	55.6	100	100	2.078	2.080	21	70 99.9
		57.5	39	39	2.014	2.010	312	40 99.9
		64.4	6	6	1.818	1.814	312	25 99.8
(4)	MN5C2	55.6	100	100	2.078	2.084	120	80 99.8
		57.5	39	39	2.014	2.019	213	100 99.9
		58.4	10	10	1.986	1.994	115	80 99.7
		64.4	6	6	1.818	1.818	213	60 100.0
(5)	MN5C2(PD5B2)	55.6	100	100	2.078	2.078	21	100 100.0
		57.5	39	39	2.014	2.016	312	80 100.0
		58.4	10	10	1.986	1.990	511	80 99.9
		64.4	6	6	1.818	1.820	312	70 99.9
(6)	FE7C3(2)	57.5	39	100	2.014	2.019	121	100 99.9
		58.4	10	26	1.986	1.989	300	16 99.9
		64.4	6	15	1.818	1.820	301	10 99.9
		65.0	23	59	1.803	1.807	22	20 99.9
(7)	CR7C3(2)	57.5	39	100	2.014	2.020	121	100 99.8
		58.4	10	26	1.986	1.990	300	20 99.9
		64.4	6	15	1.818	1.820	301	30 99.9
(8)	CR7C3	57.5	39	100	2.014	2.020	0	50 99.8
		65.0	23	59	1.803	1.810	431	70 99.7
(9)	FE8SI2C	55.6	100	100	2.078	2.070	210	80 99.8
		57.5	39	39	2.014	2.010	322	100 99.9
		58.4	10	10	1.986	1.980	114	60 99.8
		62.3	4	4	1.873	1.880	331	60 99.7
		64.4	6	6	1.818	1.820	31	20 99.9
(10)	MN15C4	65.0	23	23	1.803	1.810	15	20 99.7
		57.5	39	100	2.014	2.012	6	50 99.9
		62.3	4	12	1.873	1.873	220	20 100.0
								20 99.9

Martensite additionally present

TABLE-6.11 SUMMARY TABLE OF DIFFRACTOGRAM INDEXING

ALLOY: C2		H/T TEMPERATURE: 850°C														SOAKING DURATION: 6 HOURS															
DIFF. ANGLE	PHASE(S)														INT																
	1	3	5	7	9	11	13	15	17	19	21	23	25	27		29															
47.0	0	0	0	0	0	1	0	0	1	0	0	0	0	0	0	0	0	0	0	0	0	0	0	0	0	0	0	1	4.8		
50.5	0	0	0	0	0	1	0	1	1	1	1	1	1	0	0	0	0	0	0	0	0	0	0	0	0	0	1	1	1	0	5.6
54.5	0	0	0	0	0	0	0	0	1	1	1	0	1	1	1	0	0	1	0	0	0	0	0	0	0	0	0	0	0	1	5.8
54.6	0	0	0	0	0	0	1	0	0	0	0	0	0	0	0	0	0	1	1	0	1	0	0	0	0	0	0	0	0	1	86.0
57.0	1	0	0	0	0	0	0	1	1	1	0	0	1	1	1	0	0	0	0	0	0	0	0	0	0	0	0	1	1	0	6.8
59.0	0	0	0	0	0	1	0	0	0	1	0	0	1	0	0	0	0	0	0	0	0	0	0	0	0	0	1	1	1	0	8.6
62.7	0	0	0	0	0	1	0	0	0	0	0	0	0	0	0	0	0	1	0	1	0	0	0	0	0	0	0	0	0	0	8.8
64.0	0	0	0	0	0	0	1	0	1	1	0	0	0	0	0	0	0	0	0	0	0	0	0	0	0	0	0	1	0	0	10.0
64.6	0	0	0	0	0	0	1	0	1	1	1	1	1	1	0	0	1	0	0	0	0	0	1	0	0	1	1	0	0	0	12.2
97.4	0	0	0	0	1	0	0	0	0	0	0	0	0	0	0	0	0	0	0	0	0	0	0	0	0	0	0	0	0	0	5.8
98.3	0	0	0	0	0	0	0	0	0	0	0	0	0	0	0	0	0	0	0	0	0	0	1	0	1	0	0	0	0	0	7.0
125.2	0	0	0	0	0	0	0	1	0	0	0	0	0	0	0	0	0	0	0	0	0	0	0	0	0	0	1	0	0	0	12.2
126.2	0	0	0	0	1	0	0	0	0	0	0	0	0	0	0	0	0	0	0	0	0	0	0	0	0	0	0	0	0	0	6.6
0 0 0 0 2 3 4 3 5 7 3 2 7 3 3 0 4 2 2 0 0 3 0 0 3 2 3 3 2 3																															

0 = ABSENT 1 = PRESENT * = PROBABLE DIFF. ANGLE FOR K-BETA RADIATION

DETAILED ANALYSIS OF PHASE(S) ACTUALLY PRESENT

S.N.	PHASE PRESENT	DIFF. ANGLE	PEAK INT	D I/10	D MEAS	D STD	DIFF PLANE	INT STD	CONF LIMIT
(1)	FE3C(CEMENTITE)	50.5	6	63	2.272	2.260	200	25	99.7
		59.0	10	97	1.968	1.970	211	55	99.9
		62.7	10	100	1.862	1.870	113	30	99.7
(2)	FE5C2	47.0	5	5	2.430	2.421	311	15	99.8
		54.6	100	100	2.113	2.112	112	25	100.0
		64.0	11	11	1.828	1.821	511	20	99.7
		64.6	14	14	1.813	1.814	312	25	100.0
(3)	MN5C2	50.5	6	45	2.272	2.277	20	40	99.9
		54.5	6	47	2.116	2.121	211	80	99.9
		57.0	7	55	2.031	2.034	204	60	99.9
		64.0	11	81	1.828	1.831	115	60	99.9
		64.6	14	100	1.813	1.818	213	60	99.8
(4)	FE7C3(2)	50.5	6	45	2.272	2.270	2	8	100.0
		54.5	6	47	2.116	2.122	12	40	99.8
		64.6	14	100	1.813	1.807	22	20	99.7
		50.5	6	45	2.272	2.280	411	70	99.8
(5)	CR7C3	54.5	6	47	2.116	2.120	202	70	99.9
		57.0	7	55	2.031	2.040	421	100	99.7
		59.0	10	70	1.968	1.960	511	70	99.7
		64.6	14	100	1.813	1.810	431	70	99.9
		97.4	6	47	1.290	1.290	0	60	100.0
		98.3	8	57	1.281	1.280	0	60	99.9
		54.5	6	47	2.116	2.120	202	60	99.9
(6)	(CR,FE)7C3	57.0	7	55	2.031	2.040	122	100	99.7
		64.6	14	100	1.813	1.810	431	60	99.9
		59.0	10	70	1.968	1.960	224	60	99.7
(7)	FE8SI2C	64.6	14	100	1.813	1.810	15	20	99.9
		50.5	6	65	2.272	2.272	2	60	100.0
(8)	CRMN3	57.0	7	79	2.031	2.036	202	70	99.8
		59.0	10	100	1.968	1.970	420	100	99.9
		50.5	6	82	2.272	2.262	105	50	99.8
(9)	MN15C4	57.0	7	100	2.031	2.037	302	100	99.8

Martensite additionally present

TABLE-6.12 SUMMARY TABLE OF DIFFRACTOGRAM INDEXING

ALLOY: C2	H/T TEMPERATURE: 900°C																SOAKING DURATION: 6 HOURS													
DIFF. ANGLE	PHASE(S)																INT													
	1	3	5	7	9	11	13	15	17	19	21	23	25	27	29															
50.6	0	0	0	0	1	0	1	1	0	1	1	0	0	0	0	0	0	0	0	0	1	0	0	0	0	1	1	1	0	3.0
55.3	0	1	0	0	0	0	1	0	1	1	0	0	0	0	0	0	0	0	0	0	0	0	0	1	1	0	0	1	0	16.0
58.5	0	0	0	0	0	0	0	1	0	1	1	1	0	0	0	0	1	0	0	0	0	0	1	0	0	1	0	0	0	5.0
64.6	0	0	0	0	0	0	1	0	1	1	1	1	1	0	0	1	0	0	0	0	1	0	0	1	1	0	0	0	0	5.6
92.0	0	0	0	0	0	0	0	0	0	1	0	1	1	1	0	0	0	0	0	1	0	0	0	0	0	0	0	0	0	2.0
93.8	0	0	0	0	1	0	0	0	0	0	0	1	0	0	0	1	0	0	0	0	0	0	0	0	0	1	0	0	0	4.0
0 0 0 0 0 0 2 2 3 3 4 3 3 2 0 0 3 0 0 0 0 2 0 0 2 3 2 0 2 0																														

0 = ABSENT 1 = PRESENT * = PROBABLE DIFF. ANGLE FOR K-BETA RADIATION

DETAILED ANALYSIS OF PHASE(S) ACTUALLY PRESENT

S.N.	PHASE PRESENT	DIFF. ANGLE	PEAK INT	I/10	D MEAS	D STD	DIFF PLANE	INT STD	CONF LIMIT
(1)	FE5C2	55.3	100	100	2.088	2.080	21	70	99.8
		64.6	34	34	1.813	1.814	312	25	100.0
(2)	FE5C2(HAGG)	50.6	18	59	2.267	2.260	20	50	99.8
		58.5	31	100	1.983	1.980	511	20	99.9
(3)	MN5C2	50.6	18	18	2.267	2.277	20	40	99.8
		55.3	100	100	2.088	2.084	120	80	99.9
		64.6	34	34	1.813	1.818	213	60	99.8
(4)	MN5C2(PD5B2)	55.3	100	100	2.088	2.078	21	100	99.7
		58.5	31	31	1.983	1.990	511	80	99.8
		64.6	34	34	1.813	1.820	312	70	99.7
(5)	FE7C3(2)	50.6	18	53	2.267	2.255	120	30	99.7
		58.5	31	89	1.983	1.989	300	16	99.8
		64.6	34	100	1.813	1.807	22	20	99.7
		92.0	12	35	1.347	1.349	23	8	99.8
(6)	CR7C3(2)	50.6	18	53	2.267	2.270	120	50	99.9
		58.5	31	89	1.983	1.990	300	20	99.8
		64.6	34	100	1.813	1.820	301	30	99.7
(7)	CR7C3	64.6	34	100	1.813	1.810	431	70	99.9
		92.0	12	35	1.347	1.350	641	80	99.7
		93.8	25	71	1.327	1.330	0	50	99.7
(8)	(CR,FE)7C3	64.6	34	100	1.813	1.810	431	60	99.9
		92.0	12	35	1.347	1.350	403	20	99.7
(9)	CR3C2	58.5	31	89	1.983	1.990	420	20	99.8
		64.6	34	100	1.813	1.810	130	30	99.9
		93.8	25	71	1.327	1.325	630	20	99.8
(10)	COPPER	55.3	100	100	2.088	2.088	111	100	100.0
		64.6	34	34	1.813	1.808	200	46	99.8
(11)	FE8SI2C	55.3	100	100	2.088	2.080	131	80	99.8
		58.5	31	31	1.983	1.980	114	60	99.9
		64.6	34	34	1.813	1.810	15	20	99.9
(12)	FE-CR	50.6	18	75	2.267	2.261	2	10	99.8
		93.8	25	100	1.327	1.327	522	1	100.0
(13)	MN15C4	50.6	18	18	2.267	2.262	105	50	99.9
		55.3	100	100	2.088	2.094	213	100	99.8

TABLE-8.13 SUMMARY TABLE OF DIFFRACTOGRAM INDEXING

ALLOY: C2		H/T TEMPERATURE: 950°C														SOAKING DURATION: 6 HOURS																						
DIFF. ANGLE	PHASE(S)														INT																							
	1	3	5	7	9	11	13	15	17	19	21	23	25	27		29																						
48.0	0	0	0	1	1	1	0	1	0	0	0	0	0	0	1	0	0	0	0	0	0	0	0	0	0	0	0	0	0	0	0	0	0	0	0	0	0	4
55.3	0	1	0	0	0	0	1	0	1	1	0	0	0	0	0	0	0	0	0	0	0	0	0	0	1	1	0	0	1	0	0	0	0	0	0	0	0	75
56.2	0	0	1	1	1	1	1	1	1	1	0	0	0	0	0	0	0	0	1	0	0	0	1	0	0	0	1	1	0	0	0	0	0	0	0	0	6	
57.3	1	0	1	0	0	1	0	1	1	1	1	1	0	0	0	0	0	0	0	1	0	0	0	0	0	0	0	1	0	1	0	0	0	0	0	0	4	
* 63.9	0	0	0	0	0	0	0	0	1	1	0	0	0	0	0	0	0	0	0	1	0	1	0	0	0	0	0	1	1	0	0	0	0	0	0	0	4	
64.8	0	0	0	0	0	0	1	0	0	0	1	0	1	1	0	0	1	0	0	0	0	0	0	0	1	1	0	0	0	0	0	0	0	0	0	0	20	
98.8	0	0	0	0	0	0	0	0	0	0	0	0	0	0	0	0	0	0	0	0	0	0	0	0	1	0	0	0	0	0	0	0	0	0	0	0	84	
99.4	0	1	0	0	0	0	0	1	0	0	0	0	1	0	0	0	0	0	0	0	0	0	0	1	0	0	0	0	0	0	0	0	0	0	0	0	4	
118.9	0	0	0	0	0	0	0	0	0	0	0	0	0	0	0	0	0	0	0	0	0	0	0	0	0	0	0	0	0	0	0	0	0	0	0	0	6	
119.2	0	0	0	0	0	0	0	0	0	0	0	0	0	0	0	0	0	0	0	0	0	0	0	0	1	1	0	0	0	0	0	0	0	0	0	0	4	
124.8	0	0	0	0	0	0	0	0	0	0	0	0	0	0	0	0	0	0	0	0	0	0	0	0	0	0	0	0	0	0	0	0	0	0	0	0	14	
125.8	0	0	0	0	1	0	0	0	0	0	0	0	0	0	0	0	0	0	0	0	0	0	0	1	0	0	0	0	0	0	0	0	0	0	0	1	5	
0 2 2 2 3 3 3 4 4 4 2 0 3 0 0 0 0 2 0 0 0 3 2 0 3 3 3 0 2 0																																						

0 = ABSENT 1 = PRESENT * = PROBABLE DIFF. ANGLE FOR K-BETA RADIATION

DETAILED ANALYSIS OF PHASE(S) ACTUALLY PRESENT

S.N.	PHASE PRESENT	DIFF. ANGLE	PEAK INT	D I/10	D MEAS	D STD	DIFF PLANE	INT STD	CONF LIMIT
(1)	AUSTENITE	55.3	89	100	2.088	2.080	111	100	99.8
		99.4	5	6	1.270	1.270	220	50	100.0
(2)	FE3C(CEMENTITE)	48.0	4	69	2.382	2.380	112	65	100.0
		56.2	7	100	2.057	2.060	210	70	99.9
		57.3	5	80	2.021	2.020	22	60	100.0
(3)	FE5C2	55.3	89	100	2.088	2.080	21	70	99.8
		56.2	7	7	2.057	2.049	510	100	99.8
		64.8	23	26	1.808	1.814	312	25	99.8
(4)	FE5C2(HAGG)	48.0	4	69	2.382	2.390	202	20	99.8
		56.2	7	100	2.057	2.060	510	100	99.9
		57.3	5	80	2.021	2.030	312	100	99.7
		99.4	5	78	1.270	1.270	531	20	100.0
(5)	MN5C2	55.3	89	100	2.088	2.084	120	80	99.9
		56.2	7	7	2.057	2.060	15	80	99.9
		57.3	5	6	2.021	2.019	213	100	99.9
		63.9	4	5	1.831	1.831	115	60	100.0
(6)	MN5C2(PD5B2)	55.3	89	100	2.088	2.078	21	100	99.7
		56.2	7	7	2.057	2.058	510	80	100.0
		57.3	5	6	2.021	2.016	312	80	99.8
		63.9	4	5	1.831	1.829	511	70	99.9
(7)	FE7C3(2)	57.3	5	24	2.021	2.019	121	100	99.9
		64.8	23	100	1.808	1.807	22	20	99.9
(8)	CR7C3	57.3	5	24	2.021	2.020	0	50	100.0
		64.8	23	100	1.808	1.810	431	70	99.9
		99.4	5	23	1.270	1.270	0	30	100.0
(9)	COPPER	55.3	89	89	2.088	2.088	111	100	100.0
		64.8	23	23	1.808	1.808	200	46	100.0
		98.8	100	100	1.276	1.278	220	20	99.8
(10)	FE8SI2C	55.3	89	100	2.088	2.080	131	80	99.8
		56.2	7	7	2.057	2.050	121	80	99.8
		64.8	23	26	1.808	1.810	15	20	99.9
(11)	MN15C4	55.3	89	100	2.088	2.094	213	100	99.8
		57.3	5	6	2.021	2.012	6	50	99.7

TABLE-6.16 SUMMARY TABLE OF DIFFRACTOGRAM INDEXING

ALLOY: C3 AS-CAST																																													
DIFF. ANGLE	PHASE(S)														INT																														
	1	3	5	7	9	11	13	15	17	19	21	23	25	27		29																													
47.5	0	0	0	0	0	0	0	0	0	0	0	0	0	0	0	1	0	1	0	0	0	0	1	0	0	0	0	0	1	1	4.8														
50.3	0	0	0	0	0	0	1	0	1	1	1	1	0	0	0	0	0	0	0	0	0	0	1	0	0	0	0	0	0	1	1	0	6.2												
51.4	0	0	0	0	0	0	0	0	0	0	0	0	0	0	0	0	0	0	0	0	0	0	0	0	0	0	0	0	0	0	0	0	3.6												
54.4	0	0	0	0	0	0	1	0	1	1	1	0	1	1	1	0	0	1	0	1	0	0	0	0	0	0	0	0	1	0	1	1	6.8												
54.9	0	0	0	0	0	1	0	0	0	0	0	1	0	0	0	1	1	0	1	0	0	0	0	0	0	0	0	0	0	1	1	18.6													
56.1	0	0	1	0	1	1	0	1	1	1	0	0	0	0	0	0	0	1	0	0	1	0	0	0	0	0	1	1	1	0	0	3.8													
61.9	0	0	0	1	1	0	0	0	0	0	0	0	0	0	0	0	1	0	0	0	0	0	0	1	0	0	1	1	1	0	0	3.8													
62.8	0	0	0	0	0	0	0	0	0	0	0	0	0	0	0	1	0	1	0	0	0	0	0	0	0	0	0	0	0	0	0	0	4.0												
64.1	0	0	0	0	0	0	1	0	1	1	1	1	0	0	0	0	0	1	0	0	0	0	0	0	0	0	1	1	0	0	0	50.0													
98.0	0	0	0	0	0	0	0	0	0	0	0	0	0	0	0	0	0	0	0	0	0	0	0	0	1	0	0	0	0	0	0	10.2													
113.0	0	0	0	0	0	0	0	1	0	0	0	0	0	1	0	0	1	0	0	0	1	0	0	0	0	0	0	0	0	0	0	3.2													
124.4	0	0	0	0	0	0	0	0	0	0	0	0	0	0	0	0	0	0	0	0	0	0	0	0	0	0	0	0	0	0	0	41.0													
126.2	0	0	0	0	1	0	0	0	0	0	0	0	0	0	0	0	0	0	0	0	0	0	0	1	0	0	0	0	0	0	0	6.0													
127.0	0	1	0	0	0	0	0	0	0	0	0	0	0	0	0	0	0	0	0	0	0	0	0	1	0	0	0	0	0	0	0	3.0													
															0	0	0	0	3	2	3	2	4	4	3	3	2	2	2	2	5	3	2	0	3	0	4	0	0	3	4	3	4	3	

0 = ABSENT 1 = PRESENT * = PROBABLE DIFF. ANGLE FOR K-BETA RADIATION

DETAILED ANALYSIS OF PHASE(S) ACTUALLY PRESENT

S.N.	PHASE PRESENT	DIFF. ANGLE	PEAK INT	I/10	D MEAS	D STD	DIFF PLANE	INT STD	CONF LIMIT
(1)	FE3C(CEMENTITE)	54.9	37	100	2.102	2.100	121	60	99.9
		56.1	7	20	2.061	2.060	210	70	100.0
(2)	FE5C2	50.3	12	12	2.280	2.287	20	20	99.8
		54.4	13	13	2.120	2.112	112	25	99.8
		64.1	100	100	1.826	1.821	511	20	99.8
(3)	FE5C2(HAGG)	56.1	7	100	2.061	2.060	510	100	100.0
		113.0	6	84	1.162	1.160	423	20	99.7
(4)	MN5C2(PD5B2)	50.3	12	12	2.280	2.282	20	70	100.0
		54.4	13	13	2.120	2.117	112	70	99.9
		56.1	7	7	2.061	2.058	510	80	99.9
		64.1	100	100	1.826	1.820	312	70	99.8
(5)	FE7C3(2)	50.3	12	12	2.280	2.270	2	8	99.8
		54.4	13	13	2.120	2.122	12	40	99.9
		64.1	100	100	1.826	1.820	301	10	99.8
(6)	CR7C3(2)	50.3	12	12	2.280	2.270	120	50	99.8
		54.9	37	37	2.102	2.100	12	60	99.9
		64.1	100	100	1.826	1.820	301	30	99.8
(7)	(CR7C3+MN7C3)	54.4	13	100	2.120	2.120	555	100	100.0
		62.8	7	58	1.860	1.860	888	100	100.0
(8)	FE8SI2C	56.1	7	7	2.061	2.070	210	80	99.7
		61.9	7	7	1.884	1.880	331	60	99.9
		64.1	100	100	1.826	1.820	31	20	99.8
(9)	CRMN3	50.3	12	100	2.280	2.272	2	60	99.8
		56.1	7	61	2.061	2.069	330	100	99.8
		61.9	7	61	1.884	1.888	777	90	99.9
(10)	MN15C4	47.5	9	25	2.406	2.404	211	50	100.0
		50.3	12	33	2.280	2.273	212	50	99.8
		54.4	13	36	2.120	2.129	301	10	99.7
		54.9	37	100	2.102	2.094	213	100	99.8

Martensite additionally present

TABLE-6.17 SUMMARY TABLE OF DIFFRACTOGRAM INDEXING

ALLOY: C3		H/T TEMPERATURE: 800°C														SOAKING DURATION: 6 HOURS														
DIFF. ANGLE	PHASE(S)															INT														
	1	3	5	7	9	11	13	15	17	19	21	23	25	27	29															
48.2	0	0	0	1	1	1	0	0	0	0	0	0	0	0	0	0	0	0	0	0	0	0	0	0	0	0	0	0	6.0	
51.0	0	0	0	0	0	1	0	1	0	0	1	0	0	0	0	0	0	0	0	0	0	0	0	0	0	0	0	0	0	4.2
55.5	0	1	0	0	0	0	1	0	1	1	0	0	0	0	0	0	0	0	0	0	0	0	0	0	0	1	0	1	0	80.0
57.8	0	0	0	0	0	1	1	0	0	0	0	0	0	0	0	0	0	0	0	0	0	0	0	0	0	1	1	0	0	10.0
58.3	0	0	0	0	0	0	0	1	1	1	1	1	0	0	0	0	1	0	0	0	0	0	1	0	0	1	0	0	0	4.0
62.8	0	0	0	0	0	0	0	0	0	0	0	0	0	0	0	1	0	1	0	0	0	0	0	0	0	0	0	0	0	4.0
65.3	0	1	0	1	1	0	0	1	0	0	0	1	0	0	0	0	0	0	0	1	0	0	0	0	0	1	0	0	1	18.0
98.5	0	0	0	0	0	0	0	0	0	0	0	0	0	0	0	1	0	0	0	0	0	0	0	0	0	0	0	0	0	5.2
125.4	0	0	0	0	0	0	0	1	0	0	0	0	0	0	0	0	0	0	0	0	0	0	0	0	0	1	0	0	0	9.8
126.2	0	0	0	0	1	0	0	0	0	0	0	0	0	0	0	0	0	0	0	0	0	0	0	0	1	0	0	0	0	4.2
0 2 0 2 3 3 2 4 2 2 2 2 0 0 2 0 3 0 0 0 0 0 2 0 3 4 0 0 3 0																														

0 = ABSENT 1 = PRESENT * = PROBABLE DIFF. ANGLE FOR K-BETA RADIATION

DETAILED ANALYSIS OF PHASE(S) ACTUALLY PRESENT

S.N.	PHASE PRESENT	DIFF. ANGLE	PEAK INT	D I/10	D MEAS	D STD	DIFF PLANE	INT STD	CONF LIMIT
(1)	AUSTENITE	55.5	100	100	2.081	2.080	111	100	100.0
		65.3	22	22	1.796	1.800	200	80	99.8
(2)	FE3C(CEMENTITE)	48.2	7	59	2.373	2.380	112	65	99.8
		51.0	5	41	2.251	2.260	200	25	99.8
		57.8	12	100	2.005	2.010	103	100	99.8
(3)	FE5C2	55.5	100	100	2.081	2.080	21	70	100.0
		57.8	12	12	2.005	2.010	312	40	99.8
(4)	FE5C2(HAGG)	51.0	5	23	2.251	2.260	20	50	99.8
		58.3	5	22	1.989	1.980	511	20	99.7
		65.3	22	100	1.796	1.800	312	70	99.8
		125.4	12	54	1.090	1.090	404	20	100.0
(5)	MN5C2	55.5	100	100	2.081	2.084	120	80	99.9
		58.3	5	5	1.989	1.994	115	80	99.8
(6)	MN5C2(PD5B2)	55.5	100	100	2.081	2.078	21	100	99.9
		58.3	5	5	1.989	1.990	511	80	100.0
(7)	FE7C3(2)	51.0	5	100	2.251	2.255	120	30	99.9
		58.3	5	95	1.989	1.989	300	16	100.0
(8)	CR7C3(2)	58.3	5	22	1.989	1.990	300	20	100.0
		65.3	22	100	1.796	1.790	22	50	99.8
(9)	CR3C2	58.3	5	76	1.989	1.990	420	20	100.0
		62.8	5	76	1.860	1.860	221	30	100.0
		98.5	6	100	1.279	1.280	531	5	99.9
(10)	CU2S(1)	58.3	5	76	1.989	1.980	110	100	99.7
		98.5	6	100	1.279	1.281	114	11	99.7
(11)	COPPER	55.5	100	100	2.081	2.088	111	100	99.8
		98.5	6	6	1.279	1.278	220	20	99.9
		125.4	12	12	1.090	1.090	311	17	100.0
(12)	FE8SI2C	55.5	100	100	2.081	2.080	131	80	100.0
		57.8	12	12	2.005	2.010	322	100	99.8
		58.3	5	5	1.989	1.980	114	60	99.7
		65.3	22	22	1.796	1.794	312	20	99.9
(13)	MN15C4	51.0	5	23	2.251	2.262	105	50	99.7
		57.8	12	55	2.005	2.012	6	50	99.8
		65.3	22	100	1.796	1.789	222	50	99.7

Martensite additionally present

TABLE-6.19 SUMMARY TABLE OF DIFFRACTOGRAM INDEXING

ALLOY: C3	H/T TEMPERATURE: 900°C															SOAKING DURATION: 6 HOURS																			
DIFF. ANGLE	PHASE(S)															INT																			
	1	3	5	7	9	11	13	15	17	19	21	23	25	27	29																				
48.2	0	0	0	1	1	1	0	0	0	0	0	0	0	1	0	0	1	0	0	0	0	0	0	0	0	0	0	0	0	0	0	0	0	0	4.0
55.7	0	1	0	0	0	0	1	0	1	1	0	0	0	0	0	0	0	0	0	0	1	0	0	0	0	1	0	1	0	0	0	0	0	0	76.0
56.4	0	0	0	1	1	1	1	1	1	1	0	0	0	0	0	0	0	1	0	0	0	1	0	0	0	1	0	0	0	0	0	0	0	0	8.0
57.8	0	0	0	0	0	1	1	0	0	0	0	0	0	0	0	0	0	0	0	0	0	0	0	0	0	1	0	0	1	0	0	0	0	8.0	
58.9	0	0	0	0	0	1	0	0	0	1	0	0	0	0	0	0	0	0	0	0	0	0	0	0	0	1	1	1	0	0	0	0	0	4.2	
63.5	0	0	0	0	0	0	0	0	0	0	0	0	0	1	0	0	0	0	0	0	0	0	0	1	0	1	0	1	0	0	0	0	0	3.6	
64.9	0	0	0	0	0	0	0	0	0	0	0	0	0	1	0	1	1	0	0	1	0	0	0	0	1	1	0	0	0	0	0	0	0	5.6	
65.1	0	1	0	1	1	0	0	1	0	0	0	0	0	0	0	0	0	0	0	0	0	0	0	0	1	1	0	0	0	0	0	0	0	5.8	
125.3	0	0	0	0	0	0	0	1	0	0	0	0	0	0	0	0	0	0	0	0	0	0	0	0	1	0	0	0	0	0	0	0	0	12.0	
0 2 0 3 3 4 3 3 2 3 0 0 2 0 0 0 0 2 0 0 2 0 0 0 2 7 0 3 2 0																																			

0 = ABSENT 1 = PRESENT * = PROBABLE DIFF. ANGLE FOR K-BETA RADIATION

DETAILED ANALYSIS OF PHASE(S) ACTUALLY PRESENT

S.N.	PHASE PRESENT	DIFF. ANGLE	PEAK INT	D I/10	D MEAS	D STD	DIFF PLANE	INT STD	CONF LIMIT
(1)	AUSTENITE	55.7	100	100	2.074	2.080	111	100	99.8
		65.1	7	7	1.801	1.800	200	80	100.0
(2)	CR23C6	48.2	5	50	2.373	2.370	420	50	99.9
		56.4	10	100	2.050	2.050	511	100	100.0
		65.1	7	72	1.801	1.800	531	50	100.0
(3)	MN23C6	48.2	5	50	2.373	2.380	420	50	99.8
		56.4	10	100	2.050	2.053	511	100	99.9
		65.1	7	72	1.801	1.799	531	50	99.9
(4)	FE3C(CEMENTITE)	48.2	5	50	2.373	2.380	112	65	99.8
		56.4	10	100	2.050	2.060	210	70	99.7
		57.8	10	100	2.005	2.010	103	100	99.8
		58.9	5	52	1.971	1.970	211	55	100.0
(5)	FE5C2(HAGG)	56.4	10	66	2.050	2.060	510	100	99.7
		65.1	7	48	1.801	1.800	312	70	100.0
		125.3	15	100	1.091	1.090	404	20	99.9
(6)	MN5C2(PD5B2)	55.7	100	100	2.074	2.078	21	100	99.9
		56.4	10	10	2.050	2.058	510	80	99.8
		58.9	5	5	1.971	1.972	600	80	100.0
(7)	CR7C3	63.5	4	64	1.841	1.840	601	60	99.9
		64.9	7	100	1.806	1.810	431	70	99.8
(8)	COPPER	64.9	7	46	1.806	1.808	200	46	99.9
		125.3	15	100	1.091	1.090	311	17	99.9
(9)	FE8SI2C	55.7	100	100	2.074	2.070	210	80	99.9
		56.4	10	10	2.050	2.050	121	80	100.0
		57.8	10	10	2.005	2.010	322	100	99.8
		58.9	5	5	1.971	1.970	212	60	100.0
		63.5	4	4	1.841	1.840	15	60	99.9
		64.9	7	7	1.806	1.810	15	20	99.8
		65.1	7	7	1.801	1.794	312	20	99.7
(10)	CRMN3	55.7	100	100	2.074	2.069	330	100	99.8
		58.9	5	5	1.971	1.970	420	100	100.0
		63.5	4	4	1.841	1.838	222	40	99.9
(11)	MN15C4	57.8	10	100	2.005	2.012	6	50	99.8
		65.1	7	72	1.801	1.800	310	20	100.0

TABLE-6.14 SUMMARY TABLE OF DIFFRACTOGRAM INDEXING

ALLOY:C2		H/T TEMPERATURE:1000°C														SOAKING DURATION: 6 HOURS	
DIFF. ANGLE	1	3	5	7	9	11	13	15	17	19	21	23	25	27	29	INT	
48.1	0	0	0	1	1	1	0	1	0	0	0	0	0	0	0	0	4.5
55.0	0	0	0	0	0	1	0	0	0	0	0	0	0	0	0	0	25.6
55.5	0	1	0	0	0	0	1	0	1	1	0	0	0	0	0	0	10.0
64.4	0	0	0	0	0	0	1	0	1	1	1	1	0	0	0	0	9.0
65.3	0	1	0	1	1	0	0	1	0	0	0	0	0	0	0	0	4.0
110.4	0	0	0	0	0	0	0	0	0	0	0	0	0	0	0	0	6.0
114.0	0	0	0	0	0	0	0	0	0	0	0	0	0	0	0	0	4.0
116.1	0	0	0	0	0	0	1	0	0	0	0	0	0	0	0	0	4.0
116.9	0	0	0	0	0	0	0	0	0	0	0	0	0	0	0	0	4.0
118.4	0	0	0	0	0	0	0	0	0	0	0	0	0	0	0	0	3.0
121.2	0	0	0	0	0	0	0	0	0	0	0	0	0	0	0	0	3.6
123.2	0	0	0	0	0	0	0	0	0	0	0	0	0	0	0	0	4.0
124.7	0	0	0	0	0	0	0	0	0	0	0	0	0	0	0	0	9.6
125.0	0	0	0	0	0	0	0	0	0	0	0	0	0	0	0	0	7.6
126.0	0	0	0	0	1	0	0	0	0	0	0	0	0	0	0	0	6.0
129.2	0	0	0	0	0	0	0	0	0	0	0	0	0	0	0	0	5.6
0 2 0 2 3 2 2 3 2 2 0 4 0 0 2 0 0 0 3 2 2 2 0 0 0 4 0 0 2 3																	

0 = ABSENT 1 = PRESENT * = PROBABLE DIFF. ANGLE FOR K-BETA RADIATION

DETAILED ANALYSIS OF PHASE(S) ACTUALLY PRESENT

S.N.	PHASE PRESENT	DIFF. ANGLE	PEAK INT	D I/10	D MEAS	D STD	DIFF PLANE	INT STD	CONF LIMIT
(1)	AUSTENITE	55.5	39	100	2.081	2.080	111	100	100.0
		65.3	15	40	1.796	1.800	200	80	99.8
(2)	FE3C(CEMENTITE)	48.1	17	17	2.378	2.380	112	65	99.9
		55.0	100	100	2.098	2.100	121	60	100.0
(3)	FE5C2(HAGG)	48.1	17	100	2.378	2.390	202	20	99.7
		65.3	15	88	1.796	1.800	312	70	99.8
		116.1	15	88	1.142	1.140	821	20	99.7
(4)	MN5C2	55.5	39	100	2.081	2.084	120	80	99.9
		64.4	35	89	1.818	1.818	213	60	100.0
(5)	CR7C3(2)	55.0	100	100	2.098	2.100	12	60	100.0
		64.4	35	35	1.818	1.820	301	30	99.9
		65.3	15	15	1.796	1.790	22	50	99.8
		114.0	15	15	1.155	1.154	999	30	99.8
(6)	(CR7C3+MN7C3)	48.1	17	75	2.378	2.380	333	80	99.9
		110.4	23	100	1.180	1.180	888	100	100.0
(7)	FE8SI2C	55.0	100	100	2.098	2.090	130	80	99.8
		55.5	39	39	2.081	2.080	131	80	100.0
		64.4	35	35	1.818	1.820	31	20	99.9
		65.3	15	15	1.796	1.794	312	20	99.9
(8)	MN15C4	55.0	100	100	2.098	2.094	213	100	99.9
		65.3	15	15	1.796	1.789	222	50	99.7
(9)	FE2C	55.0	100	100	2.098	2.103	101	100	99.9
		114.0	15	15	1.155	1.156	201	20	99.9
		126.0	23	23	1.087	1.088	4	6	99.9

TABLE-6.16 SUMMARY TABLE OF DIFFRACTOGRAM INDEXING

ALLOY: C3 AS-CAST

DIFF. ANGLE	PHASE(S)																INT																
	1	3	5	7	9	11	13	15	17	19	21	23	25	27	29																		
47.5	0	0	0	0	0	0	0	0	0	0	0	0	0	0	0	1	0	1	0	0	0	0	1	0	0	0	0	0	1	1	4.8		
50.3	0	0	0	0	0	0	1	0	1	1	1	1	0	0	0	0	0	0	0	0	0	0	0	0	0	0	0	0	1	1	0	6.2	
51.4	0	0	0	0	0	0	0	0	0	0	0	0	0	0	0	0	0	0	0	0	0	0	0	0	0	0	0	0	0	0	0	3.6	
54.4	0	0	0	0	0	0	1	0	1	1	1	0	1	1	1	0	0	1	0	1	0	0	0	0	0	0	0	0	0	0	0	6.8	
54.9	0	0	0	0	0	1	0	0	0	0	0	0	1	0	0	0	0	1	0	0	0	0	0	0	0	0	0	0	0	1	1	18.6	
56.1	0	0	1	0	1	1	0	1	1	1	0	0	0	0	0	0	0	0	1	0	0	1	0	0	0	0	1	1	1	0	0	3.8	
61.9	0	0	0	1	1	0	0	0	0	0	0	0	0	0	0	0	0	0	1	0	0	0	0	0	0	0	0	1	1	1	0	0	3.8
62.8	0	0	0	0	0	0	0	0	0	0	0	0	0	0	0	0	0	1	0	1	0	0	0	0	0	0	0	0	0	0	0	0	4.0
64.1	0	0	0	0	0	0	1	0	1	1	1	1	0	0	0	0	0	0	1	0	0	0	0	0	0	0	0	1	1	0	0	0	50.0
98.0	0	0	0	0	0	0	0	0	0	0	0	0	0	0	0	0	0	0	0	0	0	0	0	0	0	0	0	0	0	0	0	0	10.2
113.0	0	0	0	0	0	0	0	1	0	0	0	0	0	0	0	0	0	0	0	0	0	0	0	0	0	0	0	0	0	0	0	0	3.2
124.4	0	0	0	0	0	0	0	0	0	0	0	0	0	0	0	0	0	0	0	0	0	0	0	0	0	0	0	0	0	0	0	0	41.0
126.2	0	0	0	0	1	0	0	0	0	0	0	0	0	0	0	0	0	0	0	0	0	0	0	0	0	0	0	0	0	0	0	0	6.0
127.0	0	1	0	0	0	0	0	0	0	0	0	0	0	0	0	0	0	0	0	0	0	0	0	0	0	0	0	0	0	0	0	0	3.0
0 0 0 0 3 2 3 2 4 4 3 3 2 2 2 2 5 3 2 0 3 0 4 0 0 3 4 3 4 3																																	

0 = ABSENT 1 = PRESENT * = PROBABLE DIFF. ANGLE FOR K-BETA RADIATION

DETAILED ANALYSIS OF PHASE(S) ACTUALLY PRESENT

S.N.	PHASE PRESENT	DIFF. ANGLE	PEAK INT	D I/10	D MEAS	D STD	DIFF PLANE	INT STD	CONF LIMIT
(1)	FE3C(CEMENTITE)	54.9	37	100	2.102	2.100	121	60	99.9
		56.1	7	20	2.061	2.060	210	70	100.0
(2)	FE5C2	50.3	12	12	2.280	2.287	20	20	99.8
		54.4	13	13	2.120	2.112	112	25	99.8
		64.1	100	100	1.826	1.821	511	20	99.8
(3)	FE5C2(HAGG)	56.1	7	100	2.061	2.060	510	100	100.0
		113.0	6	84	1.162	1.160	423	20	99.7
(4)	MN5C2(PD5B2)	50.3	12	12	2.280	2.282	20	70	100.0
		54.4	13	13	2.120	2.117	112	70	99.9
		56.1	7	7	2.061	2.058	510	80	99.9
		64.1	100	100	1.826	1.820	312	70	99.8
(5)	FE7C3(2)	50.3	12	12	2.280	2.270	2	8	99.8
		54.4	13	13	2.120	2.122	12	40	99.9
		64.1	100	100	1.826	1.820	301	10	99.8
(6)	CR7C3(2)	50.3	12	12	2.280	2.270	120	50	99.8
		54.9	37	37	2.102	2.100	12	60	99.9
		64.1	100	100	1.826	1.820	301	30	99.8
(7)	(CR7C3+MN7C3)	54.4	13	100	2.120	2.120	555	100	100.0
		62.8	7	58	1.860	1.860	888	100	100.0
(8)	FE8SI2C	56.1	7	7	2.061	2.070	210	80	99.7
		61.9	7	7	1.884	1.880	331	60	99.9
		64.1	100	100	1.826	1.820	31	20	99.8
(9)	CRMN3	50.3	12	100	2.280	2.272	2	60	99.8
		56.1	7	61	2.061	2.069	330	100	99.8
		61.9	7	61	1.884	1.888	777	90	99.9
(10)	MN15C4	47.5	9	25	2.406	2.404	211	50	100.0
		50.3	12	33	2.280	2.273	212	50	99.8
		54.4	13	36	2.120	2.129	301	10	99.7
		54.9	37	100	2.102	2.094	213	100	99.8

Martensite additionally present

TABLE-6.17 SUMMARY TABLE OF DIFFRACTOGRAM INDEXING

ALLOY:C3	H/T TEMPERATURE: 800°C															SOAKING DURATION: 6 HOURS																												
DIFF. ANGLE	PHASE(S)															INT																												
	1	3	5	7	9	11	13	15	17	19	21	23	25	27	29																													
48.2	0	0	0	1	1	1	0	0	0	0	0	0	0	0	0	0	0	0	0	0	0	0	0	0	0	0	0	6.0																
51.0	0	0	0	0	0	1	0	1	0	0	1	0	0	0	0	0	0	0	0	0	0	0	0	0	0	1	0	1	0	4.2														
55.5	0	1	0	0	0	0	1	0	1	1	0	0	0	0	0	0	0	0	0	0	0	0	0	1	1	0	0	0	0	80.0														
57.8	0	0	0	0	0	1	1	0	0	0	0	0	0	0	0	0	0	0	0	0	0	0	0	0	1	0	0	1	0	10.0														
58.3	0	0	0	0	0	0	0	1	1	1	1	1	0	0	0	0	1	0	0	0	0	0	1	0	0	1	0	0	0	0	4.0													
62.8	0	0	0	0	0	0	0	0	0	0	0	0	0	0	1	0	1	0	0	0	0	0	0	0	0	0	0	0	0	0	4.0													
65.3	0	1	0	1	1	0	0	1	0	0	0	1	0	0	0	0	0	0	1	0	0	0	0	0	1	0	0	1	0	18.0														
98.5	0	0	0	0	0	0	0	0	0	0	0	1	0	0	0	1	0	0	0	0	0	0	1	0	1	0	0	0	0	5.2														
125.4	0	0	0	0	0	0	0	1	0	0	0	0	0	0	0	0	0	0	0	0	0	0	0	0	1	0	0	0	0	9.8														
126.2	0	0	0	0	1	0	0	0	0	0	0	0	0	0	0	0	0	0	0	0	0	0	1	0	0	0	0	0	0	4.2														
															0	2	0	2	3	3	2	4	2	2	2	2	0	0	2	0	3	0	0	0	0	0	2	0	3	4	0	0	3	0

0 = ABSENT 1 = PRESENT * = PROBABLE DIFF. ANGLE FOR K-BETA RADIATION

DETAILED ANALYSIS OF PHASE(S) ACTUALLY PRESENT

S.N.	PHASE PRESENT	DIFF. ANGLE	PEAK INT	D I/O	D MEAS	D STD	DIFF PLANE	INT STD	CONF LIMIT
(1)	AUSTENITE	55.5	100	100	2.081	2.080	111	100	100.0
		65.3	22	22	1.796	1.800	200	80	99.8
(2)	FE3C(CEMENTITE)	48.2	7	59	2.373	2.380	112	65	99.8
		51.0	5	41	2.251	2.260	200	25	99.8
		57.8	12	100	2.005	2.010	103	100	99.8
(3)	FE5C2	55.5	100	100	2.081	2.080	21	70	100.0
		57.8	12	12	2.005	2.010	312	40	99.8
(4)	FE5C2(HAGG)	51.0	5	23	2.251	2.260	20	50	99.8
		58.3	5	22	1.989	1.980	511	20	99.7
		65.3	22	100	1.796	1.800	312	70	99.8
		125.4	12	54	1.090	1.090	404	20	100.0
(5)	MN5C2	55.5	100	100	2.081	2.084	120	80	99.9
		58.3	5	5	1.989	1.994	115	80	99.8
(6)	MN5C2(PD5B2)	55.5	100	100	2.081	2.078	21	100	99.9
		58.3	5	5	1.989	1.990	511	80	100.0
(7)	FE7C3(2)	51.0	5	100	2.251	2.255	120	30	99.9
		58.3	5	95	1.989	1.989	300	16	100.0
(8)	CR7C3(2)	58.3	5	22	1.989	1.990	300	20	100.0
		65.3	22	100	1.796	1.790	22	50	99.8
(9)	CR3C2	58.3	5	76	1.989	1.990	420	20	100.0
		62.8	5	76	1.860	1.860	221	30	100.0
		98.5	6	100	1.279	1.280	531	5	99.9
(10)	CU2S(1)	58.3	5	76	1.989	1.980	110	100	99.7
		98.5	6	100	1.279	1.281	114	11	99.7
(11)	COPPER	55.5	100	100	2.081	2.088	111	100	99.8
		98.5	6	6	1.279	1.278	220	20	99.9
		125.4	12	12	1.090	1.090	311	17	100.0
(12)	FE8SI2C	55.5	100	100	2.081	2.080	131	80	100.0
		57.8	12	12	2.005	2.010	322	100	99.8
		58.3	5	5	1.989	1.980	114	60	99.7
		65.3	22	22	1.796	1.794	312	20	99.9
(13)	MN15C4	51.0	5	23	2.251	2.262	105	50	99.7
		57.8	12	55	2.005	2.012	6	50	99.8
		65.3	22	100	1.796	1.789	222	50	99.7

Martensite additionally present

TABLE-6.18 SUMMARY TABLE OF DIFFRACTOGRAM INDEXING

ALLOY: C3	H/T TEMPERATURE: 850°C														SOAKING DURATION: 6 HOURS																				
DIFF. ANGLE	PHASE(S)														INT																				
	1	3	5	7	9	11	13	15	17	19	21	23	25	27	29																				
49.5	0	0	0	0	0	0	0	0	0	0	0	0	0	0	0	1	0	0	0	0	0	0	0	0	0	0	0	0	0	0	0	0	0	4.0	
54.6	0	0	0	0	0	0	1	0	1	1	1	0	1	1	1	1	1	0	0	0	0	0	0	0	0	0	0	0	0	0	0	0	0	1	3.8
55.5	0	1	0	0	0	0	1	0	1	1	0	0	0	0	0	0	0	0	0	0	0	0	0	0	0	1	1	0	0	0	0	0	0	90.0	
56.8	0	0	0	0	0	0	0	1	1	1	0	0	1	1	1	0	0	0	0	0	0	0	0	0	0	0	0	0	0	1	1	0	3.0		
* 63.3	0	0	0	0	0	1	0	0	0	0	0	0	1	0	1	0	0	0	0	0	0	0	0	0	0	1	0	1	0	0	0	0	3.2		
64.3	0	0	0	0	0	0	1	0	1	1	1	1	0	0	0	0	0	0	0	0	0	0	0	0	1	0	0	0	0	0	0	0	6.8		
65.4	0	1	0	1	1	0	0	1	0	0	0	1	0	0	0	0	0	0	0	0	0	0	0	0	1	0	0	0	1	0	0	1	0	3.2	
98.5	0	0	0	0	0	0	0	0	0	0	0	0	0	0	0	0	0	0	0	0	0	0	0	0	1	0	1	0	0	0	0	0	0	4.0	
125.2	0	0	0	0	0	0	0	0	0	0	0	0	0	0	0	0	0	0	0	0	0	0	0	0	0	0	0	0	0	0	0	0	0	18.0	
125.6	0	0	0	0	0	0	0	1	0	0	0	0	0	0	0	0	0	0	0	0	0	0	0	0	0	0	0	0	0	0	0	0	1	12.8	
	0	2	0	0	0	0	3	3	4	4	2	2	4	2	3	0	2	0	3	2	0	0	0	0	0	3	5	0	0	2	2				

0 = ABSENT 1 = PRESENT * = PROBABLE DIFF. ANGLE FOR K-BETA RADIATION
 DETAILED ANALYSIS OF PHASE(S) ACTUALLY PRESENT

S.N.	PHASE PRESENT	DIFF. ANGLE	PEAK INT	D I/10	D MEAS	D STD	DIFF PLANE	INT STD	CONF LIMIT
(1)	AUSTENITE	55.5	100	100	2.081	2.080	111	100	100.0
		65.4	3	3	1.794	1.800	200	80	99.7
(2)	FE5C2	54.6	4	4	2.113	2.112	112	25	100.0
		55.5	100	100	2.081	2.080	21	70	100.0
		64.3	7	7	1.821	1.814	312	25	99.7
(3)	FE5C2(HAGG)	56.8	3	23	2.037	2.030	312	100	99.8
		65.4	3	25	1.794	1.800	312	70	99.7
		125.6	14	100	1.089	1.090	404	20	99.8
(4)	MN5C2	54.6	4	4	2.113	2.121	211	80	99.8
		55.5	100	100	2.081	2.084	120	80	99.9
		56.8	3	3	2.037	2.034	204	60	99.9
		64.3	7	7	1.821	1.818	213	60	99.9
(5)	MN5C2(PD5B2)	54.6	4	4	2.113	2.117	112	70	99.9
		55.5	100	100	2.081	2.078	21	100	99.9
		56.8	3	3	2.037	2.035	402	70	99.9
		64.3	7	7	1.821	1.820	312	70	100.0
(6)	FE7C3(2)	54.6	4	55	2.113	2.122	12	40	99.7
		64.3	7	100	1.821	1.820	301	10	100.0
(7)	CR7C3	54.6	4	94	2.113	2.120	202	70	99.8
		56.8	3	75	2.037	2.040	421	100	99.9
		63.3	3	80	1.847	1.840	601	60	99.7
		98.5	4	100	1.279	1.280	0	60	99.9
(8)	(CR7C3+MN7C3)	54.6	4	100	2.113	2.120	555	100	99.8
		56.8	3	78	2.037	2.040	666	100	99.9
		63.3	3	84	1.847	1.850	999	80	99.9
(9)	COPPER	55.5	100	100	2.081	2.088	111	100	99.8
		98.5	4	4	1.279	1.278	220	20	99.9
		125.6	14	14	1.089	1.090	311	17	99.8
(10)	FE8SI2C	49.5	4	4	2.314	2.320	104	40	99.9
		55.5	100	100	2.081	2.080	131	80	100.0
		63.3	3	3	1.847	1.840	15	60	99.7
		64.3	7	7	1.821	1.820	31	20	100.0
		65.4	3	3	1.794	1.794	312	20	100.0
(11)	MN15C4	56.8	3	93	2.037	2.037	302	100	100.0
		65.4	3	100	1.794	1.789	222	50	99.8

Martensite additionally present

TABLE-6.20 SUMMARY TABLE OF DIFFRACTOGRAM INDEXING

ALLOY:C3	H/T TEMPERATURE: 950°C																SOAKING DURATION: 6 HOURS										
DIFF. ANGLE	PHASE(S)																INT										
	1	3	5	7	9	11	13	15	17	19	21	23	25	27	29												
55.3	0	1	0	0	0	0	1	0	1	1	0	0	0	0	0	0	0	0	0	0	1	1	0	0	1	0	39.5
64.3	0	0	0	0	0	0	1	0	1	1	1	1	0	0	0	0	0	0	0	0	1	0	0	0	0	0	3.0
64.6	0	0	0	0	0	0	1	0	0	0	1	0	1	1	0	0	1	0	0	0	1	0	0	1	1	0	6.5
73.1	0	0	0	1	0	0	0	0	0	0	0	0	0	0	0	0	0	0	0	0	0	0	0	1	0	0	2.0
77.5	0	0	0	0	0	0	0	0	0	0	0	0	0	0	0	0	0	0	0	0	0	0	0	0	0	0	1.0
77.6	0	0	0	0	0	0	0	0	0	0	0	0	0	0	0	0	0	0	0	0	1	0	0	0	0	0	3.0
89.4	0	0	0	0	0	0	0	0	0	0	0	0	0	0	0	0	0	0	0	0	0	0	0	0	0	0	1.5
101.4	0	0	0	0	1	0	0	1	0	0	0	0	0	0	0	0	0	0	0	0	0	0	0	0	0	1	3.0
102.5	0	0	0	0	0	0	0	0	0	0	0	1	0	0	0	0	0	0	0	0	0	0	0	0	0	1	4.5
0 0 0 0 0 0 0 3 0 2 2 2 0 2 0 0 0 0 0 0 0 0 2 0 0 2 4 0 2 2 3																											

0 = ABSENT 1 = PRESENT * = PROBABLE DIFF. ANGLE FOR K-BETA RADIATION

DETAILED ANALYSIS OF PHASE(S) ACTUALLY PRESENT

S.N.	PHASE PRESENT	DIFF. ANGLE	PEAK INT	D I/10	D MEAS	D STD	DIFF PLANE	INT STD	CONF LIMIT
(1)	FE5C2	55.3	100	100	2.088	2.080	21	70	99.8
		64.3	7	7	1.821	1.821	511	20	100.0
		64.6	16	16	1.813	1.814	312	25	100.0
(2)	MN5C2	55.3	100	100	2.088	2.084	120	80	99.9
		64.3	7	7	1.821	1.818	213	60	99.9
(3)	MN5C2(PD5B2)	55.3	100	100	2.088	2.078	21	100	99.7
		64.3	7	7	1.821	1.820	312	70	100.0
(4)	FE7C3(2)	64.3	7	46	1.821	1.820	301	10	100.0
		64.6	16	100	1.813	1.807	22	20	99.7
(5)	CR7C3	64.6	16	100	1.813	1.810	431	70	99.9
		102.5	11	69	1.242	1.240	0	20	99.7
(6)	CR2O3	64.6	16	100	1.813	1.816	24	40	99.9
		102.5	11	69	1.242	1.240	220	18	99.7
(7)	COPPER	55.3	100	100	2.088	2.088	111	100	100.0
		64.6	16	16	1.813	1.808	200	46	99.8
		55.3	100	100	2.088	2.080	131	80	99.8
(8)	FE8SI2C	64.3	7	7	1.821	1.820	31	20	100.0
		64.6	16	16	1.813	1.810	15	20	99.9
		73.1	5	5	1.627	1.625	124	20	99.9
(9)	CRMN3	101.4	7	66	1.252	1.251	413	40	99.9
		102.5	11	100	1.242	1.240	333	40	99.7
(10)	MN15C4	55.3	100	100	2.088	2.094	213	100	99.8
		73.1	5	5	1.627	1.622	400	10	99.7
(11)	FE2C	73.1	5	44	1.627	1.622	112	16	99.7
		89.4	3	33	1.377	1.378	110	16	100.0
		102.5	11	100	1.242	1.243	103	16	99.9

TABLE-6.20 SUMMARY TABLE OF DIFFRACTOGRAM INDEXING

ALLOY: C3	H/T TEMPERATURE: 950°C																SOAKING DURATION: 6 HOURS				INT											
DIFF. ANGLE	PHASE(S)																INT															
	1	3	5	7	9	11	13	15	17	19	21	23	25	27	29																	
55.3	0	1	0	0	0	0	1	0	1	1	0	0	0	0	0	0	0	0	0	0	0	1	1	0	0	1	0	39.5				
64.3	0	0	0	0	0	0	1	0	1	1	1	1	0	0	0	0	0	0	0	0	0	0	0	1	0	0	0	0	3.0			
64.6	0	0	0	0	0	0	1	0	0	0	1	0	1	1	0	0	1	0	0	0	0	1	0	0	1	1	0	0	0	6.5		
73.1	0	0	0	1	0	0	0	0	0	0	0	0	0	0	0	0	0	0	0	0	0	0	0	0	0	1	0	0	1	1	2.0	
77.5	0	0	0	0	0	0	0	0	0	0	0	0	0	0	0	0	0	0	0	0	0	0	0	0	0	0	0	0	0	0	1.0	
77.6	0	0	0	0	0	0	0	0	0	0	0	0	0	0	0	0	0	0	0	0	0	0	0	0	0	0	0	0	0	0	3.0	
89.4	0	0	0	0	0	0	0	0	0	0	0	0	0	0	0	0	0	0	0	0	0	0	0	0	0	0	0	0	0	0	1.5	
101.4	0	0	0	0	1	0	0	1	0	0	0	0	0	0	0	0	0	0	0	0	0	0	0	0	0	0	0	0	1	0	0	3.0
102.5	0	0	0	0	0	0	0	0	0	0	0	0	1	0	0	0	0	0	0	0	0	0	0	0	0	0	0	0	1	0	1	4.5

0 0 0 0 0 0 3 0 2 2 2 0 2 0 0 0 0 0 0 0 0 0 0 2 0 0 2 4 0 2 2 3

0 = ABSENT 1 = PRESENT * = PROBABLE DIFF. ANGLE FOR K-BETA RADIATION

DETAILED ANALYSIS OF PHASE(S) ACTUALLY PRESENT

S.N.	PHASE PRESENT	DIFF. ANGLE	PEAK INT	D I/I0	D MEAS	D STD	DIFF. PLANE	INT STD	CONF LIMIT
(1)	FE5C2	55.3	100	100	2.088	2.080	21	70	99.8
		64.3	7	7	1.821	1.821	511	20	100.0
		64.6	16	16	1.813	1.814	312	25	100.0
(2)	MN5C2	55.3	100	100	2.088	2.084	120	80	99.9
		64.3	7	7	1.821	1.818	213	60	99.9
(3)	MN5C2(PD5B2)	55.3	100	100	2.088	2.078	21	100	99.7
		64.3	7	7	1.821	1.820	312	70	100.0
(4)	FE7C3(2)	64.3	7	46	1.821	1.820	301	10	100.0
		64.6	16	100	1.813	1.807	22	20	99.7
(5)	CR7C3	64.6	16	100	1.813	1.810	431	70	99.9
		102.5	11	69	1.242	1.240	0	20	99.7
(6)	CR203	64.6	16	100	1.813	1.816	24	40	99.9
		102.5	11	69	1.242	1.240	220	18	99.7
(7)	COPPER	55.3	100	100	2.088	2.088	111	100	100.0
		64.6	16	16	1.813	1.808	200	46	99.8
(8)	FE8SI2C	55.3	100	100	2.088	2.080	131	80	99.8
		64.3	7	7	1.821	1.820	31	20	100.0
		64.6	16	16	1.813	1.810	15	20	99.9
		73.1	5	5	1.627	1.625	124	20	99.9
(9)	CRMN3	101.4	7	66	1.252	1.251	413	40	99.9
		102.5	11	100	1.242	1.240	333	40	99.7
(10)	MN15C4	55.3	100	100	2.088	2.094	213	100	99.8
		73.1	5	5	1.627	1.622	400	10	99.7
(11)	FE2C	73.1	5	44	1.627	1.622	112	16	99.7
		89.4	3	33	1.377	1.378	110	16	100.0
		102.5	11	100	1.242	1.243	103	16	99.9

TABLE-6.21 SUMMARY TABLE OF DIFFRACTOGRAM INDEXING

ALLOY: C3		H/T TEMPERATURE: 1000°C														SOAKING DURATION: 6 HOURS																					
DIFF. ANGLE	PHASE(S)														INT																						
	1	3	5	7	9	11	13	15	17	19	21	23	25	27		29																					
46.4	0	0	0	0	0	0	0	0	0	0	0	0	0	0	0	0	0	0	0	0	0	0	0	0	0	0	0	0	0	0	0	0	0	1	0	5.6	
48.2	0	0	0	1	1	1	0	0	0	0	0	0	0	0	1	0	0	1	0	0	0	0	0	0	0	0	0	0	0	0	0	0	0	0	0	0	4.0
50.6	0	0	0	0	0	1	0	1	1	0	1	1	0	0	0	0	0	0	0	0	0	0	0	0	1	0	0	0	0	1	1	1	0	0	0	3.0	
52.6	0	0	0	0	1	0	1	1	0	1	0	0	0	0	0	0	0	0	0	0	0	0	0	1	0	0	0	1	0	0	0	0	0	0	0	4.0	
54.6	0	0	0	0	0	0	1	0	1	1	1	0	1	1	1	1	1	1	1	0	0	0	0	0	0	0	0	0	0	0	0	0	0	0	0	4.0	
55.1	0	0	0	0	0	1	0	0	0	0	0	1	0	0	0	0	0	0	0	0	0	0	0	0	0	0	0	0	0	0	0	0	0	0	0	11.0	
62.8	0	0	0	0	0	0	0	0	0	0	0	0	0	0	1	0	1	0	0	0	0	0	0	0	0	0	0	0	0	0	0	0	0	0	0	4.0	
64.4	0	0	0	0	0	0	1	0	1	1	1	1	0	0	0	0	0	0	0	0	0	0	0	1	0	0	1	0	0	0	1	0	0	0	0	3.0	
67.4	0	0	0	0	0	0	0	0	0	0	0	0	0	0	0	1	0	0	0	0	0	0	0	0	0	0	0	0	0	0	0	0	0	0	0	3.6	
98.2	0	0	0	0	0	0	0	0	0	0	0	0	0	0	0	0	0	0	0	0	0	0	0	0	0	0	0	0	0	0	0	0	0	0	0	5.0	
125.0	0	0	0	0	0	0	0	0	0	0	0	0	0	0	0	0	0	0	0	0	0	0	0	0	0	0	0	0	0	0	0	0	0	0	0	7.6	
126.4	0	0	0	0	0	0	0	0	0	0	0	0	0	0	0	0	0	0	0	0	0	0	0	0	0	0	0	0	0	0	0	0	0	0	0	3.0	
127.0	0	1	0	0	0	0	0	0	0	0	0	0	0	0	0	0	0	0	0	0	0	0	0	0	0	0	0	0	0	0	0	0	0	0	0	4.0	
0 0 0 0 2 3 3 2 3 3 3 3 3 2 3 0 4 2 2 0 0 3 2 0 0 4 0 0 3 2																																					

0 = ABSENT 1 = PRESENT * = PROBABLE DIFF. ANGLE FOR K-BETA RADIATION

DETAILED ANALYSIS OF PHASE(S) ACTUALLY PRESENT

S.N.	PHASE PRESENT	DIFF. ANGLE	PEAK INT	I/I0	D MEAS	D STD	DIFF PLANE	INT STD	CONF LIMIT
(1)	MN23C6	48.2	36	100	2.373	2.380	420	50	99.8
		52.6	36	100	2.187	2.177	422	60	99.7
(2)	FE3C(CEMENTITE)	48.2	36	36	2.373	2.380	112	65	99.8
		50.6	27	27	2.267	2.260	200	25	99.8
		55.1	100	100	2.095	2.100	121	60	99.9
(3)	FE5C2	52.6	36	100	2.187	2.190	202	30	99.9
		54.6	36	100	2.113	2.112	112	25	100.0
		64.4	27	75	1.818	1.814	312	25	99.8
(4)	MN5C2(PD5B2)	52.6	36	100	2.187	2.198	202	70	99.7
		54.6	36	100	2.113	2.117	112	70	99.9
		64.4	27	75	1.818	1.820	312	70	99.9
(5)	FE7C3(2)	50.6	27	75	2.267	2.255	120	30	99.7
		54.6	36	100	2.113	2.122	12	40	99.7
		64.4	27	75	1.818	1.820	301	10	99.9
(6)	CR7C3	54.6	36	80	2.113	2.120	202	70	99.8
		67.4	32	71	1.746	1.750	412	70	99.8
		98.2	45	100	1.282	1.280	0	60	99.8
(7)	(CR, FE)7C3	54.6	36	100	2.113	2.120	202	60	99.8
		67.4	32	89	1.746	1.740	322	60	99.7
(8)	CR3C2	54.6	36	80	2.113	2.110	510	20	99.9
		62.8	36	80	1.860	1.860	221	30	100.0
		67.4	32	71	1.746	1.750	230	10	99.8
		98.2	45	100	1.282	1.280	531	5	99.8
(9)	FE8SI2C	52.6	36	36	2.187	2.180	113	40	99.8
		55.1	100	100	2.095	2.090	130	80	99.9
		64.4	27	27	1.818	1.820	31	20	99.9
		67.4	32	32	1.746	1.740	225	20	99.7
(10)	MN15C4	46.4	50	50	2.460	2.452	210	10	99.8
		50.6	27	27	2.267	2.262	105	50	99.9
		55.1	100	100	2.095	2.094	213	100	100.0

ALLOY: C3	H/T TEMPERATURE: 1050°C																SOAKING DURATION: 6 HOURS													
DIFF. ANGLE	PHASE(S)																INT													
	1	3	5	7	9	11	13	15	17	19	21	23	25	27	29															
54.7	0	0	0	0	0	1	0	0	1	0	0	0	0	0	1	1	0	1	0	0	0	0	0	0	0	0	0	0	1	8.0
55.1	0	0	0	0	0	1	0	0	0	0	0	1	0	0	0	0	0	0	0	0	0	0	0	1	1	0	0	1	0	6.0
64.5	0	0	0	0	0	0	1	0	1	1	1	1	1	0	0	1	0	0	0	0	1	0	0	0	1	0	0	0	0	4.6
96.6	0	0	0	0	0	0	0	0	0	0	0	0	0	0	0	1	1	0	0	0	1	1	0	0	0	0	0	0	0	6.0
98.2	0	0	0	0	0	0	0	0	0	0	0	1	0	0	0	1	0	0	0	0	0	1	0	0	0	0	0	0	0	4.0
0 0 0 0 0 0 2 0 0 2 0 2 2 0 0 0 4 0 0 0 0 2 2 0 0 2 0 0 0 0																														

0 = ABSENT 1 = PRESENT * = PROBABLE DIFF. ANGLE FOR K-BETA RADIATION

DETAILED ANALYSIS OF PHASE(S) ACTUALLY PRESENT

S.N.	PHASE PRESENT	DIFF. ANGLE	PEAK INT	D I/IO	D MEAS	D STD	DIFF PLANE	INT STD	CONF LIMIT
(1)	FE5C2	54.7	100	100	2.109	2.112	112	25	99.9
		64.5	57	57	1.816	1.814	312	25	99.9
(2)	MN5C2(PD5B2)	54.7	100	100	2.109	2.117	112	70	99.8
		64.5	57	57	1.816	1.820	312	70	99.8
(3)	CR7C3(2)	55.1	75	100	2.095	2.100	12	60	99.9
		64.5	57	76	1.816	1.820	301	30	99.8
(4)	CR7C3	64.5	57	100	1.816	1.810	431	70	99.8
		98.2	50	86	1.282	1.280	0	60	99.8
(5)	CR3C2	54.7	100	100	2.109	2.110	510	20	100.0
		64.5	57	57	1.816	1.810	130	30	99.8
		96.6	75	75	1.298	1.298	340	5	100.0
		98.2	50	50	1.282	1.280	531	5	99.8
(6)	CR2O3	64.5	57	76	1.816	1.816	24	40	100.0
		96.6	75	100	1.298	1.296	101	20	99.8
(7)	CU2S(1)	96.6	75	100	1.298	1.296	210	3	99.9
		98.2	50	66	1.282	1.281	114	11	100.0
(8)	FE8SI2C	55.1	75	100	2.095	2.090	130	80	99.9
		64.5	57	76	1.816	1.810	15	20	99.8

Table 6.23

Summary of X-ray diffractometric data (Alloy C1)

	Matrix	M ₃ C	M ₇ C ₃	M ₅ C ₂	Fe ₈ Si ₂ C	CrMn ₃	Cu	Mn ₁₅ C ₄
As-Cast	A+M	P	P	P	P	-	P	P
800-6	A+M	P	P	P	S	S	-	S
850-6	A+M	S	P	S	S	S	S	S
900-6	A	P	P	P	P	S	-	S
950-6	A	S	S	S	S	-	-	-
1000-6	A	-	P	S	S	T	T	T
1050-6	A	T	S	T	T	T	S	T

Table 6.24 Summary of X-ray diffractometric data (Alloy C2)

	Matrix	M ₃ C	M ₇ C ₃	M ₅ C ₂	Fe ₈ Si ₂ C	CrMn ₃	Cu	Mn ₁₅ C ₄
As-Cast	A+M	P	P	P	S	-	S	S
800-6	A+M	P	P	P	-	P	-	-
850-6	A+M	S	P	S	S	P	S	S
900-6	A	-	P	P	P	-	P	S
950-6	A	P	P	P	P	-	S	S
1000-6	A	S	P	S	S	-	T	S
1050-6	A	-	P	S	S	-	F	-

Table 6.25 Summary of X-ray diffractometric data (Alloy C3)

	Matrix	M ₃ C	M ₇ C ₃	M ₅ C ₂	Fe ₈ Si ₂ C	CrMn ₃	Cu	Mn ₁₅ C ₄
As-Cast	A+M	S	P	P	S	S	-	P
800-6	A+M	P	P	S	P	-	P	S
850-6	A+M	T?	P	P	P	-	P	S
900-6	A	P	P	P	P	P	S	S
950-6	A	-	P	S	S	S	P	S
1000-6	A	T	S	S	S	-	T	S
1050-6	A	-	P	T	S	-	T	-

Table-6.26a Element distribution into the matrix (weight %) as influenced by heat treatment

H/T	Fe	C	Mn	Cr	Cu	Si
C1 AS-CAST	82.611	1.646	8.499	3.029	1.592	2.623
C1 1000 2	84.036	.850	8.688	2.324	1.550	2.552
C1 1000 10	83.320	1.175	8.182	2.678	2.008	2.637
C1 1050 2	83.630	1.834	8.974	2.340	1.609	2.260
C1 1050 10	83.919	1.771	8.790	2.485	1.406	2.894
C2 AS-CAST	83.308	1.775	7.232	2.295	3.241	2.431
C2 950 2	82.859	1.633	7.294	2.982	3.308	2.092
C2 950 10	83.603	1.347	7.291	2.907	3.354	2.141
C2 1000 2	83.547	1.331	6.988	2.940	3.035	2.801
C2 1000 10	83.762	1.214	7.475	2.125	3.399	2.217
C2 1050 2	83.796	1.485	6.978	2.377	3.259	2.106
C3 AS-CAST	82.958	1.277	7.433	2.730	4.495	2.704
C3 950 2	82.622	.945	7.085	2.558	4.422	2.368
C3 950 10	82.602	.889	8.765	2.609	4.501	2.634
C3 1000 2	82.490	.249	7.209	1.889	4.867	2.296
C3 1000 10	82.118	.000	7.991	2.414	4.557	2.565
C3 1050 2	82.131	.161	7.781	2.640	4.818	2.569
C3 1050 10	82.765	.146	7.532	2.245	4.580	2.731

Table-6.26b Element distribution into matrix (atom %) as influenced by heat treatment

H/T	Fe	C	Mn	Cr	Cu	Si
C1 AS-CAST	75.949	7.036	7.943	2.991	1.286	4.795
C1 1000 2	79.465	3.737	8.351	2.360	1.288	4.799
C1 1000 10	77.880	5.106	7.774	2.688	1.649	4.902
C1 1050 2	76.234	7.773	8.316	2.291	1.289	4.097
C1 1050 10	75.775	7.435	8.068	2.410	1.116	5.196
C2 AS-CAST	76.387	7.567	6.741	2.260	2.612	4.433
C2 950 2	76.625	7.021	6.857	2.962	2.688	3.847
C2 950 10	77.695	5.820	6.888	2.901	2.739	3.957
C2 1000 2	77.191	5.718	6.563	2.917	2.464	5.146
C2 1000 10	78.515	5.291	7.123	2.139	2.800	4.133
C2 1050 2	78.023	6.429	6.605	2.377	2.667	3.899
C3 AS-CAST	76.311	5.462	6.951	2.697	3.634	4.946
C3 950 2	78.270	4.162	6.823	2.602	3.681	4.461
C3 950 10	76.738	3.840	8.278	2.603	3.675	4.866
C3 1000 2	80.993	1.137	7.195	1.992	4.200	4.483
C3 1000 10	80.556	.000	7.969	2.543	3.929	5.004
C3 1050 2	79.764	.727	7.682	2.753	4.112	4.961
C3 1050 10	80.380	.659	7.436	2.341	3.909	5.274

Table-6.27a Element distribution into the massive carbide (weight %) as influenced by heat treatment

H/T	Fe	C	Mn	Cr	Cu	Si
C1 AS-CAST	56.201	12.244	12.994	19.698	.087	.000
C1 1000 2	56.322	9.225	13.542	20.838	.038	.036
C1 1000 10	58.267	8.484	13.391	19.793	.040	.024
C1 1050 2	58.776	9.758	12.224	19.475	.064	.000
C1 1050 10	59.367	9.674	12.125	20.515	.140	.000
C2 AS-CAST	61.148	10.329	12.705	17.154	.122	.013
C2 950 2	60.031	8.857	11.067	19.985	.029	.031
C2 950 10	61.024	9.639	11.658	19.259	.061	.017
C2 1000 2	61.569	8.390	11.518	19.495	.005	.022
C2 1000 10	60.186	10.525	10.478	19.262	.117	.000
C2 1050 2	60.693	10.077	11.196	18.710	.221	.102
C3 AS-CAST	58.655	10.773	11.482	19.638	.189	.000
C3 950 2	60.381	9.373	11.821	18.318	.064	.043
C3 950 10	60.207	8.864	12.032	18.878	.000	.019
C3 1000 2	60.291	9.371	11.836	18.366	.136	.000
C3 1000 10	58.943	8.907	13.560	19.510	.040	.047
C3 1050 2	60.121	9.279	10.875	19.590	.128	.007
C3 1050 10	60.927	9.039	11.663	18.736	.089	.000

Table-6.27b Element distribution into massive carbide (atom %) as influenced by heat treatment

H/T	Fe	C	Mn	Cr	Cu	Si
C1 AS-CAST	38.085	38.577	8.951	14.335	.052	.000
C1 1000 2	41.577	31.663	10.162	16.520	.025	.053
C1 1000 10	43.920	29.734	10.261	16.023	.026	.036
C1 1050 2	42.733	32.986	9.035	15.206	.041	.000
C1 1050 10	42.763	32.399	8.879	15.870	.089	.000
C2 AS-CAST	43.477	34.146	9.183	13.099	.076	.018
C2 950 2	44.796	30.729	8.395	16.015	.019	.046
C2 950 10	44.073	32.367	8.559	14.938	.039	.024
C2 1000 2	46.198	29.270	8.786	15.710	.003	.033
C2 1000 10	42.818	34.814	7.578	14.717	.073	.000
C2 1050 2	43.533	33.606	8.164	14.412	.139	.145
C3 AS-CAST	41.402	35.355	8.239	14.886	.117	.000
C3 950 2	44.466	32.093	8.849	14.487	.041	.063
C3 950 10	44.943	30.764	9.130	15.134	.000	.028
C3 1000 2	44.418	32.099	8.864	14.531	.088	.000
C3 1000 10	43.590	30.626	10.194	15.495	.026	.069
C3 1050 2	44.375	31.843	8.160	15.528	.083	.010
C3 1050 10	45.128	31.129	8.782	14.904	.058	.000

Table-6.28a Element distribution in the massive carbide (grey)
(weight %) as influenced by heat treatment

H/T	Fe	C	Mn	Cr	Cu	Si
C2 AS-CAST	73.612	7.762	12.595	8.457	.171	.000
C2 950 2	68.077	10.717	11.657	9.324	.187	.038
C2 950 10	71.912	7.365	11.567	8.964	.172	.021
C2 1000 2	72.860	4.837	13.035	9.242	.003	.023
C2 1050 2	71.300	9.381	12.097	6.817	.219	.125
C3 950 2	72.965	7.367	12.123	7.393	.121	.031
C3 950 10	72.068	7.808	11.815	8.105	.174	.030
C3 1000 2	72.882	6.300	12.227	8.427	.138	.026
C3 1050 2	71.005	8.205	12.063	8.608	.107	.011

Table-6.28b Element distribution in massive carbide (grey)
(atom %) as influenced by heat treatment

H/T	Fe	C	Mn	Cr	Cu	Si
C2 AS-CAST	55.878	27.395	9.719	6.894	.114	.000
C2 950 2	48.623	35.589	8.464	7.152	.117	.054
C2 950 10	56.298	26.808	9.206	7.537	.118	.033
C2 1000 2	61.447	18.967	11.175	8.371	.002	.039
C2 1050 2	52.824	32.314	9.111	5.424	.143	.184
C3 950 2	57.161	26.833	9.654	6.220	.083	.048
C3 950 10	55.738	28.077	9.289	6.732	.118	.046
C3 1000 2	58.858	23.655	10.038	7.309	.098	.042
C3 1050 2	54.295	29.171	9.377	7.069	.072	.017

Table-6.29a Element distribution within flower type carbide (weight %)

H/T	Fe	C	Mn	Cr	Cu	Si
C1 AS-CAST	57.544	12.451	14.344	18.915	.093	.000
C2 AS-CAST	56.621	12.120	13.847	19.178	.081	.000

Table-6.30a Element distribution within grey phase (weight %)

H/T	Fe	C	Mn	Cr	Cu	Si
C1 1050 10	74.910	8.979	5.787	2.981	6.522	4.019
C2 1050 2	70.460	10.085	7.868	2.776	7.115	3.330

Table-6.31a Element distribution within DC (globular feature)
(weight %)

H/T	Fe	C	Mn	Cr	Cu	Si
C3 1000 10	59.592	9.091	11.809	19.478	.000	.030
C3 1050 10	58.882	8.826	12.232	19.985	.049	.025

Table-6.32a Element distribution within Copper- rich phase (weight %)

H/T	Fe	C	Mn	Cr	Cu	Si
C3 AS-CAST	4.009	.000	9.462	.218	88.221	.120
C3 950 2	2.075	.000	8.279	.048	89.791	.182
C3 950 10	2.082	.795	7.454	.000	89.332	.337

Table-6.29b Element distribution within flower type carbide (atom %)

H/T	Fe	C	Mn	Cr	Cu	Si
C1 AS-CAST	38.258	38.488	9.695	13.505	.054	.000
C2 AS-CAST	38.331	38.149	9.529	13.943	.048	.000

Table-6.30b Element distribution within grey phase (atom %)

H/T	Fe	C	Mn	Cr	Cu	Si
C1 - 1050 10	53.712	29.934	4.218	2.295	4.110	5.731
C2 1050 2	49.899	33.207	5.664	2.111	4.428	4.690

Table-6.31b Element distribution within DC (globular feature)
(atom %)

H/T	Fe	C	Mn	Cr	Cu	Si
C3 1000 10	44.194	31.346	8.903	15.513	.000	.044
C3 1050 10	43.972	30.645	9.286	16.028	.032	.037

Table-6.32b Element distribution within Copper-rich phase (atom %)

H/T	Fe	C	Mn	Cr	Cu	Si
C3 AS-CAST	4.375	.000	10.497	.256	84.612	.260
C3 950 2	2.310	.000	9.371	.057	87.859	.403
C3 950 10	2.250	3.995	8.189	.000	84.842	.724

Table 6.33 Partitioning ratios of Mn and Cr between carbide and matrix.

H/T	Mn carbide/Mn matrix			Cr carbide/Cr matrix		
	C1	C2	C3	C1	C2	C3
As-cast	1.52	1.75	1.54	6.50	7.47	7.19
950,2	-	1.51	1.66	-	6.70	7.16
950,10	-	1.59	1.37	-	6.62	7.23
1000,2	1.55	1.64	1.64	8.96	6.63	9.72
1000,10	1.63	1.40	1.69	7.39	9.06	8.08
1050,2	1.36	1.60	1.39	8.32	7.87	7.42
1050,10	1.37	-	1.54	8.25	-	8.34

Table-6.34 Transformation temperature, °C

Alloy designation	Transformation temperature, °C			
	I	II	III	IV
C1	575	744	900	968
C2	560	760	-	980
C3	540	-	-	972

Table-6.35 DTA, μV

Alloy designation	DTA, μV			
	I	II	III	IV
C1	-3.26	1.60	3.40	13.50
C2	-2.66	-1.40	-	10.86
C3	-4.60	-	-	18.00

Table-6.36 Effect of heat treating on the % TG

Alloy	RT	Temperature, °C										
		100	200	300	400	500	600	700	800	900	1000	1060
C1	0.00	1.63	2.32	2.68	3.01	3.37	3.96	5.36	7.69	10.71	16.54	24.44
C2	0.00	1.89	2.52	2.94	3.36	3.78	4.58	5.09	6.94	9.26	15.57	21.93
C3	0.00	1.41	2.05	2.60	2.97	3.36	3.73	4.18	4.94	6.34	11.95	18.89

Table-6.37 Percent increase in % TG on heat treating in the different temperature ranges

Alloy	I	II	III	IV	Temperature range						
					V	VI	VII	VIII	IX	X	XI
C1	...	42.32	15.29	12.48	11.82	17.39	35.43	43.36	39.24	54.40	47.78
C2	...	33.36	16.66	14.28	12.50	21.11	11.00	36.37	33.33	68.17	40.81
C3	...	44.98	26.98	14.19	13.10	10.98	12.06	18.14	28.21	88.36	58.08

Table-7.1 Effect of heat treatment on compressive behaviour
ALLOY C1

H/T condition	Compressive Strength	
	TSI	MN/m ²
As-Cast	128.16	1986.54
900, 2	150.59	2334.28
950, 6	134.12	2078.91
1000, 2	164.48	2549.59
1000, 6	137.29	2128.13
1000, 10	141.27	2189.75
1050, 2	149.24	2313.33
1050, 6	133.00	2061.64
1050, 10	131.23	2034.12

Table-7.3 Effect of heat treatment on compressive behaviour
ALLOY C3

H/T condition	Compressive Strength	
	TSI	MN/m ²
As-Cast	133.21	2064.82
900, 6	128.21	1987.39
950, 6	169.32	2624.46
950, 10	158.98	2464.24
1000, 2	130.49	2022.71
1000, 6	148.90	2308.05
1000, 10	184.66	2862.31
1050, 2	170.09	2636.47
1050, 6	157.73	2444.88
1050, 10	186.23	2886.59

Table 7.4 Summary table of the predicted and experimentally determined compressive strength values (based on Equations 7.2-7.4)

	Hardness	CSexp	Rexp	Rpred	CSpred	%error
<u>ALLOY C1</u>						
900,2	561	2334.28	4.16	4.09	2295.40	-1.69
950,6	529	2078.91	3.93	4.37	2311.79	10.07
1000,2	512	2549.59	4.98	4.46	2283.72	-11.64
1000,6	487	2128.13	4.37	4.52	2201.44	3.33
1000,10	487	2189.75	4.50	4.52	2201.44	.53
1050,2	491	2313.33	4.71	4.52	2217.66	-4.31
1050,6	480	2061.64	4.30	4.52	2170.41	5.01
1050,10	451	2034.12	4.51	4.45	2009.09	-1.25
<u>ALLOY C2</u>						
900,2	557	2535.32	4.55	4.86	2707.72	6.37
900,10	517	2830.66	5.48	4.63	2391.67	-18.35
950,2	516	2004.80	3.89	4.63	2386.61	16.00
950,6	526	2791.14	5.31	4.64	2443.14	-14.24
1000,2	482	2094.23	4.34	4.74	2285.81	8.38
1000,6	451	2318.47	5.14	5.10	2298.48	-.87
1000,10	387	2553.34	6.60	6.57	2543.89	-.37
1050,2	454	2357.71	5.19	5.05	2293.53	-2.80
1050,6	444	2278.23	5.13	5.21	2312.79	1.49
1050,10	356	2743.27	7.71	7.65	2723.44	-.73
<u>ALLOY C3</u>						
900,6	519	1987.39	3.83	3.77	1959.15	-1.44
950,6	452	2624.46	5.81	5.23	2361.95	-11.11
950,10	444	2464.24	5.55	5.42	2408.38	-2.32
1000,2	471	2022.71	4.29	4.78	2249.22	10.07
1000,6	429	2308.05	5.38	5.81	2493.14	7.42
1000,10	377	2862.31	7.59	7.30	2752.85	-3.98
1050,2	429	2636.47	6.15	5.81	2493.14	-5.75
1050,6	406	2444.88	6.02	6.44	2615.62	6.53
1050,10	335	2886.59	8.62	8.67	2905.65	.66

Table- 7.5 Corrosion data in 5% NaCl solution

ALLOY DESIG- NATION	HEAT TREAT- MENT	AREA SQ. CM	WEIGHT LOSS (GMS)	CORROSION RATE	
				MDD	IPY
C1	AS-CAST	4.175	0.00704	21.33010	0.00393
C1	900 2	4.808	0.00772	22.93796	0.00422
C1	900 10	5.3182	0.00691	18.56159	0.00342
C1	950 2	6.6802	0.00859	18.36985	0.00338
C1	950 10	6.2128	0.00757	17.40646	0.00320
C1	1000 2	7.3192	0.00808	15.77065	0.00290
C1	1000 10	7.2630	0.00720	14.16179	0.00260
C1	1050 2	5.2562	0.00505	13.72528	0.00252
C1	1050 10	5.7156	0.00486	12.14720	0.00223
C2	AS-CAST	4.3630	0.00631	20.65791	0.00380
C2	900 2	5.5268	0.00828	21.40220	0.00394
C2	900 10	4.1830	0.00529	18.06632	0.00332
C2	950 2	6.5408	0.00807	17.62562	0.00324
C2	950 10	5.5028	0.00630	16.35531	0.00301
C2	1000 2	5.2312	0.00558	15.23824	0.00280
C2	1000 10	4.4400	0.00455	14.63964	0.00269
C2	1050 2	5.0950	0.00488	13.68288	0.00252
C2	1050 10	5.2026	0.00462	12.68596	0.00233
C3	AS-CAST	4.5620	0.00599	18.75743	0.00345
C3	900 2	6.5106	0.00881	19.33111	0.00356
C3	900 10	5.1710	0.00666	18.39931	0.00339
C3	950 2	6.6268	0.00792	17.07352	0.00314
C3	950 10	5.9704	0.00702	16.79715	0.00309
C3	1000 2	5.8210	0.00610	14.97042	0.00275
C3	1000 10	5.6318	0.00570	14.45871	0.00266
C3	1050 2	5.9702	0.00510	12.20346	0.00224
C3	1050 10	5.6122	0.00485	12.34555	0.00227

Table-7.6 Comparative corrosion rates (in mdd) of the experimental alloys in the heat treated condition

ALLOY	900°C		950°C		1000°C		1050°C	
	2 h	10 h	2 h	10 h	2 h	10 h	2 h	10 h
C 1	22.93	18.56	18.36	17.40	15.77	14.16	13.72	12.14
C 2	21.40	18.06	17.62	16.35	15.23	14.63	13.68	12.68
C 3	19.33	18.39	17.07	16.79	14.97	14.45	12.20	12.34

Table 7.7 Summary table of predicted vs experimentally determined CR values based on NOP (based on Equations 7.14-7.16)

H/T	CR _{exp}	I factor	II factor	CR _{pre}	%error
Alloy C1					
900,2	22.938	36.561	0.572	20.924	9.63
900,10	18.562	29.961	0.649	19.452	4.58
950,2	18.370	34.979	0.572	20.019	8.24
950,10	17.406	22.622	0.689	15.594	11.62
1000,2	15.771	29.276	0.554	16.233	2.85
1000,10	14.162	20.143	0.745	14.999	5.58
Alloy C2					
900,2	21.402	12.173	1.678	20.428	4.77
900,10	18.066	10.598	1.639	17.369	4.01
950,2	17.626	11.390	1.678	19.113	7.78
950,10	16.355	9.852	1.549	15.258	7.19
1000,2	15.238	10.459	1.549	16.199	5.93
1000,10	14.640	9.657	1.549	14.957	2.12
Alloy C3					
900,2	19.331	11.098	1.755	19.478	0.75
900,10	18.399	10.095	1.755	17.718	3.85
950,2	17.074	10.701	1.522	16.292	4.79
950,10	16.797	9.806	1.674	16.419	2.30
1000,2	14.970	10.216	1.629	16.640	10.03
1000,10	14.459	8.893	1.629	14.484	0.18

Table 7.8 Summary table of predicted vs experimentally determined CR values based on NOP (unified model) [based on Equation 7.17]

H/T	CR _{exp}	I factor	II factor	CR _{pre}	%error
Alloy C1					
900,2	22.938	19.204	1.099	21.098	8.72
900,10	18.562	17.023	1.076	18.309	1.38
950,2	18.370	18.499	1.099	20.324	9.62
950,10	17.406	14.336	1.065	15.264	14.04
1000,2	15.771	15.937	1.105	17.602	10.41
1000,10	14.162	13.939	1.051	14.649	3.32
Alloy C2					
900,2	21.402	18.344	1.110	20.358	5.13
900,10	18.066	15.334	1.105	16.936	6.67
950,2	17.626	17.242	1.110	19.135	7.89
950,10	16.355	14.262	1.092	15.575	5.01
1000,2	15.238	15.768	1.092	17.219	11.50
1000,10	14.640	13.939	1.092	15.221	3.82
Alloy C3					
900,2	19.331	16.150	1.115	18.000	7.39
900,10	18.399	15.305	1.115	17.058	7.86
950,2	17.074	15.801	1.084	17.135	0.36
950,10	16.797	14.277	1.105	15.769	6.52
1000,2	14.970	14.934	1.099	16.407	8.75
1000,10	14.459	14.117	1.099	15.509	6.77

Table 7.9 Summary table of predicted vs experimentally determined CR values based on DF (based on Equations 7.18-7.20)

H/T	CR _{exp}	I factor	II factor	CR _{pre}	%error
Alloy C1					
900,2	22.938	17.970	1.164	20.918	9.66
900,10	18.562	15.448	1.260	19.463	4.63
950,2	18.370	17.168	1.164	19.985	8.08
950,10	17.406	11.919	1.304	15.546	11.97
1000,2	15.771	14.124	1.155	16.316	3.34
1000,10	14.162	10.992	1.364	14.990	5.52
Alloy C2					
900,2	21.402	27.024	0.743	20.069	6.64
900,10	18.066	22.008	0.754	16.603	8.81
950,2	17.626	25.121	0.768	19.302	8.68
950,10	16.355	20.572	0.762	15.678	4.32
1000,2	15.238	22.684	0.732	16.594	8.17
1000,10	14.640	20.630	0.732	15.092	2.99
Alloy C3					
900,2	19.331	17.140	1.115	19.112	1.15
900,10	18.399	15.606	1.071	16.707	10.13
950,2	17.074	16.504	1.081	17.846	4.33
950,10	16.797	13.782	1.152	15.882	5.76
1000,2	14.970	14.938	1.107	16.531	9.44
1000,10	14.459	13.513	1.107	14.954	3.31

Table 7.10 Summary table of predicted vs experimentally determined CR values based on DF (with constraints) [based on Equations 7.21-7.23]

H/T	CR _{exp}	I factor	II factor	CR _{pre}	%error
Alloy C1					
900,2	22.938	17.406	1.192	20.754	10.52
900,10	18.562	15.102	1.307	19.734	5.94
950,2	18.370	16.685	1.192	19.894	7.66
950,10	17.406	11.534	1.360	15.687	10.96
1000,2	15.771	13.837	1.182	16.353	3.56
1000,10	14.162	10.304	1.432	14.757	4.03
Alloy C2					
900,2	21.402	18.334	1.078	19.755	8.34
900,10	18.066	15.918	1.073	17.085	5.74
950,2	17.626	17.557	1.068	18.757	6.03
950,10	16.355	14.498	1.071	15.521	5.38
1000,2	15.238	16.343	1.082	17.677	13.80
1000,10	14.640	13.277	1.082	14.361	1.94
Alloy C3					
900,2	19.331	16.760	1.133	18.992	1.78
900,10	18.399	15.526	1.081	16.790	9.58
950,2	17.074	16.271	1.094	17.798	4.07
950,10	16.797	13.570	1.177	15.970	5.18
1000,2	14.970	14.912	1.123	16.752	10.63
1000,10	14.459	13.112	1.123	14.730	1.84

Table 7.11 Summary table of predicted vs experimentally determined CR values based on DF (unified model) [based on Equation 7.24]

H/T	CR _{exp}	I factor	II factor	CR _{pre}	%error
Alloy C1					
900,2	22.938	19.886	1.053	20.933	9.58
900,10	18.562	17.626	1.081	19.057	2.60
950,2	18.370	19.167	1.053	20.176	8.95
950,10	17.406	14.494	1.094	15.855	9.78
1000,2	15.771	16.444	1.050	17.266	8.66
1000,10	14.162	13.697	1.110	15.211	6.90
Alloy C2					
900,2	21.402	19.007	1.075	20.433	4.74
900,10	18.066	15.757	1.071	16.874	7.06
950,2	17.626	17.858	1.066	19.039	7.43
950,10	16.355	14.386	1.068	15.369	6.42
1000,2	15.238	16.255	1.079	17.538	13.11
1000,10	14.640	13.670	1.079	14.749	0.74
Alloy C3					
900,2	19.331	16.681	1.078	17.978	7.52
900,10	18.399	15.723	1.048	16.478	11.66
950,2	17.074	16.292	1.055	17.192	0.69
950,10	16.797	14.407	1.102	15.884	5.75
1000,2	14.970	15.279	1.072	16.382	8.61
1000,10	14.459	14.152	1.072	15.174	4.71

Table 7.12 Experimentally determined and predicted compressive strength values (based on Equations 7.25-7.27)

H/T	CR	CSexp	CSpre	CSexp-CSpre
ALLOY C1				
900,2	21.33000	2334.28000	2434.38200	-100.10160
1000,2	15.77000	2549.59000	2293.01200	256.57840
1000,10	14.16000	2189.75000	2252.07500	-62.32544
1050,2	13.72000	2313.33000	2240.88800	72.44214
1050,10	12.14000	2034.12000	2200.71400	-166.59440
ALLOY C2				
900,2	21.40000	2535.32000	2436.28600	99.03369
900,10	18.06000	2830.66000	2442.26400	388.39580
950,2	17.62000	2004.80000	2443.05200	-438.25150
1000,2	15.23000	2094.23000	2447.32900	-353.09910
1000,10	14.63000	2553.34000	2448.40300	104.93730
1050,2	13.68000	2357.71000	2450.10300	-92.39331
1050,10	12.68000	2743.27000	2451.89300	291.37720
ALLOY C3				
950,10	17.07000	2464.24000	2333.84300	130.39700
1000,2	14.97000	2022.71000	2510.27600	-487.56620
1000,10	14.45000	2862.31000	2553.96400	308.34570
1050,2	12.20000	2636.47000	2743.00000	-106.52980
1050,10	12.34000	2886.59000	2731.23800	155.35250

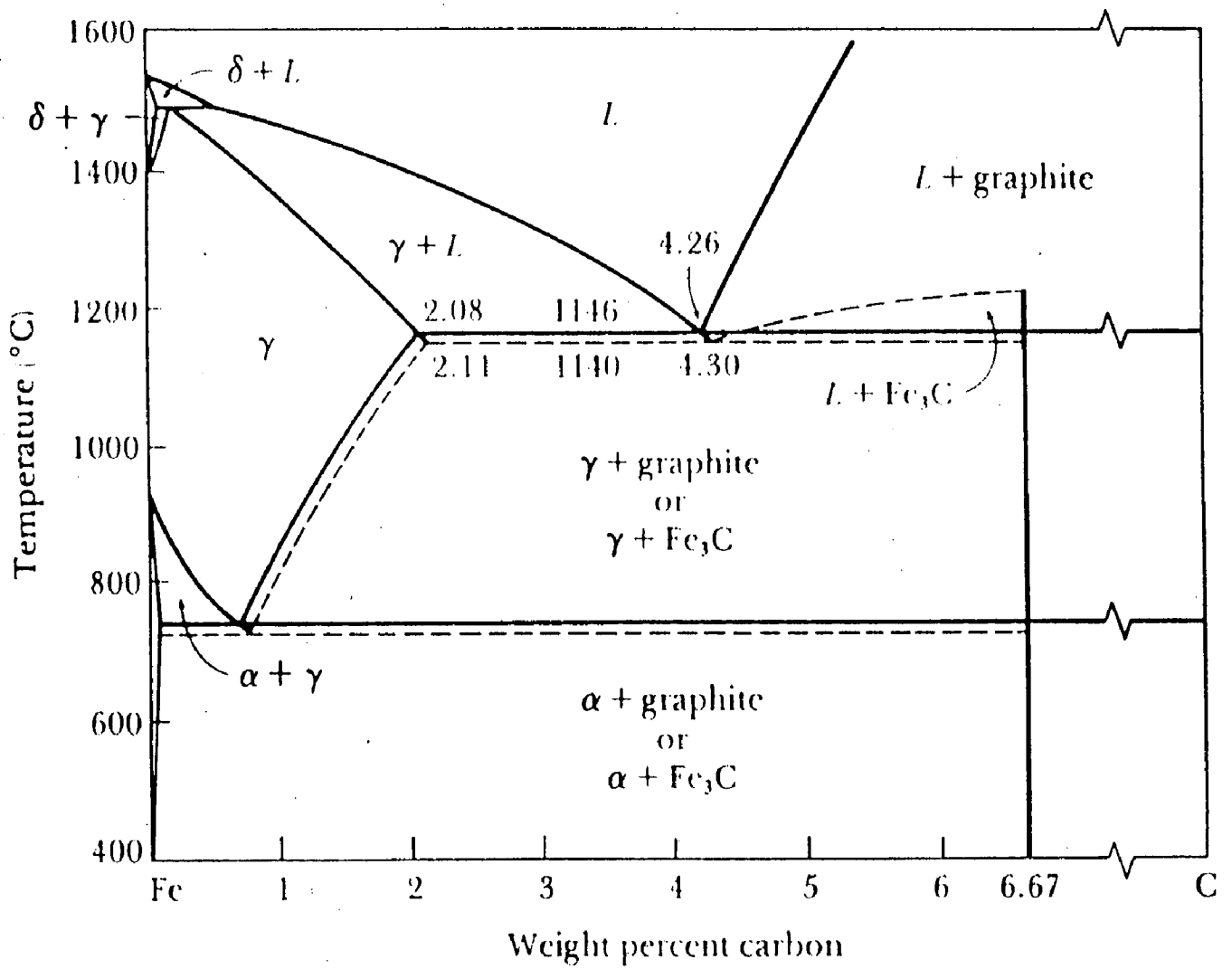


Fig. 1.1 : The iron-carbon phase diagram showing the relationship between the stable iron-graphite equilibria (solid lines) and the metastable iron-cementite reaction (dashed lines)

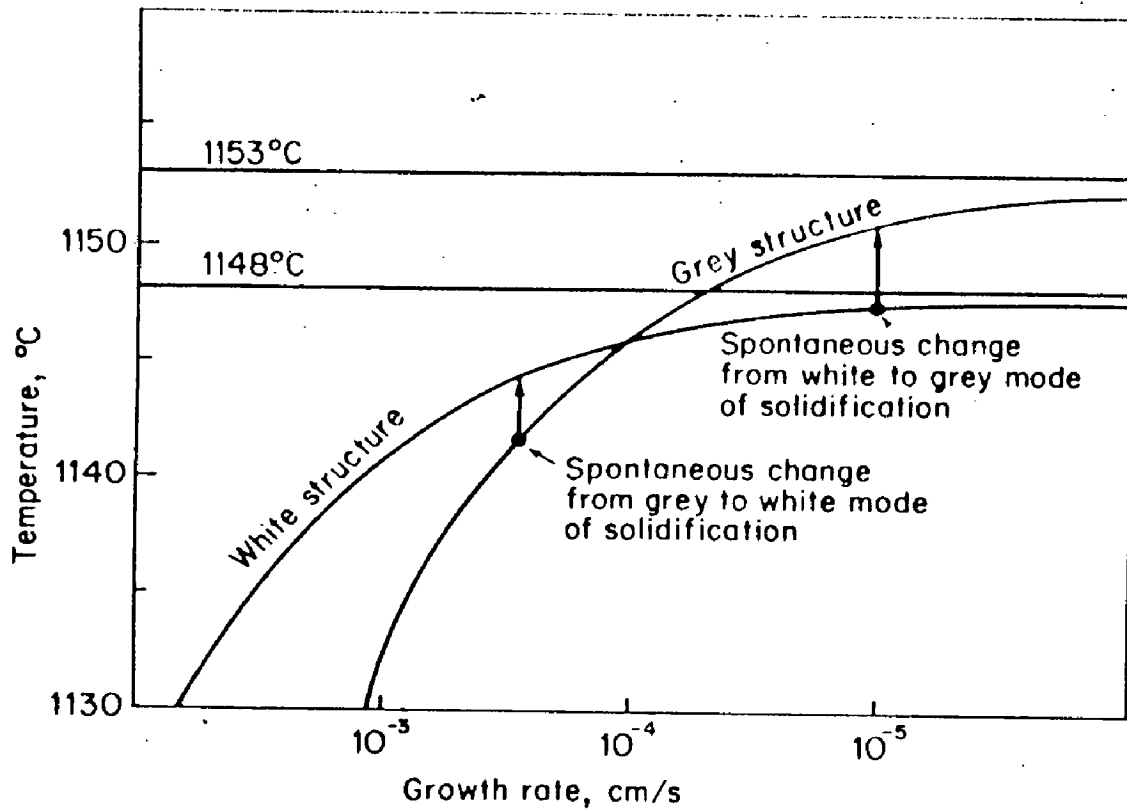


Fig. 1.2 : Variation of growth kinetics of graphite and carbide eutectics

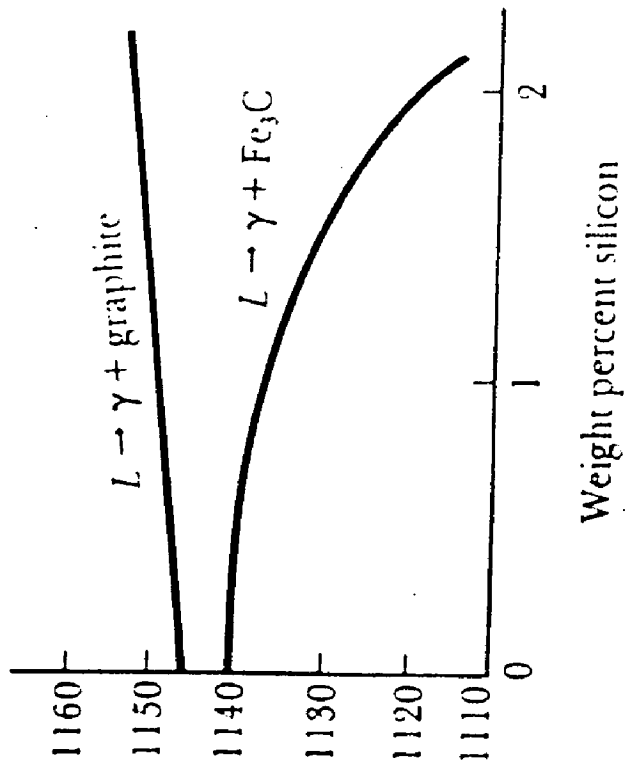
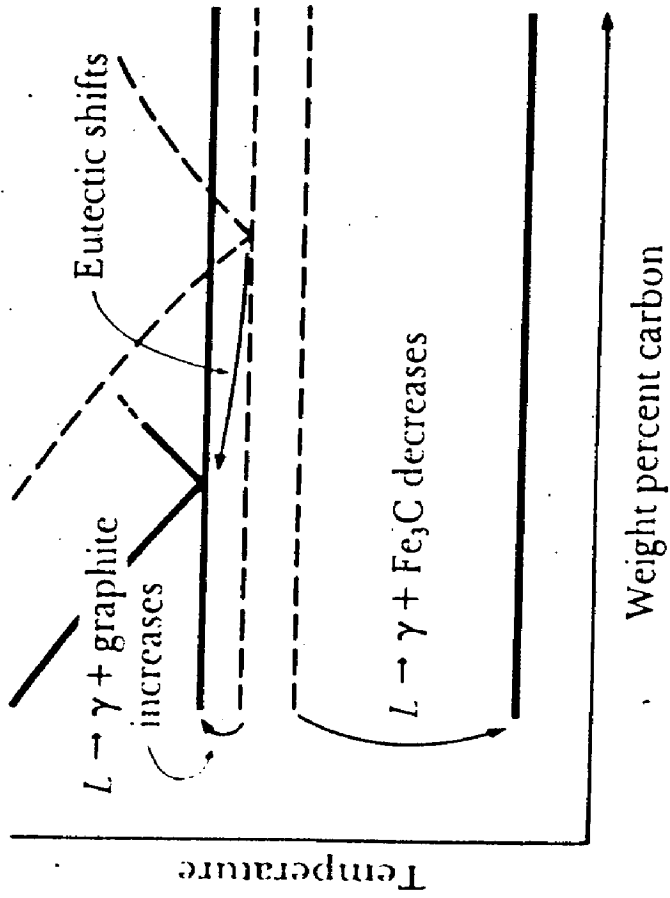


Fig. 1.3: The effect of silicon (a) the eutectic temperature and (b) the phase

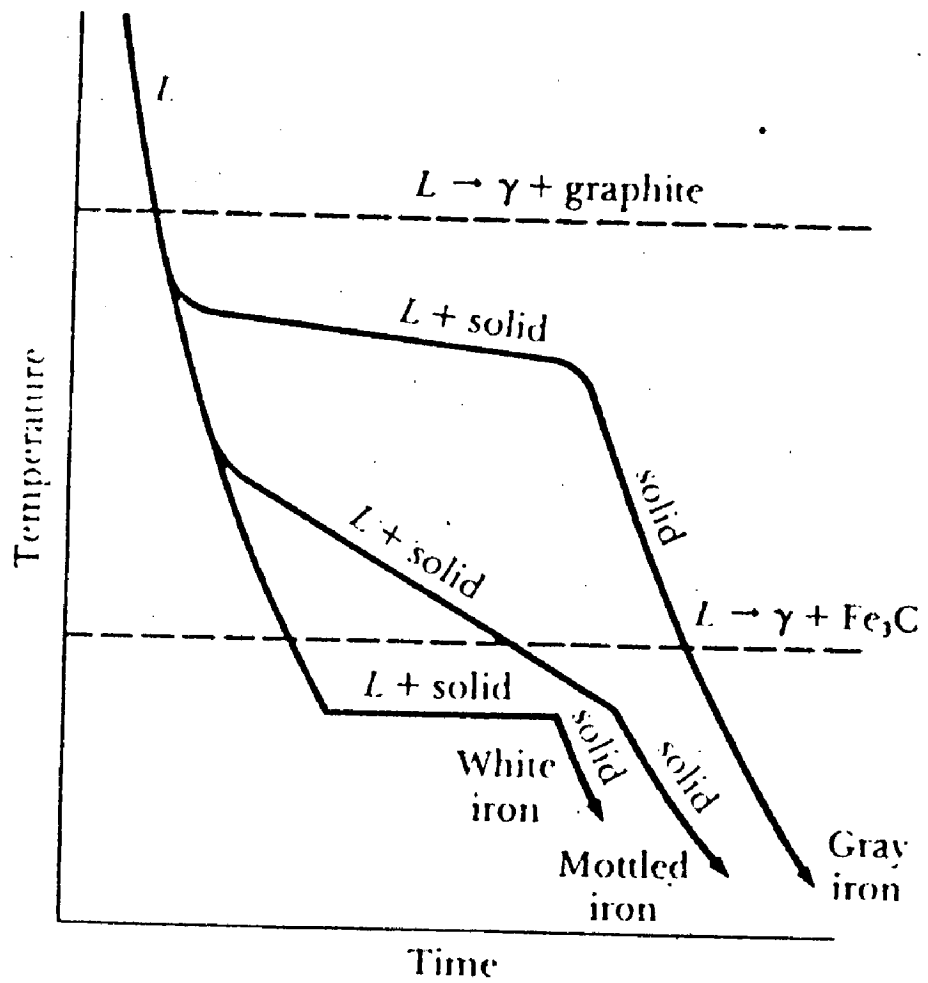


Fig. 1.4 : Cooling curves superimposed on the eutectic temperatures of cast iron

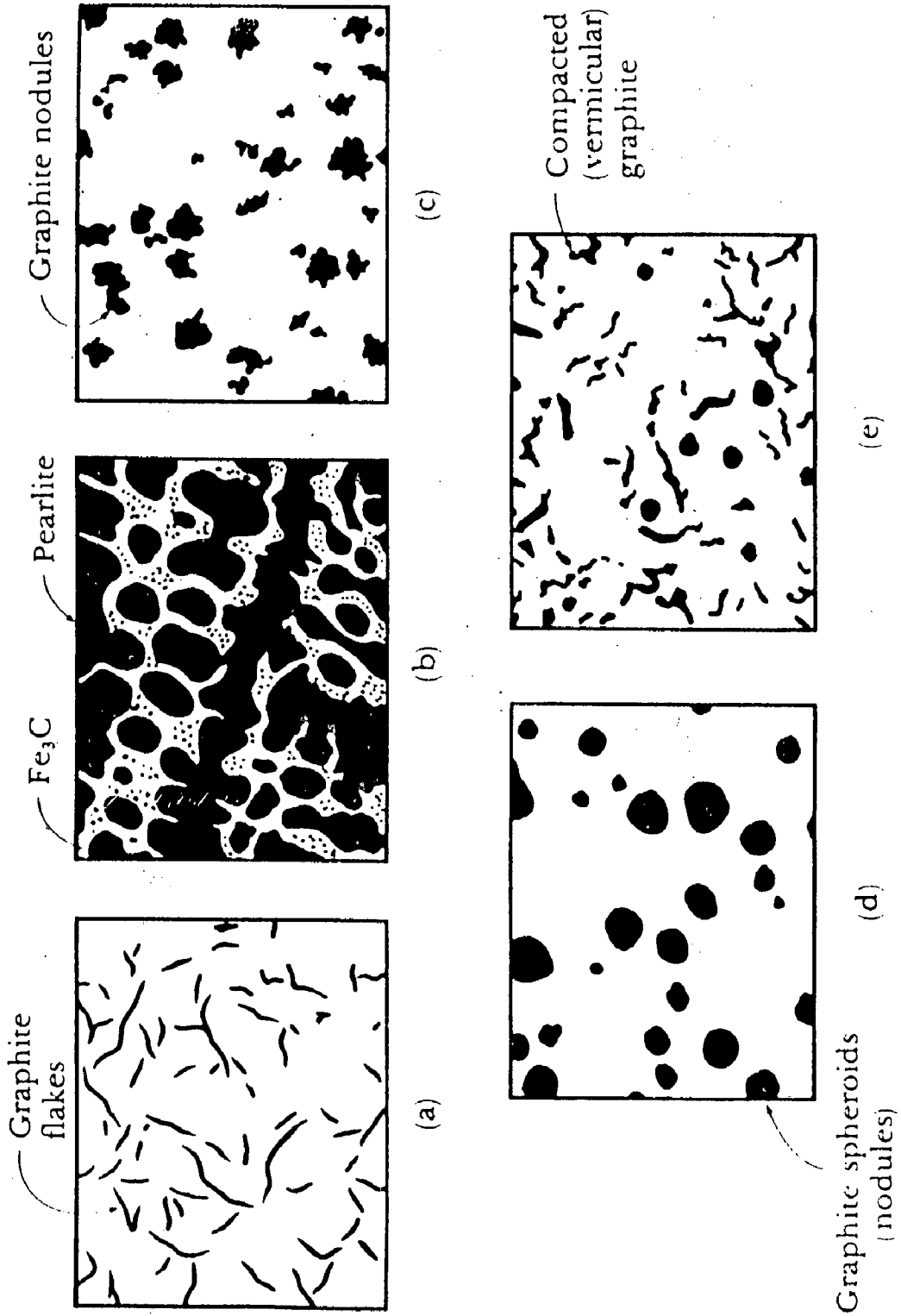


Fig. 1.5 : Schematic drawings of the five types of cast iron : (a) gray iron, (b) white iron, (c) malleable iron, (d) ductile iron, and (e) compacted graphite iron

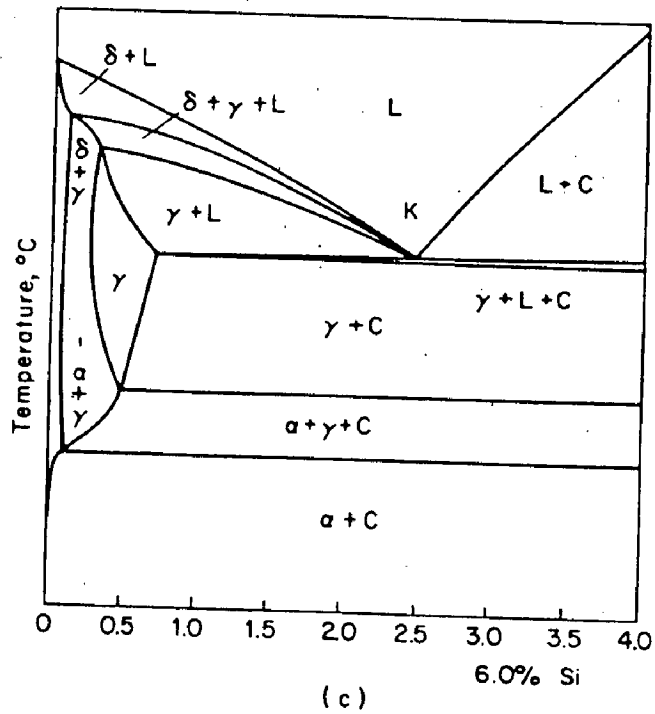
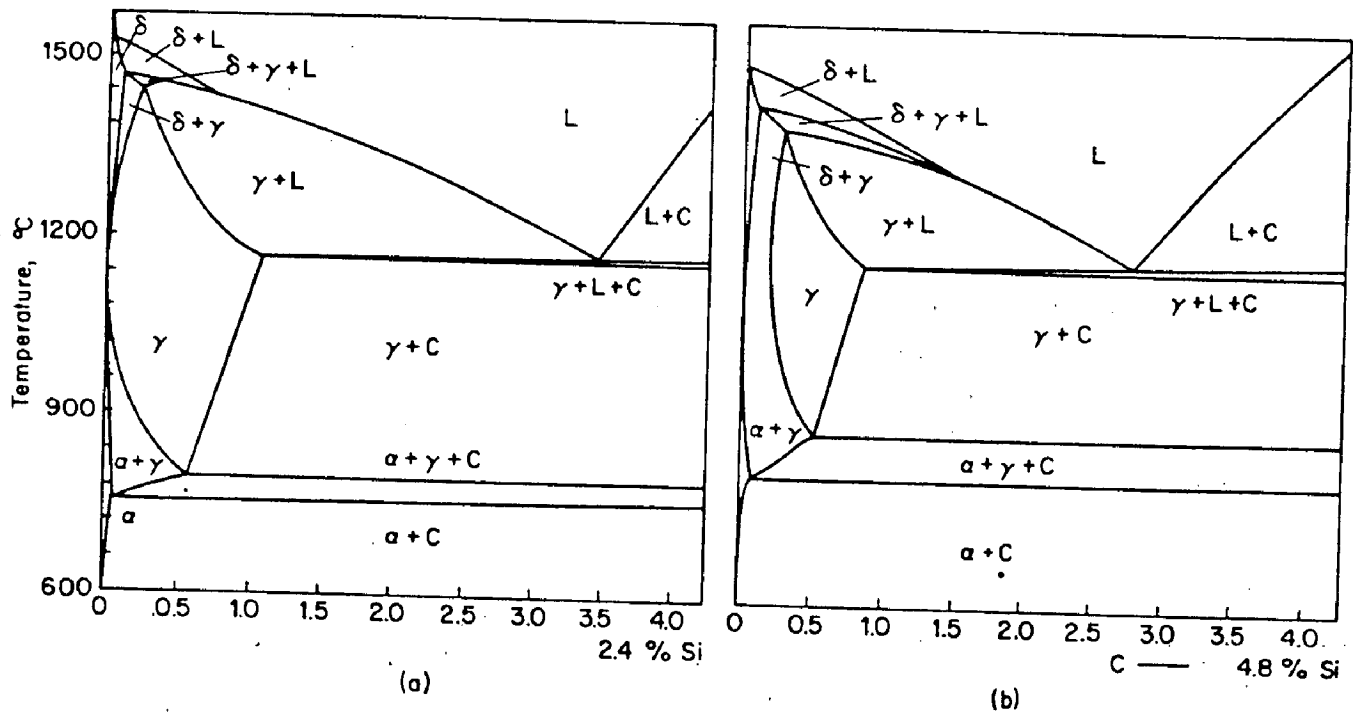


Fig. 2.1 : Vertical Sections in Fe-C-Si system

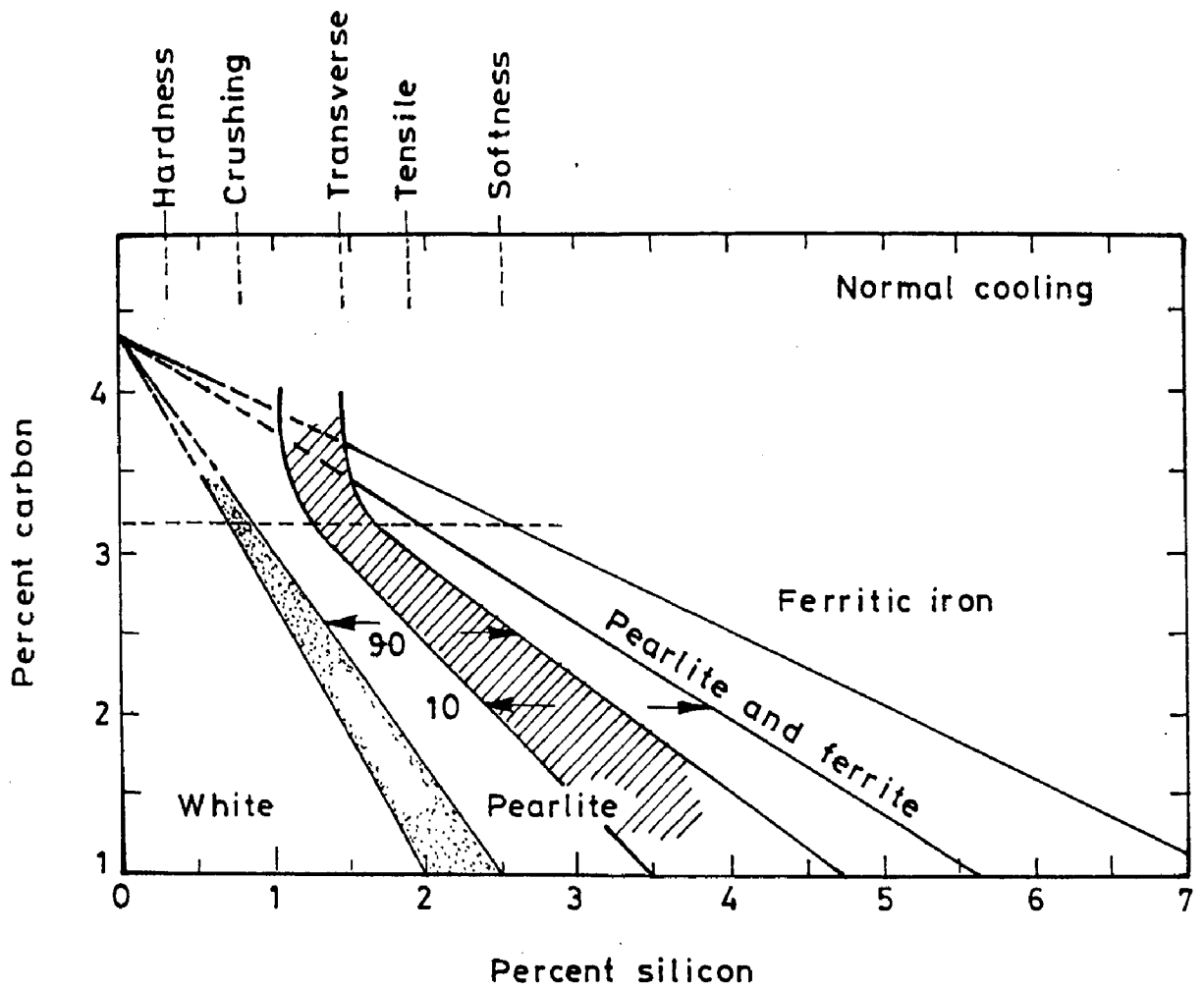


Fig. 2.2 Maurer diagram

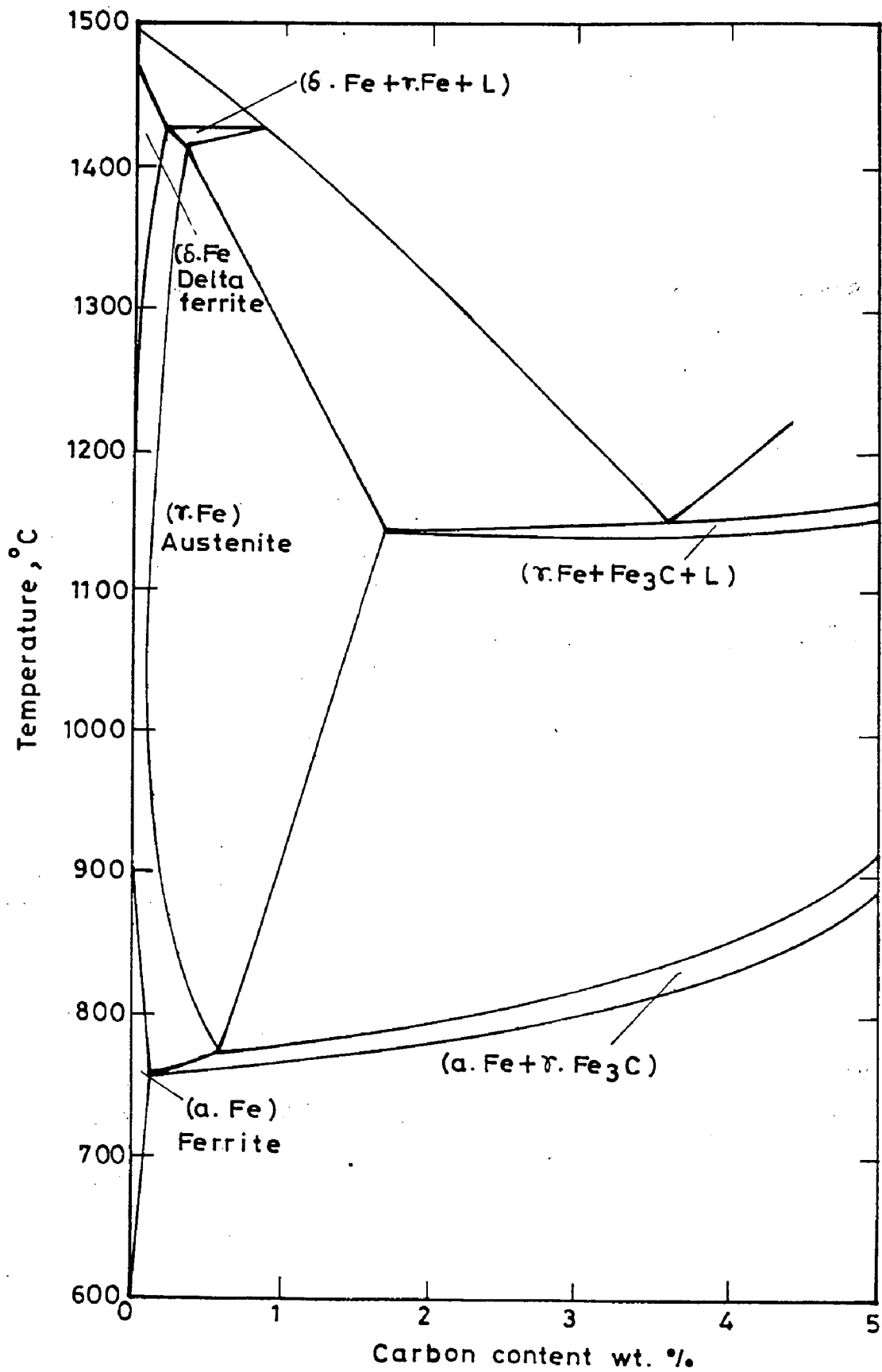


Fig. 2.3 Section through the Iron - iron carbide-silicon ternary equilibrium diagram at 2% silicon

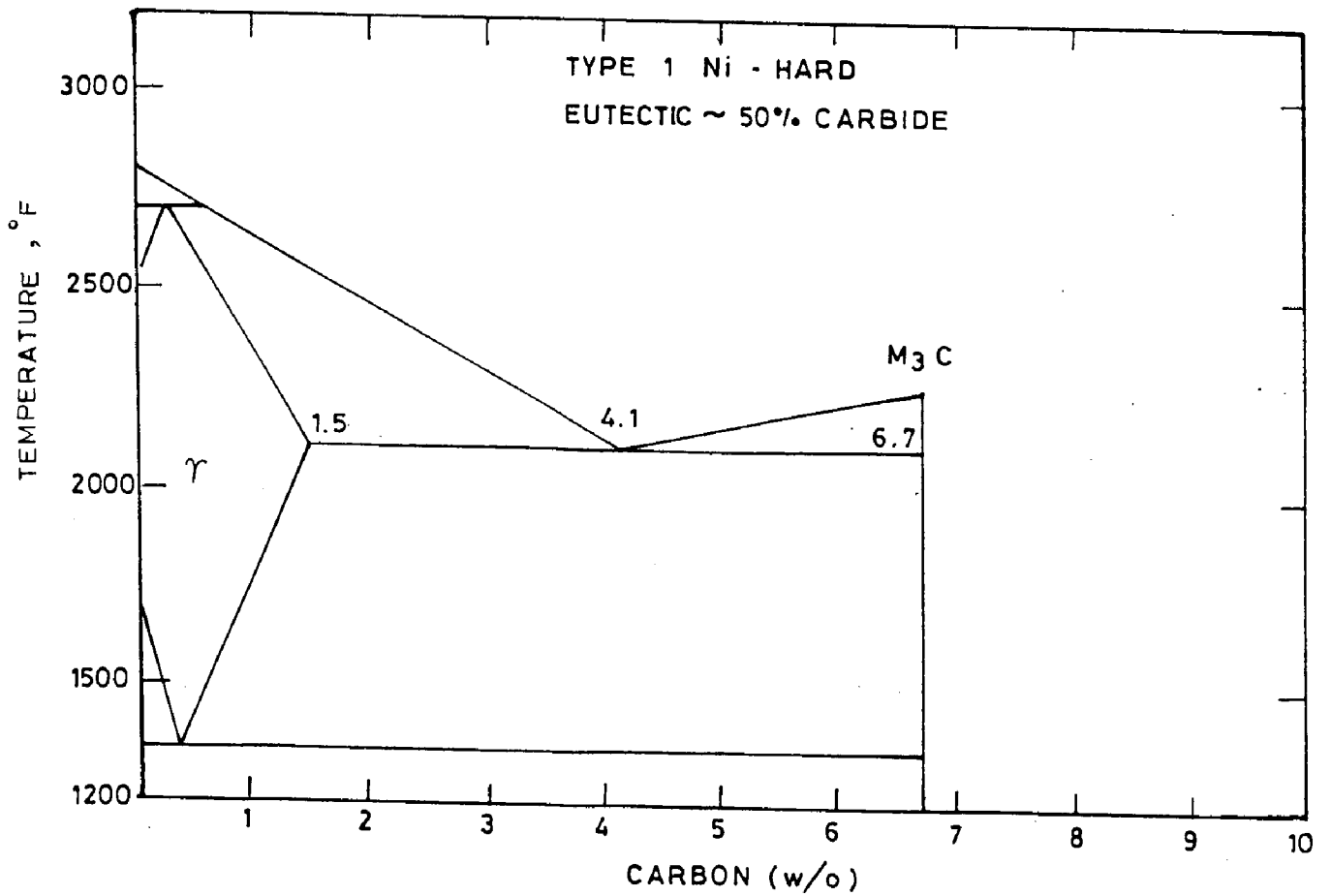
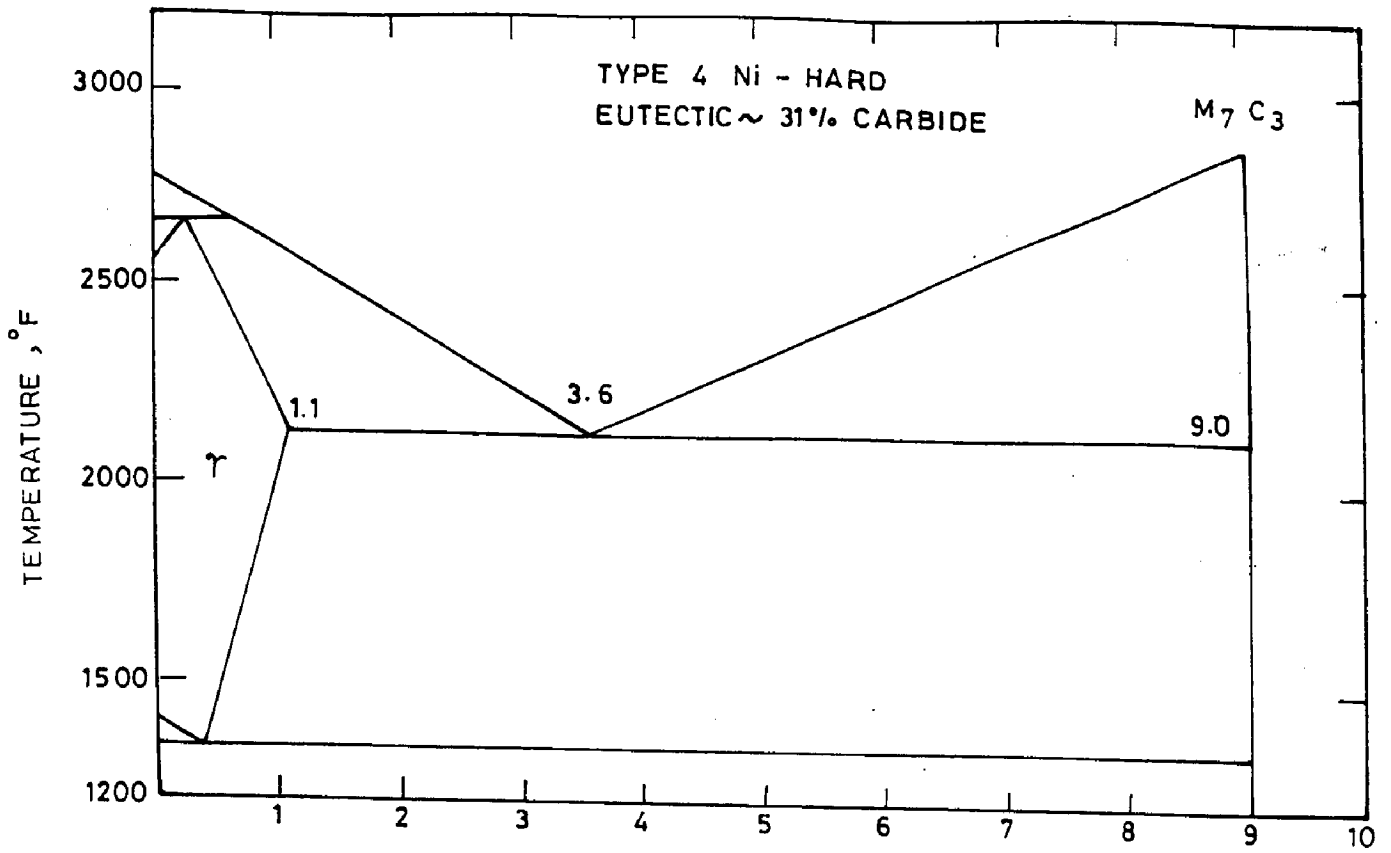


FIG. 2.4 Pseudo-binary phase diagrams of Ni-Hard Irons

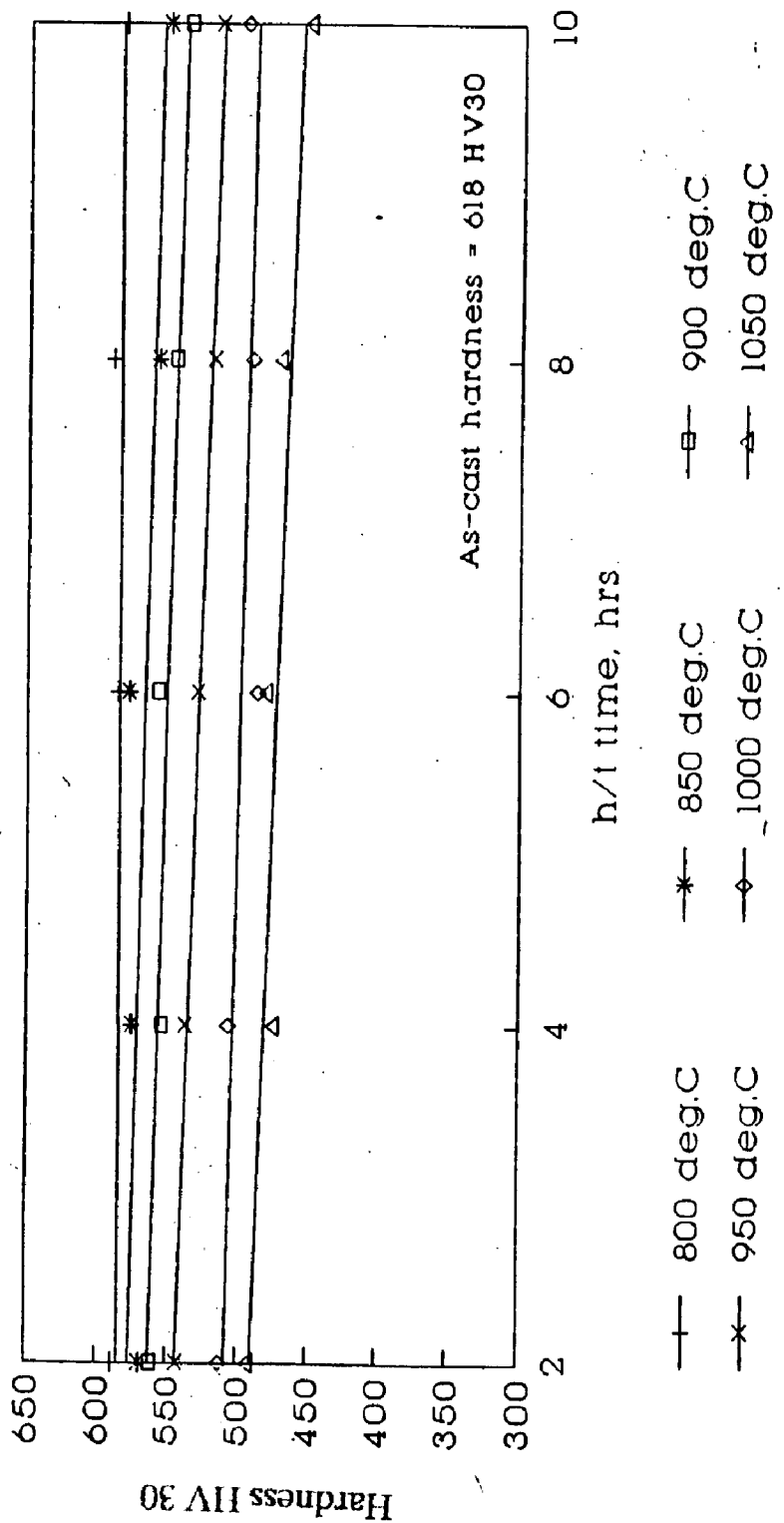


Fig. 5.1 : Effect of h/t time on hardness (base curves)
Alloy C1

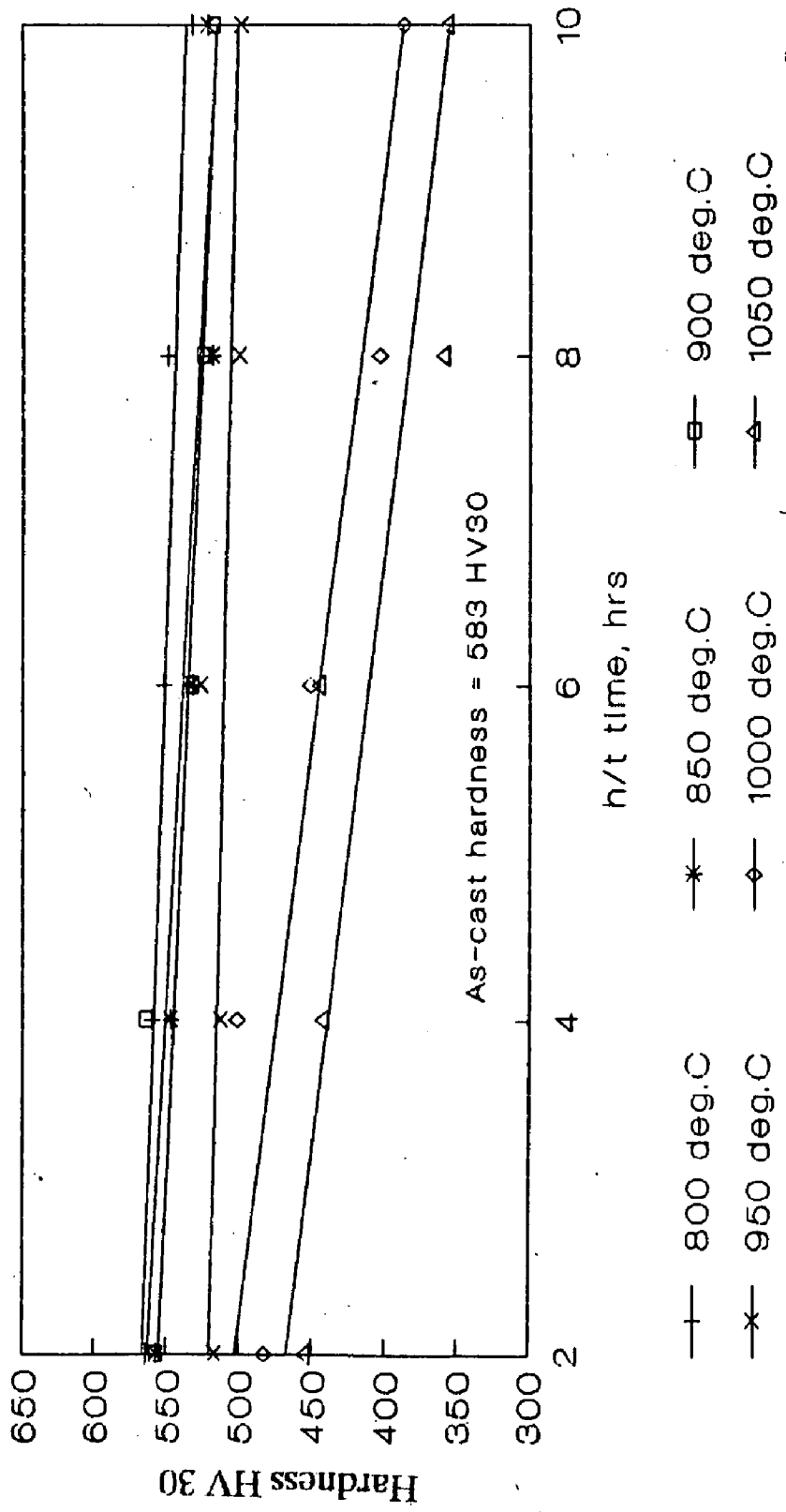


Fig. 5.2 : Effect of h/t time on hardness (base curves)
Alloy C2

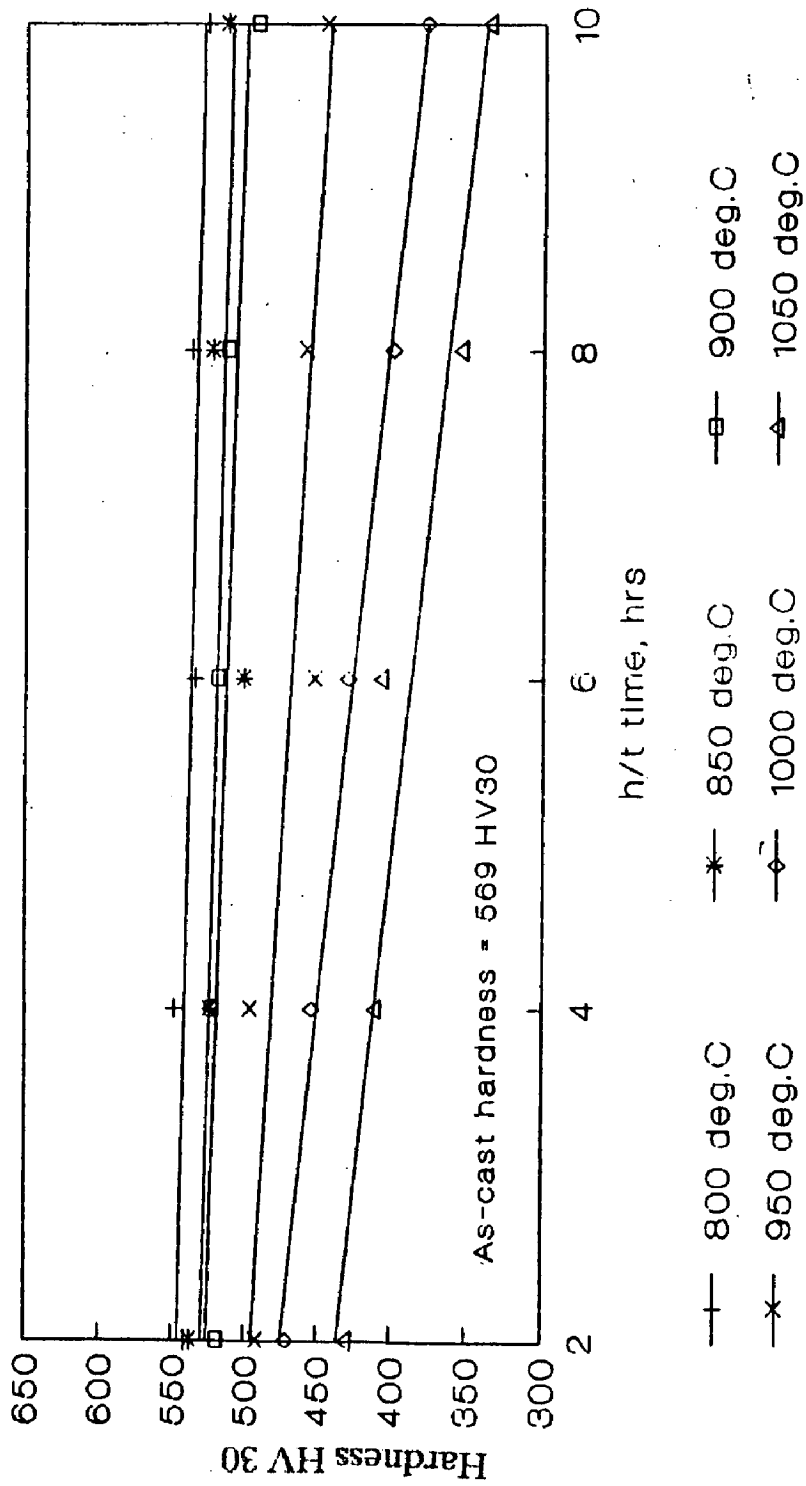


Fig. 5.3 : Effect of h/t time on hardness (base curves)
Alloy C3

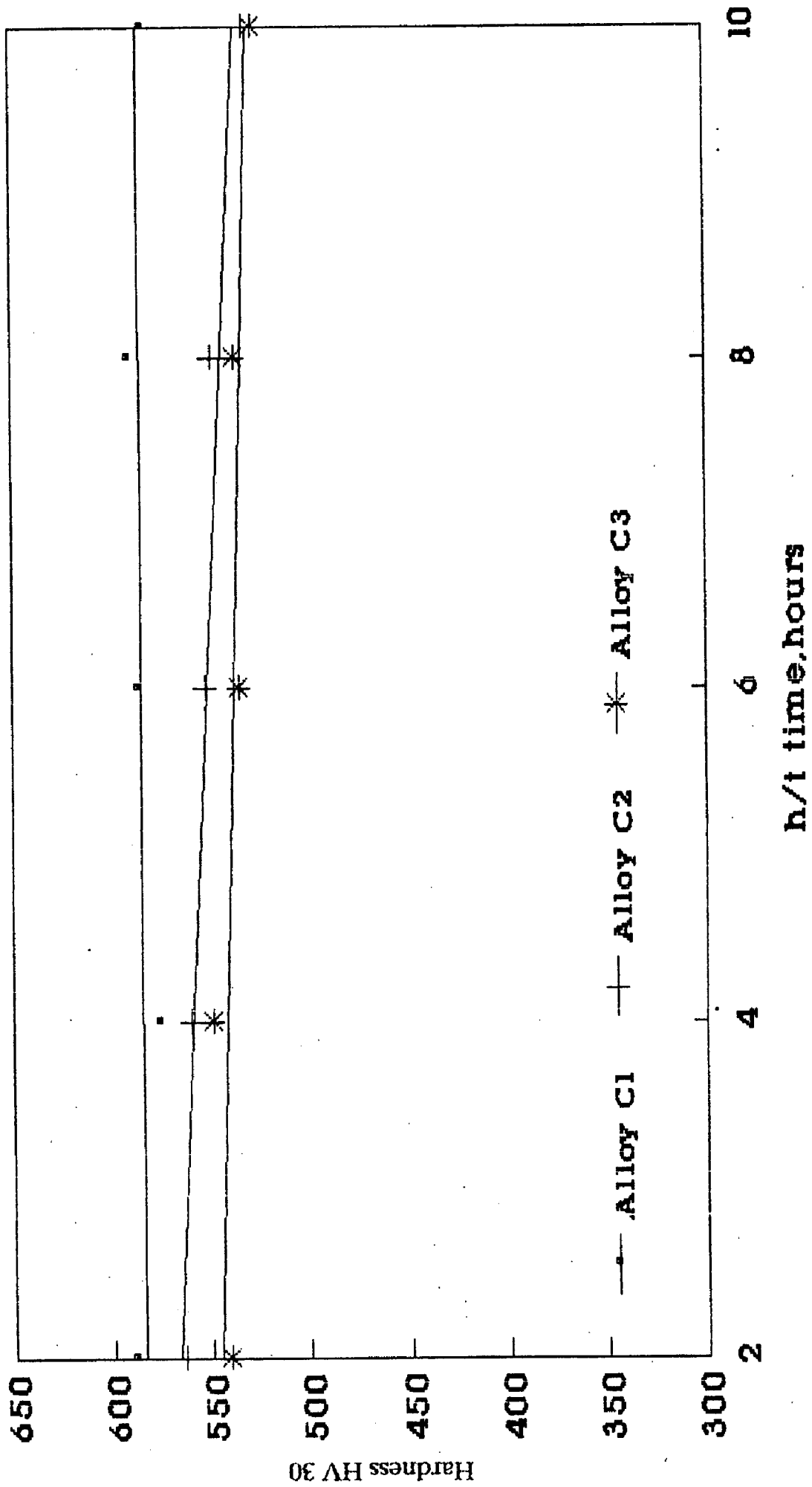


Fig. 5.4 : Effect of h/t time on hardness (comparative plots)
(800 deg C)

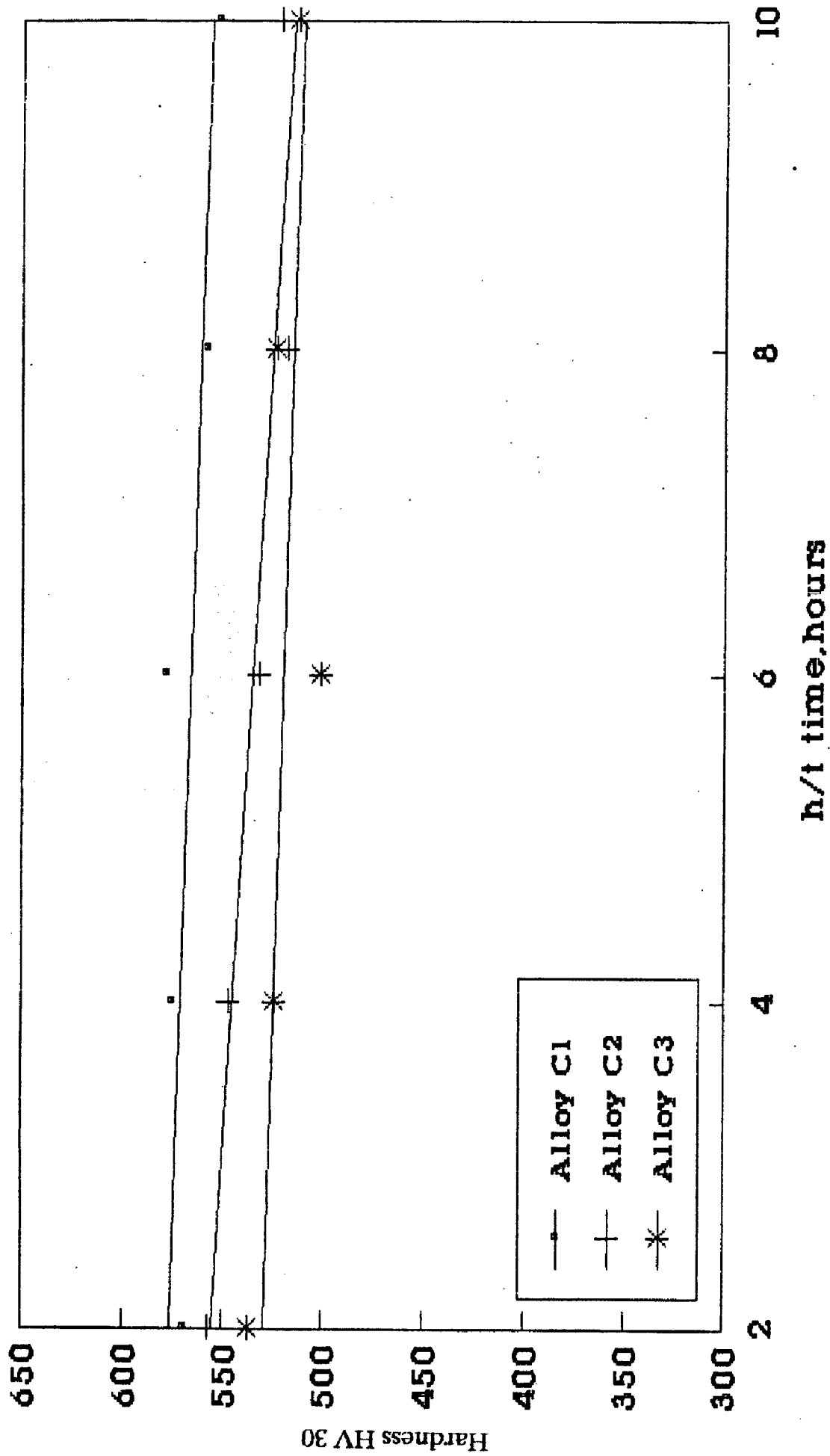


Fig. 5.5 : Effect of h/t time on hardness (comparative plots)
(850 deg C)

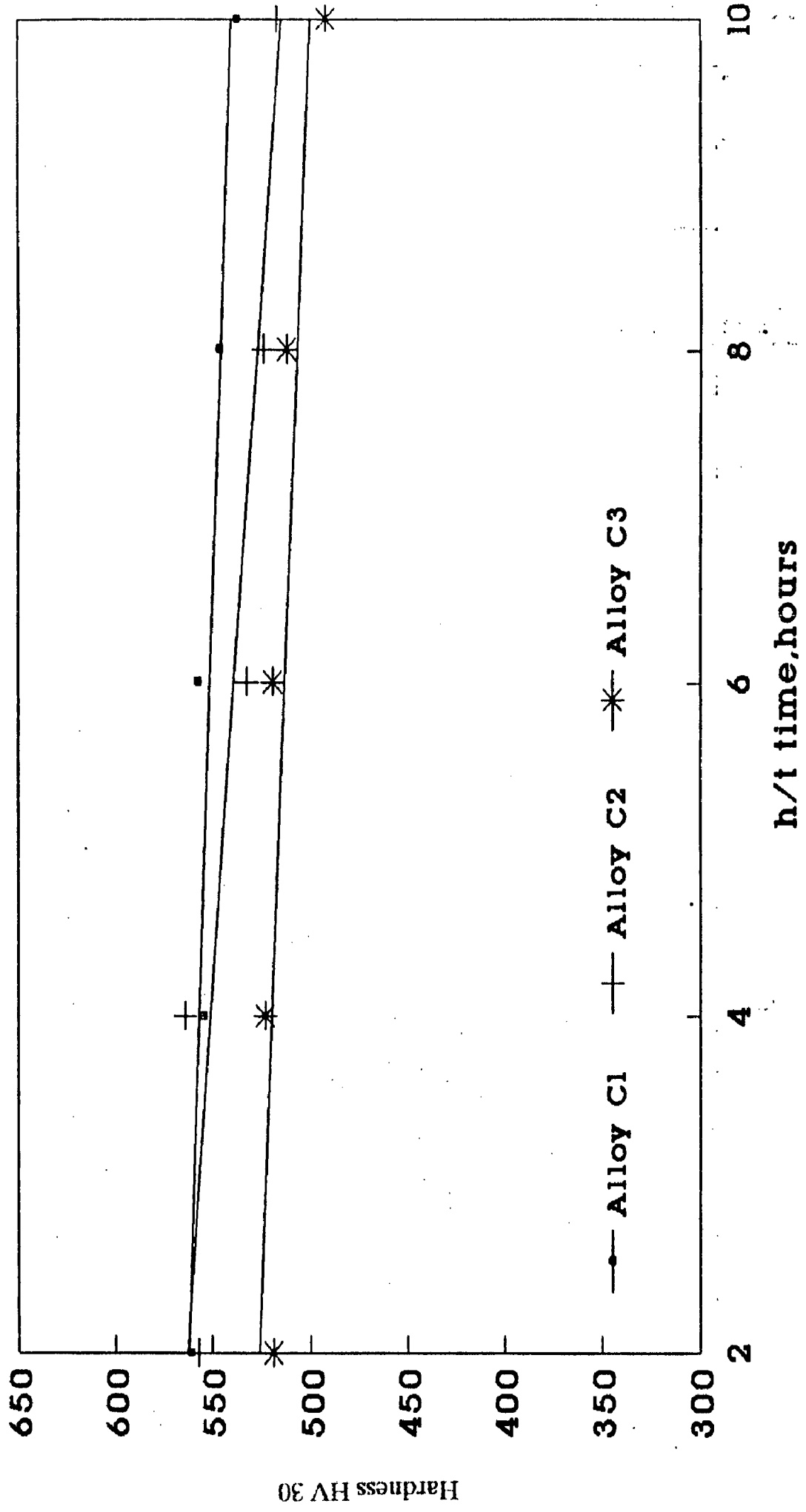


Fig. 5.6 : Effect of h/t time on hardness (comparative plots)
(900 deg C)

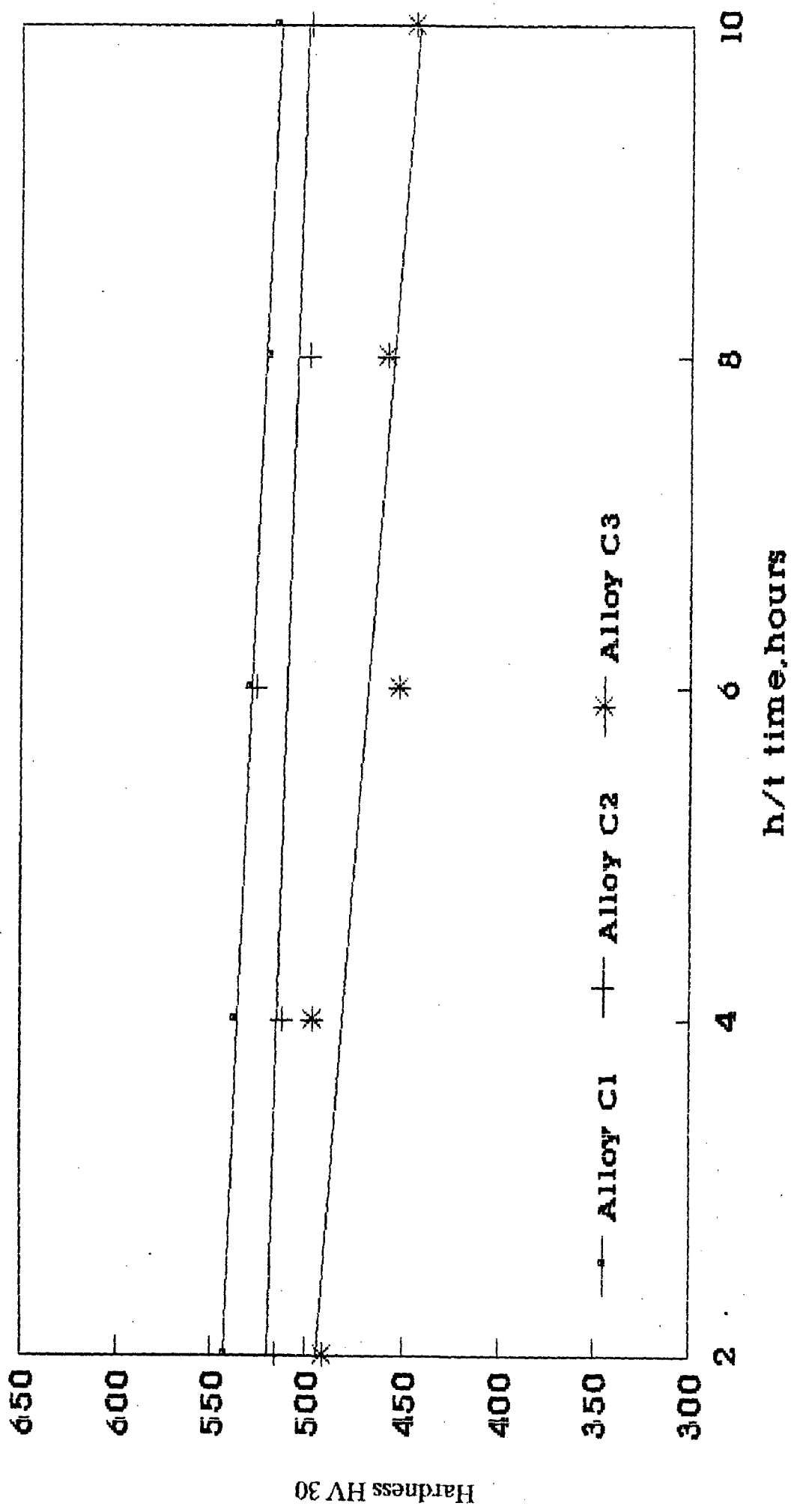


Fig. 5.7 : Effect of h/t time on hardness (comparative plots)
(950 deg C)

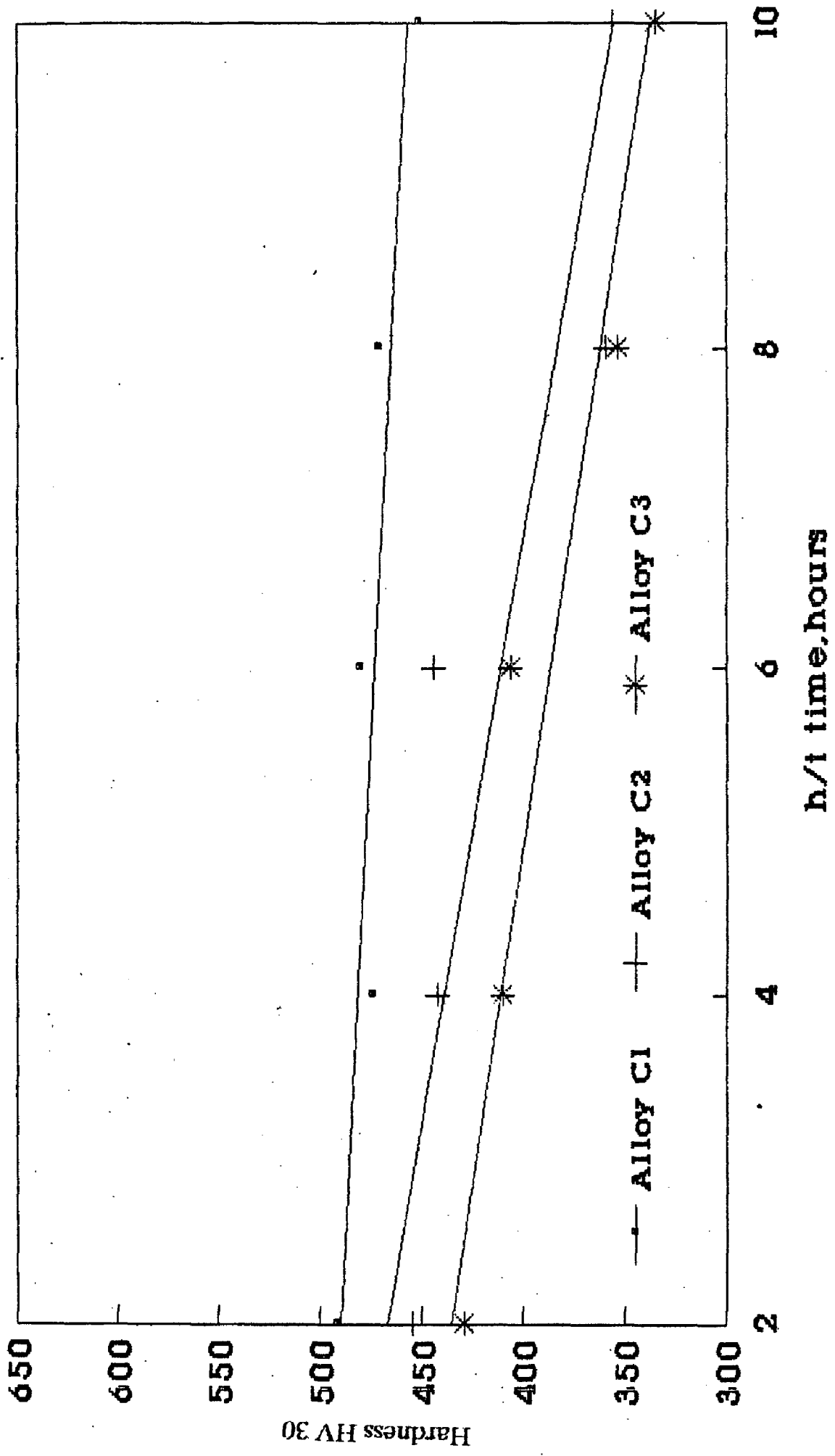


Fig. 5.9 : Effect of h/t time on hardness (comparative plots)
(1050 deg C)

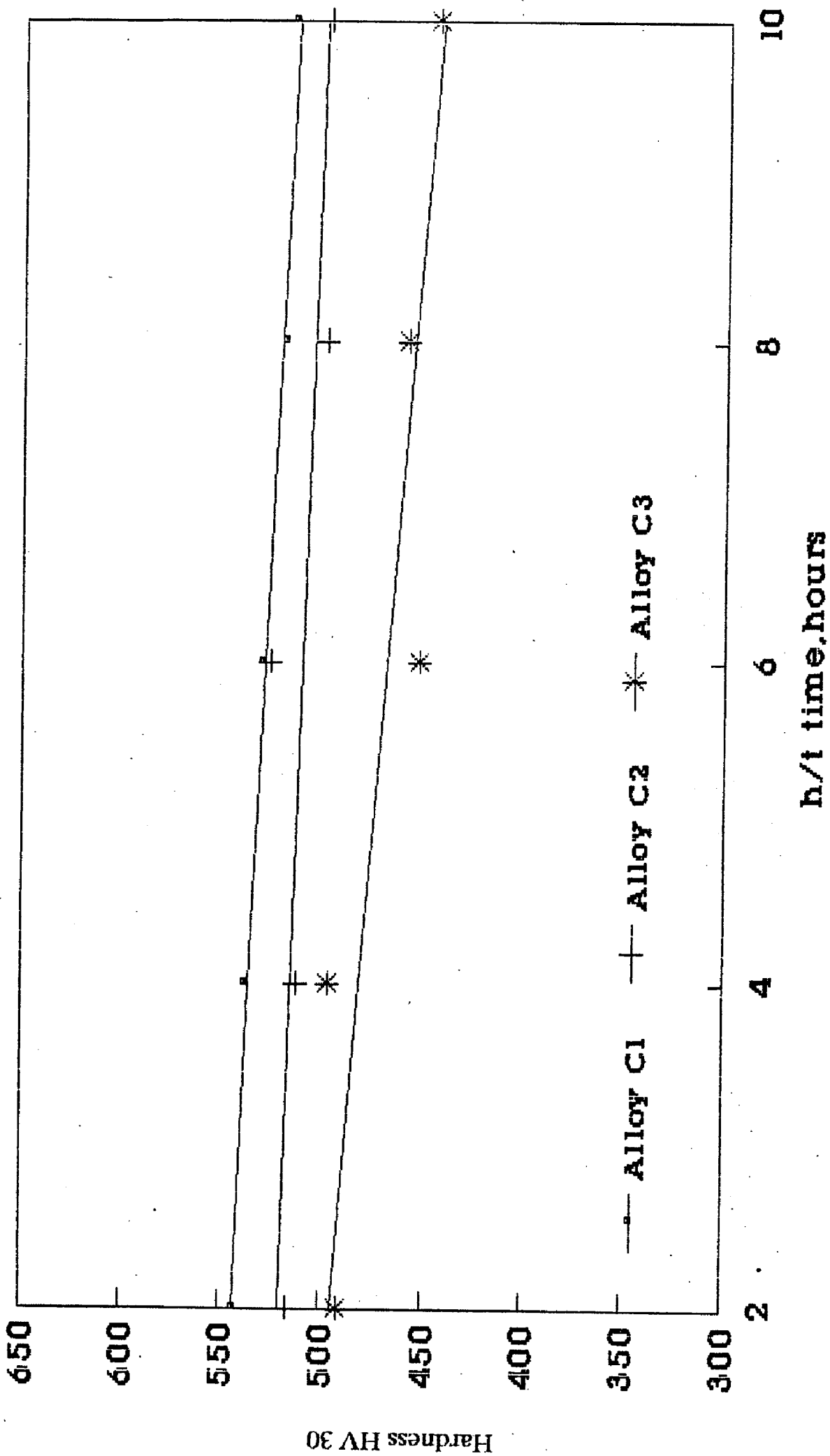


Fig. 5.7 : Effect of h/t time on hardness (comparative plots)
(950 deg C)

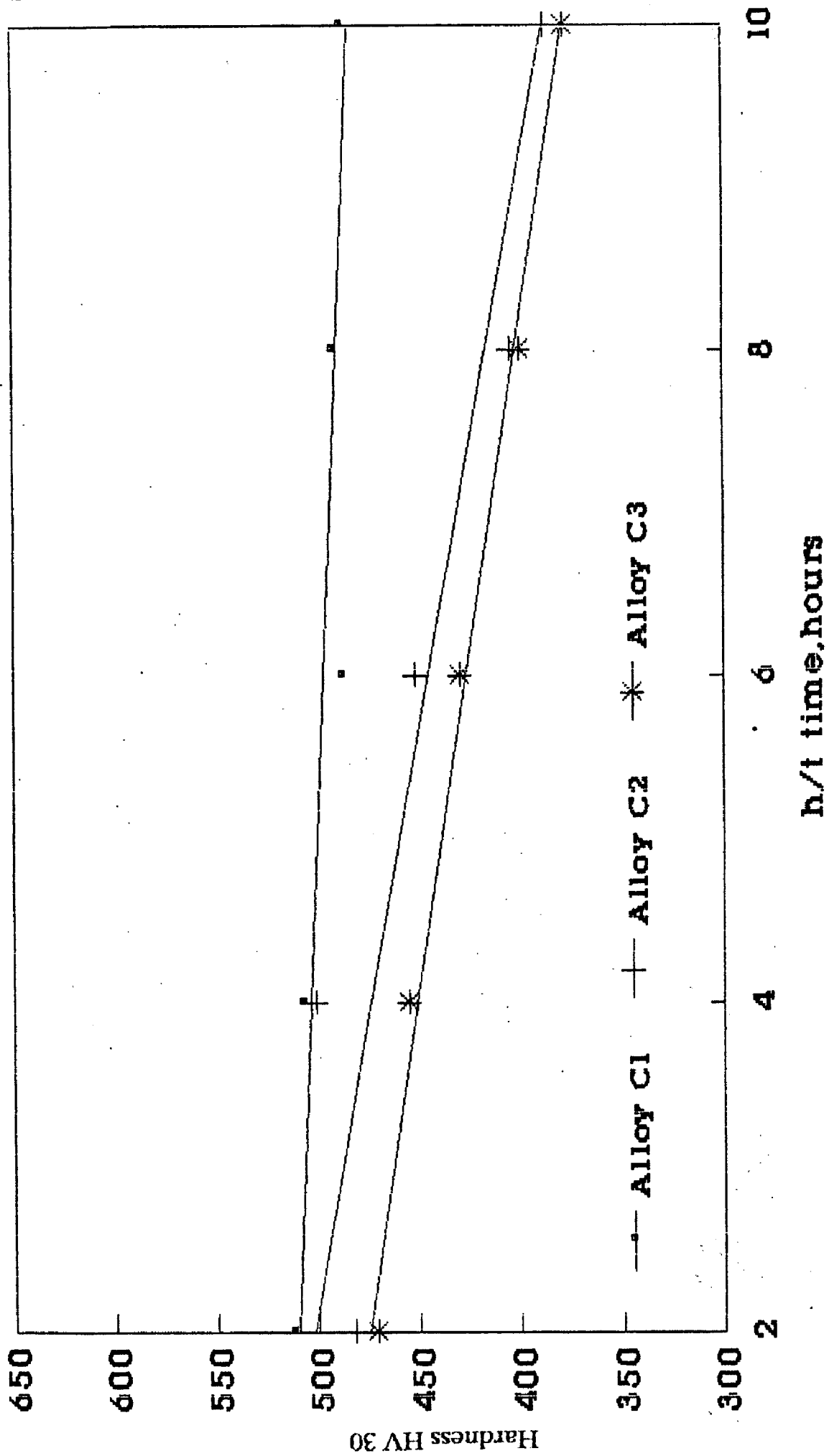


Fig. 5.8 : Effect of h/t time on hardness (comparative plots)
(1000 deg C)

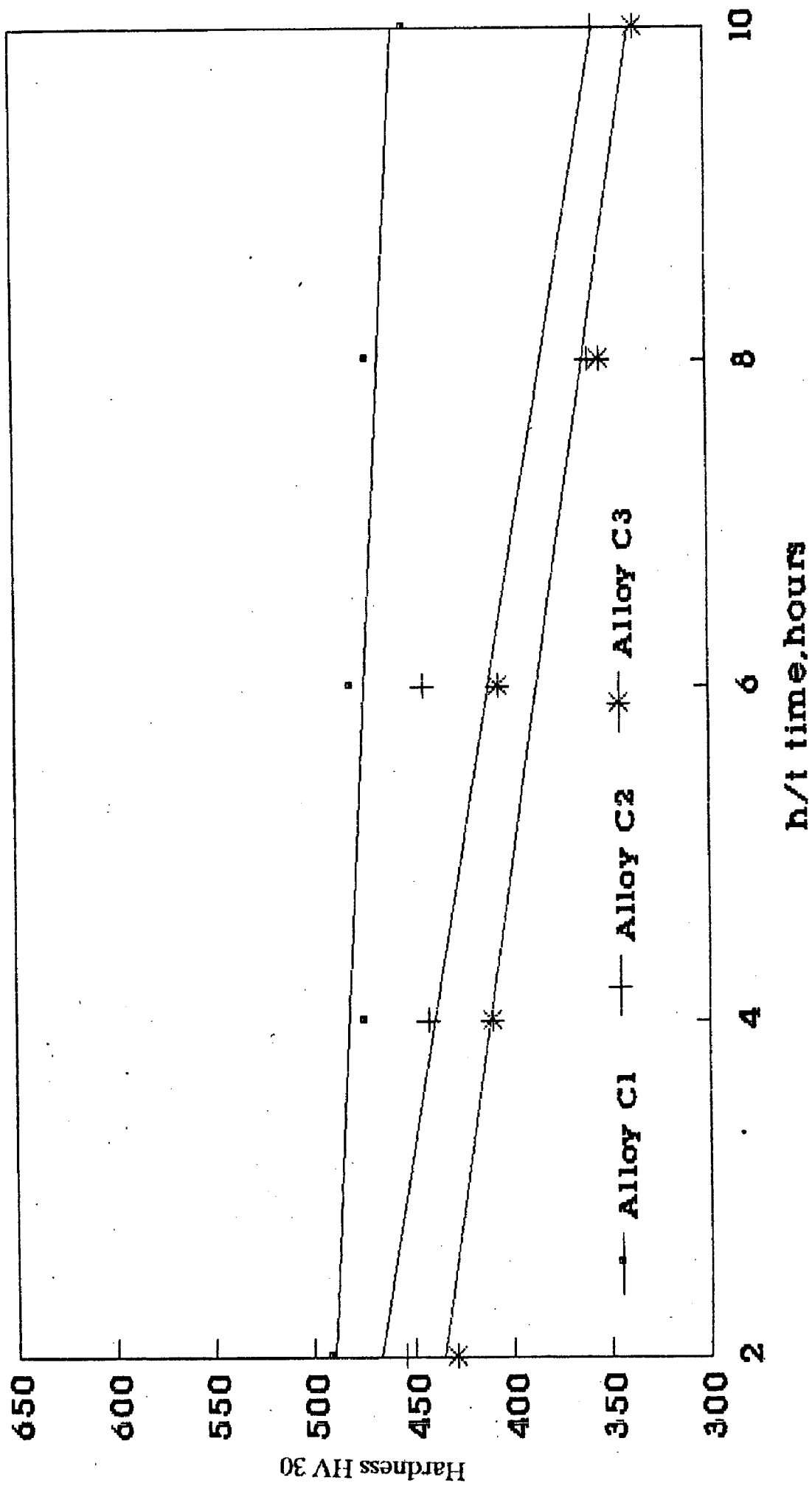
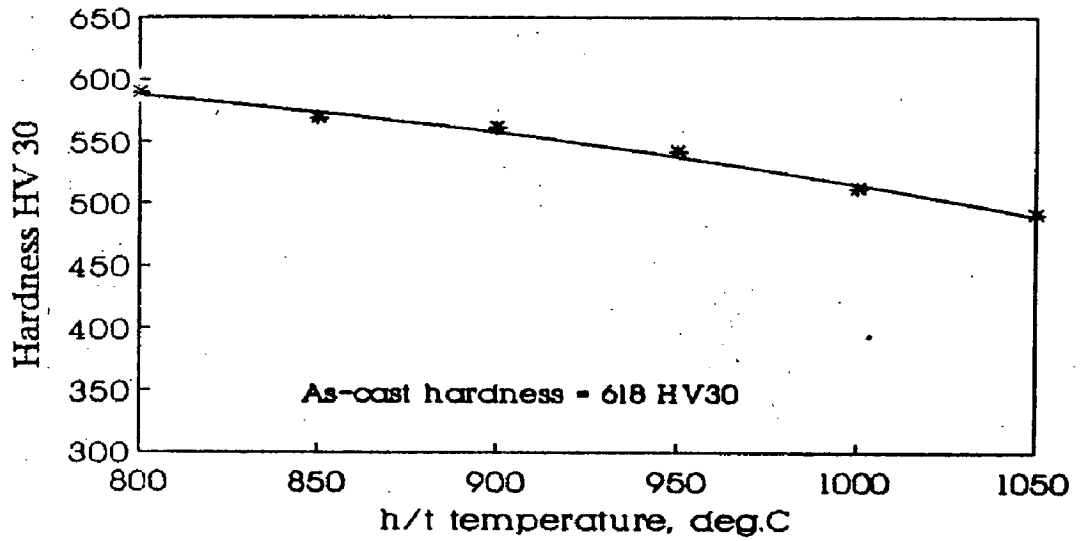
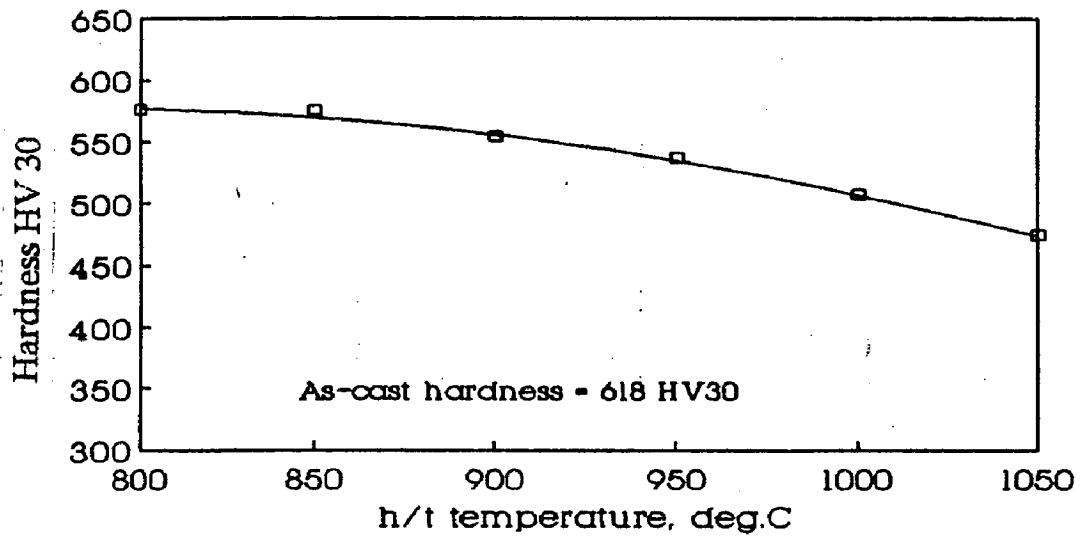


Fig. 5.9 : Effect of h/t time on hardness (comparative plots)
(1050 deg C)

2 hours



4 hours



6 hours

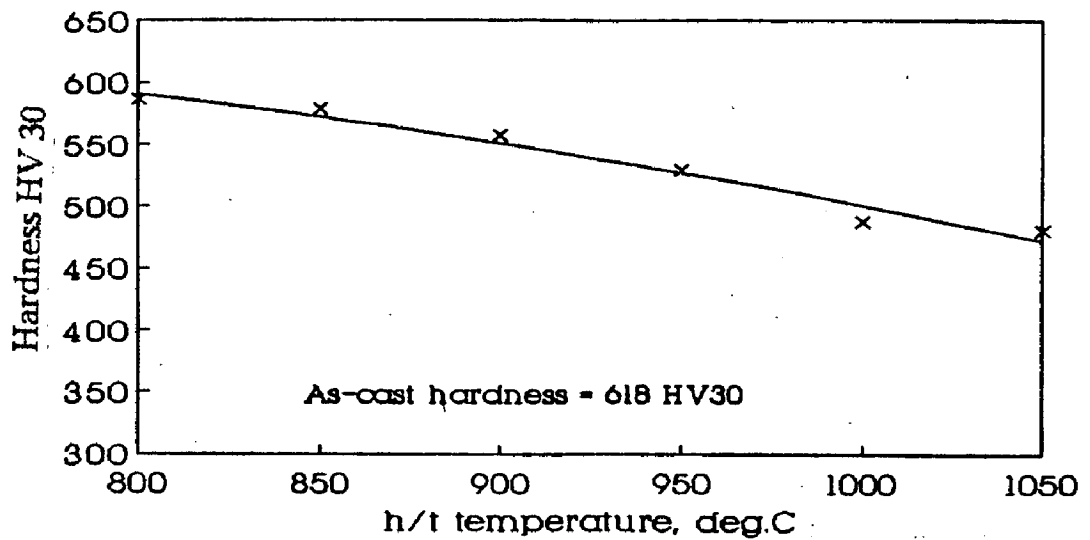


Fig. 5.10 : Effect of h/t temperature on hardness as influenced by h/t time (Alloy C1)

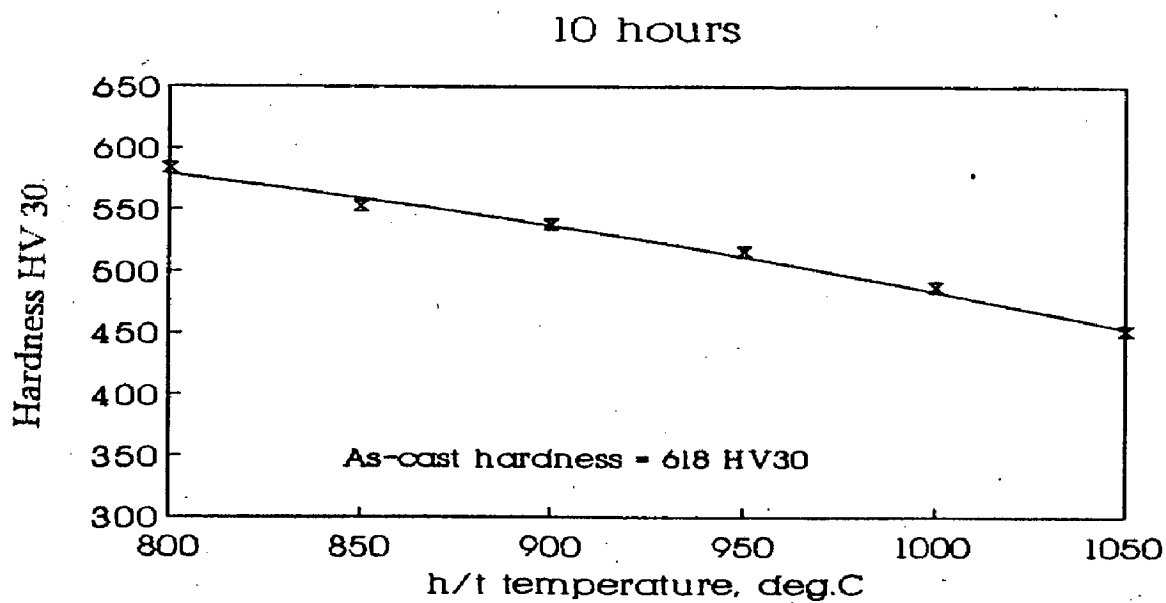
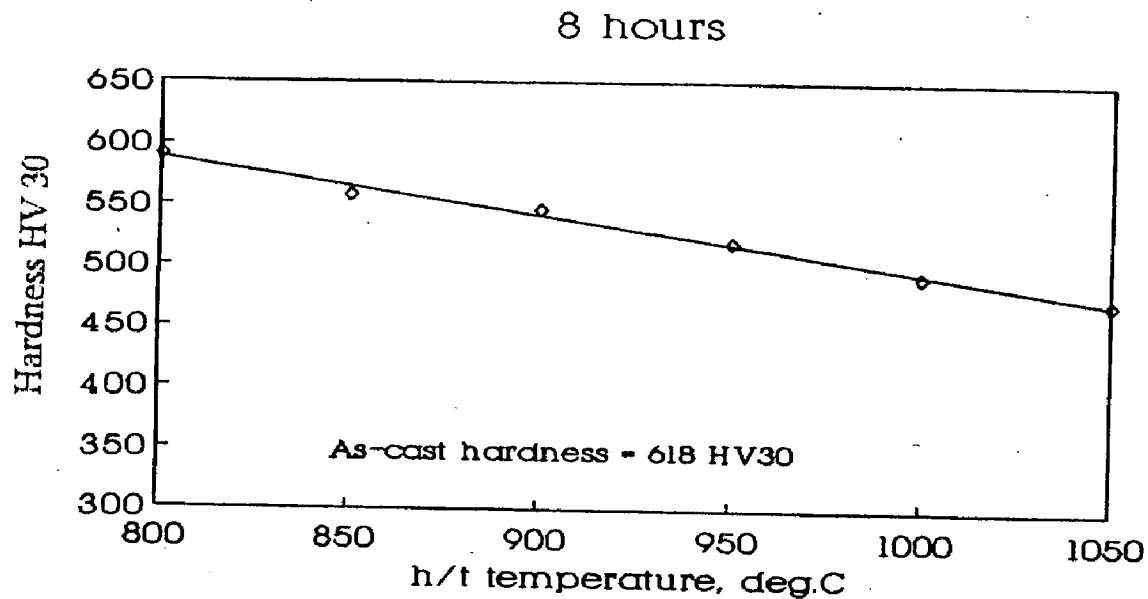
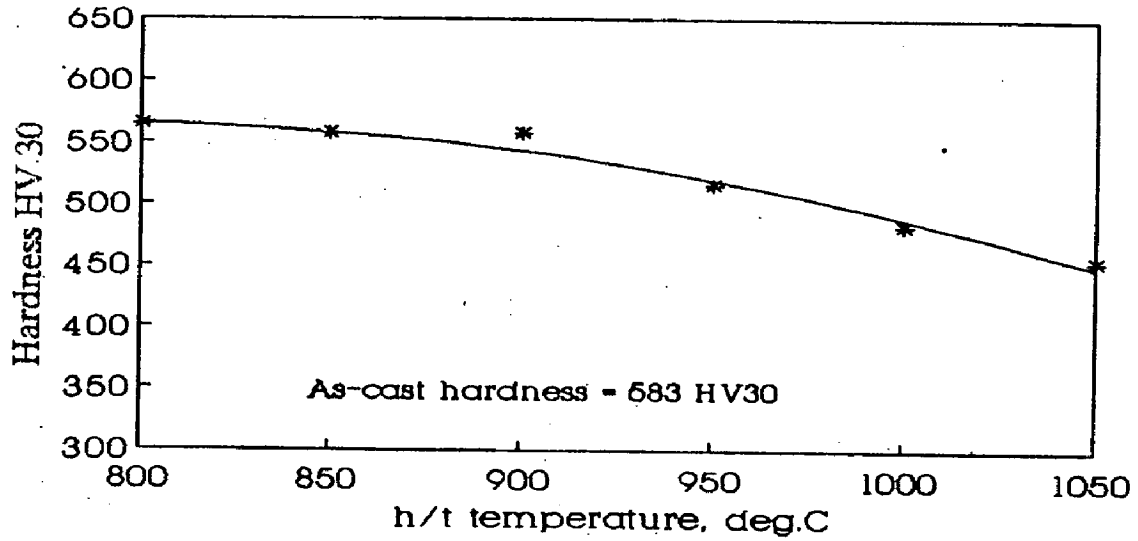
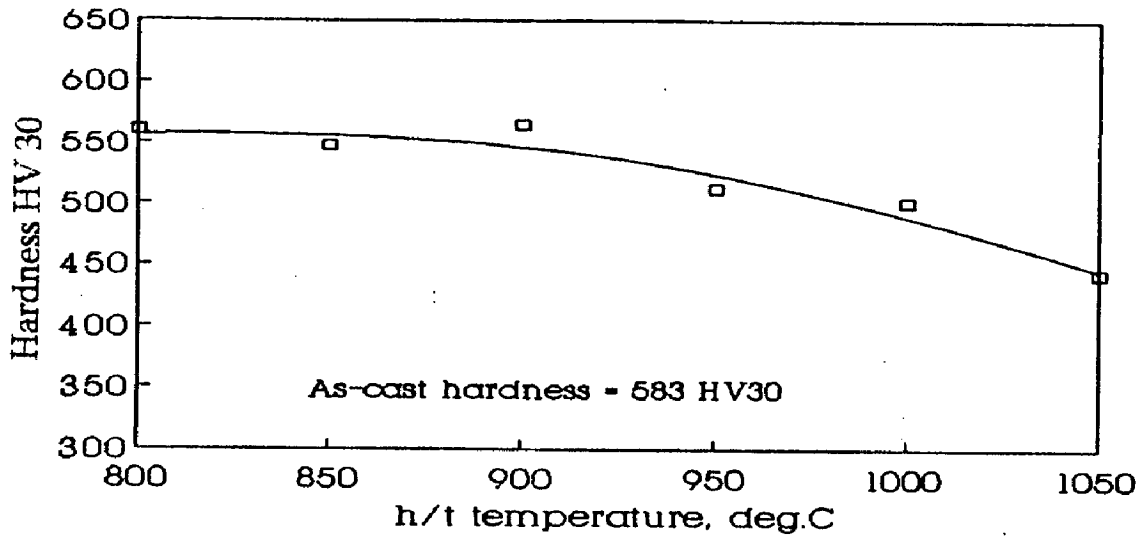


Fig. 5.10 : Effect of h/t temperature on hardness as influenced by h/t time (Alloy C1)

2 hours



4 hours



6 hours

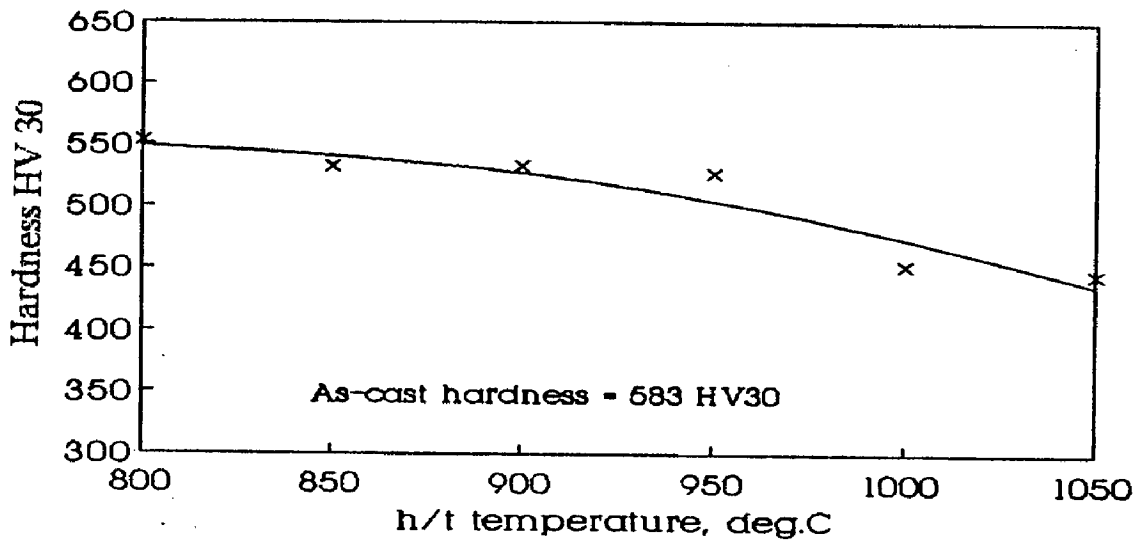


Fig. 5.11 : Effect of h/t temperature on hardness as influenced by h/t time (Alloy C2)

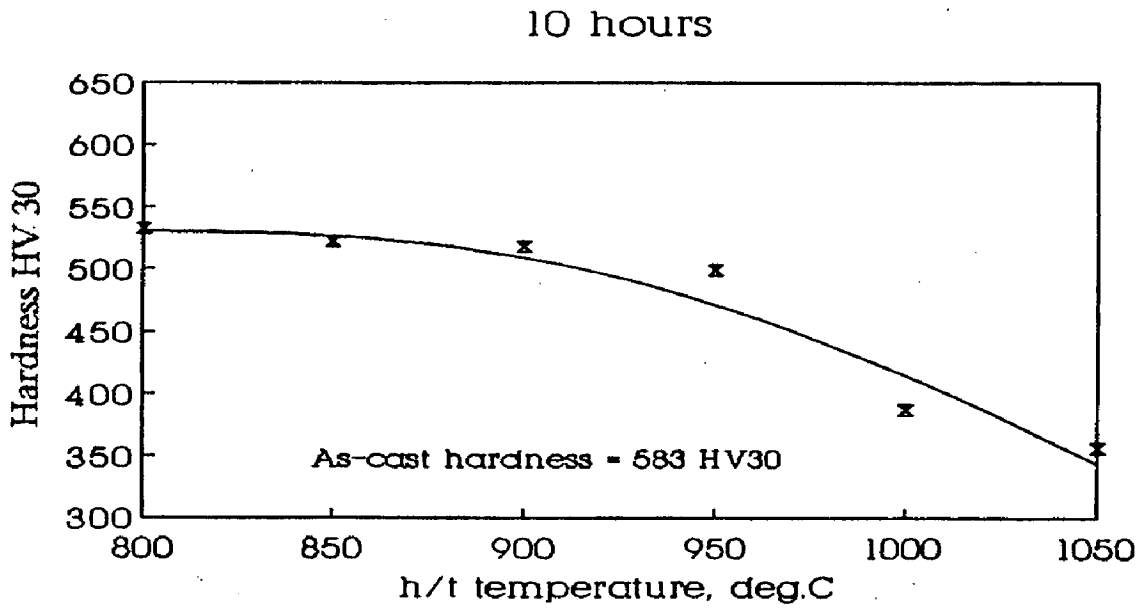
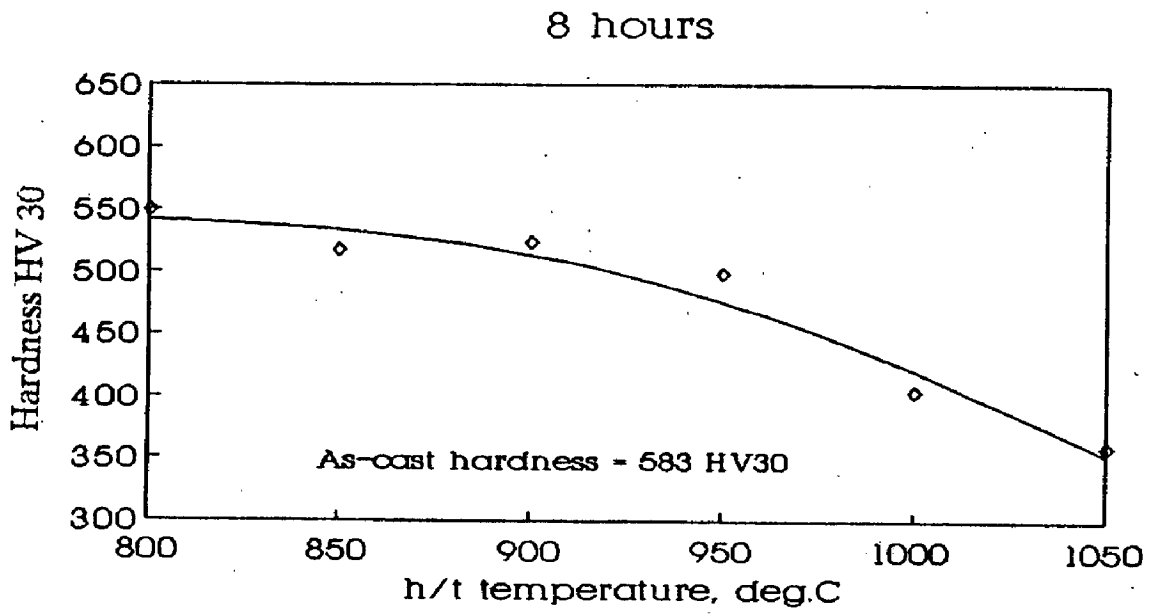


Fig. 5.11 : Effect of h/t temperature on hardness as influenced by h/t time (Alloy C2)

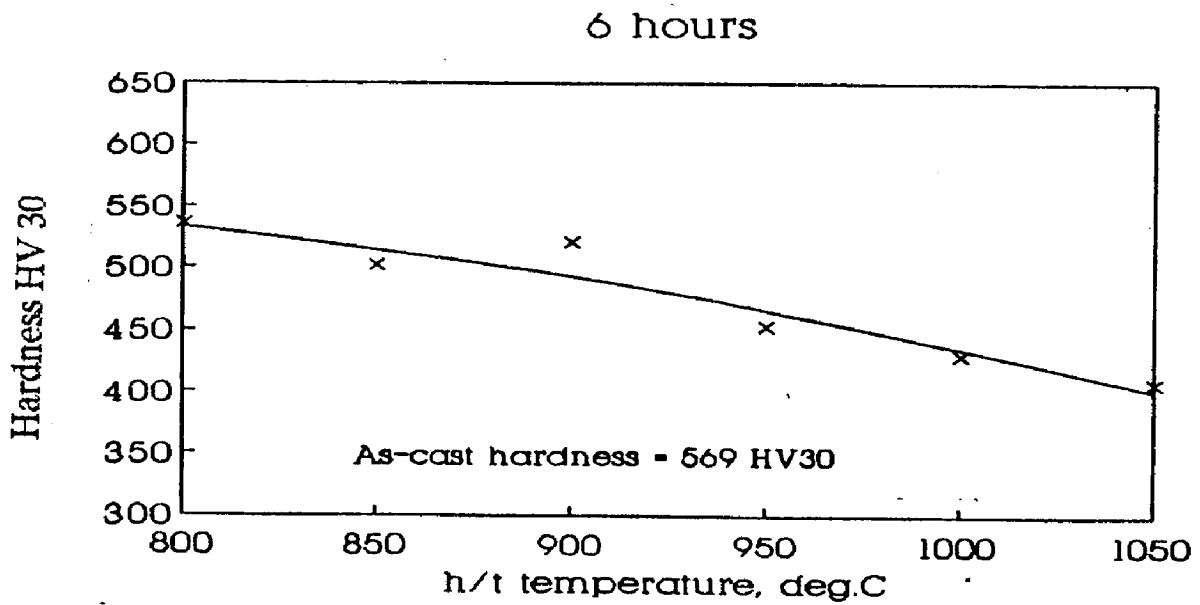
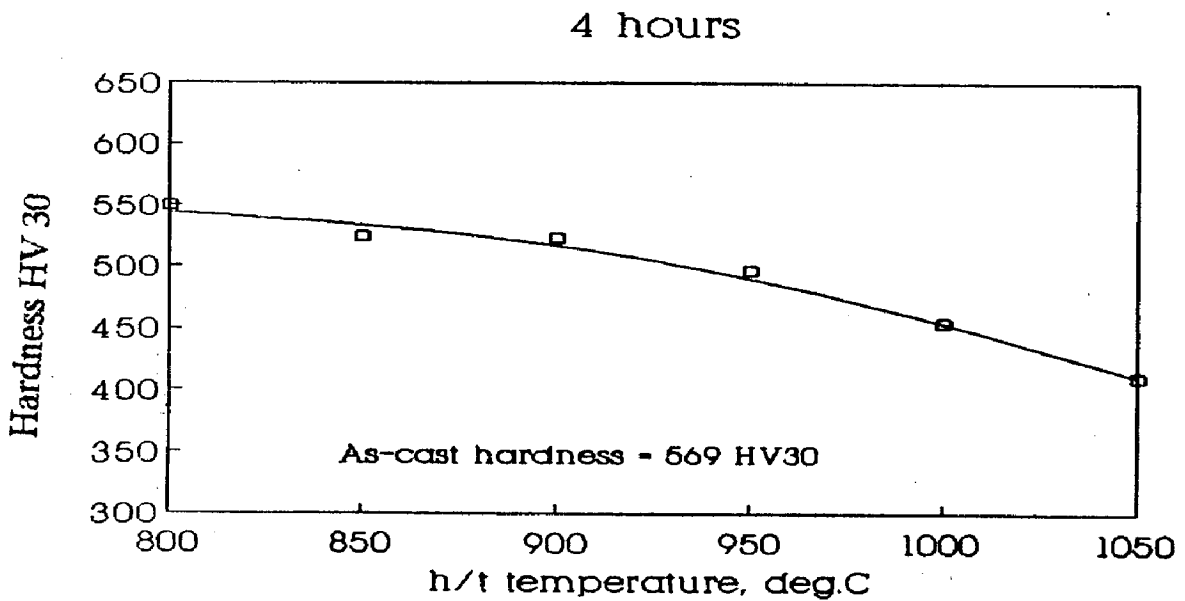
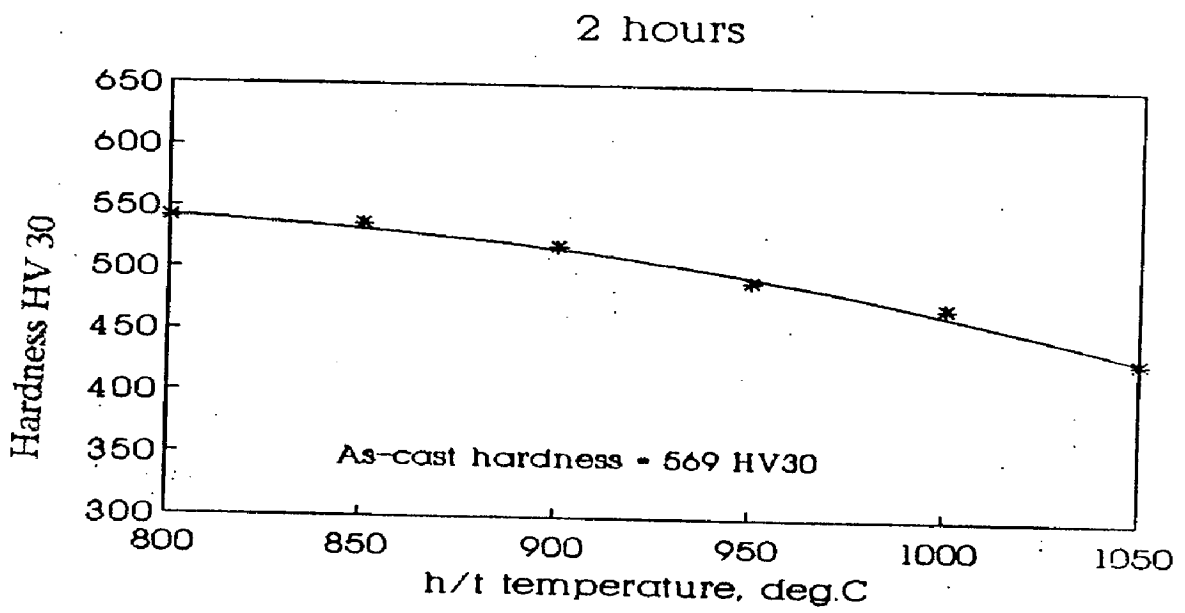


Fig. 5.12: Effect of h/t temperature on hardness as influenced by h/t time (Alloy C3)

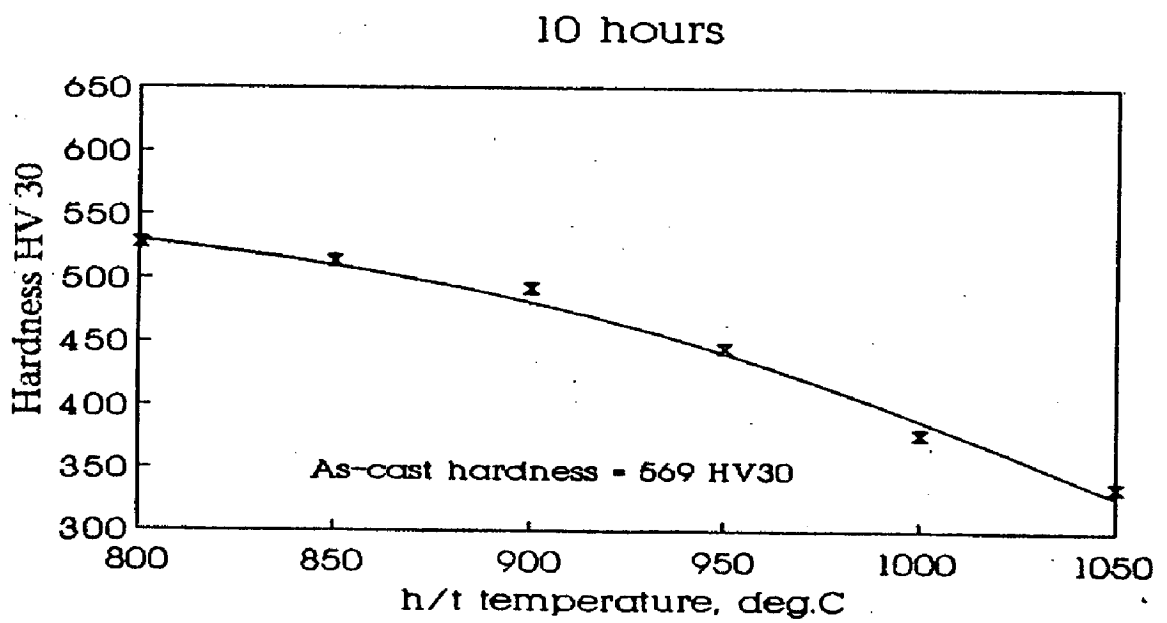
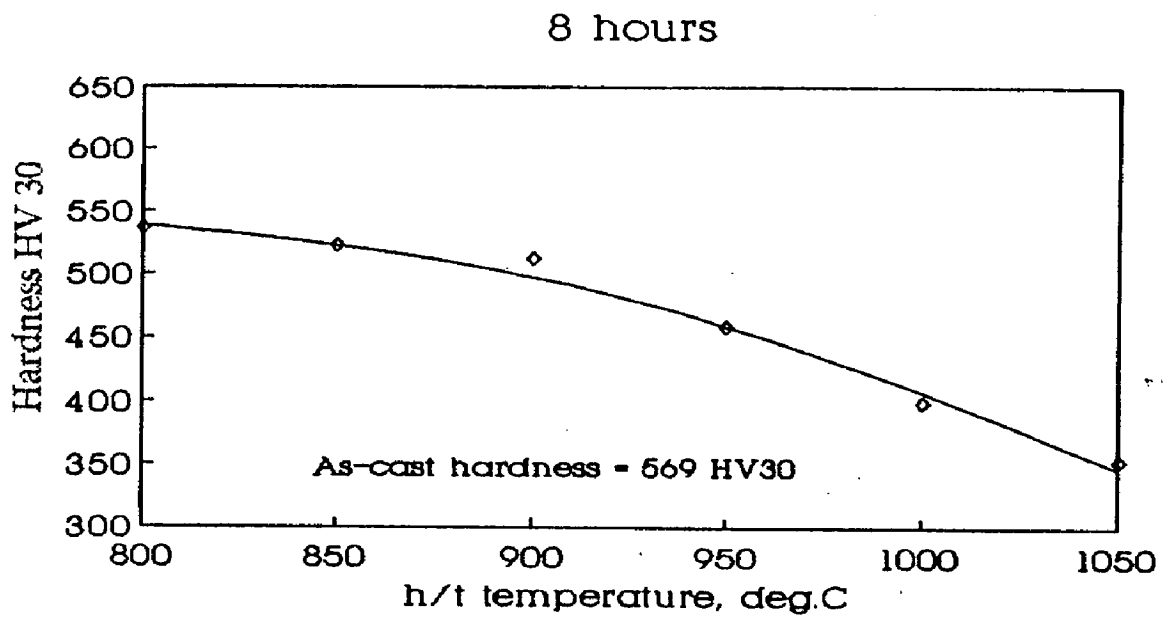


Fig. 5.12 : Effect of h/t temperature on hardness as influenced by h/t time (Alloy C3)

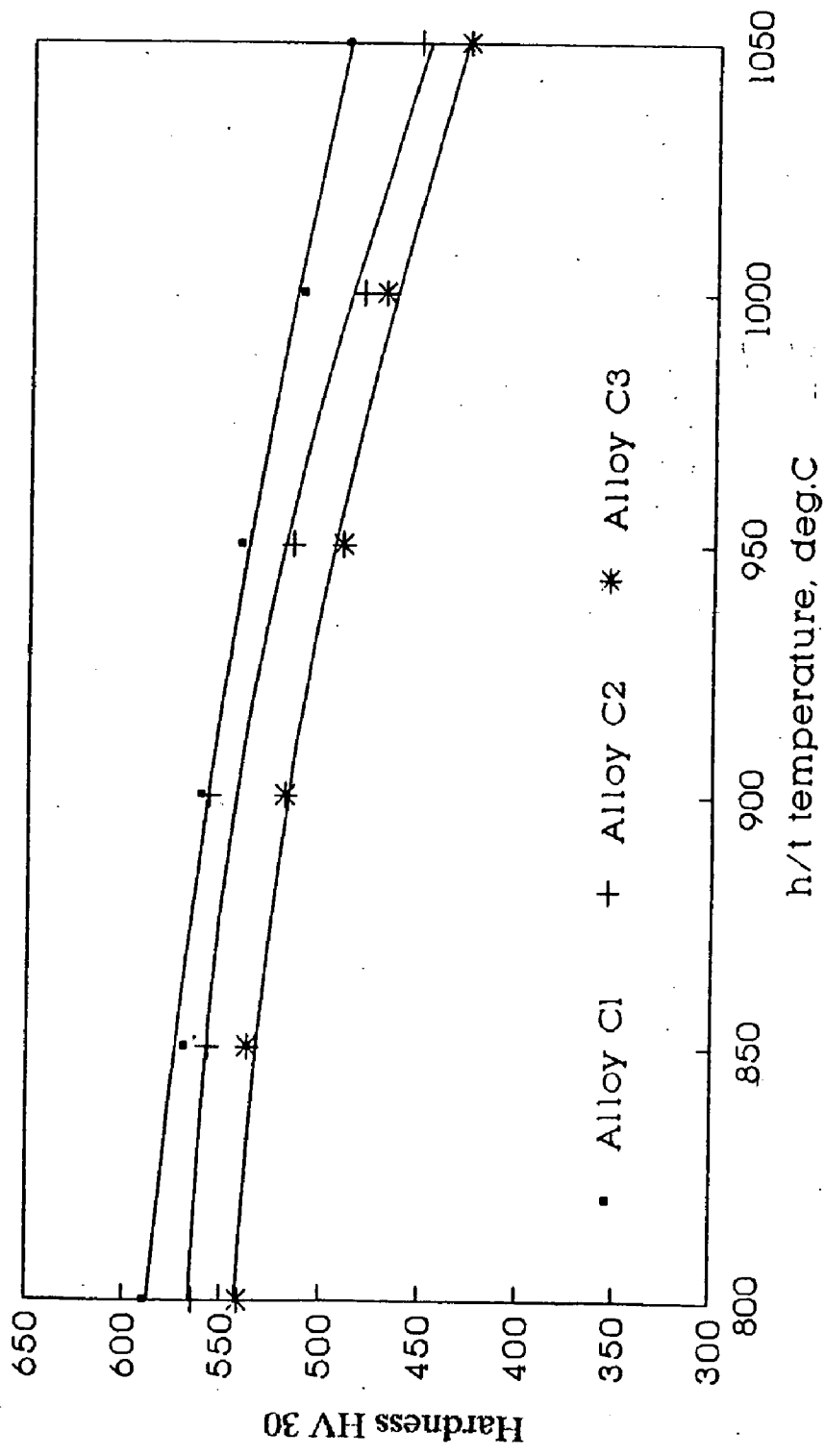


Fig. 5.13 : Effect of h/t temperature on hardness (2 hours)

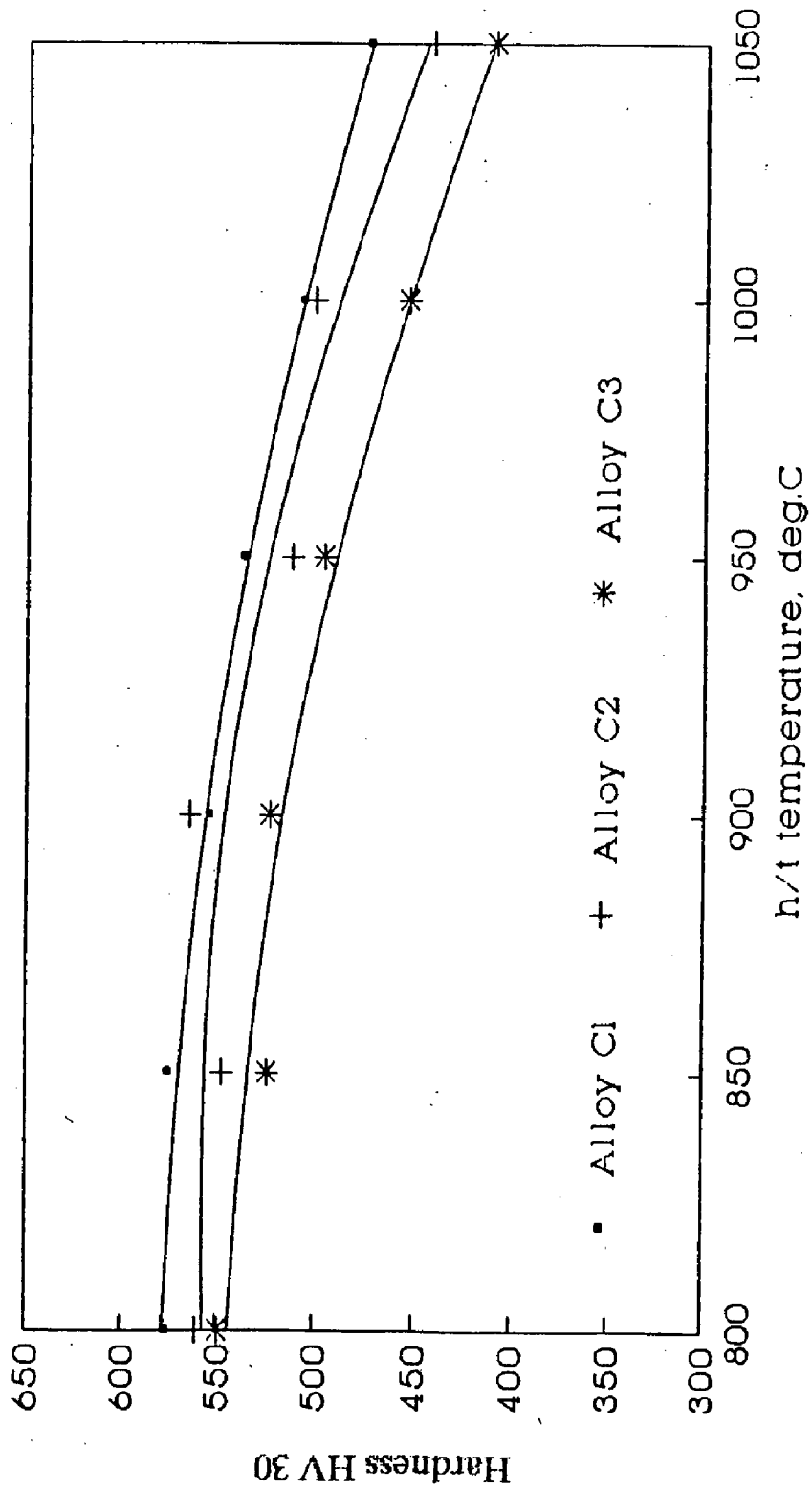


Fig. 5.14 : Effect of h/t temperature on hardness (4 hours)

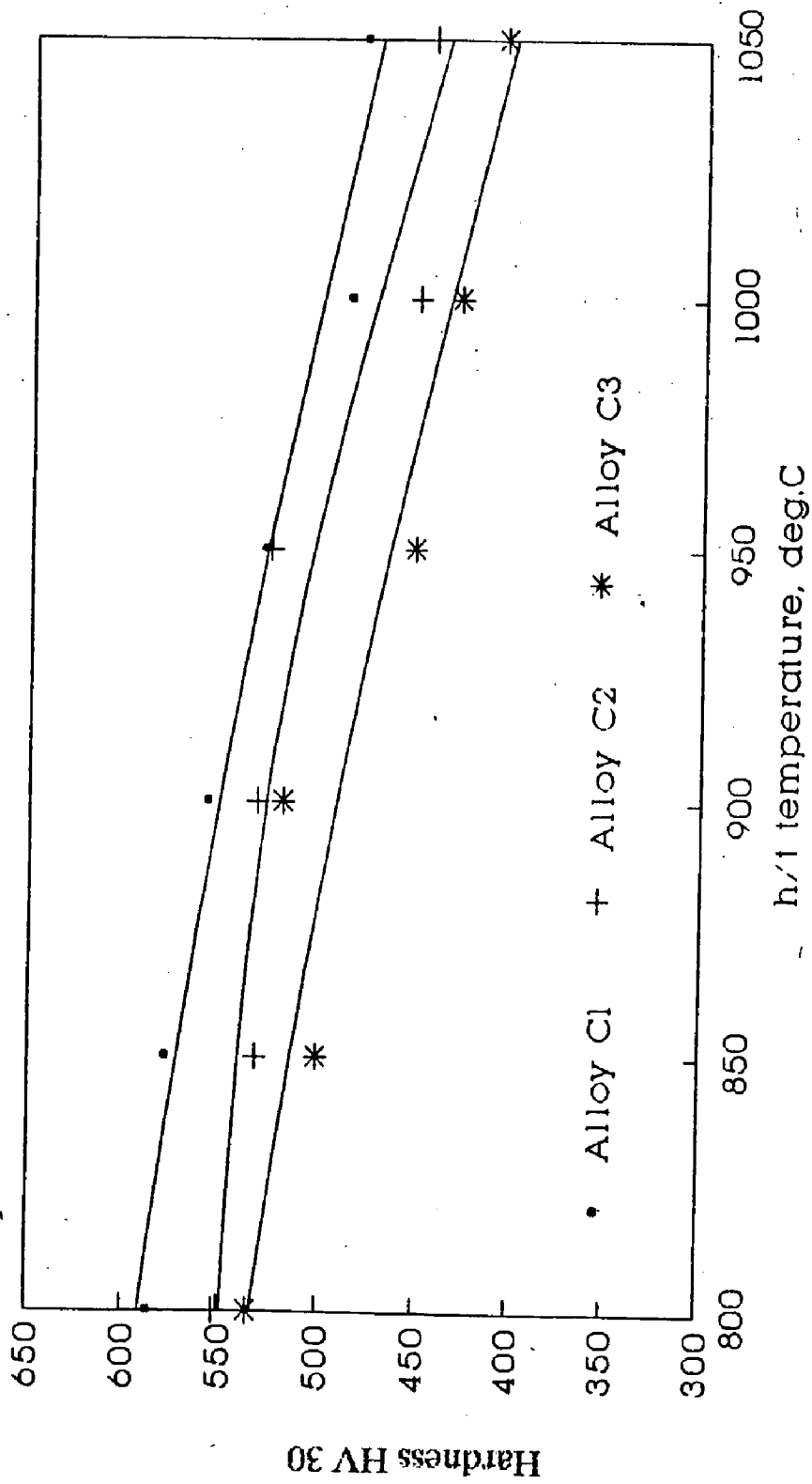


Fig. 5.15 : Effect of h/t temperature on hardness (6 hours)

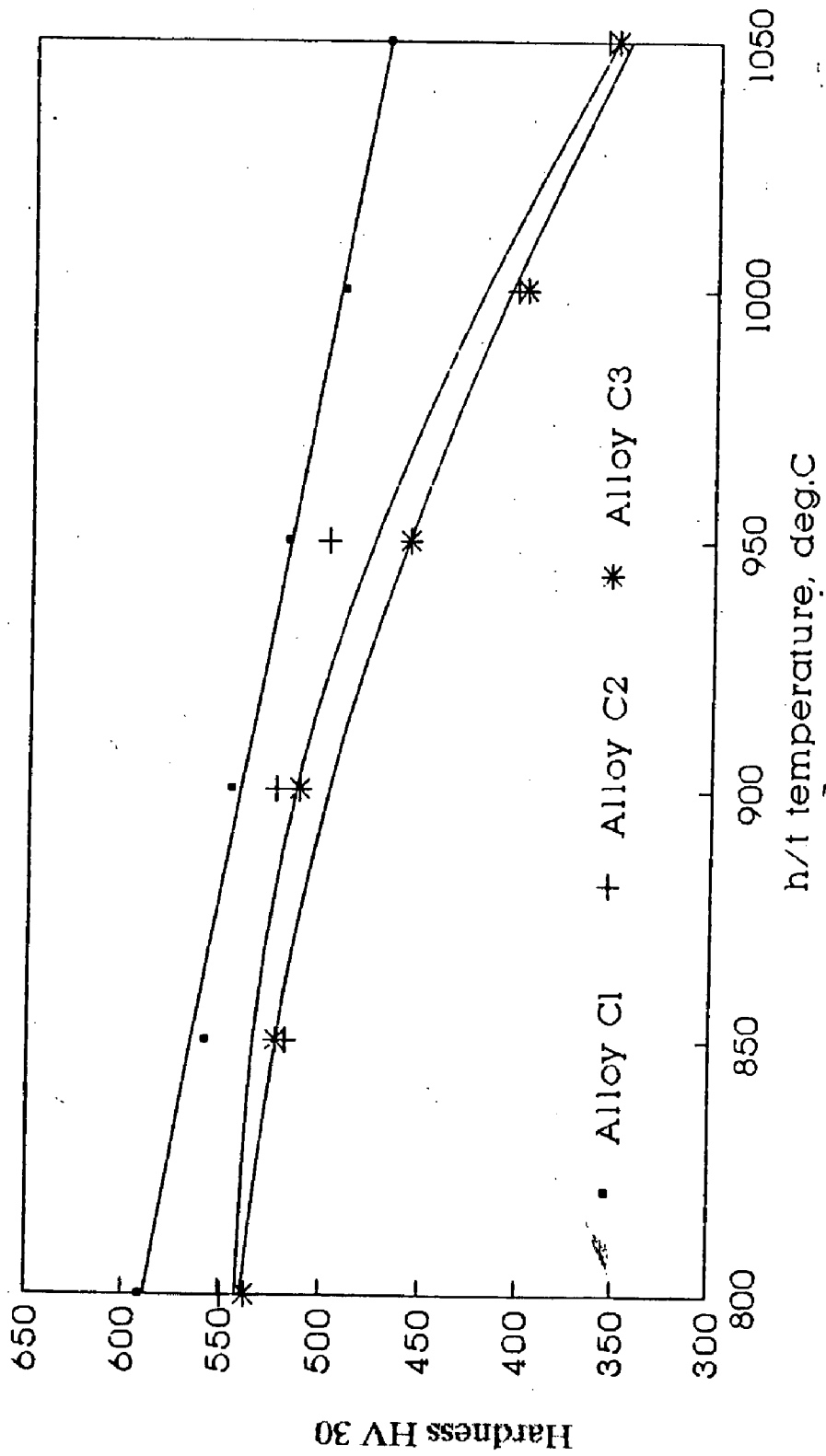


Fig. 5.16 : Effect of h/t temperature on hardness (8 hours)

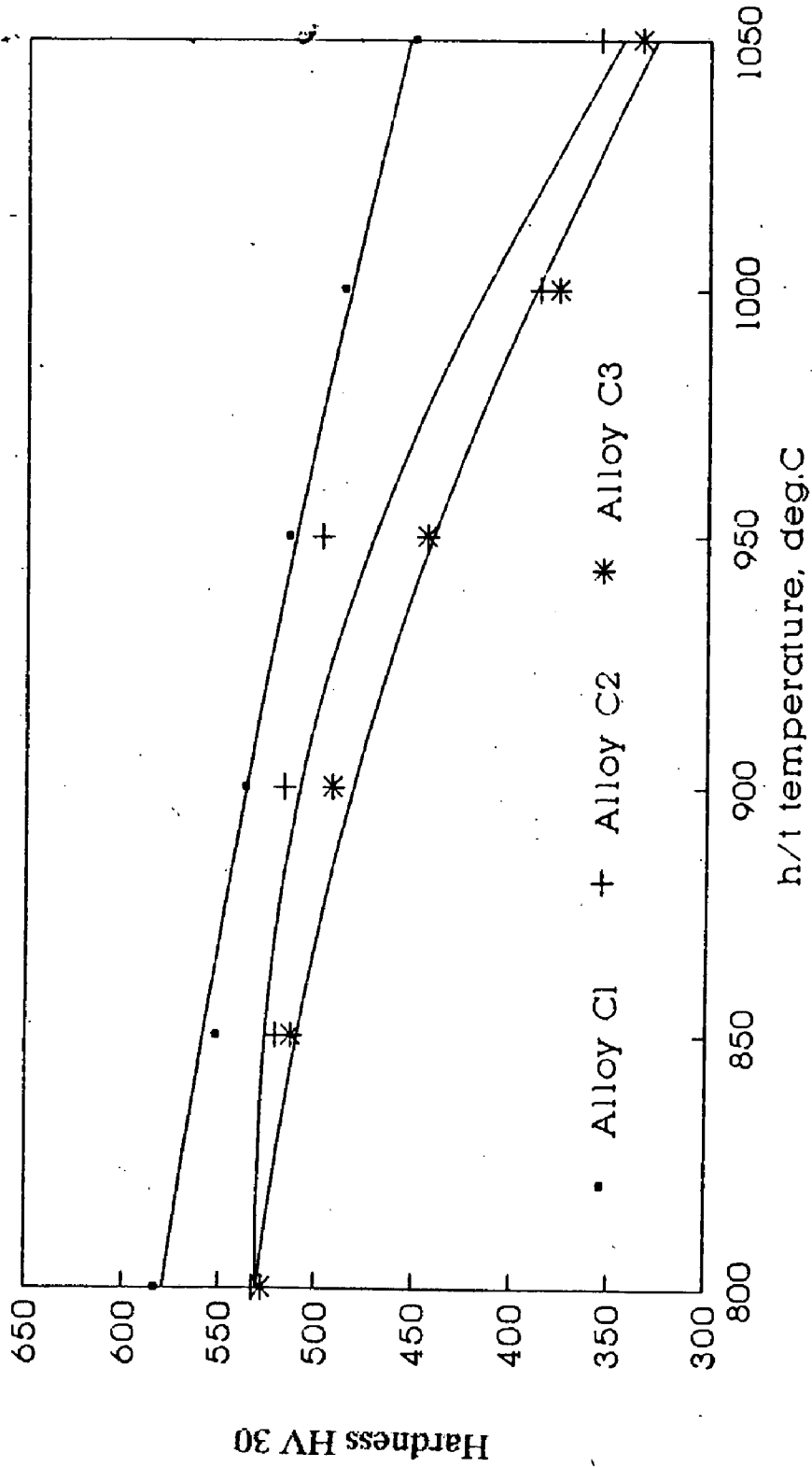


Fig. 5.17 : Effect of h/t temperature on hardness (10 hours)

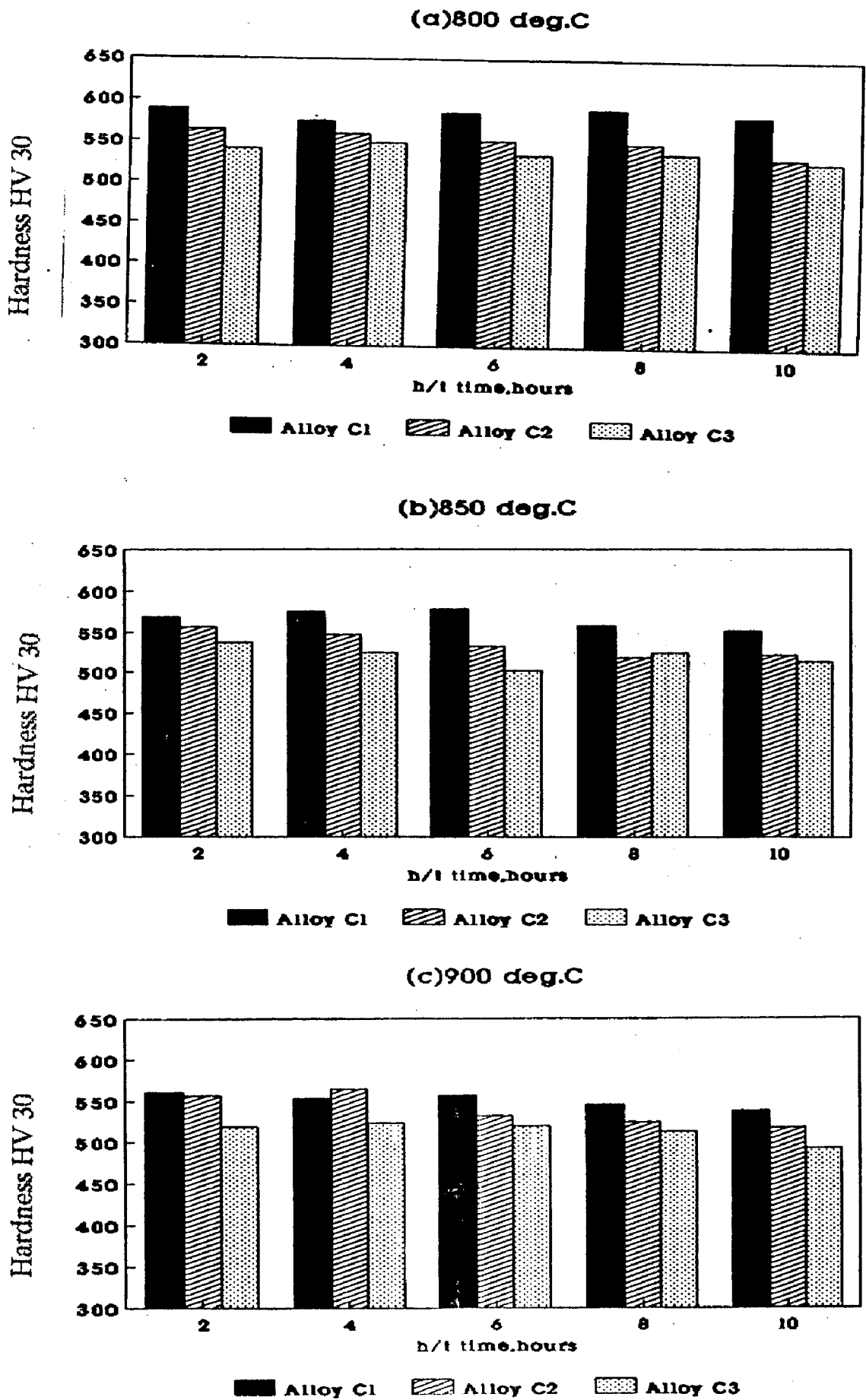
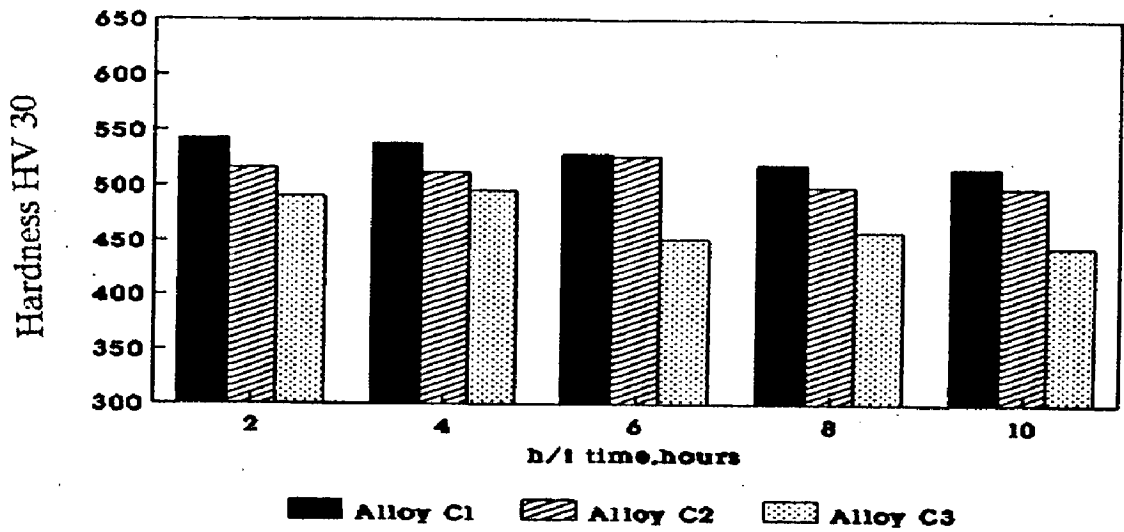
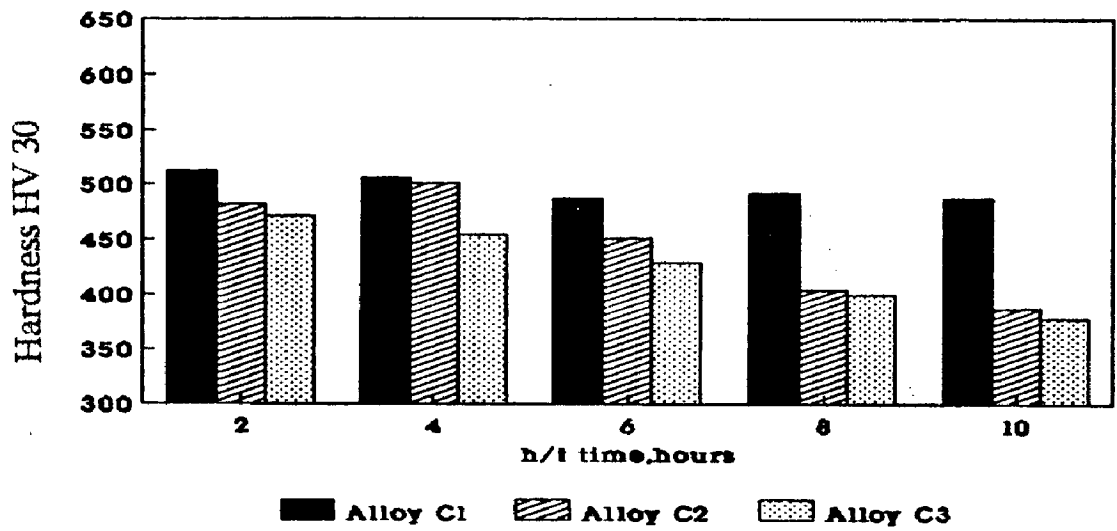


Fig. 5.18 : Summary bar diagram depicting the effect of alloy composition on hardness (variable h/t temperature)

(d) 950 deg.C



(e) 1000 deg.C



(f) 1050 deg.C

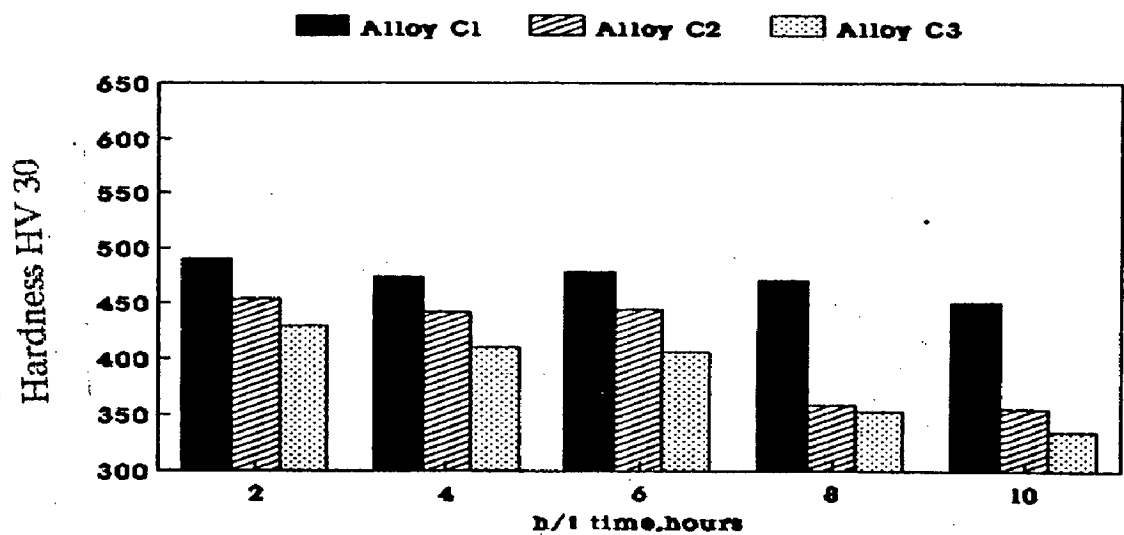
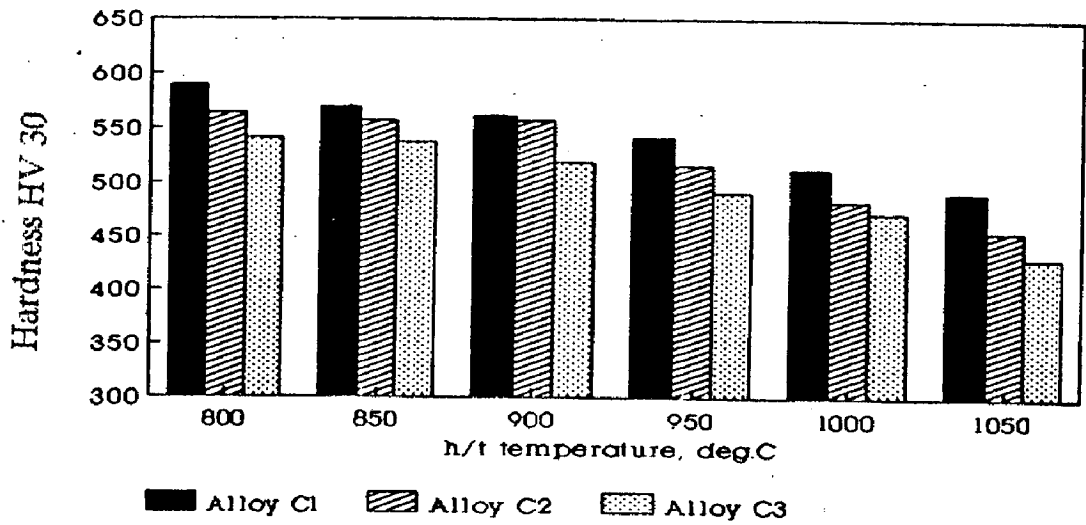
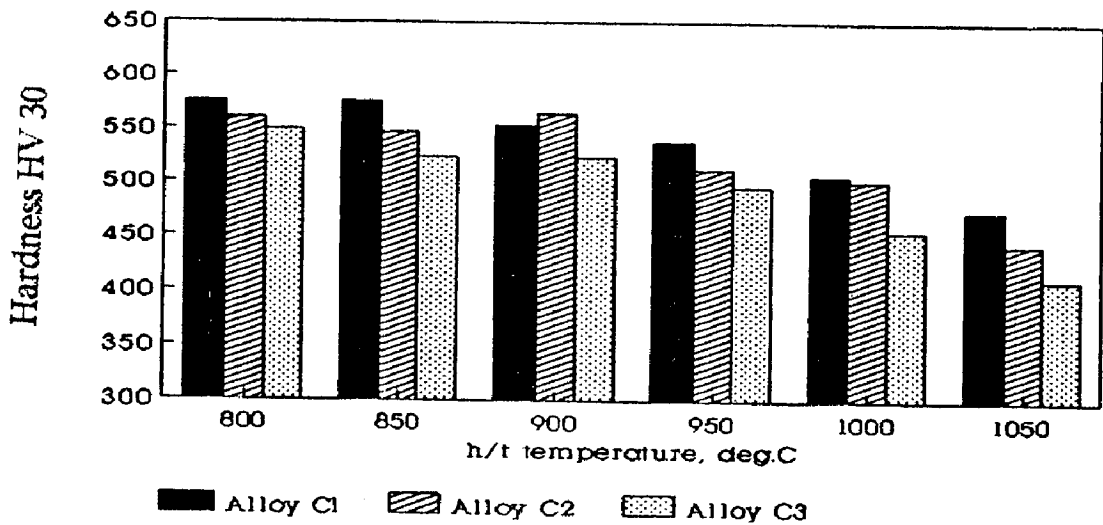


Fig. 5.18 : Summary bar diagram depicting the effect of alloy composition on hardness (variable h/t temperature)

(a) 2 hours



(b) 4 hours



(c) 6 hours

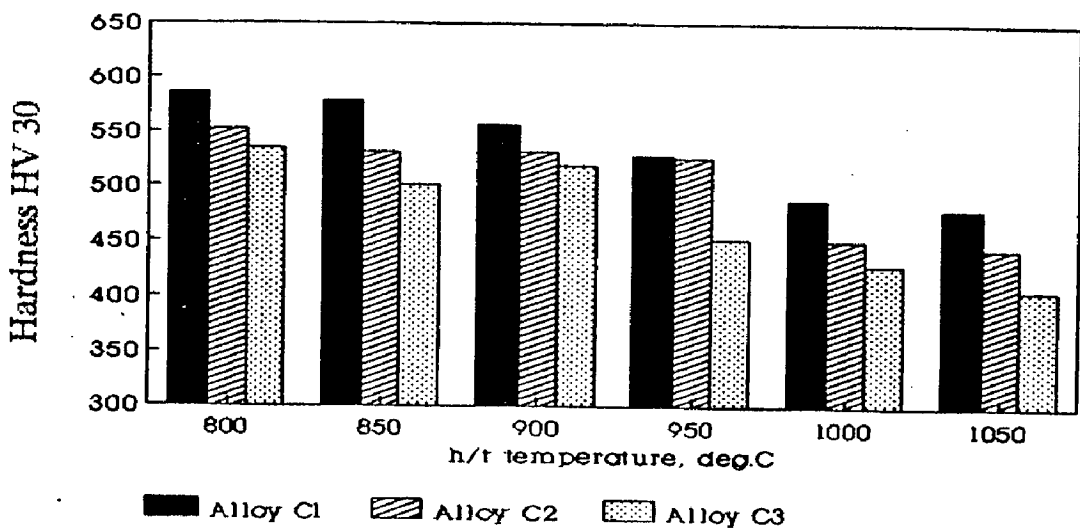


Fig. 5.19 : Summary bar diagrams depicting the effect of alloy composition on hardness (variable h/t time)

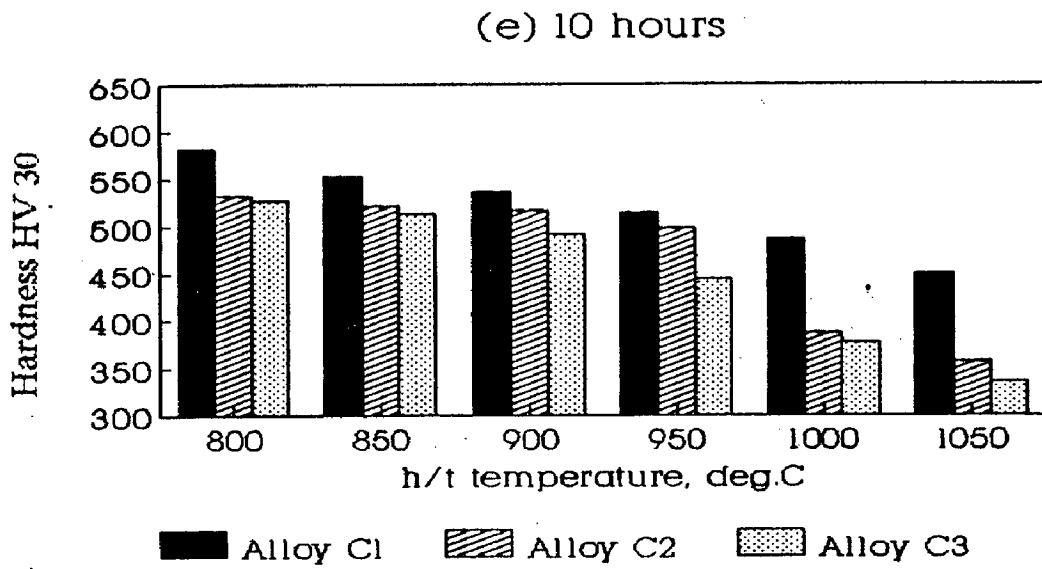
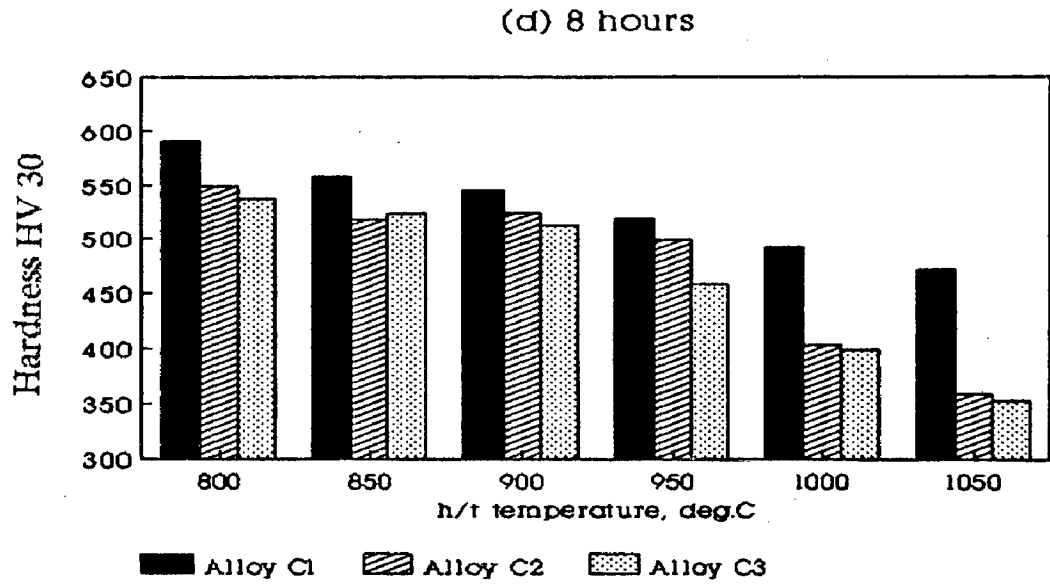


Fig. 5.19 : Summary bar diagrams depicting the effect of alloy composition on hardness (variable h/t time)

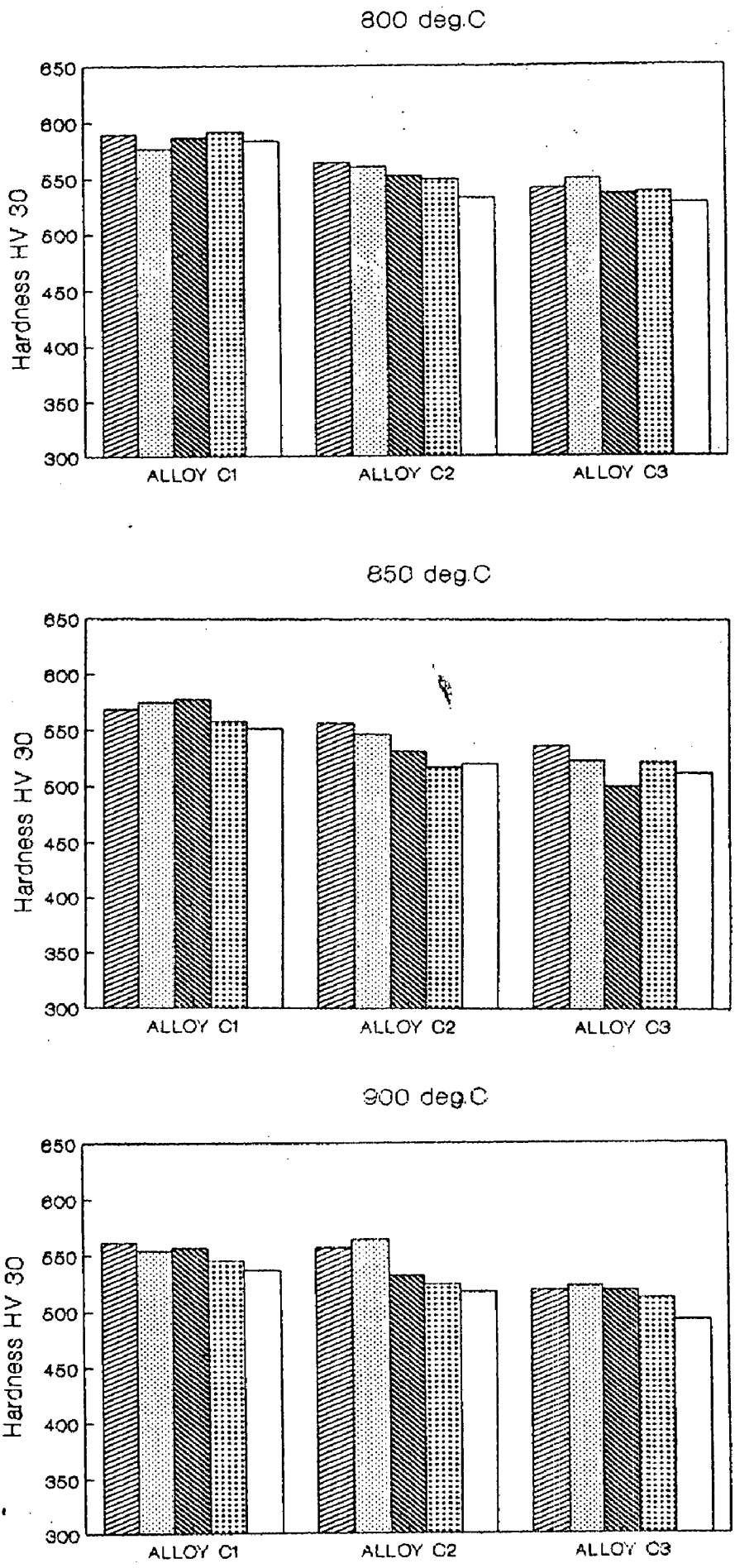


Fig. 5.20 : Summary bar diagrams depicting the effect of h/t time on hardness (variable h/t temperature)

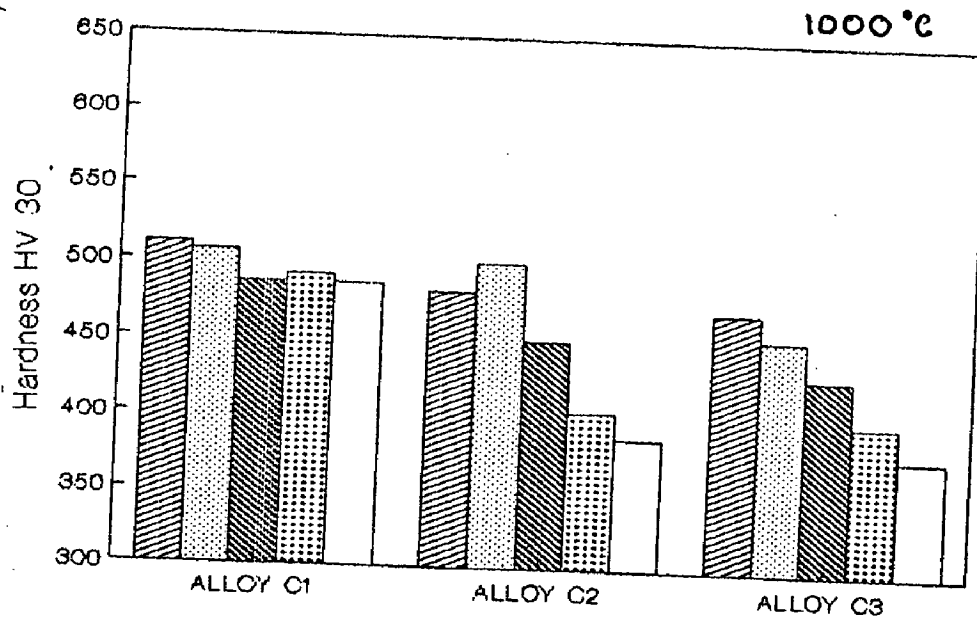
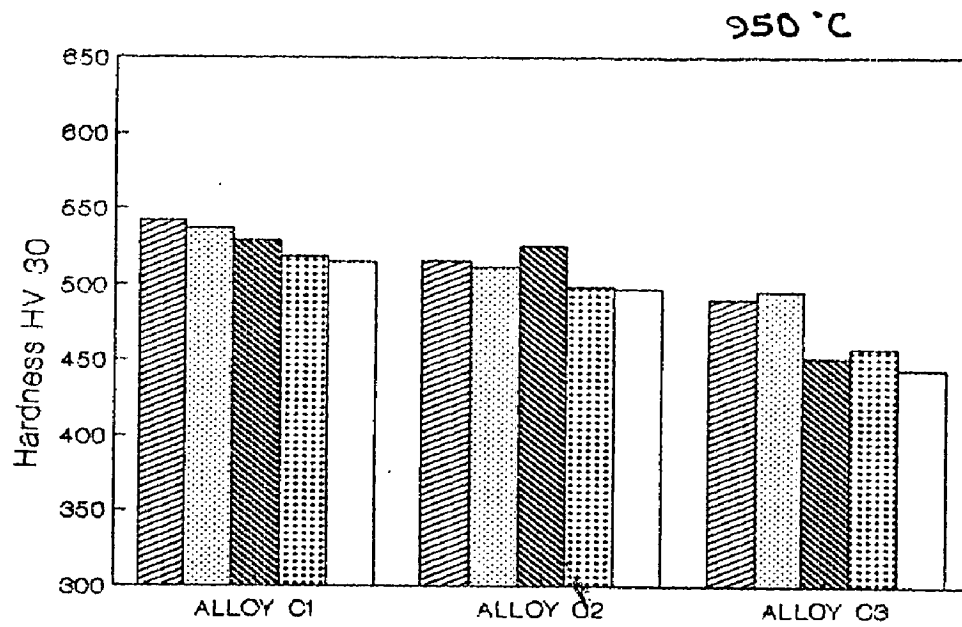


Fig. 5.20 : Summary bar diagrams depicting the effect of h/t time on hardness (variable h/t temperature)

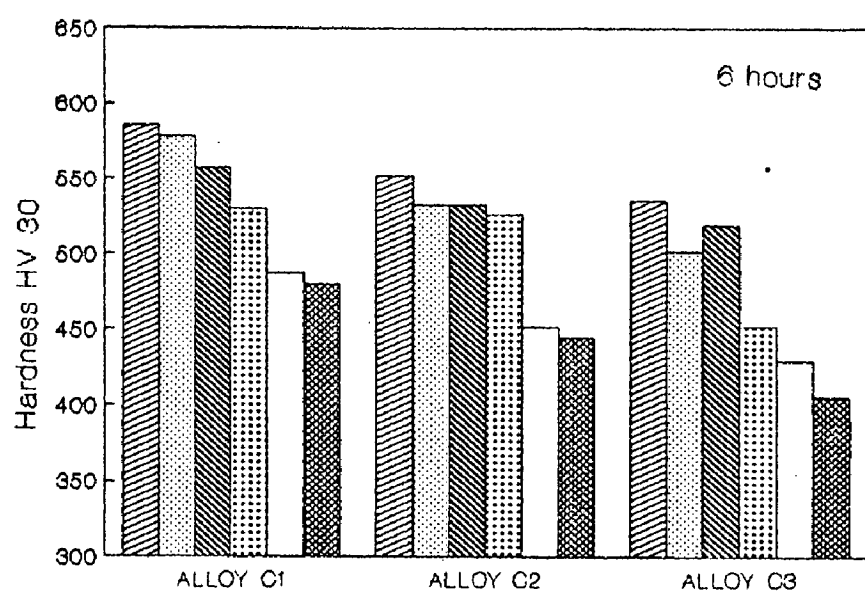
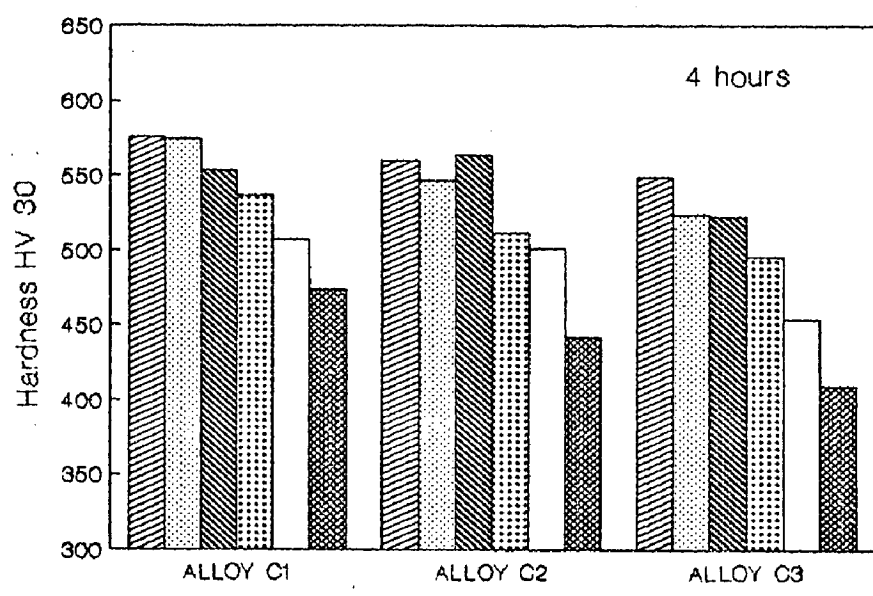
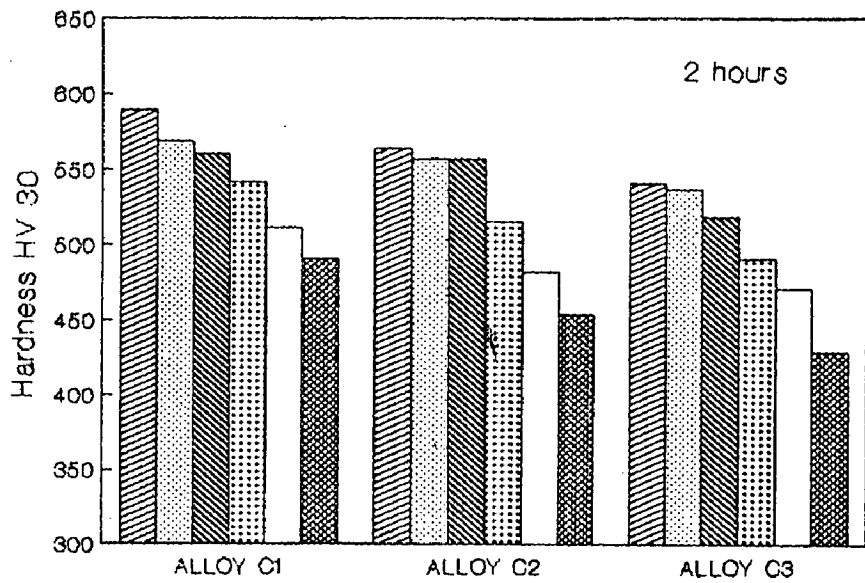


Fig. 5.21 : Summary bar diagrams depicting the effect of h/t temperature on hardness (variable h/t time)

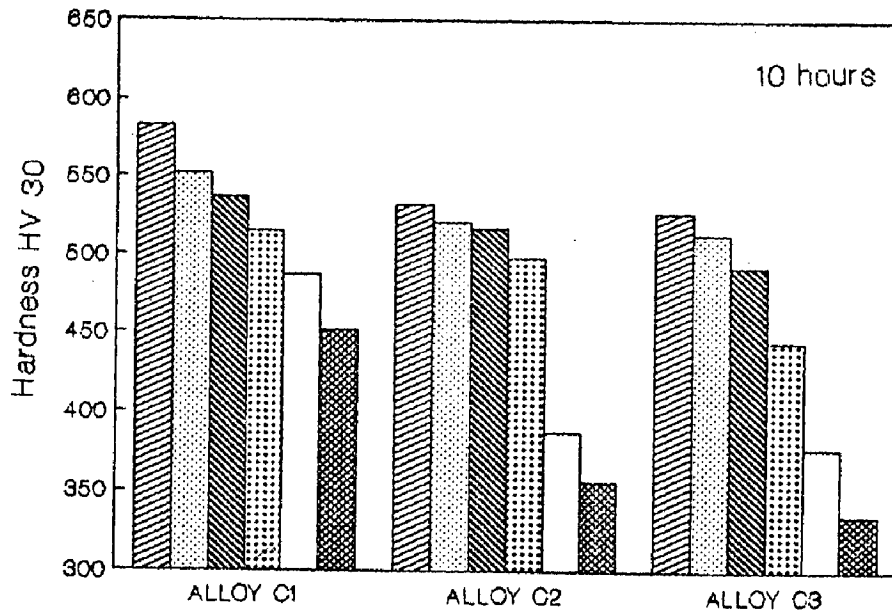
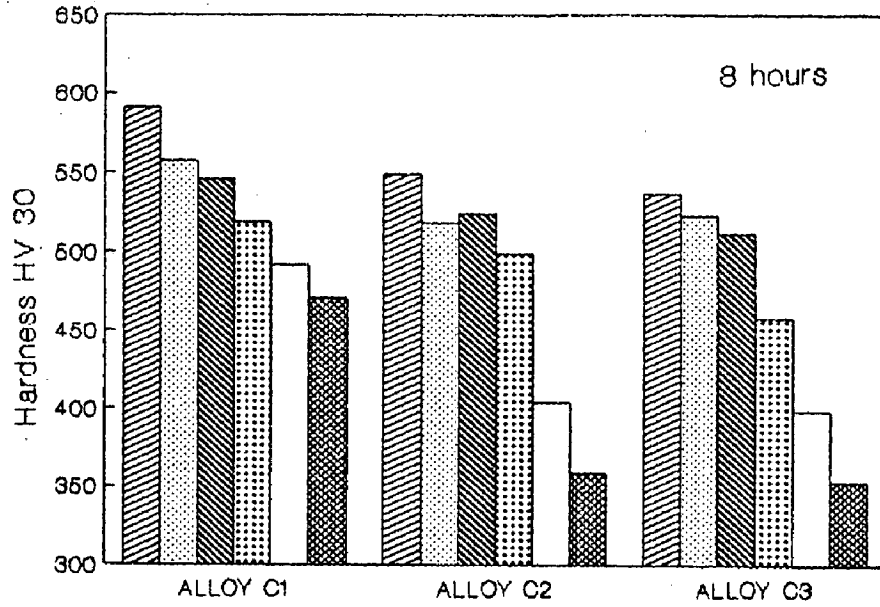


Fig. 5.21 : Summary bar diagrams depicting the effect of h/t temperature on hardness (variable h/t time)

Figure 5.22

- (a) C1, As cast
x 200
- (b) C1, As cast
x 200
- (c) C1, As cast
x 1000

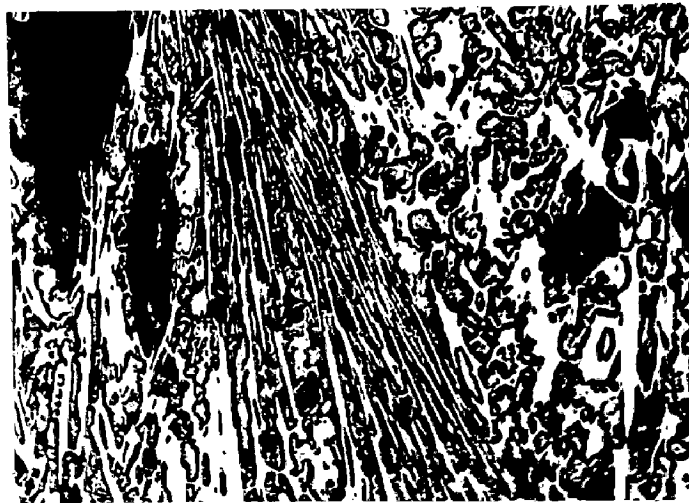
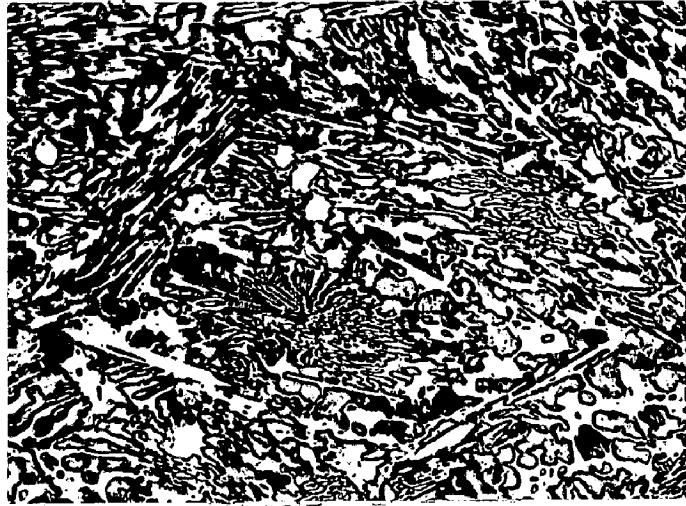


Figure 5.23

- | | |
|---------------------------|---------------------------|
| (a) C1, 800, 2
x 200 | (b) C1, 800, 2
x 1000 |
| (c) C1, 800, 6
x 200 | (d) C1, 800, 6
x 1000 |
| (e) C1, 800, 10
x 200 | (f) C1, 800, 10
x 1000 |
| (g) C1, 800, 10
x 1000 | |

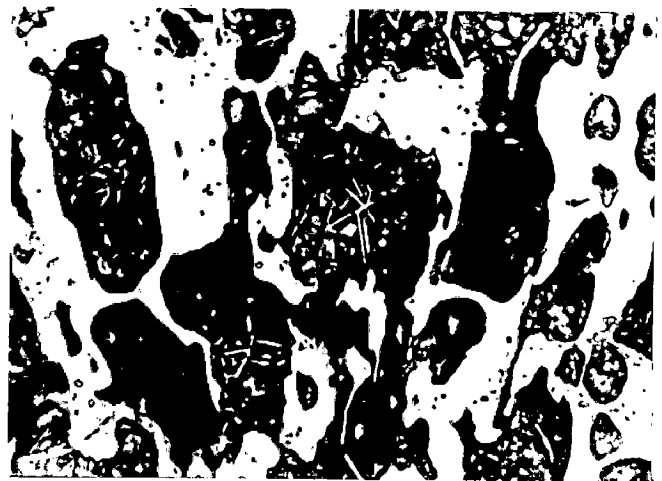
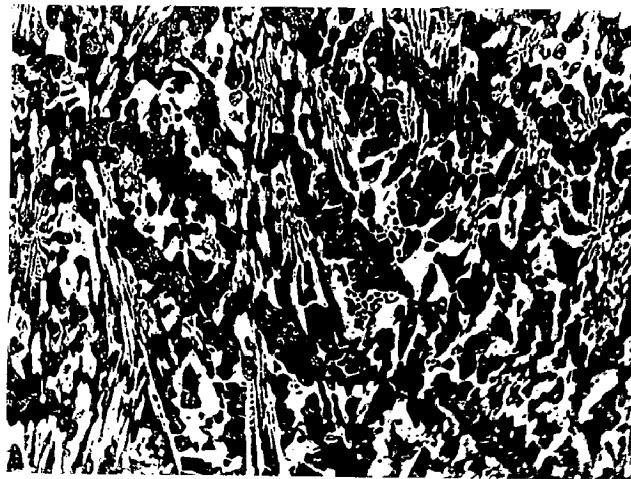
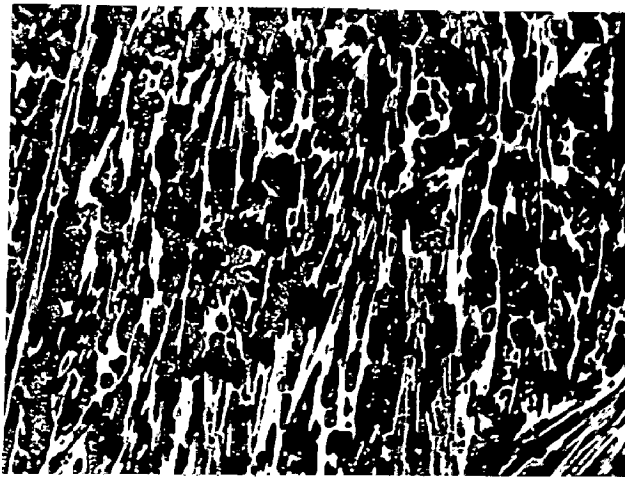
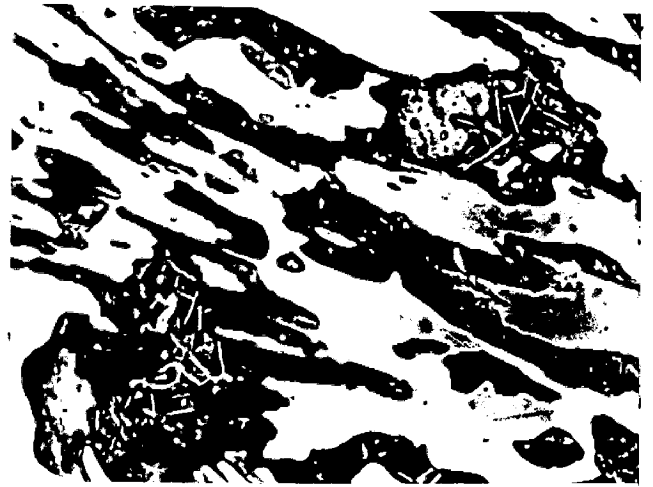


Figure 5.24

- (a) C1, 850, 2
x 1000
- (b) C1, 850, 2
x 1000
- (c) C1, 850, 2
x 200
- (d) C1, 800, 6
x 200
- (e) C1, 800, 6
x 1000

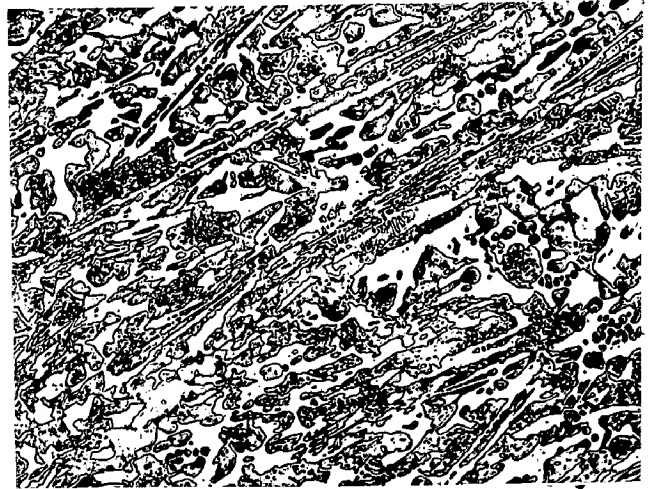
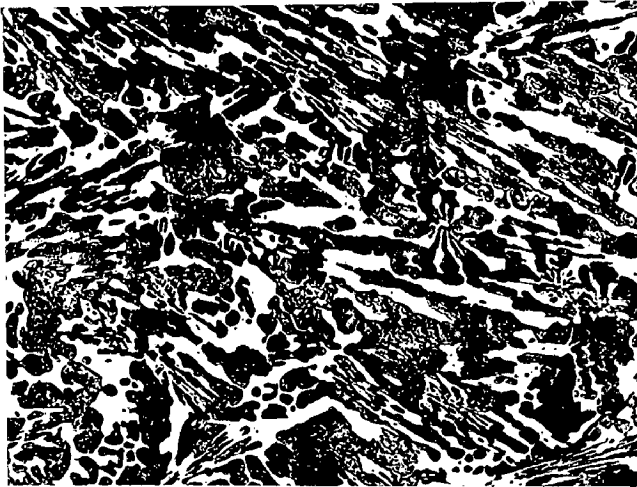
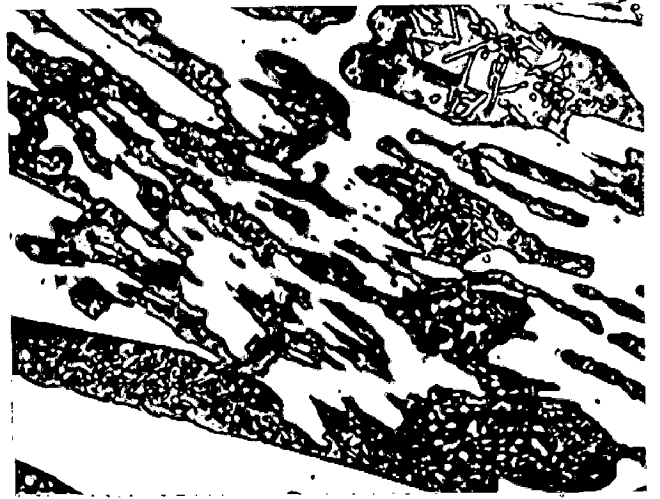
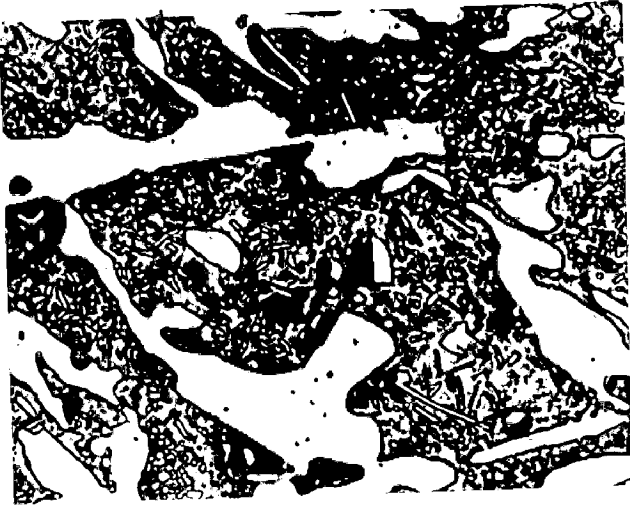


Figure 5.24

(f)	C1, 850, 6 x 1000	(g)	C1, 850, 10 x 200
(h)	C1, 850, 10 x 800	(i)	C1, 850, 10 x 1000

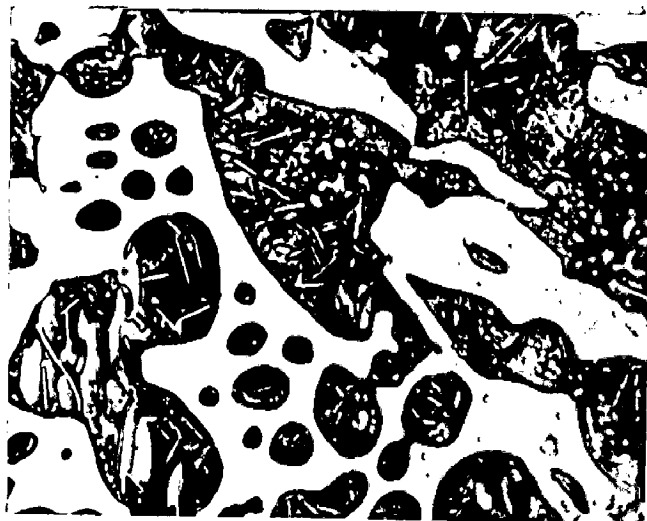
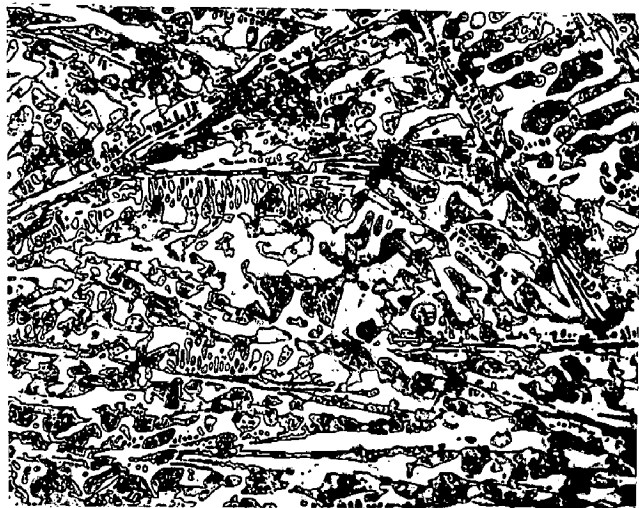
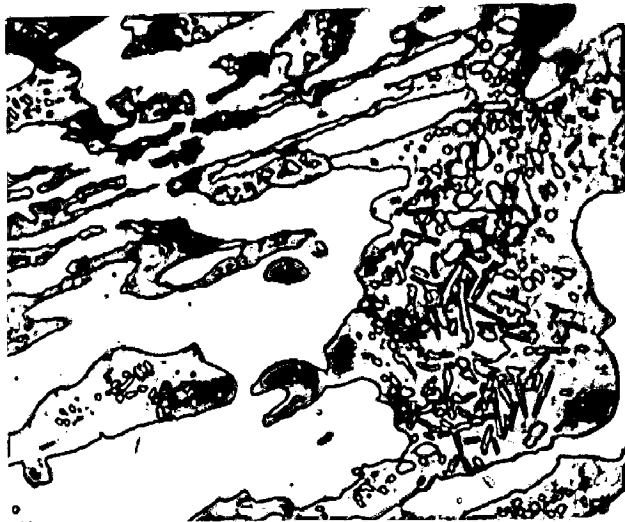


Figure 5.25

- | | |
|---------------------------|---------------------------|
| (a) C1, 900, 2
x 200 | (b) C1, 900, 2
x 1000 |
| (c) C1, 900, 6
x 200 | (d) C1, 900, 6
x 1000 |
| (e) C1, 900, 10
x 200 | (f) C1, 900, 10
x 1000 |
| (g) C1, 900, 10
x 1000 | |

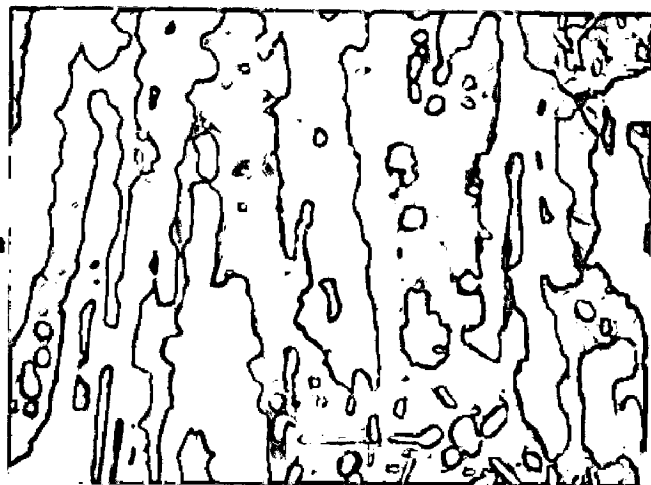
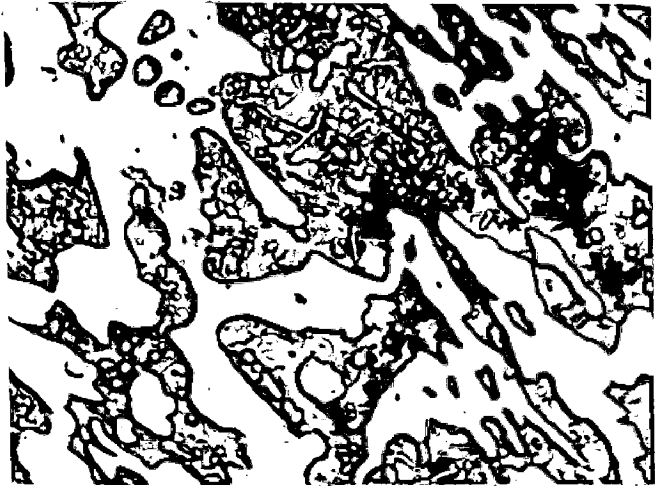
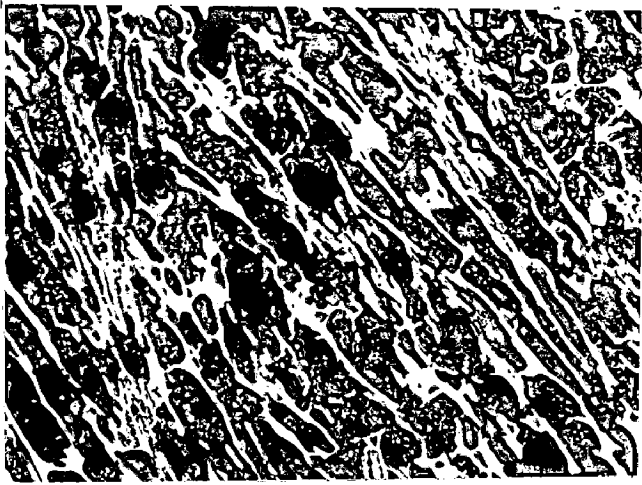


Figure 5.26

(a) C1, 950, 2
x 200

(b) C1, 950, 2
x 1000

(c) C1, 950, 6
x 200

(d) C1, 950, 6
x 1000

(e) C1, 950, 10
x 200

(f) C1, 950, 10
x 1000

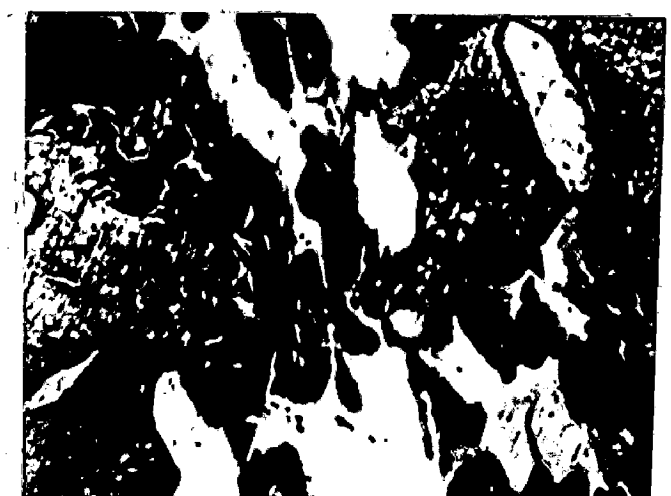
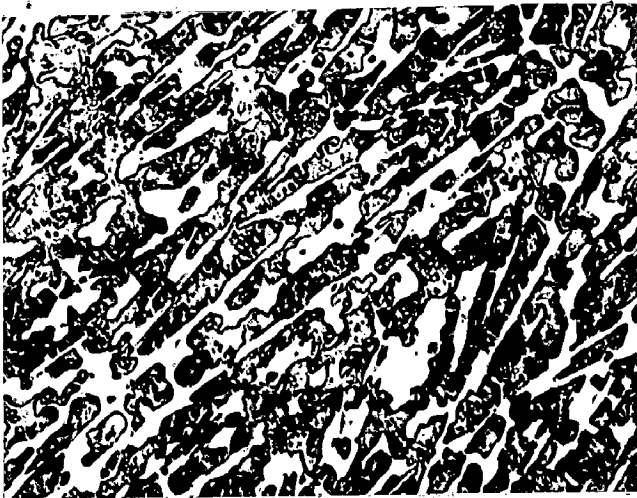
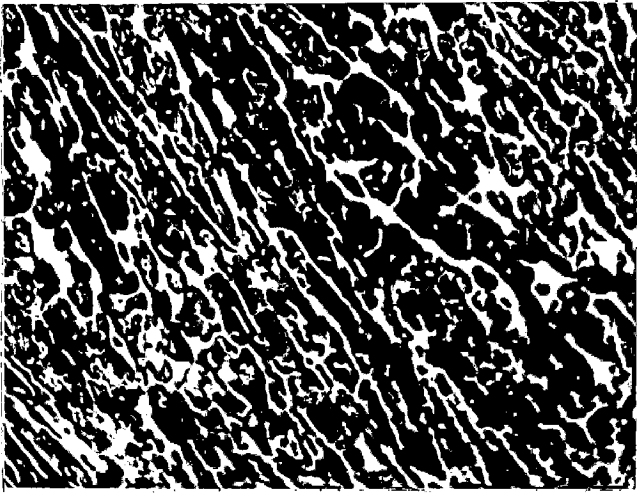


Figure 5.27

- | | |
|---------------------------|----------------------------|
| (a) C1, 1000, 2
x 200 | (b) C1, 1000, 2
x 1000 |
| (c) C1, 1000, 6
x 200 | (d) C1, 1000, 6
x 1000 |
| (e) C1, 1000, 10
x 200 | (f) C1, 1000, 10
x 1000 |
| | (g) C1, 1000, 10
x 1000 |



Figure 5.28

- | | |
|---------------------------|---------------------------|
| (a) C1, 1050, 2
x 200 | (b) C1, 1050, 2
x 1000 |
| (c) C1, 1050, 2
x 1000 | (d) C1, 1050, 6
x 200 |
| (e) C1, 1050, 6
x 1000 | (f) C1, 1050, 6
x 1000 |

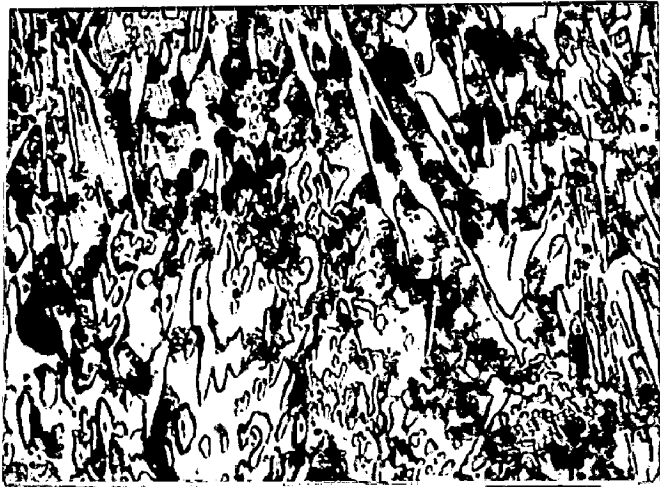


Figure 5.28

(g)	C1, 1050, 10 x 200	(h)	C1, 1050, 10 x 200
(i)	C1, 1050, 10 x 1000	(j)	C1, 1050, 10 x 1000

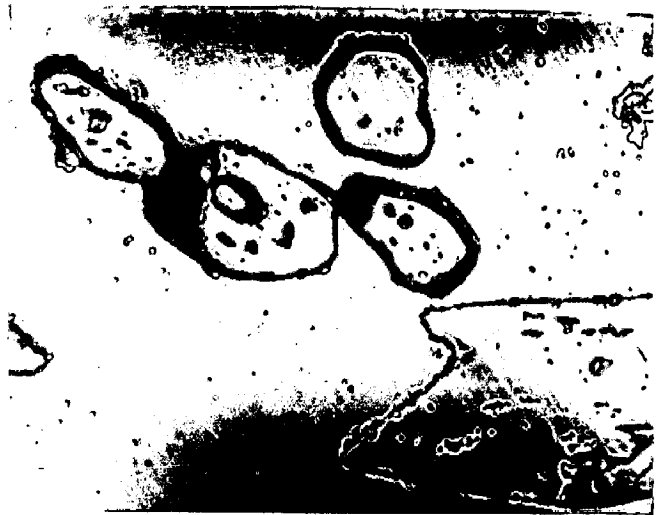
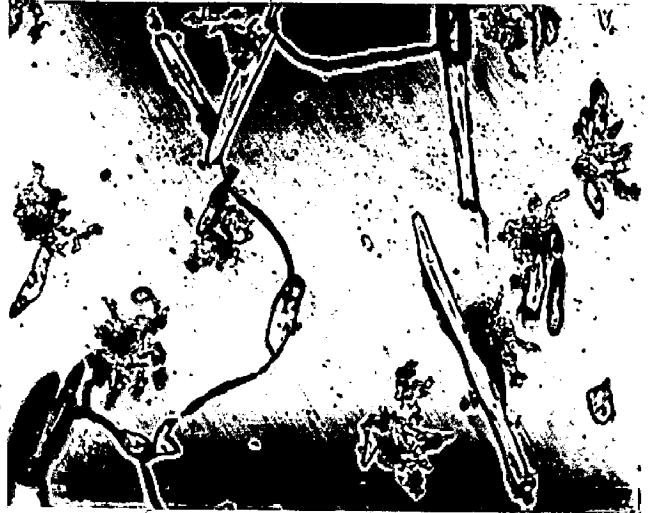
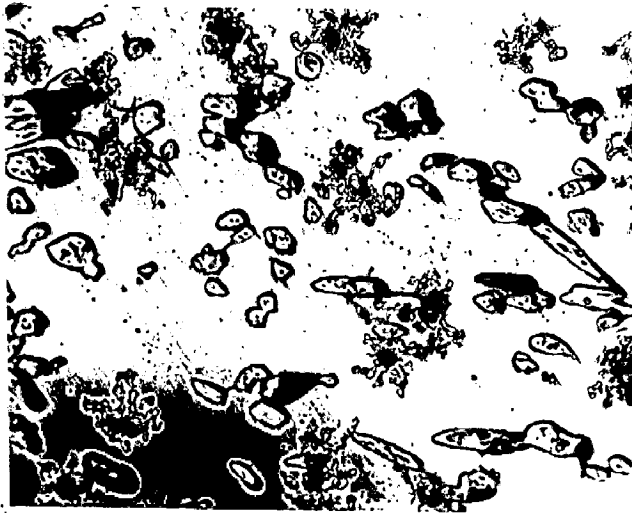


Figure 5.29

- | | |
|---------------------------|---------------------------|
| (a) C2, As cast
x 200 | (b) C2, As cast
x 200 |
| (c) C2, As cast
x 1000 | (d) C2, As cast
x 1000 |



Figure 5.30

- | | |
|--------------------------|--------------------------|
| (a) C2, 800, 2
x 200 | (b) C2, 800, 2
x 1000 |
| (c) C2, 800, 6
x 200 | (d) C2, 800, 6
x 1000 |
| (e) C2, 800, 6
x 1000 | (f) C2, 800, 10
x 200 |

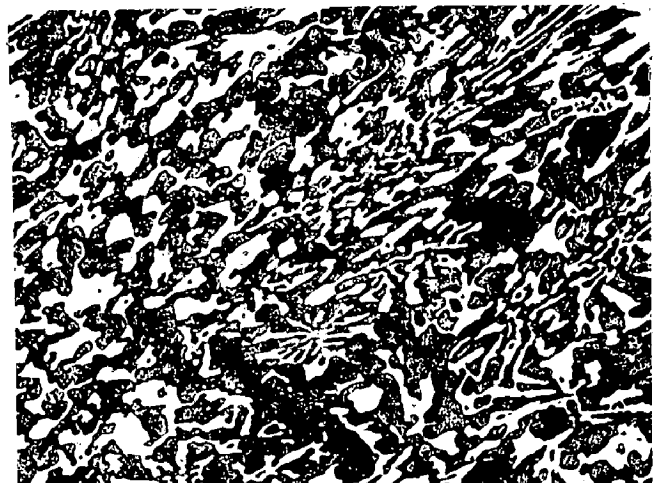
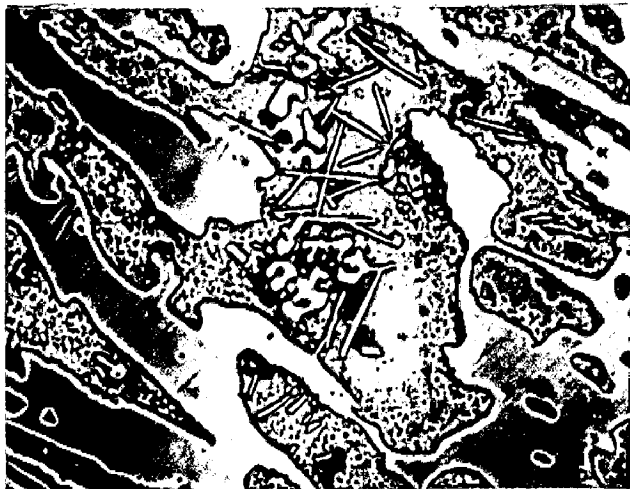
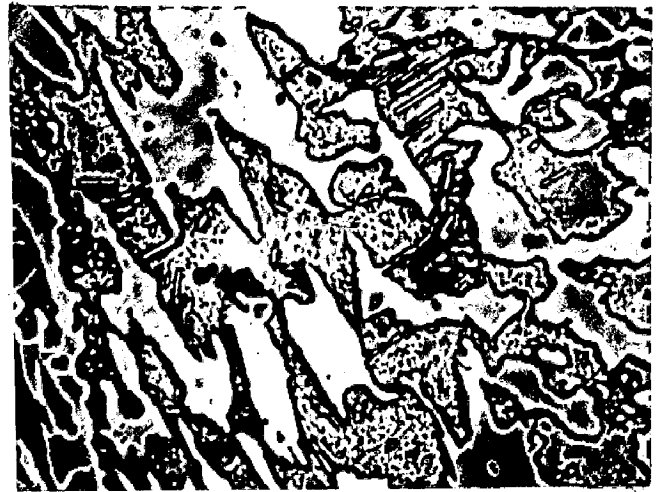
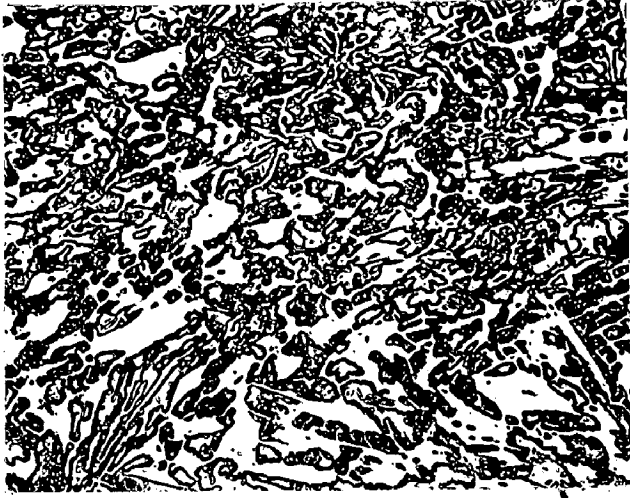


Figure 5.31

- | | |
|---------------------------|---------------------------|
| (a) C2, 850, 2
x 200 | (b) C2, 850, 6
x 200 |
| (c) C2, 850, 6
x 1000 | (d) C2, 850, 6
x 1000 |
| (e) C2, 850, 10
x 200 | (f) C2, 850, 10
x 1000 |
| (g) C2, 850, 10
x 1000 | |

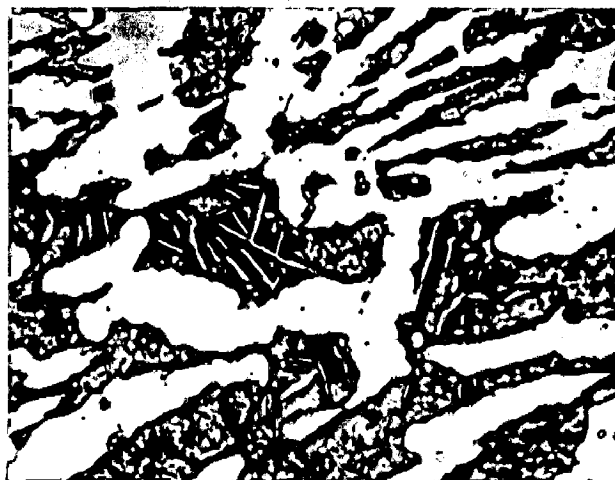
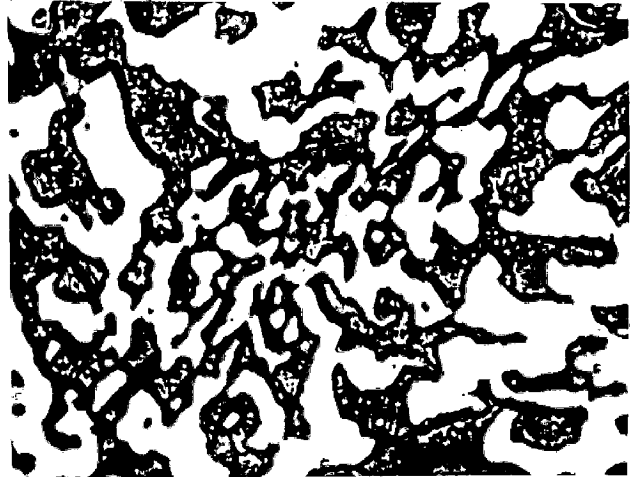
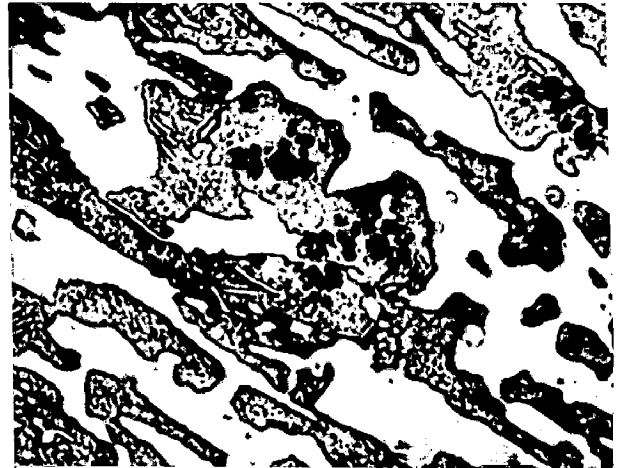
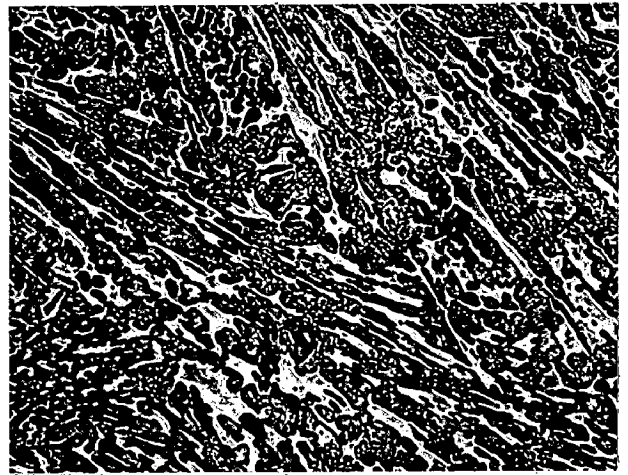
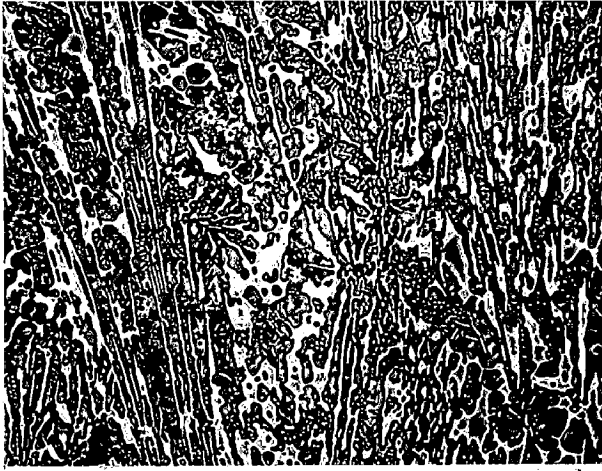


Figure 5.32

(a) C2, 900, 2
x 200

(b) C2, 900, 2
x 1000

(c) C2, 900, 2
x 1000

(d) C2, 900, 2
x 1000

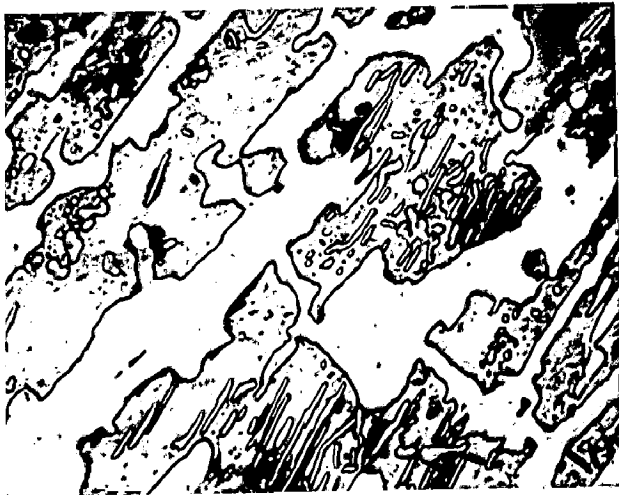


Figure 5.32

(e)	C2, 900, 6 x 200	(f)	C2, 900, 6 x 1000
(g)	C2, 900, 6 x 1000	(h)	C2, 900, 6 x 200
(i)	C2, 900, 10 x 1000	(j)	C2, 900, 10 x 1000

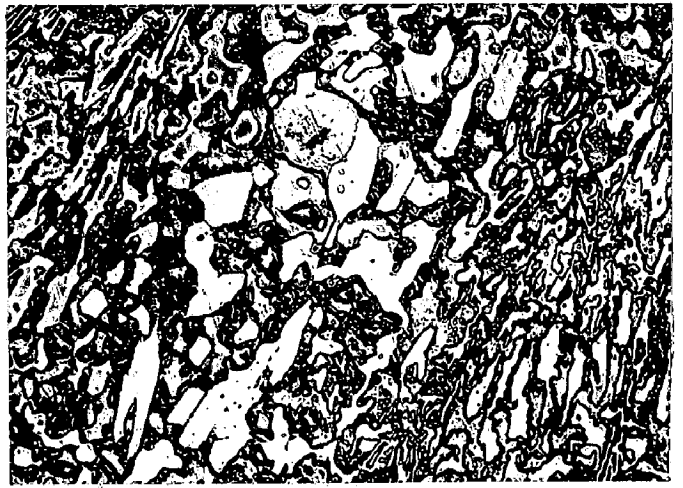
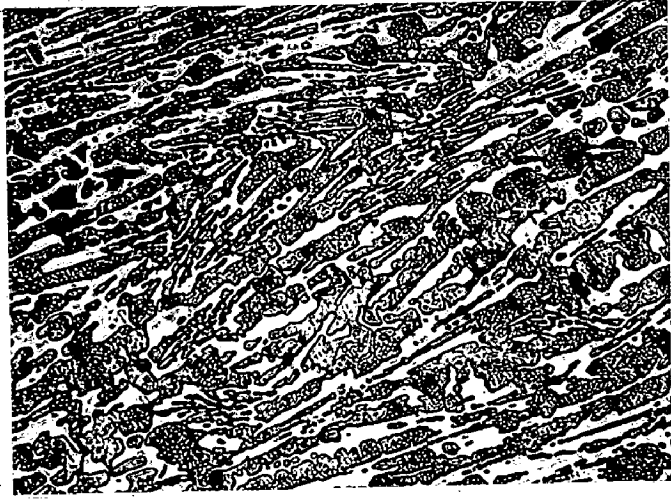


Figure 5.33

- | | | | |
|-----|----------------------|-----|----------------------|
| (a) | C2, 950, 2
x 200 | (b) | C2, 950, 2
x 1000 |
| (c) | C2, 950, 2
x 1000 | (d) | C2, 950, 6
x 200 |
| (e) | C2, 950, 6
x 1000 | (f) | C2, 950, 6
x 200 |

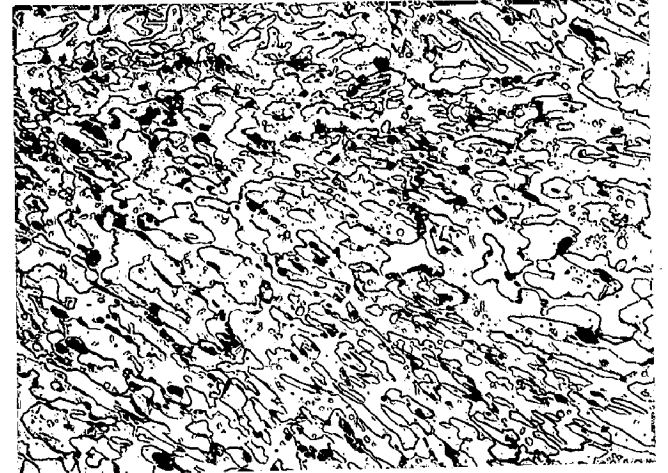
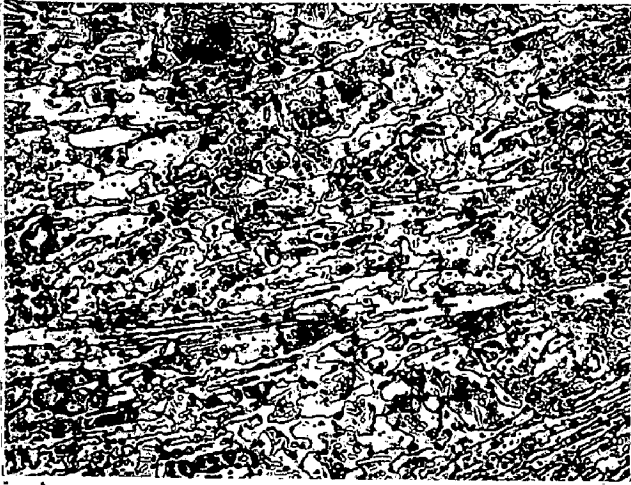


Figure 5.33

(g) C2, 950, 10
x 200

(h) C2, 950, 10
x 1000

(i) C2, 950, 10
x 1000

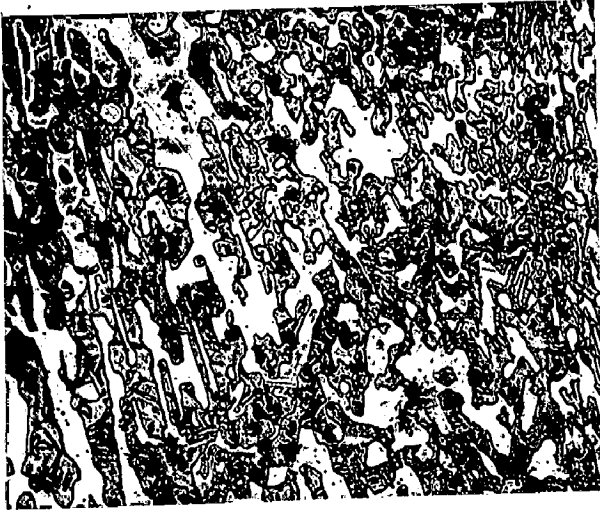


Figure 5.34

- (a) C2, 1000, 2
x 200
- (b) C2, 1000, 2
x 1000
- (c) C2, 1000, 2
x 1000
- (d) C2, 1000, 6
x 1000
- (e) C2, 1000, 6
x 1000



Figure 5.34

- | | | | |
|-----|------------------------|-----|------------------------|
| (f) | C2, 1000, 6
x 200 | (g) | C2, 1000, 10
x 1000 |
| (h) | C2, 1000, 10
x 1000 | (i) | C2, 1000, 10
x 1000 |

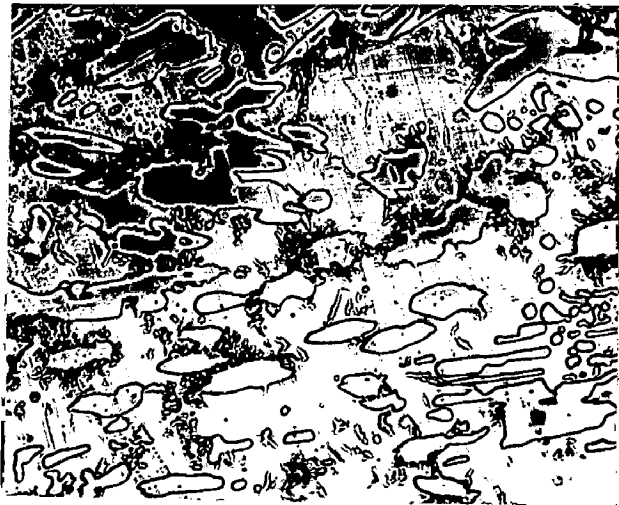


Figure 5.35

(a) C2, 1050, 2
x 200

(b) C2, 1050, 2
x 200

(c) C2, 1050, 2
x 1000

(d) C2, 1050, 2
x 1000

(e) C2, 1050, 6
x 1000

(f) C2, 1050, 6
x 1000

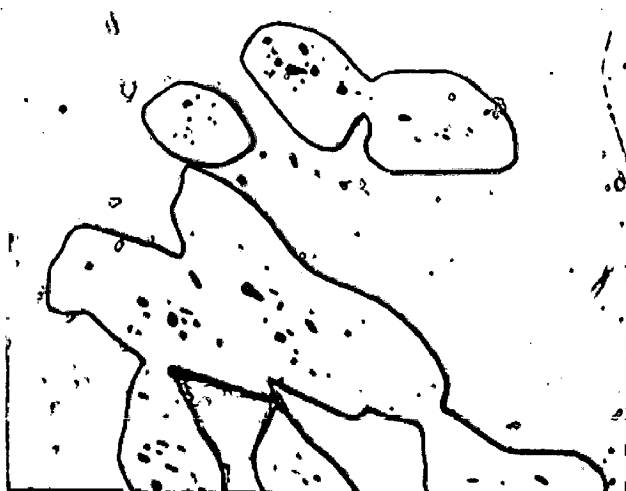
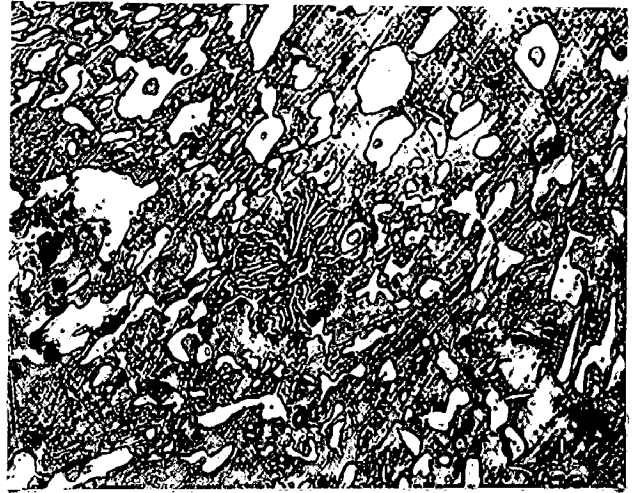


Figure 5.35.

- | | |
|----------------------------|----------------------------|
| (g) C2, 1050, 6
x 1000 | (h) C2, 1050, 6
x 1000 |
| (i) C2, 1050, 10
x 200 | (j) C2, 1050, 10
x 200 |
| (k) C2, 1050, 10
x 1000 | (l) C2, 1050, 10
x 1000 |

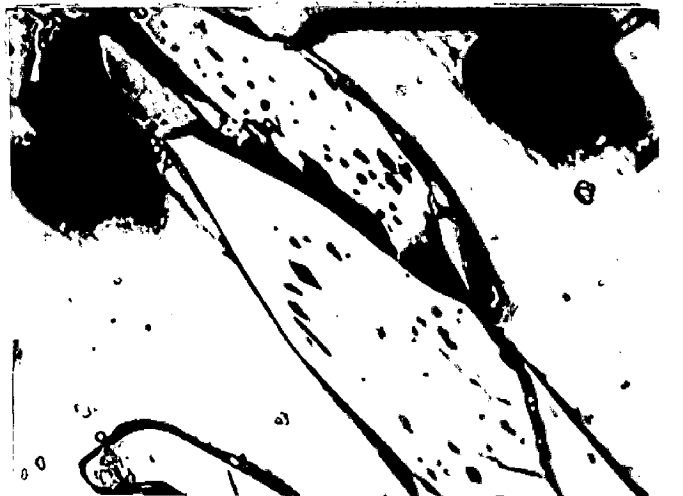
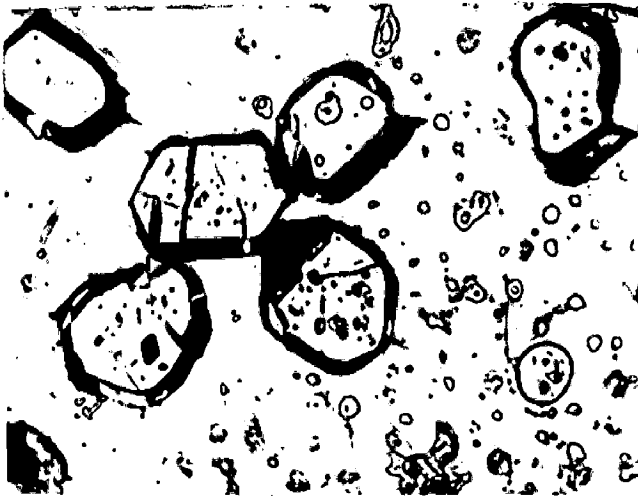
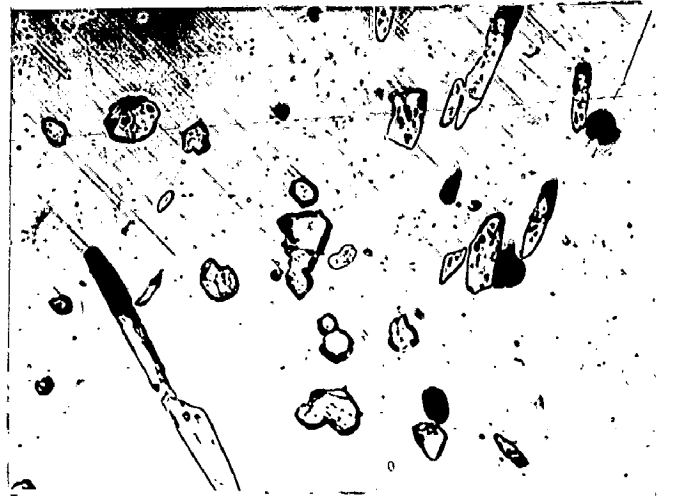
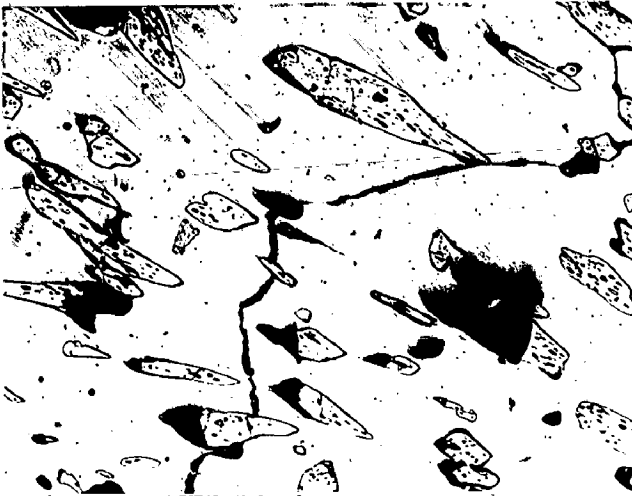


Figure 5.36

- (a) C3, As cast
x 200
- (b) C3, As cast
x 200
- (c) C3, As cast
x 1000

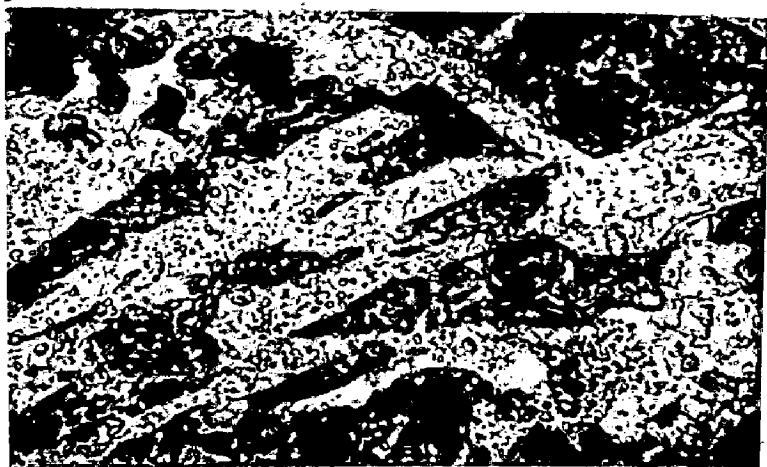
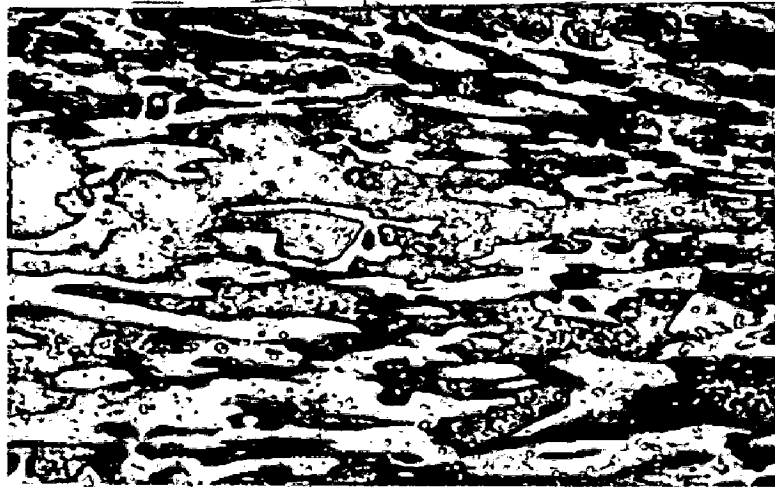


Figure 5.37

- | | |
|---------------------------|---------------------------|
| (a) C3, 800, 2
x 200 | (b) C3, 800, 2
x 1000 |
| (c) C3, 800, 6
x 200 | (d) C3, 800, 6
x 1000 |
| (e) C3, 800, 6
x 1000 | (f) C3, 800, 10
x 200 |
| (g) C3, 800, 10
x 1000 | (h) C3, 800, 10
x 1000 |

Figure 5.38

- | | |
|-------------------------|---------------------------|
| (a) C3, 850, 2
x 200 | (b) C3, 850, 2
x 1000 |
| (c) C3, 850, 6
x 200 | (d) C3, 850, 6
x 1000 |
| (e) C3, 850, 6
x 200 | (f) C3, 850, 10
x 1000 |

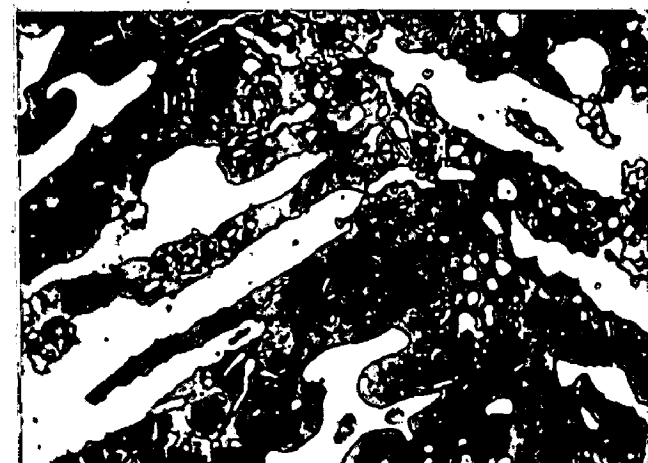
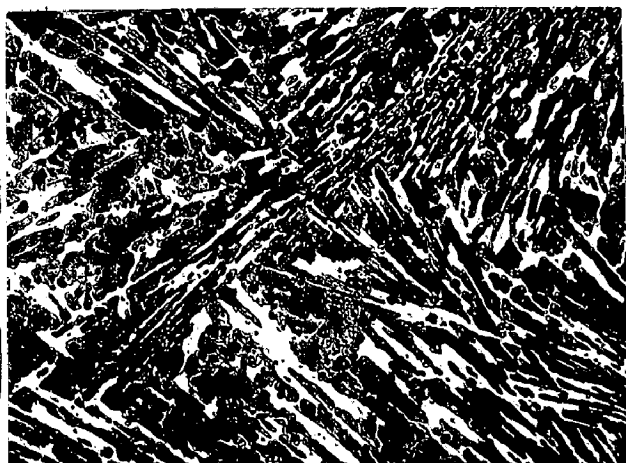
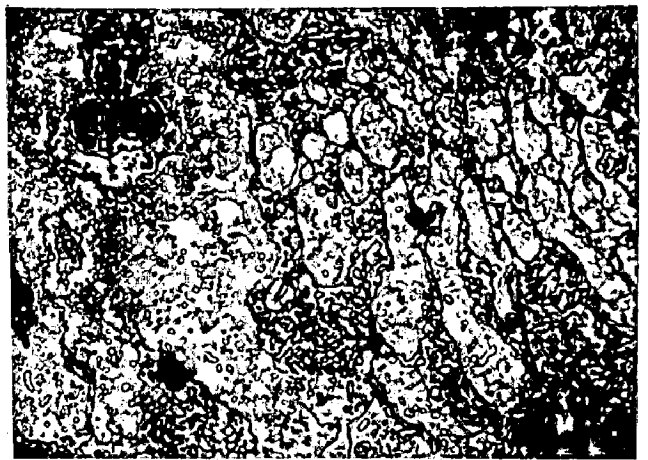
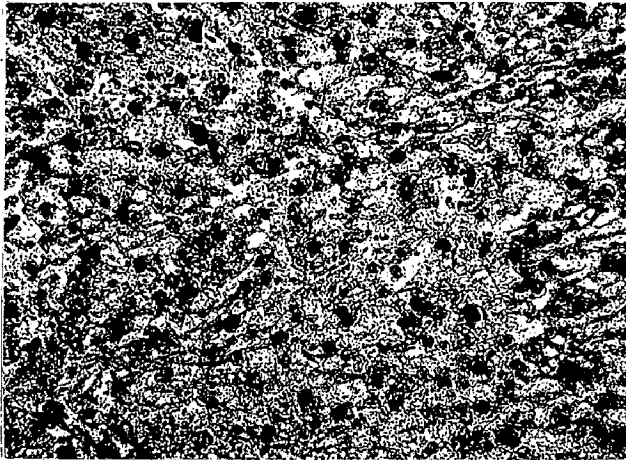


Figure 5.39

- (a) C3, 900, 2
x 200
- (b) C3, 900, 2
x 1000
- (c) C3, 900, 2
x 1000
- (d) C3, 900, 6
x 200
- (e) C3, 900, 6
x 1000

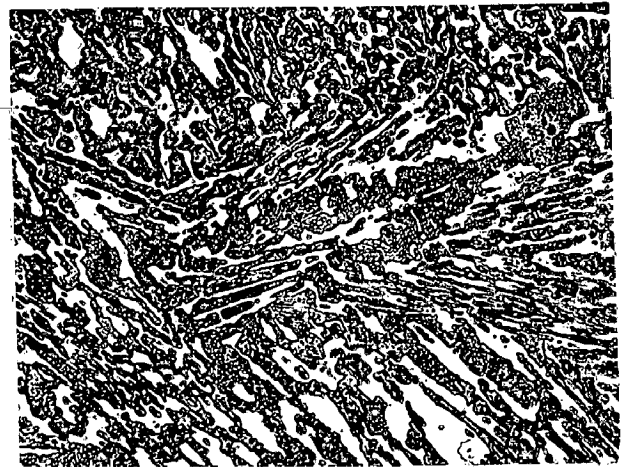
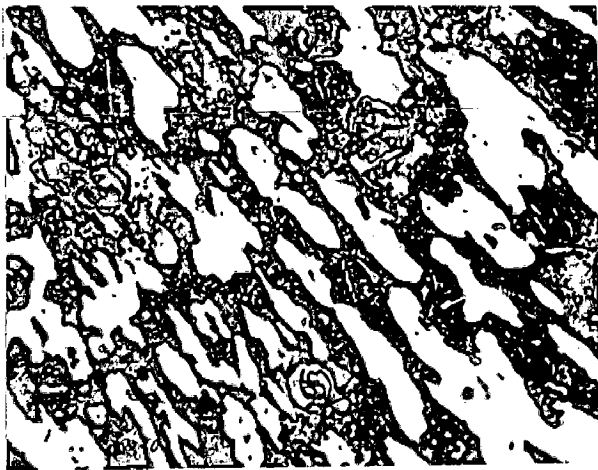
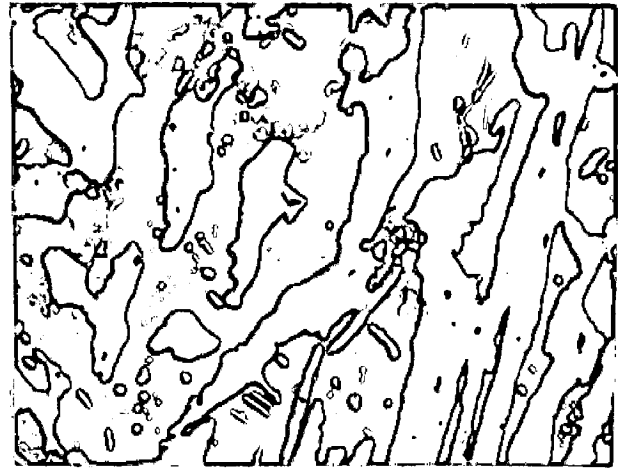
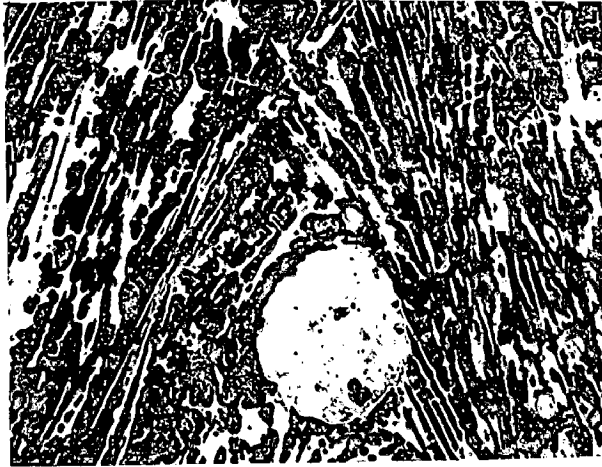


Figure 5.39

(f)	C3, 900, 6 x 1000	(g)	C3, 900, 10 x 200
(h)	C3, 900, 10 x 1000	(i)	C3, 900, 10 x 1000

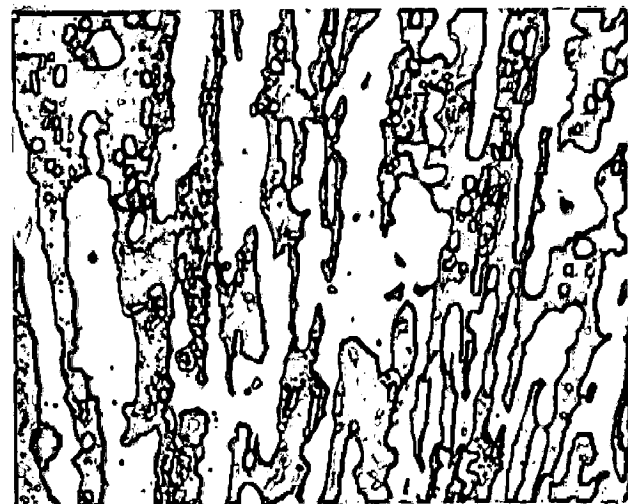
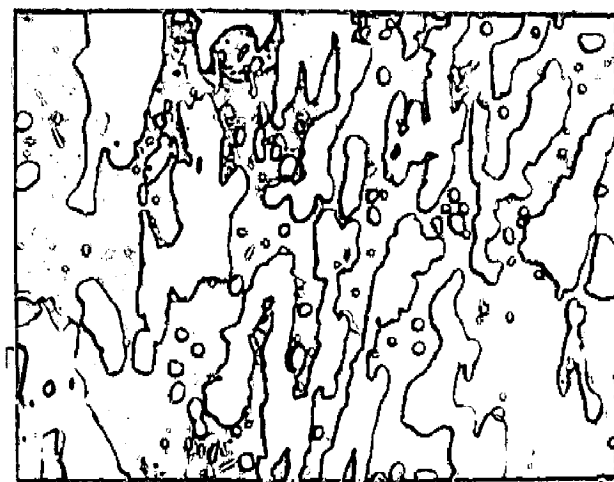
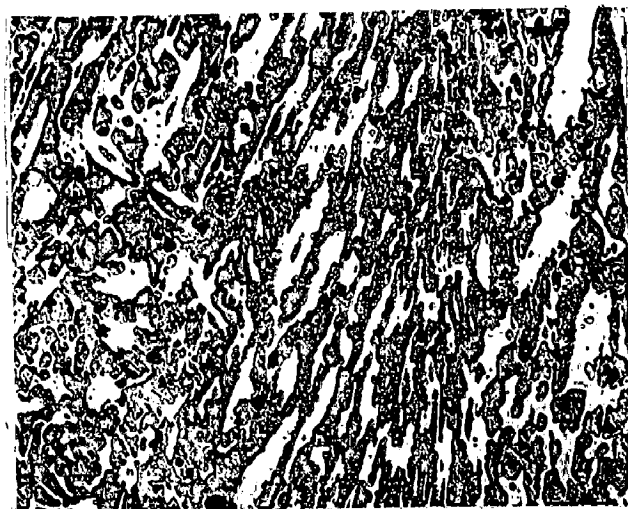
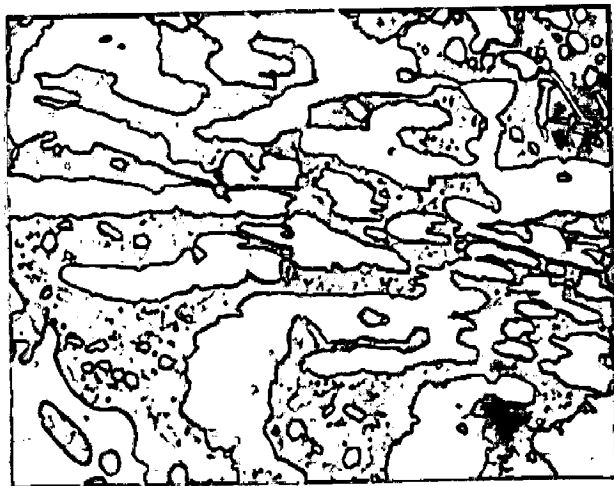


Figure 5.40

- | | |
|---------------------------|--------------------------|
| (a) C3, 950, 2
x 200 | (b) C3, 950, 2
x 1000 |
| (c) C3, 950, 6
x 200 | (d) C3, 950, 6
x 200 |
| (e) C3, 950, 6
x 1000 | (f) C3, 950, 10
x 200 |
| (g) C3, 950, 10
x 1000 | |

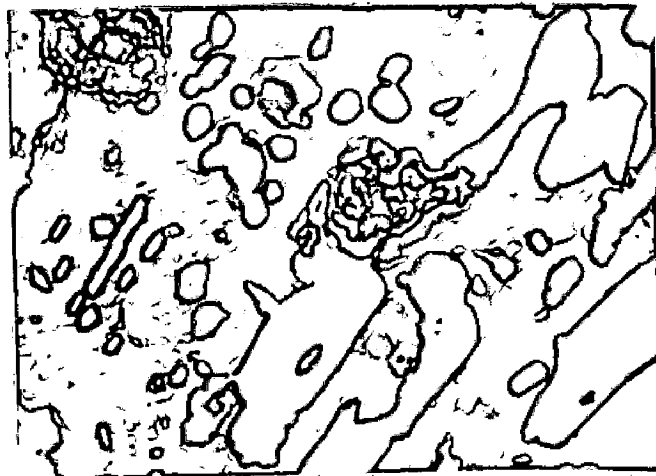
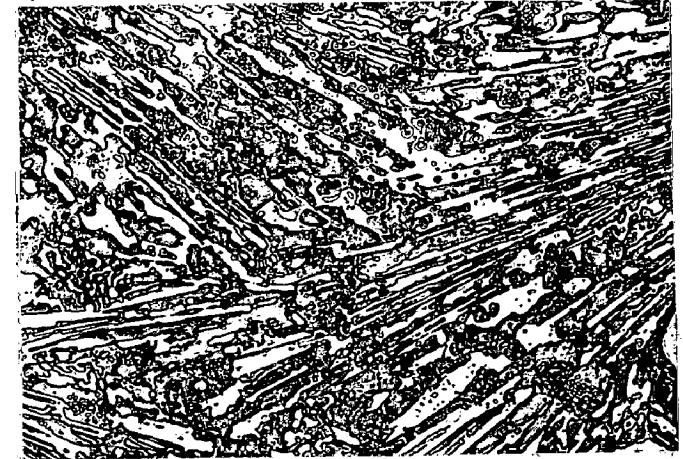
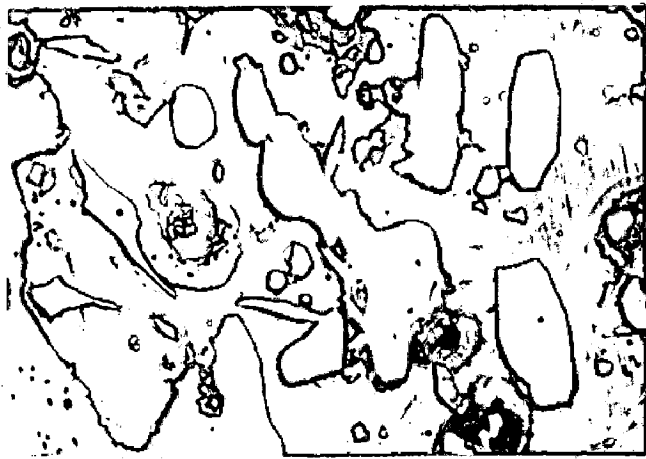
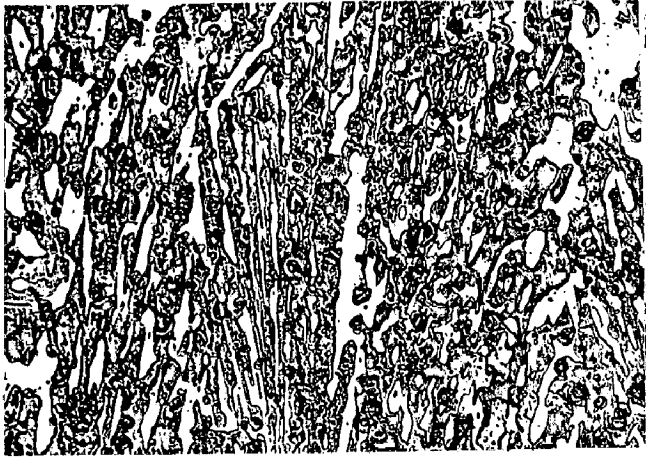
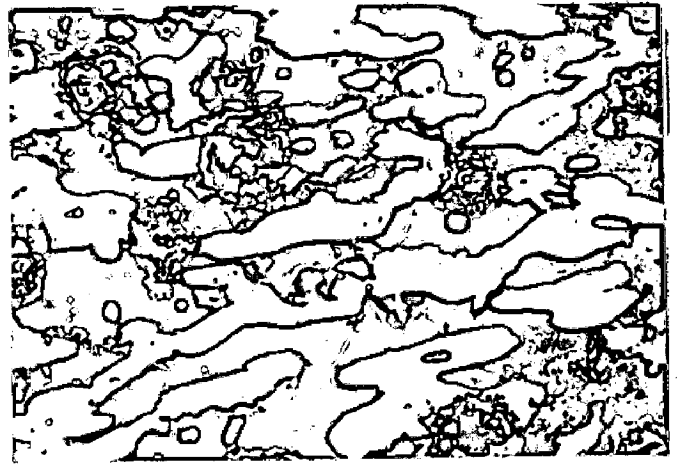
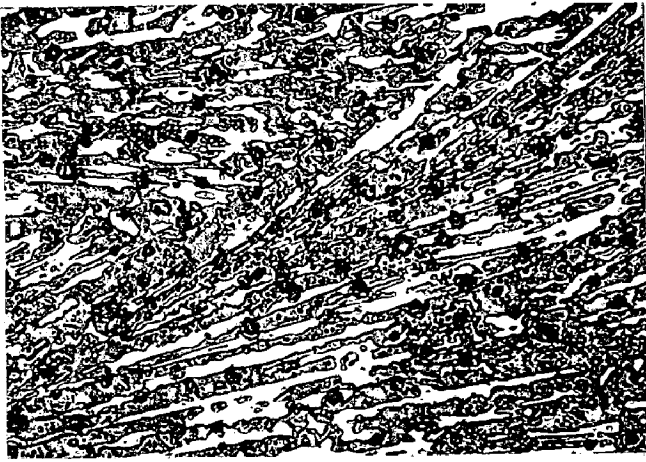


Figure 5.41

- | | |
|----------------------------|----------------------------|
| (a) C3, 1000, 2
x 200 | (b) C3, 1000, 2
x 1000 |
| (c) C3, 1000, 2
x 1000 | (d) C3, 1000, 6
x 200 |
| (e) C3, 1000, 6
x 1000 | (f) C3, 1000, 10
x 200 |
| (g) C3, 1000, 10
x 1000 | (h) C3, 1000, 10
x 1000 |

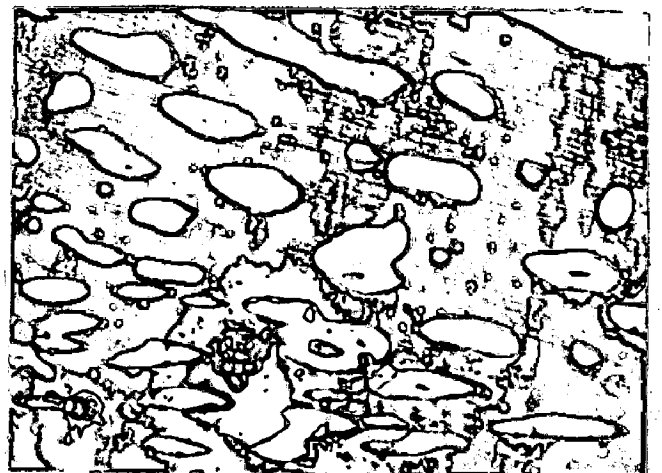
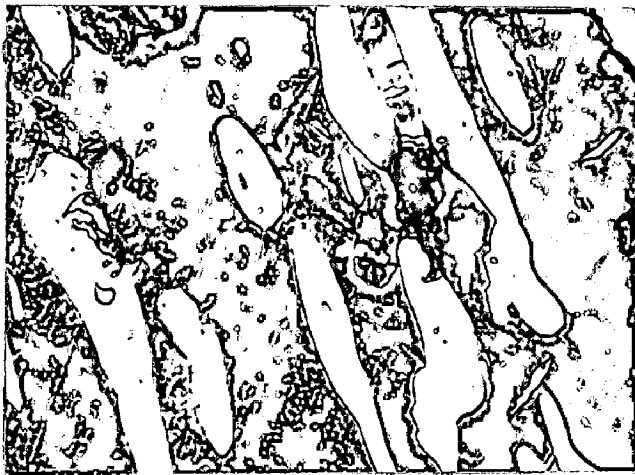
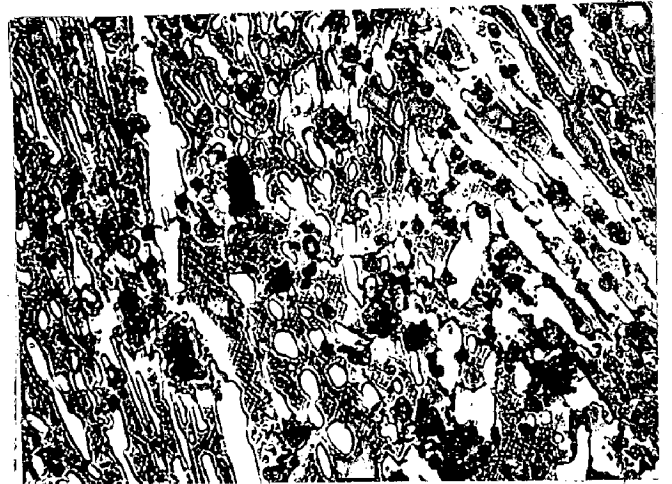
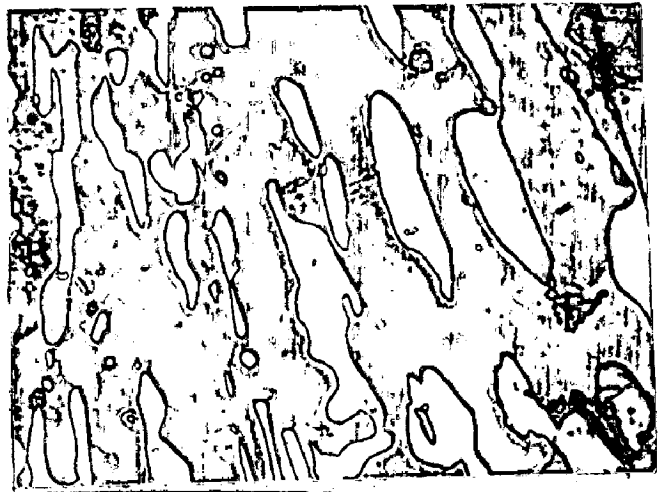


Figure 5.42

- | | |
|---------------------------|---------------------------|
| (a) C3, 1050, 2
x 200 | (b) C3, 1050, 2
x 200 |
| (c) C3, 1050, 2
x 1000 | (d) C3, 1050, 2
x 1000 |
| (e) C3, 1050, 2
x 1000 | (f) C3, 1050, 6
x 200 |

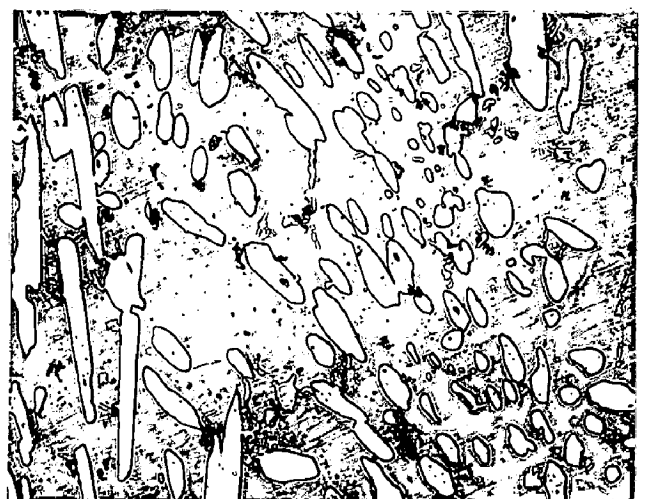
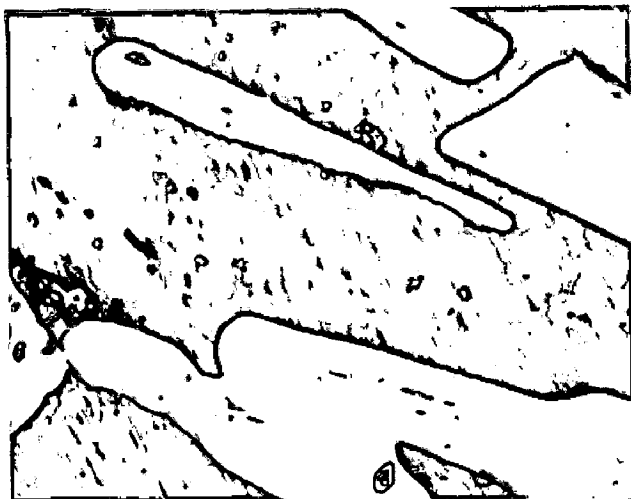
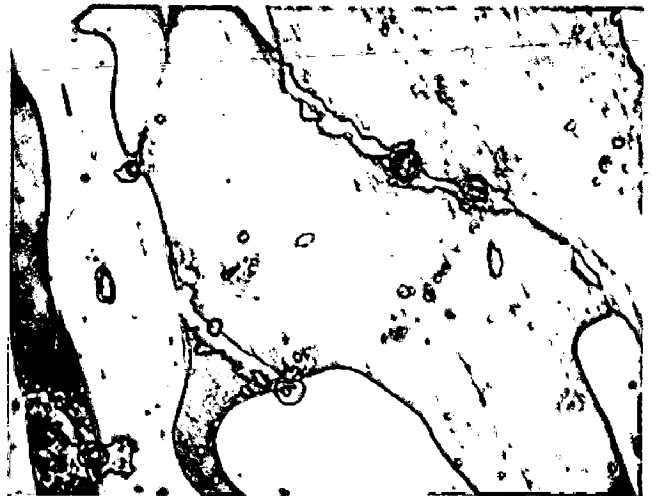
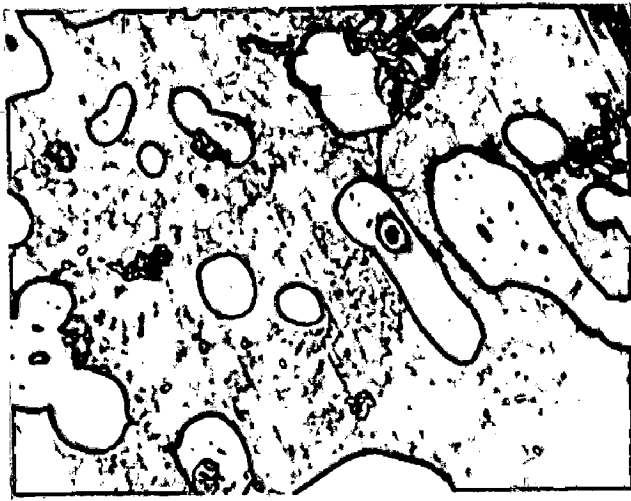
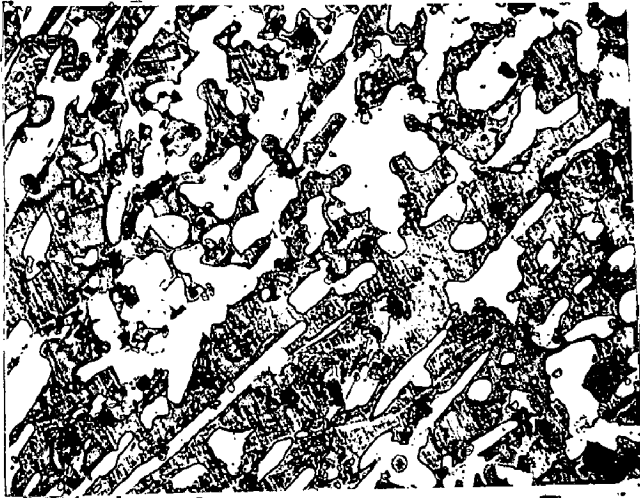
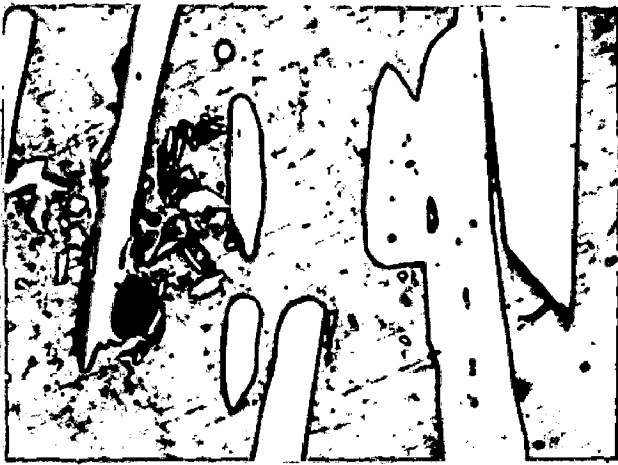
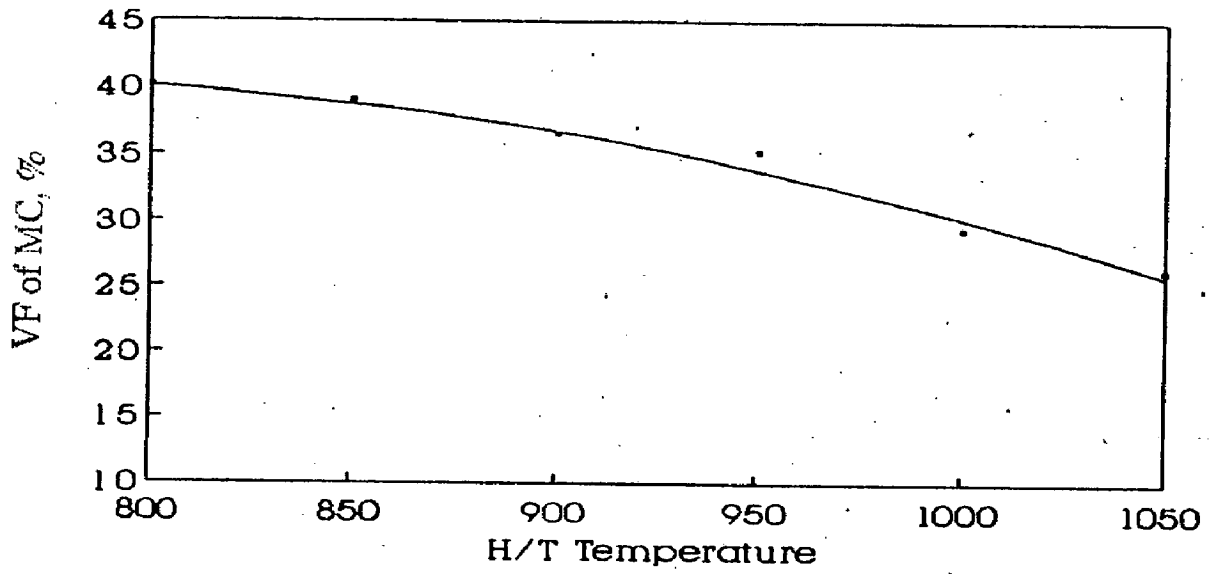


Figure 5.42

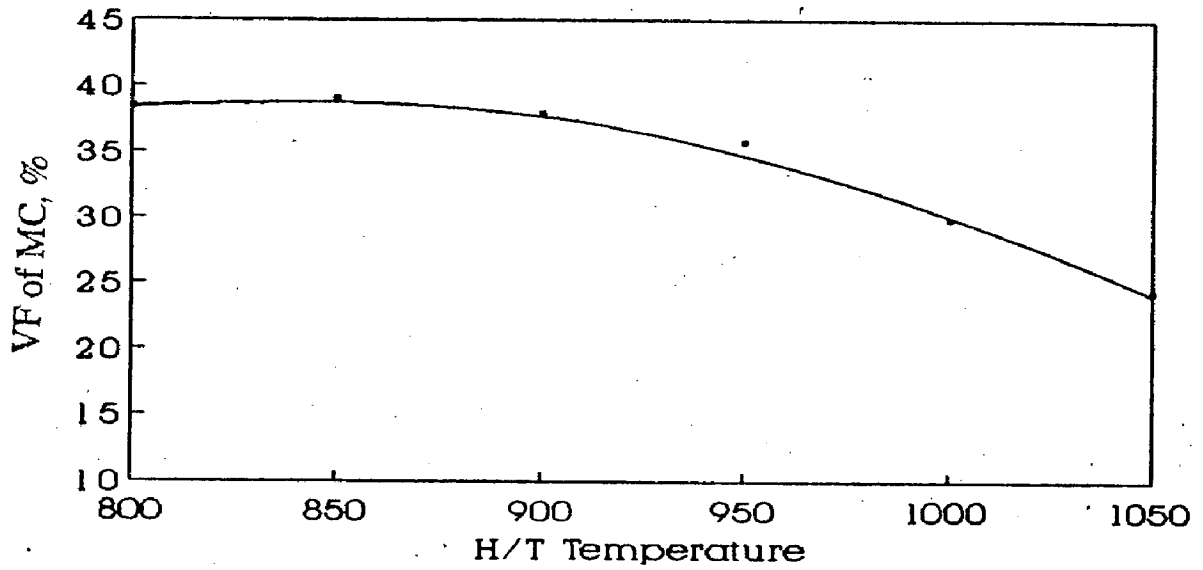
- | | | | |
|-----|------------------------|-----|------------------------|
| (g) | C3, 1050, 6
x 1000 | (h) | C3, 1050, 6
x 1000 |
| (i) | C3, 1050, 10
x 1000 | (j) | C3, 1050, 10
x 200 |
| (k) | C3, 1050, 10
x 200 | (l) | C3, 1050, 10
x 1000 |
| | (m) | | C3, 1050, 10 |



C1,2 HOURS



C1,4 HOURS



C1,6 HOURS

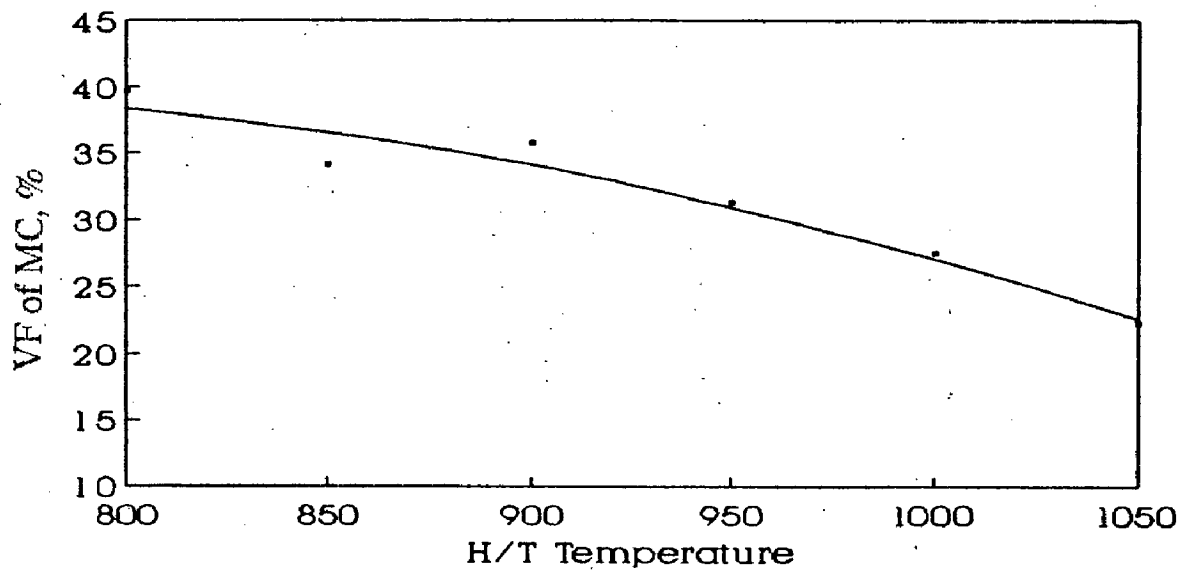
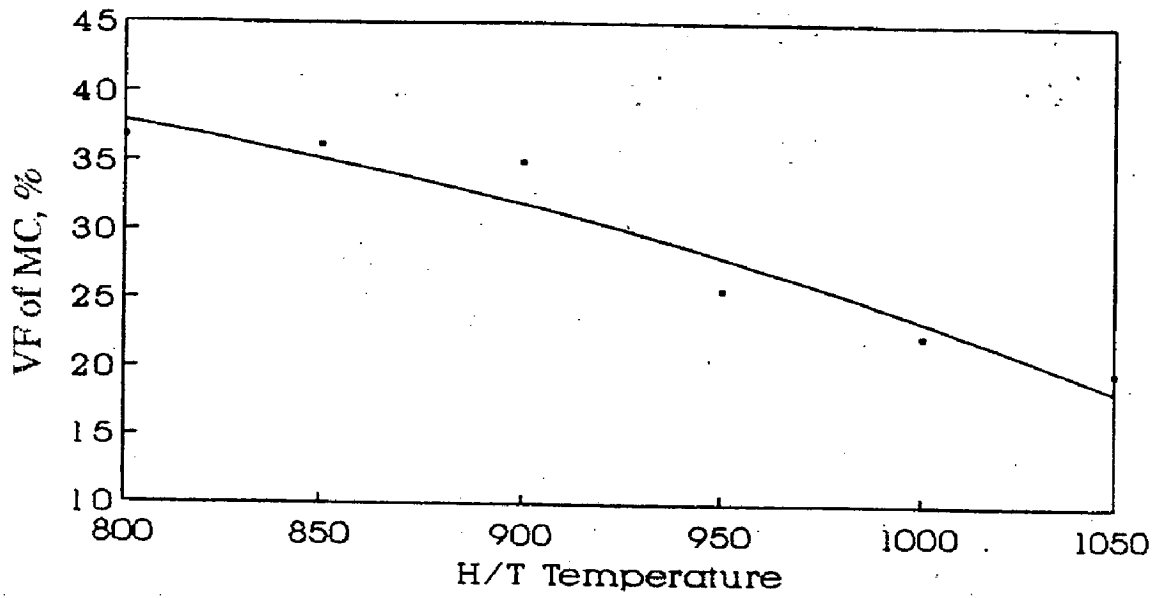


Fig. 5.43 : Effect of heat treatment on volume fraction of massive carbide (Alloy C1)

C1, 8 HOURS



C1, 10 HOURS

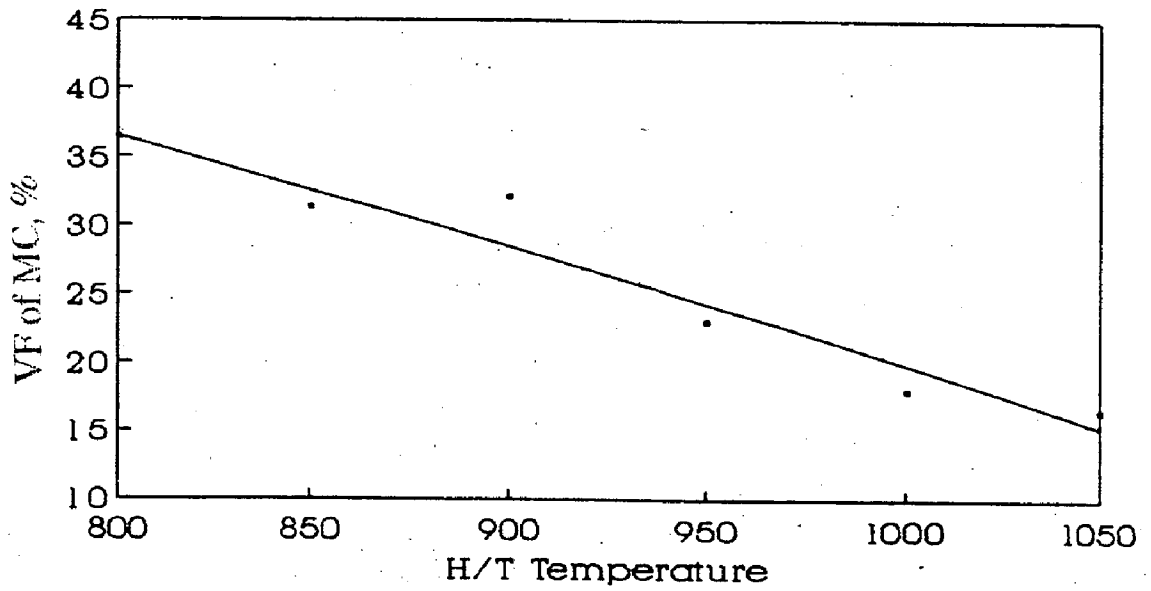
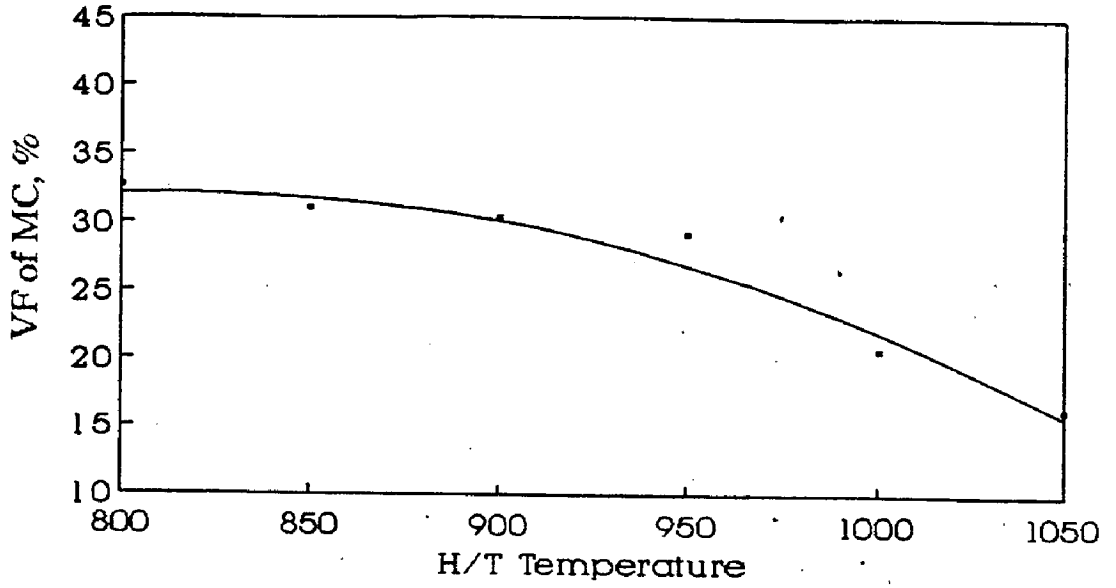


Fig. 5.43 : Effect of heat treatment on volume fraction of massive carbide (Alloy C1)

C2,8 HOURS



C2,10 HOURS

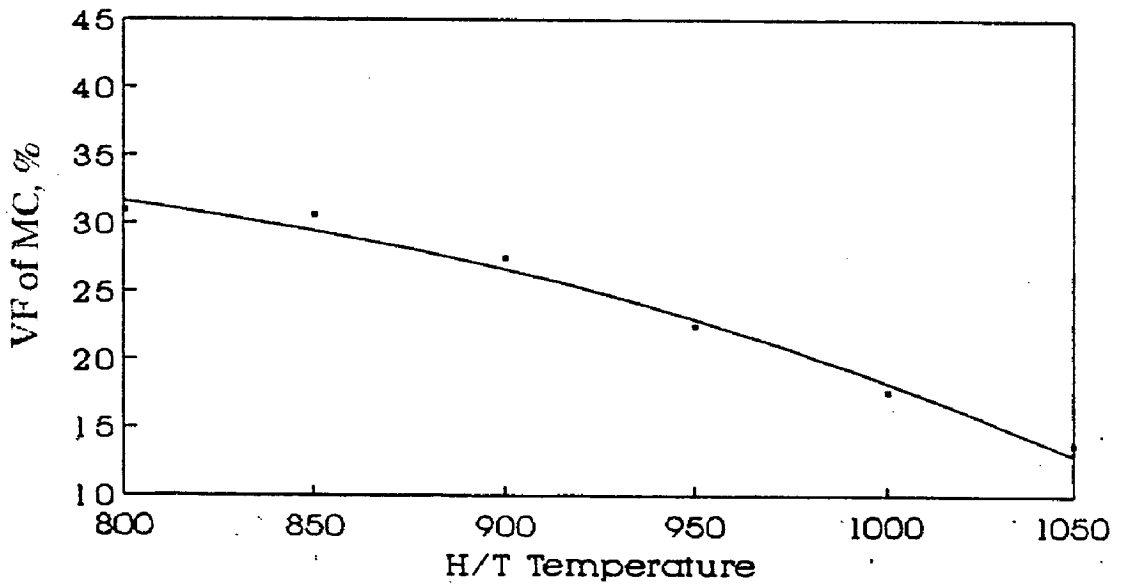
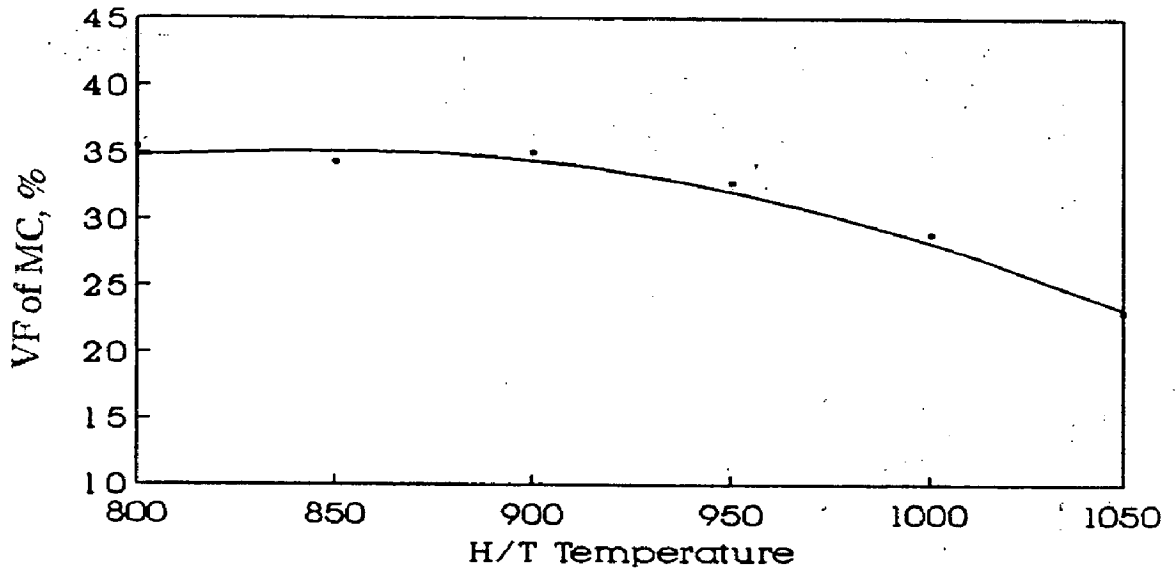
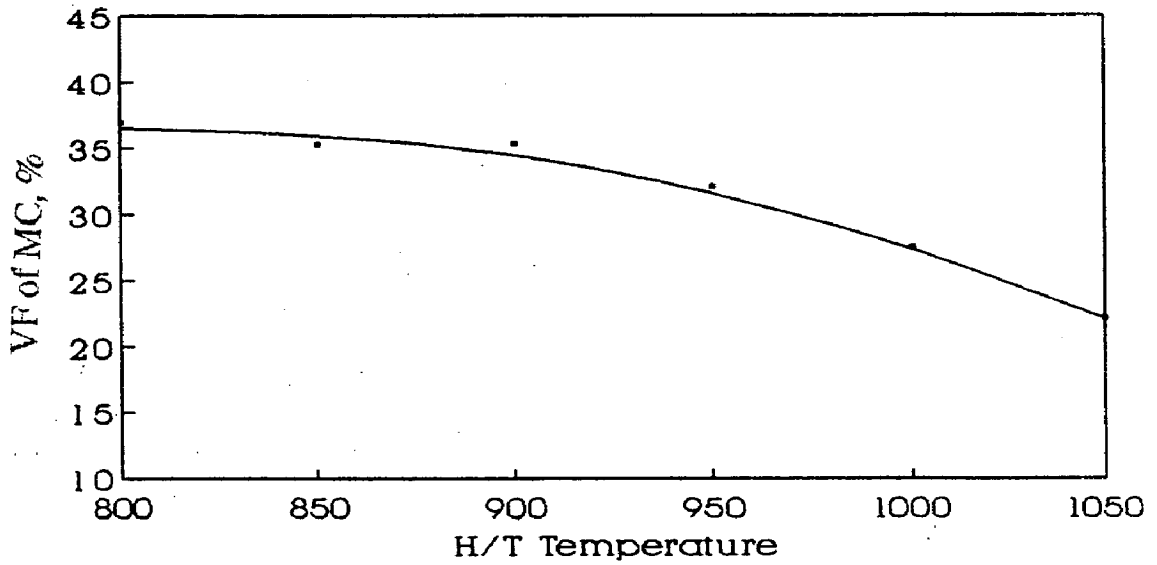


Fig. 5.44 : Effect of heat treatment on volume fraction of massive carbide (Alloy C2)

C2,2 HOURS



C2,4 HOURS



C2,6 HOURS

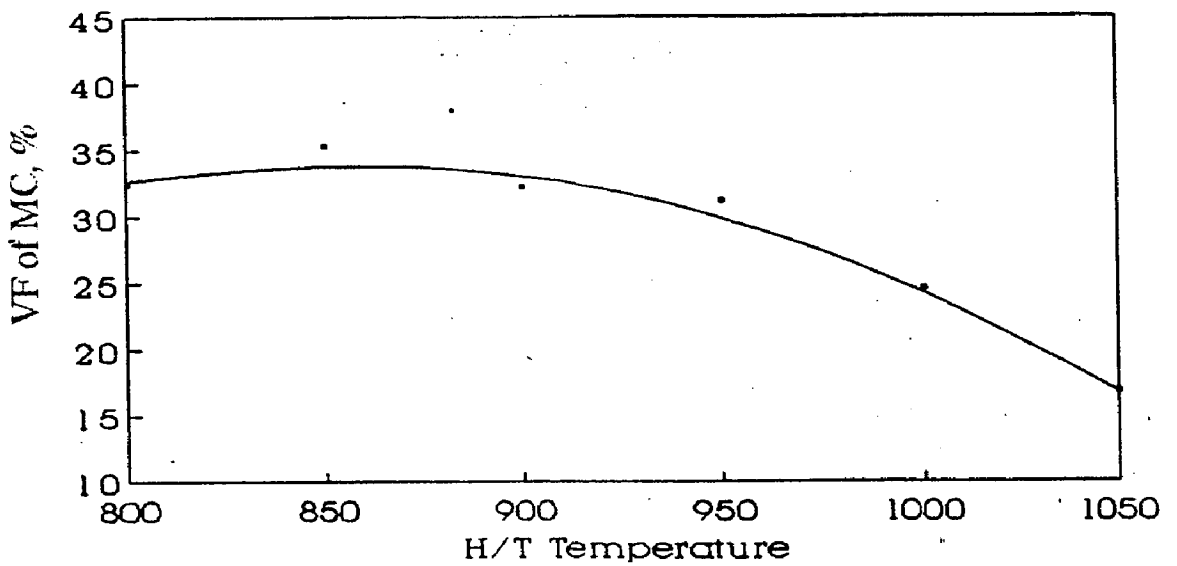
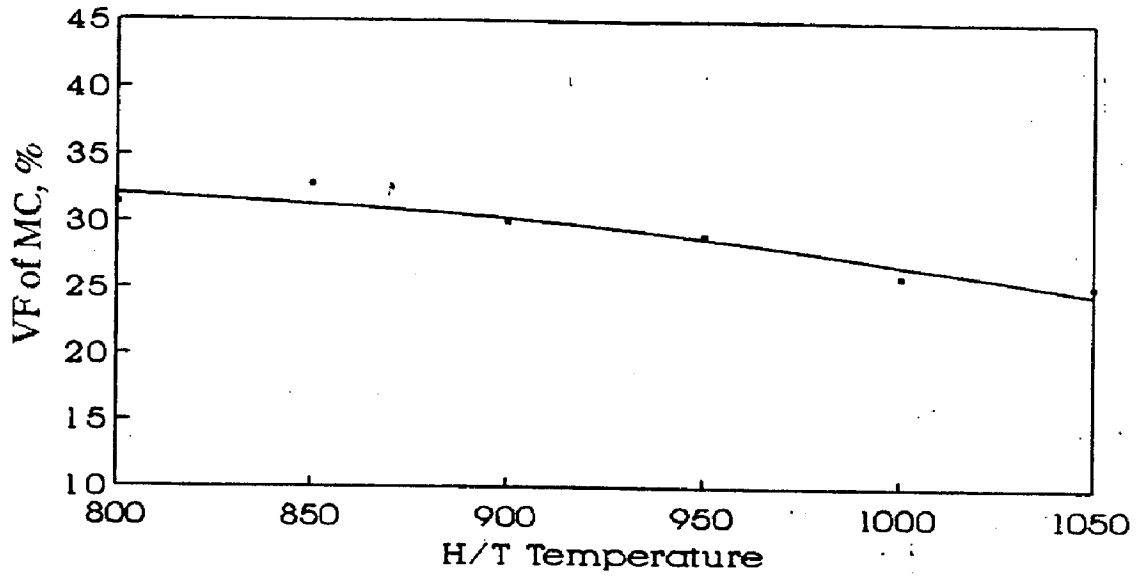
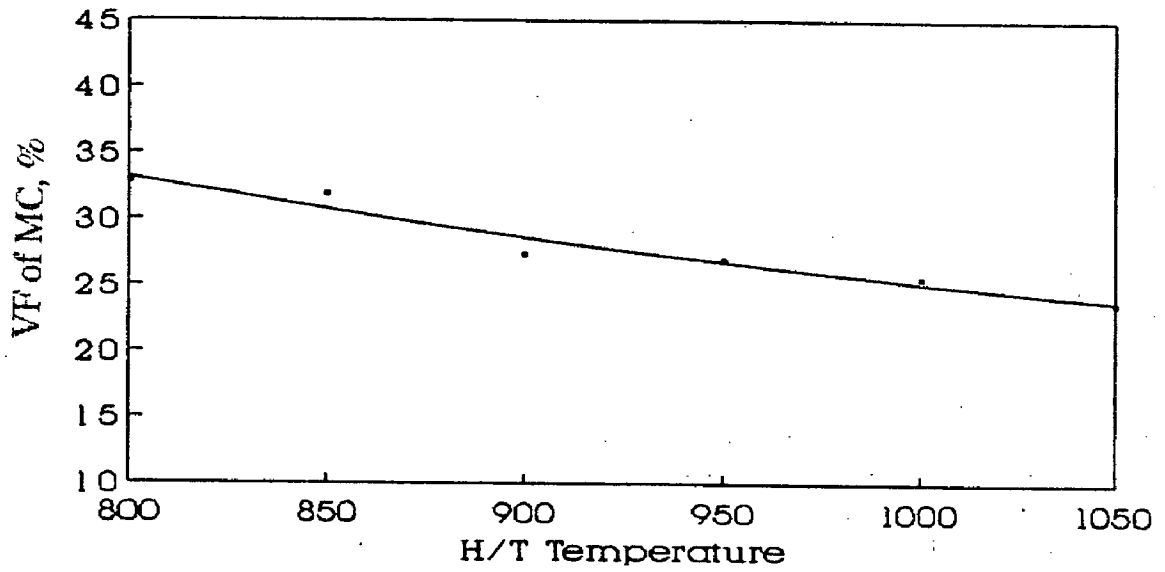


Fig. 5.44 : Effect of heat treatment on volume fraction of massive carbide (Alloy C2)

C3,2 HOURS



C3,4 HOURS



C3,6 HOURS

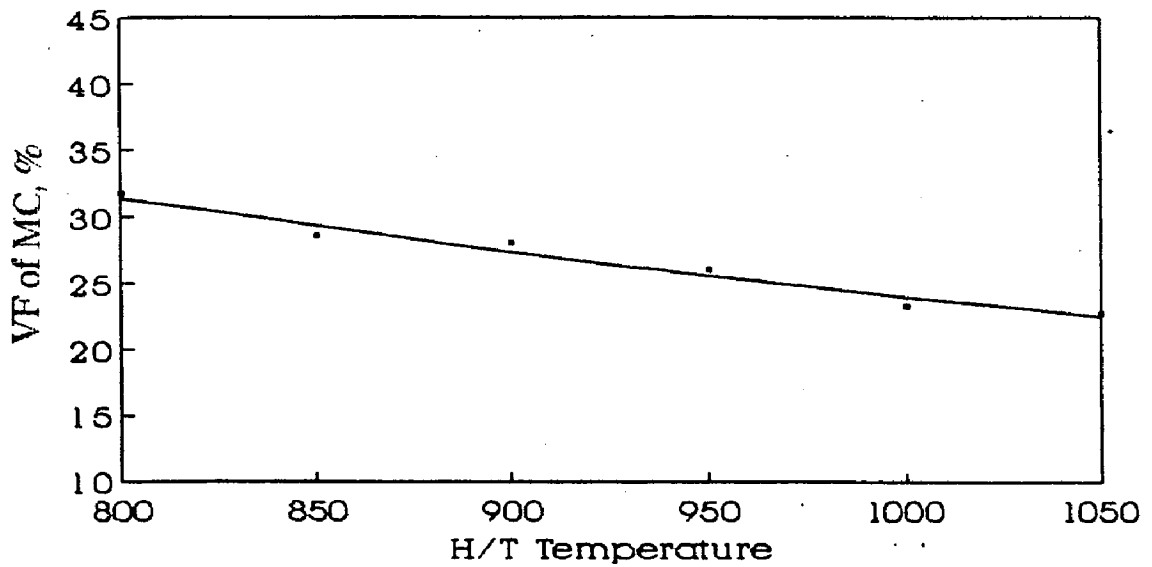
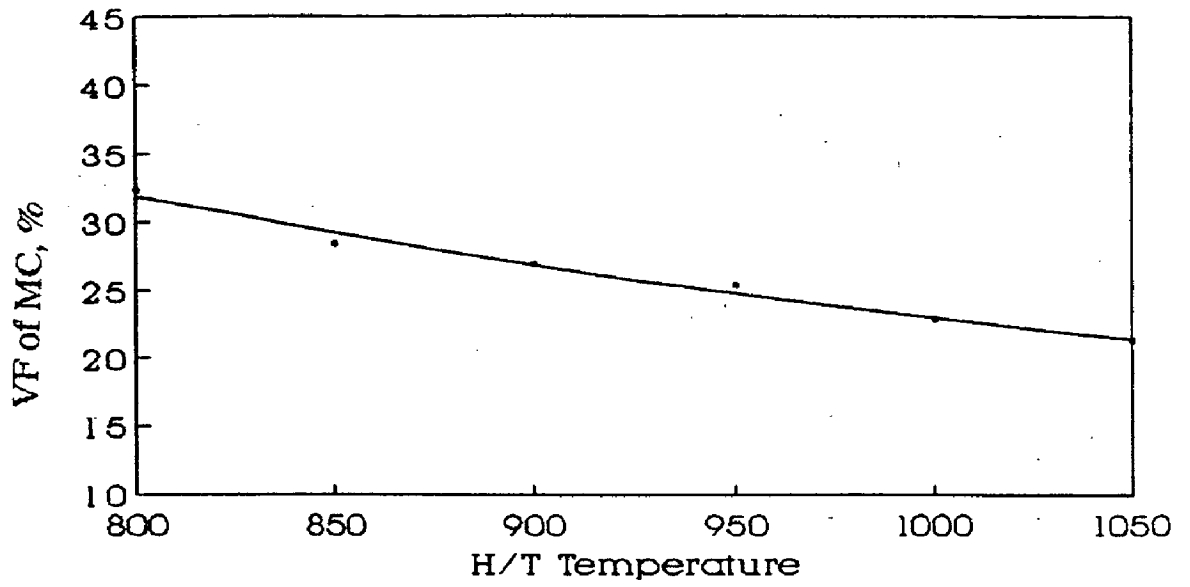


Fig. 5.45 : Effect of heat treatment on volume fraction of massive carbide (Alloy C3)

C3,8 HOURS



C3,10 HOURS

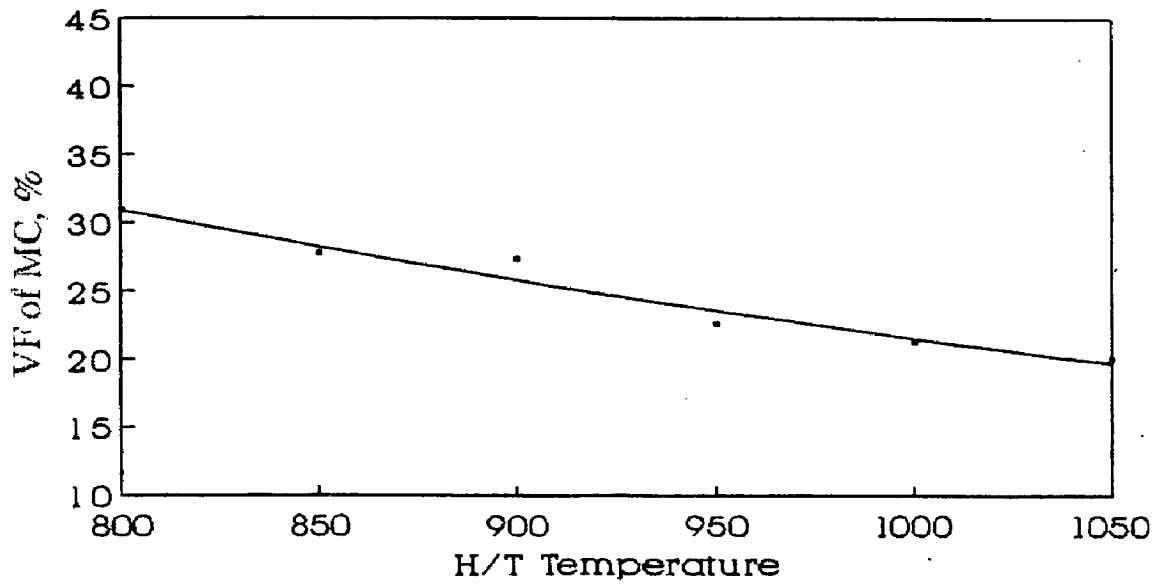
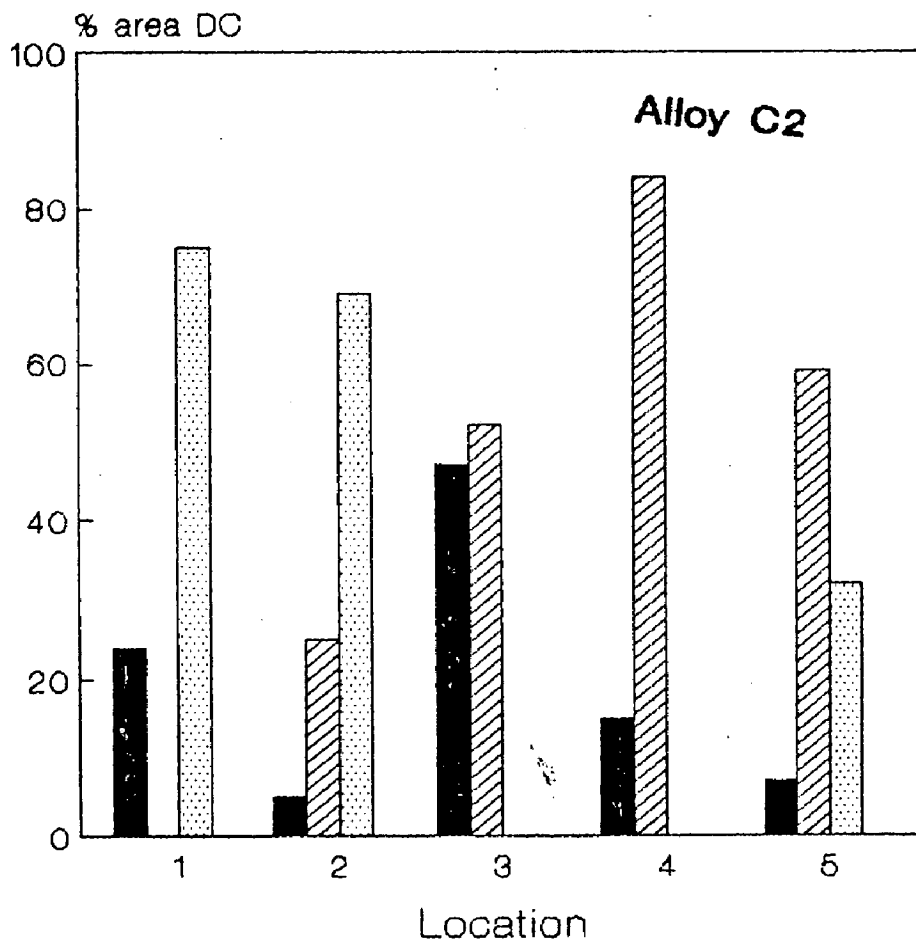
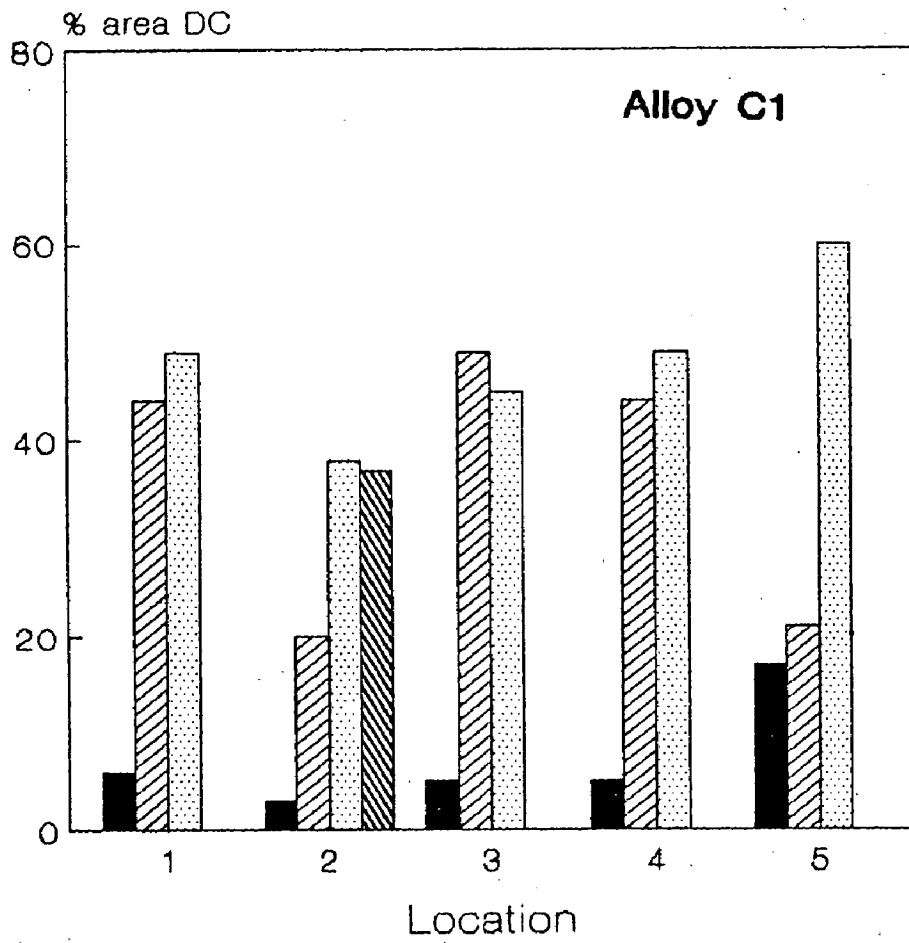


Fig. 5.45 : Effect of heat treatment on volume fraction of massive carbide (Alloy C3)

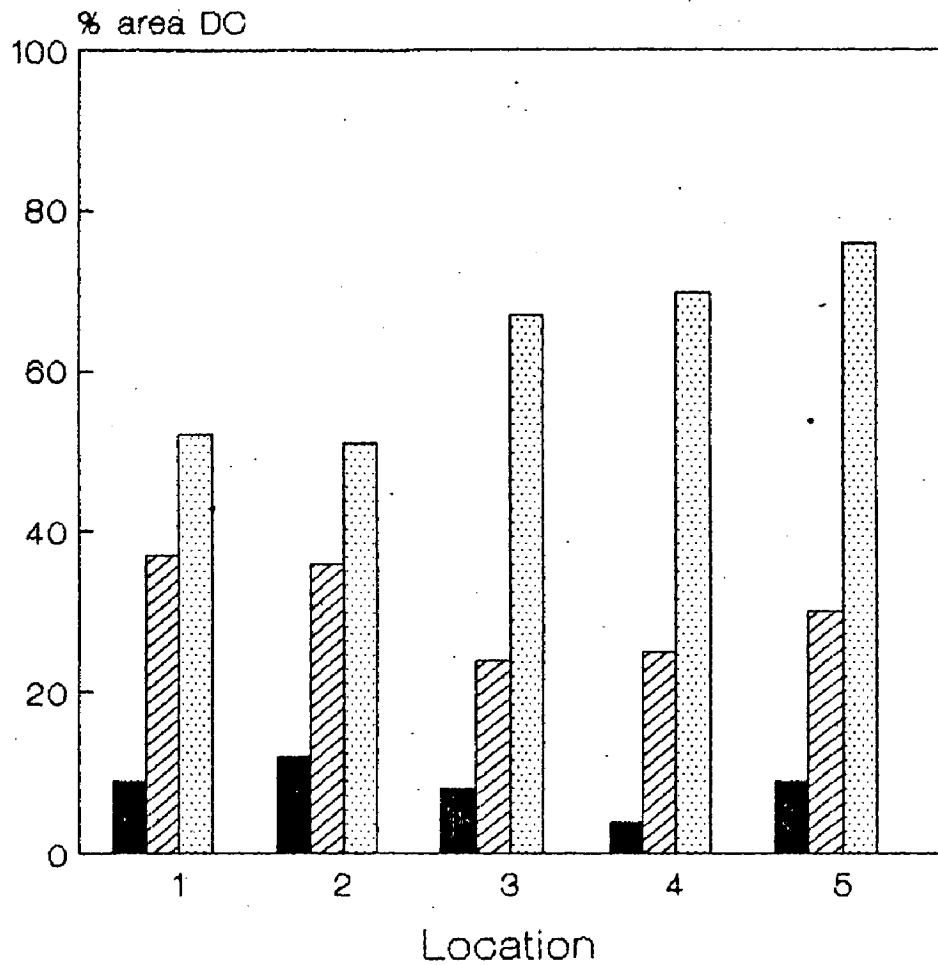


(a) 850 deg C, 10 hours heat treatment

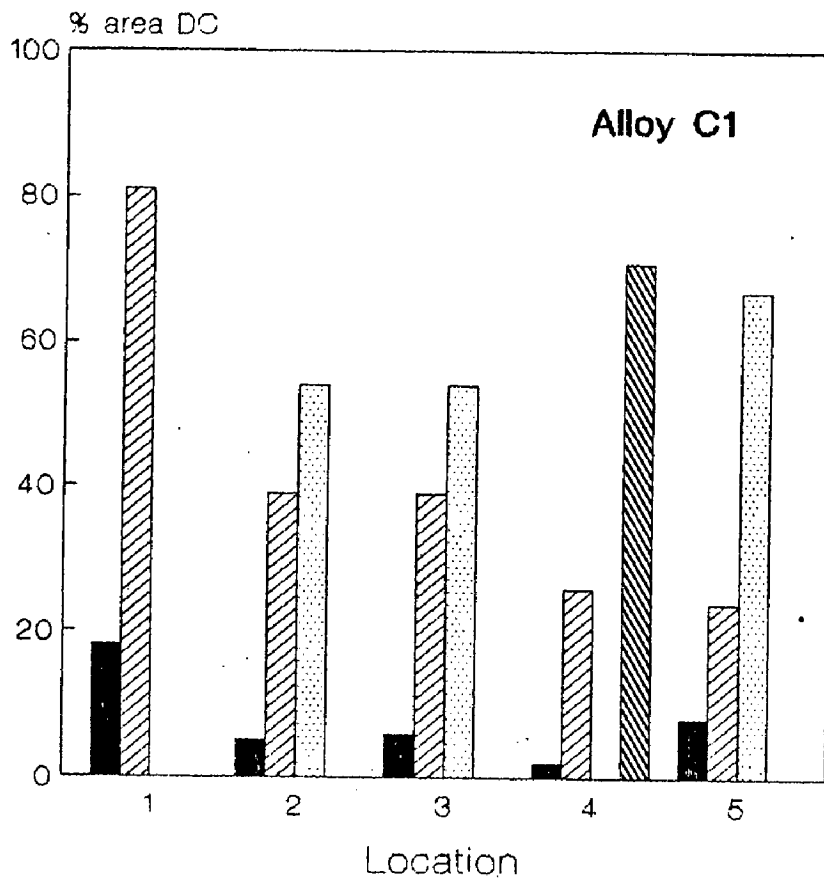
F73

Fig. 5.46 : % area of DCs in different classes at different locations,

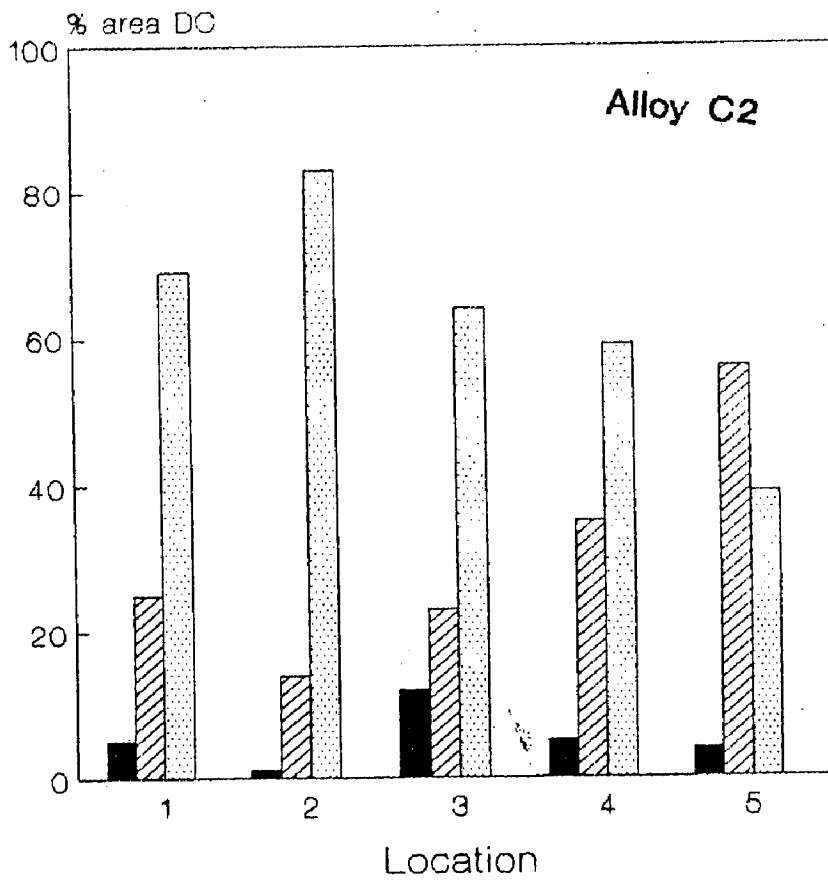
Fig. 5.46 : % area of DCs in different classes at different locations, Alloy C3



(a) 850 deg C, 10 hours heat treatment

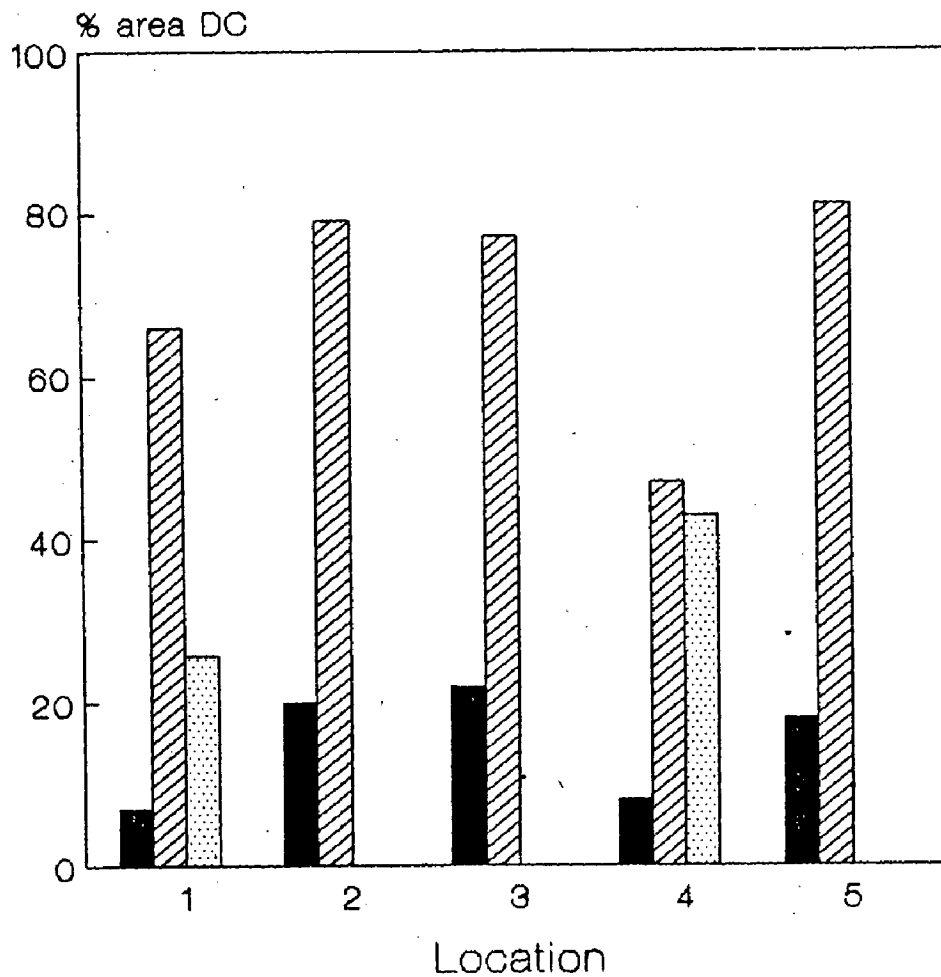


(a) 900 deg C, 10 hours heat treatment



(a) 900 deg C, 10 hours heat treatment

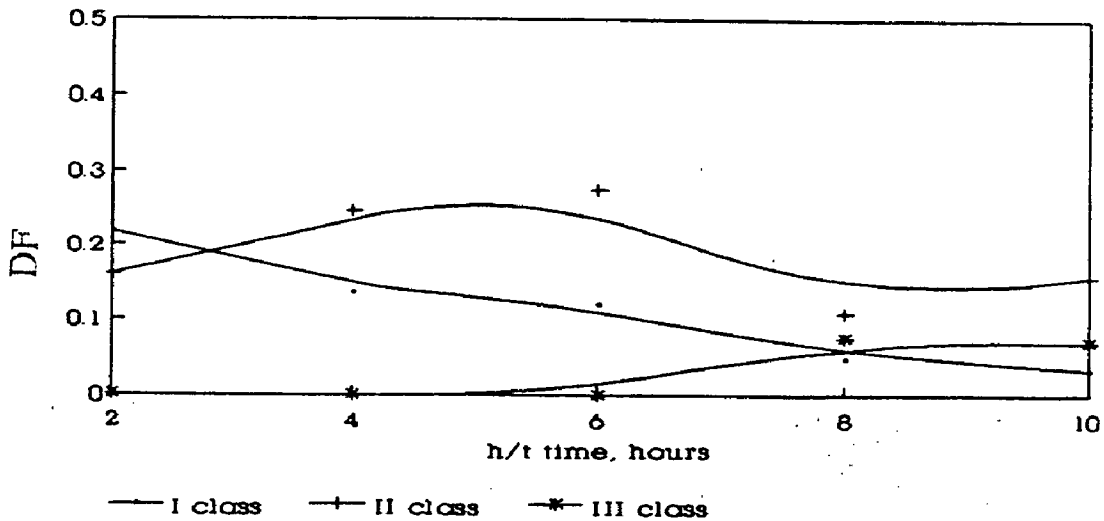
Fig. 5.47 : % area of DCs in different classes at different locations,



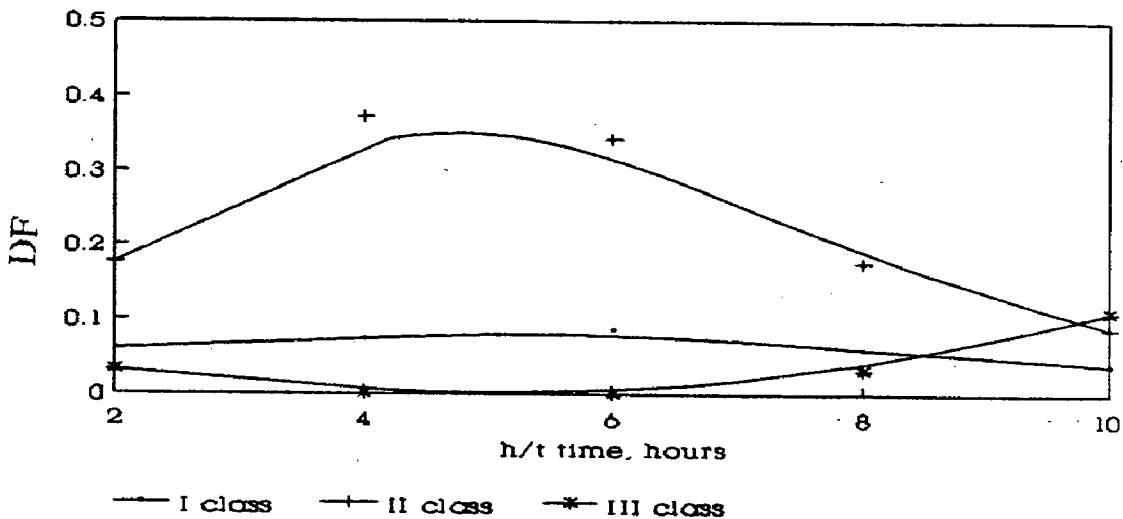
(a) 900 deg C, 10 hours heat treatment

Fig. 5.47 : % area of DCs in different classes at different locations, Alloy C3

(a) 800 deg.C



(b) 850 deg.C



(c) 900 deg.C

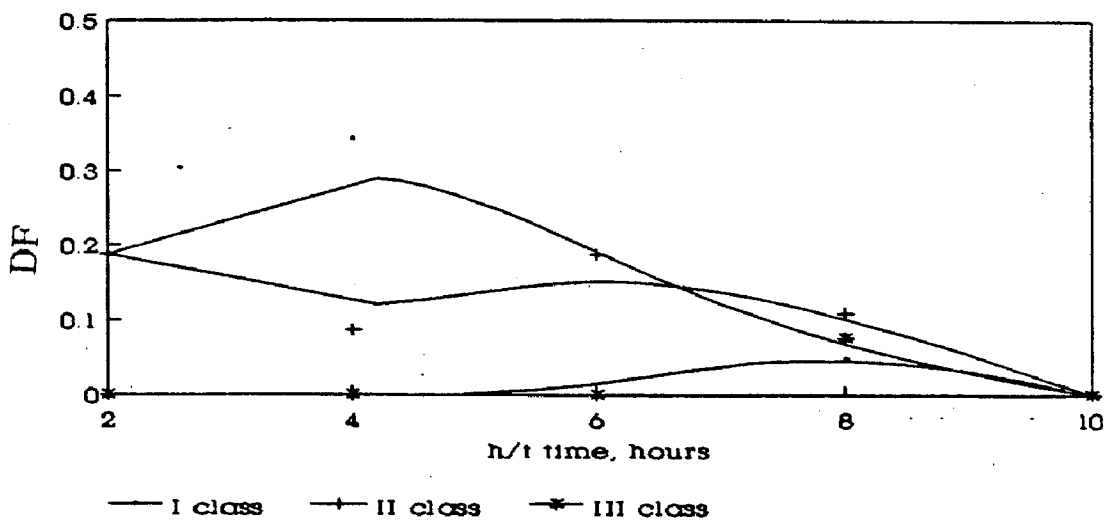


Fig. 5.48 : Effect of heat treatment on DF of DCs (Alloy C1)

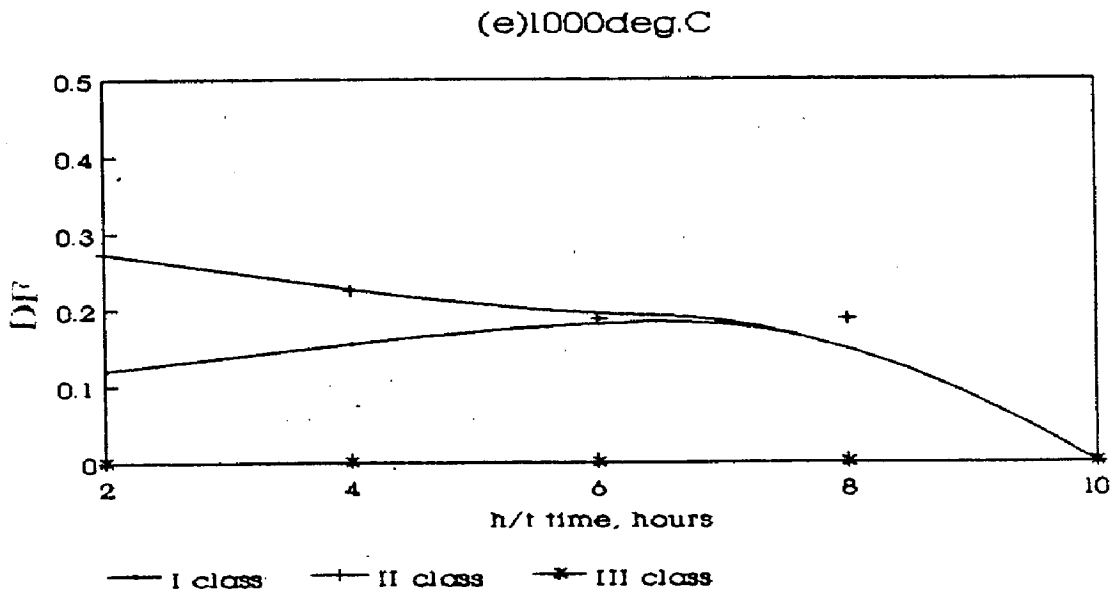
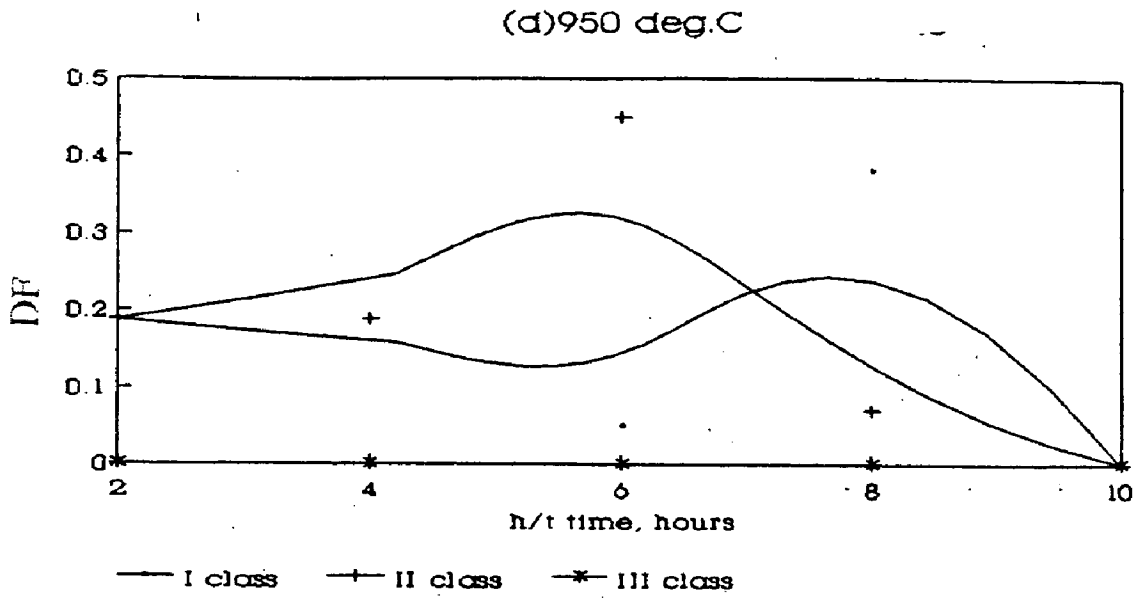
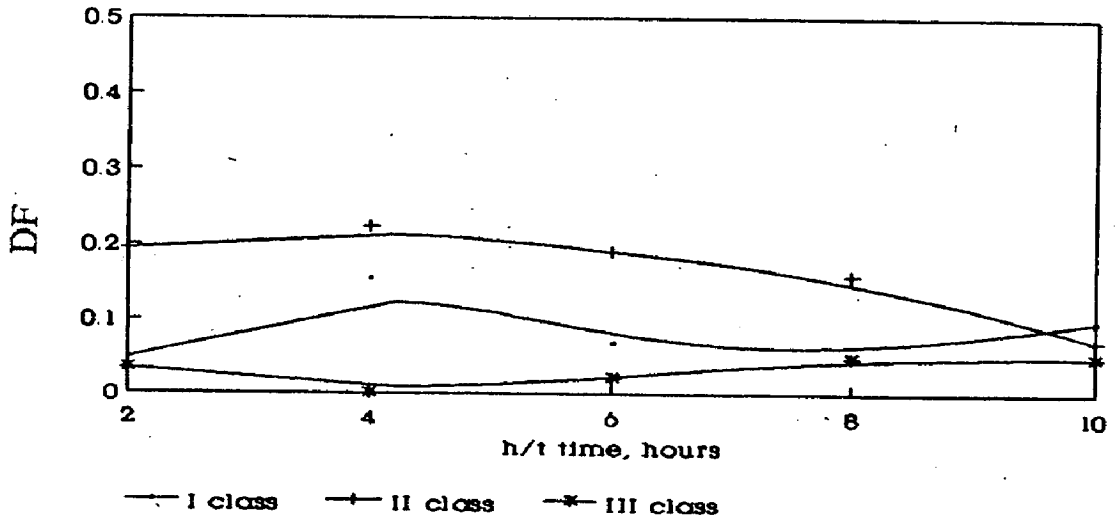
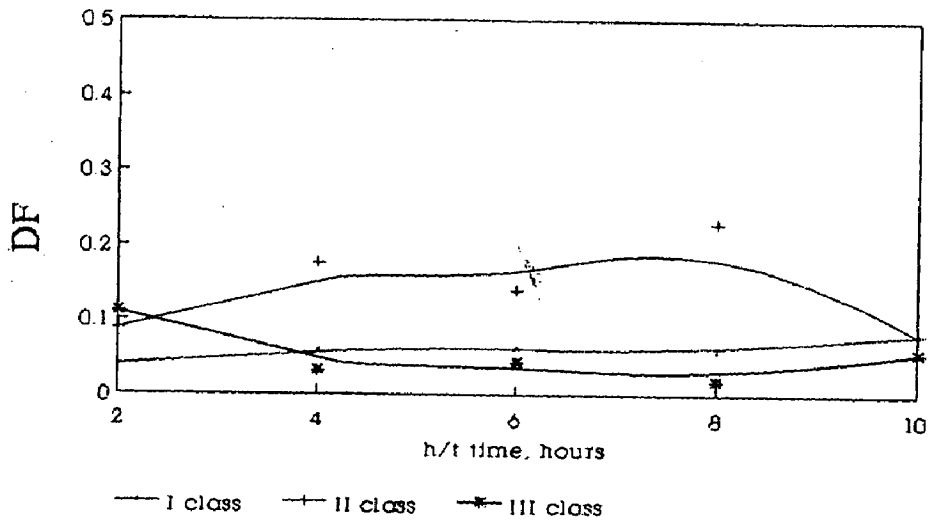


Fig. 5.48 : Effect of heat treatment on DF of DCs (Alloy C1)

Alloy C2 (a)800 deg.C



Alloy C2 (B)850 deg.C



Alloy C2 (c)900 deg.C

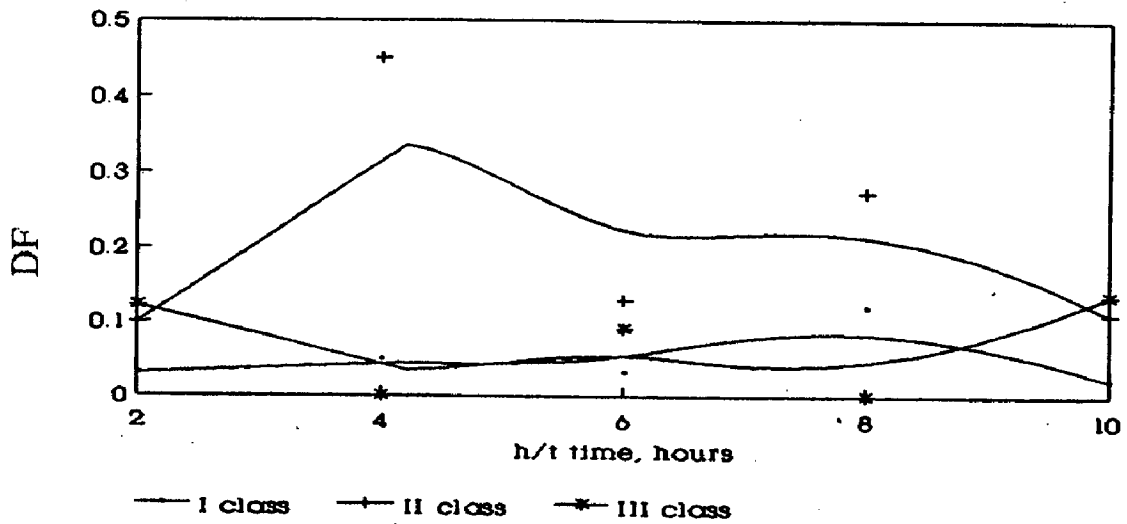
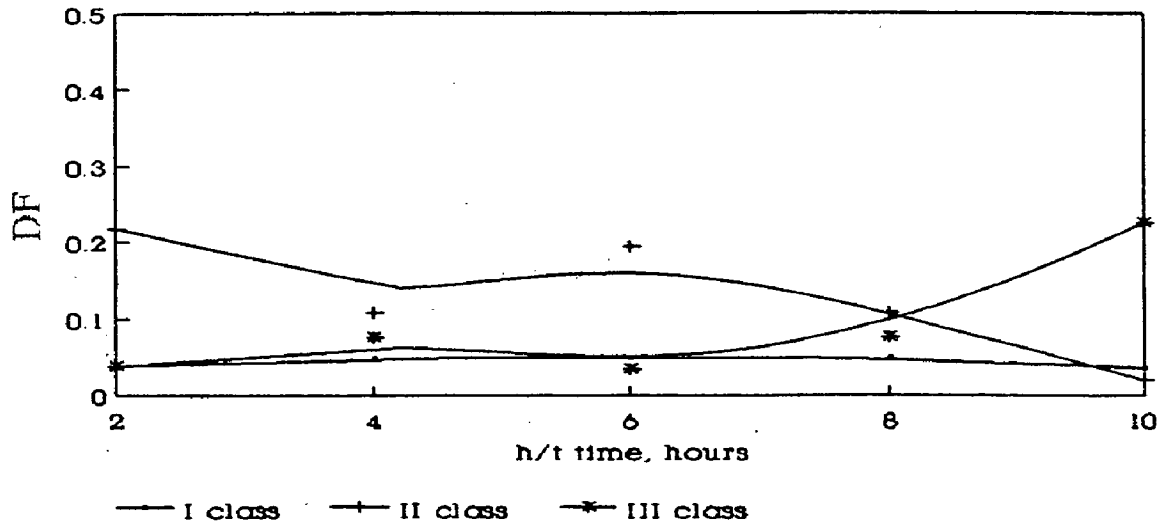


Fig. 5.49 : Effect of heat treatment on DF of DCs (Alloy C2)

Alloy C2 (d)950 deg.C



Alloy C2 (e)1000deg.C

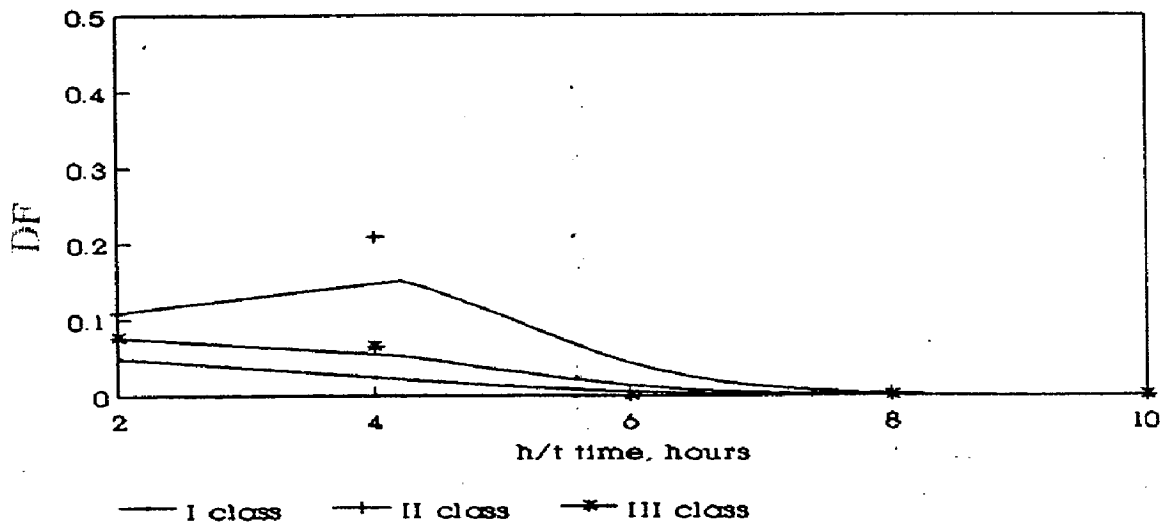
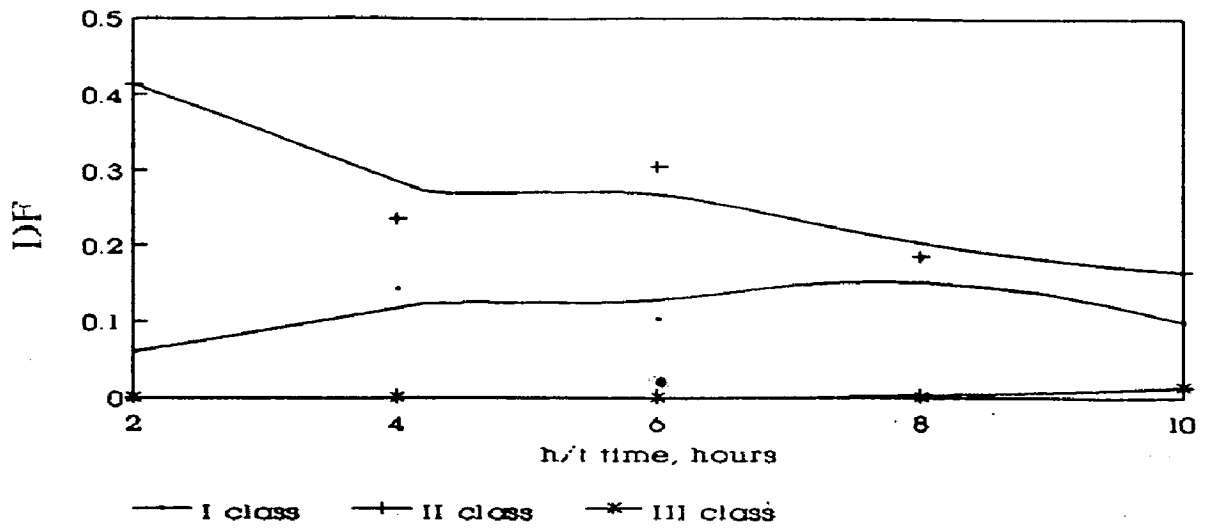
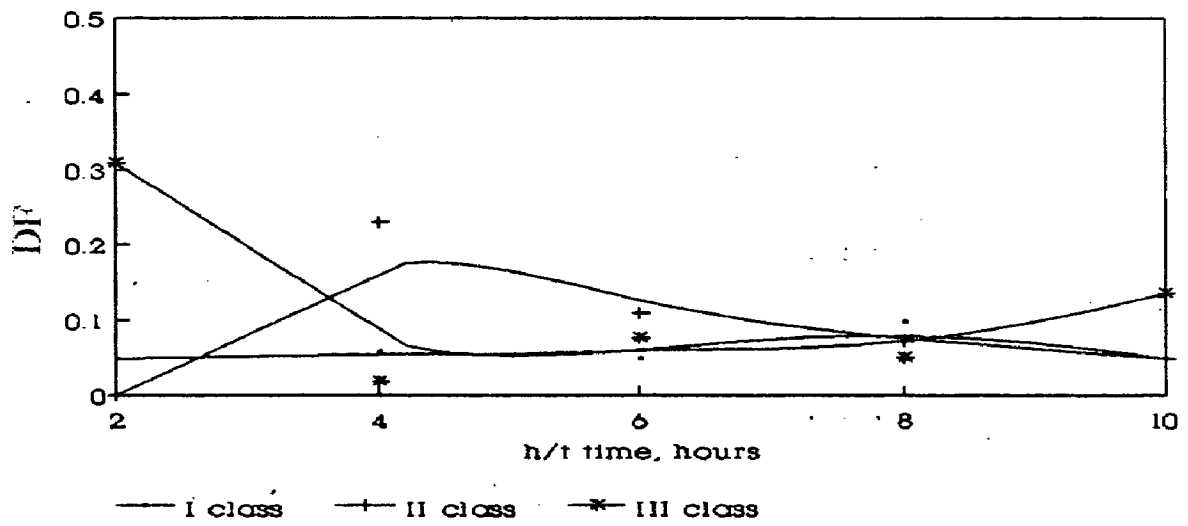


Fig. 5.49 : Effect of heat treatment on DF of DCs (Alloy C2)

Alloy C3 (a)800 deg.C



Alloy C3 (b)850 deg.C



Alloy C3 (c)900 deg.C

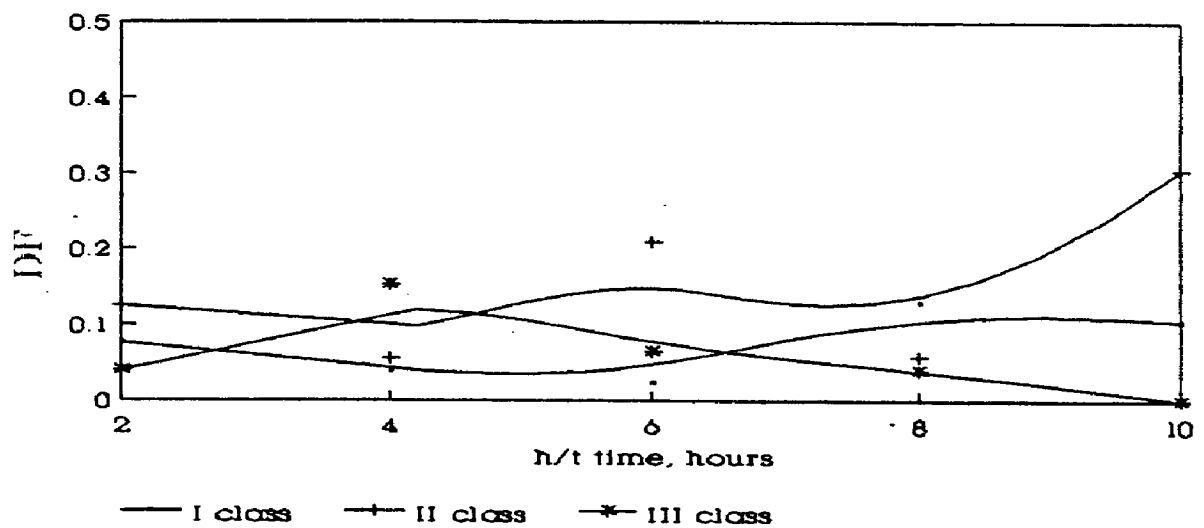
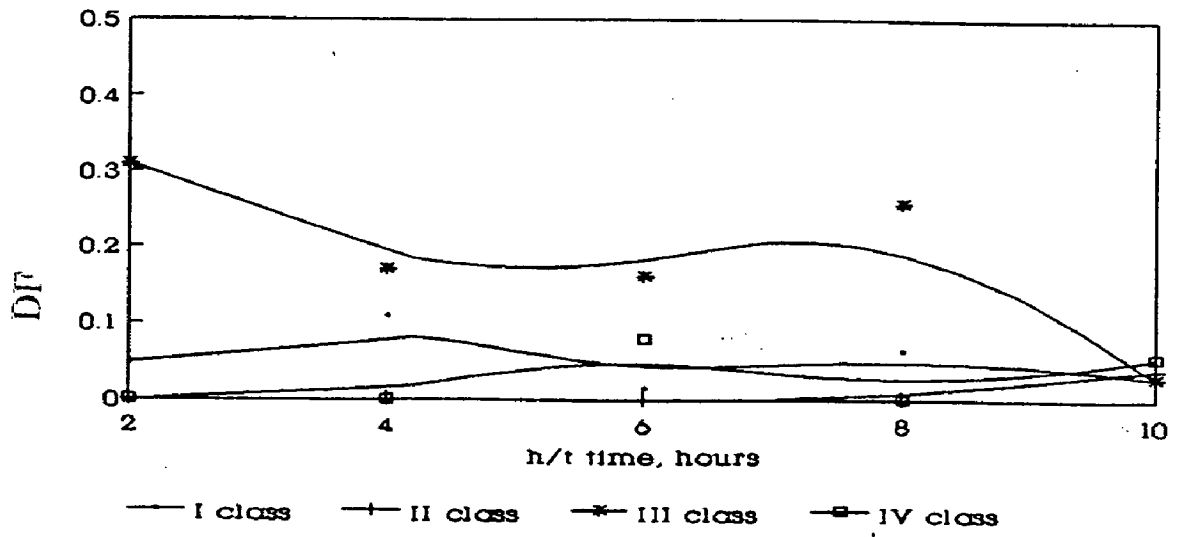


Fig. 5. 50 : Effect of heat treatment on DF of DCs (Alloy C3)

Alloy C3 (d)950 deg.C



Alloy C3 (e)1000deg.C

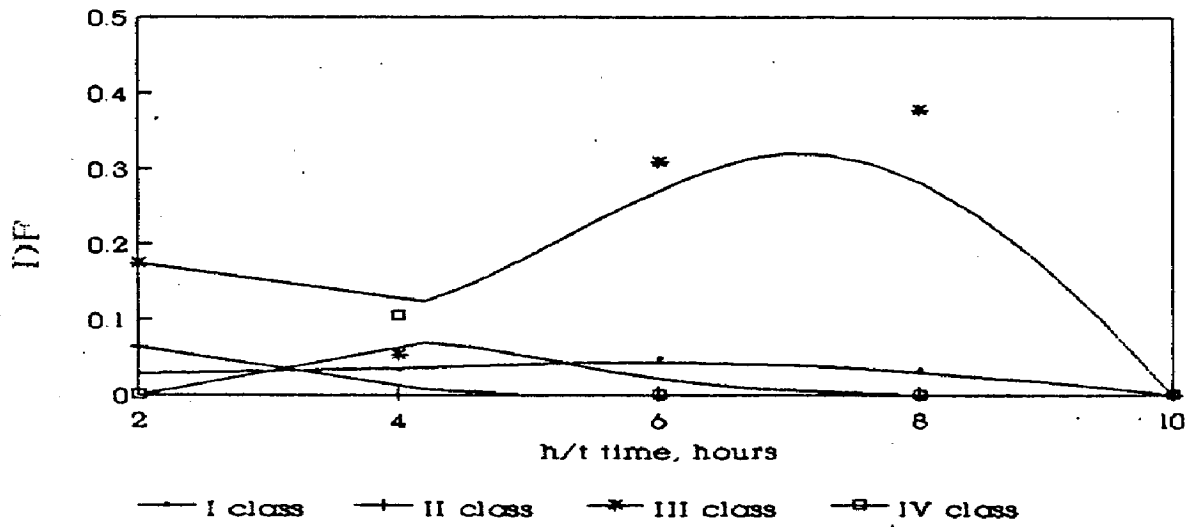


Fig. 5. 50 : Effect of heat treatment on DF of DCs (Alloy C3)

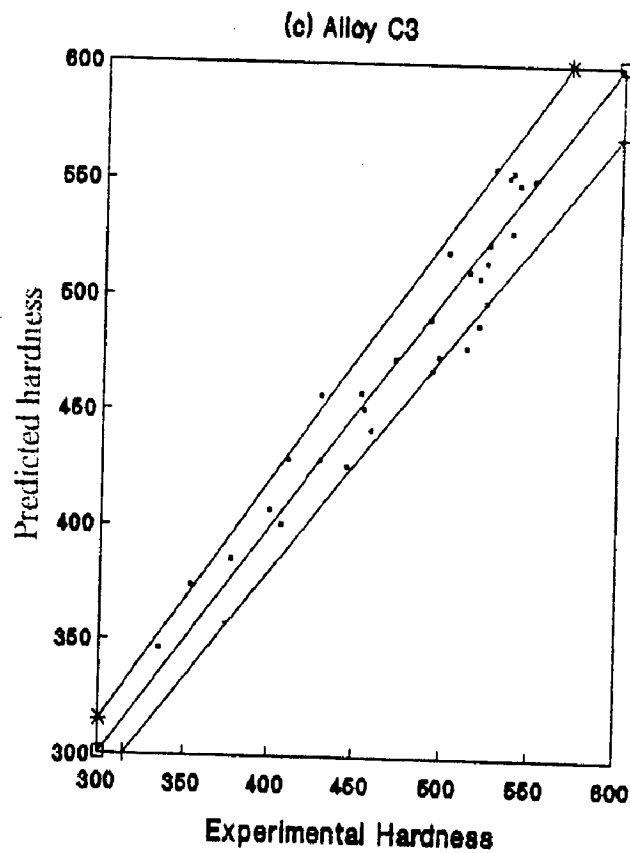
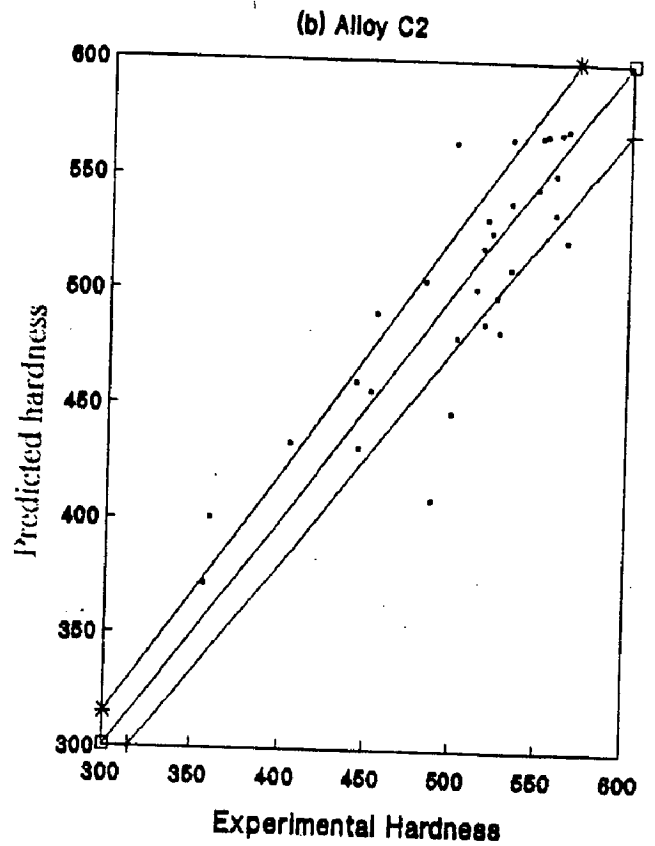
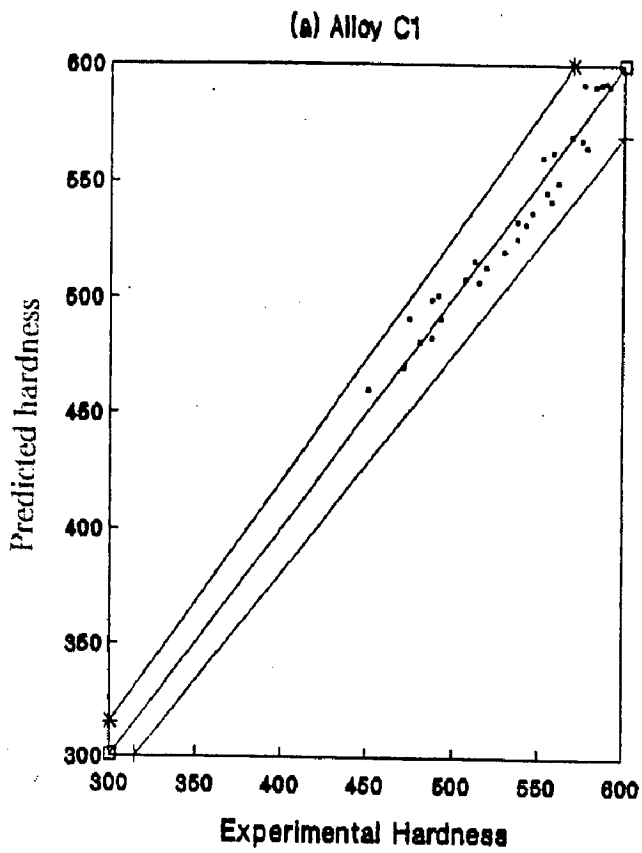


Fig. 5.51 : Experimental vs predicted hardness values of the experimental alloys

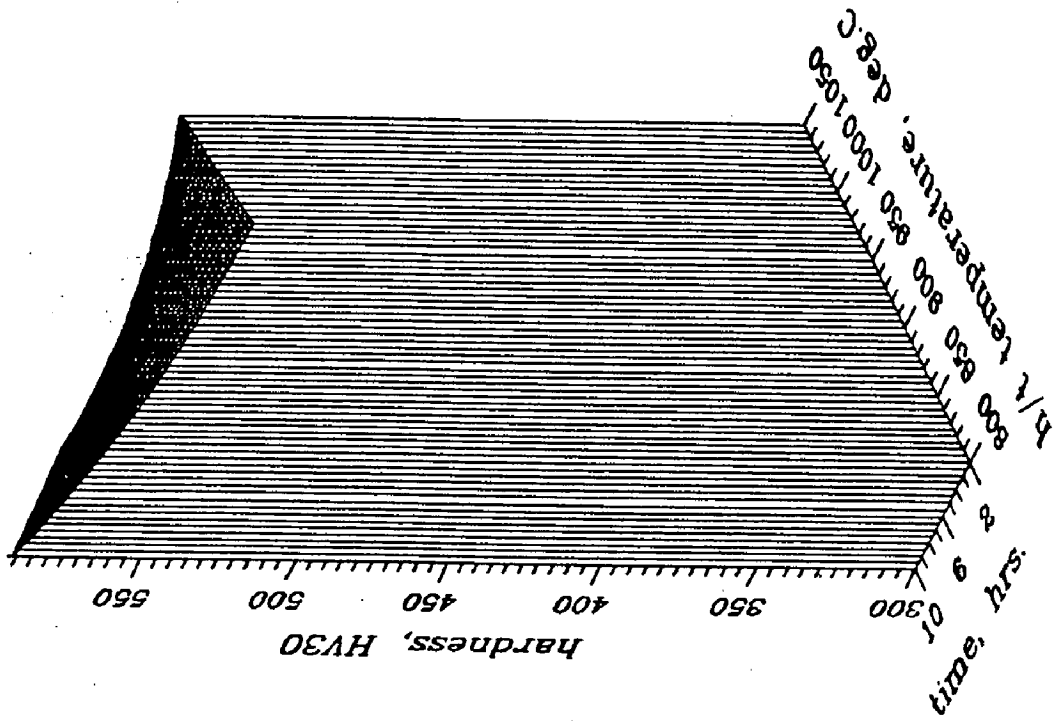
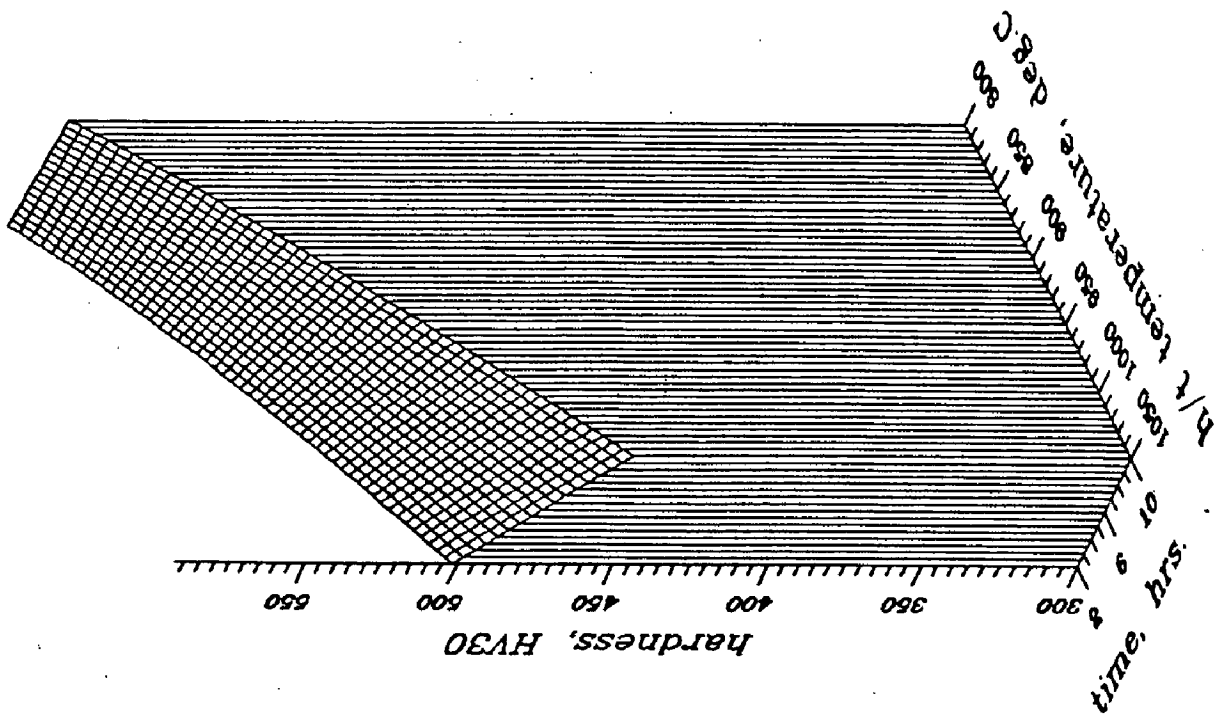


Fig. 5.52 : 3D plot depicting the effect of heat treating parameters on hardness (Alloy C1)

Fig. 5.53 : 3D plot depicting the effect of heat treating parameters on hardness (Alloy C2)

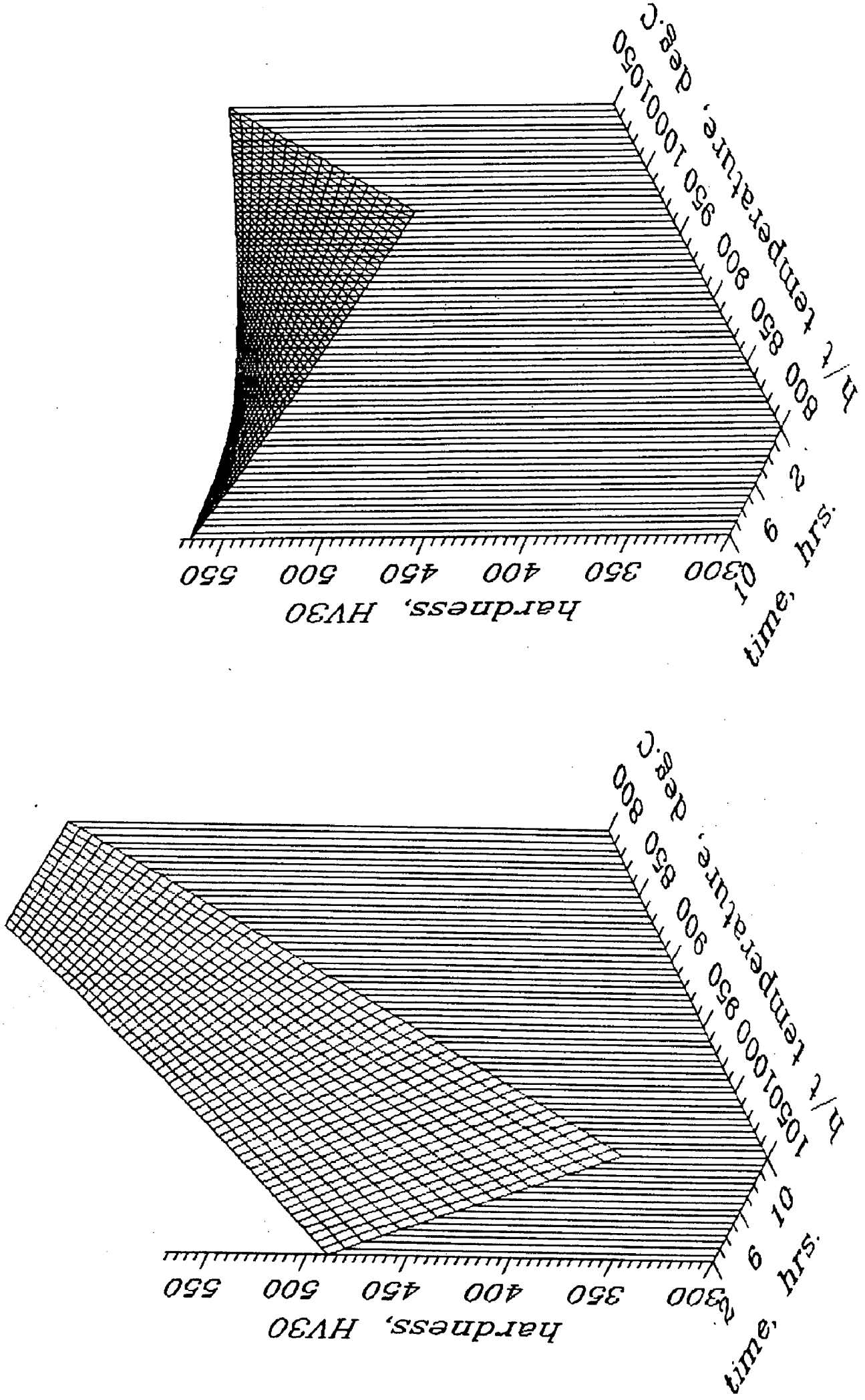
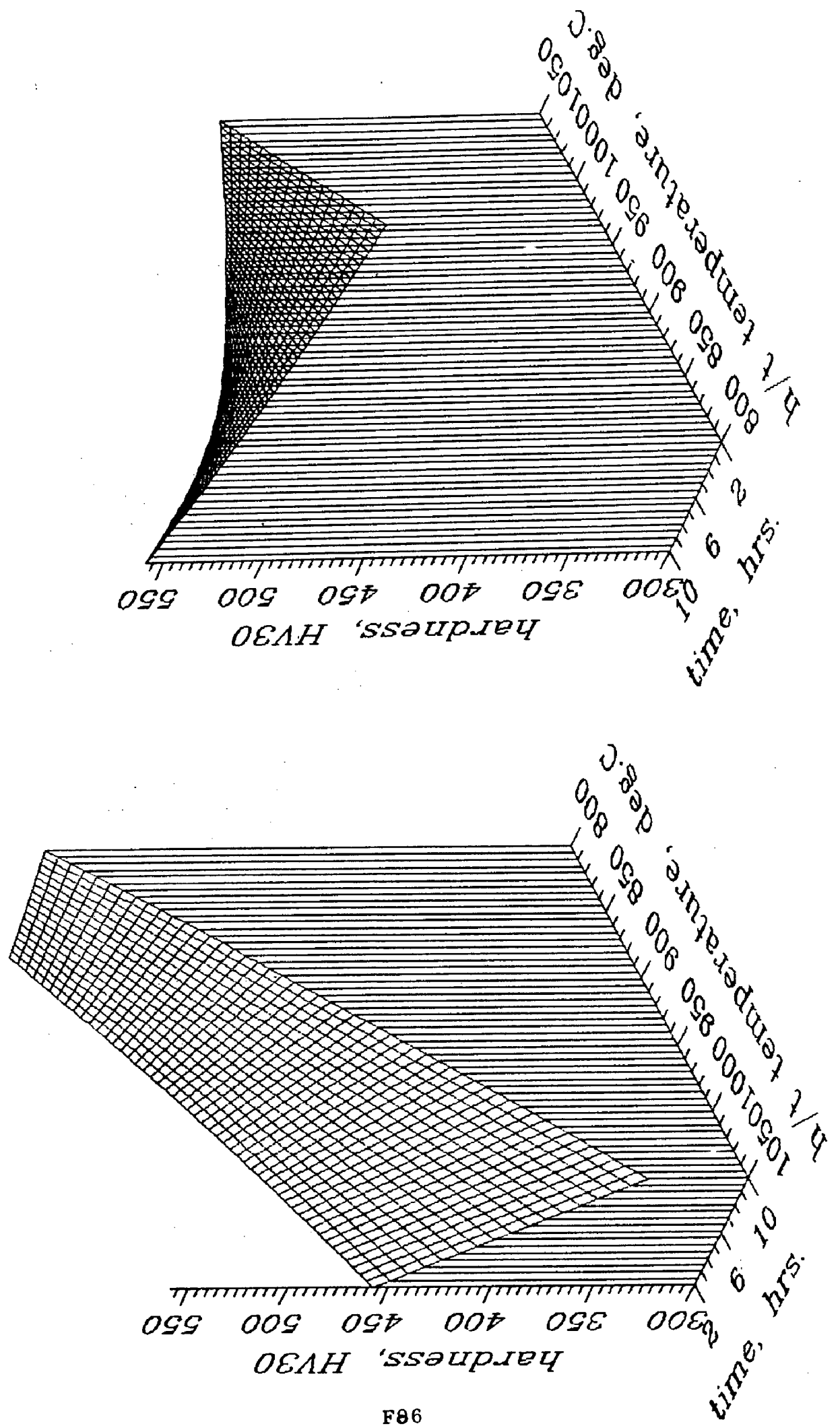


Fig. 5.24 : 3D plot depicting the effect of heat treating parameters on hardness (Alloy C3)



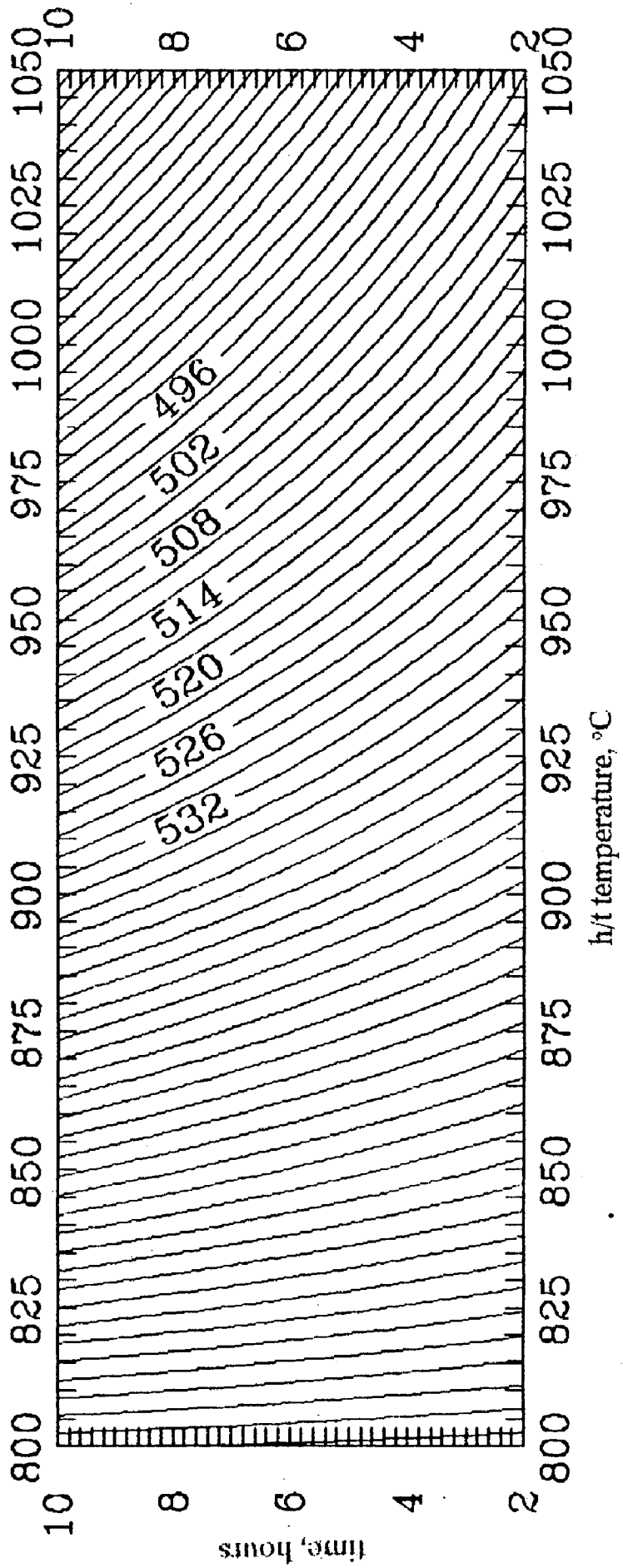


Fig. 5.55 : Iso-hardness plot of alloy C1

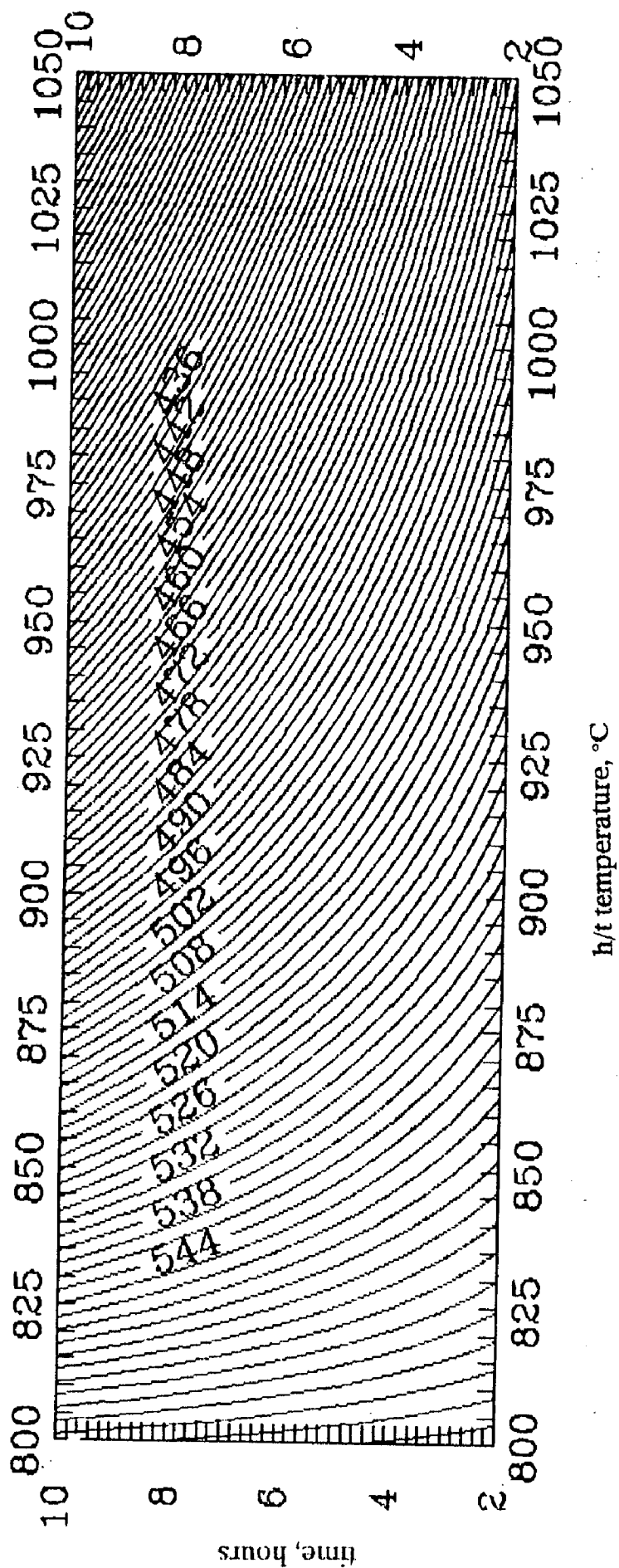


Fig. 5.56 : Iso-hardness plot of alloy C2

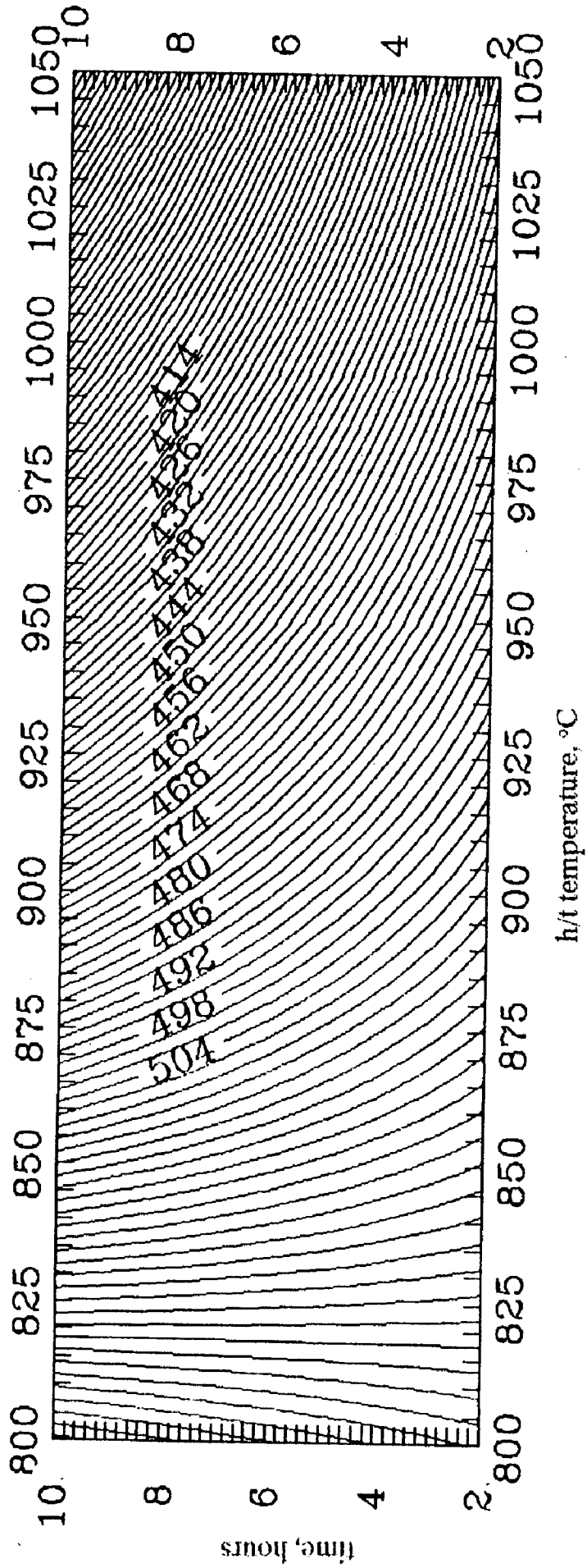


Fig. 5.57 : Iso-hardness plot of alloy C3

Figure 6.1

- | | |
|--------------------------|--|
| (a) C1, As Cast
x 200 | (b) C1, 1000, 2
x 400 |
| (c) C1, 1050, 2
x 400 | (d) C2, 950, 2
x 800 |
| (e) C2, 1000, 2
x 800 | (f) C2, 1000, 2
X-ray dot map of Cu |

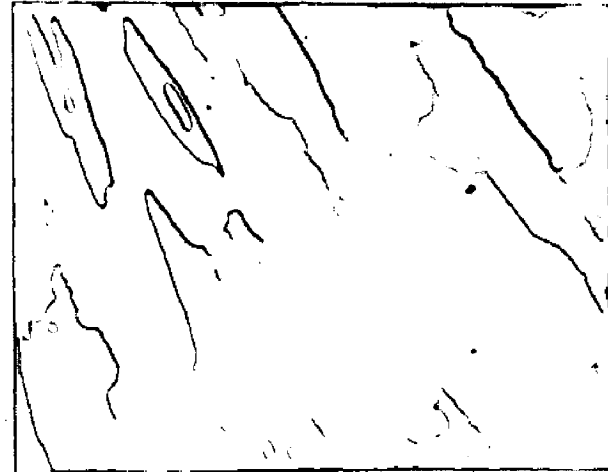
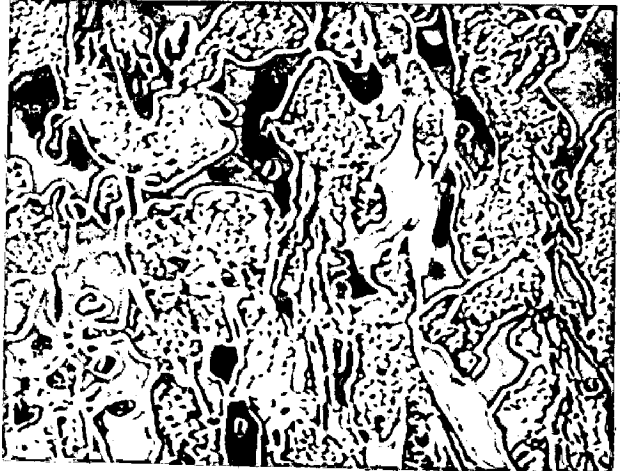
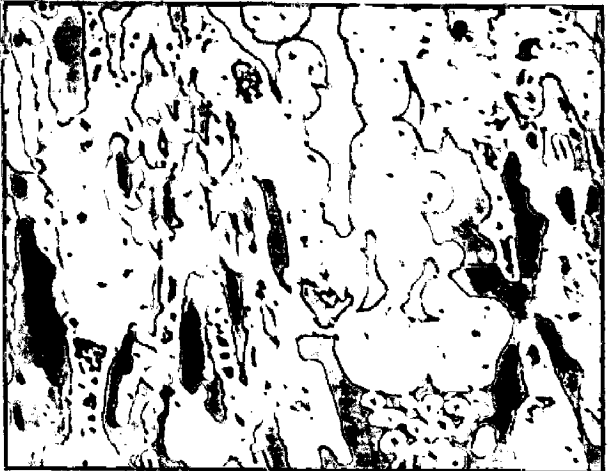
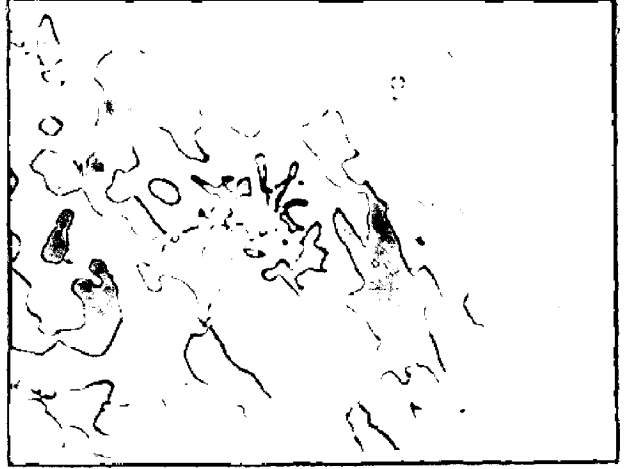
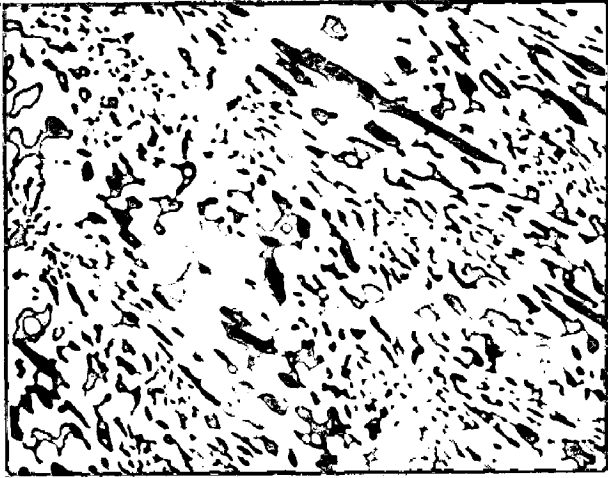


Figure 6.1

(g) C3, 950, 10
x 400

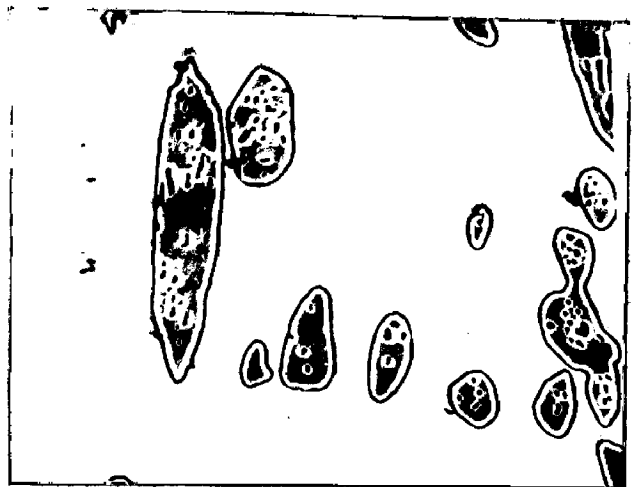
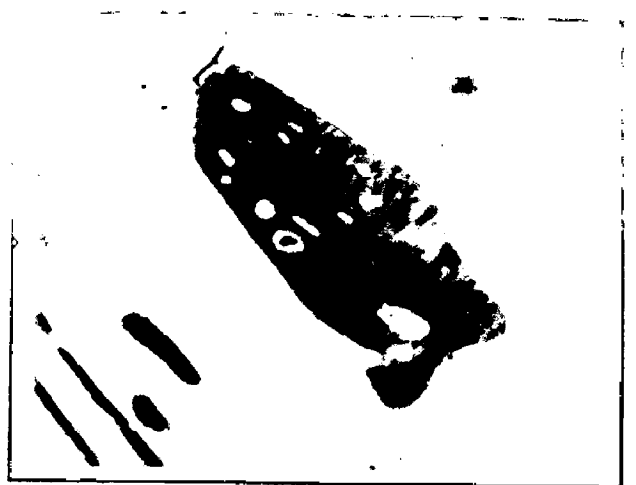
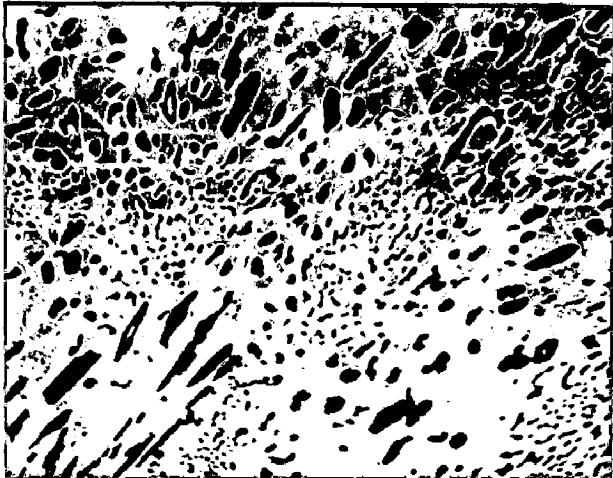
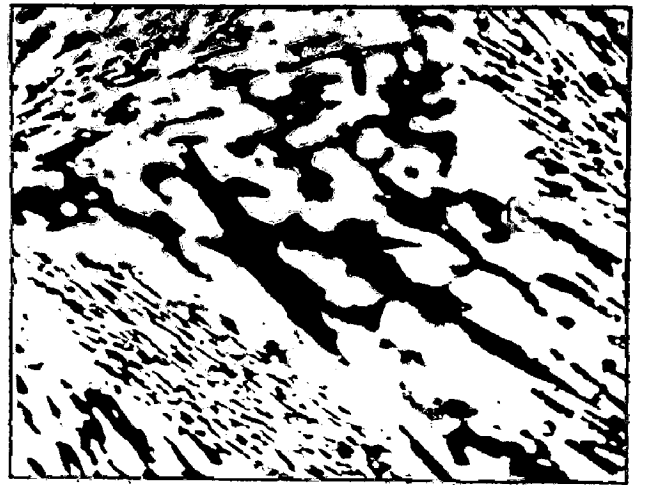
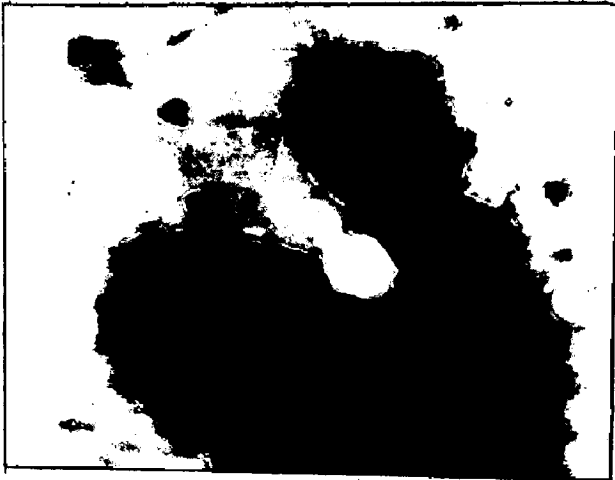
(h) C3, 1000, 2
x 400

(i) C3, 1000, 10
x 200

(j) C3, 1000, 2
x 800

(k) C3, 1050, 2
x 200

(l) C3, 1050, 10
x 800



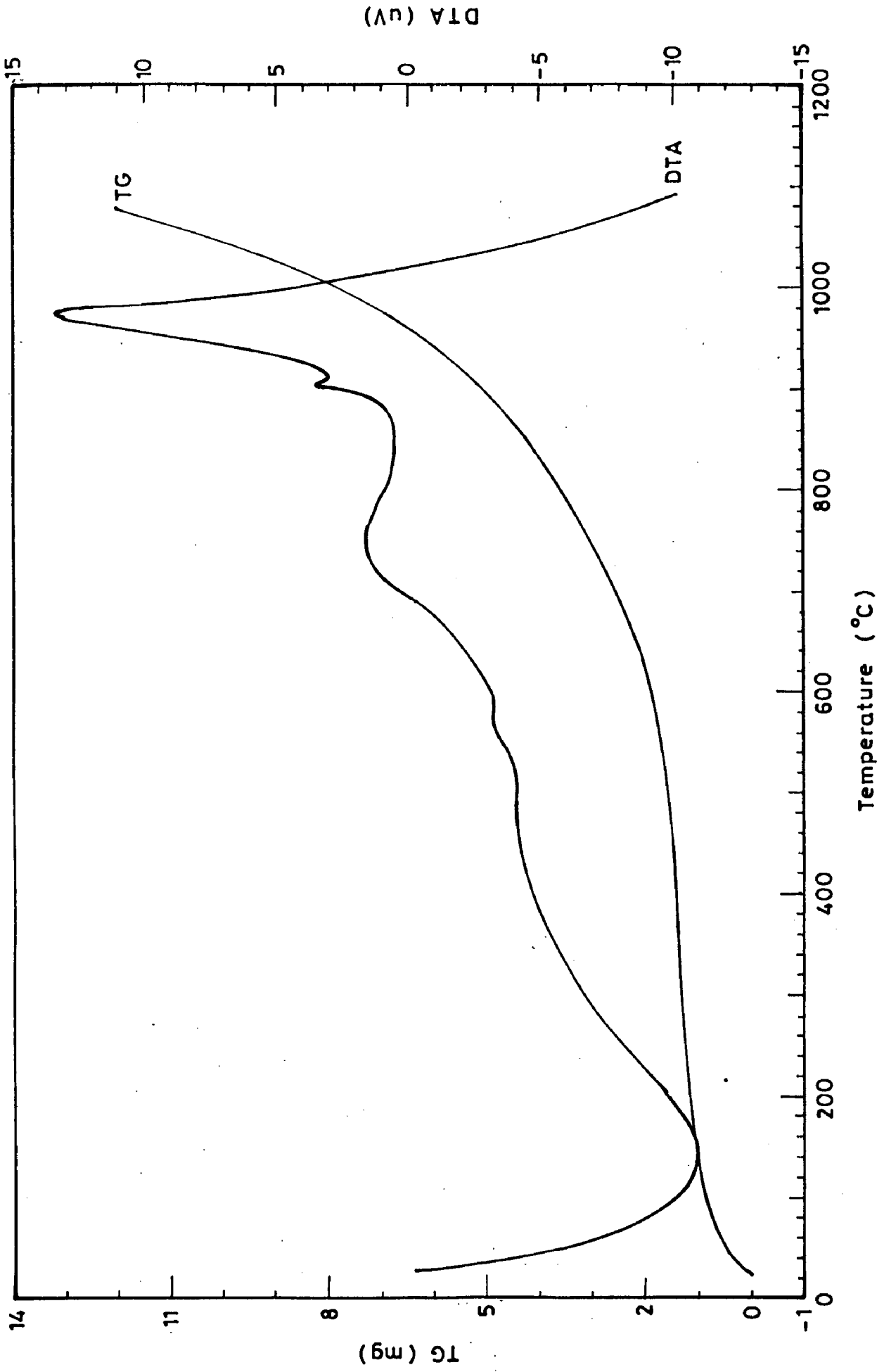


Fig. 6.2 Differential thermal analysis plot for alloy C1

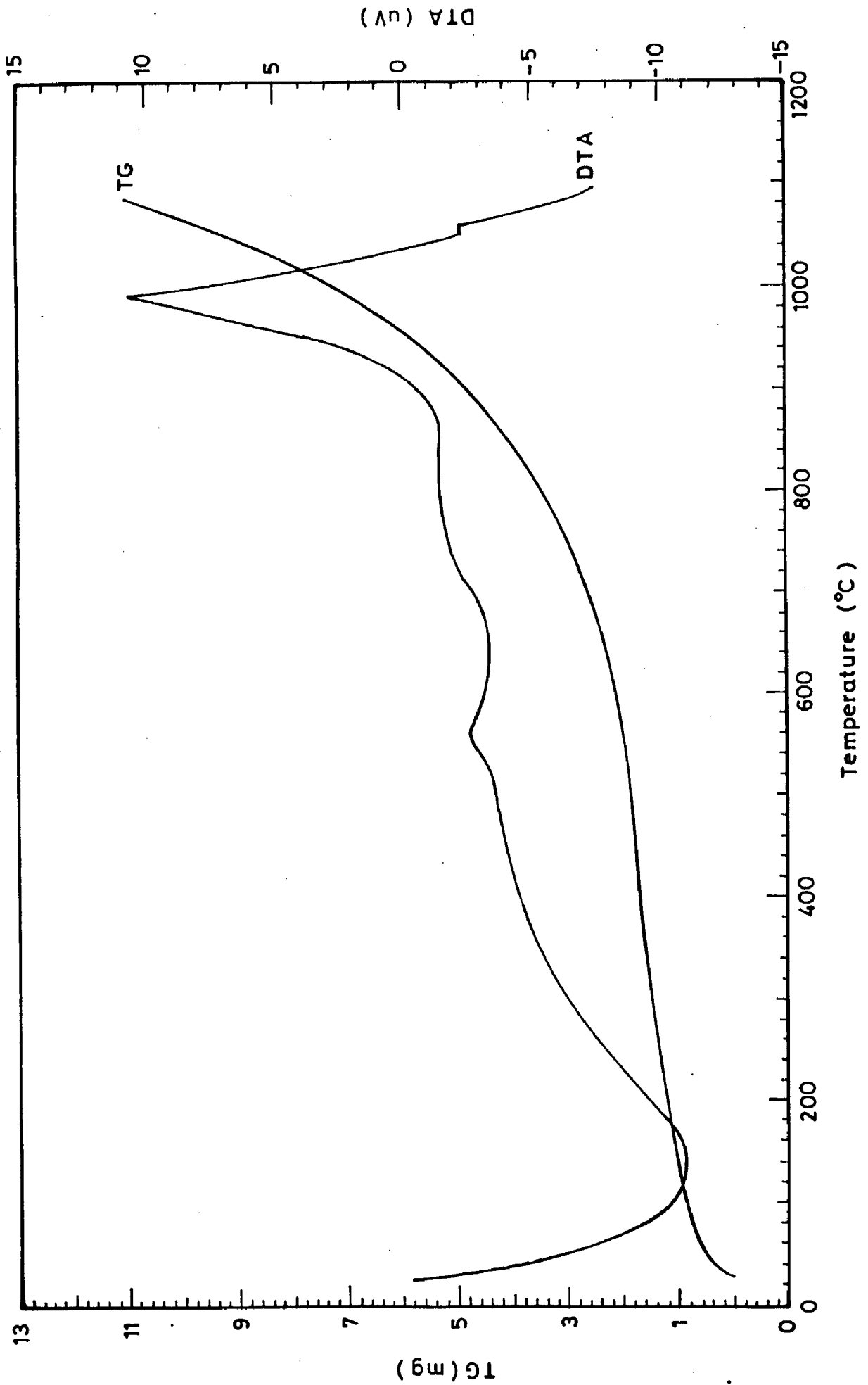


Fig. 6.3 Differential thermal analysis plot for alloy C2

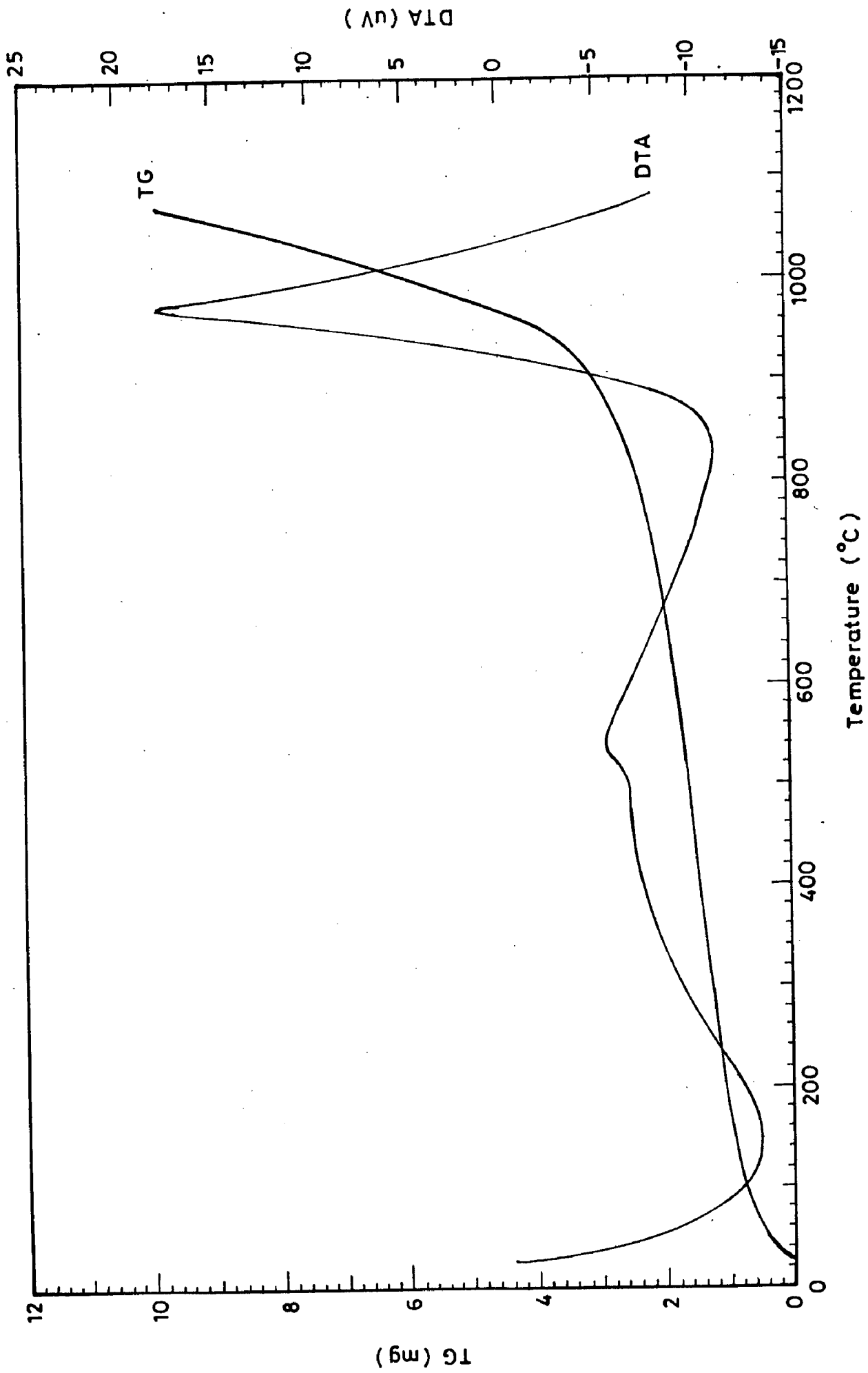


Fig.6.4 Differential thermal analysis plot for alloy C3

(a) Alloy C1

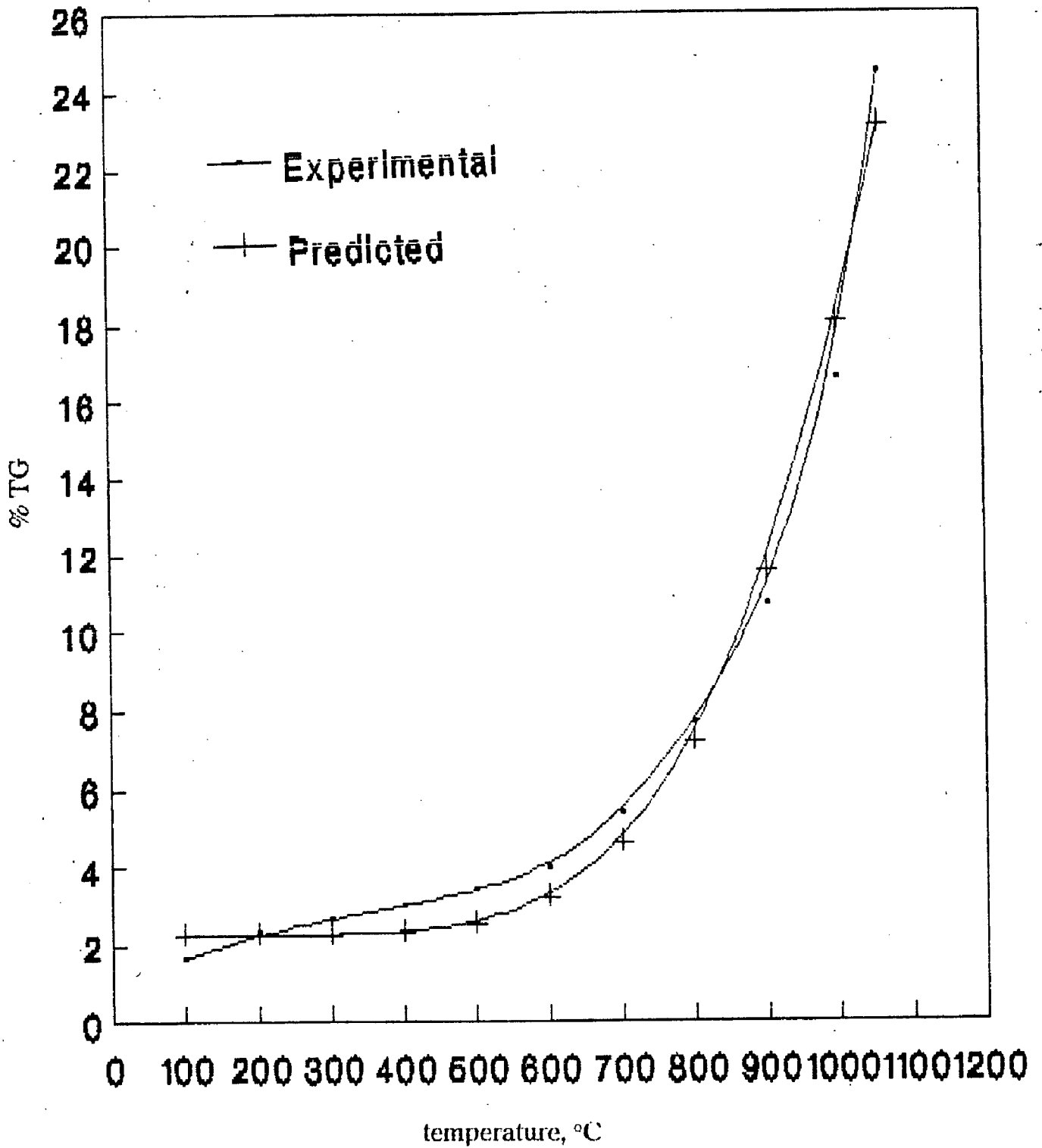


Fig. 6.5 : Experimental vs predicted %TG plots of experimental alloys.

(b) Alloy C2

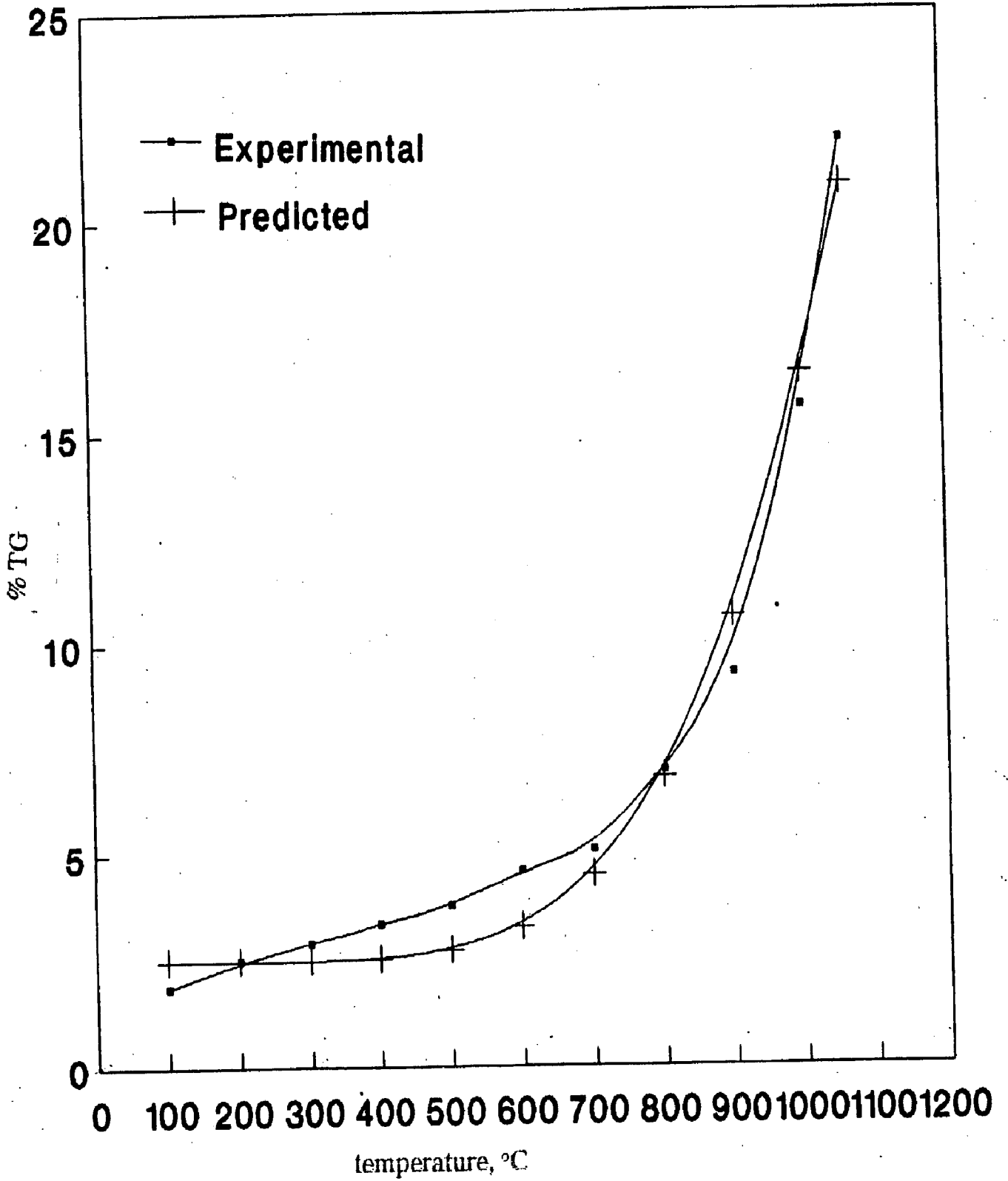


Fig. 6.5 : Experimental vs predicted %TG plots of experimental alloys

(c) Alloy C3

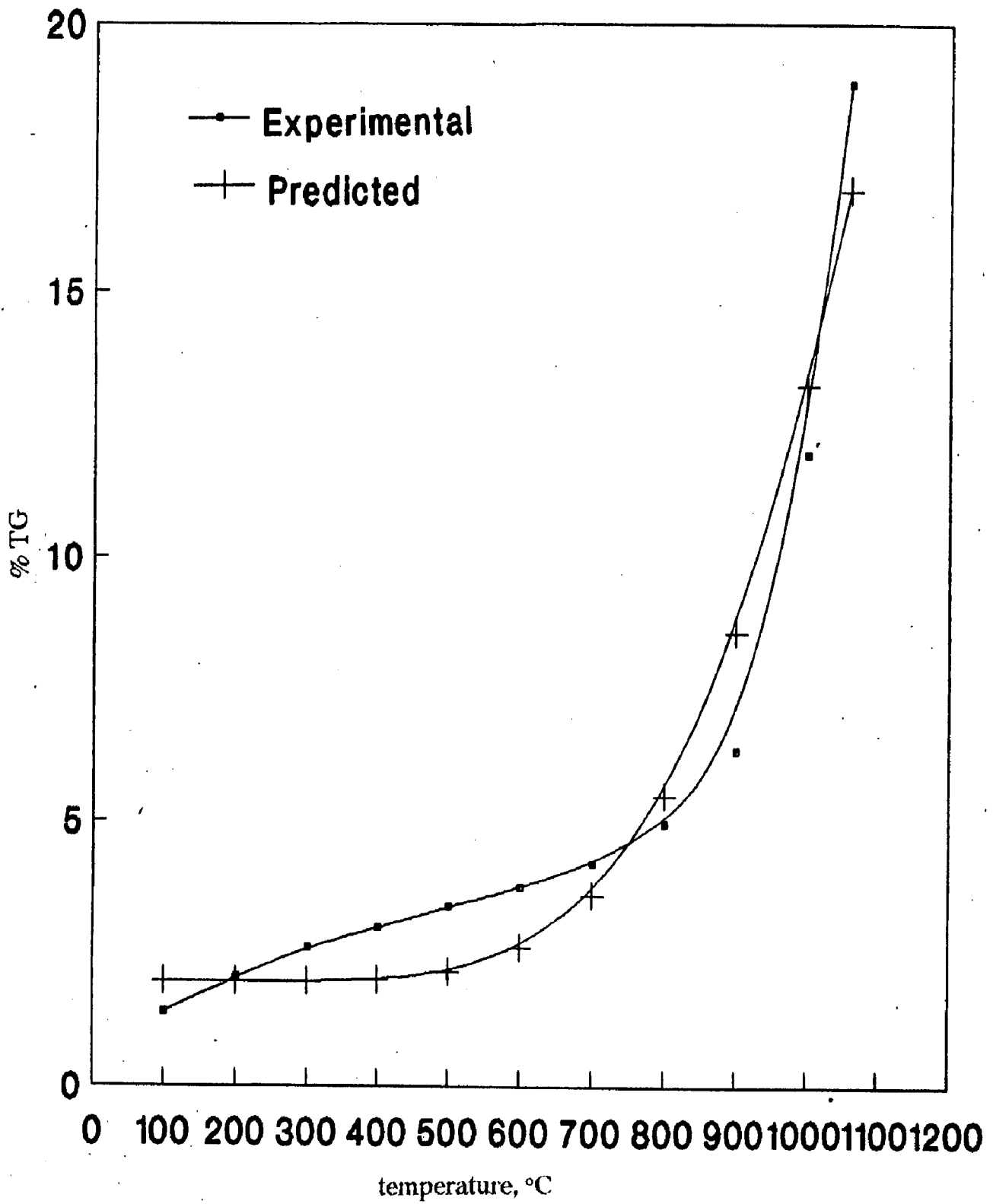


Fig. 6.5 : Experimental vs predicted %TG plots of experimental alloys

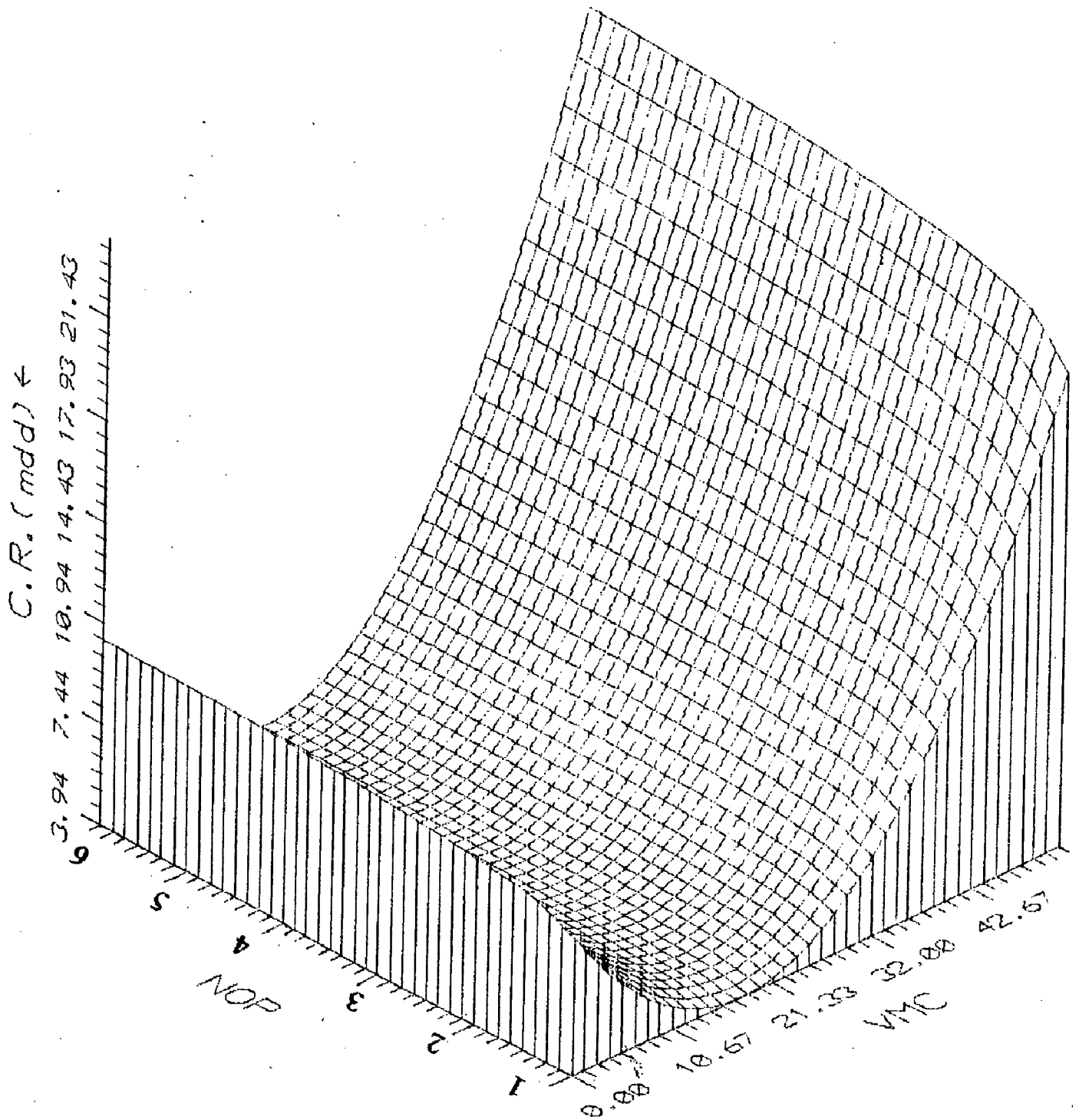


Fig. 7.9 : 3D plot depicting the effect of VMC & NOP on corrosion rate (based on equation 7.17)

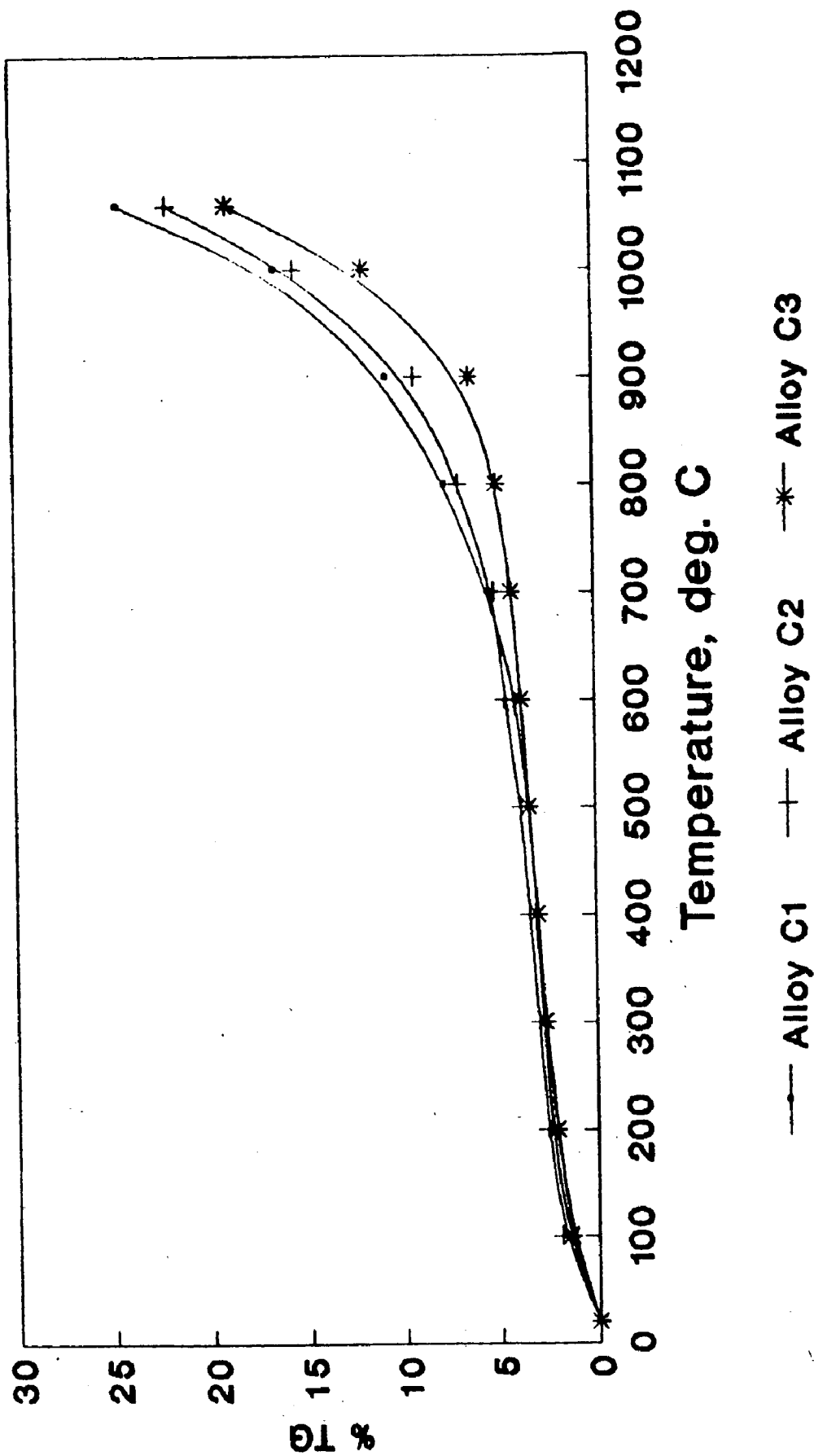


Fig. 6.6 : A summary plot of differential thermal analysis of experimental alloys

(b) 6 hours

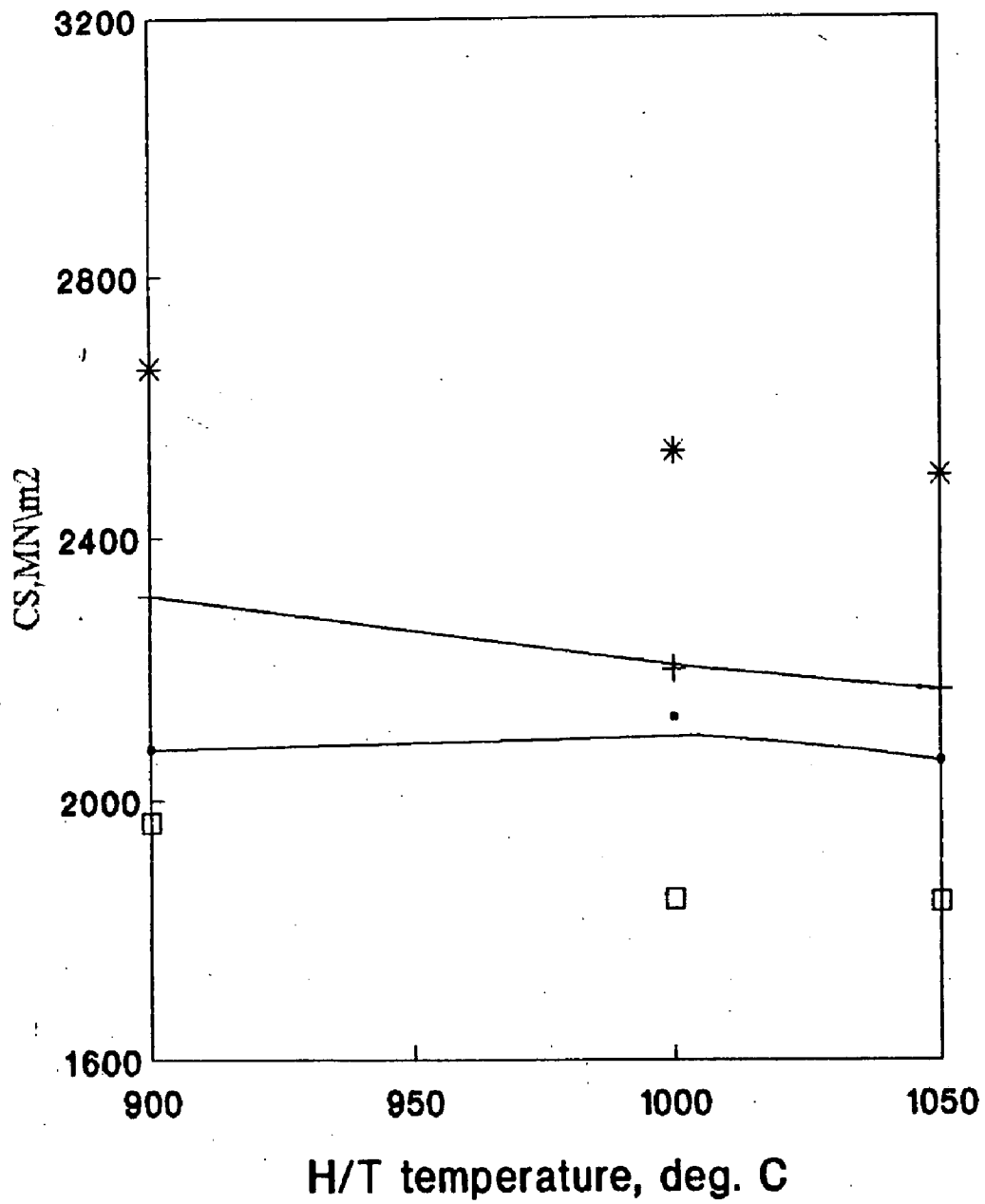


Fig. 7.1 : Variation in C.S. with temperature as influenced by soaking period (Alloy C1)

(a) 2 hours

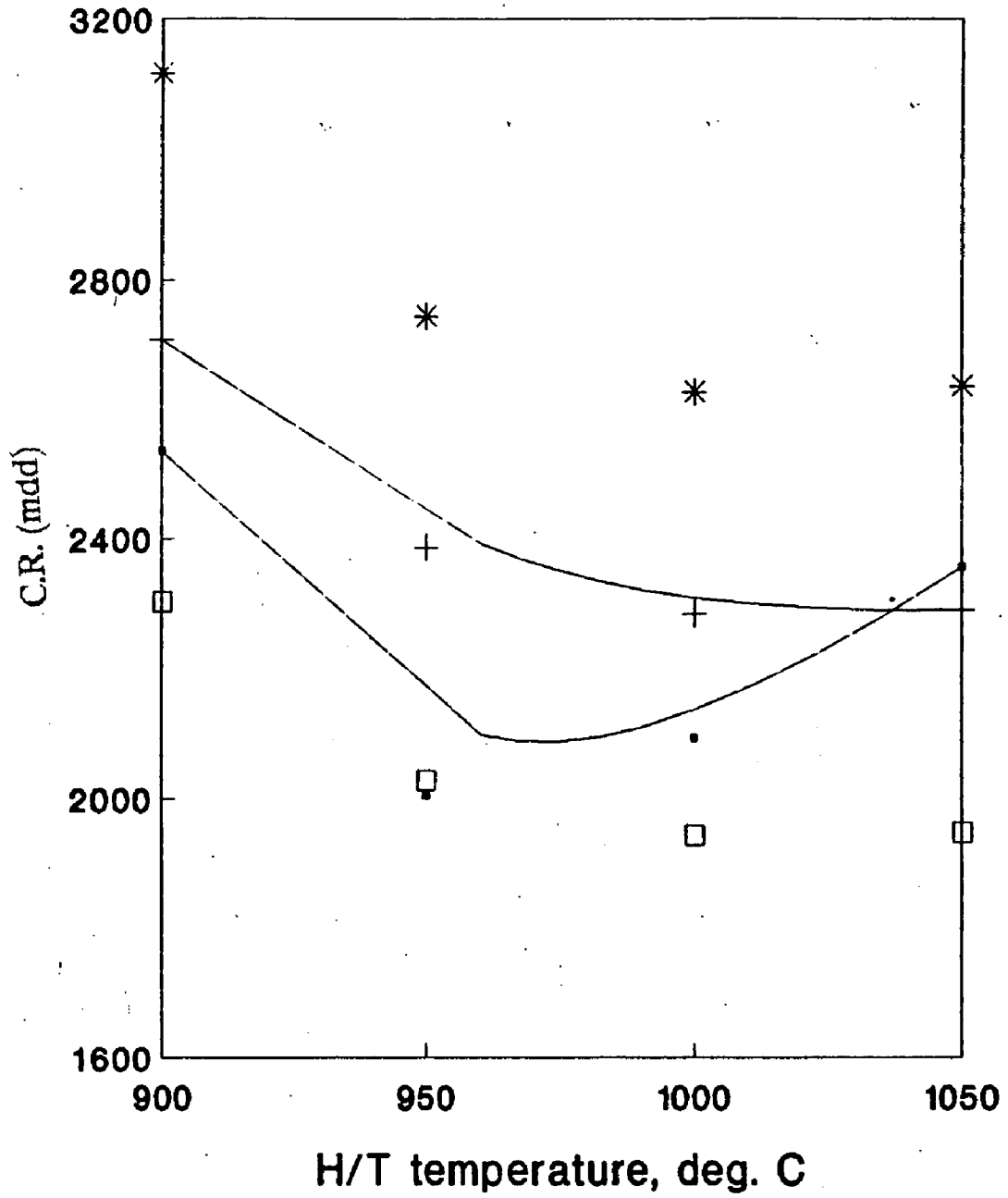


Fig. 7.2 : Variation in C.S. with temperature as influenced by soaking period (Alloy C2)

(b) 10 hours

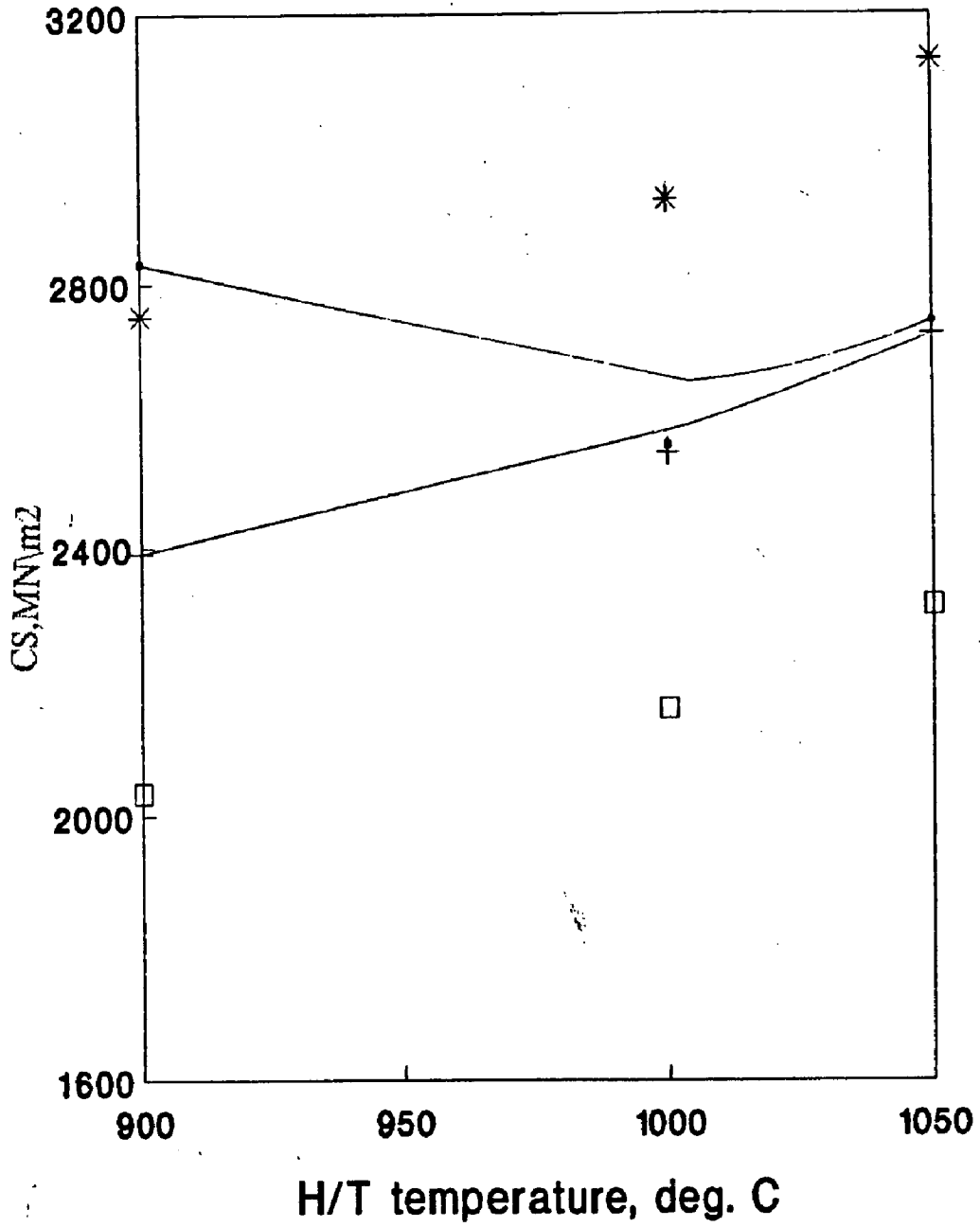


Fig. 7.2 : Variation in C.S. with temperature as influenced by soaking period (Alloy C2)

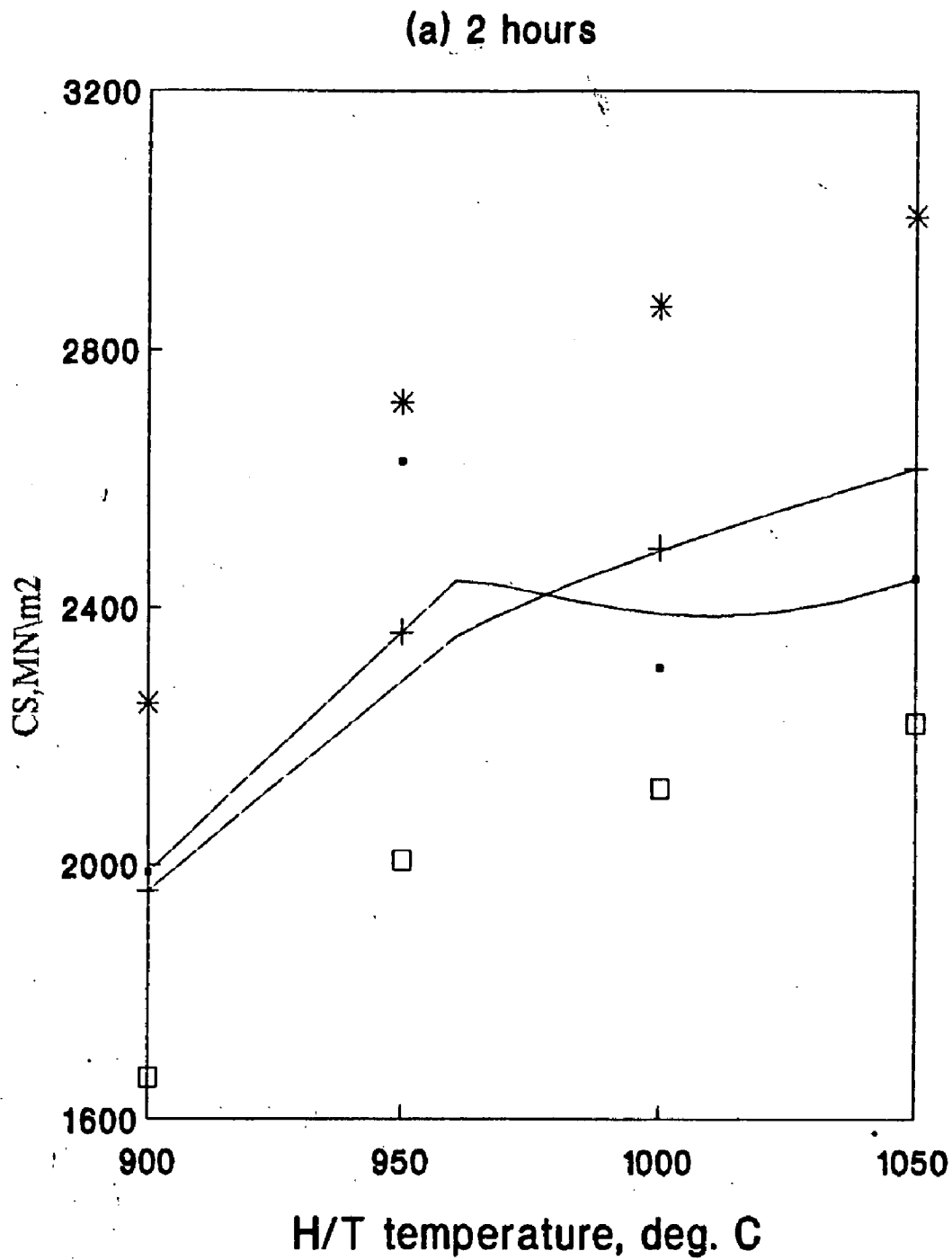


Fig. 7.3 : Variation in C.S. with temperature as influenced by soaking period (Alloy C3)

(b) 10 hours

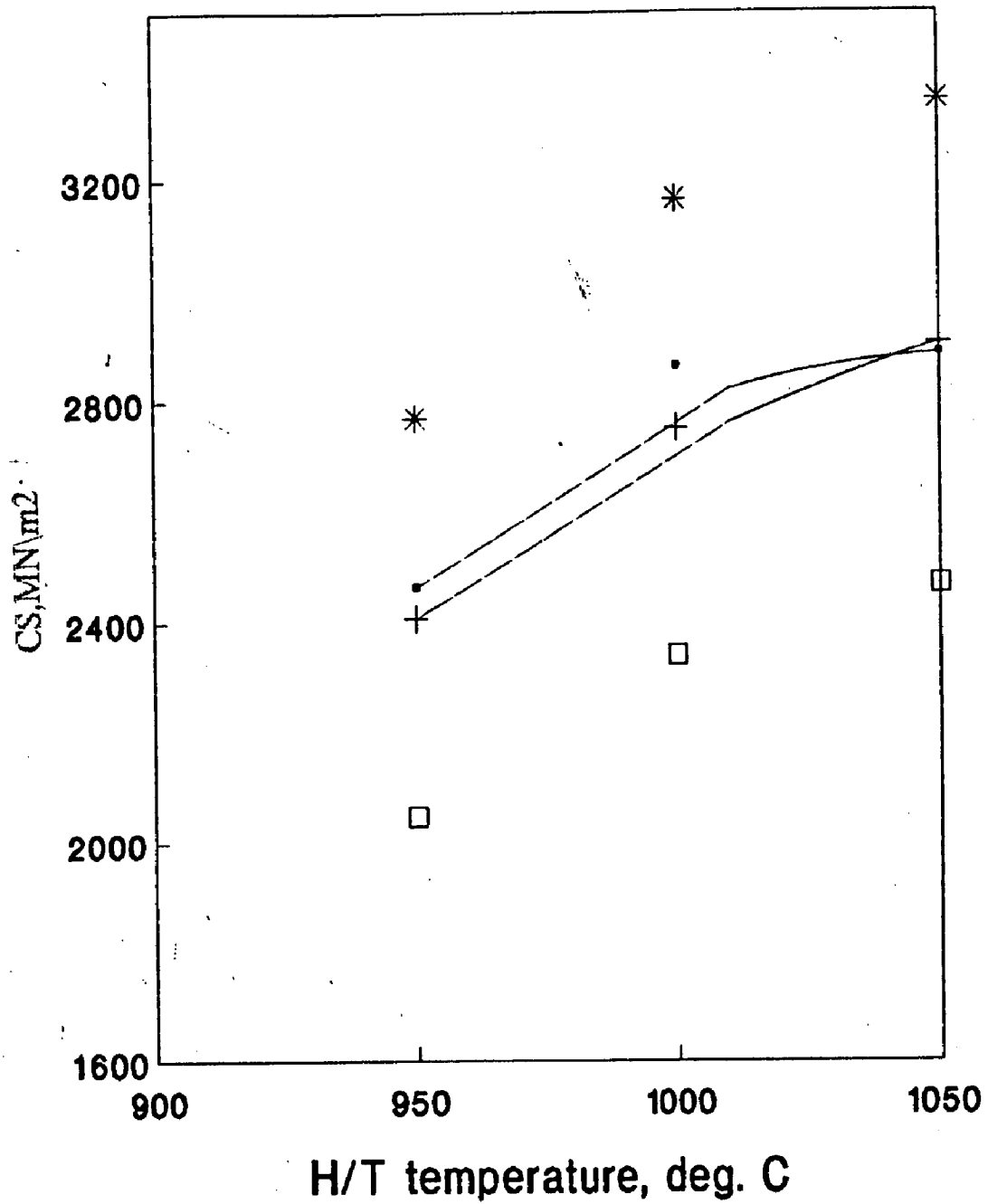


Fig. 7.3 : Variation in C.S. with temperature as influenced by soaking period (Alloy C3)

Fig. 7.4 Effect of heat treatment on corrosion behaviour (Alloy C1)

(a) 2 hours

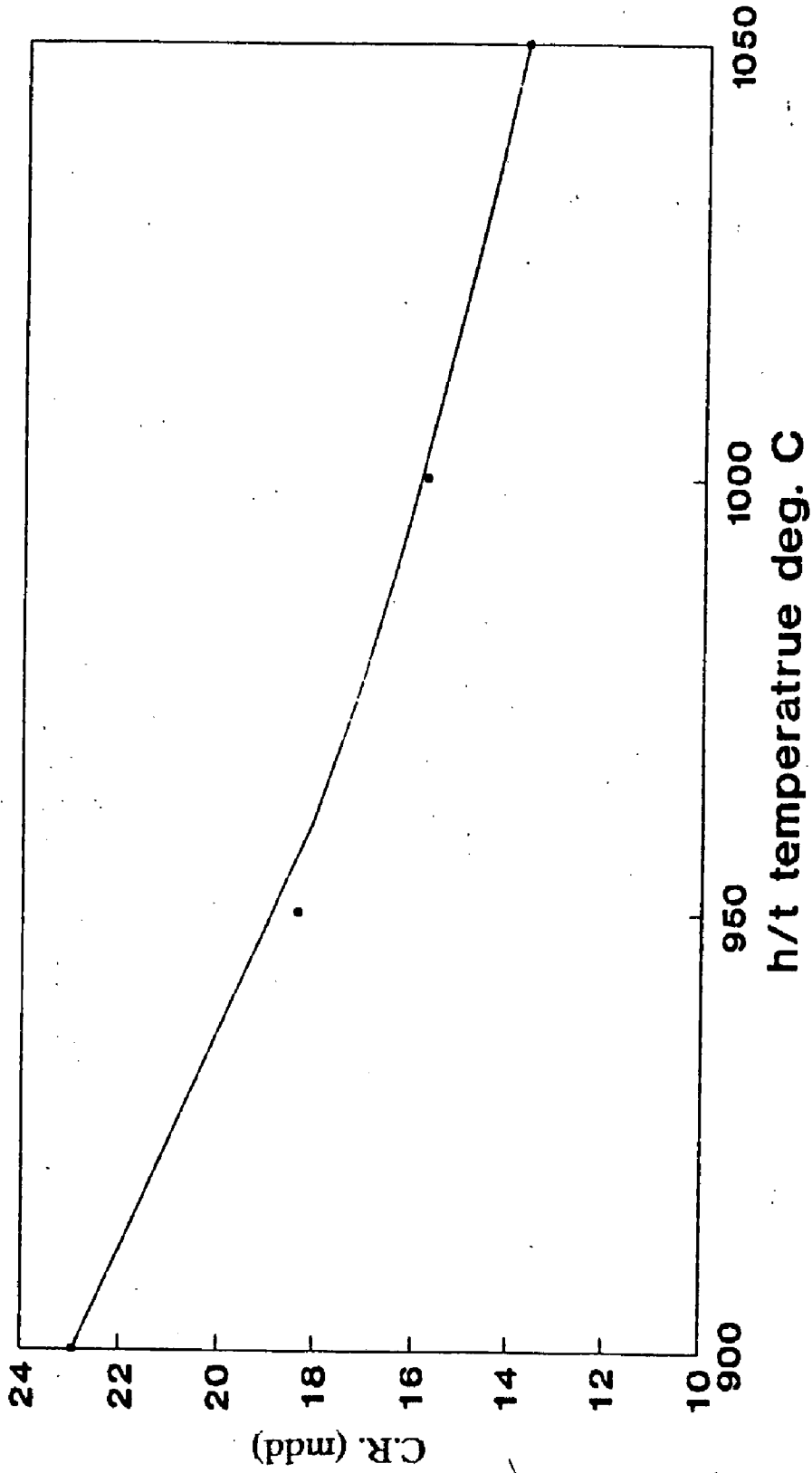


Fig. 7.4 Effect of heat treatment on corrosion behaviour (Alloy C1)
(b) 10 hours

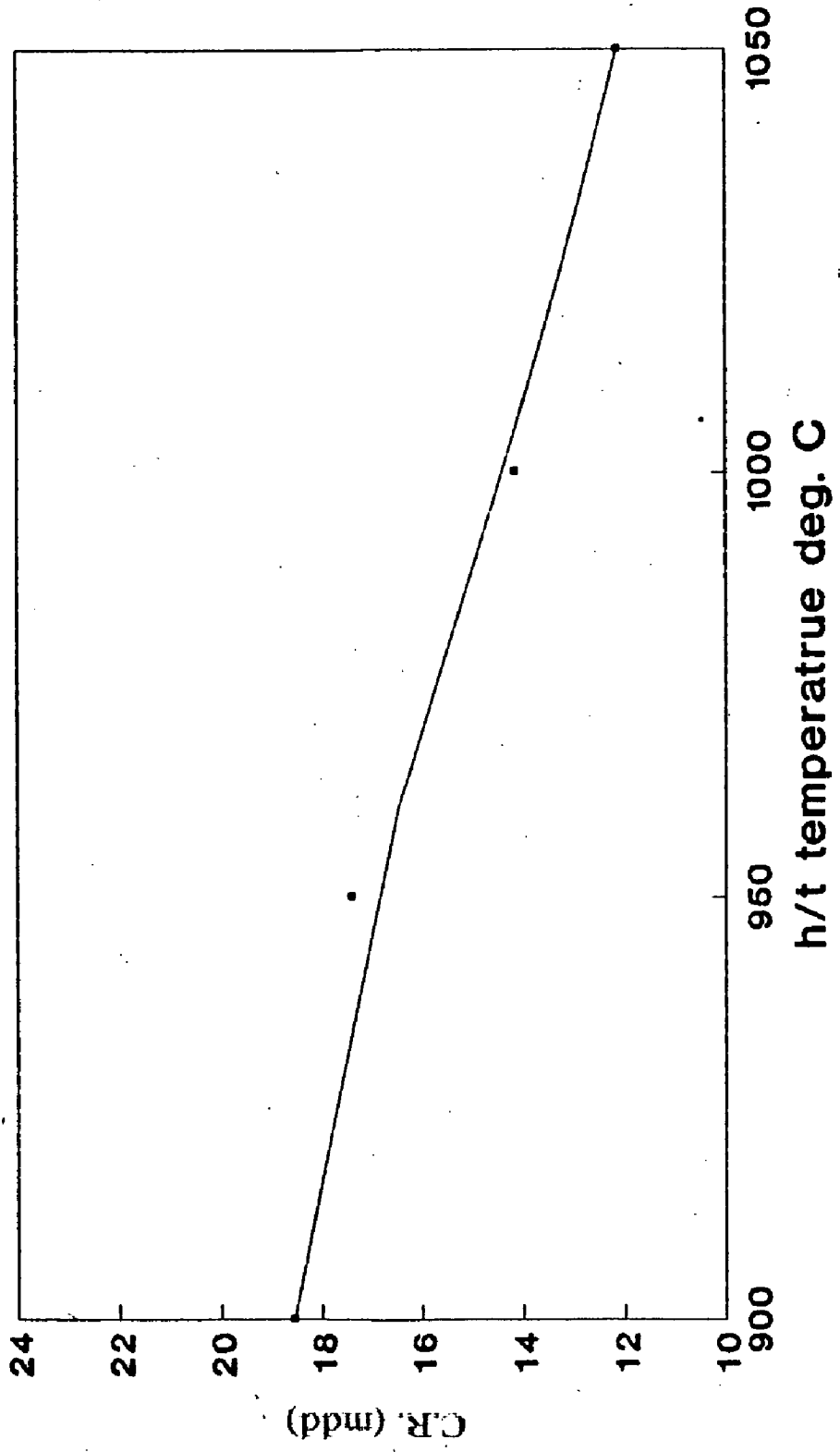


Fig. 7.5 Effect of heat treatment on corrosion behaviour (Alloy C2)

(a) 2 hours

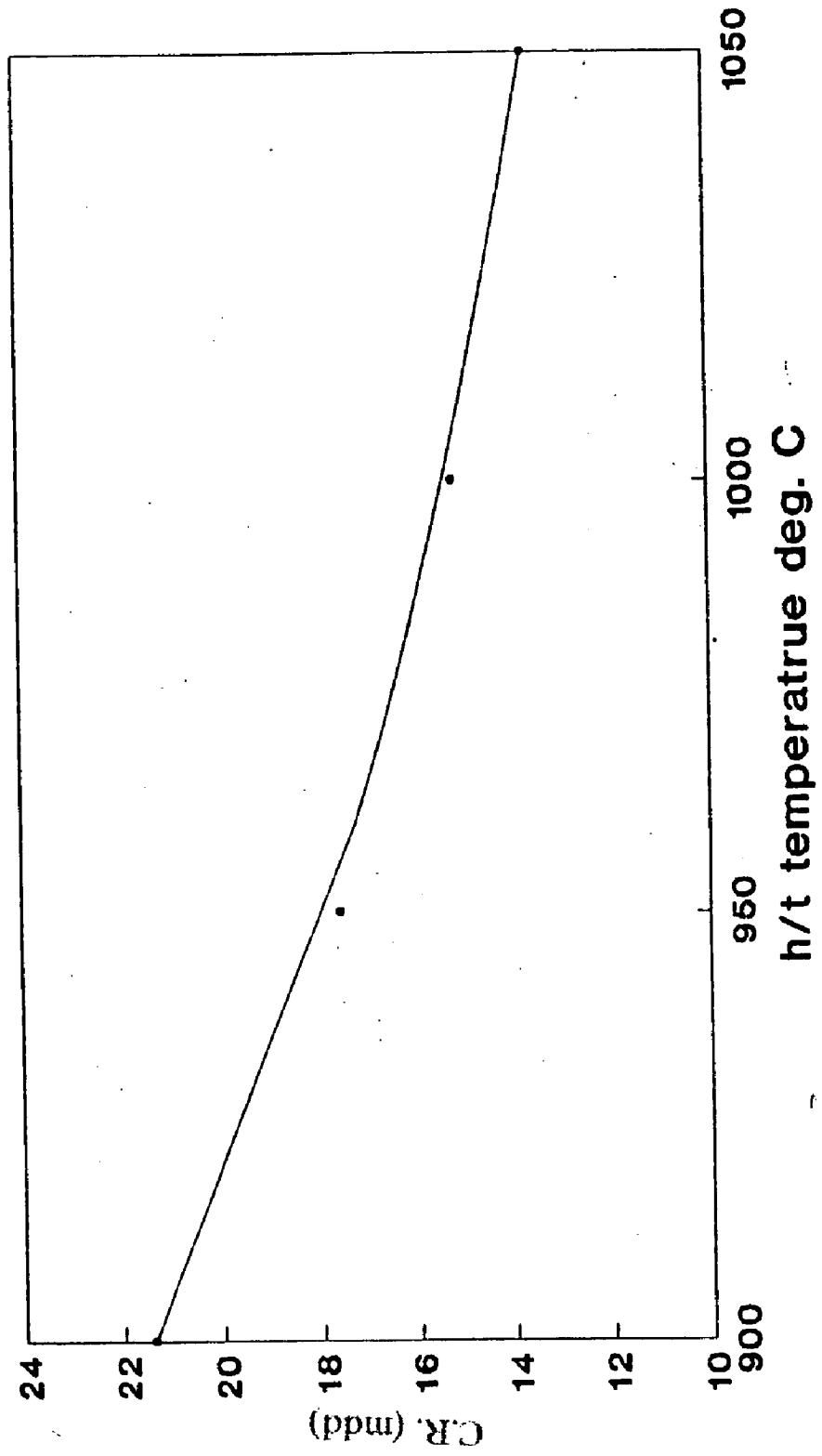


Fig. 7.5 Effect of heat treatment on corrosion behaviour (Alloy C2)
(b) 10 hours

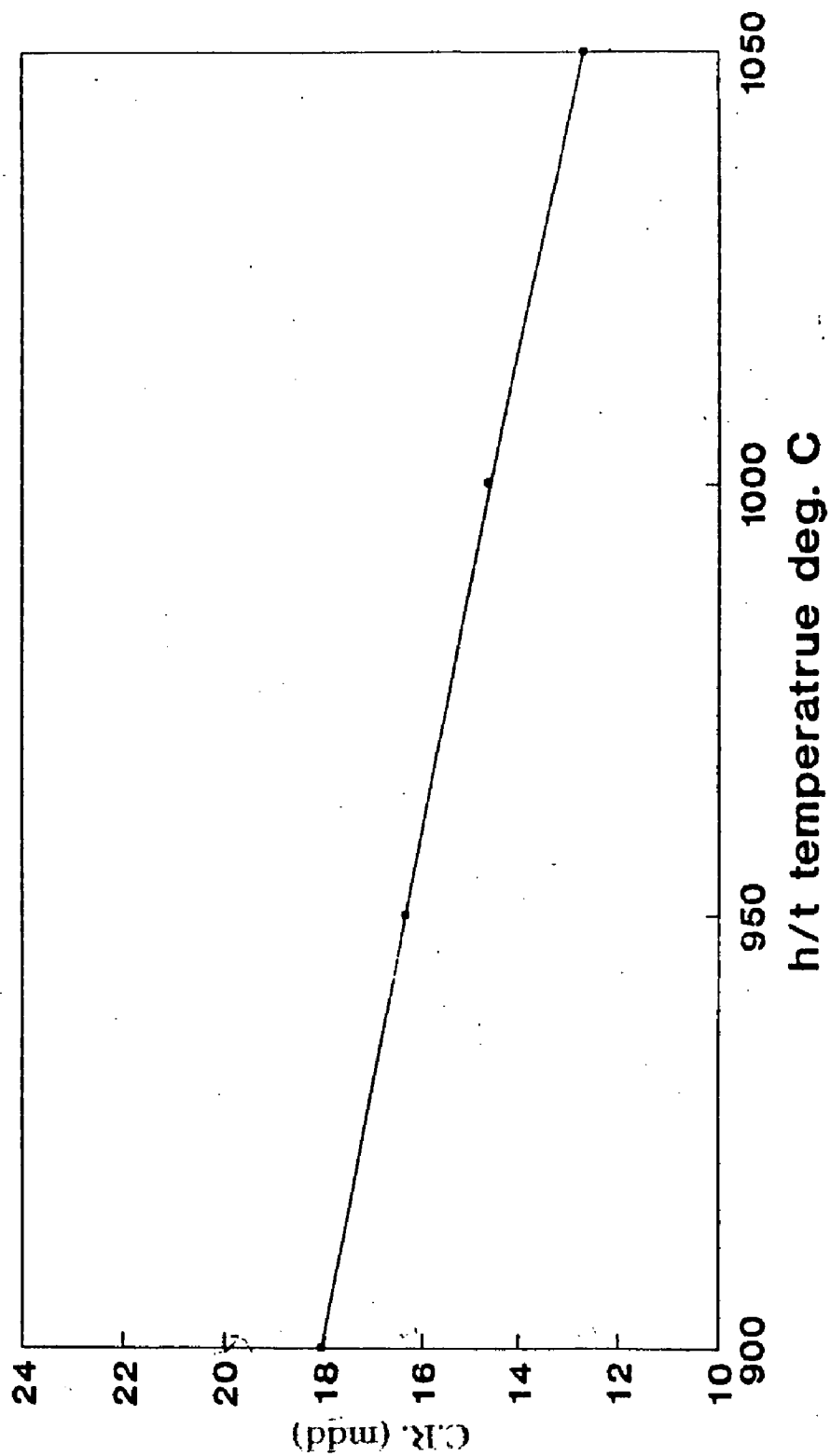


Fig. 7.6 Effect of heat treatment on corrosion behaviour (Alloy C3)
(b) 10 hours

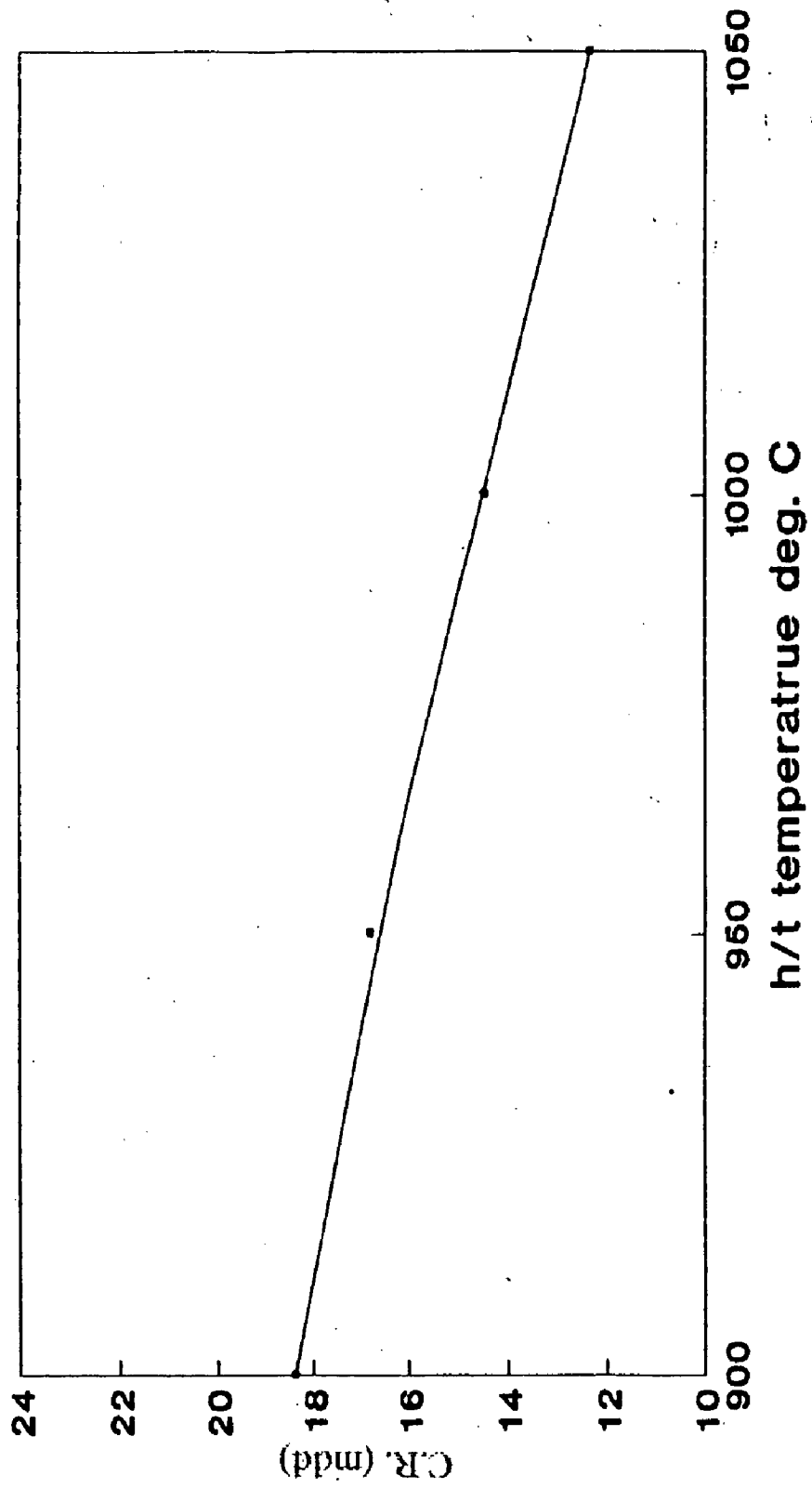
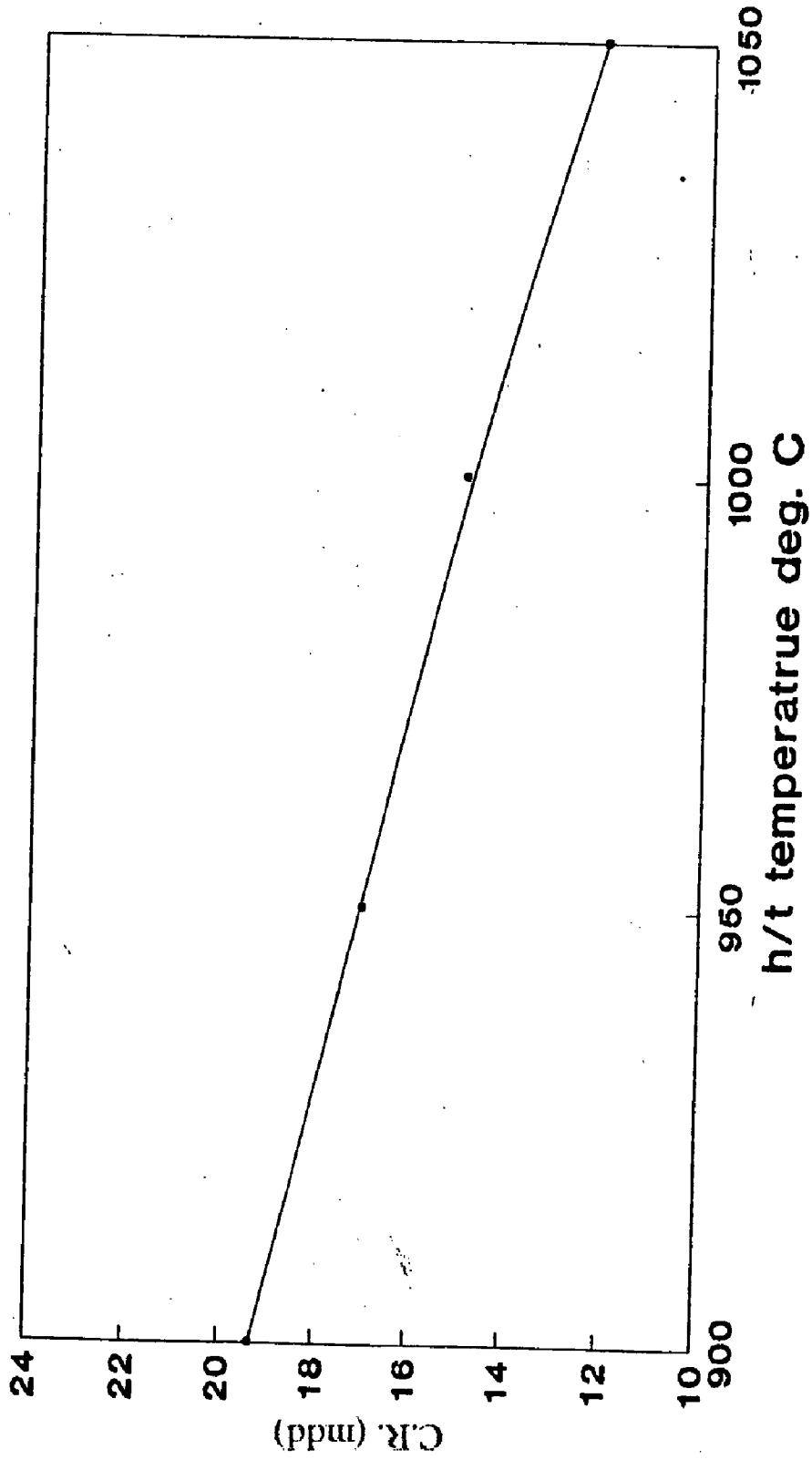


Fig. 7.8 Effect of heat treatment on corrosion behaviour (Alloy C3)

(a) 2 hours



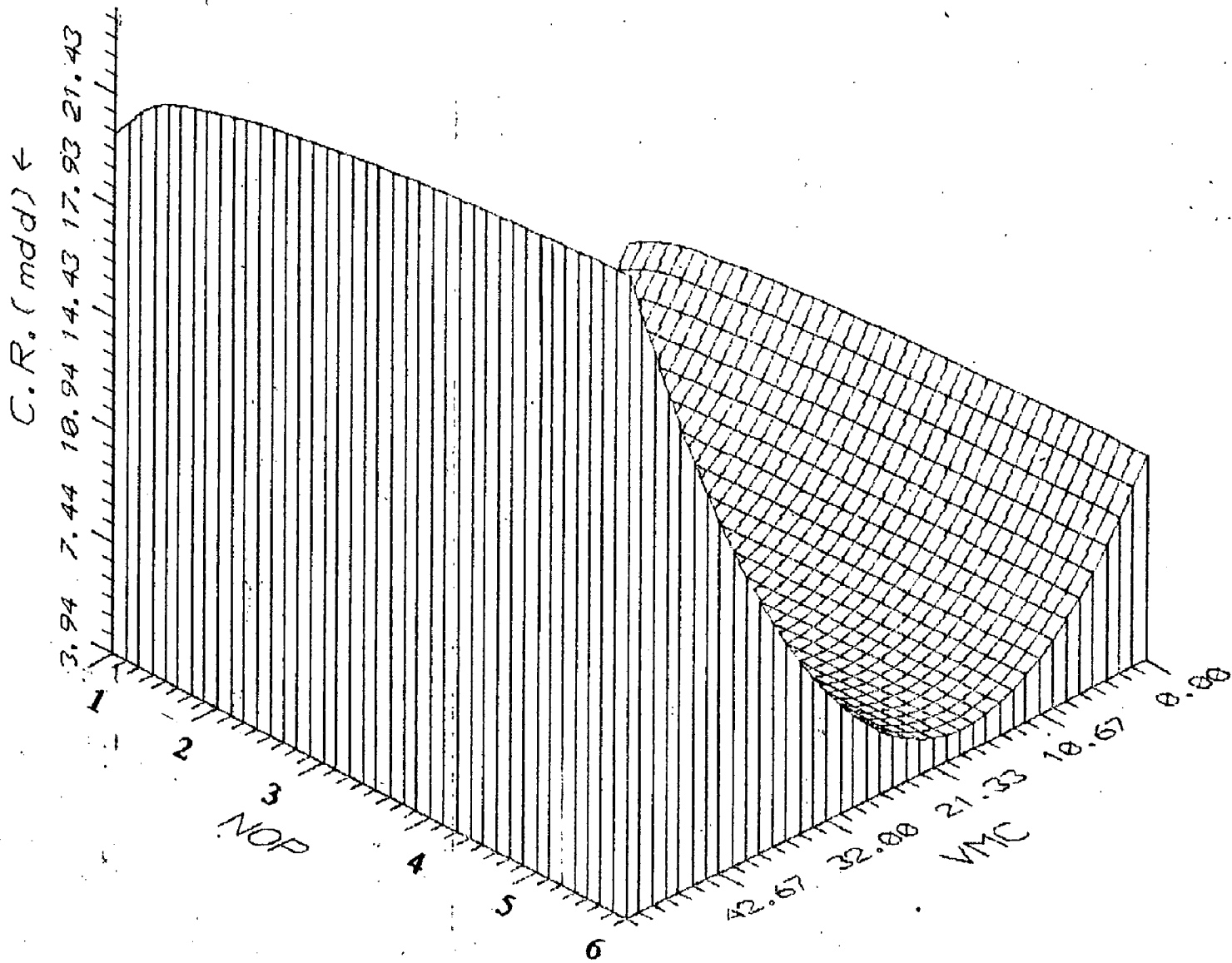


Fig. 7.7: 3D plot depicting the effect of VMC & NOP on corrosion rate (based on equation 7.17)

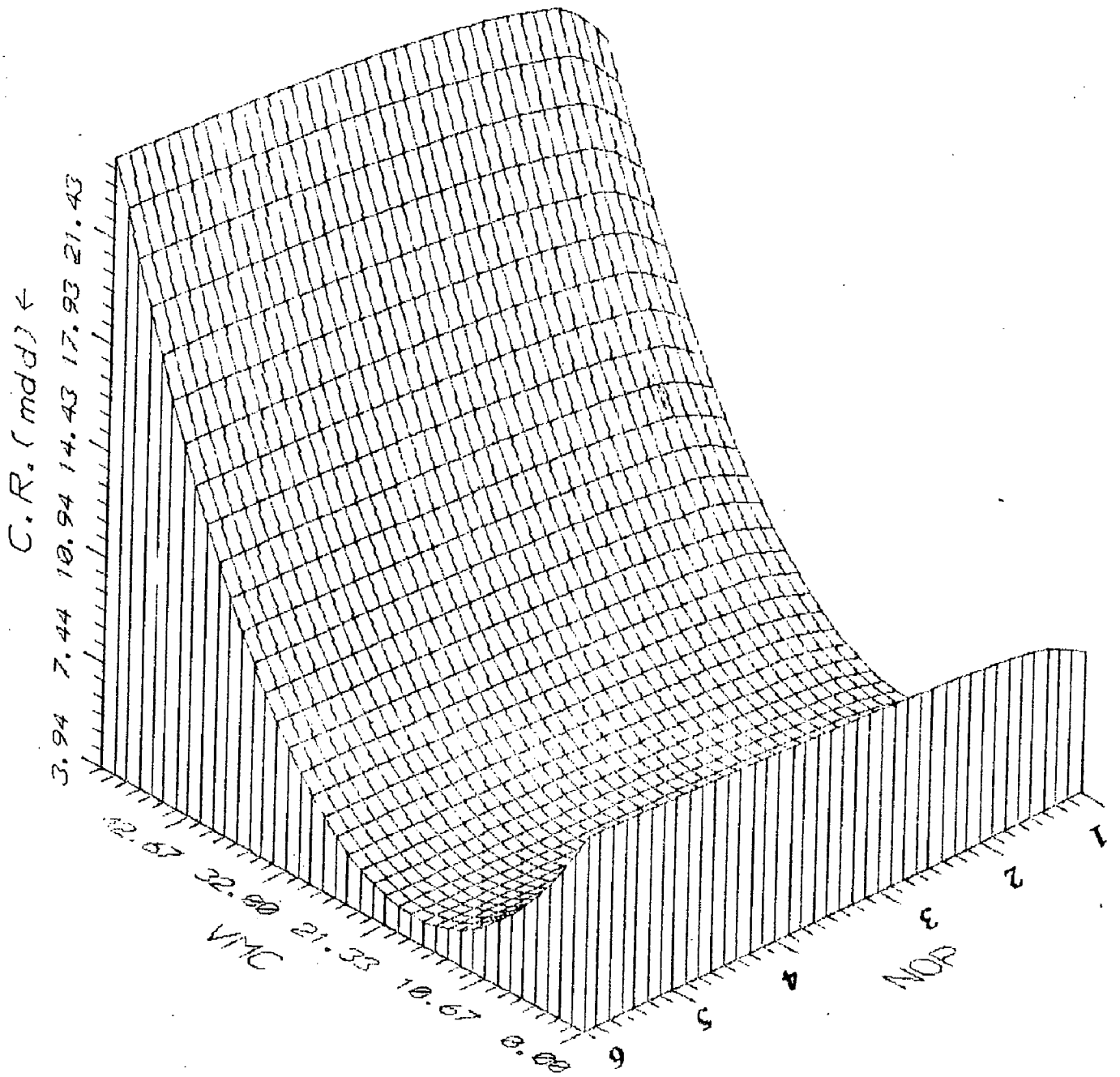


Fig. 7.8: 3D plot depicting the effect of VMC & NOP on corrosion rate (based on equation 7.17)

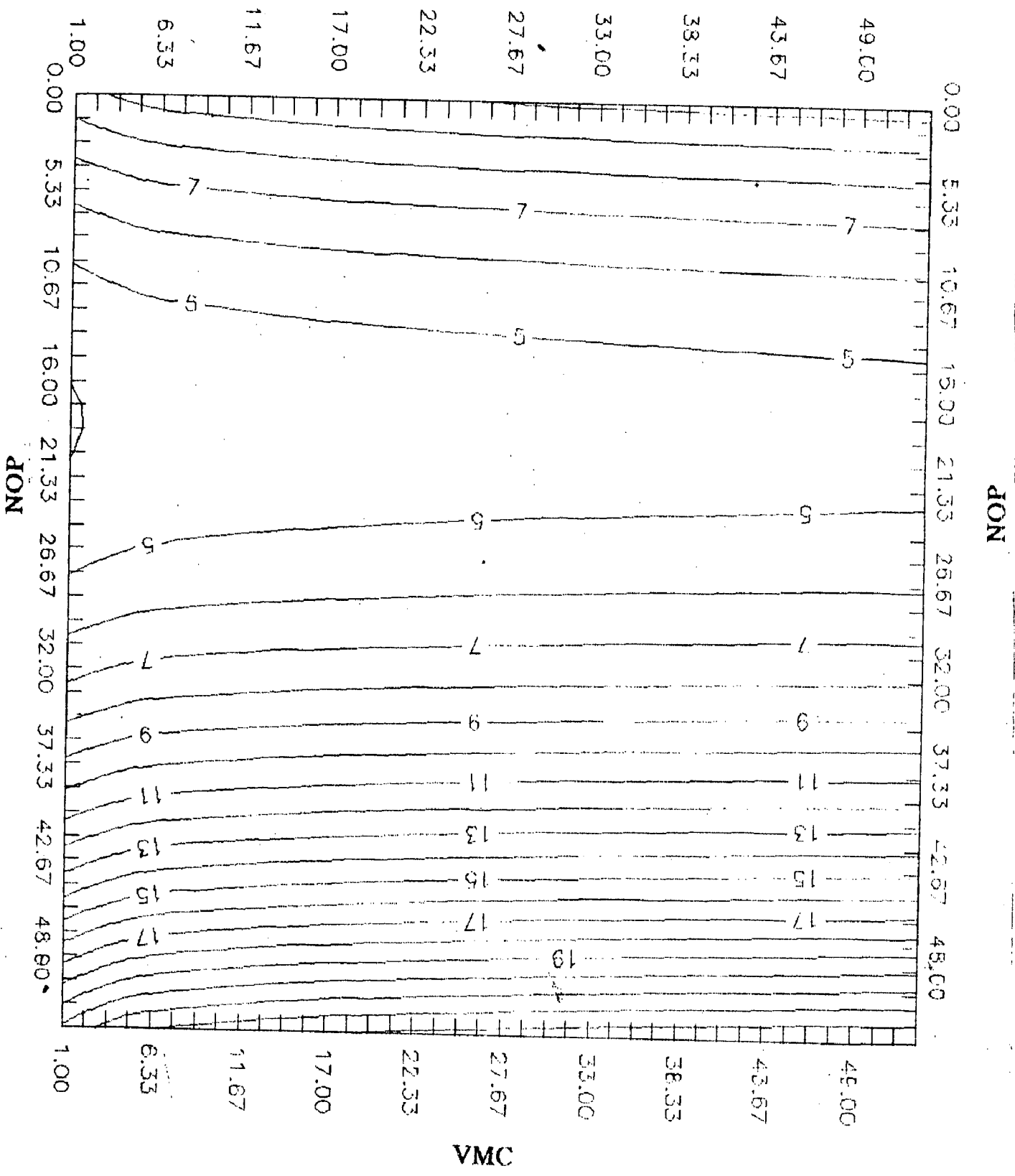


Fig. 7.10 : Contour plot depicting the combined effect of VMC & NOP on corrosion rate (based on equation 7.17)

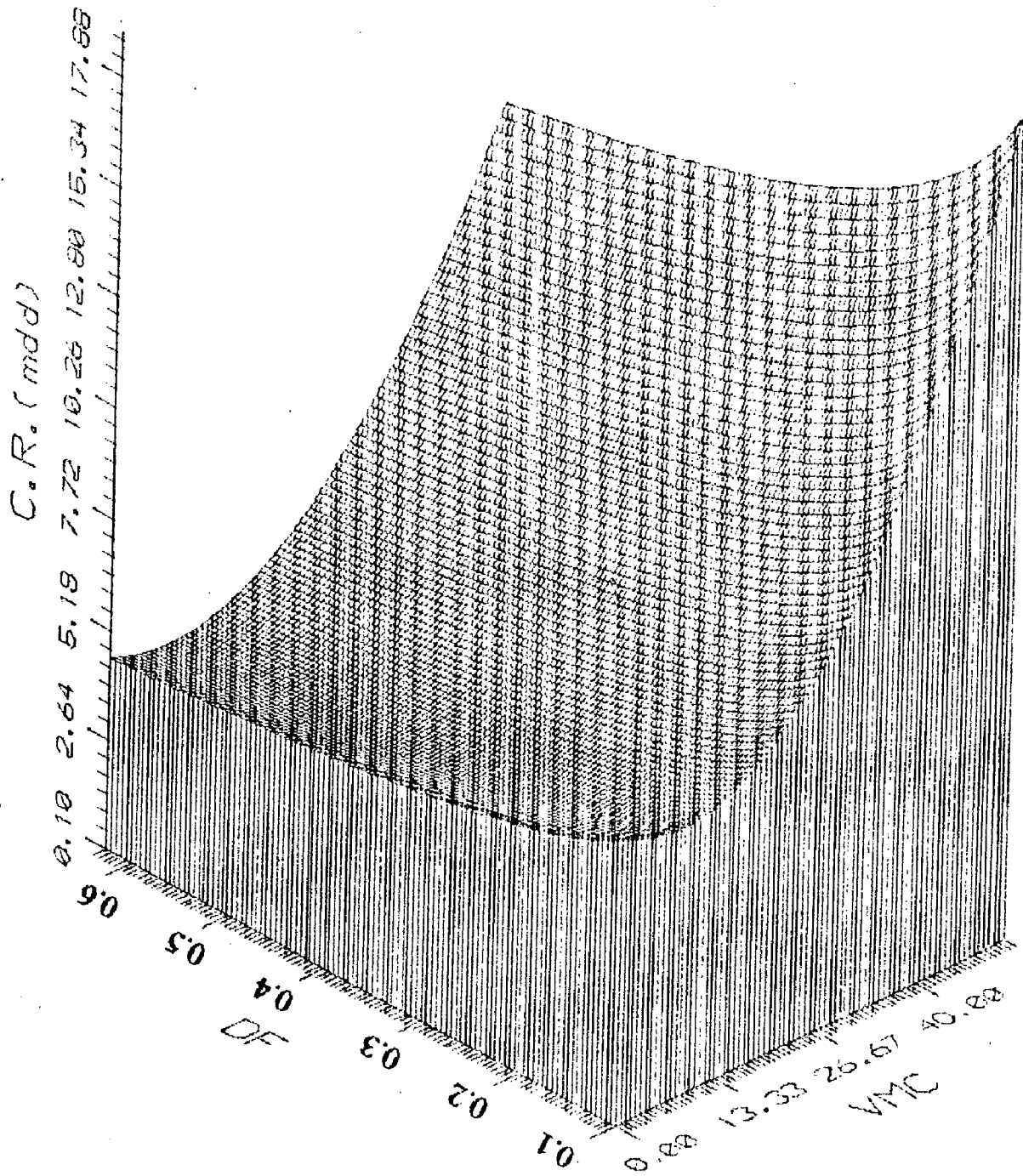


Fig. 7.12: 3D plot depicting the effect of VMC & DF on corrosion rate (based on equation 7.21)

Fig. 7.5 Effect of heat treatment on corrosion behaviour (Alloy C2)
(a) 2 hours

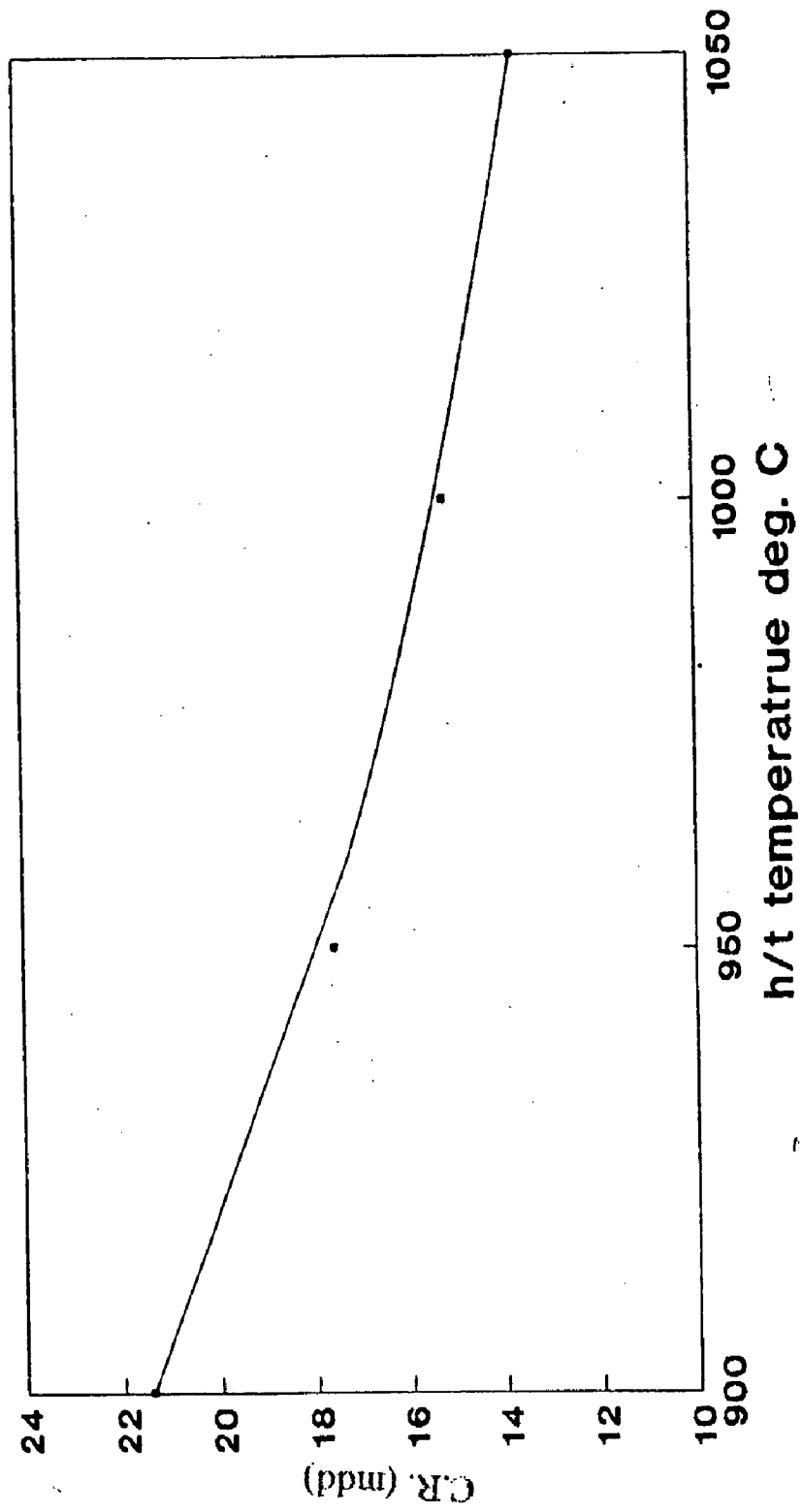


Fig. 7.6 Effect of heat treatment on corrosion behaviour (Alloy C2)
(b) 10 hours

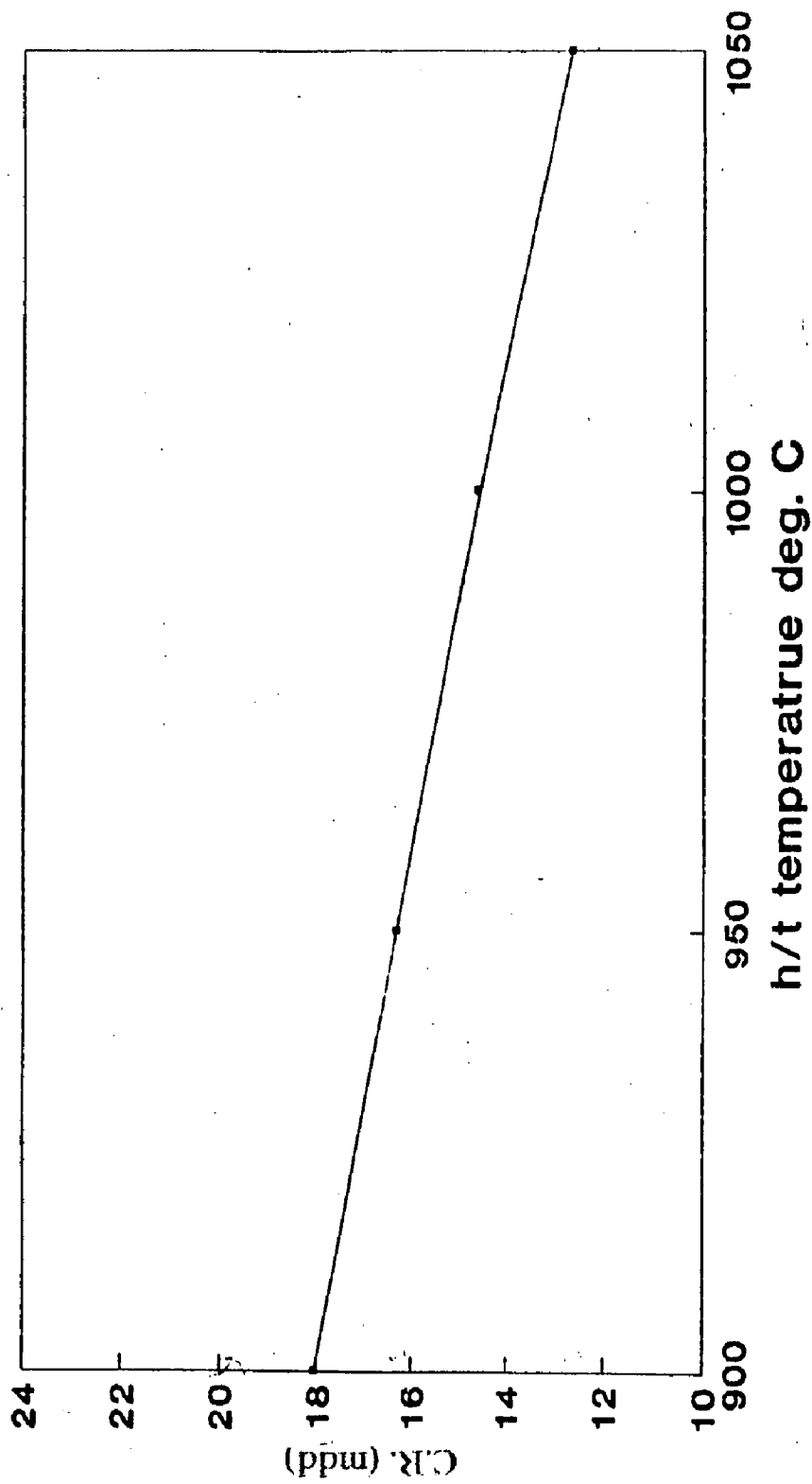


Fig. 7.6 Effect of heat treatment on corrosion behaviour (Alloy C3)
(b) 10 hours

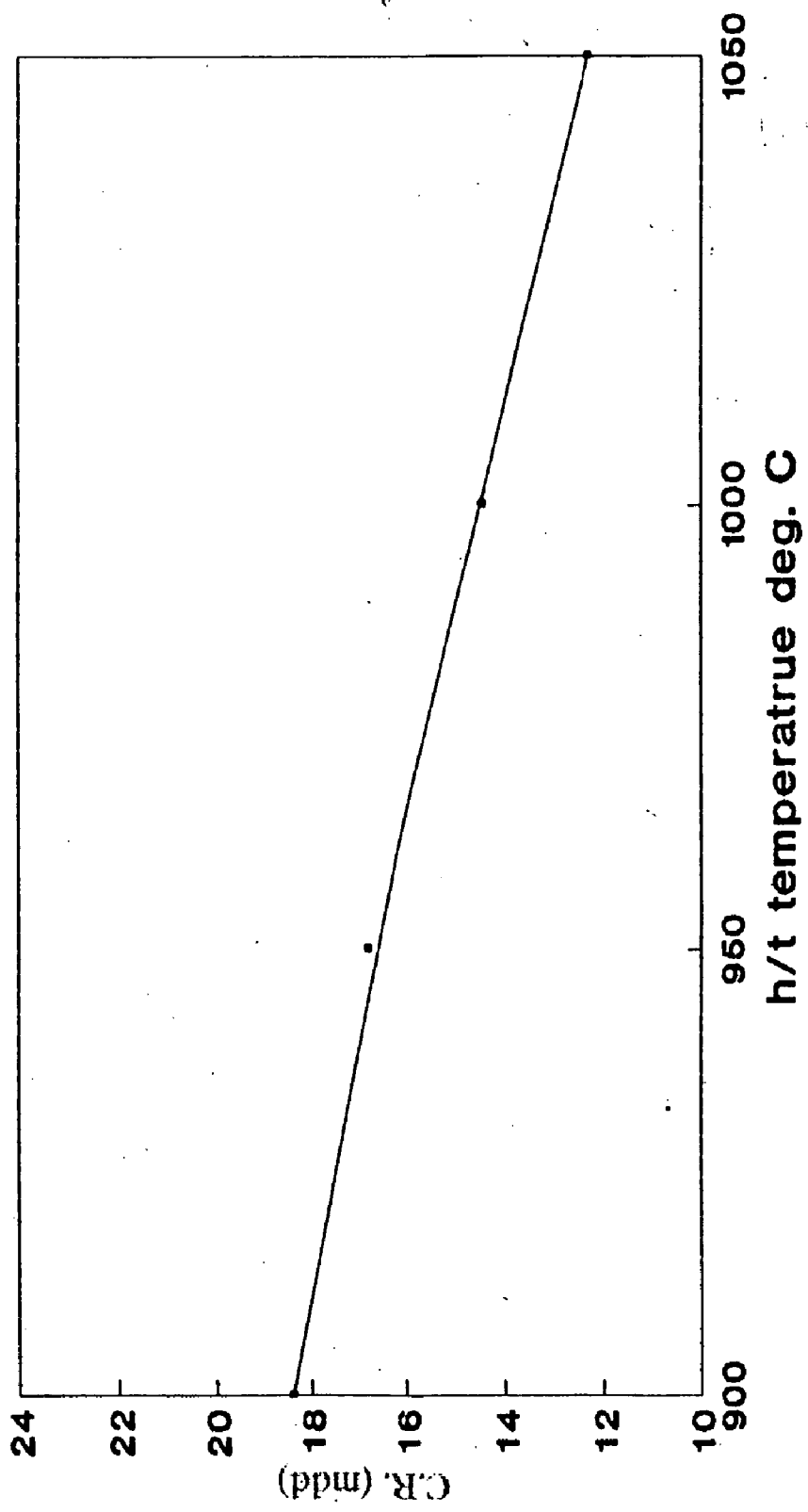
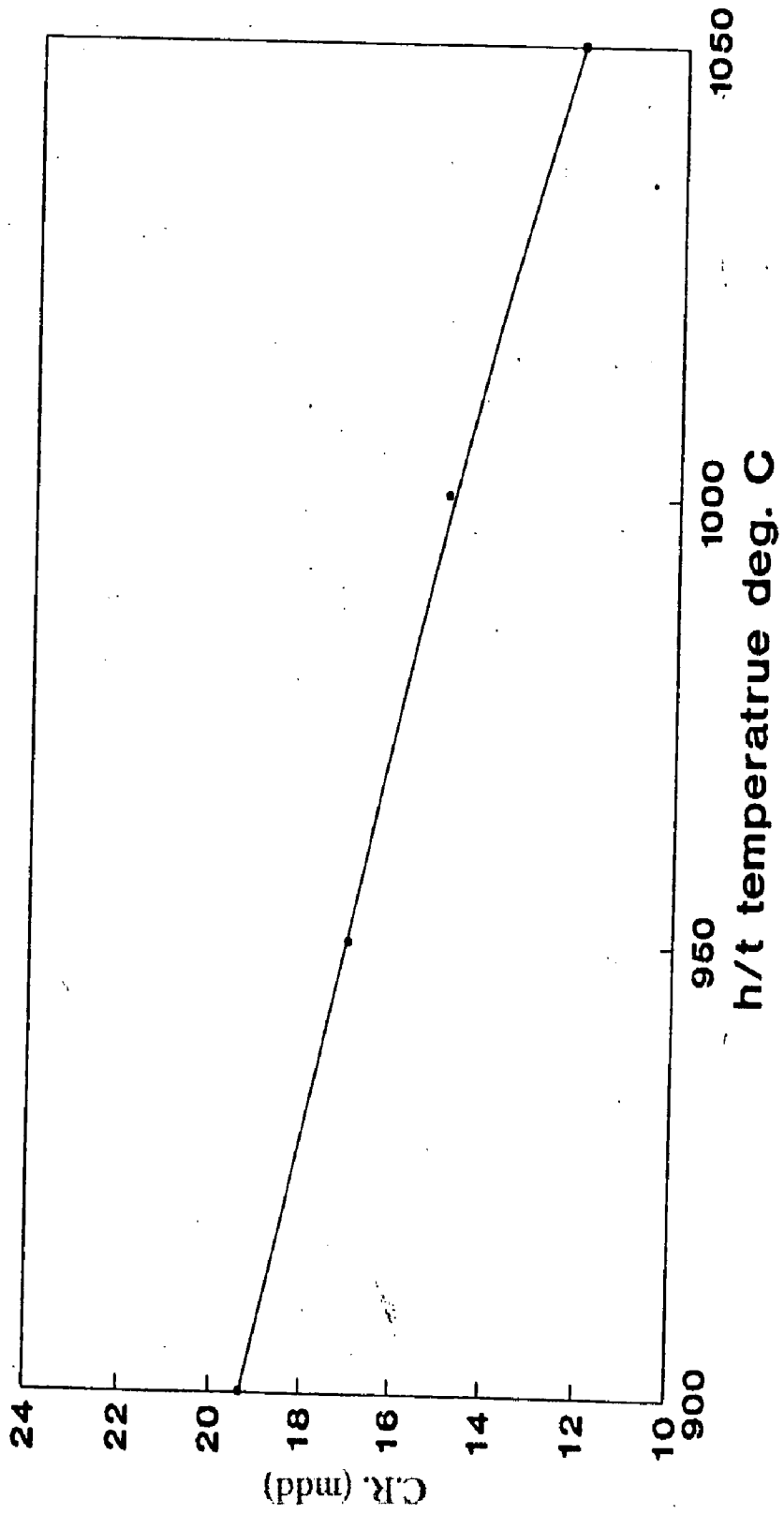


Fig. 7.8 Effect of heat treatment on corrosion behaviour (Alloy C3)
(a) 2 hours



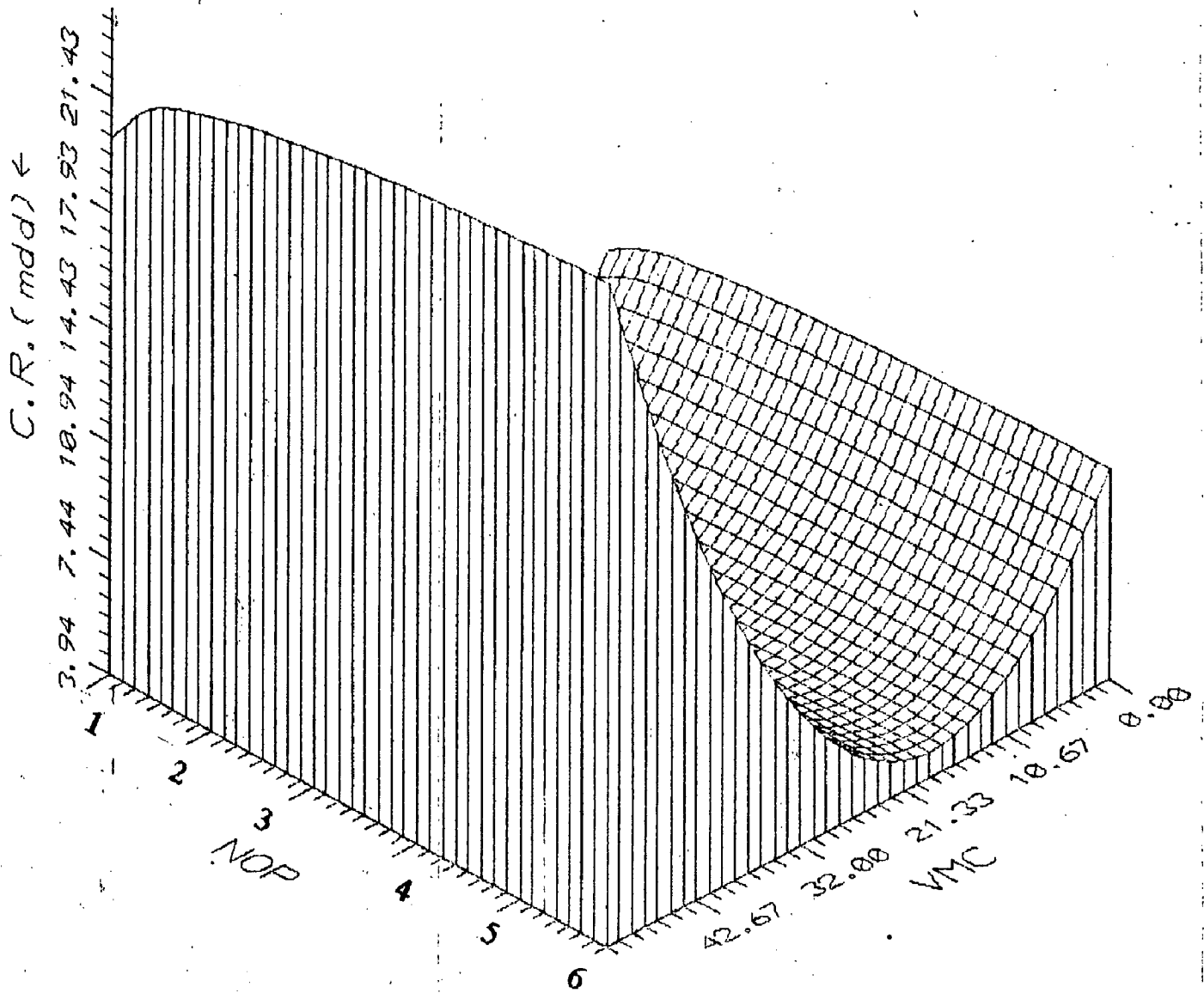


Fig. 7.7: 3D plot depicting the effect of VMC & NOP on corrosion rate (based on equation 7.17)

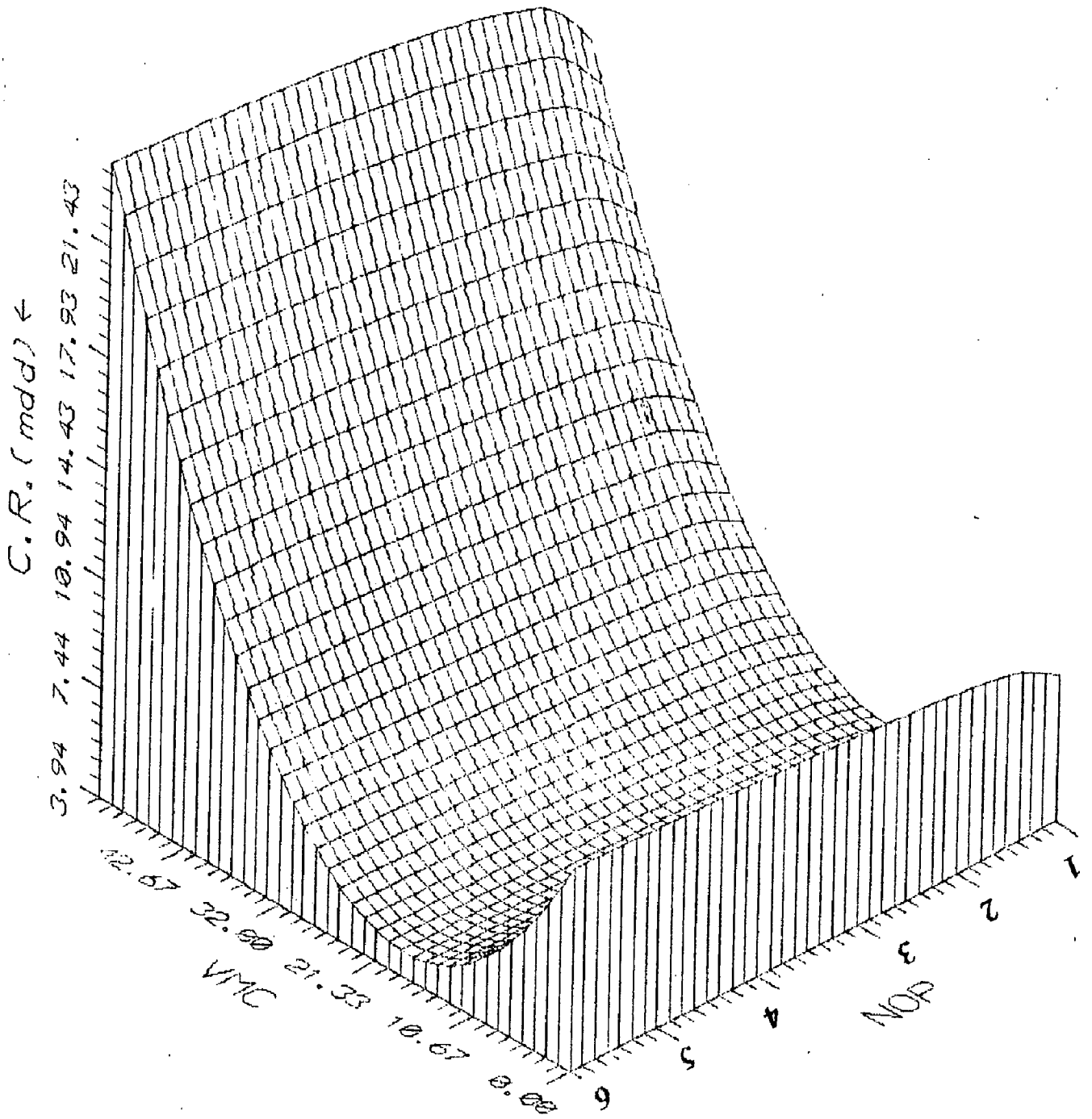


Fig. 7.8: 3D plot depicting the effect of VMC & NOP on corrosion rate (based on equation 7.17)

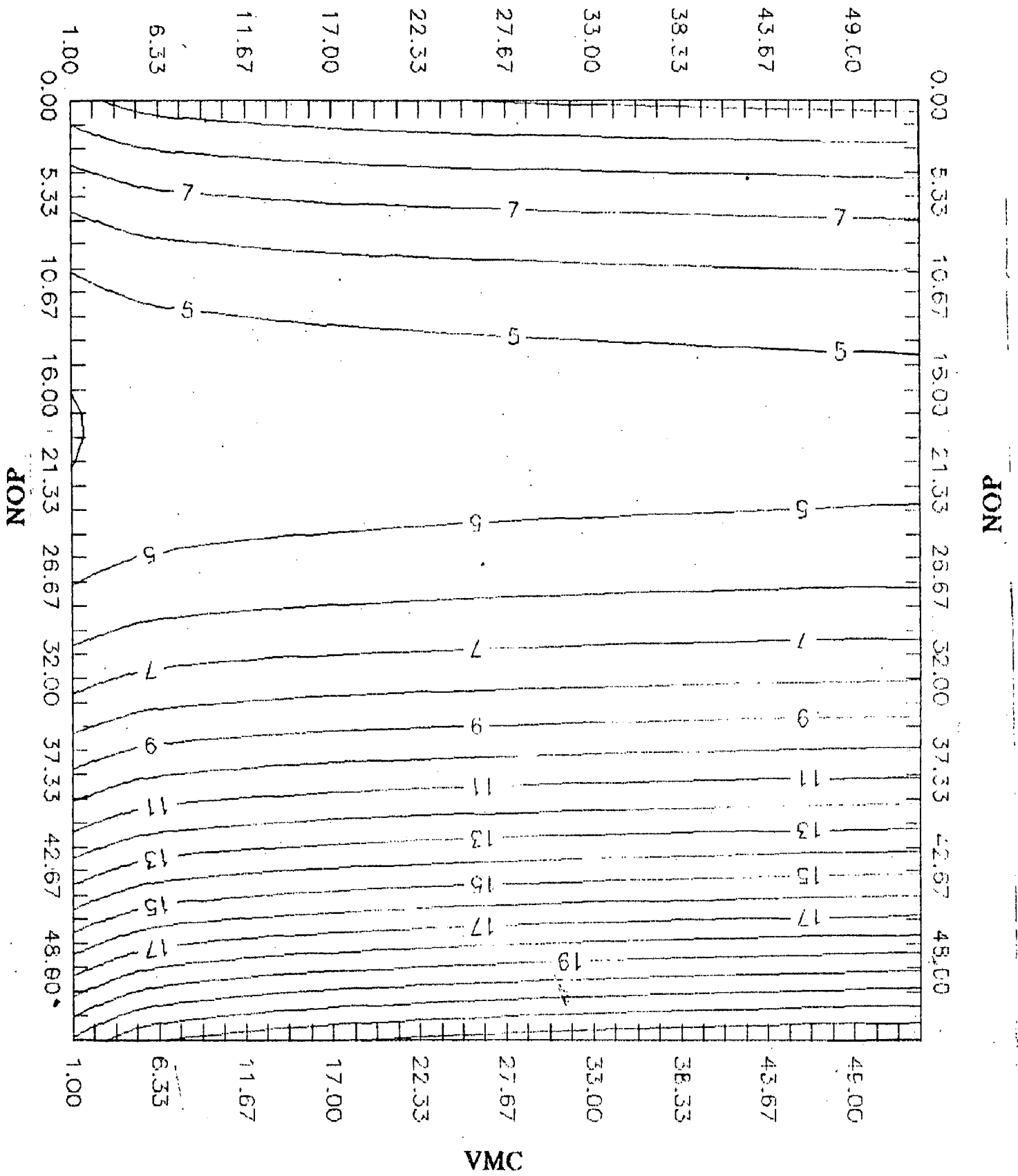


Fig. 7.10 : Contour plot depicting the combined effect of VMC & NOP on corrosion rate (based on equation 7.17)

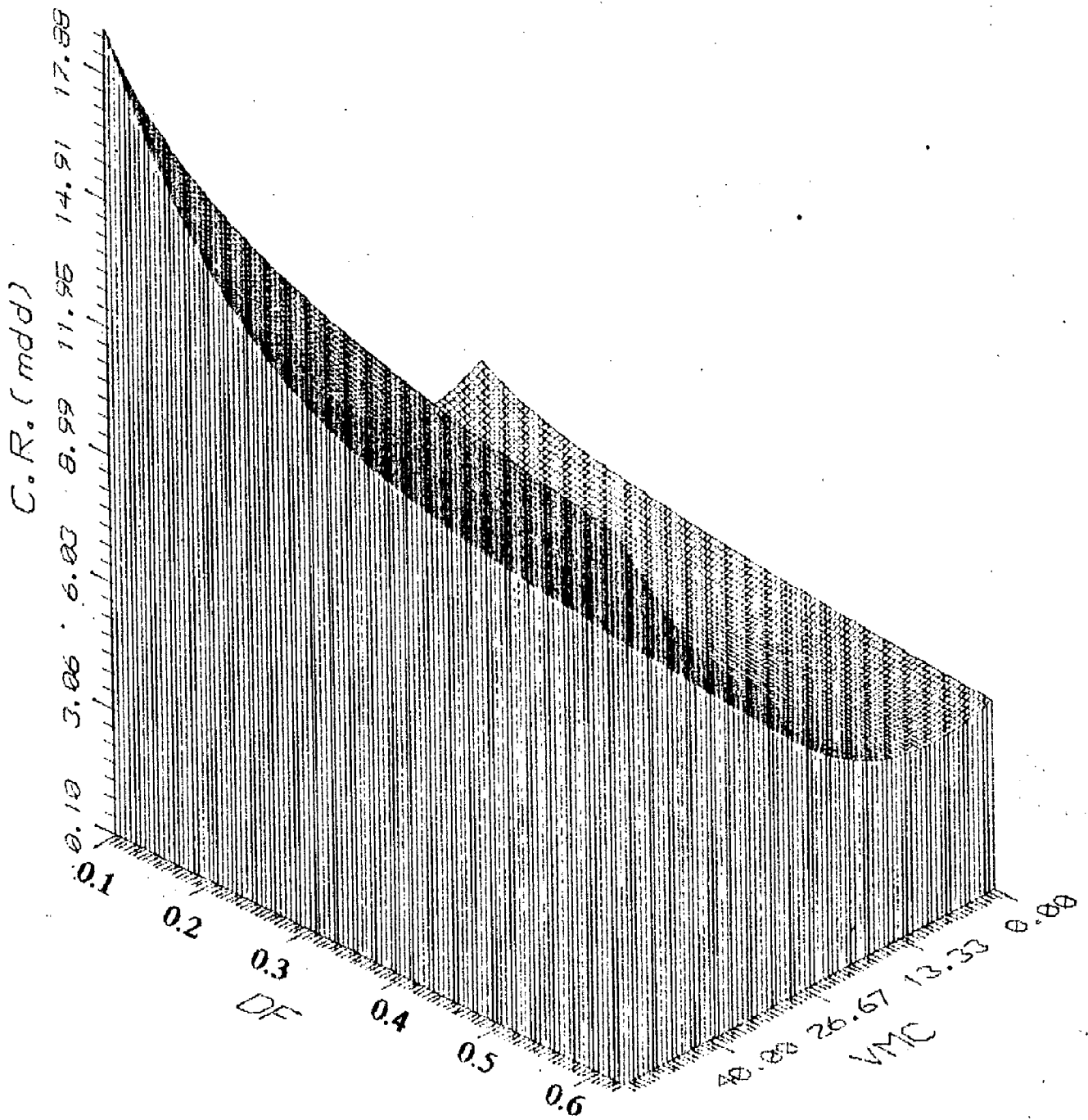


Fig. 7.11: 3D plot depicting the effect of VMC & DF on corrosion rate (based on equation 7.21)

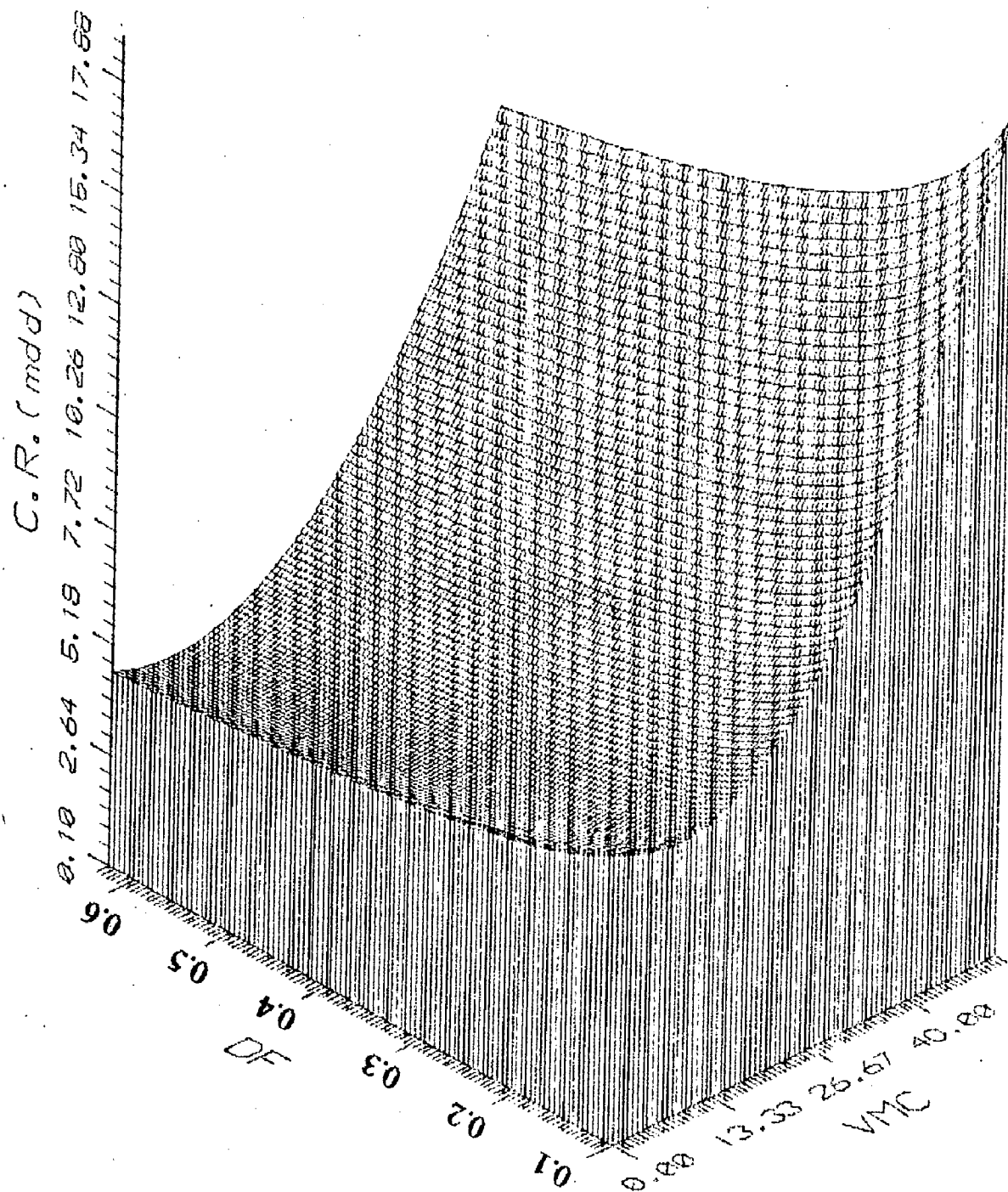


Fig. 7.12: 3D plot depicting the effect of VMC & DF on corrosion rate (based on equation 7.21)

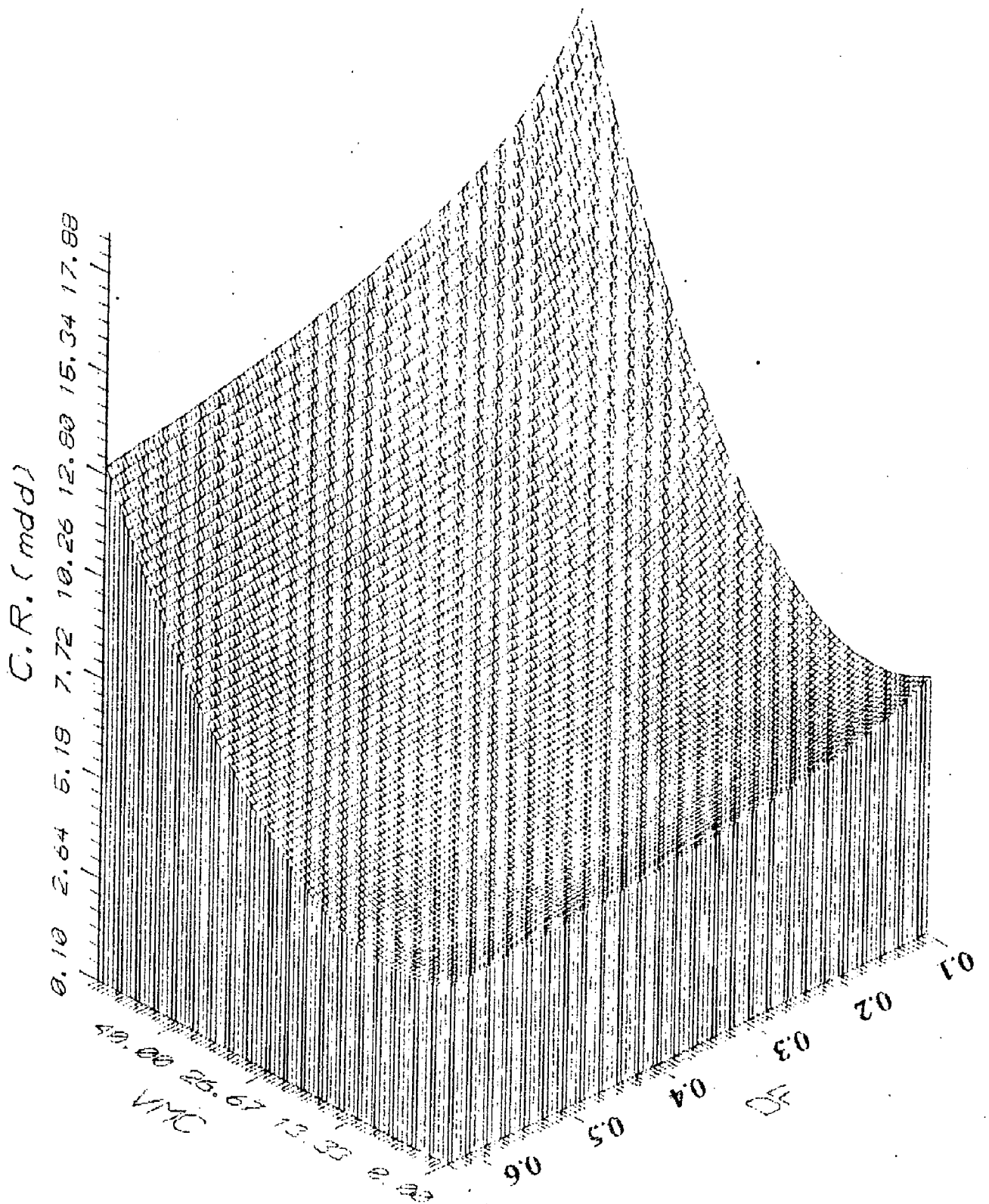


Fig. 7.13: 3D plot depicting the effect of VMC & DF on corrosion rate (based on equation 7.21)

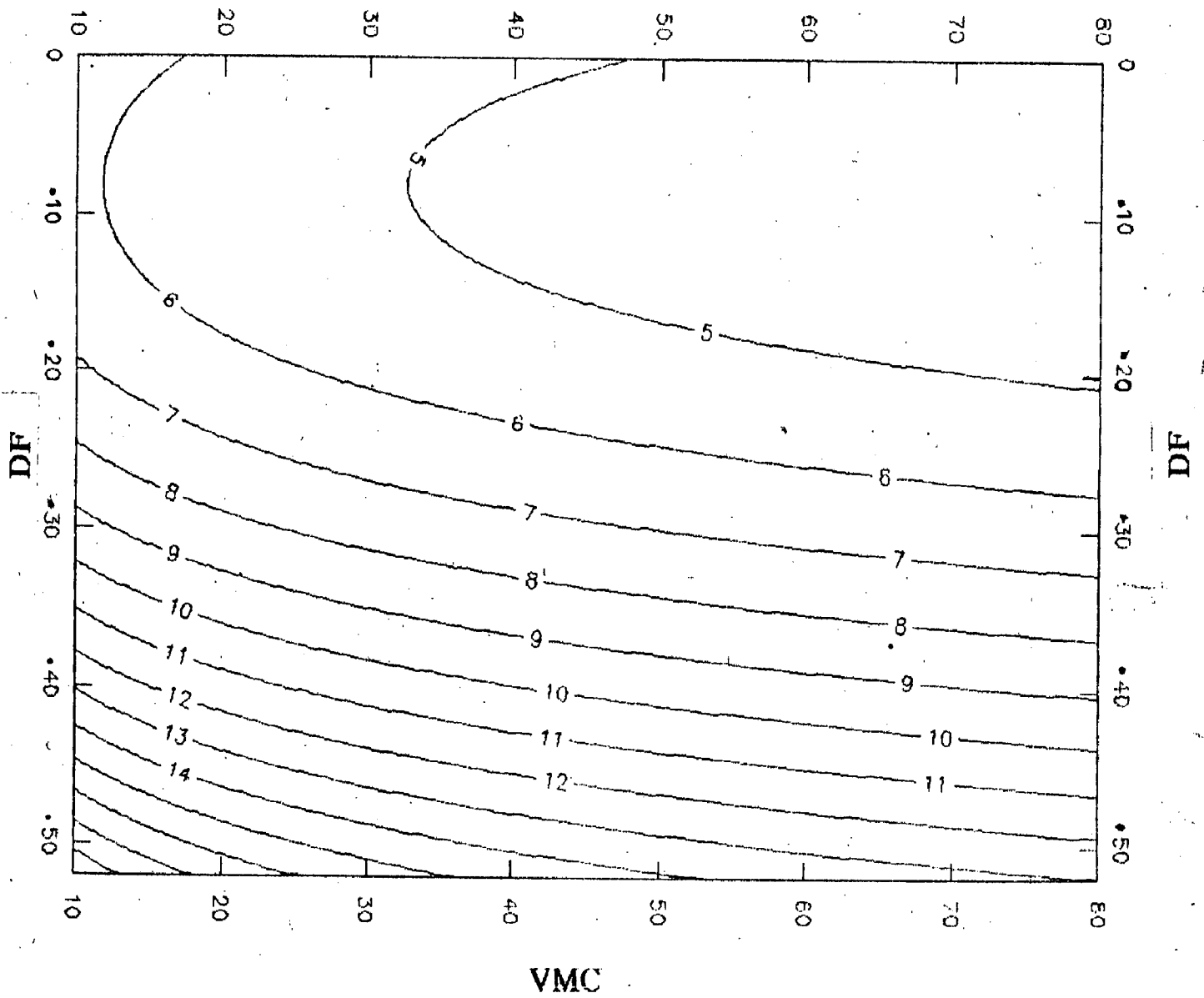


Fig. 7.14: Contour plot depicting the combined effect of F-113 VMC & DF on corrosion rate (based on equation 7.21)

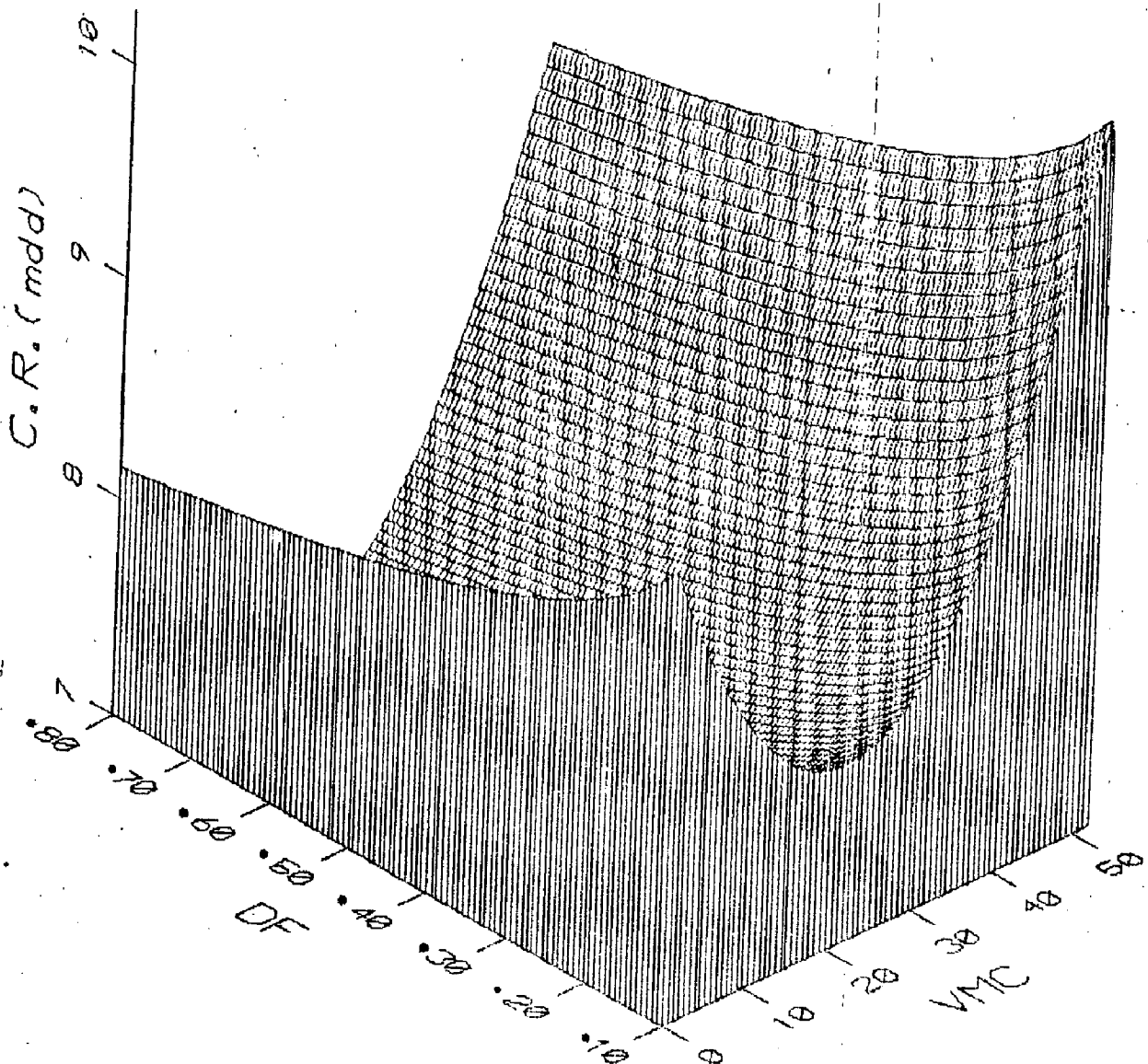


Fig. 7.15: 3D plot depicting the effect of VMC & DF on corrosion rate (based on equation 7.22)

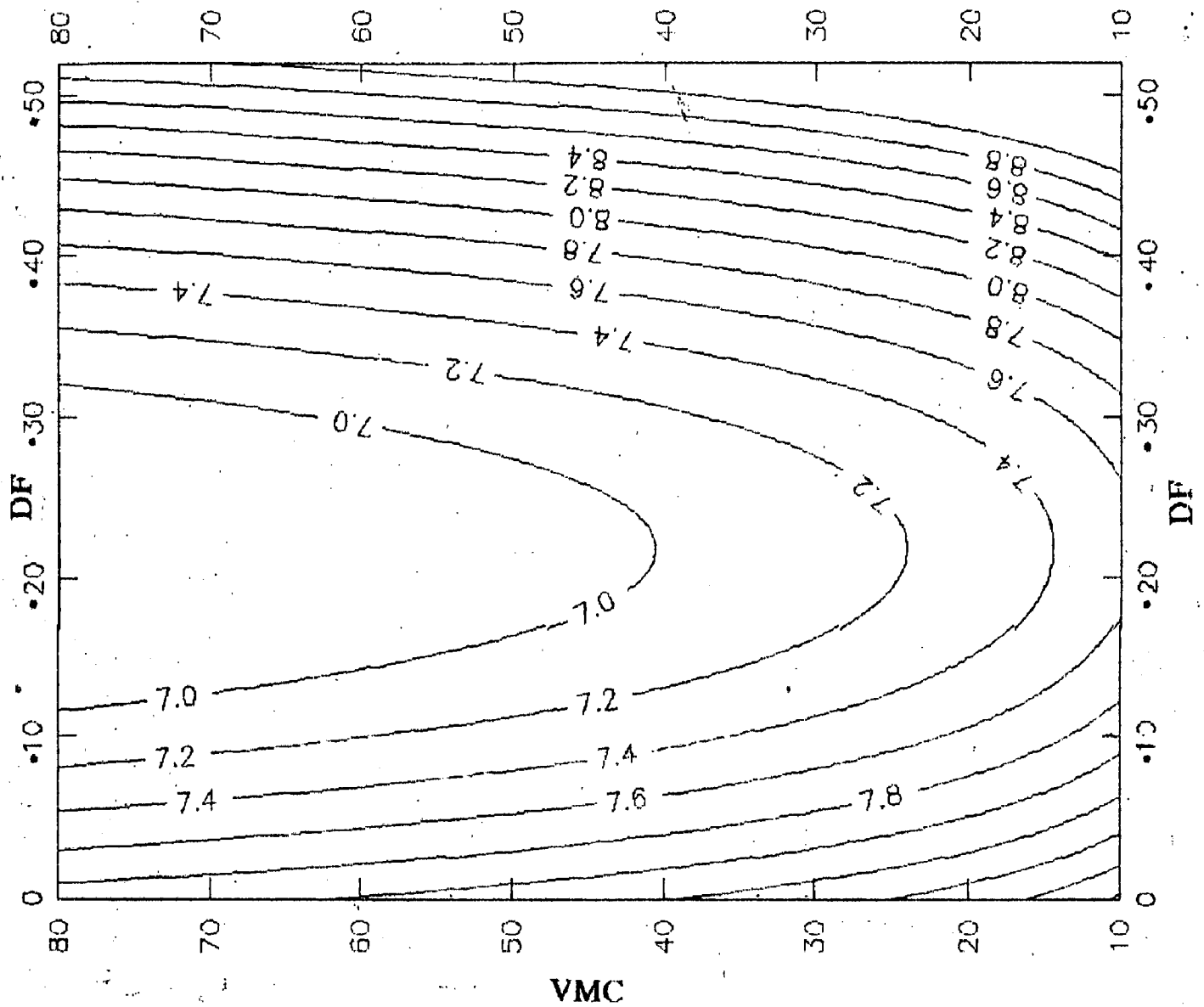


Fig. 7.16: Contour plot depicting the combined effect of F-113 VMC & DF on corrosion rate (based on equation 7.22)

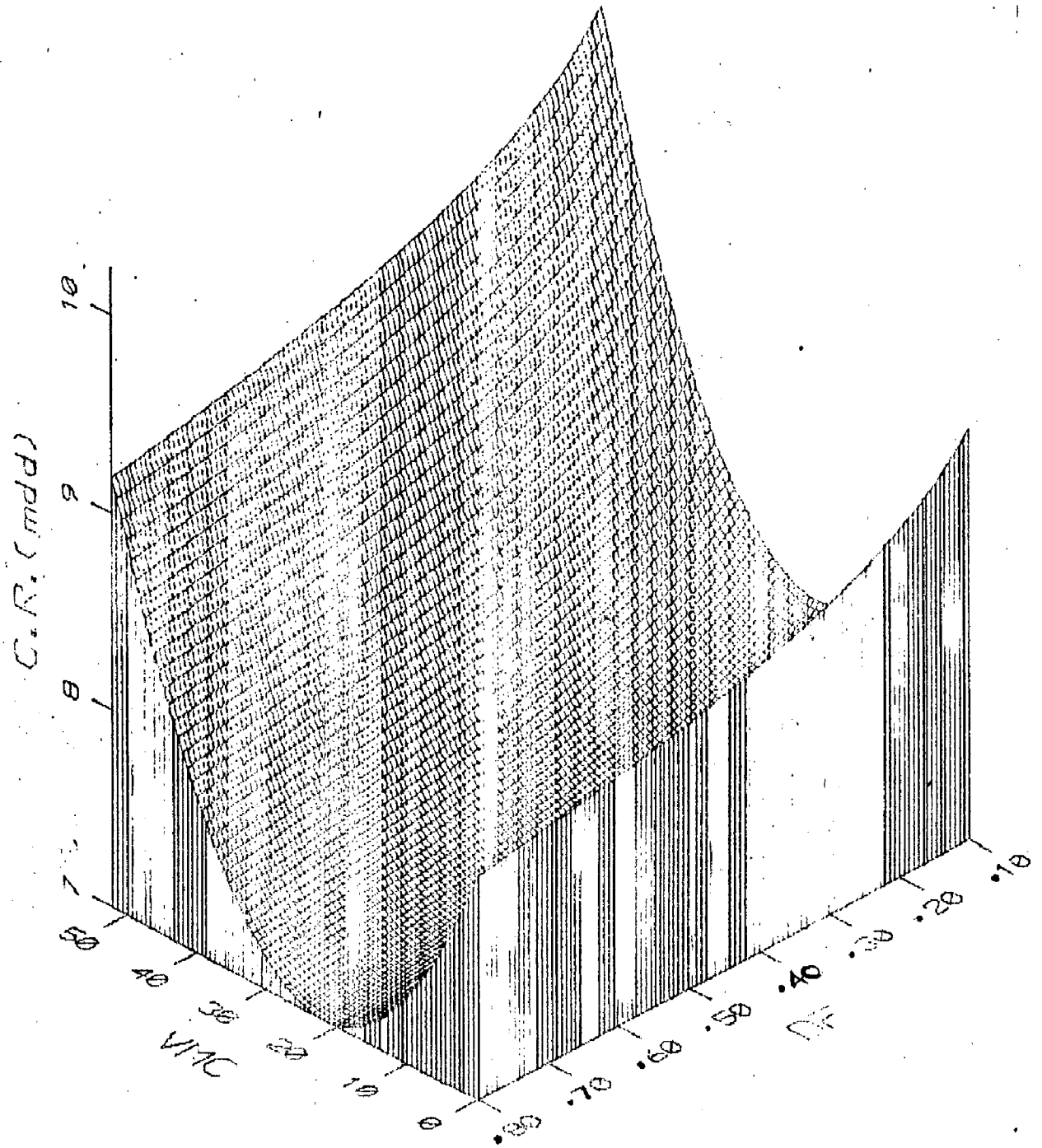


Fig. 7.17: 3D plot depicting the effect of VMC & DF on corrosion rate (based on equation 7.22)

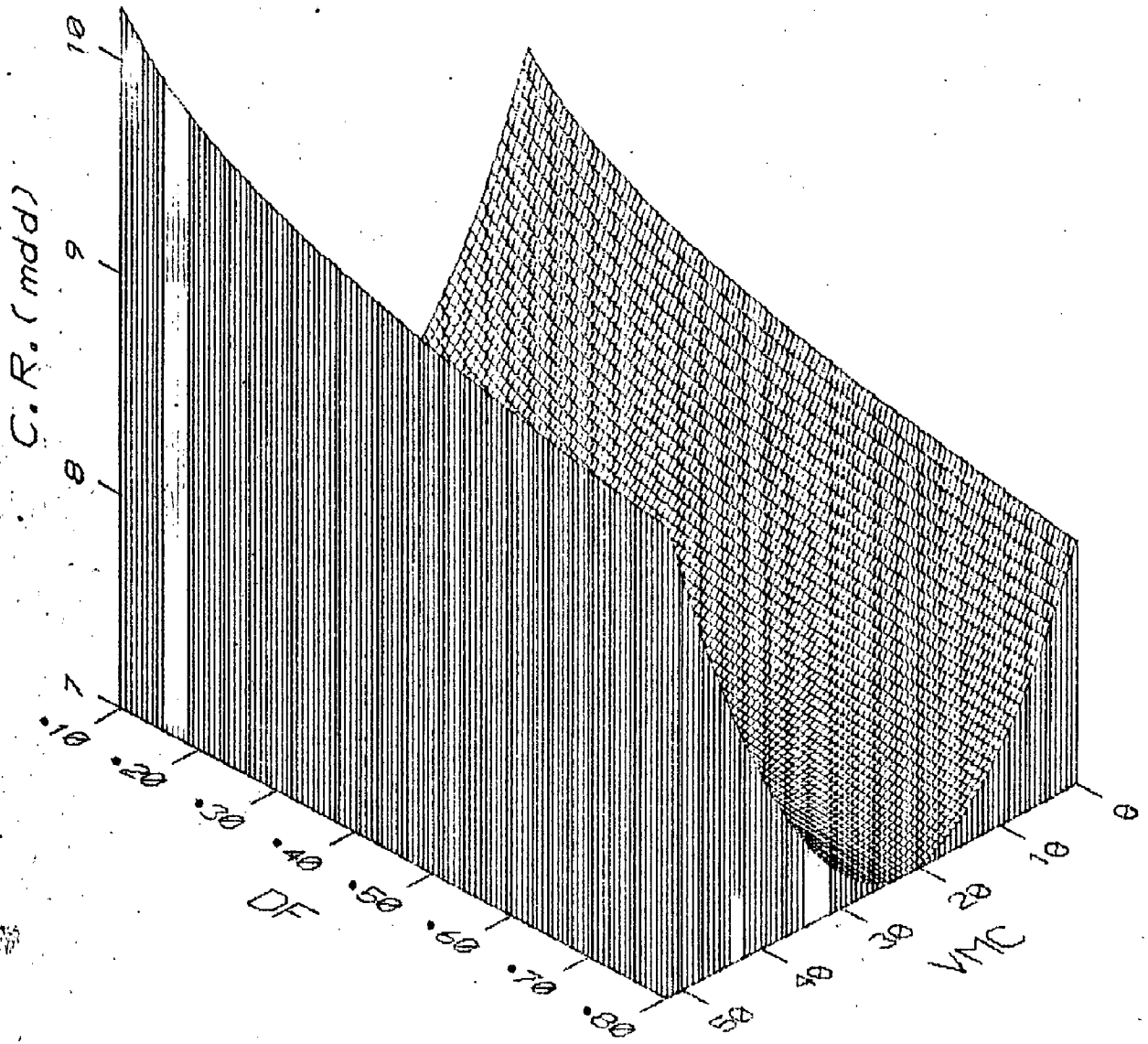


Fig. 7.18: 3D plot depicting the effect of VMC & DF on corrosion rate (based on equation 7.22)

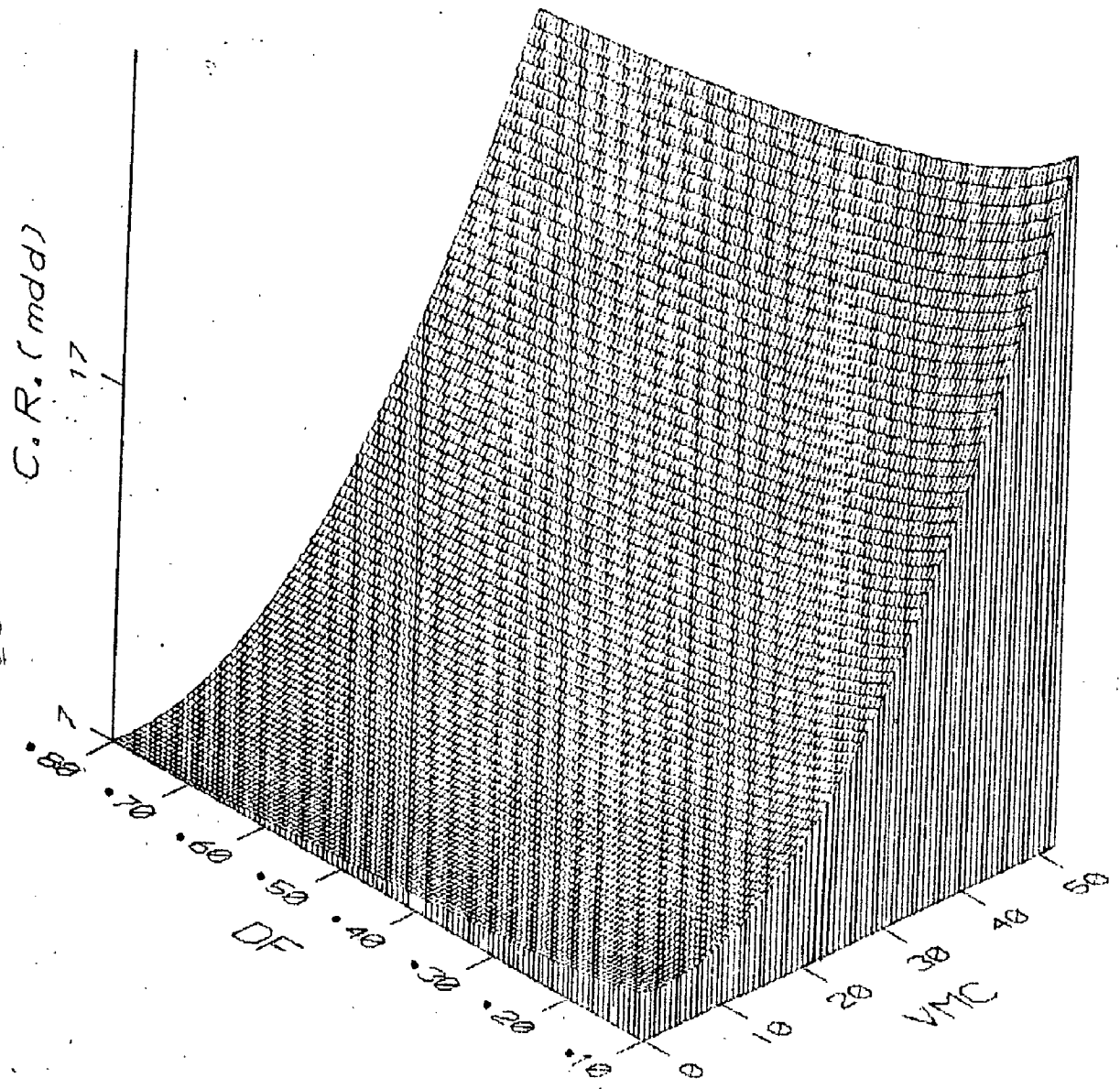


Fig. 7.19: 3D plot depicting the effect of VMC & DF on corrosion rate (based on equation 7.23).

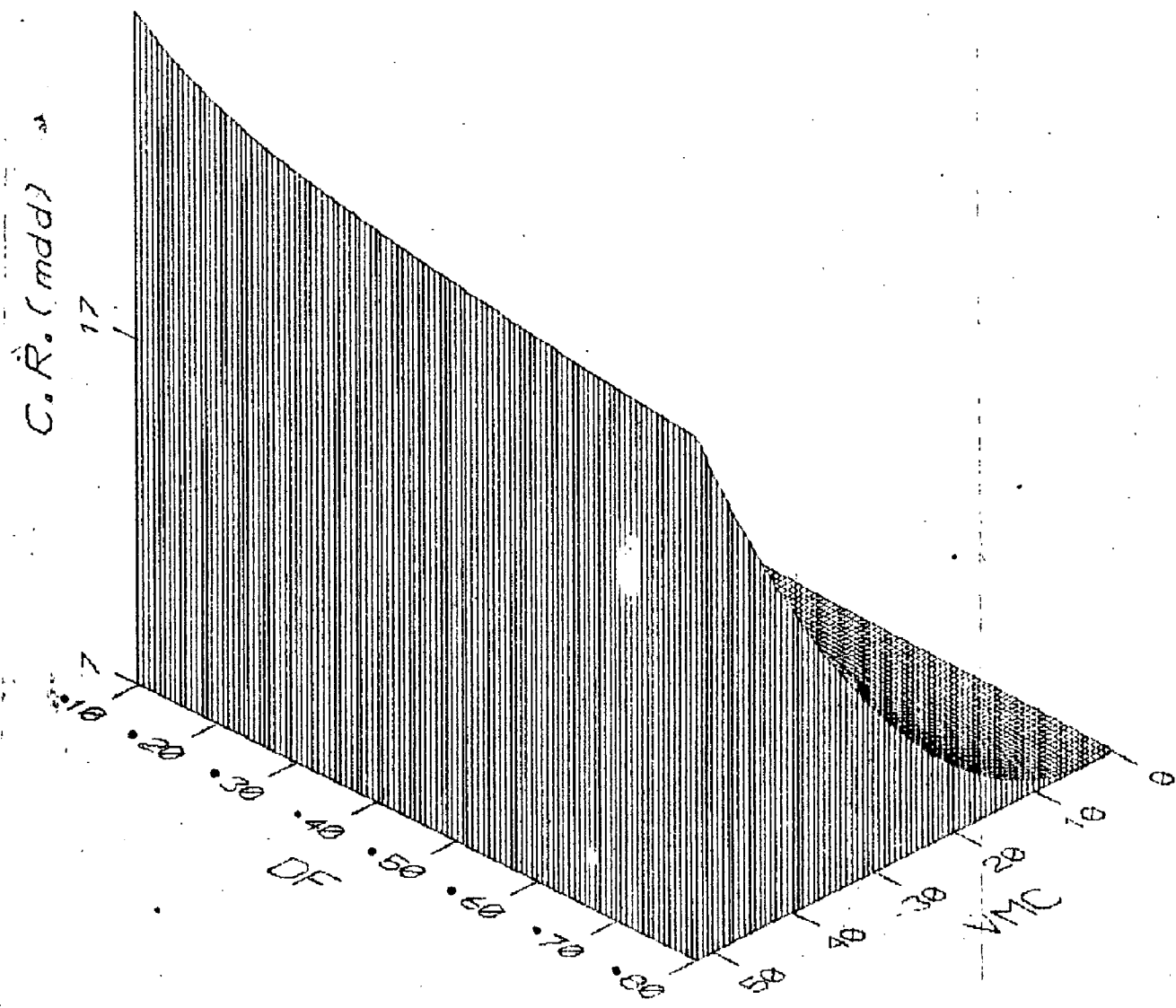


Fig. 7.20 : 3D plot depicting the effect of VMC & DF on corrosion rate (based on equation 7.23)

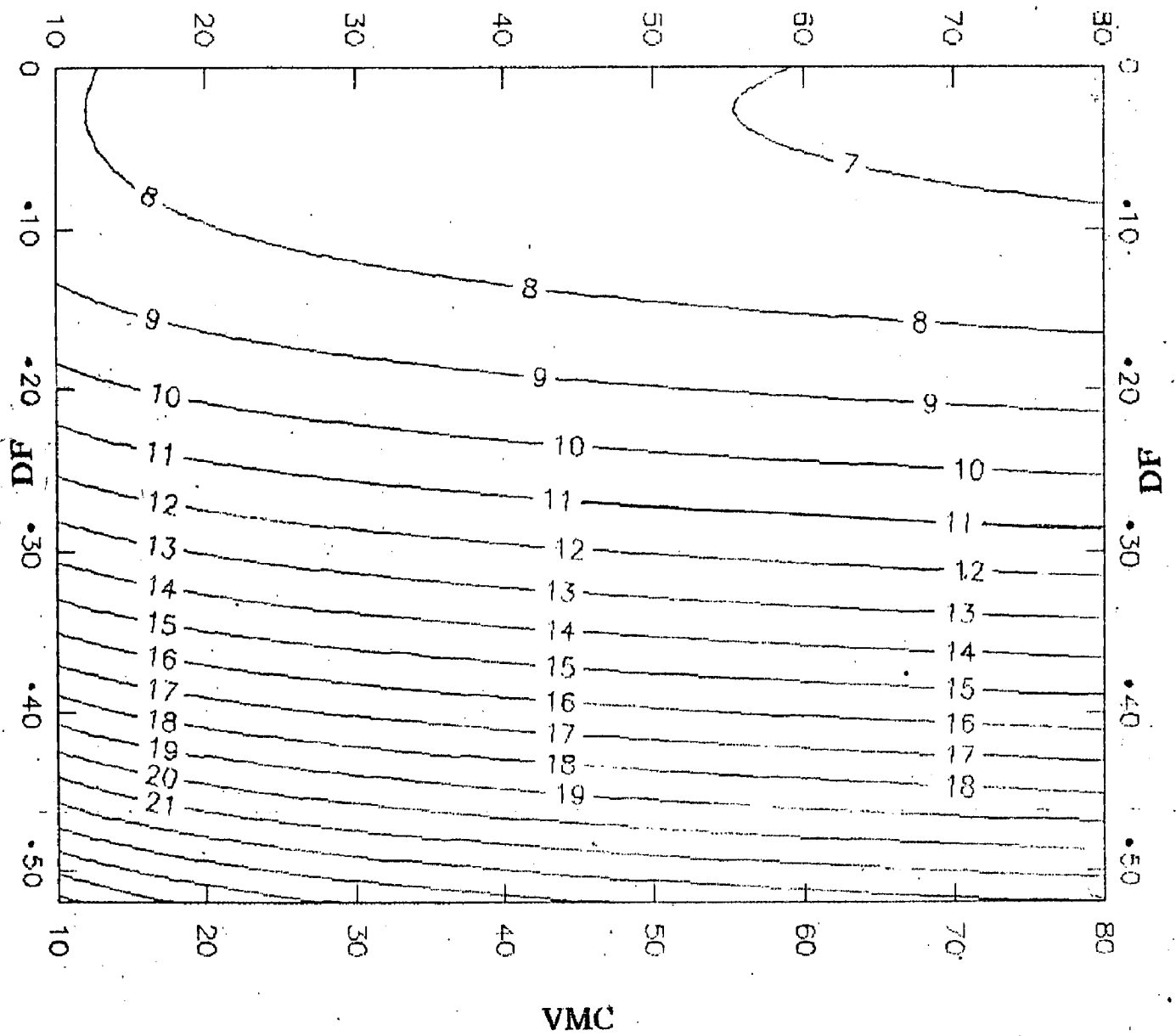


Fig. 7.21: Contour plot depicting the combined effect of F-113 VMC & DF on corrosion rate (based on equation 7.23)

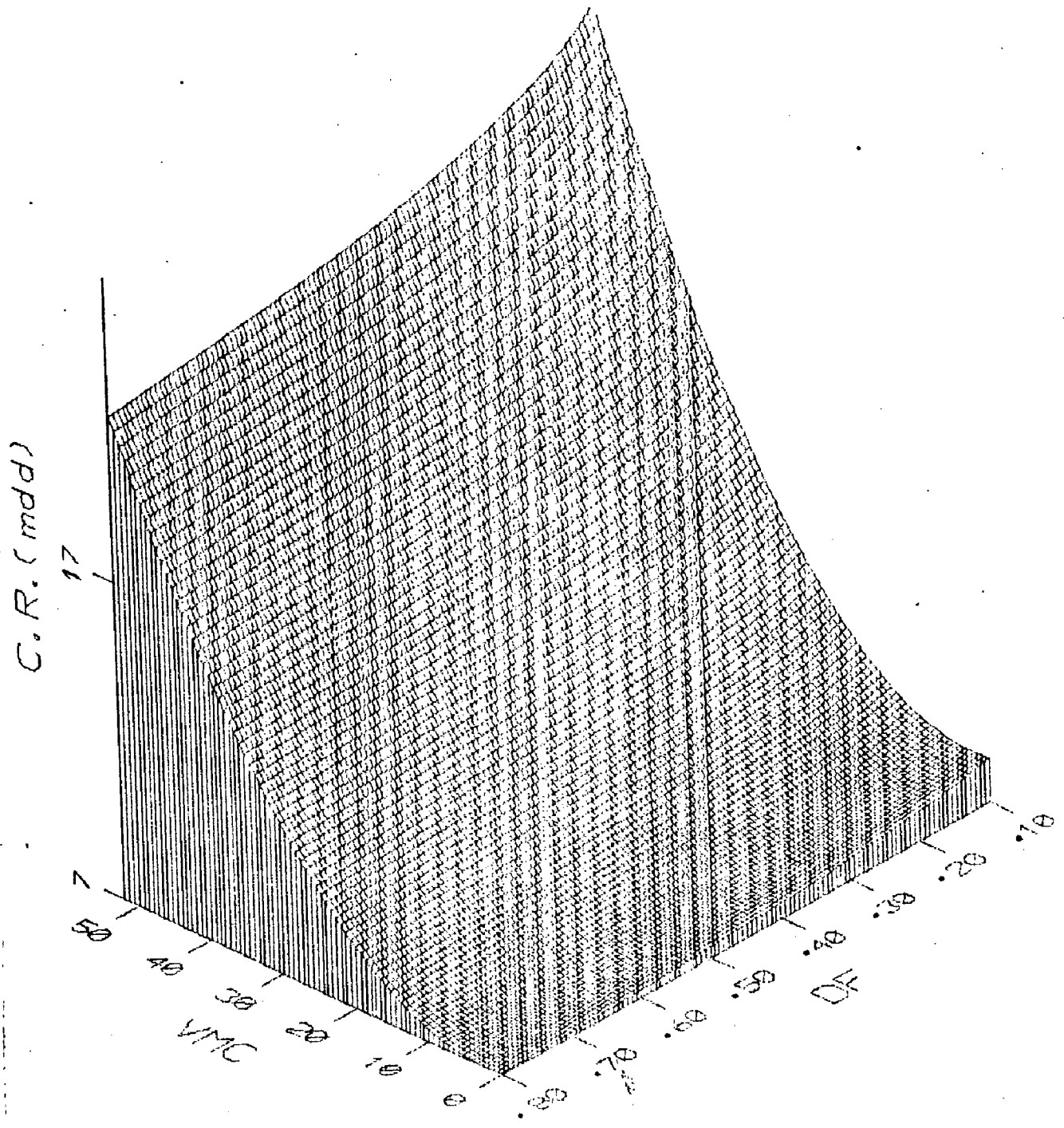


Fig. 7.22: 3D plot depicting the effect of VMC & DF on corrosion rate (based on equation 7.23)

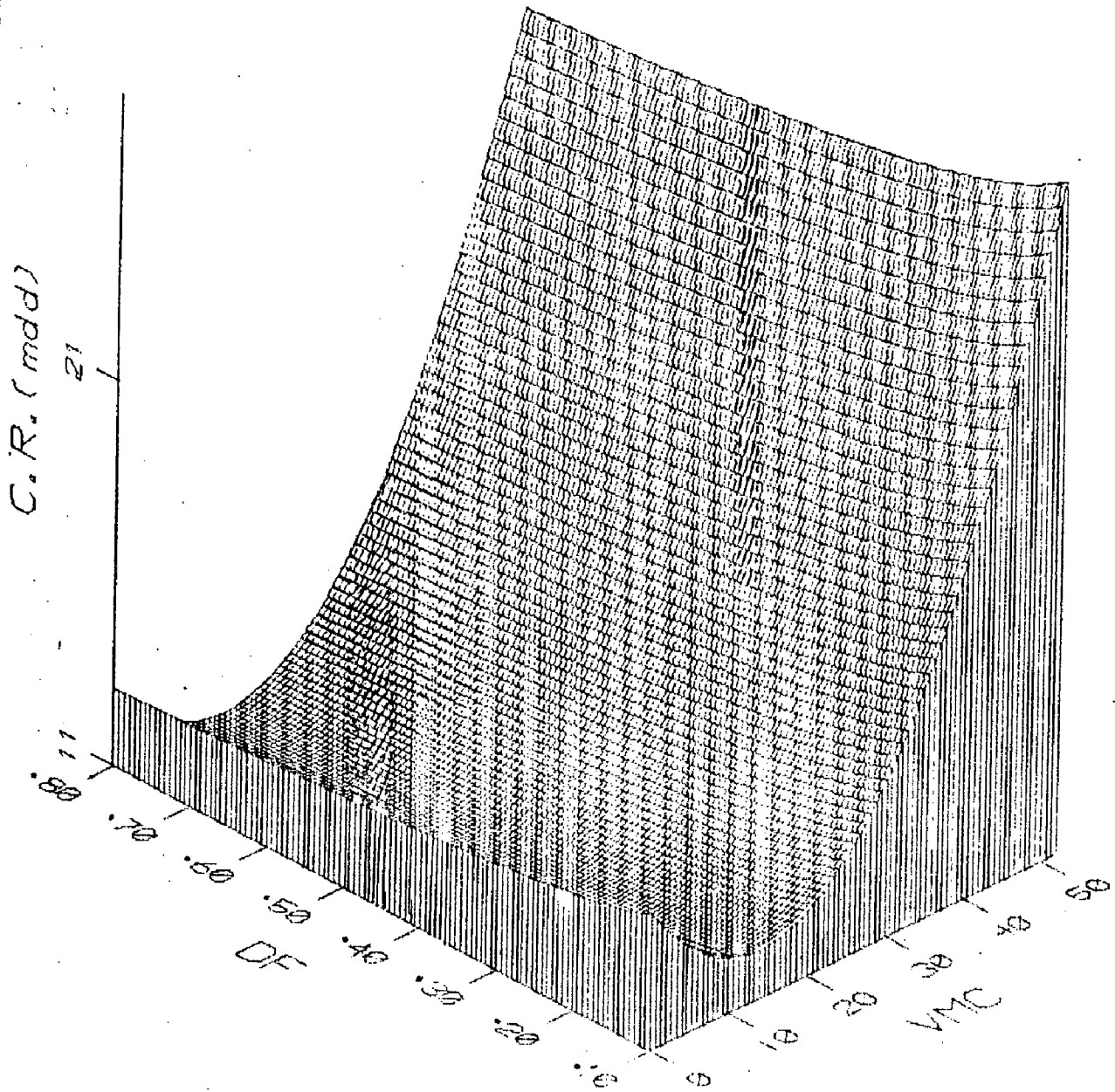


Fig. 7.23: 3D plot depicting the effect of VMC & DF on corrosion rate (based on equation 7.24)

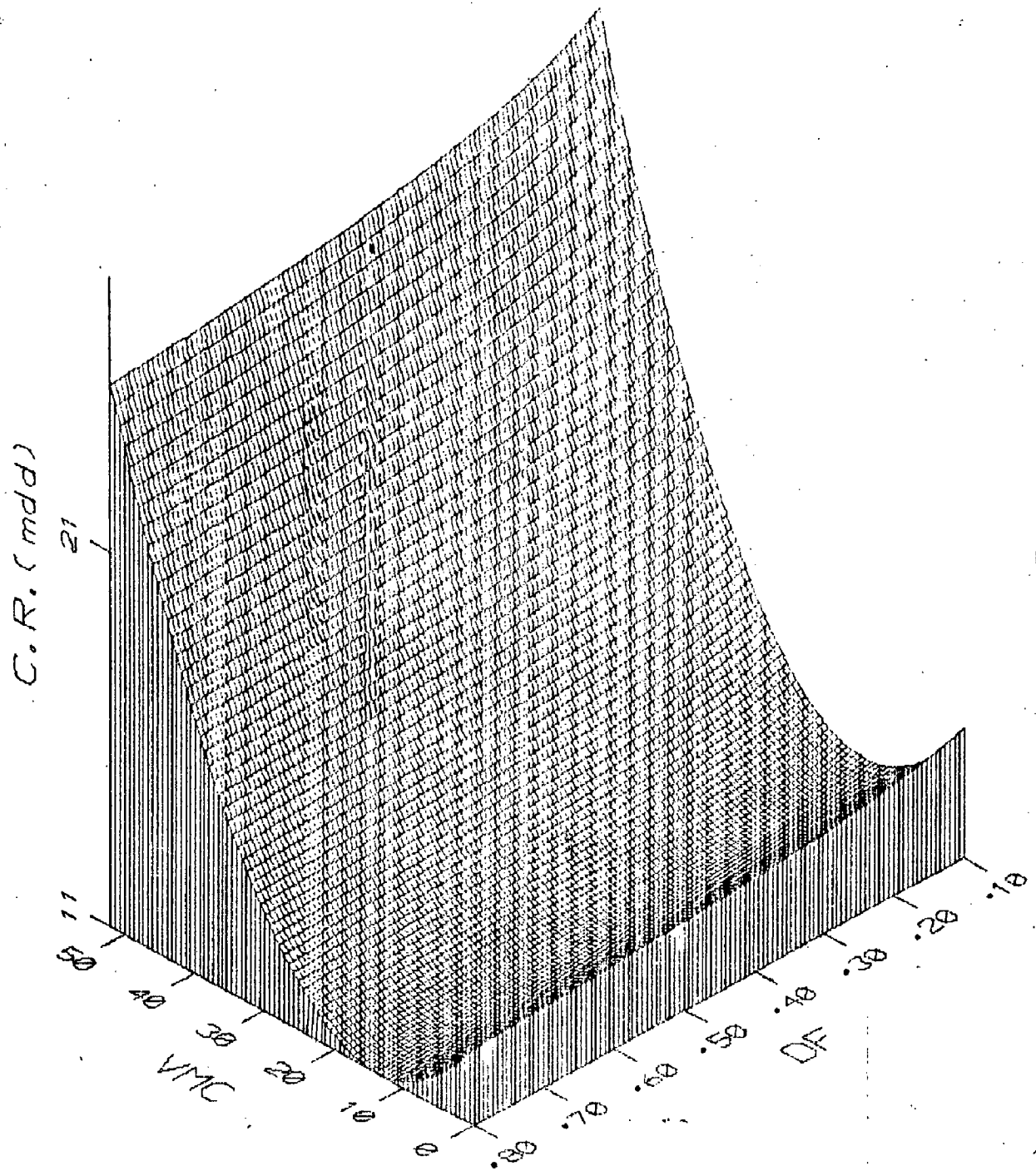


Fig. 7.24 : 3D plot depicting the effect of VMC & DF on corrosion rate (based on equation 7.24)

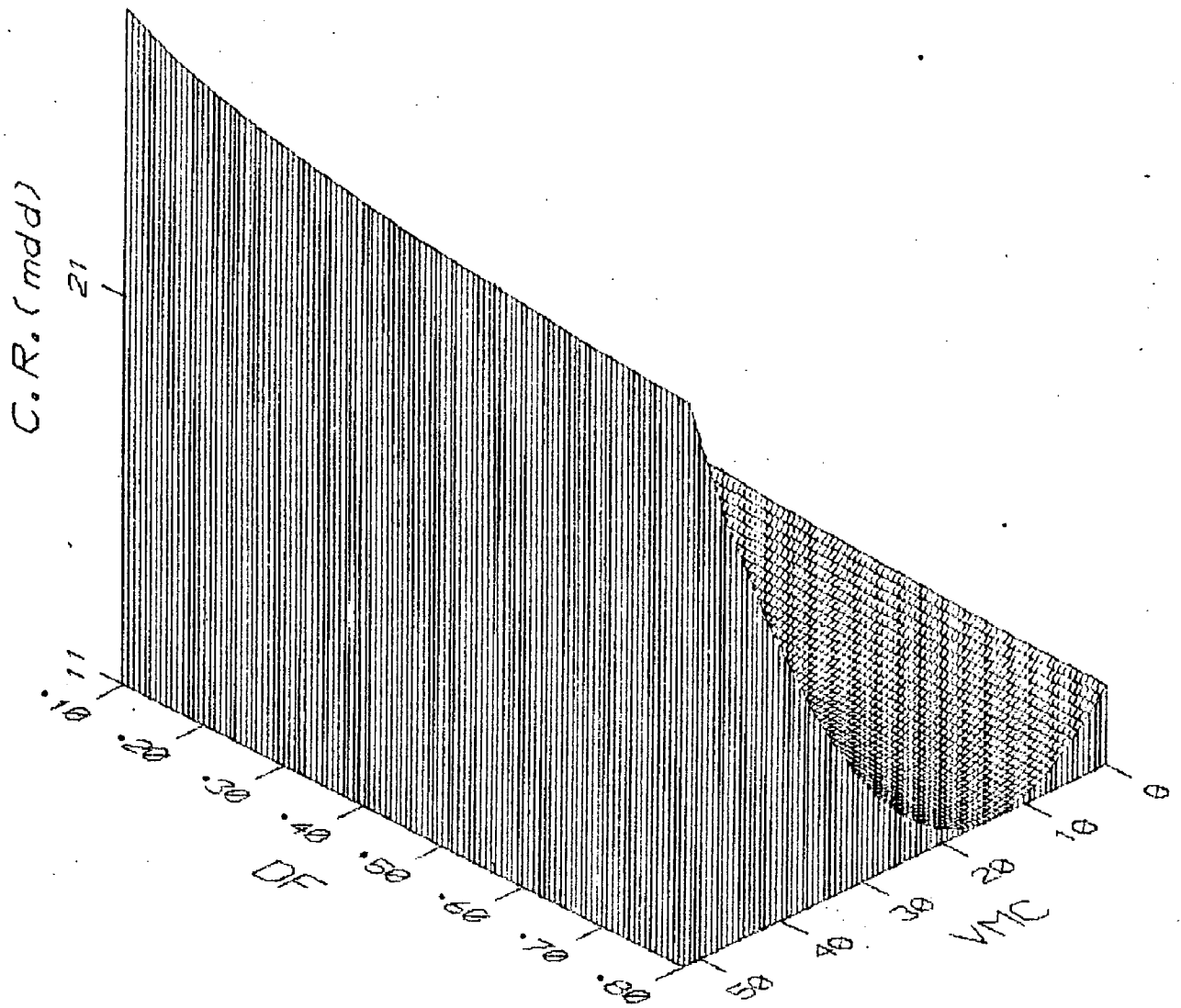


Fig. 7.25: 3D plot depicting the effect of VMC & DF on corrosion rate (based on equation 7.24)

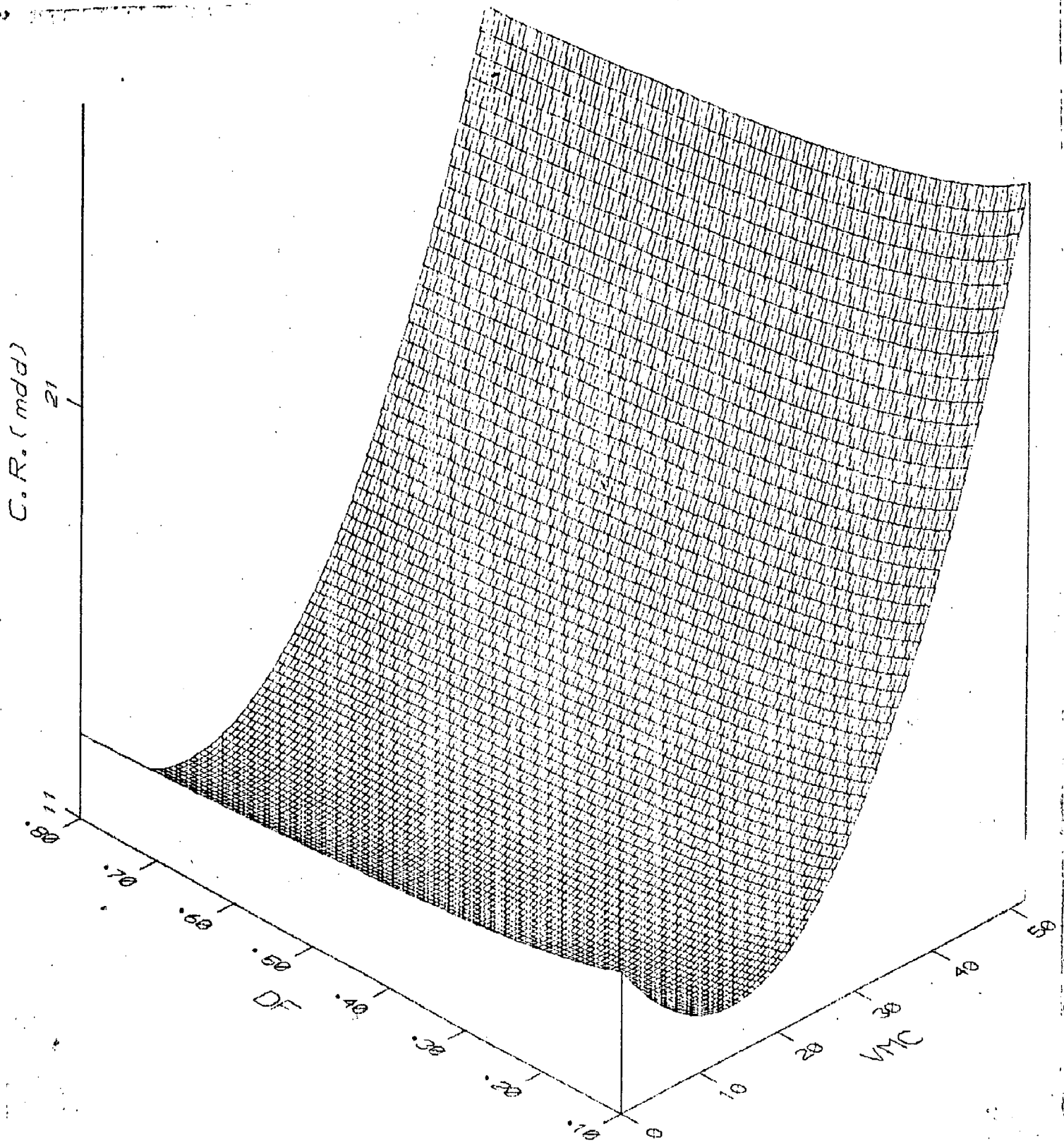


Fig. 7.26: 3D plot depicting the effect of VMC & DF on corrosion rate
(based on equation 7.24)

Appendix-A1 Percent area of particles in different classes at different locations as influenced by heat treating parameters(Alloy C1)

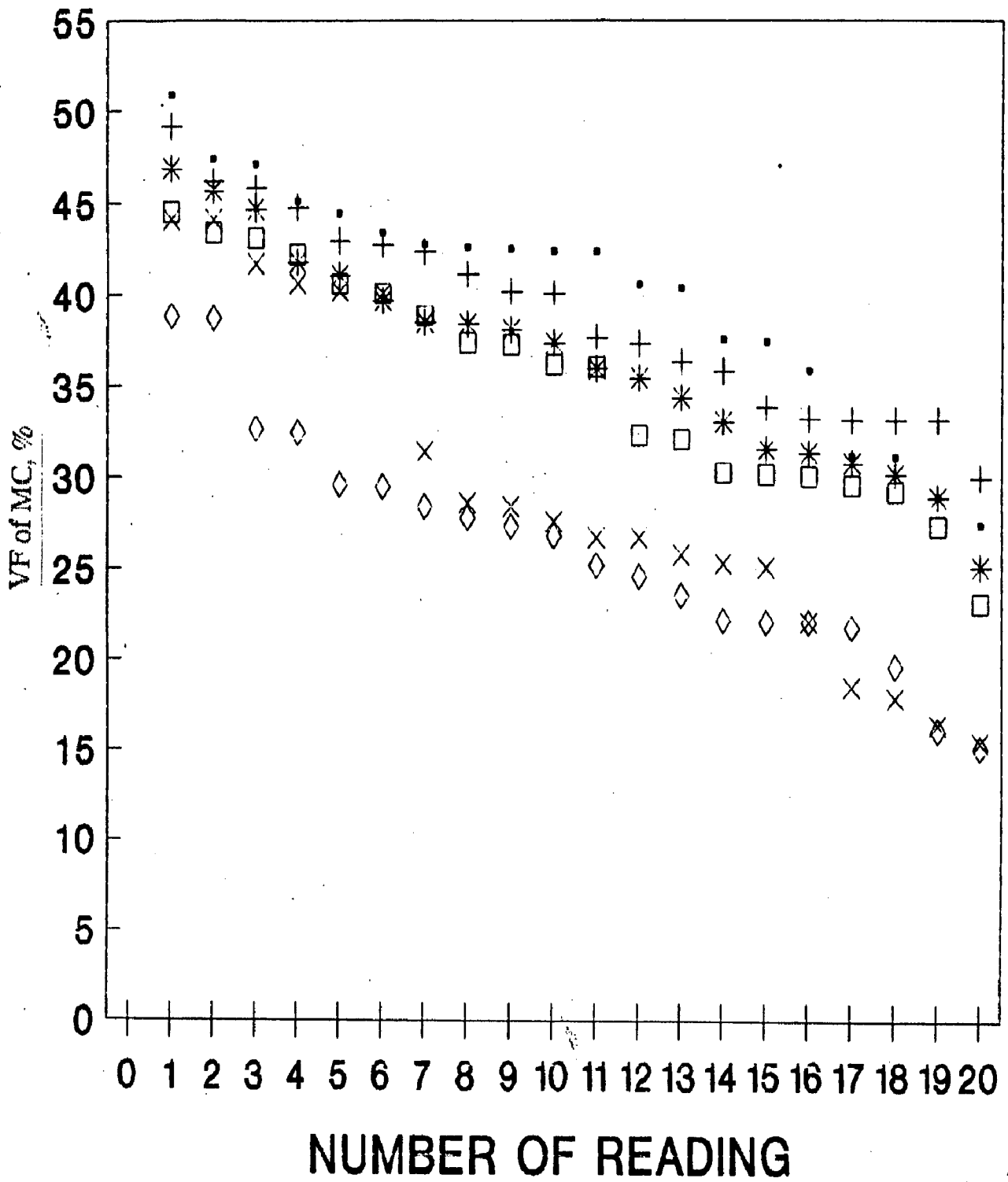
h/t	location I				location II				location III				location IV				location V				
800	2	25	74	0	0	27	71	0	0	25	75	0	0	25	74	0	0	20	80	0	0
800	4	16	83	0	0	21	78	0	0	22	77	0	0	20	79	0	0	23	76	0	0
800	6	15	84	0	0	15	84	0	0	18	81	0	0	30	69	0	0	16	83	0	0
800	8	7	59	32	0	39	59	0	0	3	50	46	0	10	23	65	0	6	39	54	0
800	10	7	34	57	0	2	44	52	0	15	35	49	0	5	30	21	41	7	63	29	0
850	2	15	35	49	0	27	71	0	0	14	85	0	0	8	62	29	0	5	39	54	0
850	4	11	88	0	0	7	92	0	0	5	94	0	0	30	69	0	0	18	81	0	0
850	6	8	24	67	0	5	94	0	0	21	78	0	0	25	74	0	0	6	39	54	0
850	8	6	48	45	0	8	38	53	0	5	39	54	0	20	79	0	0	13	35	50	0
850	10	6	44	49	0	3	20	38	37	5	49	45	0	5	44	49	0	17	21	60	0
900	2	35	64	0	0	12	87	0	0	15	22	62	0	39	59	0	0	20	79	0	0
900	4	100	0	0	0	21	78	0	0	14	85	0	0	27	71	0	0	47	52	0	0
900	6	15	22	62	0	100	0	0	0	21	78	0	0	18	81	0	0	12	87	0	0
900	8	18	81	0	0	5	39	54	0	6	39	54	0	2	26	0	71	8	24	67	0
950	2	25	74	0	0	47	52	0	0	18	81	0	0	18	81	0	0	33	66	0	0
950	4	16	83	0	0	39	59	0	0	47	52	0	0	12	87	0	0	100	0	0	0
950	6	100	0	0	0	10	90	0	0	2	25	71	0	100	0	0	0	0	100	0	0
950	8	100	0	0	0	14	85	0	0	21	78	0	0	52	47	0	0	30	69	0	0
1000	2	16	83	0	0	8	47	43	0	16	83	0	0	30	69	0	0	22	77	0	0
1000	4	25	74	0	0	6	39	54	0	25	74	0	0	18	81	0	0	10	46	43	0
1000	6	18	81	0	0	13	44	41	0	35	64	0	0	10	37	52	0	22	77	0	0
1000	8	33	66	0	0	10	90	0	0	100	0	0	0	100	0	0	0	10	90	0	0

Appendix-A2 Percent area of particles in different classes at different locations as influenced by heat treating parameters(Alloy C2)

h/t	location I				location II				location III				location IV				location V			
800 2	9	13	76	0	14	85	0	0	10	90	0	0	9	89	0	0	6	35	19	38
800 4	43	56	0	0	14	85	0	0	100	0	0	0	25	74	0	0	8	53	37	0
800 6	7	63	29	0	10	46	43	0	12	87	0	0	13	55	30	0	21	78	0	0
800 8	21	78	0	0	3	25	70	0	11	88	0	0	2	40	56	0	22	77	0	0
800 10	19	21	59	0	11	45	42	0	28	71	0	0	25	74	0	0	5	31	21	42
850 2	4	44	50	0	5	30	64	0	11	56	31	0	3	10	86	0	13	35	50	0
850 4	5	52	41	0	6	55	38	0	32	0	67	0	7	48	44	0	11	52	36	0
850 6	8	38	53	0	7	9	82	0	10	37	52	0	8	47	43	0	9	58	32	0
850 8	13	86	0	0	7	66	26	0	9	58	32	0	13	55	30	0	11	56	31	0
850 10	24	0	75	0	5	25	69	0	47	52	0	0	15	84	0	0	7	59	32	0
900 2	4	33	61	0	4	40	55	0	12	23	64	0	3	18	26	51	7	59	32	0
900 4	14	85	0	0	11	88	0	0	8	62	29	0	10	90	0	0	7	92	0	0
900 6	10	90	0	0	6	14	79	0	0	26	73	0	21	78	0	0	7	48	44	0
900 8	10	37	52	0	18	81	0	0	10	90	0	0	17	21	60	0	14	85	0	0
900 10	5	25	69	0	1	14	83	0	12	23	64	0	5	35	59	0	4	56	39	0
950 2	11	88	0	0	6	55	38	0	15	84	0	0	7	32	60	0	4	25	70	0
950 4	9	13	76	0	6	14	79	0	1	34	64	0	30	69	0	0	15	84	0	0
950 6	14	85	0	0	8	53	37	0	6	48	45	0	20	80	0	0	18	81	0	0
950 8	8	38	53	0	5	49	45	0	4	7	44	43	2	25	71	0	21	78	0	0
950 10	10	23	65	0	10	37	52	0	4	14	80	0	6	10	28	55	1	10	88	0
1000 2	7	54	37	0	5	25	69	0	10	23	65	0	18	81	0	0	4	14	80	0
1000 4	4	40	55	0	8	38	53	0	10	90	0	0	0	51	48	0	8	24	67	0
1000 6	100	0	0	0	100	0	0	0	100	0	0	0	0	0	0	100	4	14	80	0

Appendix-A3 Percent area of particles in different classes at different locations as influenced by heat treating parameters(Alloy C3)

h/t	location I				location II				location III				location IV				location V			
800 2	13	86	0	0	10	90	0	0	12	87	0	0	8	91	0	0	10	46	43	0
800 4	14	85	0	0	14	44	40	0	25	75	0	0	7	92	0	0	7	24	22	44
800 6	22	77	0	0	11	88	0	0	10	57	32	0	27	71	0	0	8	47	43	0
800 8	20	33	46	0	27	72	0	0	16	83	0	0	20	80	0	0	17	34	48	0
800 10	10	68	21	0	13	66	20	0	25	74	0	0	6	24	68	0	19	51	28	0
850 2	5	0	94	0	2	0	97	0	5	0	94	0	3	0	96	0	100	0	0	0
850 4	12	36	51	0	4	36	60	0	12	87	0	0	13	86	0	0	10	68	21	0
850 6	18	81	0	0	16	83	0	0	4	25	70	0	6	39	54	0	8	38	53	0
850 8	10	0	89	0	19	0	80	0	8	24	67	0	9	46	43	0	10	57	32	0
850 10	9	37	52	0	12	36	51	0	8	24	67	0	4	25	70	0	9	13	76	0
900 2	18	81	0	0	14	50	35	0	17	21	60	0	25	74	0	0	7	38	53	0
900 4	11	23	64	0	3	44	52	0	3	0	96	0	9	0	0	90	7	0	92	0
900 6	8	91	0	0	10	37	52	0	1	34	64	0	9	0	90	0	1	26	24	47
900 8	13	55	30	0	23	32	44	0	25	74	0	0	21	78	0	0	26	19	54	0
900 10	7	66	26	0	20	79	0	0	22	77	0	0	8	47	43	0	18	81	0	0
950 2	1	0	59	38	7	0	92	0	9	0	90	0	5	0	32	62	5	25	69	0
950 4	3	0	96	0	13	0	86	0	24	0	75	0	10	0	89	0	1	0	33	65
950 6	1	0	59	38	5	0	94	0	1	0	33	65	2	10	29	57	8	24	67	0
950 8	21	0	78	0	19	0	80	0	6	0	93	0	13	0	86	0	3	0	96	0
950 10	5	18	25	50	5	0	0	94	4	25	35	34	19	0	80	0	6	55	38	0
1000 2	7	32	60	0	10	0	89	0	3	31	65	0	8	24	67	0	6	39	54	0
1000 4	1	15	42	41	2	0	19	77	100	0	0	0	2	0	49	48	4	0	48	47
1000 6	16	0	83	0	2	0	97	0	13	0	86	0	6	0	93	0	10	0	89	0
1000 8	6	0	93	0	6	0	93	0	3	0	96	0	3	0	96	0	5	0	94	0



• 800 DEG C + 850 DEG C * 900 DEG C
 □ 950 DEG C × 1000 DEG C ◇ 1050 DEG C

Fig. A-4 : Variation in Vf of MC as influenced by h/t temperature (2 hours soaking period) Alloy C1

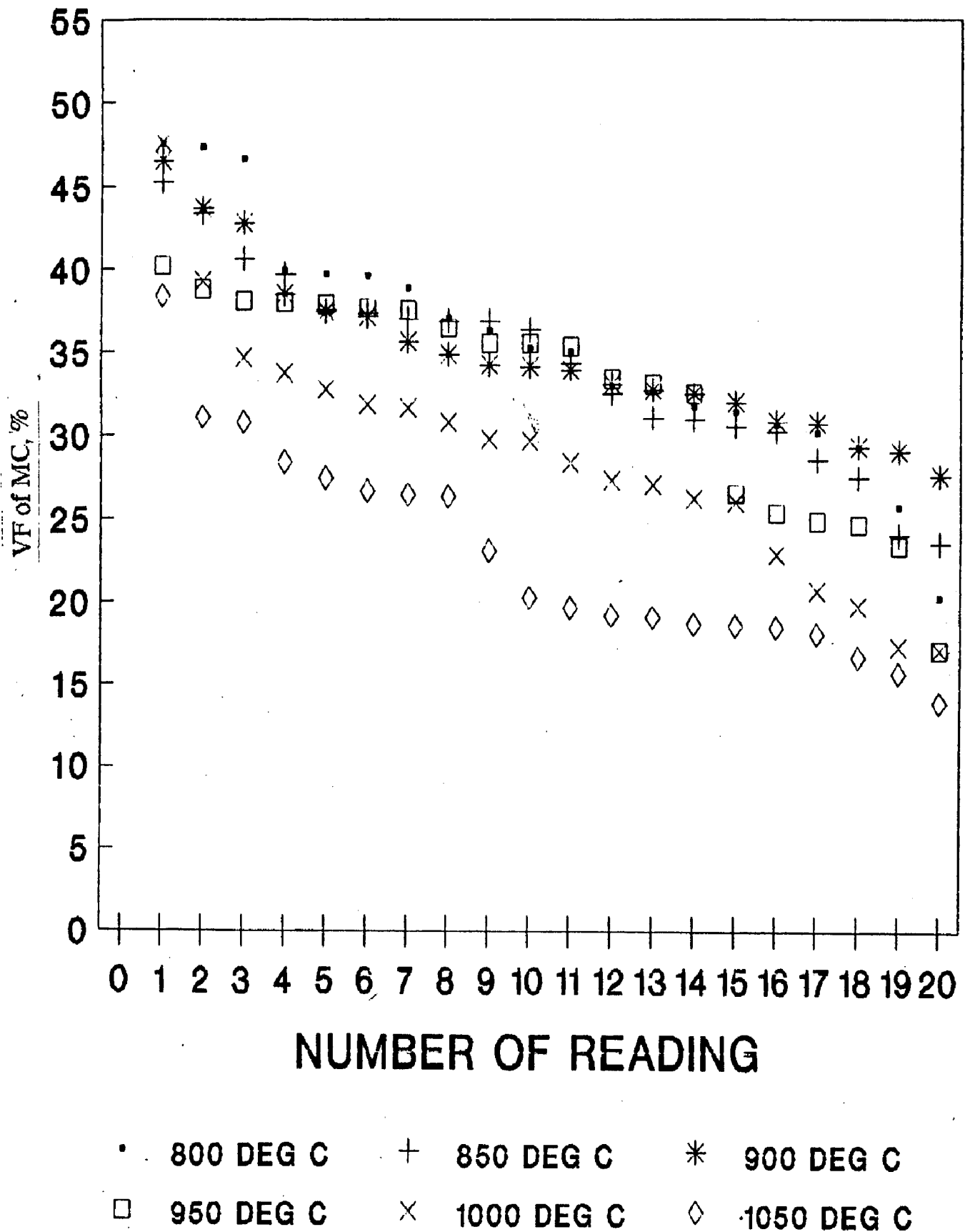
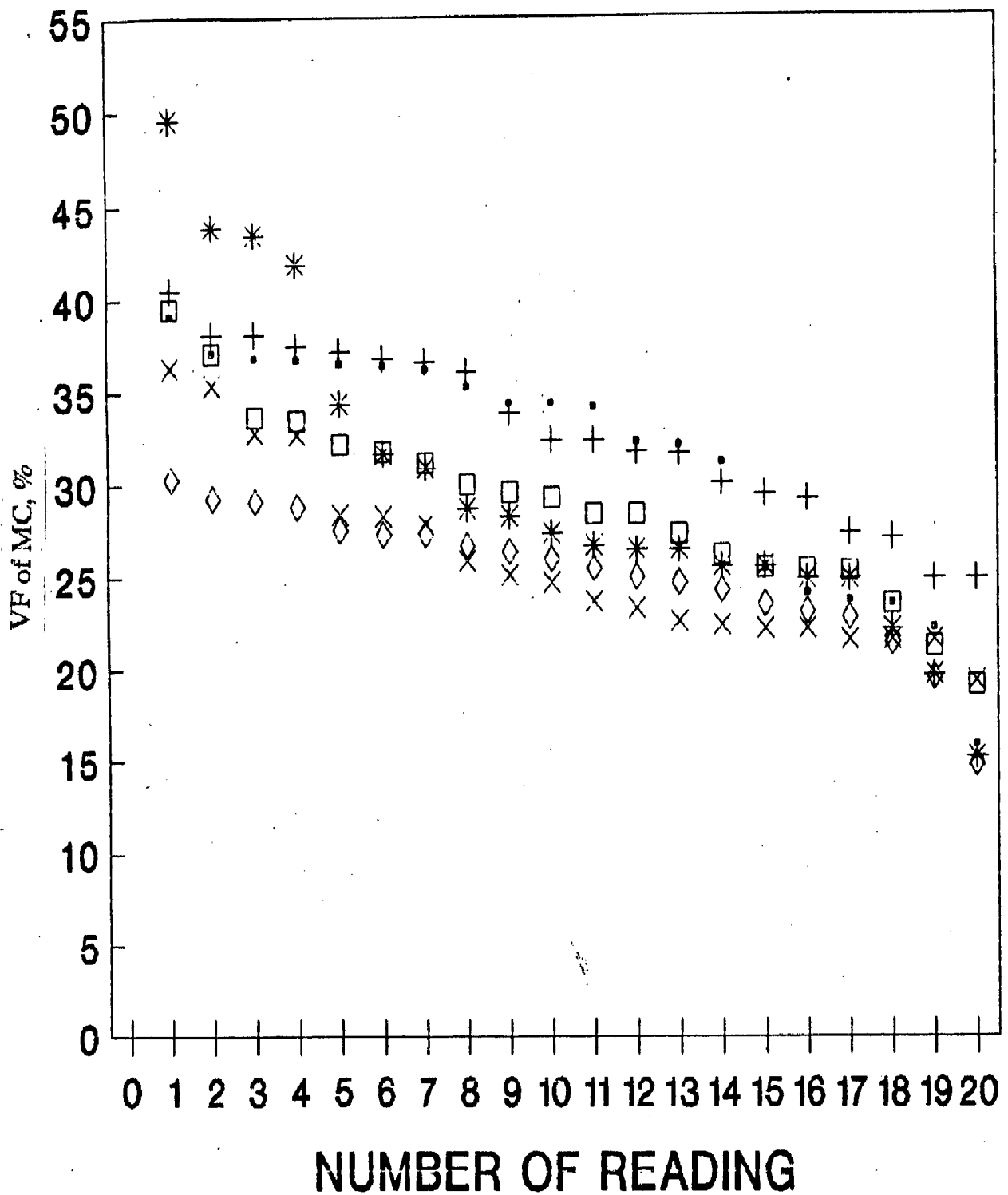
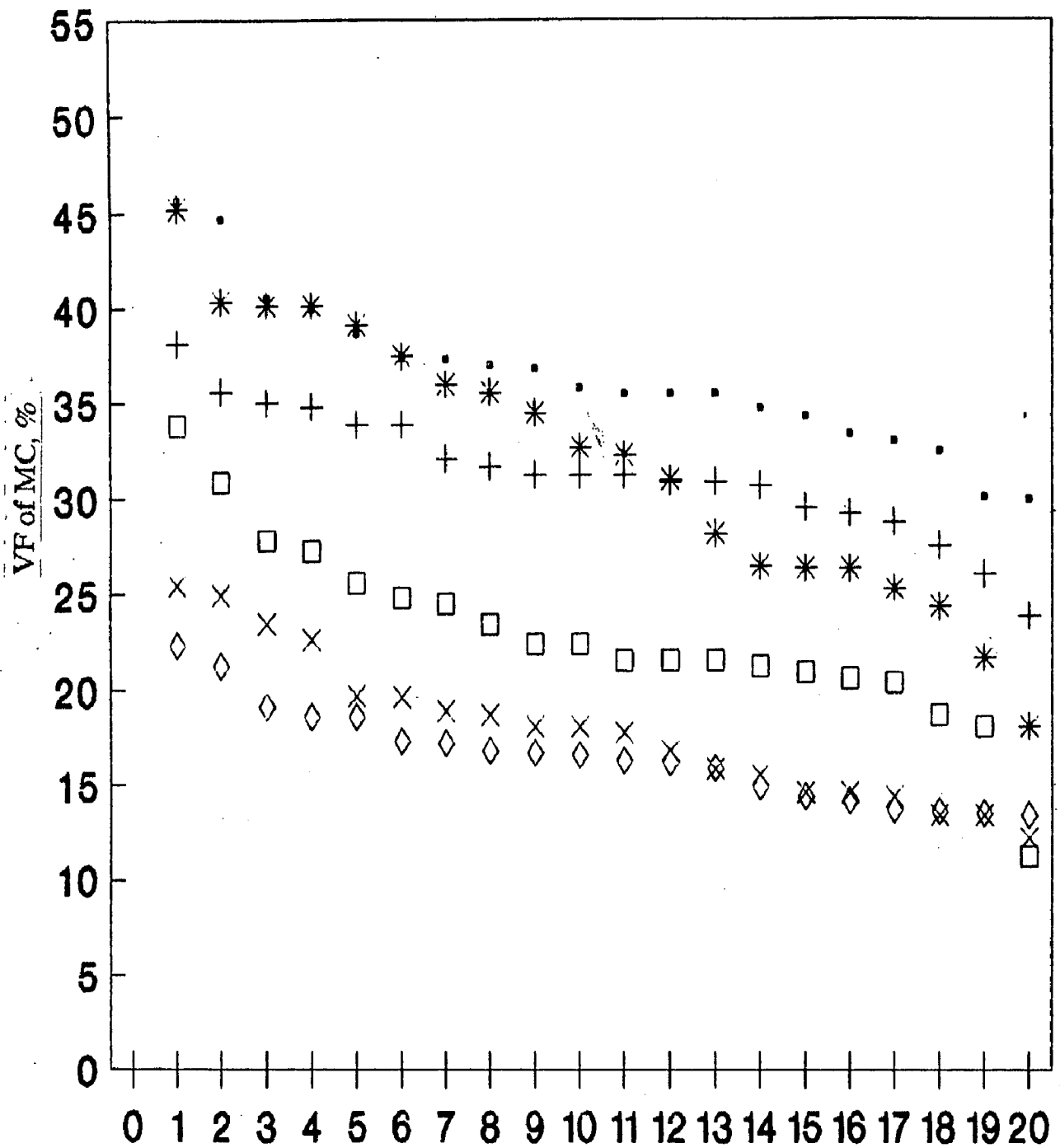


Fig. A-5 : Variation in Vf of MC as influenced by h/t temperature (2 hours soaking period) Alloy C2



• 800 DEG C + 850 DEG C * 900 DEG C
 □ 950 DEG C x 1000 DEG C ◇ 1050 DEG C

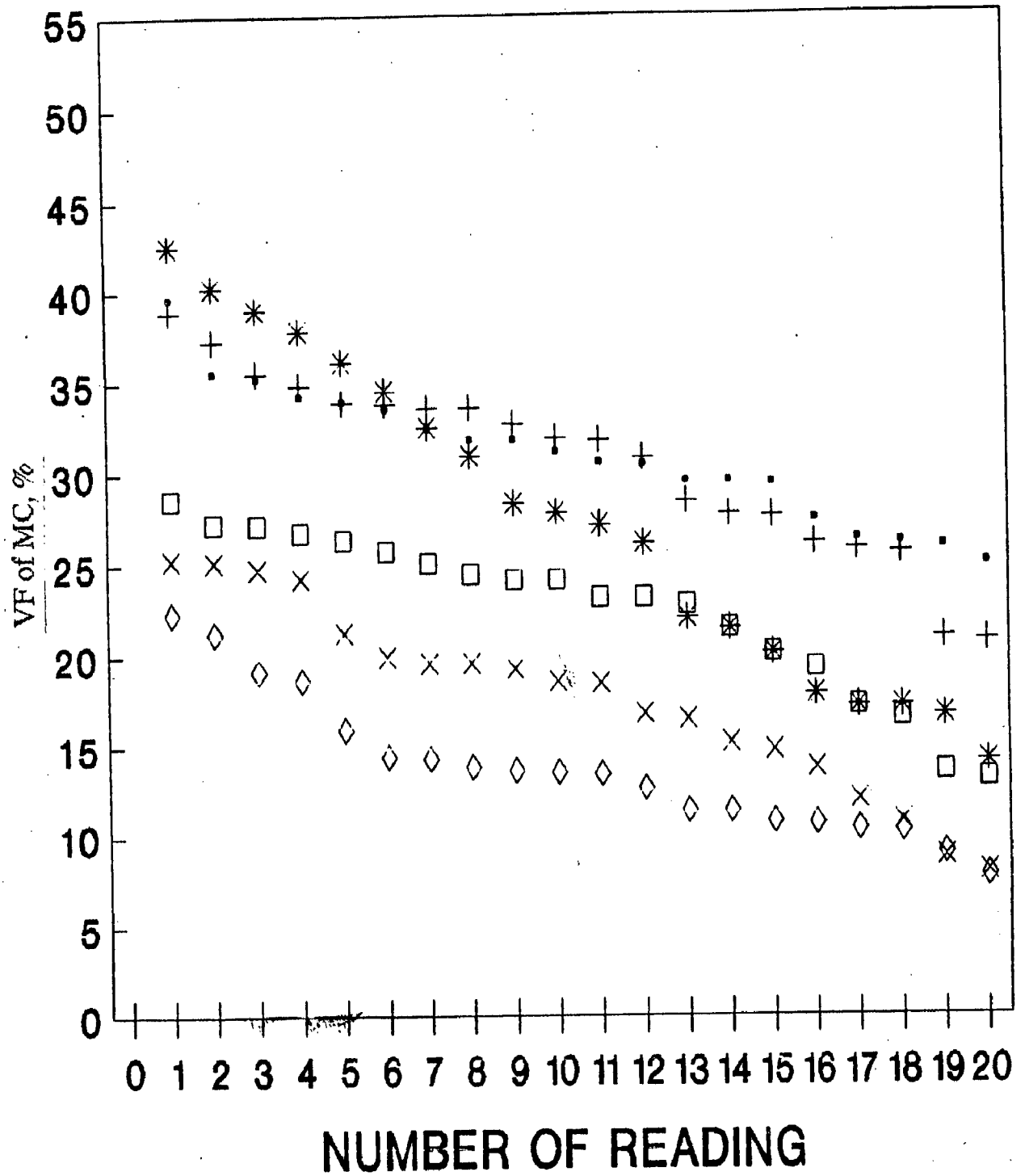
Fig. A-6 : Variation in Vf of MC as influenced by h/t temperature (2 hours soaking period) Alloy C3



NUMBER OF READING

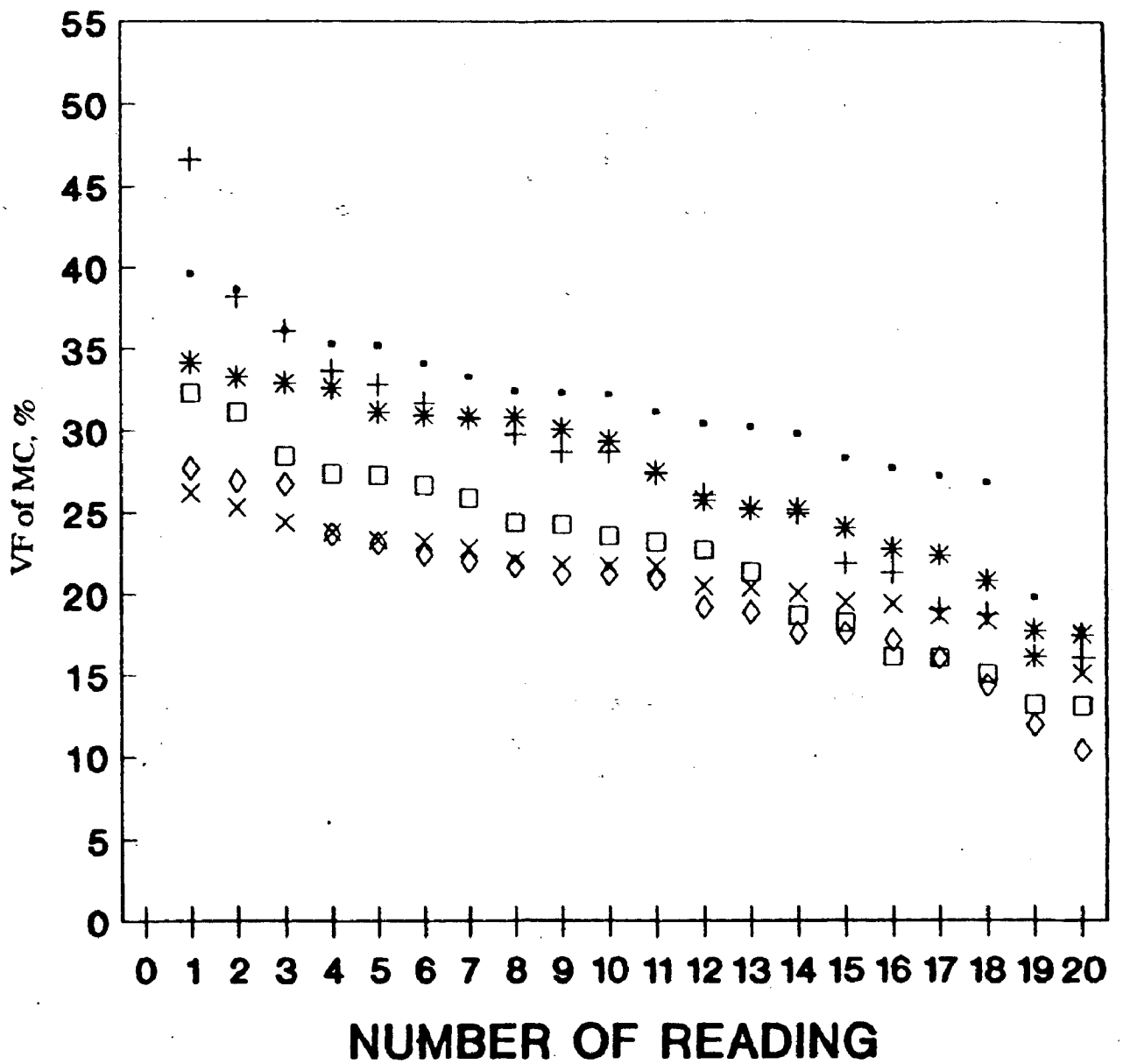
- 800 DEG C + 850 DEG C * 900 DEG C
- 950 DEG C x 1000 DEG C ◇ 1050 DEG C

Fig. A-7 : Variation in Vf of MC as influenced by h/t temperature (10 hours soaking period) Alloy C1



• 800 DEG C + 850 DEG C * 900 DEG C
 □ 950 DEG C × 1000 DEG C ◇ 1050 DEG C

Fig. A-8 : Variation in Vf of MC as influenced by h/t temperature (10 hours soaking period) Alloy C2



• 800 DEG C + 850 DEG C * 900 DEG C
 □ 950 DEG C x 1000 DEG C ◇ 1050 DEG C

Fig. A-9 : Variation in Vf of MC as influenced by h/t temperature (10 hours soaking period) Alloy C3

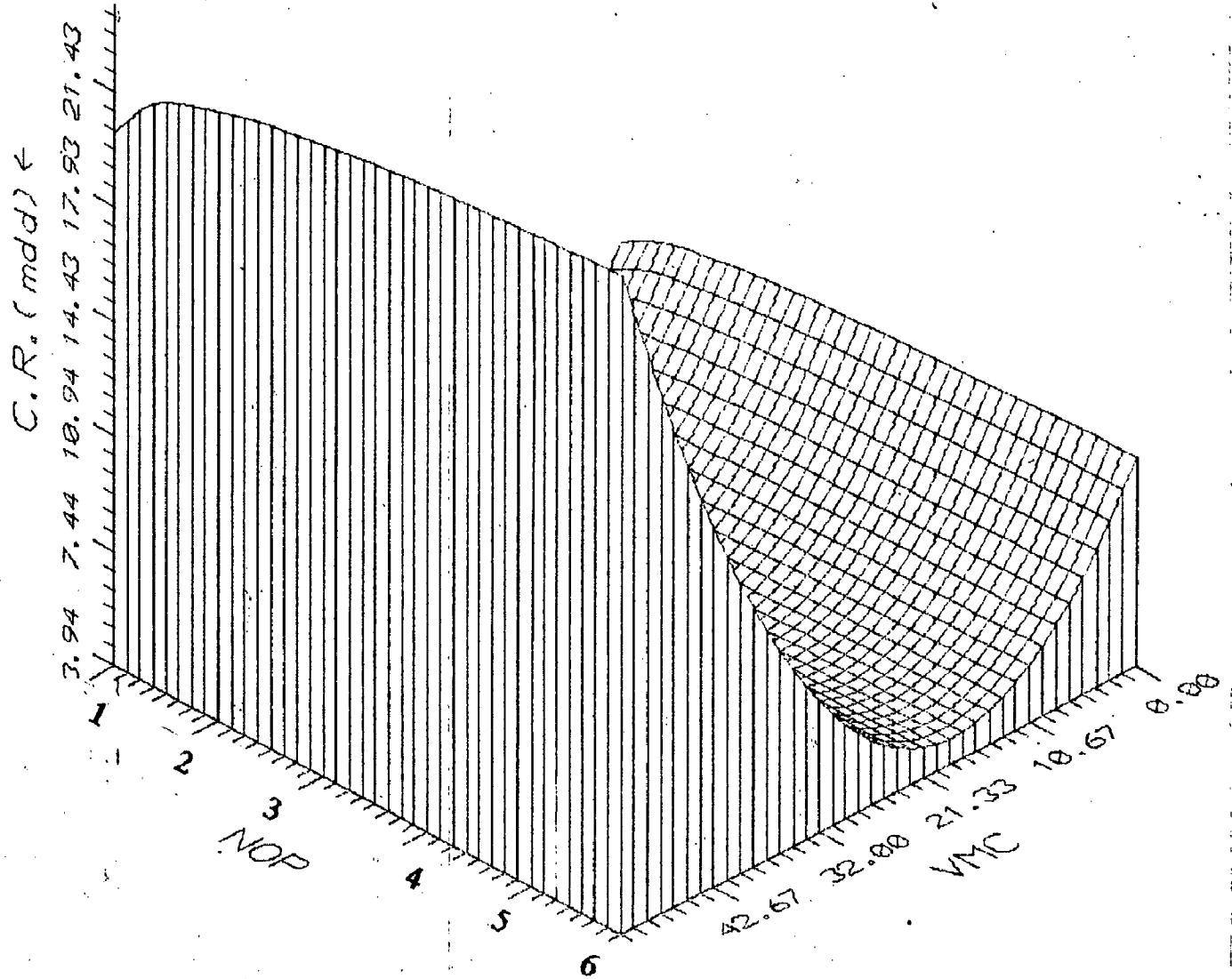


Fig. 7.7: 3D plot depicting the effect of VMC & NOP on corrosion rate (based on equation 7.17)

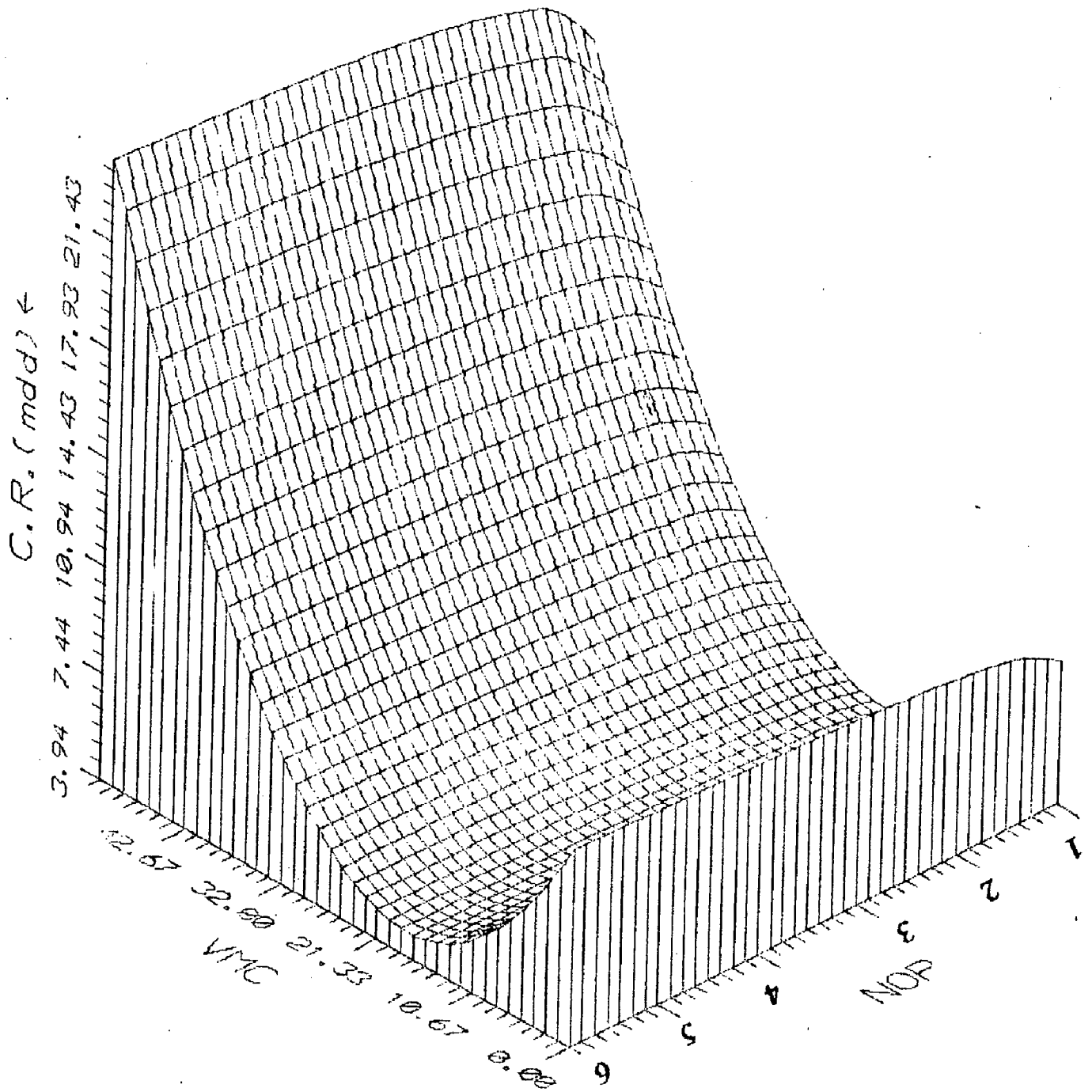


Fig. 7.8: 3D plot depicting the effect of VMC & NOP on corrosion rate (based on equation 7.17)

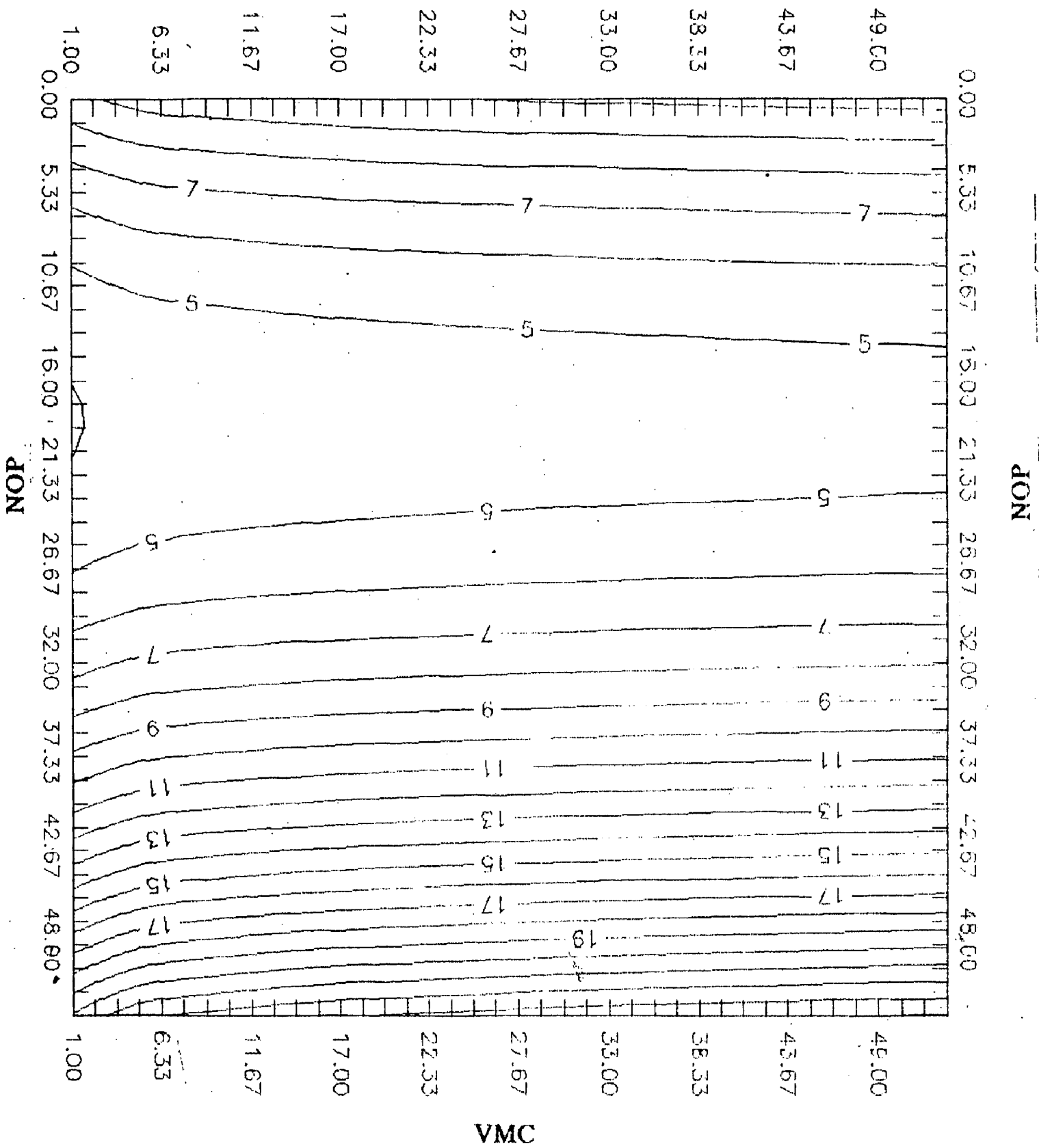


Fig. 7.10 : Contour plot depicting the combined effect of VMC & NOP on corrosion rate (based on equation 7.17)

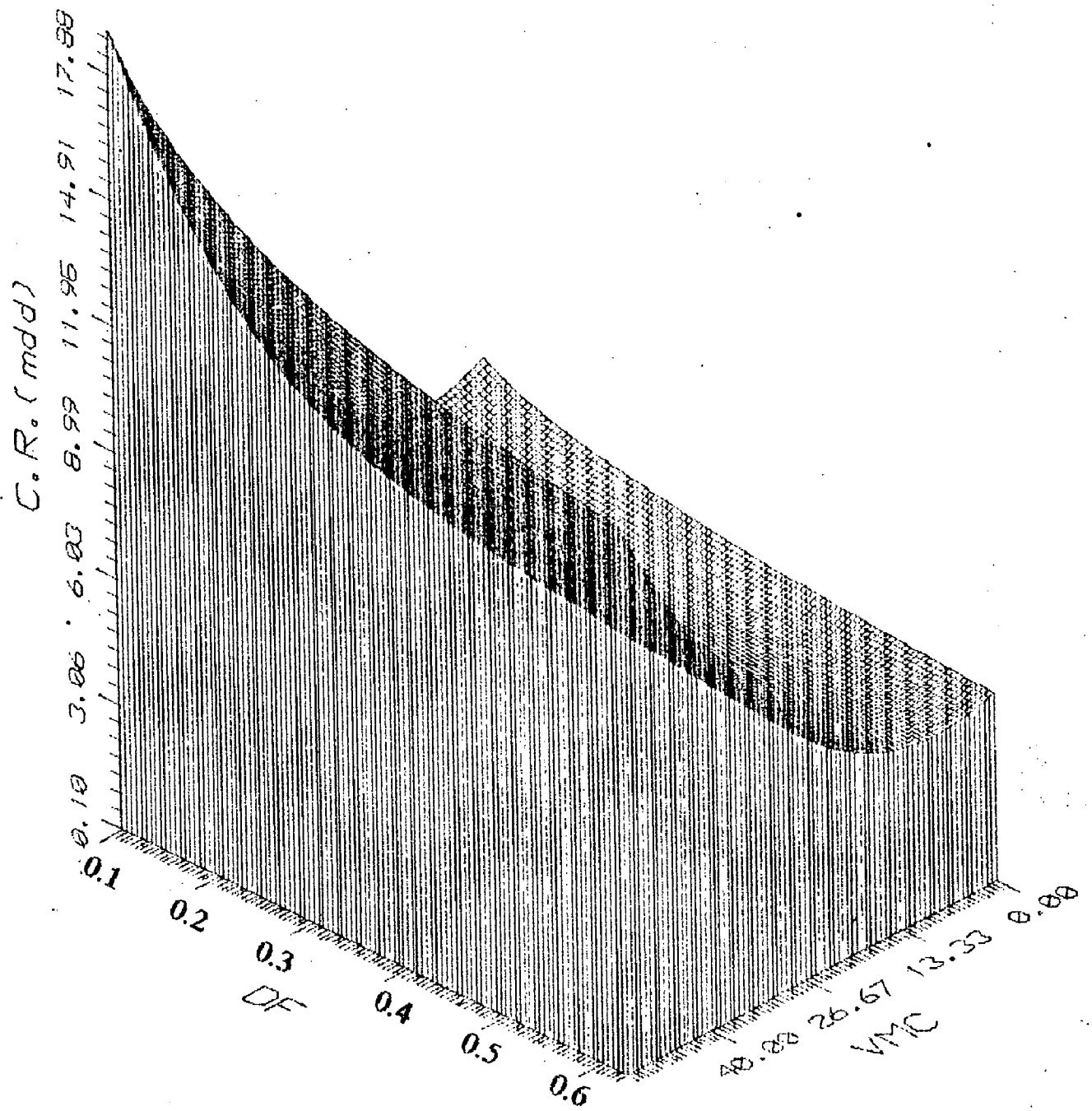


Fig. 7.11: 3D plot depicting the effect of VMC & DF on corrosion rate (based on equation 7.21)

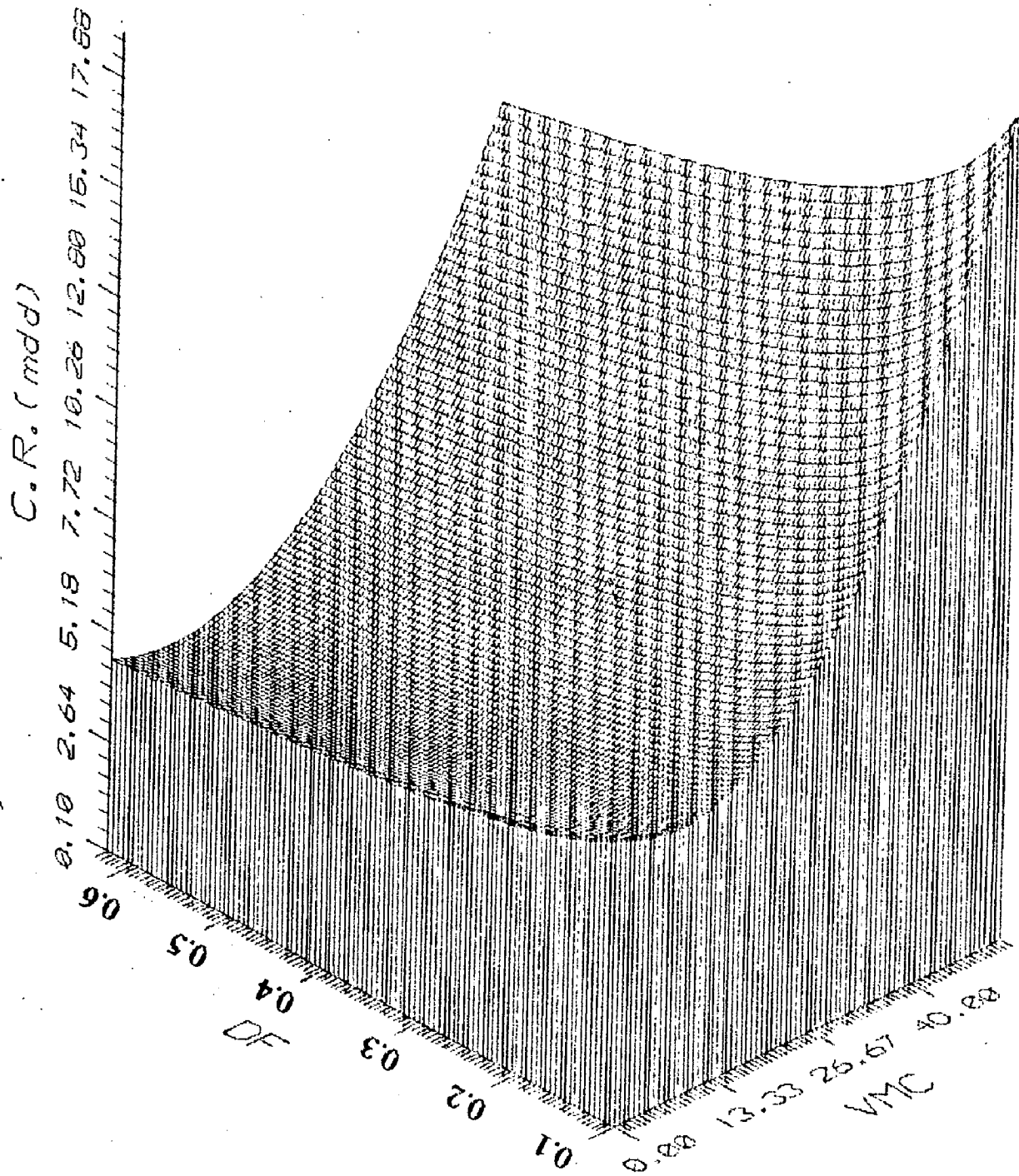


Fig. 7.12: 3D plot depicting the effect of VMC & DF on corrosion rate (based on equation 7.21)

C. R. (mdd)

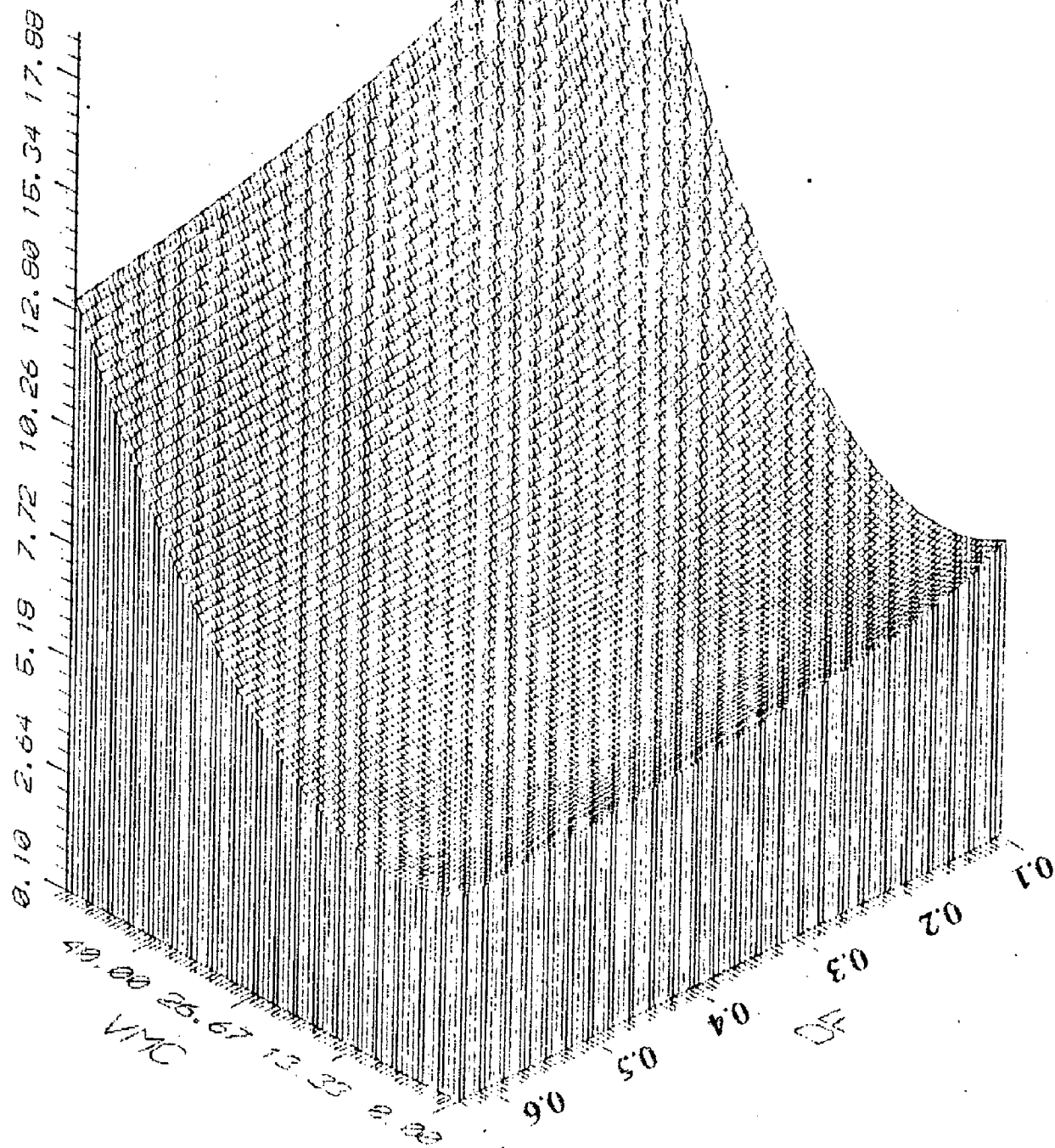


Fig. 7.13: 3D plot depicting the effect of VMC & DF on corrosion rate (based on equation 7.21)

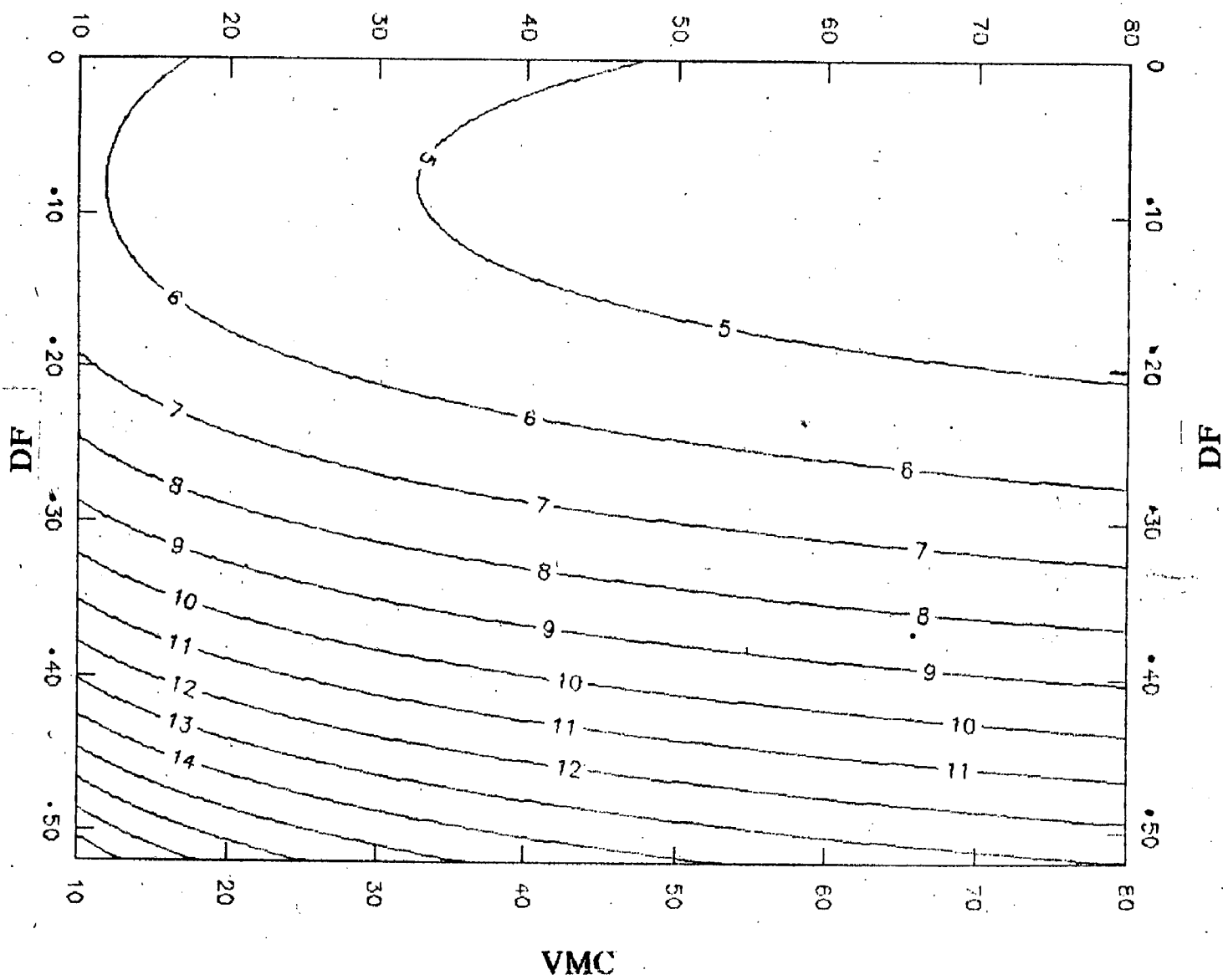


Fig. 7.14 : Contour plot depicting the combined effect of F-113 VMC & DF on corrosion rate (based on equation 7.21)

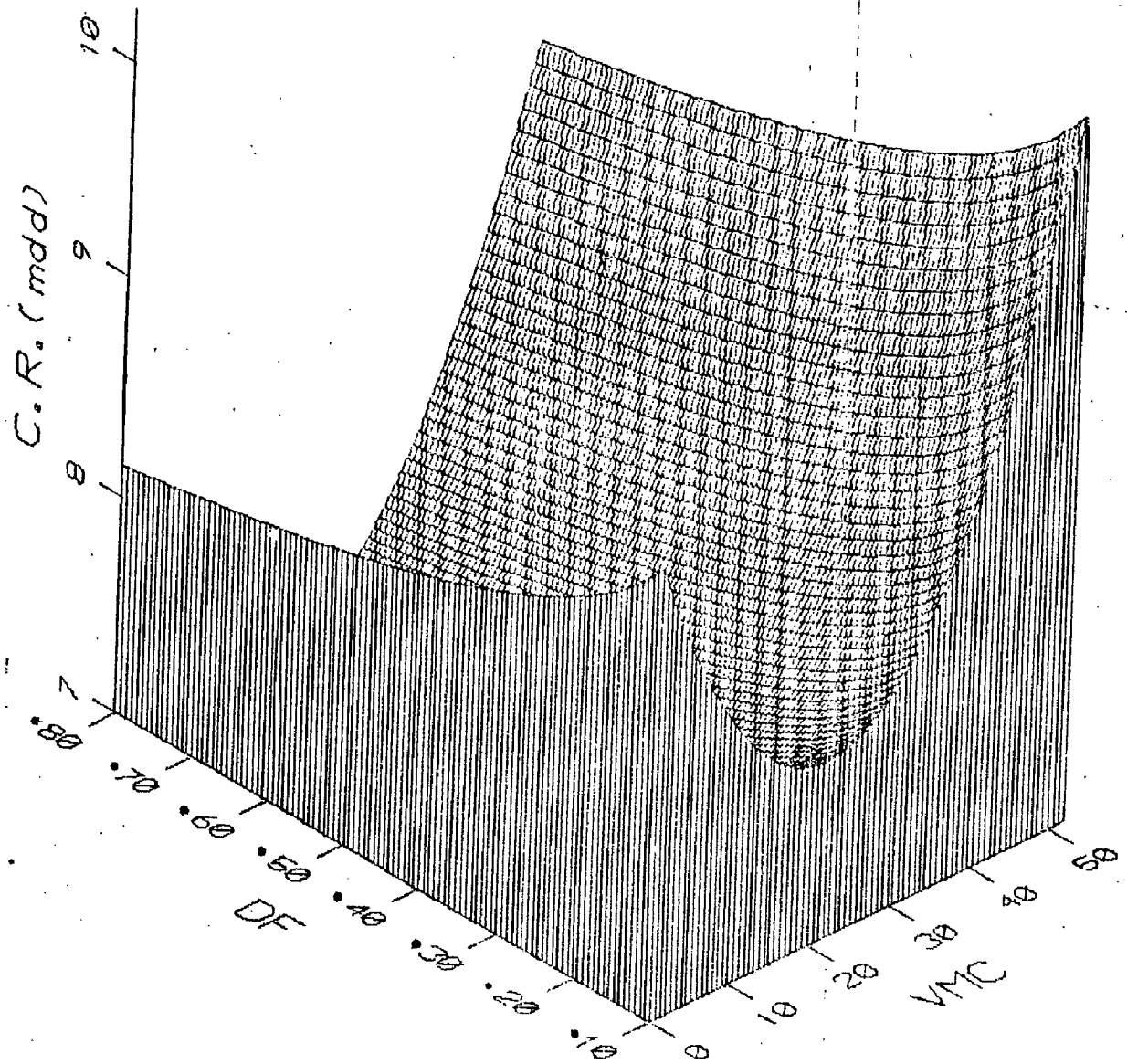


Fig. 7.15: 3D plot depicting the effect of VMC & DF on corrosion rate (based on equation 7.22)

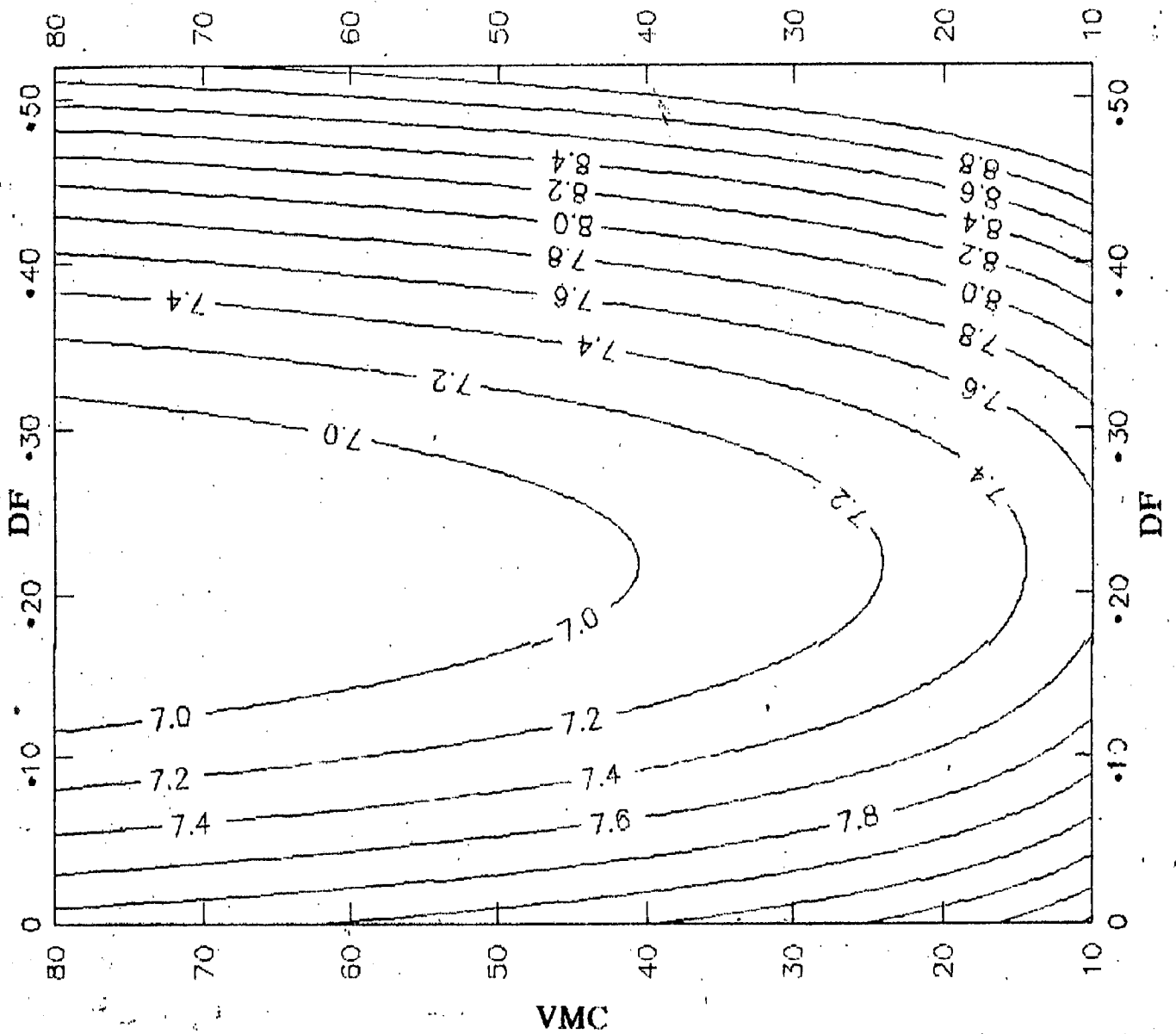


Fig. 7.16: Contour plot depicting the combined effect of F-113 VMC & DF on corrosion rate (based on equation 7.22)

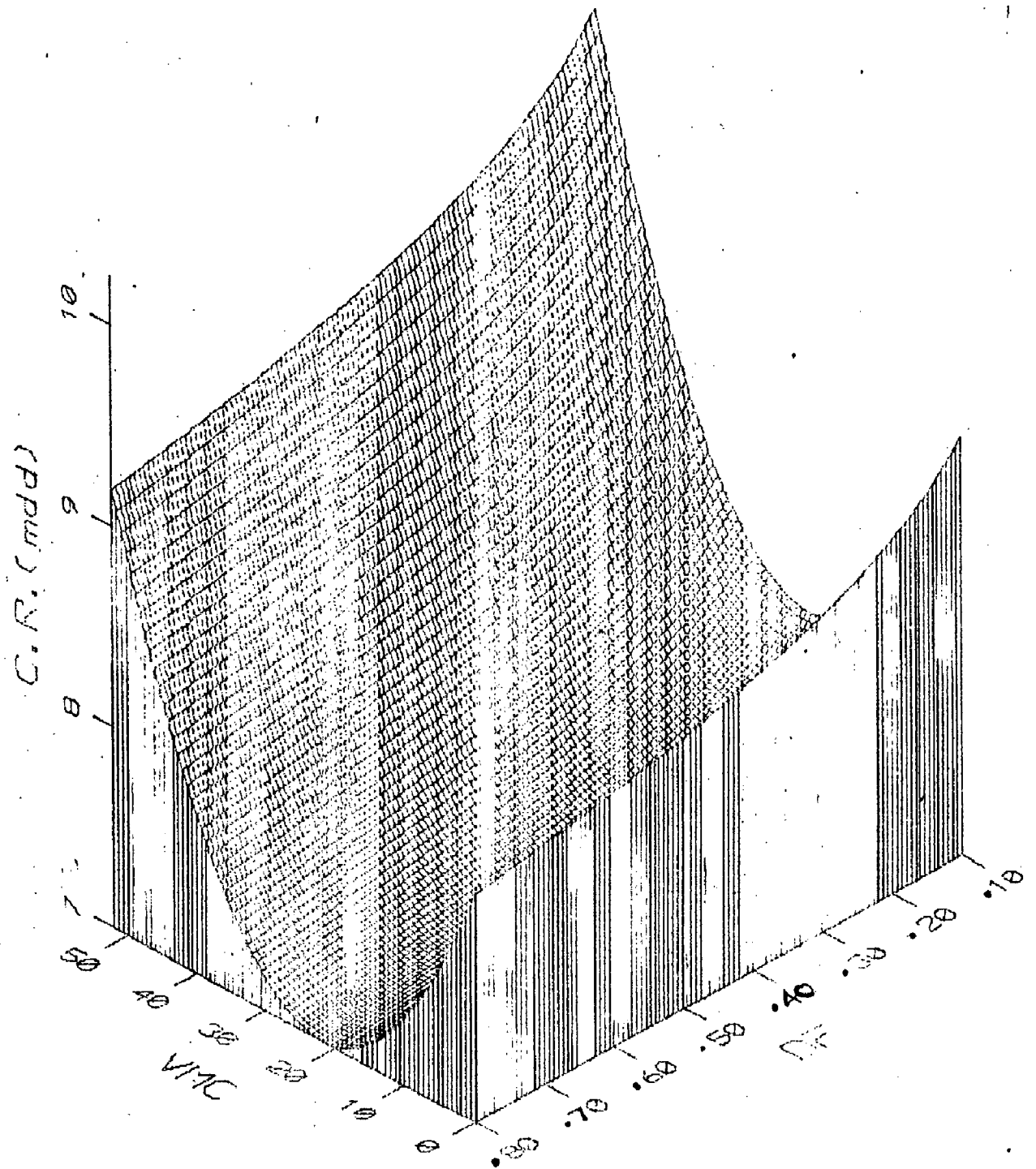


Fig. 7.17: 3D plot depicting the effect of VMC & DF on corrosion rate (based on equation 7.22)

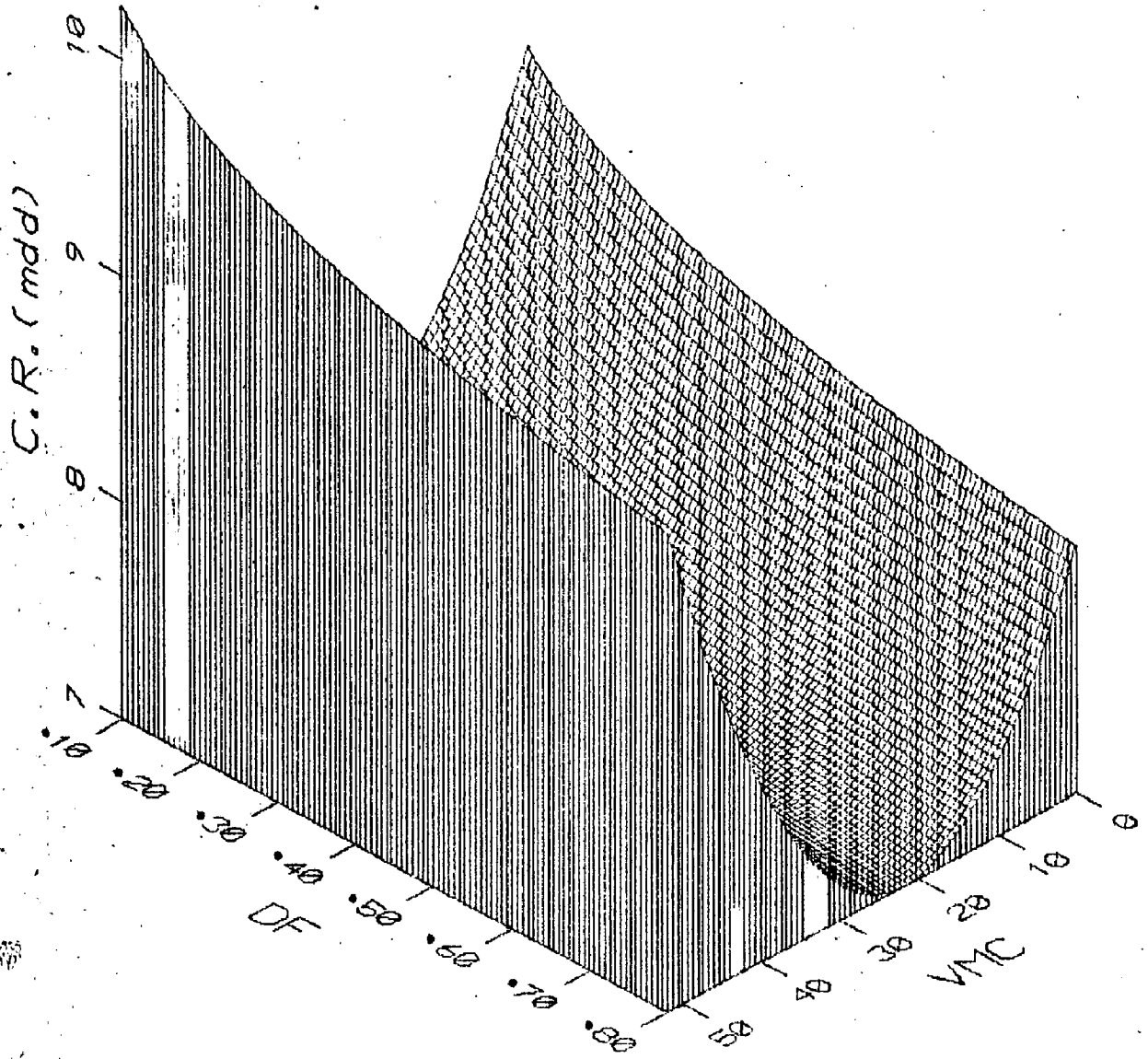


Fig. 7.18: 3D plot depicting the effect of VMC & DF on corrosion rate (based on equation 7.22)

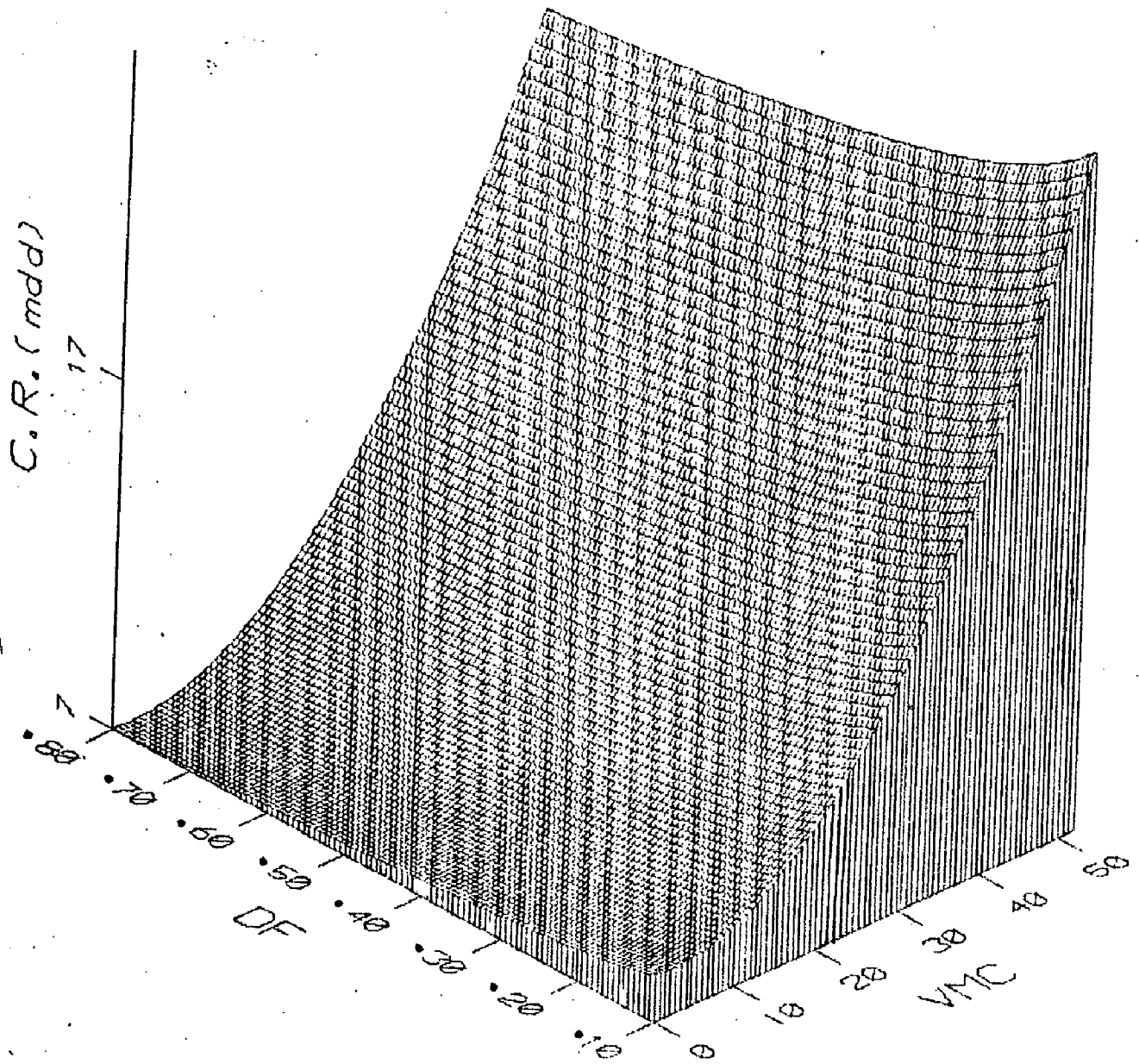


Fig. 7.19: 3D plot depicting the effect of VMC & DF on corrosion rate (based on equation 7.23).

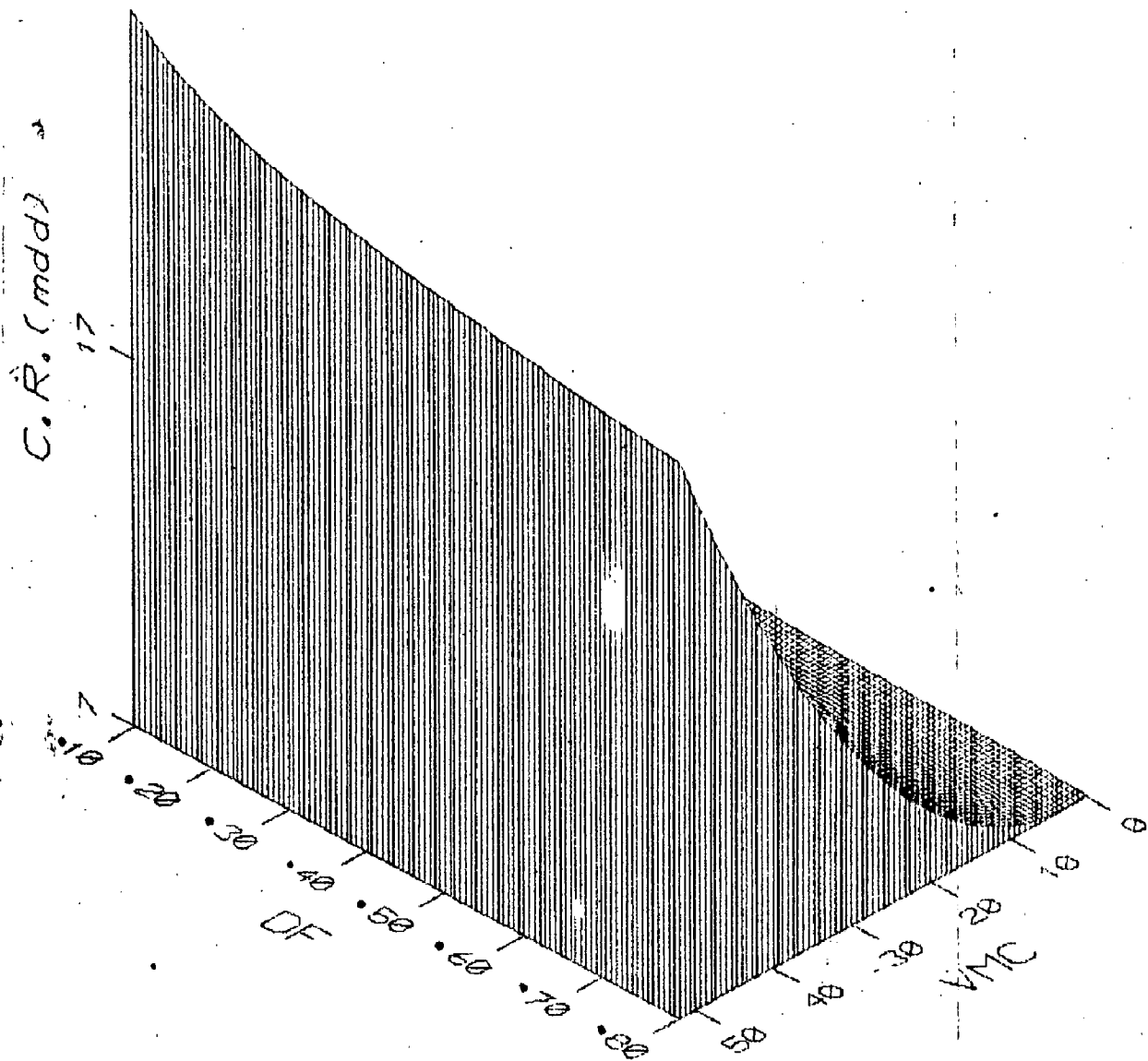


Fig. 7.20: 3D plot depicting the effect of VMC & DF on corrosion rate (based on equation 7.23)

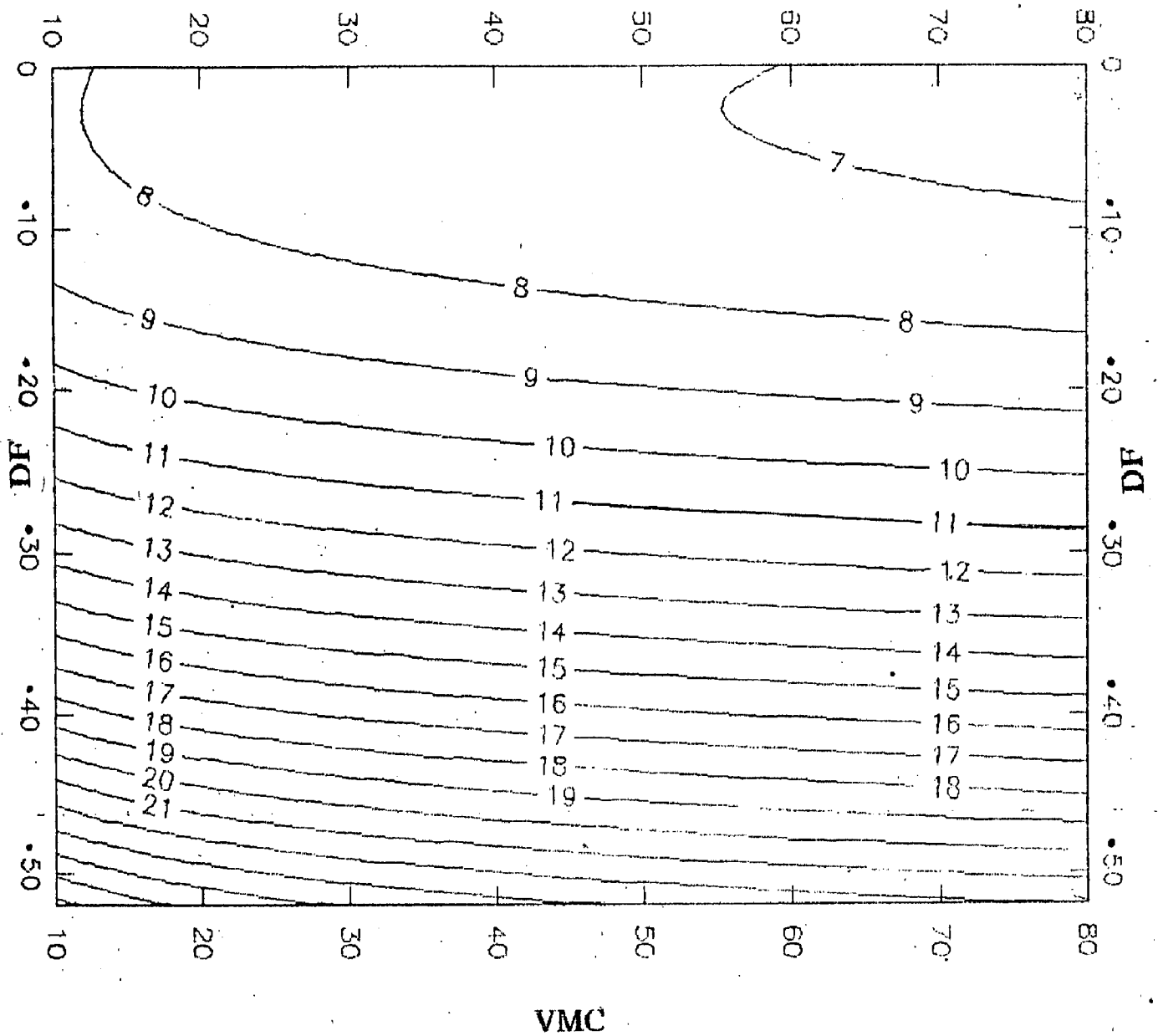


Fig. 7.21: Contour plot depicting the combined effect of F-113 VMC & DF on corrosion rate (based on equation 7.23)

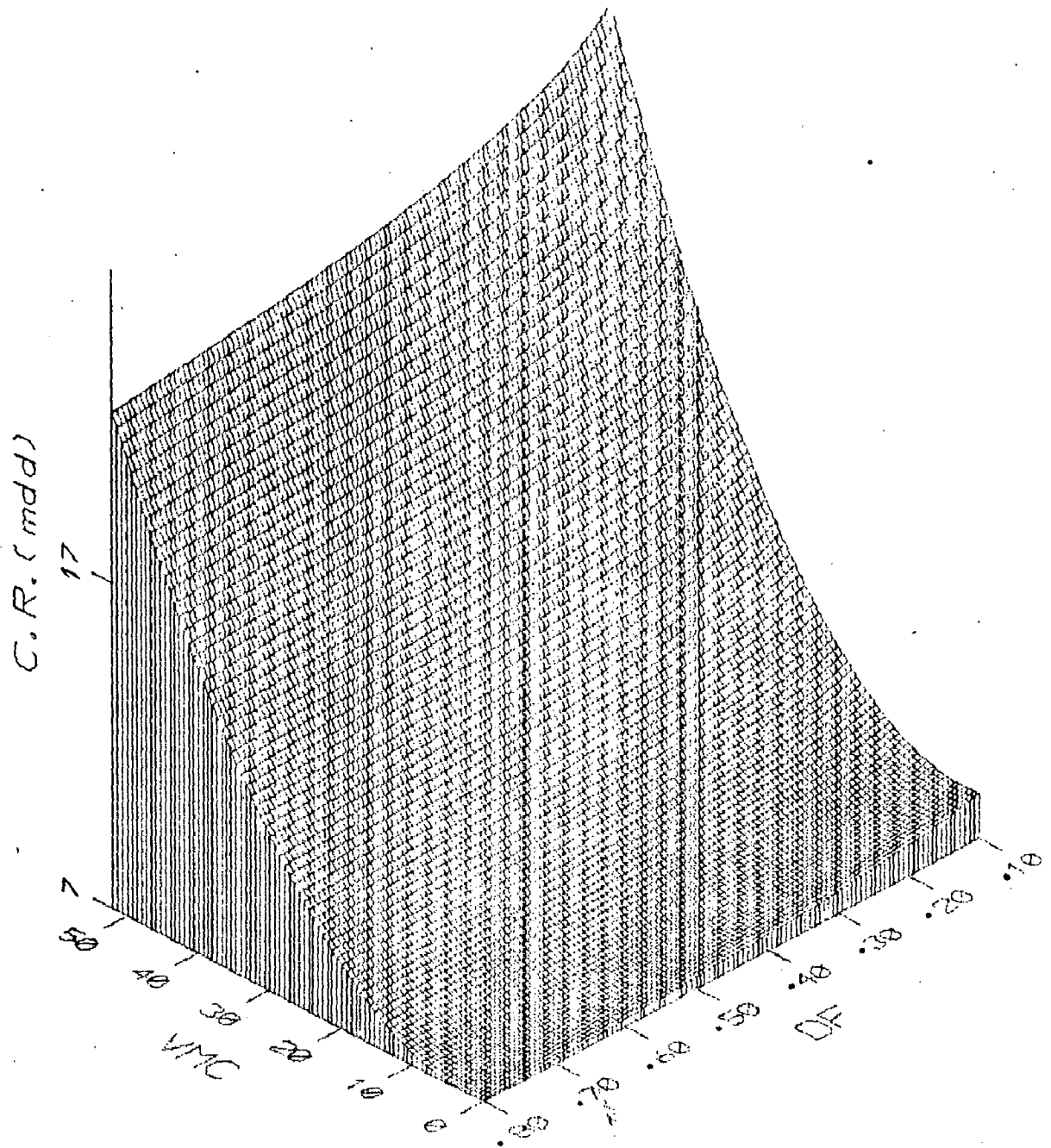


Fig. 7.22: 3D plot depicting the effect of VMC & DF on corrosion rate (based on equation 7.23)

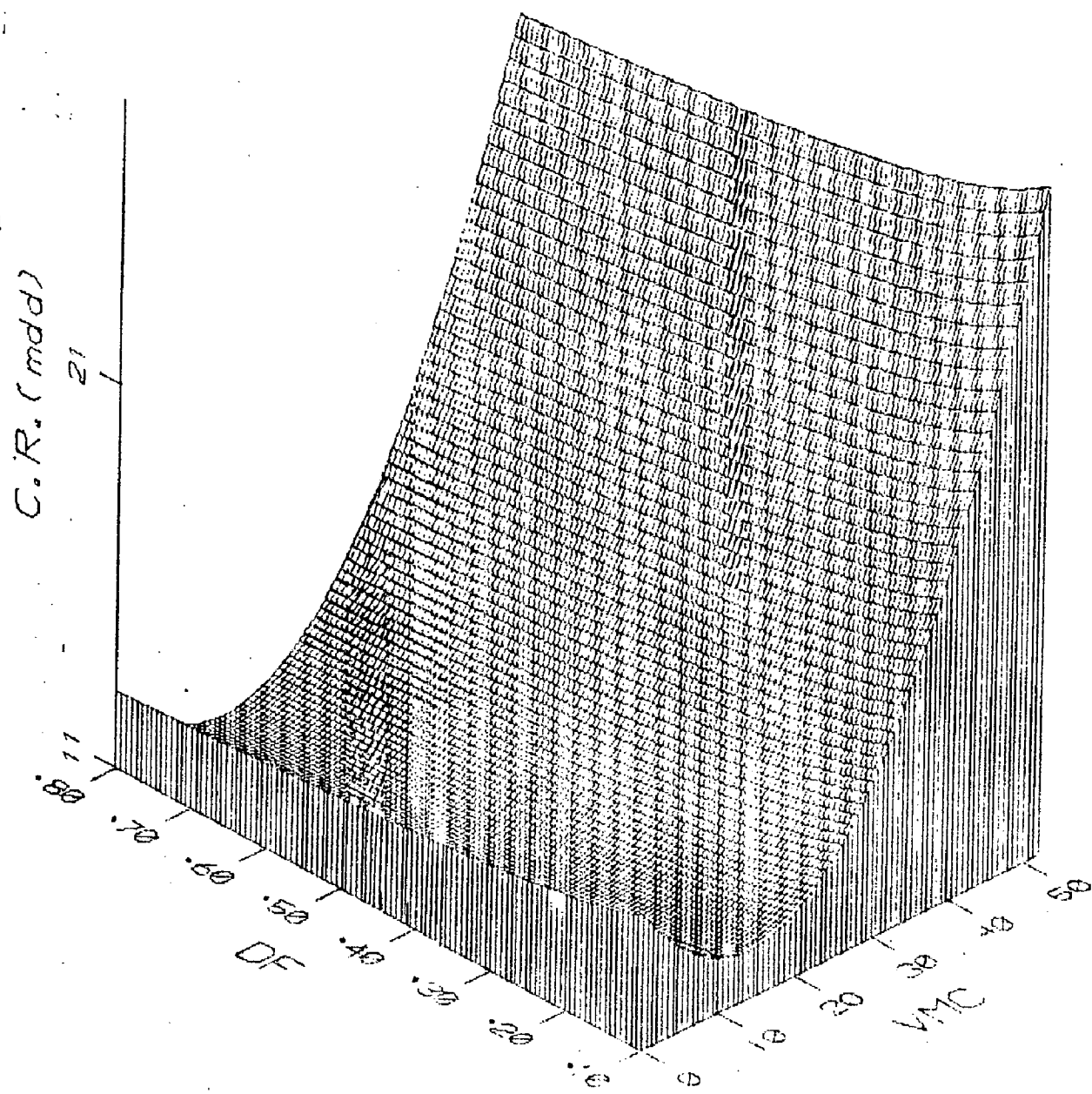


Fig. 7.23: 3D plot depicting the effect of VMC & DF on corrosion rate (based on equation 7.24)

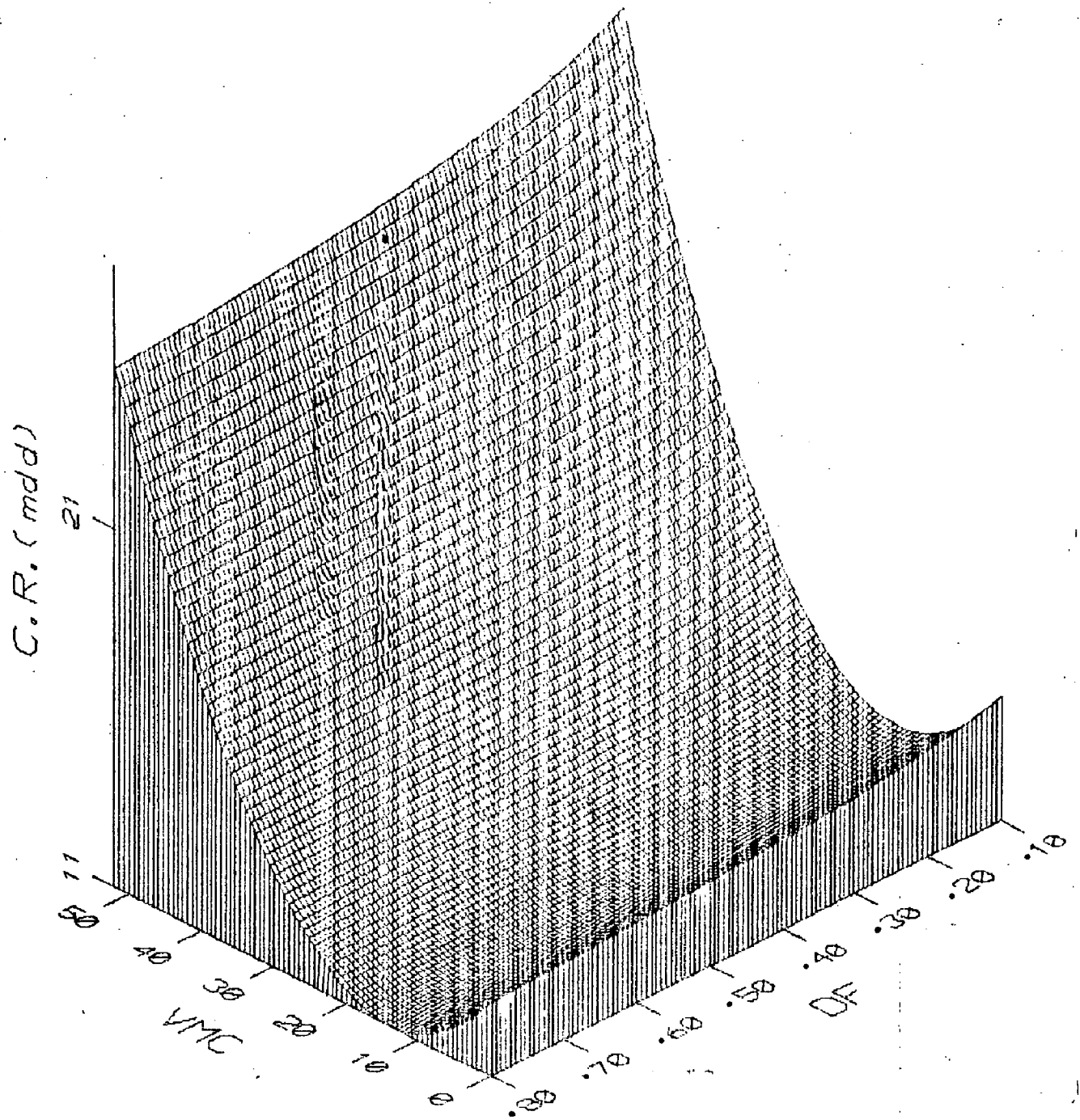


Fig. 7.24: 3D plot depicting the effect of VMC & DF on corrosion rate (based on equation 7.24)

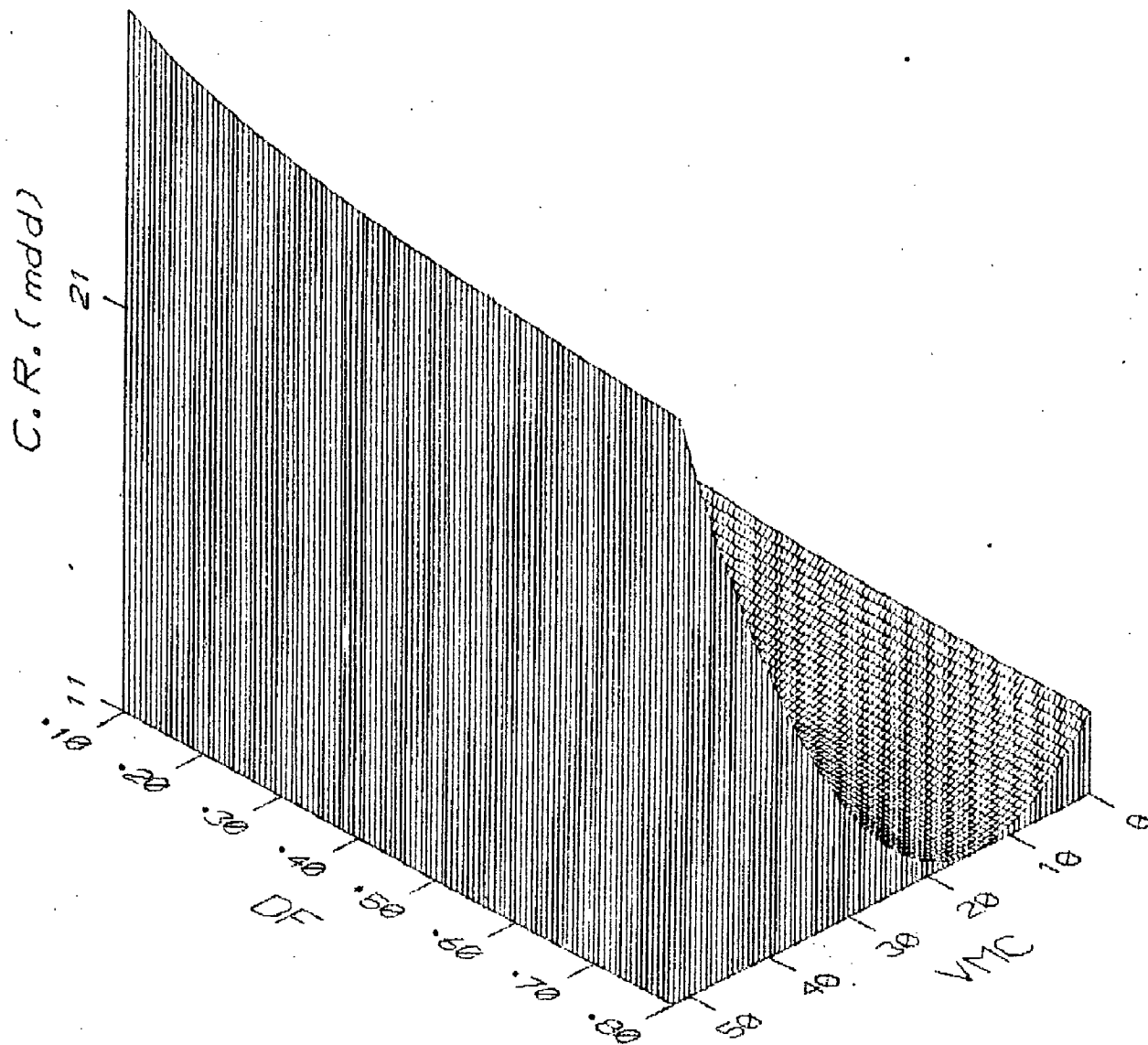


Fig. 7.25 : 3D plot depicting the effect of VMC & DF on corrosion rate (based on equation 7.24)

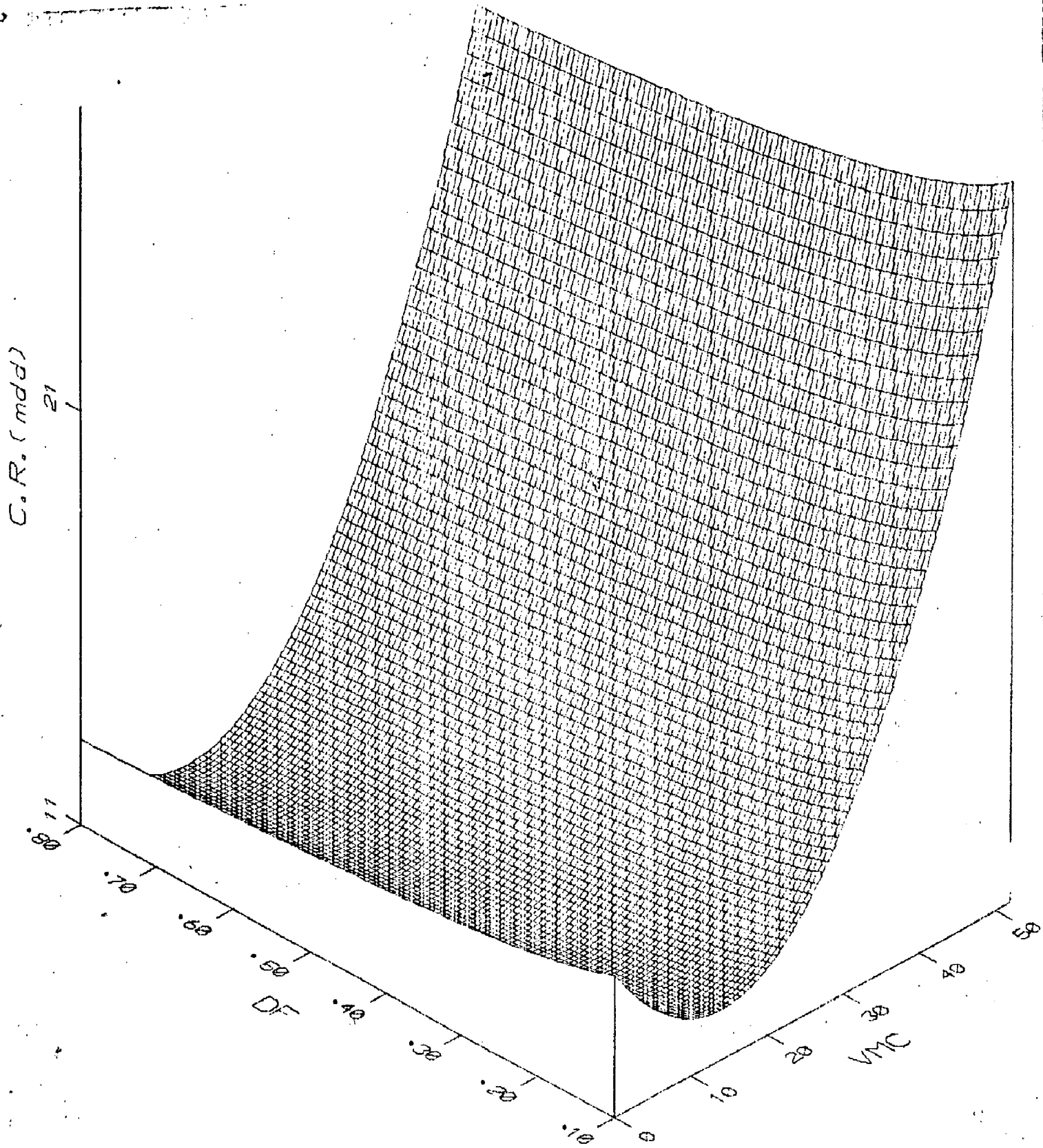


Fig. 7.26: 3D plot depicting the effect of VMC & DF on corrosion rate (based on equation 7.24)

Appendix-A1 Percent area of particles in different classes at different locations as influenced by heat treating parameters(Alloy C1)

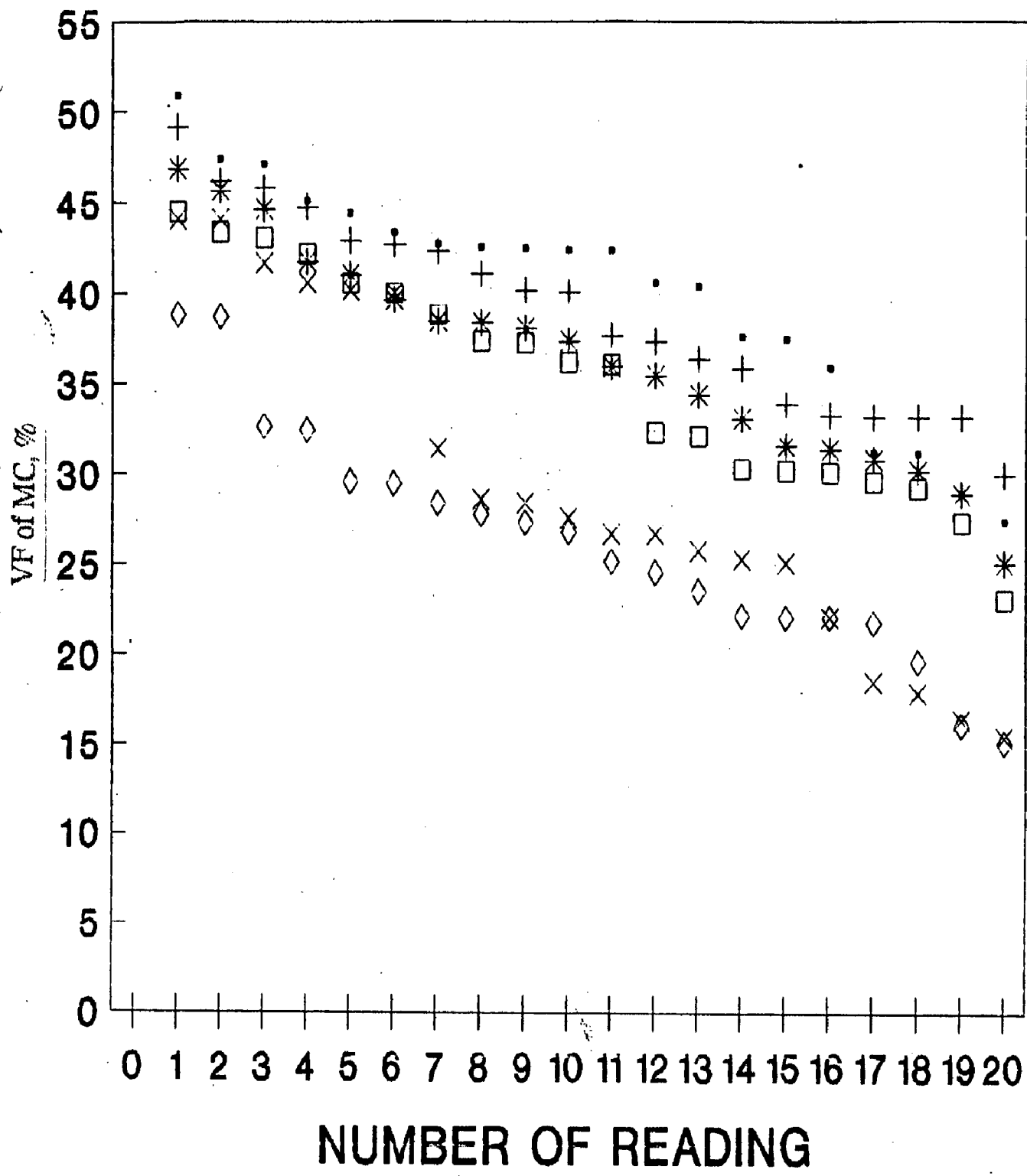
h/t	location I				location II				location III				location IV				location V				
800	2	25	74	0	0	27	71	0	0	25	75	0	0	25	74	0	0	20	80	0	0
800	4	16	83	0	0	21	78	0	0	22	77	0	0	20	79	0	0	23	76	0	0
800	6	15	84	0	0	15	84	0	0	18	81	0	0	30	69	0	0	16	83	0	0
800	8	7	59	32	0	39	59	0	0	3	50	46	0	10	23	65	0	6	39	54	0
800	10	7	34	57	0	2	44	52	0	15	35	49	0	5	30	21	41	7	63	29	0
850	2	15	35	49	0	27	71	0	0	14	85	0	0	8	62	29	0	5	39	54	0
850	4	11	88	0	0	7	92	0	0	5	94	0	0	30	69	0	0	18	81	0	0
850	6	8	24	67	0	5	94	0	0	21	78	0	0	25	74	0	0	6	39	54	0
850	8	6	48	45	0	8	38	53	0	5	39	54	0	20	79	0	0	13	35	50	0
850	10	6	44	49	0	3	20	38	37	5	49	45	0	5	44	49	0	17	21	60	0
900	2	35	64	0	0	12	87	0	0	15	22	62	0	39	59	0	0	20	79	0	0
900	4	100	0	0	0	21	78	0	0	14	85	0	0	27	71	0	0	47	52	0	0
900	6	15	22	62	0	100	0	0	0	21	78	0	0	18	81	0	0	12	87	0	0
900	8	18	81	0	0	5	39	54	0	6	39	54	0	2	26	0	71	8	24	67	0
950	2	25	74	0	0	47	52	0	0	18	81	0	0	18	81	0	0	33	66	0	0
950	4	16	83	0	0	39	59	0	0	47	52	0	0	12	87	0	0	100	0	0	0
950	6	100	0	0	0	10	90	0	0	2	25	71	0	100	0	0	0	0	100	0	0
950	8	100	0	0	0	14	85	0	0	21	78	0	0	52	47	0	0	30	69	0	0
1000	2	16	83	0	0	8	47	43	0	16	83	0	0	30	69	0	0	22	77	0	0
1000	4	25	74	0	0	6	39	54	0	25	74	0	0	18	81	0	0	10	46	43	0
1000	6	18	81	0	0	13	44	41	0	35	64	0	0	10	37	52	0	22	77	0	0
1000	8	33	66	0	0	10	90	0	0	100	0	0	0	100	0	0	0	10	90	0	0

Appendix-A2 Percent area of particles in different classes at different locations as influenced by heat treating parameters(Alloy C2)

h/t		location I				location II				location III				location IV				location V			
800	2	9	13	76	0	14	85	0	0	10	90	0	0	9	89	0	0	6	35	19	38
800	4	43	56	0	0	14	85	0	0	100	0	0	0	25	74	0	0	8	53	37	0
800	6	7	63	29	0	10	46	43	0	12	87	0	0	13	55	30	0	21	78	0	0
800	8	21	78	0	0	3	25	70	0	11	88	0	0	2	40	56	0	22	77	0	0
800	10	19	21	59	0	11	45	42	0	28	71	0	0	25	74	0	0	5	31	21	42
850	2	4	44	50	0	5	30	64	0	11	56	31	0	3	10	86	0	13	35	50	0
850	4	5	52	41	0	6	55	38	0	32	0	67	0	7	48	44	0	11	52	36	0
850	6	8	38	53	0	7	9	82	0	10	37	52	0	8	47	43	0	9	58	32	0
850	8	13	86	0	0	7	66	26	0	9	58	32	0	13	55	30	0	11	56	31	0
850	10	24	0	75	0	5	25	69	0	47	52	0	0	15	84	0	0	7	59	32	0
900	2	4	33	61	0	4	40	55	0	12	23	64	0	3	18	26	51	7	59	32	0
900	4	14	85	0	0	11	88	0	0	8	62	29	0	10	90	0	0	7	92	0	0
900	6	10	90	0	0	6	14	79	0	0	26	73	0	21	78	0	0	7	48	44	0
900	8	10	37	52	0	18	81	0	0	10	90	0	0	17	21	60	0	14	85	0	0
900	10	5	25	69	0	1	14	83	0	12	23	64	0	5	35	59	0	4	56	39	0
950	2	11	88	0	0	6	55	38	0	15	84	0	0	7	32	60	0	4	25	70	0
950	4	9	13	76	0	6	14	79	0	1	34	64	0	30	69	0	0	15	84	0	0
950	6	14	85	0	0	8	53	37	0	6	48	45	0	20	80	0	0	18	81	0	0
950	8	8	38	53	0	5	49	45	0	4	7	44	43	2	25	71	0	21	78	0	0
950	10	10	23	65	0	10	37	52	0	4	14	80	0	6	10	28	55	1	10	88	0
1000	2	7	54	37	0	5	25	69	0	10	23	65	0	18	81	0	0	4	14	80	0
1000	4	4	40	55	0	8	38	53	0	10	90	0	0	0	51	48	0	8	24	67	0
1000	6	100	0	0	0	100	0	0	0	100	0	0	0	0	0	0	100	4	14	80	0

Appendix-A3 Percent area of particles in different classes at different locations as influenced by heat treating parameters(Alloy C3)

h/t	location I				location II				location III				location IV				location V				
800	2	13	86	0	0	10	90	0	0	12	87	0	0	8	91	0	0	10	46	43	0
800	4	14	85	0	0	14	44	40	0	25	75	0	0	7	92	0	0	7	24	22	44
800	6	22	77	0	0	11	88	0	0	10	57	32	0	27	71	0	0	8	47	43	0
800	8	20	33	46	0	27	72	0	0	16	83	0	0	20	80	0	0	17	34	48	0
800	10	10	68	21	0	13	66	20	0	25	74	0	0	6	24	68	0	19	51	28	0
850	2	5	0	94	0	2	0	97	0	5	0	94	0	3	0	96	0	100	0	0	0
850	4	12	36	51	0	4	36	60	0	12	87	0	0	13	86	0	0	10	68	21	0
850	6	18	81	0	0	16	83	0	0	4	25	70	0	6	39	54	0	8	38	53	0
850	8	10	0	89	0	19	0	80	0	8	24	67	0	9	46	43	0	10	57	32	0
850	10	9	37	52	0	12	36	51	0	8	24	67	0	4	25	70	0	9	13	76	0
900	2	18	81	0	0	14	50	35	0	17	21	60	0	25	74	0	0	7	38	53	0
900	4	11	23	64	0	3	44	52	0	3	0	96	0	9	0	0	90	7	0	92	0
900	6	8	91	0	0	10	37	52	0	1	34	64	0	9	0	90	0	1	26	24	47
900	8	13	55	30	0	23	32	44	0	25	74	0	0	21	78	0	0	26	19	54	0
900	10	7	66	26	0	20	79	0	0	22	77	0	0	8	47	43	0	18	81	0	0
950	2	1	0	59	38	7	0	92	0	9	0	90	0	5	0	32	62	5	25	69	0
950	4	3	0	96	0	13	0	86	0	24	0	75	0	10	0	89	0	1	0	33	65
950	6	1	0	59	38	5	0	94	0	1	0	33	65	2	10	29	57	8	24	67	0
950	8	21	0	78	0	19	0	80	0	6	0	93	0	13	0	86	0	3	0	96	0
950	10	5	18	25	50	5	0	0	94	4	25	35	34	19	0	80	0	6	55	38	0
1000	2	7	32	60	0	10	0	89	0	3	31	65	0	8	24	67	0	6	39	54	0
1000	4	1	15	42	41	2	0	19	77	100	0	0	0	2	0	49	48	4	0	48	47
1000	6	16	0	83	0	2	0	97	0	13	0	86	0	6	0	93	0	10	0	89	0
1000	8	6	0	93	0	6	0	93	0	3	0	96	0	3	0	96	0	5	0	94	0



• 800 DEG C	+ 850 DEG C	* 900 DEG C
□ 950 DEG C	× 1000 DEG C	◇ 1050 DEG C

Fig. A-4 : Variation in Vf of MC as influenced by h/t temperature
(2 hours soaking period) Alloy C1

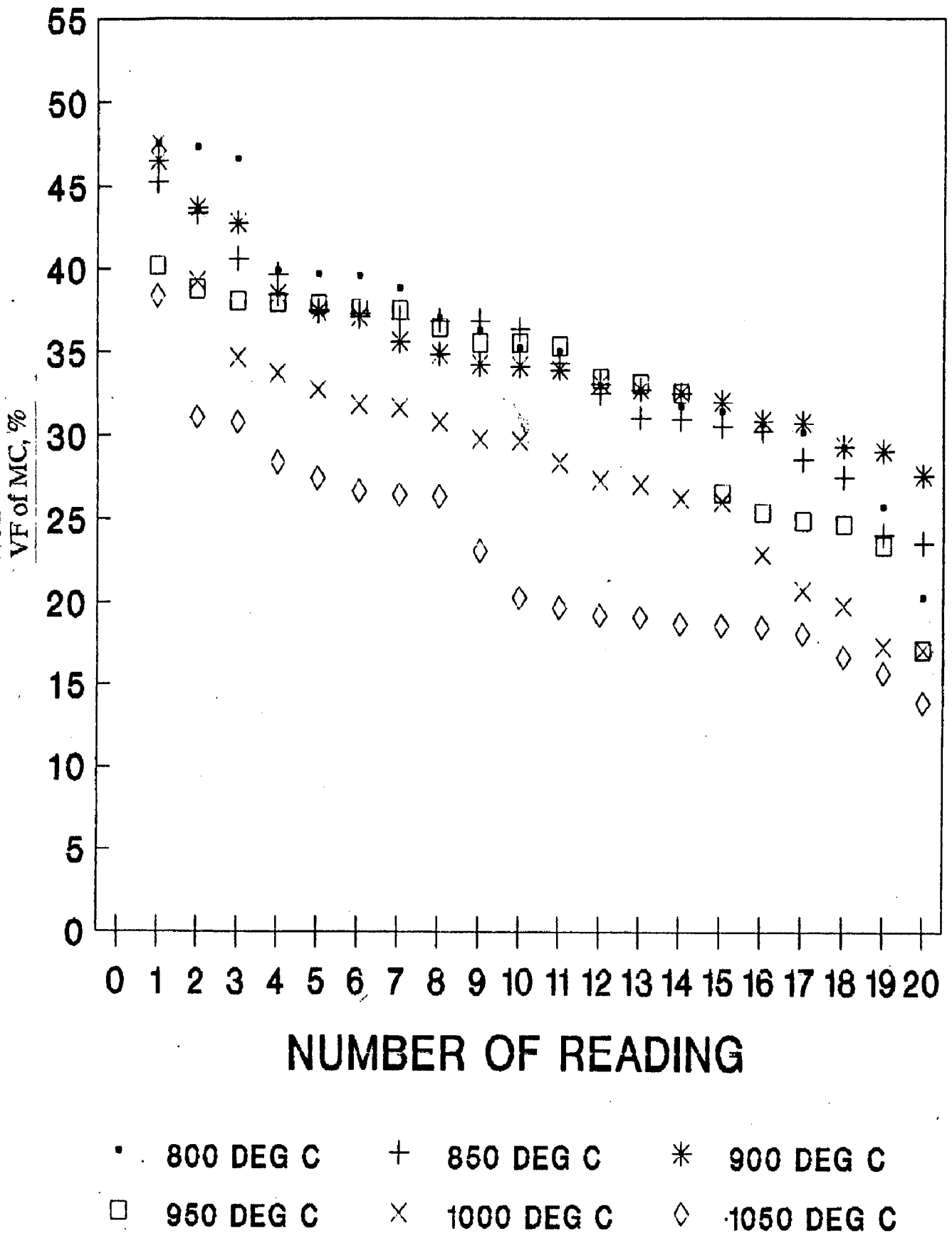
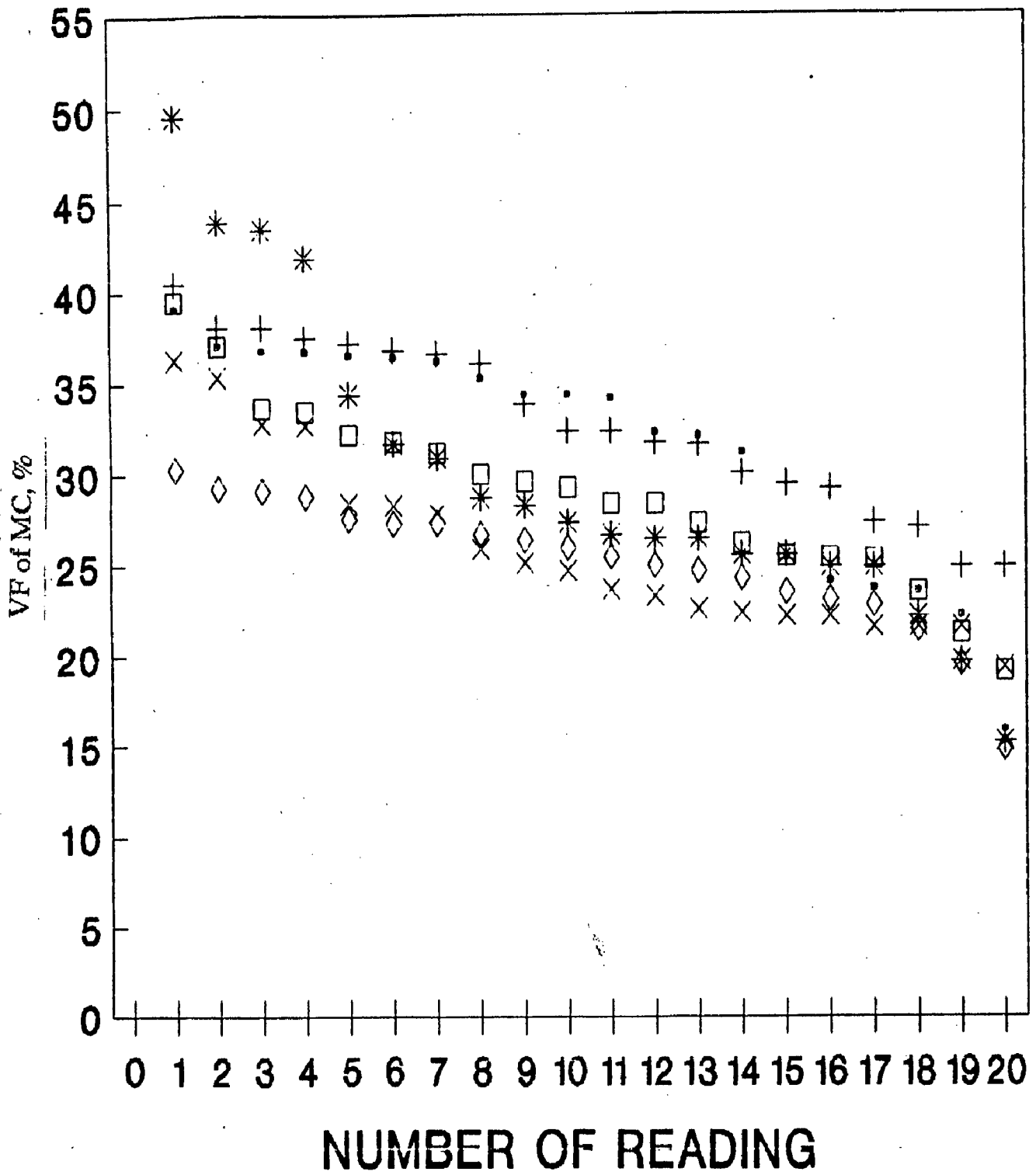


Fig. A-5 : Variation in Vf of MC as influenced by h/t temperature (2 hours soaking period) Alloy C2



• 800 DEG C + 850 DEG C * 900 DEG C
 □ 950 DEG C × 1000 DEG C ◇ 1050 DEG C

Fig. A-6 : Variation in Vf of MC as influenced by h/t temperature (2 hours soaking period) Alloy C3

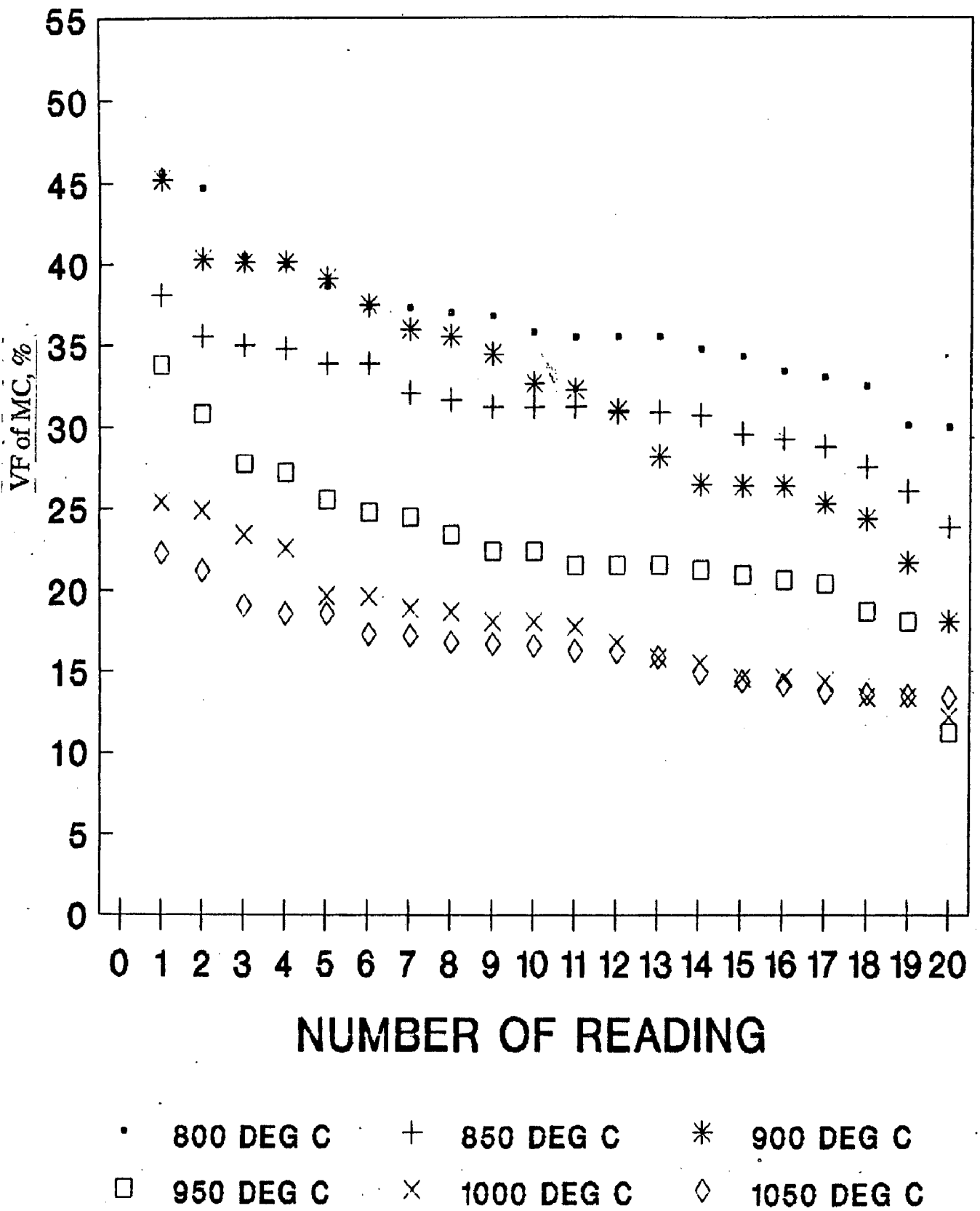
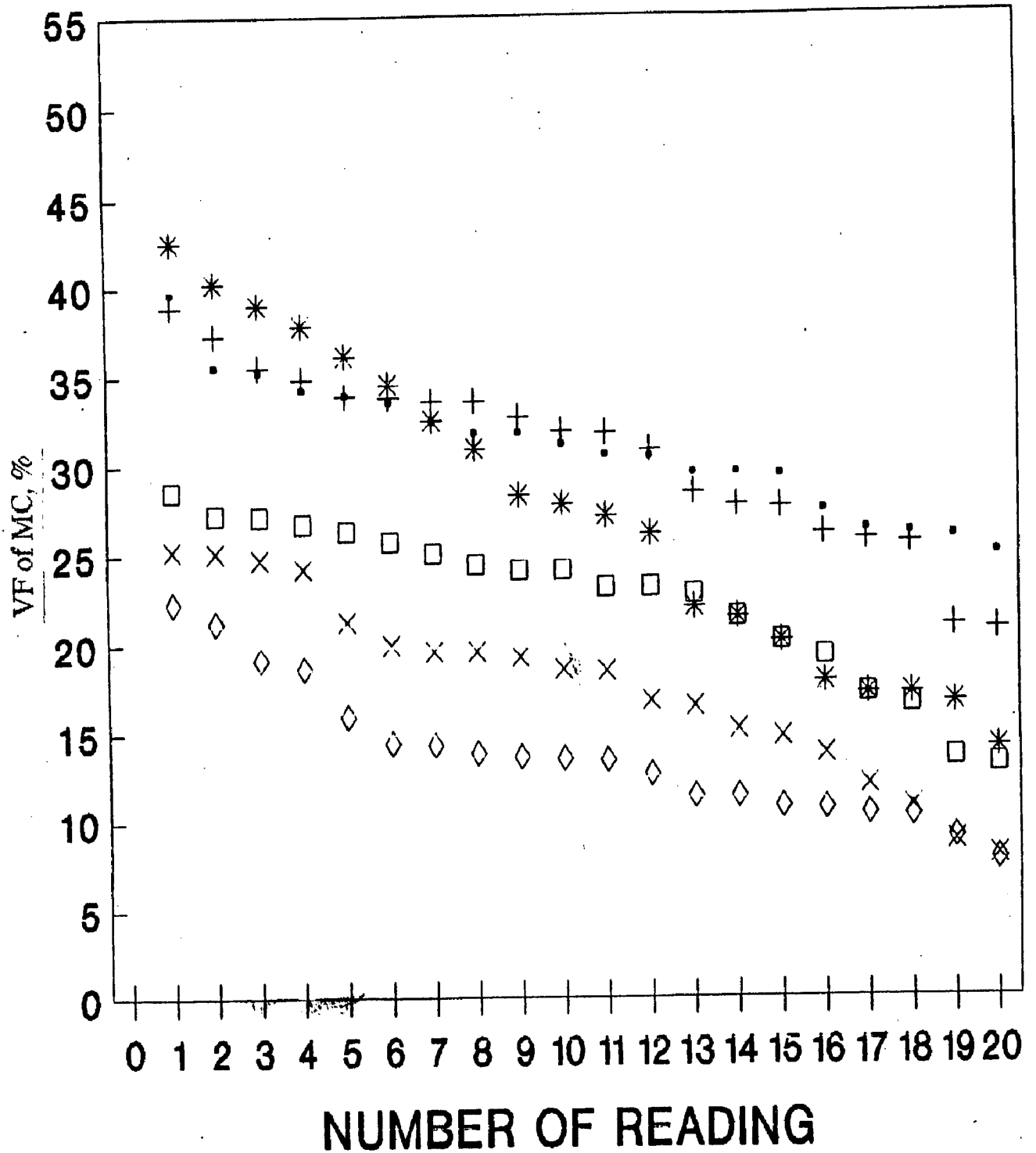
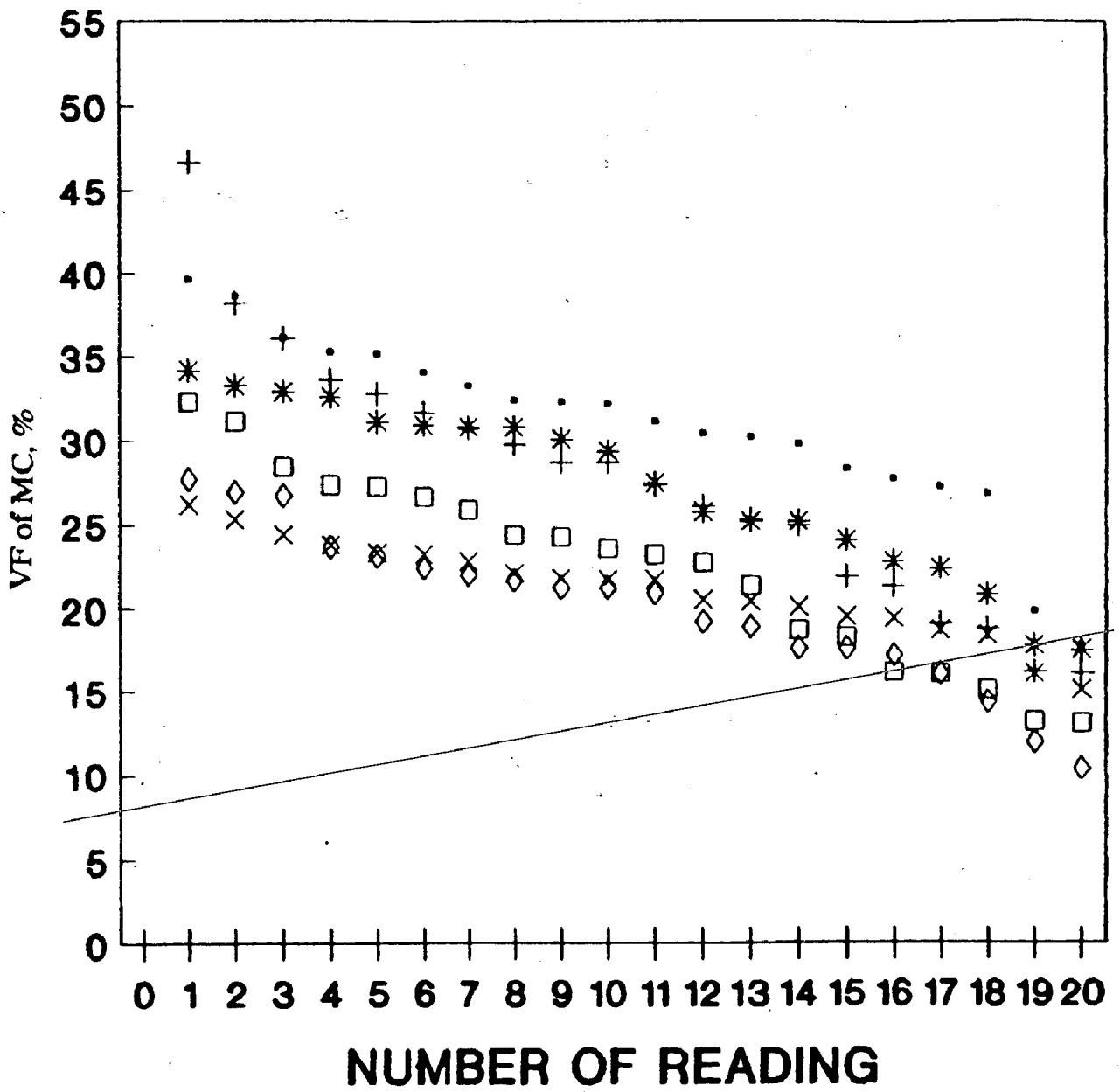


Fig. A-7 : Variation in Vf of MC as influenced by h/t temperature (10 hours soaking period) Alloy C1



• 800 DEG C	+ 850 DEG C	* 900 DEG C
□ 950 DEG C	× 1000 DEG C	◇ 1050 DEG C

Fig. A-8 : Variation in Vf of MC as influenced by h/t temperature
(10 hours soaking period) Alloy C2



• 800 DEG C + 850 DEG C * 900 DEG C
 □ 950 DEG C x 1000 DEG C ◇ 1050 DEG C

Fig. A-9 : Variation in VF of MC as influenced by h/t temperature (10 hours soaking period) Alloy C3